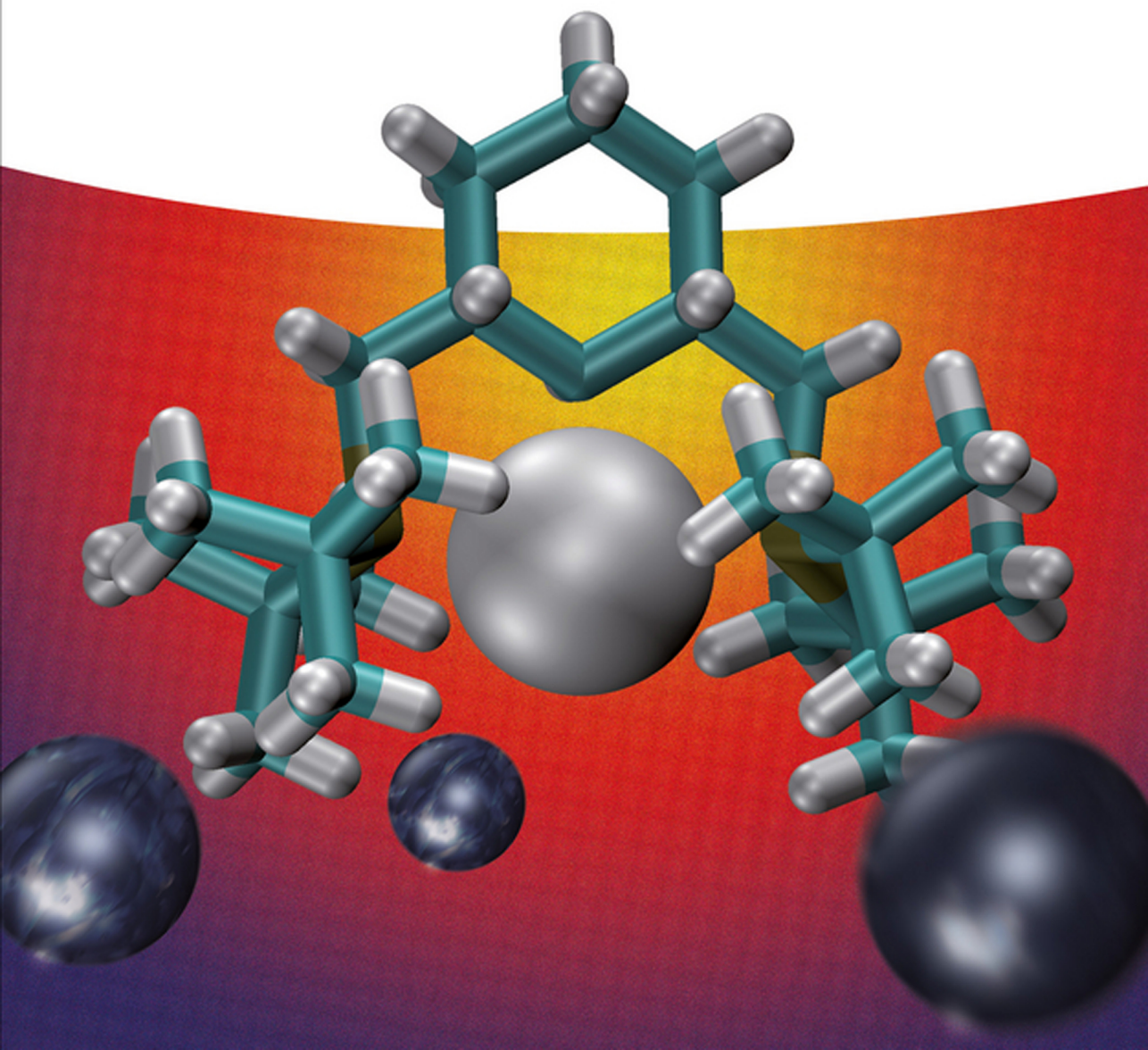


Kálmán J. Szabó and Ola F. Wendt

Pincer and Pincer-Type Complexes

Applications in Organic Synthesis and Catalysis



Edited by
Kálmán J. Szabó and
Ola F. Wendt

Pincer and Pincer-Type Complexes

Related Titles

Nolan, S.P. (ed.)

N-Heterocyclic Carbenes-Effective Tools for Organometallic Synthesis

2014

Print ISBN: 978-3-527-33490-2, also available in
digital formats

Andersson, P.G. (ed.)

Innovative Catalysis in Organic Synthesis

**Oxidation, Hydrogenation, and C-X Bond
Forming Reactions**

2012

Print ISBN: 978-3-527-33097-3, also available in
digital formats

de Meijere, A., Bräse, S., Oestreich, M.
(eds.)

Metal-Catalyzed Cross-Coupling Reactions and More

2014

Print ISBN: 978-3-527-33154-3, also available in
digital formats

Kuhl, O.

Functionalised N-Heterocyclic Carbene Complexes

2010

Print ISBN: 978-0-470-71215-3, also available in
digital formats

Molnár, Á. (ed.)

Palladium-Catalyzed Coupling Reactions

2013

Print ISBN 978-3-527-33254-0, also available in
digital formats

Edited by Kálmán J. Szabó and Ola F. Wendt

Pincer and Pincer-Type Complexes

Applications in Organic Synthesis and Catalysis

WILEY-VCH
Verlag GmbH & Co. KGaA

The Editors

Prof. Kálmán J. Szabó

Stockholm University
Arrhenius Laboratory
106 91 Stockholm
Sweden

Prof. Ola F. Wendt

Lund University
Organic Chemistry
221 00 Lund
Sweden

All books published by **Wiley-VCH** are carefully produced. Nevertheless, authors, editors, and publisher do not warrant the information contained in these books, including this book, to be free of errors. Readers are advised to keep in mind that statements, data, illustrations, procedural details or other items may inadvertently be inaccurate.

Library of Congress Card No.: applied for

British Library Cataloguing-in-Publication Data

A catalogue record for this book is available from the British Library.

Bibliographic information published by the Deutsche Nationalbibliothek

The Deutsche Nationalbibliothek lists this publication in the Deutsche Nationalbibliografie; detailed bibliographic data are available on the Internet at <<http://dnb.d-nb.de>>.

© 2014 Wiley-VCH Verlag GmbH & Co. KGaA, Boschstr. 12, 69469 Weinheim, Germany

All rights reserved (including those of translation into other languages). No part of this book may be reproduced in any form – by photoprinting, microfilm, or any other means – nor transmitted or translated into a machine language without written permission from the publishers. Registered names, trademarks, etc. used in this book, even when not specifically marked as such, are not to be considered unprotected by law.

Print ISBN: 978-3-527-33442-1
ePDF ISBN: 978-3-527-68132-7
ePub ISBN: 978-3-527-68133-4
Mobi ISBN: 978-3-527-68131-0
oBook ISBN: 978-3-527-68130-3

Cover-Design Grafik-Design Schulz, Fußgönheim, Germany

Typesetting Laserwords Private Limited, Chennai, India

Printing and Binding Markono Print Media Pte Ltd, Singapore

Printed on acid-free paper

Contents

Preface XI

List of Contributors XIII

1 Catalysis by Pincer Complexes: Synthesis of Esters, Amides, and Peptides 1

Chidambaram Gunanathan and David Milstein

- 1.1 Introduction and Background 1
- 1.2 Bond Activation by Metal–Ligand Cooperation 3
- 1.3 Synthesis of Esters 4
 - 1.3.1 Synthesis of Esters from Primary Alcohols 4
 - 1.3.2 Synthesis of Cross-Esters from Primary and Secondary Alcohols 9
 - 1.3.3 Synthesis of Esters by Acylation of Secondary Alcohols Using Esters 9
 - 1.3.4 Synthesis of Polyesters from Diols 11
- 1.4 Synthesis of Amides 15
 - 1.4.1 Synthesis of Amides from Alcohols and Amines 15
 - 1.4.2 Synthesis of Amides from Esters and Amines 18
 - 1.4.3 Synthesis of Polyamides from Diols and Diamines 20
- 1.5 Synthesis of Peptides from β -Amino Alcohols 24
- 1.6 Concluding Remarks 26
 - Acknowledgments 26
 - References 27

2 The Role of Redox Processes in Reactions Catalyzed by Nickel and Palladium Complexes with Anionic Pincer Ligands 31

Juan Cámpora and Cristóbal Melero

- 2.1 Introduction 31
- 2.2 Pincer Complexes of Ni, Pd, and Pt in Oxidation States Different from II 34
 - 2.2.1 Complexes in the Higher Oxidation States (III, IV) 34
 - 2.2.2 Reduced Complexes of Ni, Pd, and Pt with Pincer Ligands 43
- 2.3 Catalytic Reactions Involving Redox Processes in the Pincer-Metal Framework 46

2.3.1	Atom-Transfer Radical Addition (ATRA) and Polymerization Reactions (ATRP)	46
2.3.2	The Heck Reaction	48
2.3.3	C–C Cross-Coupling Reactions	54
2.3.4	Carbon–Heteroatom Coupling Reactions	62
2.4	Concluding Remarks	65
	Acknowledgment	66
	References	66
3	Appended Functionality in Pincer Ligands	71
	<i>Cameron M. Moore and Nathaniel K. Szymczak</i>	
3.1	Introduction	71
3.1.1	Design Criteria	72
3.1.2	Motivations	72
3.1.2.1	Transition-Metal Catalysis	72
3.1.2.2	Supramolecular Architectures	73
3.2	Appended Functionality Coplanar with the Pincer Chelate	75
3.2.1	Systems that Incorporate 2,2':6',2''-Terpyridine	75
3.2.1.1	Synthetic Strategies	75
3.2.1.2	Appended Lewis Acid/Bases	77
3.2.1.3	Appended Hydrogen-Bond Acceptor/Donors	79
3.2.2	Pyridine-2,6-Dicarboxamide Systems	84
3.3	Appended Functionality Not Coplanar to the Pincer Chelate	86
3.3.1	ENE Pincer Systems	86
3.3.2	PCP Pincer Systems	88
3.3.3	PEP Pincer Systems	88
3.3.4	Pyridine-2,6-Diimine Systems	90
3.4	Future Outlook and Summary	91
	References	91
4	C–C, C–O, and C–B Bond Formation by Pincer Complexes Including Asymmetric Catalysis	95
	<i>Kálmán J. Szabó</i>	
4.1	Introduction – Pros and Cons of Using Pincer Complexes in Catalysis	95
4.2	Reaction of Imines and Isocyanoacetates	96
4.2.1	Stereoselective Synthesis of Imidazolines	96
4.2.2	Application of Chiral Pincer Complexes	99
4.2.3	Mechanistic Considerations	101
4.3	C–H Functionalization of Organonitriles	102
4.3.1	Allylation of Imines	102
4.3.2	Benzyl Amine Synthesis	103
4.4	Reactions Involving Hypervalent Iodines	107
4.4.1	Arylation of Alkenes Using Pincer Complex Catalysis	107
4.4.2	Acetoxylation with Hypervalent Iodines	109

- 4.4.3 C–H Borylation of Alkenes 112
- 4.5 Summary and Outlook 113
References 115
- 5 Nickel-Catalyzed Cross-Coupling Reactions 117**
Anubendu Adhikary and Hairong Guan
- 5.1 Introduction 117
- 5.2 Carbon–Carbon Bond-Forming Reactions 118
- 5.2.1 Kumada–Corriu–Tamao Coupling 118
- 5.2.2 Suzuki–Miyaura Coupling 129
- 5.2.3 Negishi Coupling 132
- 5.2.4 Sonogashira Coupling 139
- 5.2.5 Mizoroki–Heck Reaction 140
- 5.2.6 Other Miscellaneous Cross-Coupling Reactions 141
- 5.3 Carbon–Heteroatom Bond-Forming Reactions 143
- 5.4 Summary and Outlook 144
Acknowledgments 144
References 144
- 6 PSiP Transition-Metal Pincer Complexes: Synthesis, Bond Activation, and Catalysis 149**
Laura Turculet
- 6.1 Introduction 149
- 6.2 PSiP Ligand Syntheses 151
- 6.3 Group 8 Metal PSiP Chemistry 153
- 6.4 Group 9 Metal PSiP Chemistry 161
- 6.5 Group 10 Metal PSiP Chemistry 169
- 6.6 Group 11 Metal PSiP Chemistry 179
- 6.7 Alternative Silyl Pincers 180
- 6.8 Summary 183
References 183
- 7 Electronic Structures of Reduced Manganese, Iron, and Cobalt Complexes Bearing Redox-Active Bis(imino)pyridine Pincer Ligands 189**
Paul J. Chirik
- 7.1 Introduction 189
- 7.2 Reduced Manganese, Iron, and Cobalt Complexes with Redox-Active Bis(imino)pyridines 189
- 7.2.1 Reduced Bis(imino)pyridine Manganese Chemistry 190
- 7.2.2 Reduced Bis(imino)pyridine Iron Chemistry 193
- 7.2.3 Reduced Bis(imino)pyridine Cobalt Chemistry 200
- 7.3 Conclusions and Outlook 209
References 209

- 8 Pincer Complexes with Saturated Frameworks: Synthesis and Applications** 213
Klara J. Jonasson and Ola F. Wendt
- 8.1 Introduction 213
- 8.2 Synthesis of the Ligands 213
- 8.3 Synthesis and Coordination Behavior of Carbometallated PC(sp³)P Complexes 215
- 8.3.1 Coordination Flexibility in Acyclic PC(sp³)P Complexes 216
- 8.4 Reactivity and Catalytic Applications of PC(sp³)P Complexes 217
- 8.4.1 Ammonia Activation 217
- 8.4.2 Isotopic Labeling 219
- 8.4.3 Reactions with Coordinated Olefins 219
- 8.4.4 Carbon–Carbon Coupling Reactions 221
- 8.4.5 Hydrogenation and Dehydrogenation 223
- 8.4.6 CO₂ Activation 225
References 225
- 9 Heavier Group 14 Elements-Based Pincer Complexes in Catalytic Synthetic Transformations of Unsaturated Hydrocarbons** 229
Jun Takaya and Nobuharu Iwasawa
- 9.1 Introduction 229
- 9.2 Synthesis of Palladium Complexes Bearing PXP-Pincer Ligands (X = Si, Ge, Sn) 230
- 9.2.1 Synthesis 230
- 9.2.2 Structural Analyses 230
- 9.3 Hydrocarboxylation 231
- 9.3.1 Hydrocarboxylation of Allenes 232
- 9.3.2 Hydrocarboxylation of 1,3-Dienes 234
- 9.4 Reductive Aldol Type Reaction 235
- 9.5 Dehydrogenative Borylation 237
- 9.5.1 Dehydrogenative Borylation of Alkenes and 1,3-Dienes 237
- 9.5.2 Mechanistic Considerations 239
- 9.6 Synthesis and Reaction of η^2 -(Si–H)Pd(0) Complex as an Equivalent to PSiP-Palladium Hydride Complexes 241
- 9.6.1 Synthesis and Structure of η^2 -(Si–H)Pd(0) 241
- 9.6.2 Reaction of η^2 -(Si–H)Pd(0) Complex with an Allene 242
- 9.6.3 Reaction of η^2 -(Si–H)Pd(0) Complex with Diboron 244
- 9.7 Conclusions 245
References 246
- 10 Experimental and Theoretical Aspects of Palladium Pincer-Catalyzed C–C Cross-Coupling Reactions** 249
Christian M. Frech
- 10.1 C–C Cross-Coupling Reactions – an Indispensable Tool for the Synthesis of Complex Organic Molecules 249

10.2	Palladium Pincer Complexes as C–C Cross-Coupling Catalysts	250
10.3	The Role of Palladium Pincer Complexes in Heck Reactions	253
10.3.1	Pd ^{II} /Pd ^{IV} Cycles and Palladium Nanoparticle Formation	256
10.4	Computational Investigations on the Thermal Feasibility of Pd ^{II} /Pd ^{IV} Cycles of Palladium Pincer-Catalyzed Heck Reactions	262
10.4.1	Possible Initial Reaction Steps of Pd ^{II} /Pd ^{IV} Mechanisms	263
10.4.2	Investigations on Mechanisms Initiated by Oxidative Addition of Phenyl Bromide on the Palladium(II) Center of [C ₆ H ₃ -2,6-(NHP(piperidinyl) ₂) ₂ }Pd(Cl)] (10)	263
10.4.3	Investigations on Mechanisms Initiated by Styrene Coordination and/or Chloride Dissociation	265
10.4.4	Pd ^{II} /Pd ^{IV} Cycle Proposed for Palladium Pincer-Catalyzed Heck Reactions	270
10.4.5	Heck Reactions Catalyzed by Palladium Pincer Complexes: Pd ^{II} /Pd ^{IV} Cycles and/or Palladium Nanoparticle Formation	274
10.5	Theoretical Investigations on a Pincer-Catalyzed Negishi Cross-Coupling Reaction	275
10.6	Concluding Remarks	277
	References	278
11	Reactions of Square-Planar d⁸ Pincer Complexes with Oxygen and Hydrogen	281
	<i>Wilson D. Bailey, Marie V. Parkes, Richard A. Kemp, and Karen I. Goldberg</i>	
11.1	Introduction	281
11.2	Insertion of Molecular Oxygen into Late-Transition Metal Hydride Bonds	284
11.3	Hydrogenolysis of Late-Transition Metal Hydroxide and Alkoxide Complexes	289
11.4	Summary	294
	Acknowledgment	294
	References	295
	Index	299

Preface

Transition metal catalysis has become one of the most important tools in organic synthesis, important reasons being the high selectivities and high levels of atom economy usually achieved in catalytic transformations. Pincer and pincer-like complexes is an important class of catalysts employed in organic synthesis. The main advantage of these species is the well-defined stoichiometry, which allows conscious catalyst design and fine-tuning of the reactivity and selectivity of the catalyst. Also, the tri-dentate pincer ligand gives the metal complexes an unusual thermal stability. These properties contribute to the improvement of the usual catalytic properties of the commonly used catalysts and sometimes this can give unique catalytic features, which cannot be presented without the pincer framework of the system.

The book aims to help synthetic chemists to choose and apply pincer-complex catalysts in organic transformations. It also points out the most important pincer architectures that can be used efficiently in selective synthesis. Furthermore, it discusses reactivity and mechanisms in the elementary steps of catalytic transformation, which increases our understanding thereby pointing toward completely new applications.

Chapter 1 by Milstein and Chidambaram describes a unique pincer-complex catalyzed transformation for synthesis of esters, amides, and peptides using the aromatization–dearomatization ability of the pincer ligands. Several chapters focus on the possibility of using pincer complexes to stabilize the unusual oxidation state of the metal central atom. Chapter 2 by Campora and Melero analyze the possibilities of bringing palladium to Pd(IV) and nickel to Ni(III) states during the catalytic process. Chapter 10 by Frech is focused on application of a Pd(II)–Pd(IV) catalytic cycle in cross-coupling reactions. Chapter 3 by Szymczak and Moore describes an entirely new application area of pincer complexes, namely as scaffolds for appended functionalities, such as Lewis acids or Lewis bases (even both of these functionalities in the same complex). Another promising novel application is using saturated pincer frameworks for catalysis as described by Jonasson and Wendt in Chapter 8. Chapter 4 by Szabó is focused on pincer-complex catalyzed functionalization of imines and some C–H functionalizations including asymmetric catalysis. Chapter 5 by Adhikary and Guan describes the use of nickel pincer complexes in cross-coupling reactions and shows how these can be complementary to the traditional palladium systems. Pincer complexes

have shown very promising reactivity in the activation of small molecules, and in the contribution by Bailey, Parkes, Kemp, and Goldberg (Chapter 11), the possibilities for generation of reactive intermediates in oxidation and reduction reactions are described. In the last decade, a number of new pincer frameworks have appeared and a few of these are described in the final chapters. Although they have not always shown a lot of applications they hold a promise for completely novel transformations. Thus, Chirik in Chapter 7 describes how redox activity of the ligands can be understood and give unprecedented reactivity to base metal complexes. The use of Si, Ge, or Sn with their exceptional trans influence as the central ligating atom is explored in two chapters. Turculet in Chapter 6 gives an overview of PSiP pincer chemistry, showing the unique features of this chemistry and Takaya and Iwasawa in Chapter 9 describes the application of heavier group 14 based pincer palladium complexes in hydrocarboxylation and borylation reactions.

Hopefully, the new aspects of pincer-complex catalysis reviewed in the above chapters will contribute to a broadening of the applications of pincer complexes in organic synthesis as well as to the study of reaction mechanisms.

We would like to acknowledge the authors of this book for their enthusiasm and for sharing their knowledge on pincer chemistry with the readers and for their help in realizing the present book on applications of pincer-complex catalysis in organic synthesis.

Stockholm and Lund
December 2013

Kálmán J. Szabó
Stockholm University
Department of Organic Chemistry
Stockholm, Sweden

Ola F. Wendt
Lund University
Department of Chemistry
Centre for Analysis and Synthesis
Lund, Sweden

List of Contributors

Anubendu Adhikary

University of Cincinnati
Department of Chemistry
301 Clifton Court
Cincinnati
OH 45221-0172
USA

Wilson D. Bailey

University of Washington
Department of Chemistry
Seattle
WA 98195-1700
USA

Juan Cámpora

Instituto de Investigaciones
Químicas
CSIC–Universidad de Sevilla
c/ Américo Vespucio, 49
41092 Sevilla
Spain

Paul J. Chirik

Princeton University
Department of Chemistry
292 Frick Laboratory
Princeton
NJ 08544
USA

Christian M. Frech

Zürich University of Applied
Sciences
Department of Life Sciences and
Facility Management
Institute of Chemistry and
Biological Chemistry
Einsiedlerstrasse 31
CH-8820 Wädenswil
Switzerland

Karen I. Goldberg

University of Washington
Department of Chemistry
Seattle
WA 98195-1700
USA

Hairong Guan

University of Cincinnati
Department of Chemistry
301 Clifton Court
Cincinnati
OH 45221-0172
USA

Chidambaram Gunanathan

National Institute of Science
Education and Research (NISER)
School of Chemical Sciences
Bhubaneswar 751005
India

Nobuharu Iwasawa

Tokyo Institute of Technology
Department of Chemistry
2-12-1-E1-2 O-okayama
Tokyo 152-8551
Japan

Klara J. Jonasson

Lund University
Department of Chemistry
Centre for Analysis and Synthesis
Getingevägen 60
221 00 Lund
Sweden

Richard A. Kemp

University of New Mexico
Department of Chemistry and
Chemical Biology
Albuquerque
NM 87131
USA

and

Sandia National Laboratories
Advanced Materials Laboratory
Albuquerque
NM 87106
USA

Cristóbal Melero

Instituto de Investigaciones
Químicas
CSIC–Universidad de Sevilla
c/ Américo Vespucio, 49
41092 Sevilla
Spain

David Milstein

The Weizmann Institute of
Science
Department of Organic
Chemistry
Rehovot 76100
Israel

Cameron M. Moore

University of Michigan
Department of Chemistry
930 N. University
Ann Arbor
MI 48109-1055
USA

Marie V. Parkes

University of New Mexico
Department of Chemistry and
Chemical Biology
Albuquerque
NM 87131
USA

Kálmán J. Szabó

Stockholm University
Department of Organic
Chemistry
Svante Arrhenius väg 16C
SE-106 91 Stockholm
Sweden

Nathaniel K. Szymczak

University of Michigan
Department of Chemistry
930 N. University
Ann Arbor
MI 48109-1055
USA

Jun Takaya

Tokyo Institute of Technology
Department of Chemistry
2-12-1-E1-2 O-okayama
Tokyo 152-8551
Japan

Laura Turculet

Dalhousie University
Department of Chemistry
6274 Coburg Road
P.O. Box 15000
Halifax, Nova Scotia
B3H 4R2 Canada

Ola F. Wendt

Lund University
Department of Chemistry
Centre for Analysis and Synthesis
Getingevägen 60
221 00 Lund
Sweden

1

Catalysis by Pincer Complexes: Synthesis of Esters, Amides, and Peptides

Chidambaram Gunanathan and David Milstein

1.1

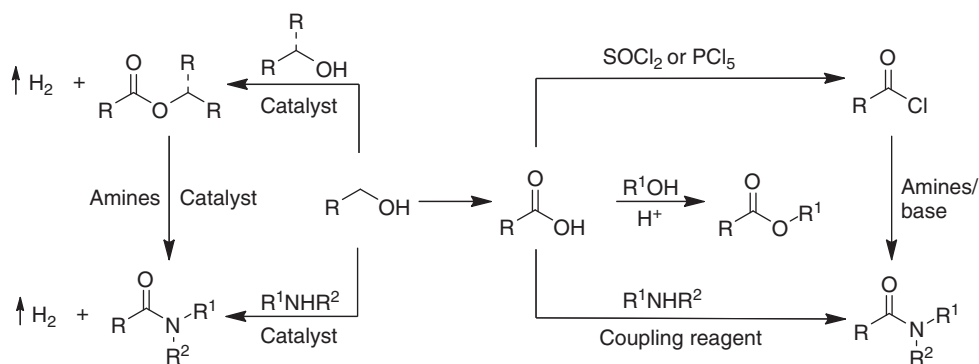
Introduction and Background

Esters, amides, amines, acetals, and peptides are important industrial chemicals. Production of these chemicals is based on multistep processes using stoichiometric amounts of acid or base promoters and coupling reagents, and involves reactive intermediates derived from alcohols or acids (Scheme 1.1), which leads to very large amounts waste [1]. Controlling overoxidation of substrates in the synthetic methods of these products is a challenge, and hence stepwise syntheses are performed (see below) [2]. Thus, green processes that can circumvent stoichiometric reagents and the generation of reactive intermediates, such as acid chlorides, and directly deliver stable and useful industrial products, such as esters and amides, in an atom-economical, selective manner without producing waste are needed.

Pincer ligands, that is, tridentate ligands that enforce meridional geometry upon complexation to transition metals, result in pincer complexes which possess a unique balance of stability versus reactivity [3]. Transition-metal complexes of bulky, electron-rich “pincer” ligands have found important applications in synthesis, bond activation, and catalysis [4, 5]. Among these, pincer complexes of ^tPr-PNP (2,6-bis-(di-*iso*-propylphosphinomethyl)pyridine), ^tBu-PNP (2,6-bis-(di-*tert*-butylphosphinomethyl)pyridine), and PNN ((2-(di-*tert*-butylphosphinomethyl)-6-diethylaminomethyl)pyridine), PNN-BPy (6-di-*tert*-butylphosphinomethyl-2,2'-bipyridine) ligands exhibit diverse reactivity [6–8]. These bulky, electron-rich pincer ligands can stabilize coordinatively unsaturated complexes and participate in unusual bond activation and catalytic processes.

In most processes, homogeneously catalyzed by metal complexes, the ligands, while imparting critical properties on the metal center, do not participate directly in bond-making and -breaking processes with the substrates. In recent years, complexes in which the ligands actively cooperate with the metal center in bond-activation processes have been developed [9]. We have devised novel catalytic systems based on pincer complexes in which the pincer ligands cooperate with the metal center in a synergistic manner and their interplay facilitates the chemical processes. The pincer complexes are based on new pyridine- and acridine-type

pincer ligands, which undergo bond-breaking and -making processes, involving aromatization–dearomatization of the pincer ligands [8]. Such cooperative pincer complexes catalyze several unique processes, as summarized in recent reviews [6–8, 10]. Here we concentrate on the selective synthesis of esters [11–13], amides [14, 15], acetals [16], amines [17], and imines [18], directly from alcohols. Using diols, polyesters were obtained [19]; diols and diamines provided polyamides [20, 21], and aminoalcohols resulted in formation of pyrazines and peptides [22]. Cooperative pincer complexes have also catalyzed the reverse reactions of esterification and amidation; thus, hydrogenation of esters [23, 24], formates, and carbonates [25] provides the corresponding alcohols, whereas amides give amines and alcohols [26] and urea provides methanol and amines [27]. Carbon dioxide also undergoes hydrogenation to formate salts [28] by pincer catalysts.



Scheme 1.1 Conventional versus catalytic synthesis of esters and amides.

Deprotonation of a pyridinylmethylenic proton of pyridine- and bipyridine-based pincer complexes can lead to dearomatization. The dearomatized complexes can then activate a chemical bond ($H-Y$, $Y = H, OH, OR, NH_2, NR_2, C$) by cooperation between the metal and the ligand, thereby regaining aromatization (Figure 1.1). The overall process does not involve a change in the metal's oxidation state [6–8]. In this chapter, we describe the novel, environmentally benign catalytic synthesis of esters, amides, and peptides that operate via this new metal–ligand cooperation based on aromatization–dearomatization processes.

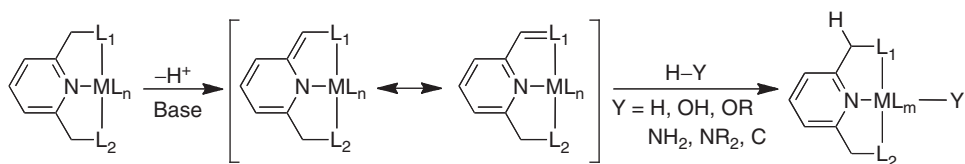
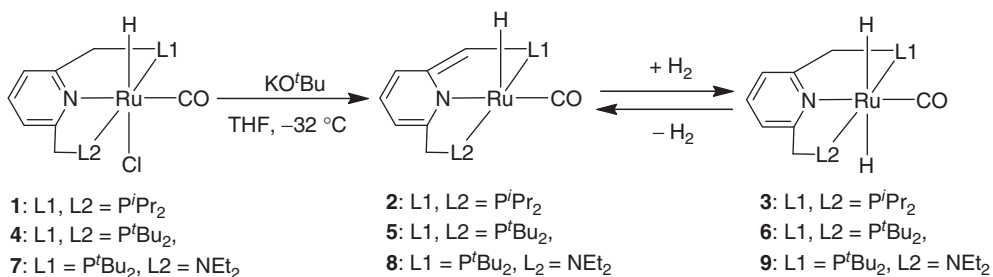


Figure 1.1 Metal–ligand cooperation based on aromatization–dearomatization.

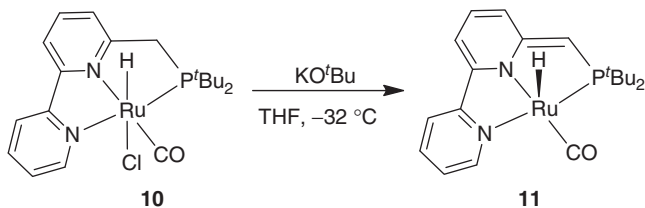
1.2 Bond Activation by Metal–Ligand Cooperation

We have discovered a new mode of bond activation by metal–ligand cooperation based on aromatization–dearomatization of pyridine- and acridine-based heteroaromatic pincer complexes (Figure 1.1) [6–8, 29]. Recently, we have observed that bipyridine-derived PNN-Bipy ligands also exhibit similar metal–ligand cooperativity (Scheme 1.2) [13, 24–27]. Such reactivity, which is not possible with the corresponding aryl-based PCP pincer complexes, is made possible in pyridine-based pincer complexes by (i) the relatively low resonance energy of pyridine (28 kcal mol⁻¹; compared to benzene, 36 kcal mol⁻¹), (ii) the acidity of pyridinyl methylene protons in the pyridine-based pincer complexes, and (iii) stabilization of the dearomatized ligand by the metal center.



Scheme 1.2 Preparation of dearomatized pyridine-based PNP and PNN pincer complexes and their reversible reaction with H₂.

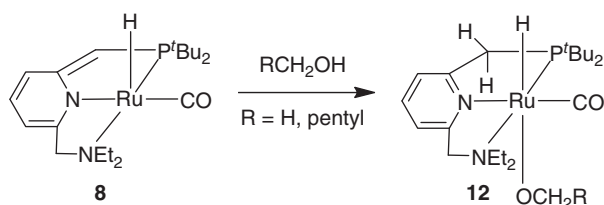
For example, the pyridine-based pincer complexes **1**, **4**, **7**, and **10** undergo smooth deprotonation to provide complexes **2**, **5**, **8**, and **11** (Schemes 1.2 and 1.3). NMR studies of **2**, **5**, **8**, and **11** indicate dearomatization, as the pyridine protons are shifted to lower frequency (olefinic region). Moreover, the structure of complex **2** is unequivocally corroborated by single-crystal X-ray diffraction studies [23]. Importantly, the dearomatized complexes of **2**, **5**, and **8** activate dihydrogen by cooperation between the ruthenium center and the deprotonated phosphine arm, resulting in aromatization to quantitatively yield the ruthenium *trans*-dihydride complexes of **3**, **6**, and **9**, respectively (Schemes 1.2). The magnetically equivalent



Scheme 1.3 Preparation of dearomatized bipyridine-derived PNN pincer complex **11**.

trans-dihydrides resonate as triplets in complexes **3** and **6** at -4.96 ppm ($^2J_{\text{PH}} = 20.0$ Hz) and -4.90 ppm ($^2J_{\text{PH}} = 17.0$ Hz), respectively, whereas they display doublets at -4.06 ppm ($^2J_{\text{PH}} = 17.0$ Hz) for complexes **9**. The *trans*-dihydride complexes **3**, **6**, and **9** slowly lose H_2 at room temperature to regenerate complexes **2**, **5**, and **8**, respectively.

In addition to the activation of dihydrogen [29d, 30], the dearomatized pyridine-derived pincer complexes also activate O–H bonds of alcohols [11–18, 31] and water [29e, 32], N–H bonds of amines and ammonia [29f,h], sp^3 C–H [29c] and sp^2 C–H bonds [29a,g], and carbon dioxide [33]. Among these various bond-activation reactions, of particular interest here is the O–H bond activation of alcohols, as complex **8** reacts with alcohols to provide the aromatic coordinatively saturated hydrido-alkoxy complexes **12** (Scheme 1.4), indicating the possibility of catalytic transformations based on dehydrogenation of alcohols.



Scheme 1.4 O–H activation by the dearomatized PNN pincer complex **8**.

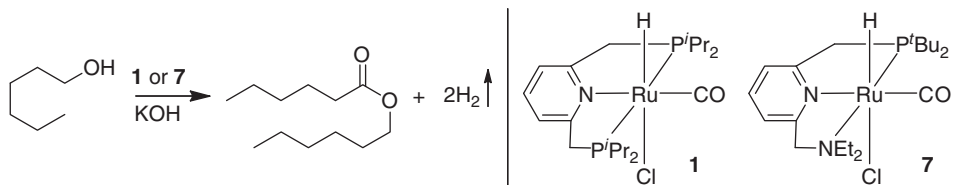
Such dearomatization and aromatization of these electron-rich ligand systems in cooperation with metal centers present new opportunities for homogeneous catalysis.

1.3 Synthesis of Esters

Esterification is an important reaction in organic synthesis. It has an assortment of applications in the production of synthetic intermediates, biologically active natural products, fragrances, polymers, polyesters, plasticizers, fatty acids, paints, and pharmaceuticals. Environmentally benign esterification methods catalyzed by pincer complexes that operate via metal–ligand cooperation are described in this section.

1.3.1 Synthesis of Esters from Primary Alcohols

When primary alcohols were heated with a catalytic amount of complex **1**, in the presence of a catalytic amount of base, an unusual dehydrogenative coupling to form esters with evolution of H_2 was observed [11]. Thus, refluxing a hexanol (bp 157°C) solution containing complex **1** and KOH (0.1 mol% each) under argon in

Table 1.1 Catalytic conversion of alcohols to esters by PNP (1) and PNN (7) complexes in the presence of catalytic base.


The reaction scheme shows 1-hexanol reacting with catalysts 1 or 7 and KOH to form hexyl hexanoate and 2H₂. The structures of the catalysts are shown below the reaction arrow:

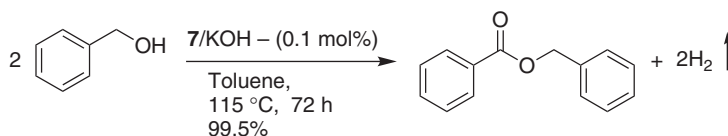
Complex 1: A ruthenium (Ru) center coordinated to a bidentate PNP ligand (1,1'-bis(diphenylphosphino)ethane), a hydride (H), a carbonyl (CO), and a chloride (Cl) ligand.

Complex 7: A ruthenium (Ru) center coordinated to a hemilabile PNN ligand (1,1'-bis(diphenylphosphino)ethane with a dimethylamino arm), a hydride (H), a carbonyl (CO), and a chloride (Cl) ligand.

Catalyst	Solvent	Time	Temperature (°C)	Yield (%)	TON
1/KOH (0.1 mol%)	—	24	157	67	670
7/KOH (0.1 mol%)	Toluene	24	115	95	950

an open system for 24 h resulted in formation of hexyl hexanoate in 67% yield. The PNN complex 7, which possesses a hemilabile amine “arm,” was a significantly better catalyst (still in the presence of an equivalent of base) than the corresponding PNP complex 1, leading to 95% (950 turnovers) hexyl-hexanoate after 24 h at 115 °C (Table 1.1) [11].

Good turnover numbers (TONs) and yields of esters were obtained with various alcohols at 115 °C. Reaction follow-up with benzyl alcohol indicated that 91% benzyl benzoate was formed already after 6 h, with turnover frequency (TOF) reaching 333 h⁻¹ at the level of 50% benzyl benzoate. Formation of the ester became very slow after 6 h, perhaps because of retardation of the reaction by the high ester concentration. However, almost quantitative formation of benzyl benzoate was obtained (Scheme 1.5).

**Scheme 1.5** Catalytic conversion of benzyl alcohol to benzyl benzoate by PNN complex 7.

Further improvement in the reaction was possible by exclusion of the need for base. Thus, reaction of complex 7 with KO^tBu resulted in the formation of the coordinatively unsaturated, 16e⁻ Ru(II) neutral complex 8. Indeed, 8 is an excellent catalyst for the dehydrogenative coupling of alcohols to esters and the reaction proceeds with liberation of H₂ under neutral conditions [11]. Table 1.2 provides a few examples. GC analysis of the reaction mixtures indicated that aldehydes were formed only in trace amounts. This catalytic reaction provided a new “green” pathway for the synthesis of esters directly from alcohols. Considerably less efficient methods had been reported previously for this transformation [34].

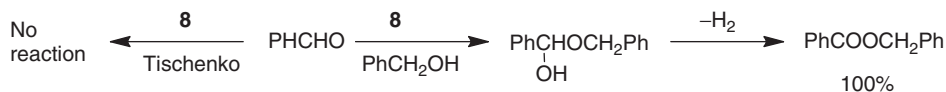
Table 1.2 Examples of dehydrogenative coupling of alcohols to form esters and dihydrogen catalyzed by dearomatized Ru PNN complex **8**.

Entry	R	Ester	Time (h)	Ester (%)
1 ^a	Propyl	Butyl butyrate	5	90
2	Pentyl	Hexyl hexanoate	6	99
3	Ph	Benzyl benzoate	4	92

Conditions: 0.01 mmol catalyst **8**, 10 mmol alcohol, and toluene (2 ml) were refluxed (115 °C) under Ar flow.

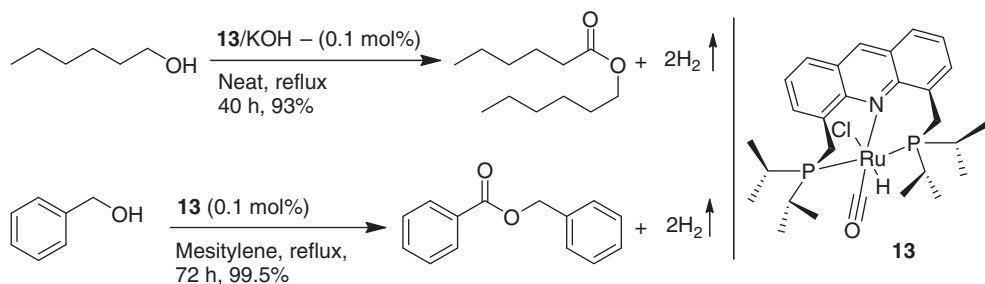
^aNeat reaction, heated at 117 °C.

There are two potential pathways by which an ester can be formed, both involving an intermediate aldehyde, namely a Tischenko-type condensation [35] or hemiacetal formation followed by its dehydrogenation [34]. Our results establish that the second pathway is operative, at least in the case of benzyl alcohol [11]. Thus, employing benzaldehyde (in absence of alcohol) did not yield any ester. On the other hand, reaction of benzaldehyde with 1 equivalent of benzyl alcohol led to quantitative formation of benzyl benzoate (Scheme 1.6).

**Scheme 1.6** Formation of ester via hemiacetal intermediary.

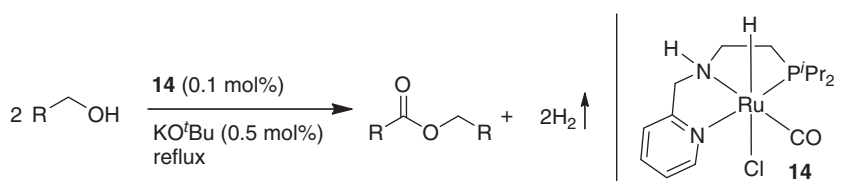
Using the acridine-derived PNP pincer complex **13**, primary alcohols can be directly transformed into acetals under neutral conditions [16, 36]. When the reactions were carried out in the presence of 1 equivalent of base (relative to complex **13**, 0.1 mol%), the corresponding esters were obtained in very good yields (Scheme 1.7). Mechanistic studies revealed that a β -hydrogen is essential for the acetal formation; thus, alcohols such as benzyl alcohol provided benzyl benzoate in 99.5% yield, rather than acetal, even under neutral conditions [16].

Recently, Gusev and coworkers [37] reported the PNN ruthenium pincer complex **14** with an aliphatic backbone, which displayed impressive catalytic activity in the presence of a base (KO^tBu , 0.5 mol%) for the conversion of simple alcohols such as ethanol and propanol. Although the reactions worked at temperatures below 100 °C, good conversions required heating at higher temperatures (Table 1.3,



Scheme 1.7 Esterification of primary alcohols by acridine PNP ruthenium pincer complex **13**.

Table 1.3 Dehydrogenative coupling of alcohols to form esters and dihydrogen catalyzed by the Ru PNN complex **14**.



Entry	R	T (°C)	Time (h)	Conversion (%)
1	Me	78	7.5	30
2	Et	96	8	73
3	Pr	118	3	78
4	<i>i</i> -Amyl	131	2.5	92
5	Hexyl	158	1	86

entries 4–5). An analogous dehalogenated osmium-based dimeric pincer complex was also reported to have comparable activity to that of complex **14**.

Though in moderate yield, the reported conversion of ethanol to ethyl acetate by complex **14** and a related osmium dimer complex [37] by Gusev generated interest in the catalytic synthesis of ethyl acetate from ethanol because it is a widely used fine chemical. Very recently, Beller *et al.* [38] screened the catalytic activity of various known pincer complexes for this transformation and found that Takasago's complex **15**, known as *Ru-MACHO catalyst*, is very efficient and the reaction in the presence of a base resulted in very good TON (Table 1.4).

Simultaneously, Spasyuk and Gusev [39] also reported a similar finding; among the various screened pincer complexes, complex **16** showed impressive reactivity with 85% conversion of ethanol (Scheme 1.8).

In addition to these transformations by well-defined pincer complexes, the complexes assembled *in situ* from the metal precursor $[\text{Ru}(\text{COD})(\text{methylallyl})_2]$ (COD, cyclooctadiene) and PNP or PNN pincer ligands (used for complexes

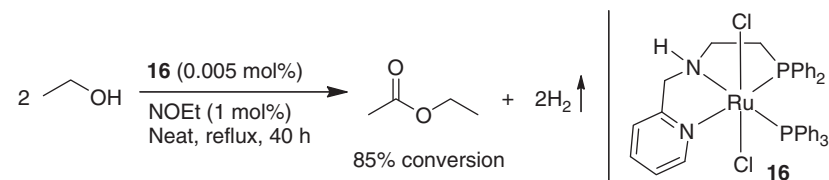
Table 1.4 Synthesis of ethyl acetate from ethanol by Ru-MACHO catalyst.

$2 \text{ CH}_3\text{CH}_2\text{OH} \xrightarrow[\text{reflux}]{\text{15 (0.05–0.005 mol\%)}, \text{NOEt (0.6–1.3 mol\%)}}$

$\rightarrow \text{CH}_3\text{COOCH}_2\text{CH}_3 + 2\text{H}_2 \uparrow$

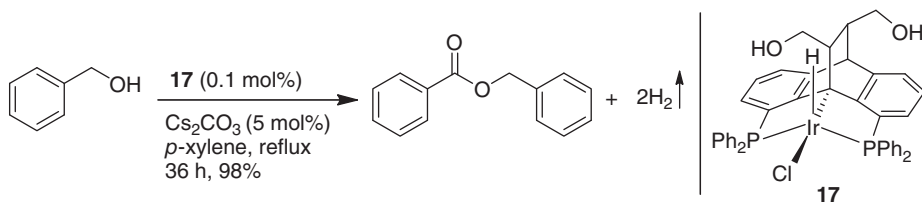
15

Entry	15 (mol%)	NaOEt (mol%)	Time (h)	T (°C)	Yield (%)	TON
1	0.05	1.3	6	90	81	1620
2	0.05	1.3	24	70	70	1400
3	0.005	0.6	46	90	77	15400

**Scheme 1.8** Synthesis of ethyl acetate from ethanol by the PNN ruthenium pincer complex **16**.

4 and 7, respectively) also catalyzed the dehydrogenative coupling of alcohol into esters successfully [40]. The catalytically active complex (which could be complex **8**, the CO ligand generated from intermediate aldehyde) displayed similar reactivity as that of complex **8**. PNP and PNN ruthenium(II) hydrido borohydride complexes [(PNX)RuH(BH₄), X = P, N] [41] and PNS ruthenium complexes [(PNS^{tBu})RuHCl(CO)] [42], analogs to complex **7**, also show catalytic reactivity for the esterification of alcohols.

In 2011, Gelman and coworkers [43] reported a PC_{Sp}³P iridium pincer complex (**17**), which exhibited efficient catalytic activity for the conversion of benzyl alcohol to benzyl benzoate (Scheme 1.9) and was suggested to operate via a novel metal–ligand cooperation mode. Both electron-withdrawing and electron-donating substituents

**Scheme 1.9** Acceptor-less dehydrogenative coupling of benzyl alcohols to form esters and dihydrogen catalyzed by the Ir(III) PC_{Sp}³P complex **17**.

on the aromatic ring are tolerated, and the corresponding esters were obtained in good yields (88–97%).

1.3.2

Synthesis of Cross-Esters from Primary and Secondary Alcohols

When a toluene solution of complex **11** (1 mol%) was refluxed with equimolar amounts of 1-hexanol and cyclohexanol, cyclohexyl hexanoate was obtained in 79% yield, together with 16% hexyl hexanoate, resulting from self-coupling of 1-hexanol, and 12% of cyclohexanone by dehydrogenation of cyclohexanol [13]. Despite the use of equimolar amounts of primary and secondary alcohols, the formation of the ester cyclohexyl hexanoate as the major product from dehydrogenative cross-esterification is noteworthy. The yield of the cross-esterification products significantly improved when an excess of secondary alcohols was used in the reaction. Thus, in a similar reaction, refluxing a toluene solution containing cyclohexanol and 1-hexanol in a molar ratio of 2.5/1 with complex **11** (1 mol%), cyclohexyl hexanoate was obtained in 93% yield (based on 1-hexanol). Cyclohexanone (34%) was also formed, and the products were isolated by column chromatography. The synthetic potential and substrate scope of this selective dehydrogenative cross-esterification process were demonstrated [13] with various cyclic and acyclic secondary alcohols and other primary alcohols, and the results are summarized in Table 1.5.

1.3.3

Synthesis of Esters by Acylation of Secondary Alcohols Using Esters

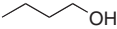
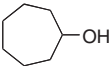
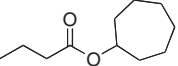
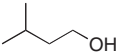
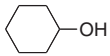
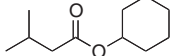
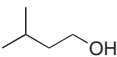
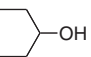
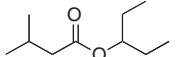
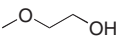
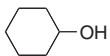
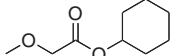
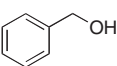
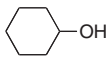
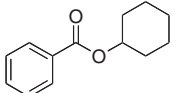
The transesterification reaction is a useful transformation that converts esters to other esters upon reaction with alcohols, as a result of exchange of alkoxy groups, avoiding the use of air- and moisture-sensitive reagents, such as acid chlorides. Further, ester-to-ester transformation is particularly useful when the carboxylic acid and their activated derivatives are not readily available [44]. In general, transesterification of secondary alcohols is slower than that of primary alcohols. The reaction is not atom-economical, as it produces, in addition to the desired ester, an equivalent of alcohol. Circumventing this undesired path, we have devised a novel method for transesterification in which dihydrogen is formed as the only byproduct, rather than alcohols, upon reaction of symmetrical esters with secondary alcohols.

Thus, refluxing a benzene solution of complex **8** (1 mol%), ethyl acetate (5 mmol) and cyclohexanol (15 mmol) under an argon atmosphere for 28 h resulted in complete consumption of ethyl acetate [12]. Cyclohexyl acetate was the only product formed (95%, Table 1.6) as observed by GC analysis and further confirmed by characterization of the isolated product. Similarly, refluxing a toluene solution containing 1 equivalent of an ester, such as hexyl hexanoate, pentyl pentanoate, and butyl butyrate, and 3 equivalent of various secondary alcohols in the presence of 1 mol% of complex **8** resulted in cross-esters in very good yields (Table 1.6). Somewhat lower yields of products were obtained when only 2 equivalent of secondary alcohols was used.

Table 1.5 Dehydrogenative cross-coupling of primary and secondary alcohols catalyzed by **11**.^a

Entry	1° alcohol	2° alcohol	Cross ester	Time (h)	Yield (%)
$\text{R}^1\text{CH}_2\text{OH} + \text{R}^2\text{CH}(\text{OH})\text{R}^3 \xrightarrow[\text{Toluene, reflux}]{\mathbf{11} (1 \text{ mol}\%)} \text{R}^1\text{COCH}(\text{R}^2)\text{R}^3 + 2\text{H}_2 \uparrow$ <div style="display: inline-block; vertical-align: middle; margin-left: 20px;"> <p style="text-align: center;">11</p> </div>					
1				24	93
2				26	63
3				26	90
4				26	93
5				26	58
6				25	95
7				24	96
8				38	46
9				25	95
10				26	93

Table 1.5 (Continued)

Entry	1° alcohol	2° alcohol	Cross ester	Time (h)	Yield (%)
11				26	70
12				25	99
13				25	95
14				24	98
15				24	91

^aComplex 11 (0.03 mmol), primary alcohol (3 mmol), secondary alcohol (7.5 mmol), and toluene (2 ml) were refluxed under argon. Yields of products were determined by GC using *m*-xylene as an internal standard.

When the unsymmetrical ester ethyl butyrate was reacted with 3-pentanol in the presence of **8** (1 mol%) under refluxing toluene, 75% conversion of ethyl butyrate took place to yield 73% of 3-pentyl butyrate (entry 14, Table 1.6). 3-Pentyl acetate, which was expected to be formed from the ethanol intermediate, was observed only in trace amounts, perhaps as a result of the loss of ethanol under reflux conditions. Likewise, the reaction of methyl hexanoate with cyclohexanol results in 42% conversion with the formation of 42% cyclohexyl hexanoate (entry 15).

Dehydrogenation of the secondary alcohol to the corresponding ketone is a slower reaction than the dehydrogenative coupling of the primary alcohol to ester, and thus most of the secondary alcohol reacts with the ester, although some ketone formation is observed as excess of alcohol is used. When symmetrical esters are used, both acyl and alkoxy parts of the substrate ester are incorporated into the product ester with liberation of hydrogen, providing an atom-economical and environmentally benign method for the transesterification reactions [12].

1.3.4

Synthesis of Polyesters from Diols

Polyesters are generally synthesized by a step-growth polycondensation reaction or through chain-growth ring-opening polymerization. However, achieving high molecular weights by the known methods for the synthesis of polyesters is

Table 1.6 Acylation of secondary alcohols catalyzed by the complex **8**.^a

Entry	Ester	Alcohol	Cross-esters	Time	Conversion	Yield (%)
$2 \text{ R}^2\text{-CH(OH)-R}^1 + \text{R-CO-O-R} \xrightarrow[\text{Toluene, reflux}]{\mathbf{8} \text{ (1 mol\%)}} 2 \text{ R}^2\text{-CH(O-CO-R)-R}^1 + 2\text{H}_2 \uparrow$ <div style="display: inline-block; vertical-align: middle; margin-left: 20px;"> <p style="text-align: center;">8</p> </div>						
1 ^b				28	100	95
2				26	96	95
3				26	71	70
4				36	50	49
5				26	91	90
6				36	93	93
7				36	87	85
8				18	51	49
9				26	91	90

Table 1.6 (Continued)

Entry	Ester	Alcohol	Cross-esters	Time	Conversion	Yield (%)
10				34	93	92
11				28	75	74
12				36	41	39
13				18	77	76
14 ^c				20	75	73
15				17	42	42

^aComplex **8** (0.05 mmol), ester (5 mmol), and toluene (3 ml) were refluxed under argon. Conversion and yields are based on GC analysis using internal standard.

^bBenzene was used as solvent.

^c*m*-Xylene was used as solvent.

challenging [45]. Further, the byproducts (H₂O, CH₃OH, HCl, salts) that are produced during a polycondensation can be challenging to remove from a viscous polymer solution, resulting in low conversion and poor polymer properties. By using complex **8** as a catalyst, Robertson [19] achieved the synthesis of high molecular weight polyesters from diols in a remarkable process that used complex **8** as a catalyst. Concomitantly generated dihydrogen was efficiently removed by performing the polymerization reaction under reduced pressure, leading to the formation of high molecular weight polyesters.

Complex **8** (0.2 mol%), generated *in situ* by deprotonation of complex **7** (Scheme 1.2), catalyzed polymerization of diols (higher than pentanediol) by heating under vacuum. Comparison of the molecular weight versus reaction time for the polymerization of 1,10-decanediol under vacuum versus nitrogen purge (Figure 1.2) revealed that polymer growth occurred faster and reached a higher molecular weight when the reaction was performed under reduced pressure.

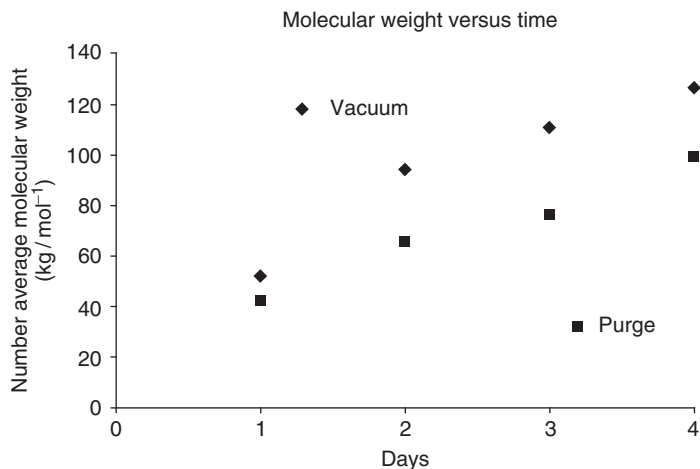


Figure 1.2 Plot of M_n versus reaction time for the polymerization of 1,10-decanediol under vacuum compared to using a nitrogen purge. (Reproduced with permission. Copyright © 2012 Wiley-VCH [19].)

Molecular weights higher than $125\,000\text{ g mol}^{-1}$ were attained. Considering the reaction conditions, which involve vacuum and rapidly lose solvent and become highly viscous with the reaction's progress, achieving such high molecular weights is noteworthy. The better performance under vacuum is attributed to the efficient removal of the hydrogen byproduct (which in turn helps to drive the equilibrium toward further polymerization) from the highly viscous molten polymer solution.

Diols such as 1,10-decanediol, 1,9-nonanediol, 1,8-octanediol, 1,6-hexanediol, and 1,5-pentanediol were polymerized using a catalyst loading of 0.2 mol% of complex **8** under vacuum. Table 1.7 summarizes the yields and some properties of the polymers. Polymerization of 1,10-decanediol leads to a polymer with M_n approaching $140\,000\text{ g mol}^{-1}$ and a degree of polymerization over 800 (entry 1). The molecular weights of the polymers and the degree of polymerization decrease as the molecular weight and length of the monomer decrease, which may be due to the viscosity differences of the molten polymer. The dehydrogenation of 1,5-pentanediol resulted in the predominant formation of thermodynamically stable and kinetically favored six-membered δ -valerolactone and 29% of polyester (entry 6). The reaction of 1,4-butanediol with complex **8** provided γ -butyrolactone exclusively.

In general, a range of esters is accessible directly from alcohols by dehydrogenative coupling and also from esters via transesterification catalyzed by ruthenium pincer complexes. The dearomatized complex **8** efficiently catalyzes the formation of polyesters from diols under vacuum. Although low catalyst loading and nonpurified monomeric diols were used, high degrees of polymerizations were achieved. These reactions take place with the liberation of dihydrogen (the only byproduct) under mild and neutral conditions, thus providing highly atom-economical processes for the formation esters and polyesters.

Table 1.7 Polymerization of linear aliphatic diols catalyzed by the complex **8** under vacuum and nitrogen purge.^a

Entry	<i>n</i> (diol)	<i>M_n</i> (kg mol ⁻¹) ^b	<i>M_w</i> / <i>M_n</i> ^b	Degree of polymerization	<i>T_m</i> (°C) ^c	Yield (%)
1	8	138	2.7	811	51	78
2	7	91.8	3.1	587	42	85
3	6	76.6	2.3	538	40	95
4 ^d	4	55.5	2.0	486	13	70
5 ^e	4	29.4	1.6	258	14	97
6	3	57.7	2.9	576	-2	29 ^f
7	2	—	—	—	—	90 ^g

Taken from Robertson *et al.* [19].

^aComplex **8** (0.2 mol%) and monomeric diol were heated at 150 °C with a 3 h purge and 5 day vacuum.

^bDetermined by gel permeation chromatography (GPC) using polystyrene standard.

^cDetermined by differential scanning calorimetry (DSC).

^dNitrogen purge instead of vacuum.

^e5 h nitrogen purge prior to vacuum to promote oligomerization and minimize loss of monomer.

^fIsolated yield of polymer. Remaining volatiles in vacuum trap were solvent and lactone.

^gYield of lactone.

1.4

Synthesis of Amides

Amide formation plays a very important role in chemical synthesis [1, 46]. Preparation of amides under neutral conditions and without generation of waste is a challenging goal [46–48]. Applying our pyridine-based ruthenium pincer complexes as catalysts, amides were synthesized directly from amines and alcohols or esters; polyamides were obtained from diols and diamines, as delineated in this section.

1.4.1

Synthesis of Amides from Alcohols and Amines

Direct catalytic conversion of alcohols and amines into amides and dihydrogen is a desirable method for the synthesis of amides. Using this environmentally benign reaction [14], an assortment of simple alcohols and amines were converted

into amides, with high atom economy. The liberated hydrogen gas shifts the equilibrium toward the completion of the reaction.

The reaction mixtures were refluxed under a flow of argon to facilitate the formation of product amides by hydrogen removal. When simple linear alcohols such as 1-hexanol and 1-pentanol were used, the corresponding amides were obtained in very good yields. 2-Methoxyethanol reacted with diverse amines to generate the amides in almost quantitative yields. When aniline was subjected to acylation with 1-pentanol, the amide was obtained in 58% yield. The lower reactivity of aniline may be attributed to its lower nucleophilicity as compared with that of alkylamines. The amidation reactions are sensitive to steric hindrance at the alcohol or the amine. Thus, when 2-methyl-1-butanol reacted with benzylamine, the corresponding amide was obtained in 70% yield, the rest of the alcohol being converted to the ester 2-methylbutyl-2-methylbutanoate. A similar pattern was also observed when 2-methylhexamine was reacted with 1-hexanol, leading to 72% yield of the corresponding amide (Table 1.8).

Amino alcohols also undergo amidation reactions. Gratifyingly, when chiral amino alcohols were used, the amide products were obtained with the retention of configuration. For example, reaction of (*S*)-2-amino-3-phenylpropan-1-ol, benzylamine, and 1 mol% of the complex **8** in toluene at reflux for 6 h led to (*S*)-2-amino-*N*-benzyl-3-phenylpropanamide in 58% yield after column chromatography (Scheme 1.10) [22]. The specific rotation of the product amide (+16.08) obtained from this catalysis reaction is essentially the same as reported [49]. The neutral reaction conditions likely help to prevent racemization.

Secondary amines do not react under these conditions. Thus, heating dibenzylamine with 1-hexanol under the experimental conditions resulted in a quantitative yield of hexyl hexanoate (entry 6, Table 1.8). The scope of this method was extended to the bis-acylation processes with diamines. Upon refluxing a slight excess of a primary alcohol and catalyst **1** with diamines (500 equivalent relative to **1**) in toluene under argon, bis-amides were produced in high yields (Table 1.9). The high selectivity of the dehydrogenative amidation reaction to primary amine functionalities enabled the direct bis-acylation of diethylenetriamine with 1-hexanol to provide the bis-amide in 88% yield without the need to protect the secondary amine functionality [14].

This is a fundamentally new chemical transformation. The reaction mechanism likely involves metal–ligand cooperation that operates in complex **8**. The reaction plausibly proceeds via a hemiaminal intermediate (Scheme 1.11) formed by the nucleophilic attack of the amine on an intermediate aldehyde that is either coordinated to the metal or free in solution [7, 32, 50].

The discovery of the catalytic amide formation with liberation of dihydrogen provides the most atom-economical method to make amides directly from amines and alcohols; as such, it elicited much research interest in this direction and diverse catalytic systems were reported, although generally in significantly lower catalyst turnovers [51].

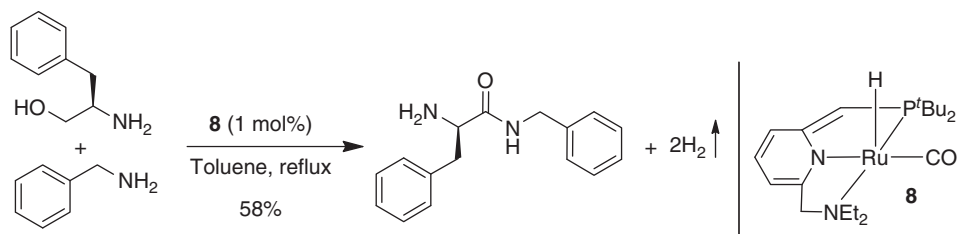
Table 1.8 Synthesis of amides directly from alcohols and amines.^a

Entry	R ¹ CH ₂ OH	R ² NH ₂	Time (h)	Amides	Yield (%) ^b
$ \begin{array}{c} \text{R}^1\text{CH}_2\text{OH} \\ + \\ \text{R}^2\text{NH}_2 \end{array} \xrightarrow[\text{Toluene, reflux}]{\mathbf{8} \text{ (0.1 mol\%)}} \begin{array}{c} \text{O} \\ \parallel \\ \text{R}^1\text{C}-\text{N}-\text{R}^2 \\ \\ \text{H} \end{array} + 2\text{H}_2\uparrow $					
1			7		96
2			7		97
3			9		99
4			12		70 ^c
5			8		78 ^c
6			8		0 ^c
7			8		58 ^c
8			8		99
9			8		72 ^c
10			8		99

^aConditions: Catalyst **8** (0.01 mmol), alcohol (10 mmol), amine (10 mmol), and toluene (3 ml) were refluxed under argon flow.

^bIsolated yields.

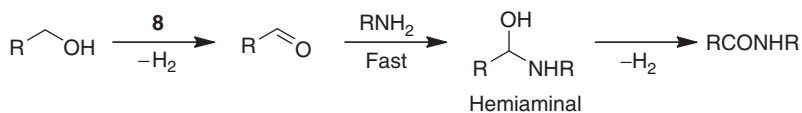
^cThe remaining alcohol was converted into the corresponding ester. In the reactions involving hexanol and pentanol, trace amounts of the corresponding secondary amines were detected (GC-MS).



Scheme 1.10 Synthesis of a chiral amide from amino alcohol and benzylamine.

Table 1.9 Dehydrogenative coupling of di- and tri-amines with alcohols to form bis-amides, catalyzed by complex **8**.

Entry	Diamine	Time (h)	Bis-amide	Yield (%)
1	Ethylenediamine	9		99
2	Diethylenetriamine	8		88
3	1,6-Diaminohexane	9		95

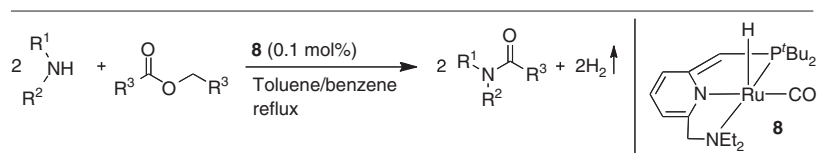


Scheme 1.11 Amide formation via hemiaminal intermediary.

1.4.2

Synthesis of Amides from Esters and Amines

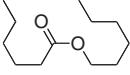
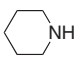
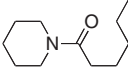
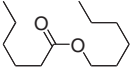
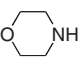
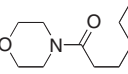
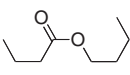
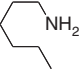
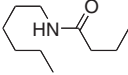
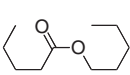
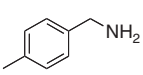
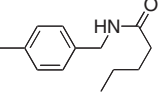
Synthesis of amides from the coupling reactions of esters and amines is a potentially attractive method; however, stoichiometric amounts of promoters or metal mediators are normally required [52]. Complex **8** also catalyzes the amide synthesis from esters and amines and the reaction is general and efficient, and proceeds under neutral conditions, thus providing an environmentally benign method [15]. As demonstrated in the alcohol acylation process (Section 1.3.3, Table 1.6), when symmetrical esters are used, acylation of amines occurs by both acyl and alkoxy parts of the esters and they are incorporated in the products, and the only byproduct generated from this reaction is H_2 .

Table 1.10 Synthesis of amides from esters and amines catalyzed by complex **8**.^a

Entry	Ester	Amine	Conversion of amine/time (%/h)	Amides	Isolated yields (%)
1 ^b			100/26		99
2 ^b			69/36		66
3 ^b			54/24		52
4			100/19		94
5			100/21		95
6			100/24		94
7			100/36		56
8			100/19		96
9			100/26		92
10			100/24		94
11			100/18		97

(continued overleaf)

Table 1.10 (Continued)

Entry	Ester	Amine	Conversion. of amine/time (%/h)	Amides	Isolated yields (%)
12			100/26		94
13			100/18		93
14			100/24		97
15			100/18		98

^aComplex **8** (0.01 mmol), ester (5 mmol), amine (10 mmol), and toluene/benzene (3 ml) were refluxed at an oil bath temperature of 135 °C in a Schlenk tube. Conversion of amine was analyzed by GC using *m*-xylene as an internal standard.

^bBenzene was used as a solvent.

When a benzene solution of complex **8** (0.1 mol%) containing pyrrolidine and ethyl acetate was refluxed under an argon atmosphere, quantitative conversion of pyrrolidine was observed by GC after 28 h, and *N*-acetylpyrrolidine was isolated in 98% yield (Table 1.10, entry 1). The same results were obtained when the reaction was carried out in refluxing toluene. The scope of the ester amidation reaction was explored with various esters and amines, and the results are summarized in Table 1.10.

The aminolysis of esters catalyzed by complex **8** is possibly initiated by N–H activation of the amine by metal–ligand cooperation involving **8**. Ester coordination followed by intramolecular nucleophilic attack by the amido ligand at the acyl functionality is thought to be a key step [15]. Overall, in one catalytic cycle, two molecules of amide and of H₂ are formed from one ester molecule.

1.4.3

Synthesis of Polyamides from Diols and Diamines

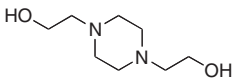
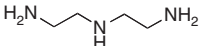
Polyamides are an important class of polymers in chemistry and biology, including biomolecules such as peptides and proteins. Synthetic polyamides have found numerous applications [53, 54] in fiber products, engineering plastics, and biomaterials. They possess high strength, toughness, and stability, and have good biocompatibility and degradability. Generally, polyamides are synthesized by

Table 1.11 Catalytic dehydrogenative polyamidation.^a

Entry	Diol	Diamine	Conversion ^b (yield ^c) %	M _n (10 ³)	PDI
1 ^d			99 (89)	11.9	3.09
2 ^d			>99 (87)	12.7	2.80
3 ^d			>99 (84)	19.8	1.86
4 ^e			>99 (88)	28.4	1.75
5 ^e			>99 (73)	19.4	1.59
6 ^e			>99 (78)	22.1	1.56
7 ^e			99 (85)	15.0	1.59
8 ^e			>99 (79)	16.5	1.69
9 ^e			>99 (76)	19.5	1.65
10 ^e			97 (65)	6.8 ^f	2.56
11 ^e			99 (70)	9.6 ^f	1.65

(continued overleaf)

Table 1.11 (Continued)

Entry	Diol	Diamine	Conversion ^b (yield ^d) %	M_n (10^3)	PDI
12 ^e			99 (72)	11.3 ^f	3.06

Taken from Guan *et al.* [21]

^aReaction conditions: 1.0 mmol diol, 1.0 mmol diamine, and the Ru catalyst were premixed in 1.5 ml solvent in a glovebox, then heated under N₂ flow for 48 h.

^bDetermined by ¹H NMR of the crude reaction mixture.

^cIsolated yield after precipitation from toluene.

^dIn anisole/DMSO (4 : 1), 2 mol% catalyst loading.

^eIn anisole, 1 mol% catalyst loading.

^fGPC taken after acylation by Ac₂O to avoid strong interaction with the GPC column gel material.

condensation of diamines and activated dicarboxylic acid derivatives [54, 55] and/or in the presence of coupling reagents [56]. In some cases, ring opening of small-ring lactams at high temperatures leads to the formation of polyamides [57]. To avoid the use of activators, waste generation, or harsh conditions, the development of atom-economical, efficient, and environmentally benign protocols are desirable.

Thus, we have developed the catalytic synthesis of polyamides [20] from diols and diamines using complex **8** as a catalyst. Prior to us, Zeng and Guan [21] reported such a transformation using (the now commercially available) complex **8**. Extensive optimization studies carried out by Zeng and Guan [21] revealed the need for polar solvents for successful polymerization of diols and diamines, and anisole was found to be a suitable polar solvent in which the catalyst remained highly active and the number averaged molecular weights (M_n) of the polyamides were dramatically increased. M_n of the polyamides was further improved by the addition of small amounts of dimethylsulfoxide (DMSO).

Using the optimized conditions, Guan and coworkers prepared a series of polyamides using various diols and diamines; selected examples are shown in Table 1.11. The anisole/DMSO mixed solvent provided better polymerization for less soluble polyamides (Table 1.11, entries 1–3), but decreased the catalytic activity of the complex **8**. Polymerizations in anisole gave longer polymers for more soluble polyamides (entries 4–12). As described in Section 1.4.1, the amidation reaction catalyzed by complex **8** is highly selective to primary amines and this offered excellent opportunity for the direct synthesis of functional polyamides containing secondary amino groups (entries 10–12) circumventing tedious protection and deprotection steps.

While Guan *et al.* disclosed the preparation of a variety of polyamides, many bearing ether spacers, with M_n in the range of 10–30 kDa, we reported the application of the amidation reaction to the synthesis of a variety of polyamides not bearing ether spacers, from simple diols and diamines, under different conditions,

Table 1.12 Catalytic polyamidation using diols and diamines.^a

Entry	Diols	Diamines	Polyamides	Isolated yield (%)	Highest Mw: MALDI-TOF (Da)	M_n (10^3)	PDI
1				82	4195	16.6 ^b	—
2				88	5000	10.3 ^b	—
3				86	7199	18.7	2.08
4				63	1849	ND	—
5				74	4583	26.9 ^c	—
6				86	3861	ND	—
7				84	3734	ND	—
8				78	1467	ND	—
9				80	5200	ND	—
10				76	4450	5.3 ^c	3.20
11				88	—	11.3 ^c	2.18
12				84	4951	ND	—

^aComplex 8 (0.01 mmol), diol (1 mmol), diamine (1 mmol), and 1,4-dioxane (2 ml) were refluxed at an oil bath temperature of 135 °C in a Schlenk tube under argon for 3 days.

^b M_n was calculated from ¹H NMR.

^c M_n was obtained from GPC analysis.

^dCatalyzed by complex 11 under solvent-free condition. ND means GPC was not performed because of insolubility in dimethyl formamide (DMF).

using 1,4-dioxane as a solvent (Table 1.12). Both complexes **8** and **11** were used as catalysts. Remarkably, using complex **11** as catalyst, the polyamidation reaction proceeded under solvent-free conditions, and only 0.2 mol% of catalyst was required, representing a perfect “green” reaction [20].

Notably, the potentially competing polyester formation [19] by dehydrogenative self-coupling of diols was not observed under these conditions. This is probably because the intermediate aldehyde reacts preferentially with the amine, which is a better nucleophile than the alcohol, forming a hemiaminal intermediate [14] (rather than a hemiacetal [11]) followed by its dehydrogenation to the amide (Schemes 1.6 and 1.11). In addition, it should be noted that complex **8** also catalyzes the formation of amides by coupling of esters with amines (Section 1.4.2) [15]; hence, even if some ester (or oligoester) were to be initially formed, it would be converted to the polyamide.

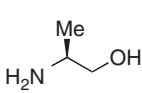
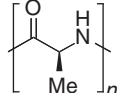
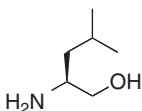
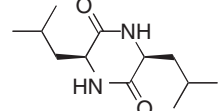
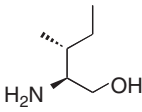
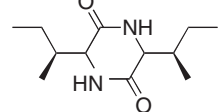
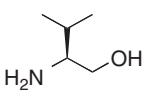
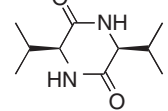
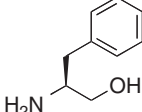
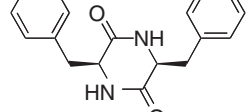
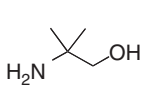
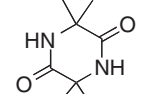
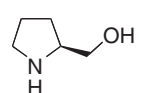
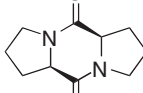
In general, an assortment of polyamides having aliphatic–aliphatic, aromatic–aromatic, aliphatic–aromatic, and aliphatic–heteroaromatic spacers were obtained in good yields using nonactivated and ether-linked/non-ether-linked diols and diamines, with liberation of H₂. Under our conditions, using dioxane as a solvent, polyamides were obtained with M_n in the range of 19–29 kDa, and, under the conditions of Zeng and Guan [21] using anisole or anisole/DMSO as solvents, $M_n = 10–30$ kDa was obtained. Both polymerization conditions catalyzed by complex **8** (as well as by complex **11**) provide synthetically useful and general methods for the preparation of a variety of polyamides under mild, neutral conditions, using no toxic reagents, not requiring preactivation of the substrates, and generating no waste.

1.5

Synthesis of Peptides from β -Amino Alcohols

Peptides constitute one of the most important families of compounds in chemistry and biology and play vital roles in living systems. Short peptides have found interesting biological and synthetic applications. For example, the conformational rigidity of cyclic peptides makes them attractive candidates for drug discovery and biomedical research [58]. Several cyclic peptides that show intriguing biological activity are found in nature [59]. Cyclic peptides have interesting applications as antibiotics [60], enzyme inhibitors [61], and receptor antagonists. Among them are the smallest cyclic peptides, 2,5-diketopiperazines derivatives, which are commonly found as natural products [62]. These peptides exhibit high-affinity binding to a large variety of receptors and show a broad range of biological activities [63], including antimicrobial, antitumor, antiviral, and neuroprotective effects. In general, 2,5-diketopiperazine derivatives are synthesized in solution or on the solid phase from commercially available and appropriately protected chiral α -amino acids in processes that are usually not atom-economical and generate considerable amounts of waste. Large libraries of cyclic peptides are accessible through solid-phase split-and-pool synthesis [64], and various methods have been developed for

Table 1.13 Synthesis of cyclic dipeptides from β -amino alcohols.^a

Entry	β -Amino alcohol	Peptides	Yield ^b (%)
1			72 ^c
2			64
3			72
4			78
5			72
6			92
7			99

^aComplex **8** (0.02 mmol), amino alcohol (2 mmol), and 1,4-dioxane (2 ml) were heated to reflux in argon (oil bath temperature of 135 °C) for 19 h.

^bYield of isolated product.

^cIncluding a minor amount of the dipeptide.

their syntheses [65]. Thus, green, atom-economical methods for the generation of peptides are highly desirable.

As complex **8** catalyzes the amidation of amines by amino alcohols with retention of configuration, we reasoned that use of amino alcohols alone might result in linear or cyclic peptides from the self-coupling reactions. Refluxing a 1,4-dioxane solution containing (*S*)-(+)-2-amino-1-propanol and complex **8** (1 mol%) for 19 h under argon flow provided a mixture of oligo-alanines containing a small amount of the cyclic dipeptide amounting together giving 72% yield (Table 1.13, entry 1). Interestingly, similar reactions of amino alcohols bearing larger substituents at the α -position of the amine group provided the corresponding cyclic dipeptides (diketopiperazines) as the only products (Table 1.13, entries 2–7) in very good yields with liberation of H₂ as the only byproduct.

1.6

Concluding Remarks

The chemistry illustrated in this chapter outlines the outstanding potential of pincer complexes for the catalytic synthesis of esters, amides, and peptides. These commonly used fine and bulk chemicals, conventionally prepared from carboxylic acids and their derivatives in multistep processes, can now be produced atom-economically directly from alcohols with liberation of molecular hydrogen (*the only byproduct*), which is valuable by itself. In addition to the higher stability associated with mer-coordination, the pincer platform offers the opportunity to fine-tune the steric and electronic properties of the metal, and, importantly, provide new opportunities for efficient metal–ligand cooperation. This has resulted in hitherto-unknown, efficient, and environmentally benign catalytic processes. In addition to the processes described here, we have developed several other reactions catalyzed by PNP and PNN pincer complexes of Ru and Fe, as briefly mentioned in Section 1.1. The PNN complex **8** and its precursor complex **7**, as well as complex **13** and the associated ligands, are commercially available (from Strem Chemicals, USA). We believe that many innovative catalysts and methodologies would emerge from this stimulating research topic.

Acknowledgments

We thank all our coworkers, whose names appear in the cited references, for their valuable contributions. Our research described in this chapter was supported by the Israel Science Foundation, by the DIP program for German-Israeli Cooperation, by the European Research Council under the FP7 framework (ERC No 246837), and by the Helen and Martin Kimmel Center for Molecular design. C.G. is a DST Ramanujan Fellow. D.M. is the holder of the Israel Matz Professorial Chair of Organic Chemistry.

References

- (a) Trost, B.M. and Fleming, I. (eds) (1992) *Comprehensive Organic Synthesis*, Pergamon Press, New York; (b) Larock, R.C. (1996) *Comprehensive Organic Transformations*, 2nd edn, Wiley-VCH Verlag GmbH, New York.
- (a) Otera, J. and Nishikido, J. (2010) *Esterification: Methods, Reactions, and Applications*, Wiley-VCH Verlag GmbH, Weinheim; (b) Otera, J. (2003) *Esterification Methods, Reactions and Applications*, Wiley-VCH Verlag GmbH, Weinheim; (c) Tojo, G. and Fernandez, M. (2006) *Oxidation of Alcohols to Aldehydes and Ketones*, Springer Science Business Media, Inc., New York; (d) Sheldon, R.A. and van Santen, R.A. (1995) *Catalytic Oxidation: Principles and Applications*, World Scientific, Singapore; (e) Sheldon, R.A., Arends, I.W.C.E., Ten Brink, G.-J., and Dijkstra, A. (2002) *Acc. Chem. Res.*, **35**, 774–781; (f) Bäckvall, J.-E. (2004) *Modern Oxidation Methods*, Wiley-VCH Verlag GmbH, Weinheim.
- (a) Van der Boom, M.E. and Milstein, D. (2003) *Chem. Rev.*, **103**, 1759–1792; (b) Morales-Morales, D. and Jensen, C.M. (eds) (2007) *The Chemistry of Pincer Compounds*, Elsevier, Amsterdam.
- Choi, J., Roy MacArthur, A.M.H., Brookhart, M., and Goldman, A.S. (2011) *Chem. Rev.*, **111**, 1761–1779.
- (a) Selander, N. and Szabó, K.K. (2011) *Chem. Rev.*, **111**, 2048–2076; (b) Schneider, S., Meiners, J., and Askevold, B. (2012) *Eur. J. Inorg. Chem.*, 412–429.
- Gunanathan, C. and Milstein, D. (2011) *Top. Organomet. Chem.*, **37**, 55–84.
- Gunanathan, C. and Milstein, D. (2011) *Acc. Chem. Res.*, **44**, 588–602.
- Milstein, D. (2010) *Top. Catal.*, **53**, 915–923.
- Ikariya, T. and Shibasaki, M. (eds) (2011) *Bifunctional Molecular Catalysis*, Springer, Heidelberg.
- Gelman, D. and Musa, S. (2012) *ACS Catal.*, **2**, 2456–2466.
- Zhang, J., Leitus, G., Ben-David, Y., and Milstein, D. (2005) *J. Am. Chem. Soc.*, **127**, 10840–10841.
- Gnanaprakasam, B., Ben-David, Y., and Milstein, D. (2010) *Adv. Synth. Catal.*, **352**, 3169–3173.
- Srimani, D., Balaraman, E., Gnanaprakasam, B., Ben-David, Y., and Milstein, D. (2012) *Adv. Synth. Catal.*, **354**, 2043–2406.
- Gunanathan, C., Ben-David, Y., and Milstein, D. (2007) *Science*, **317**, 790–792.
- Gnanaprakasam, B. and Milstein, D. (2011) *J. Am. Chem. Soc.*, **133**, 1682–1685.
- Gunanathan, C., Shimon, L.J.W., and Milstein, D. (2009) *J. Am. Chem. Soc.*, **131**, 3146–3147.
- (a) Gunanathan, C. and Milstein, D. (2008) *Angew. Chem.*, **120**, 8789–8792; *Angew. Chem. Int. Ed.*, **2008**, **47**, 8661–8664; (b) Gunanathan, C., Gnanaprakasam, B., Iron, M.A., Shimon, L.J.W., and Milstein, D. (2010) *J. Am. Chem. Soc.*, **132**, 14763–14765.
- Gnanaprakasam, B., Zhang, J., and Milstein, D. (2010) *Angew. Chem.*, **122**, 1510–1513; *Angew. Chem. Int. Ed.*, **2010**, **49**, 1468–1471.
- Hunsicker, D.M., Dauphinais, B.C., Mc Ilrath, S.P., and Robertson, N.J. (2012) *Macromol. Rapid Commun.*, **33**, 232–236.
- Gnanaprakasam, B., Balaraman, E., Gunanathan, C., and Milstein, D. (2012) *J. Polym. Sci., Part A: Polym. Chem.*, **50**, 1755–1765.
- Zeng, H. and Guan, Z. (2011) *J. Am. Chem. Soc.*, **133**, 1159–1161.
- Gnanaprakasam, B., Balaraman, E., Ben-David, Y., and Milstein, D. (2011) *Angew. Chem. Int. Ed.*, **50**, 12240–12244.
- Zhang, J., Leitus, G., Ben-David, Y., and Milstein, D. (2006) *Angew. Chem.*, **118**, 1131–1133; *Angew. Chem. Int. Ed.*, **2006**, **45**, 1113–1115.
- Balaraman, E., Fogler, E., and Milstein, D. (2010) *Chem. Commun.*, **48**, 1111–1113.
- (a) Balaraman, E., Gunanathan, C., Zhang, J., Shimon, L.J.W., and Milstein, D. (2011) *Nat. Chem.*, **3**, 609–614; (b) Huff, C.A. and Sanford, M.S. (2011) *J. Am. Chem. Soc.*, **133**, 18122–18125.

26. Balaraman, E., Gnanaprakasam, B., Shimon, L.J.W., and Milstein, D. (2010) *J. Am. Chem. Soc.*, **132**, 16756–16758.
27. Balaraman, E., Ben-David, Y., and Milstein, D. (2011) *Angew. Chem.*, **123**, 11906; *Angew. Chem. Int. Ed.*, 2011, **50**, 11702–11705.
28. (a) Tanaka, R., Yamashita, M., and Nozaki, K. (2009) *J. Am. Chem. Soc.*, **131**, 14168–14169; (b) Schmeier, T.J., Dobereiner, G.E., Crabtree, R.H., and Hazari, N. (2011) *J. Am. Chem. Soc.*, **133**, 9274–9277; (c) Langer, R., Diskin-Posner, Y., Leitus, G., Shimon, L.J.W., Ben-David, Y., and Milstein, D. (2011) *Angew. Chem. Int. Ed.*, **50**, 9948–9952.
29. (a) Ben-Ari, E., Leitus, G., Shimon, L.J.W., and Milstein, D. (2006) *J. Am. Chem. Soc.*, **128**, 15390–15391; (b) Vuzman, D., Poverenov, E., Shimon, L.J.W., Diskin-Posner, Y., and Milstein, D. (2008) *Organometallics*, **27**, 2627–2634; (c) Schwartzburd, L., Iron, M.A., Konstantinovski, L., Diskin-Posner, Y., Leitus, G., Shimon, L.J.W., and Milstein, D. (2010) *Organometallics*, **29**, 3817–3827; (d) Iron, M.A., Ben-Ari, E., Cohen, R., and Milstein, D. (2009) *Dalton Trans.*, 9433–9439; (e) Kohl, S.W., Weiner, L., Schwartzburd, L., Konstantinovski, L., Shimon, L.J.W., Ben-David, Y., Iron, M.A., and Milstein, D. (2009) *Science*, **324**, 74–77; (f) Khaskin, E., Iron, M.A., Shimon, L.J.W., Zhang, J., and Milstein, D. (2010) *J. Am. Chem. Soc.*, **132**, 8542–8543; (g) Schwartzburd, L., Iron, M.A., Konstantinovski, L., Ben-Ari, E., and Milstein, D. (2011) *Organometallics*, **30**, 2721–2729; (h) Feller, M., Diskin-Posner, Y., Shimon, L.J.W., Ben-Ari, E., and Milstein, D. (2012) *Organometallics*, **31**, 4083–4101.
30. Zeng, G., Guo, Y., and Li, S. (2009) *Inorg. Chem.*, **48**, 10257–10263.
31. Montag, M., Zhang, J., and Milstein, D. (2012) *J. Am. Chem. Soc.*, **134**, 10325–10328.
32. (a) Sandhya, K.S. and Suresh, C.H. (2011) *Organometallics*, **30**, 3888–3891; (b) Chen, Y. and Fang, W.-H. (2010) *J. Phys. Chem. A*, **114**, 10334–10338; (c) Yang, X. and Hall, M.B. (2010) *J. Am. Chem. Soc.*, **132**, 120–130; (d) Li, J., Shiota, Y., and Yoshizawa, K. (2009) *J. Am. Chem. Soc.*, **131**, 13584–13585.
33. Vogt, M., Gargir, M., Iron, M.A., Diskin-Posner, Y., Ben-David, Y., and Milstein, D. (2012) *Chem. Eur. J.*, **18**, 9194–9197.
34. (a) Blum, Y. and Shvo, Y. (1985) *J. Organomet. Chem.*, **282**:C7, 62; (b) Murahashi, S.-I., Naota, T., Ito, K., Maeda, Y., and Taki, H. (1987) *J. Org. Chem.*, **52**, 4319–4327.
35. Ito, T., Horino, H., Koshiro, Y., and Yamamoto, A. (1982) *Bull. Chem. Soc. Jpn.*, **55**, 504–512.
36. Kossoy, E., Diskin-Posner, Y., Leitus, G., and Milstein, D. (2012) *Adv. Synth. Catal.*, **354**, 497–504.
37. Spasyuk, D., Smith, S., and Gusev, D.G. (2012) *Angew. Chem. Int. Ed.*, **51**, 2772–2775.
38. Nielsen, M., Junge, H., Kammer, A., and Beller, M. (2012) *Angew. Chem. Int. Ed.*, **51**, 5711–5713.
39. Spasyuk, D. and Gusev, D.G. (2012) *Organometallics*, **31**, 5239–5242.
40. Prechtel, M.H.G., Wobser, K., Theyssen, N., Ben-David, Y., Milstein, D., and Leitner, W. (2012) *Catal. Sci. Technol.*, **2**, 2039–2042.
41. Zhang, J., Balaraman, E., Leitus, G., and Milstein, D. (2011) *Organometallics*, **30**, 5716–5724.
42. Gargir, M., Ben-David, Y., Leitus, G., Diskin-Posner, Y., Shimon, L.J.W., and Milstein, D. (2012) *Organometallics*, **31**, 6207–6214.
43. Musa, S., Shaposhnikov, I., Cohen, S., and Gelman, D. (2011) *Angew. Chem. Int. Ed.*, **50**, 3533–3537.
44. For reviews on transesterification, see: (a) Otera, J. (1993) *Chem. Rev.*, **93**, 1449–1470; (b) Otera, J. (2004) *Acc. Chem. Res.*, **37**, 288–296; (c) Grasa, G.A., Singh, R., and Nolan, S.P. (2004) *Synthesis*, **7**, 971–985; (d) Hoydonckx, H.E., De Vos, D.E., Chavan, S.A., and Jacobs, P.A. (2004) *Top. Catal.*, **27**, 83–96.
45. Nagao, Y. and Takasu, A. (2010) *J. Polym. Sci., Part A: Polym. Chem.*, **48**, 4207–4218.
46. Smith, B. (2001) *Compendium of Organic Synthetic Methods*, Vol. 9, John Wiley & Sons, Inc., New York, pp. 100–116.

47. Constable, D.J.C., Dunn, P.J., Hayler, J.D., Humphrey, G.R., Leazer, J.L. Jr., Linderman, R.J., Lorenz, K., Manley, J., Pearlman, B.A., Wells, A., Zaks, A., and Zhang, T.Y. (2007) *Green Chem.*, **9**, 411–420.
48. Pattabiraman, V.R. and Bode, J.W. (2011) *Nature*, **480**, 471–479.
49. Basso, A., Banfi, L., Riva, R., and Guanti, G. (2005) *J. Org. Chem.*, **70**, 575–579.
50. (a) Zeng, G. and Li, S. (2011) *Inorg. Chem.*, **50**, 10572–10580; (b) Li, H., Wang, X., Huang, F., Lu, G., Jiang, J., and Wang, Z. (2011) *Organometallics*, **30**, 5233–5247.
51. (a) Nordstrøm, L.U., Vogt, H., and Madsen, R. (2008) *J. Am. Chem. Soc.*, **130**, 17672–17673; (b) Zweifel, T., Naubron, J.V., and Grützmacher, H. (2009) *Angew. Chem.*, **121**, 567–571; *Angew. Chem. Int. Ed.*, 2009, **48**, 559–563; (c) Watson, A.J.A., Maxwell, A.C., and Williams, J.M.J. (2009) *Org. Lett.*, **11**, 2667–2670; (d) Ghosh, S.C., Muthaiah, S., Zhang, Y., Xu, X., and Hong, S.H. (2009) *Adv. Synth. Catal.*, **351**, 2643–2649; (e) Shimizu, K., Ohshima, K., and Satsuma, A. (2009) *Chem. Eur. J.*, **15**, 9977–9980; (f) Zhang, Y., Chen, C., Ghosh, S.C., Li, Y., and Hong, S.H. (2010) *Organometallics*, **29**, 1374–1378; (g) Muthaiah, S., Ghosh, S.C., Jee, J.-E., Chen, C., Zhang, J., and Hong, S.H. (2010) *J. Org. Chem.*, **75**, 3002–3006; (h) Schley, N.D., Dobreiner, G.E., and Crabtree, R.H. (2011) *Organometallics*, **30**, 4174–4179; (i) Chen, C., Zhang, Y., and Hong, S.H. (2011) *J. Org. Chem.*, **76**, 10005–10010.
52. (a) Ishihara, K., Kuroki, Y., Hanaki, N., Ohara, S., and Yamamoto, H. (1996) *J. Am. Chem. Soc.*, **118**, 1569–1570; (b) Kuroki, Y., Ishihara, K., Hanaki, N., Ohara, S., and Yamamoto, H. (1998) *Bull. Chem. Soc. Jpn.*, **71**, 1221–1230; (c) Porta, F., Pizzotti, M., Crotti, C., and Cenini, S. (1988) *Gazz. Chim. Ital.*, **118**, 475; (d) Han, C., Lee, J.P., Lobkovsky, E., and Porco, J.A. Jr., (2005) *J. Am. Chem. Soc.*, **127**, 10039–10044; (e) Eldred, S.E., Stone, D.A., Gellman, S.H., and Stahl, S.S. (2003) *J. Am. Chem. Soc.*, **125**, 3422–3423; (f) Hoerter, J.M., Otte, K.M., Gellman, S.H., Cui, Q., and Stahl, S.S. (2008) *J. Am. Chem. Soc.*, **130**, 647–654; (g) Stephenson, N.A., Zhu, J., Gellman, S.H., and Stahl, S.S.J. (2009) *J. Am. Chem. Soc.*, **131**, 10003–10008.
53. (a) Odian, G. (2004) *Principles of Polymerization*, 4th edn, John Wiley & Sons, Inc., Hoboken, NJ; (b) Langer, R. and Tirrell, D.A. (2004) *Nature*, **428**, 487–492; (c) Mintzer, M.A. and Simanek, E.E. (2009) *Chem. Rev.*, **109**, 259–302; (d) Place, E.S., Evans, N.D., and Stevens, M. (2009) *Nat. Mater.*, **8**, 457–470.
54. Garcia, J.M., Garcia, F.C., Serna, F., and de la Pena, J.L. (2010) *Prog. Polym. Sci.*, **35**, 623–686.
55. Zaliz, C.L.R. and Varela, O. (2005) *Tetrahedron: Asymmetry*, **16**, 97–103.
56. (a) Ueda, M., Kakuta, M., Morosumi, T., and Sato, R. (1991) *Polym. J.*, **23**, 167–176; (b) Chan, W.C. and White, P.D. (2000) *Fmoc Solid Phase Peptide Synthesis: A Practical Approach*, Oxford University Press, New York.
57. (a) Zhang, J.H., Kissounko, D.A., Lee, S.E., Gellman, S.H., and Stahl, S.S. (2009) *J. Am. Chem. Soc.*, **131**, 1589–1597; (b) Deming, T.J. (2006) *Adv. Polym. Sci.*, **202**, 1–18; (c) Ding, H. and Harris, F.W. (1995) *Pure Appl. Chem.*, **87**, 1997–2004.
58. Liu, S., Gu, W., Lo, D., Ding, X., Ujiki, M., Adrian, T.E., Soff, G.A., and Silverman, R.B. (2005) *J. Med. Chem.*, **48**, 3630–3638.
59. Hamada, Y. and Shioiri, T. (2005) *Chem. Rev.*, **105**, 4441–4482.
60. For examples see: (a) Fernandez-Lopez, S., Kim, H.S., Choi, E.C., Delgado, M., Granja, J.R., Khasanov, A., Kraehenbuehl, K., Long, G., Weinberger, D.A., Wilcoxon, K.M., and Ghadiri, M.R. (2001) *Nature*, **412**, 452–456; (b) Kohli, R.M., Walsh, C.T., and Burkart, M.D. (2002) *Nature*, **418**, 658–661; (c) Qin, C., Bu, X., Zhong, X., Ng, N.L.J., and Guo, Z.J. (2004) *J. Comb. Chem.*, **6**, 398–406; (d) Dartois, V., Sanchez-Quesada, J., Cabezas, E., Chi, E., Dubbelde, C., Dunn, C., Granja, J., Gritzen, C., Weinberger, D., Ghadiri, M.R., and Parr, T.R. Jr., (2005) *Antimicrob. Agents Chemother.*, **49**, 3302–3310.

61. For examples see: (a) McBride, J.D., Freeman, H.N., Domingo, G.J., and Leatherbarrow, R.J. (1996) *J. Mol. Biol.*, **259**, 819–827; (b) Eichler, J., Lucka, A.W., Pinilla, C., and Houghten, R.A. (1996) *Mol. Diversity*, **1**, 233–240; (c) March, D.R., Abbenante, G., Bergman, D.A., Brinkworth, R.R., Wickramasinghe, W., Begun, J., Martin, J.L., and Fairlie, D.P. (1996) *J. Am. Chem. Soc.*, **118**, 3375–3379; (d) Bratkovič, T., Lunder, M., Popovic, T., Kreft, S., Turk, B., Strukelj, B., and Urleb, U. (2005) *Biochem. Biophys. Res. Commun.*, **332**, 897–903.
62. Prasad, C. (1995) *Peptides*, **16**, 151–164.
63. (a) Martins, M.B. and Carvalho, I. (2007) *Tetrahedron*, **63**, 9923–9932; (b) Houston, D.R., Synstad, B., Eijssink, V.G.H., Stark, M.J.R., Eggleston, I.M., and van Aalten, D.M.F. (2004) *J. Med. Chem.*, **47**, 5713–5720; (c) Graz, C.J.M., Grant, G.D., Brauns, S.C., Hunt, A., Jamie, H., and Milne, P.J. (2000) *J. Pharm. Pharmacol.*, **52**, 75–82; (d) Prakash, K.R.C., Tang, Y., Kozikowski, A.P., Flippen-Anderson, J.L., Knoblach, S.M., and Faden, A.I. (2002) *Bioorg. Med. Chem.*, **10**, 3043–3048.
64. (a) Lam, K.S., Salmon, S.E., Hersh, E.M., Hruby, V.J., Kazmierski, W.M., and Knapp, R.J. (1991) *Nature*, **354**, 82–84; (b) Houghten, R.A., Pinilla, C., Blondelle, S.E., Appel, J.R., Dooley, C.T., and Cuervo, J.H. (1991) *Nature*, **354**, 84–86; (c) Furka, A., Sebestyen, F., Asgedom, M., and Dibo, G. (1991) *Int. J. Pept. Protein Res.*, **37**, 487–493.
65. (a) Fischer, P.M.J. (2003) *J. Pept. Sci.*, **9**, 9–35; (b) Dinsmore, C.J. and Beshore, D.C. (2002) *Tetrahedron*, **58**, 3297–3312; (c) Rodionov, I.L., Rodionova, L.N., Baidakova, L.K., Romashko, A.M., Balashova, T.A., and Ivanov, V.T. (2002) *Tetrahedron*, **58**, 8515–8523; (d) Rajappa, S. and Natekar, M.V. (1993) *Adv. Heterocycl. Chem.*, **57**, 187–829; (e) Ueda, T., Saito, M., Kato, T., and Izumiya, N. (1983) *Bull. Chem. Soc. Jpn.*, **56**, 568–572; (f) Suzuki, K., Sasaki, Y., Endo, N., and Mihara, Y. (1981) *Chem. Pharm. Bull.*, **29**, 233–237; (g) Eriksson, J., Arvidsson, P.I., and Davidsson, O. (1999) *Chem. Eur. J.*, **5**, 2356–2361; (h) Lee, S., Kanmera, T., Aoyagi, H., and Izumiya, N. (1979) *Int. J. Pept. Protein Res.*, **13**, 207–217.

2

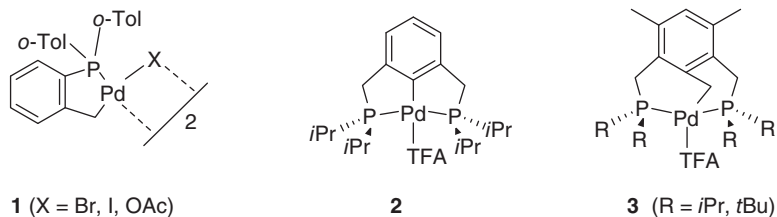
The Role of Redox Processes in Reactions Catalyzed by Nickel and Palladium Complexes with Anionic Pincer Ligands

Juan Cámpora and Cristóbal Melero

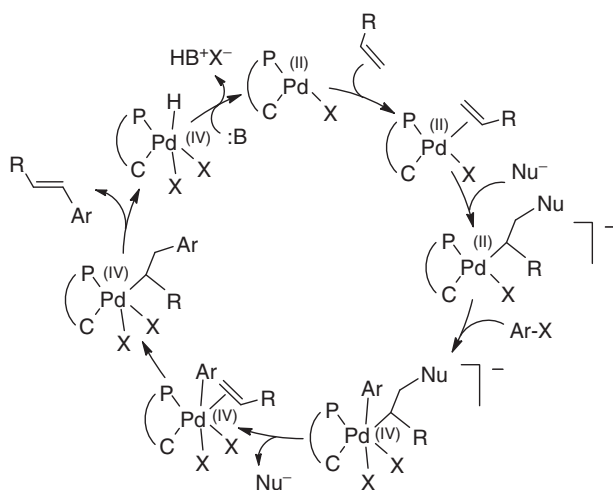
2.1

Introduction

The organometallic chemistry of Ni and Pd is dominated by oxidation states 0 and II [1]. In consequence, many of their catalytic reactions, such as the Heck [2] or cross-coupling reactions [3], typically involve cycles in which the metal alternates between these oxidation states. Thus, electrically neutral ligands that stabilize both oxidation states, namely 0 and II, such as phosphines, bipyridyls, and similar heterocyclic systems, or *N*-heterocyclic carbenes [4], have been traditionally preferred in the design of Ni and Pd catalysts. Although it is now recognized that some types of anionic Pd(0) species can play an important role in Pd-catalyzed coupling processes, σ -binding anionic ligands are rarely found in M(0) complexes and, consequently, σ -ligated species were considered mechanistically irrelevant for catalytic processes involving Pd(0)/Pd(II) cycles [5]. For example, palladacycles such as **1** ($X = \text{Br}, \text{I}$) were identified by Heck as orange-red crystalline materials formed in the course of diene arylation when palladium tris(*o*-tolyl)phosphine was used as a catalyst, but they were regarded as catalyst deactivation products [6]. In this context, the announcement by Herrmann and Beller [7] in 1995 that the complex **1** ($X = \text{OAc}$) is highly active in the Heck and Suzuki reactions was received with high interest and resulted in the rapid development of palladacycles as catalysts in cross-coupling reactions [8–12]. Compared to conventional Pd catalysts, palladacycles are much more stable and often perform without appreciable decomposition to Pd metal. In 1997, Milstein [13] reported that palladium complexes containing PCP pincer ligands **2** and **3** also achieve very high activities in the Heck coupling of olefins with aryl iodides and bromides. A variety of palladium pincer complexes have been tested as catalysts in different types of cross-coupling reactions [10–12, 14, 15], and these have turned out to be exceptionally active, often achieving fantastic turnover numbers (TONs), sometimes higher than 10^6 , at very low catalyst loadings. Recently, a number of nickel complexes bearing pincer ligands have found interesting applications in catalysis as well [16–18].



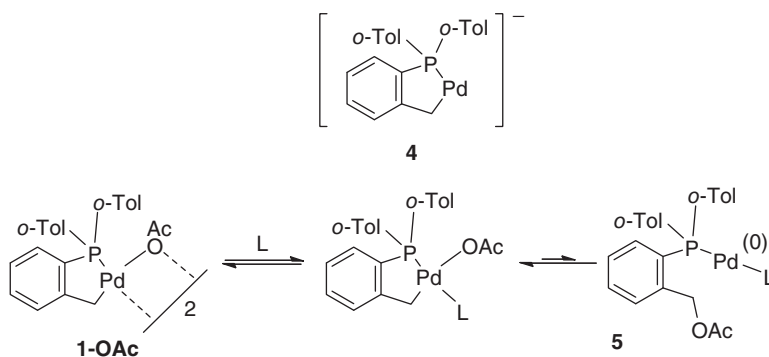
The discovery of catalysts featuring σ -M–C bonded ligands posed interesting questions regarding the mechanisms involved. The fact that palladacycles catalyze the Heck reaction without apparent decomposition to palladium black led to the idea that these could operate via a different mechanism involving Pd(II) and Pd(IV) oxidation states instead of Pd(II) and Pd(0) [19]. One of the difficulties of this proposal is the relatively low nucleophilicity of Pd(II) species (as compared to Pd(0)), which are usually unreactive toward mild electrophiles such as aryl halides. To overcome this problem, Shaw suggested that palladacycles could give rise to anionic intermediates of higher nucleophilicity. In the case of the Heck reaction, anionic palladacycles could be generated by coordination of the olefin substrate to the Pd(II) center, followed by the attack of an external nucleophile, as shown in Scheme 2.1 [20].



Scheme 2.1 Shaw's hypothetical Pd(II)/Pd(IV) mechanism for the Heck reaction catalyzed by palladacycles.

Although the active participation of Pd(IV) intermediates in catalysis is currently well established [21, 22], it has been shown that the catalytic activity of palladacycles is usually due to Pd nanoparticles or soluble Pd(0) species arising from partial or complete decomposition processes. Hartwig and Louie [23] showed that palladacycles of type 1 are reduced by amines (in aryl amination reactions) or stannanes (in the Stille coupling) to afford Pd(0) phosphine complexes. Furthermore,

Herrmann's investigation of the Heck reaction catalyzed by **1** confirmed that its catalytic activity is due to the formation of Pd(0) species. Interestingly, the author noted small but significant differences in the results obtained with catalyst **1** and two classic sources of Pd(0), ($\{\text{Pd}[\text{P}(o\text{-Tol})_3]_2\}$ or $\{\text{Pd}(\mu\text{-Br})[\text{P}(o\text{-Tol})_3]_2\}$), suggesting that these could be explained by assuming that the cyclometallated moiety of **1** is retained throughout the catalytic process, undergoing reversible reduction to the anionic σ -aryl Pd(0) complex **4** [24]. Later studies by Jutand led to the conclusion that, although a highly reactive species, thought to be **4**, can be generated by electrochemical reduction of **1**, this is not involved in catalysis. The true active species is a conventional Pd(0) complex, **5**, arising from **1** by reductive coupling of the cyclometallated phosphine and acetate ligand, as shown in Scheme 2.2 [25].



Scheme 2.2 Reversible reduction of metallacycle **1-OAc** to Pd(0).

Compared to simple palladacycles, pincer complexes such as **2** and **3** are much more likely to participate directly in catalytic processes [11], not only because of their higher thermal stability but also because the rigid metal-pincer framework is more fit to resist oxidative addition or other redox changes without collapsing [26]. This is the origin of the intense debate regarding the true nature of the catalytic species involved in reactions catalyzed by pincer complexes. However, as discussed later in this chapter, the high temperatures often required to carry out catalytic reactions with pincer complexes is probably needed to induce their degradation into catalytically active ligand-free species. On the other hand, there are also cases in which the evidence points to pincer complexes themselves as molecular catalysts.

This chapter will discuss the ability of pincer complexes of Ni and Pd to catalyze reactions undergoing redox changes without losing their structural integrity. It is worth mentioning here that the term *pincer* is usually applied to almost any tridentate ligand enforcing mer-coordination [27]. In principle, electrically neutral tridentate ligands can stabilize complexes with the metal center in both zero and divalent oxidation states, and therefore they pose no particular difficulties to *normal* M(0)/M(II) cycles. However, our focus will be on complexes containing *anionic* pincer ligands that bind to the metal through at least one non-dative metal–ligand bond (e.g., σ M–C or M–N bonds), because these are much less prone to forming

M(0) complexes, favoring the emergence of nonconventional mechanisms involving less usual oxidation states. In order to provide a background for the topic, the first part of the chapter will summarize relevant aspects of the chemistry of group 10 elements containing anionic pincer ligand complexes in oxidation states above or below the usual divalent state. The ensuing sections will deal with catalytic reactions involving redox changes in the metal-pincer framework, which includes the Kharasch and Heck reactions and other C–C and C–X bond formation processes. Rather than providing an exhaustive review of these processes ([10–18] are excellent accounts in this regard), our interest will be directed to mechanistic issues, but emphasizing their implications for their application in synthesis.

2.2

Pincer Complexes of Ni, Pd, and Pt in Oxidation States Different from II

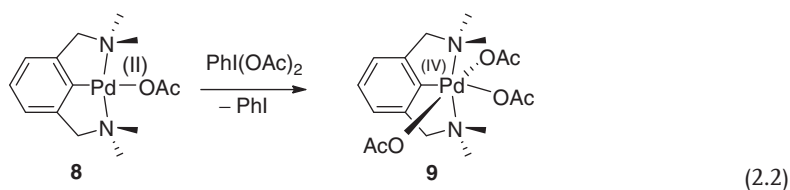
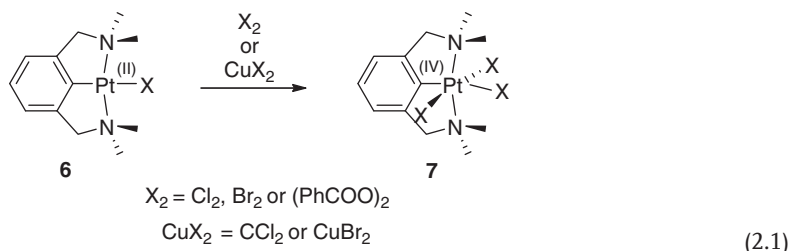
One of the most useful properties of pincer ligands is their capacity to stabilize compounds that otherwise would be reactive intermediates (e.g., complexes in unusual oxidation states), allowing the study of their properties. Organometallic derivatives of Pd in its higher oxidation state, although considerably more labile than the analogous Pt(IV) complexes [28, 29], are stabilized by pincer ligands containing hard donor sets [30]. Although a few Ni(IV) organometallic derivatives have been isolated and characterized [31], this oxidation state has only marginal importance in the chemistry of the lighter of the group 10 elements. In contrast, the existence of organometallic nickel species in intermediate oxidation states I and III has been suspected since the early days of Tsou and Kochi's studies [32] on the mechanism of the oxidative addition of aryl halides to Ni(0). As discussed later in this section, isolation and characterization of stable Ni(I) and Ni(III) organometallic compounds was made possible by the use of suitable pincer ligands.

2.2.1

Complexes in the Higher Oxidation States (III, IV)

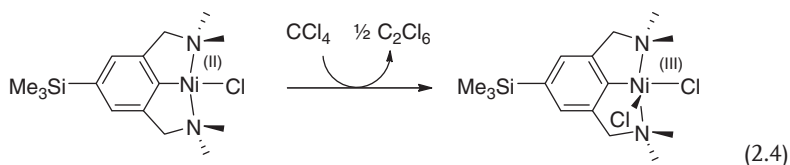
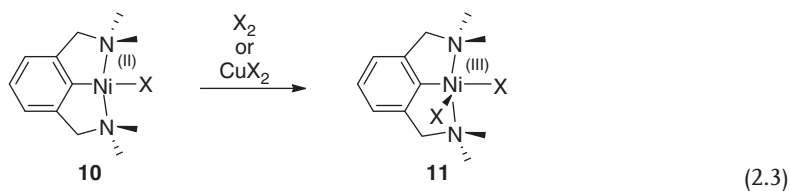
In the last two decades of the past century, studies by van Koten's group [26, 33] on the complexes of the group 10 elements with NCN pincer ligands led to the isolation of unusual high-valent organometallic complexes. As expected, the stability of the +IV oxidation state increases when descending in the group. Thus, trichloro- and tribromoplatinum(IV) pincer complexes were obtained as thermally very stable orange-red diamagnetic compounds when the corresponding Pt(II) precursors [(NCN)Pt-X], **6**, were treated with chlorine, bromine, or the corresponding Cu(II) halides [34], and similar Pt(IV) carboxylates were obtained by oxidative addition of acid anhydrides [35] (Eq. (2.1)). Several Pd(IV) complexes containing nonsymmetrical anionic pincer ligands featuring NNC [36], ONC [37, 38], and NNC [39] donor sets have been prepared by oxidative addition of halogens to the corresponding Pd(II) precursors, some of them stable enough to allow structural characterization. However, similar reactions have not been reported for

the corresponding palladium(II) NCN complexes (**8**). Iodonium(III) salts provide a more successful route to the corresponding Pd(IV) derivatives. Thus, Pd(IV) chloride complexes have been prepared using PhICl_2 [40], and although Canty and van Koten [35] mention that Pd(II) carboxylates $[(\text{NCN})\text{PdOCOPh}]$ are not nucleophilic enough to react with benzoic anhydride, Szabó [41] reported that the Pd(IV) acetate complex **9** is formed when the corresponding Pd(II) precursor reacts with $\text{PhI}(\text{OAc})_2$ (Eq. (2.2)). Different from their robust Pt(IV) analogs, Pd(IV) derivatives with NCN pincer ligands exhibit only moderate stabilities, decomposing in solution at room temperature.

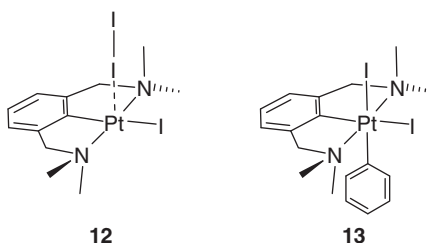


In contrast to the analogous pincer complexes of Pd or Pt, oxidation of nickel derivatives **10** with X_2 or CuX_2 ($\text{X} = \text{Cl}, \text{Br}, \text{I}$) stops at the trivalent state, affording dihalides **11** as very dark colored, air-stable crystalline solids (Eq. (2.3)) [42]. The solid-state structure of the iodide and bromide derivatives shows a pentacoordinated Ni center in a square-pyramidal coordination, with one of the halide ligands in the apical position [42, 43]. Their magnetic moments and electron paramagnetic resonance (EPR) spectra are consistent with low-spin d^7 configurations, the unpaired electron occupying the d_{z^2} orbital [44]. These complexes undergo clean substitution of the X^- ligands with silver salts. Ni(III) nitrate, nitrito, and isothiocyanate derivatives were prepared in this way [45]. Electrochemical studies have shown that one-electron oxidation of pincer derivatives of type **10** is easier than for most other Ni(II) complexes (at about 9.2–0.8 V vs Ag/AgCl). Oxidation potentials are sensitive to the nature of the anionic ligand X and to the substituents in the ring of the pincer ligand. A good correlation was found between the oxidation potentials and the Hammett parameter σ_p of the ring substituents [46]. In favorable cases, such as that shown in Eq. (2.4), the oxidation of the Ni(II) complex can be quantitatively carried out with CCl_4 [47]. The byproduct of this reaction is a trichloromethyl radical ($\cdot\text{CCl}_3$), which decays forming hexachloroethane. This is closely related to the ability of Ni pincer complexes to catalyze atom-transfer radical

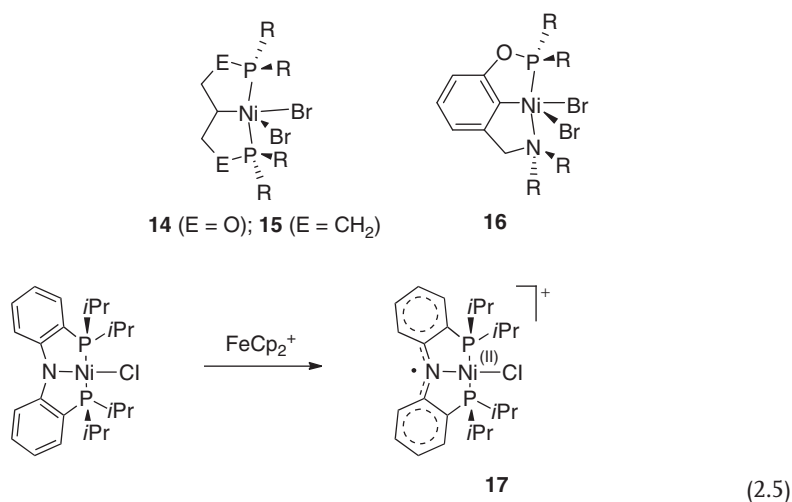
addition (ATRA) reactions, see Section 2.3.1.



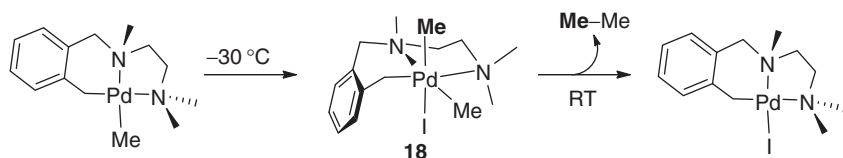
The reactivity of NCN complexes of Ni, Pd, and Pt toward I_2 provides a significant illustration of redox trends in the organometallic chemistry of group 10 elements. As mentioned, Ni(II) complexes are readily oxidized to Ni(III) by Cl_2 , Br_2 , and I_2 , while Cl_2 or Br_2 oxidize Pt(II) NCN complexes to Pt(IV). However, I_2 reacts with the iodide complex **6-I** (from now on, the number given to pincer complexes will refer to their general type, and the anionic ligand will be added to the number to distinguish between specific complexes), giving rise to a charge-transfer adduct **12**, without altering the formal oxidation state of platinum [48, 49]. The bonding in this complex arises from the overlap of a metal filled d_{z^2} and the I_2 empty σ^* orbitals. As a consequence of the transfer of electron density into the σ^* orbital, the I–I bond (2.822 Å) is significantly weakened as compared to that in the free I_2 molecule (2.715 Å). Remarkably, a Pt(IV) diiodide, **13**, is obtained when I_2 reacts with [(NCN)Pt-Ph], probably because the increased electronic density in the Pt(II) phenyl derivative allows for full electron transfer to the I_2 molecule [50]. Treatment of the NCN Pd(II) complex **8-I** with iodine led to the isolation of crystals containing two molecules of I_2 per Pd atom. However, the crystal structure of this material proved that I_2 merely cocrystallizes without interacting with the Pd(II) complex [26, 51]. It appears paradoxical that, while both the Ni(II) and Pt(II) complexes react with I_2 , the Pd(II) complex is unreactive. This indicates that, while its electron density on the Pd(II) complex is not high enough to allow the formation of a stable charge-transfer complex (similar to that formed with Pt), its partial oxidation to Pd(III) is not thermodynamically favorable, as it is in the case of Ni.



Pincer ligands containing soft donor atom sets (e.g., PCP) are less effective in stabilizing high oxidation states than those based on hard donors (N, O). No tetravalent Pt or Pd complexes with PCP pincer ligands have been reported so far in the literature, but Zargarian has reported the isolation of a series of Ni(III) complexes stabilized by PCP (**14**, **15**) [52–54] and hybrid PCN [55] pincers (**16**) by chemical oxidation of the corresponding Ni(II) precursors. The stability of Ni(III) complexes is closely related to the electrochemically measured oxidation potential of the Ni(II) complexes. Not surprisingly, these potentials are lower for PCN derivatives than for pure PCP complexes. Oxidation potentials are controlled not only by the nature of the donor atoms of the pincer ligand arms but also by their substituents and by the anionic X ligand [56]. In other cases, the electronic structure of the pincer framework plays a determinant role in the stabilization of the oxidized complex. For example, spectroscopic and structural studies indicate that complex **17** is best described as a Ni(II) complex containing an oxidized PNP pincer ligand, and therefore the redox reaction depicted in Eq. (2.5) is a ligand-centered process [57].



Oxidative addition of alkyl halides to Pd(II) or Pt(II) complexes usually leads to M(IV) complexes containing potentially reactive M–C bonds. In general, Pd(IV) compounds containing more than one M–C bond exist only as transient reaction intermediates, but pincer derivatives such as the one presented in Scheme 2.3 can be stable enough to allow spectroscopic detection [36]. In general, oxidative



Scheme 2.3 Generation of a detectable Pd(IV) pincer complex containing multiple Pd-C carbon bonds.

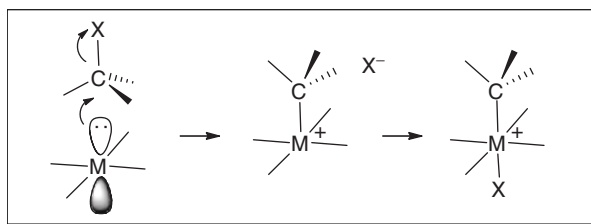
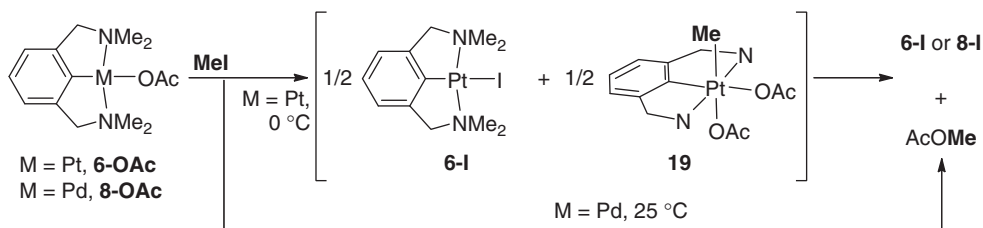


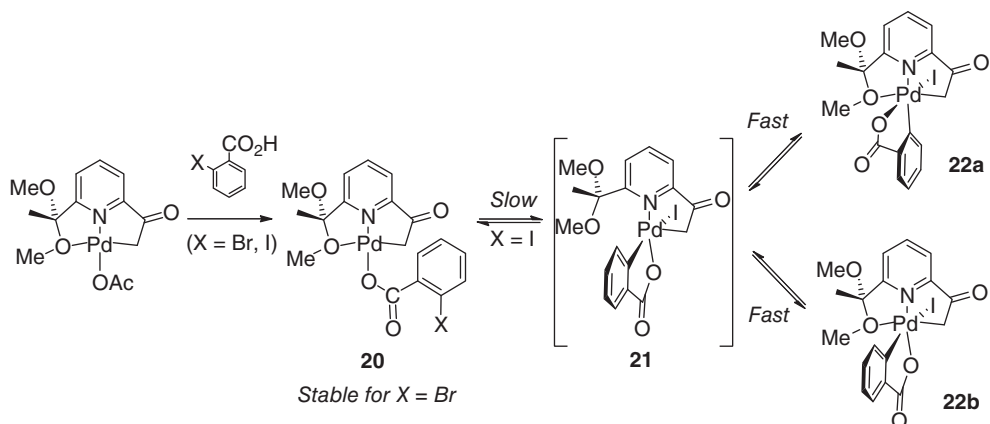
Figure 2.1 Oxidative addition of alkyl halides to d^8 metal centers.

addition of alkyl halides to square-planar d^8 metal centers proceeds via an S_N2 mechanism, as sketched in Figure 2.1 [28]. The primary product is an ion pair which later recombines into a neutral 18-electron $M(IV)$ complex. Evidence for this type of mechanism has been found in the oxidative addition of methyl iodide to the Pt derivative **6-OAc** (Scheme 2.4) [35]. Monitoring the reaction at 0°C reveals that the initial product of the reaction is a 1 : 1 mixture of Pt(II) iodide **6-I** and Pt(IV) diacetate complex **19**. It is believed that this mixture of products arises by the anion exchange between the ion pair intermediate and the starting material (**6-OAc**). At room temperature, **19** decomposes with C–O reductive coupling, affording methyl acetate. The analogous reaction of Pd acetate complex **8-OAc** with MeI takes place at room temperature without detectable intermediates, directly yielding **8-I** and methyl acetate, but it is believed that it involves a similar oxidative addition mechanism.



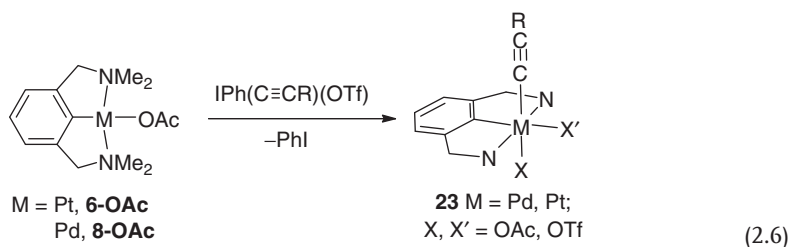
Scheme 2.4 Anion exchange involving $M(IV)$ intermediates ($M = \text{Pt}$ or Pd).

S_N2 reactions are not favored on most types of unsaturated carbon centers, and thus is not surprising that, until very recently, oxidative addition of C–X bonds containing sp^2 - or sp -hybridized carbons to Pd(II) centers were virtually unknown. Many reactions catalyzed by Pd pincer complexes are C–C couplings involving oxidative addition of aryl or alkenyl halides, and thus it is not obvious that these could take place through molecular mechanisms requiring Pd(II)/Pd(IV) cycles. However, Vicente [58] has reported a case of oxidative addition of aryl iodide to a Pd(II) complex containing a CNO pincer ligand (Scheme 2.5), which demonstrates the feasibility of this kind of processes. In order to enable the oxidative addition to proceed under mild conditions, it was forced to take place in an intramolecular manner. The complex **20**, containing a 2-iodobenzoate ligand,



Scheme 2.5 Intramolecular oxidative addition of aryl iodide to a Pd(II) center.

was generated *in situ* from the corresponding acetate precursor. This compound smoothly underwent oxidative addition of the C–I bond to afford a Pd(IV) product **22**, which was isolated and characterized by X-ray diffraction. In solution, complex **22** exists in equilibrium with small amounts of **20**, indicating that the iodoarene oxidative addition is a reversible process. Below $-20\text{ }^{\circ}\text{C}$, the NMR signals of **22** split into two sets corresponding to the geometric isomers **22a** (the one present in the X-ray structure) and **22b**. Presumably, rapid isomeric exchange takes place through an undetected intermediate **21**, resulting from the dissociation of the weakly coordinated OMe side arm. Very likely, the hemilabile behavior of the pincer ligand is important in facilitating the oxidative addition reaction, and **21** is also an intermediate in the C–I activation pathway.



As previously mentioned, oxidative addition of iodonium compounds to Pd(II) or Pt(II) centers provides one of the most effective pathways to M(IV) compounds. Canty [59] applied this method to the synthesis of Pt and Pd(IV) alkyne derivatives **23** (Eq. (2.6)). To avoid decomposition of the unstable Pd(IV) complex, the reaction of the Pd(II) complex **6** with the iodonium reagent needs to be carried out at low temperature over a long period ($-80\text{ }^{\circ}\text{C}$ /1 week). Szabó [60] has carried out density functional theory (DFT) calculations to model the addition of alkyne- and aryl-iodonium compounds to the Pd pincer complex, and compared these processes with the oxidative addition of aryl iodides (Figure 2.2). Both alkyne and aryl transfer

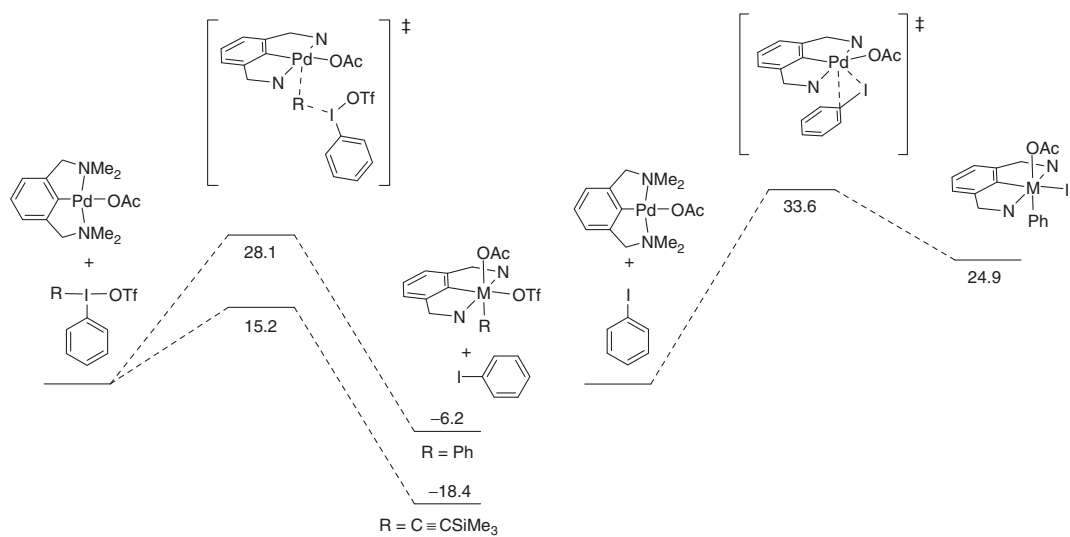


Figure 2.2 Computational energy profiles for the reaction of hypervalent iodonium and aryl iodides to Pd(II) pincer complexes. Energies are expressed in kilocalories per mol.

from iodine (III) to Pd(II) are exothermic, but it is more favorable in the former case. In addition, the activation barrier is lower for alkynyl than for aryl groups (15.2 and 28.1 kcal mol⁻¹, respectively). The favorable conditions predicted for the oxidative addition of alkynyliodonium reagents reproduce Canty's experimental results. In contrast, the oxidative addition of PhI to the Pd(II) complex was found to be endothermic by 24.9 kcal mol⁻¹, though the energy barrier is only 5.5 kcal mol⁻¹ higher than that for the phenyl transfer from diphenyliodonium(III) triflate (33.6 vs 28.1 kcal mol⁻¹). In the transition state for oxidative addition of iodonium reagents, only the I-bound carbon atom of the iodonium reagent interacts with the Pd atom. This interaction arises from the overlapping of a metal-filled d orbital with a low-energy empty σ^* orbital of the iodonium molecule, and is therefore reminiscent of the Pd-I₂ complex **12**. Therefore, this type of oxidative addition can be seen as a nucleophilic attack of the Pd(II) center on the carbon atom. In contrast, the transition state for the addition of aryl iodide contains a side-on interaction of the C-I bond with the Pd center that resembles that of the addition of aryl halides to Pd(0) [61]. The reversal of the Ar-I addition (i.e., reductive elimination of PhI) has a very low energy barrier of only 8.7 kcal mol⁻¹ (=33.6 - 24.9 see Figure 2.2), meaning that, in line with Vicente's observations, oxidative addition of haloarenes to Pd(II) is reversible. The aryl-Pd(IV) NCN pincer complex cannot be obtained by direct oxidative addition of aryl iodide because the thermodynamic balance favors the Pd(II) complex. It is worth remarking that the favorable thermodynamics associated with the oxidative addition of hypervalent iodonium compounds is due to the high energy of this type of reagents.

Although the existence of Pd(IV) species stabilized by PCP ligands remains still to be authenticated, Frech and Blacque [62, 63] used DFT methods to study the oxidative addition of Ph-Br to Pd(II) in the context of a mechanistic investigation of the Heck reaction catalyzed by [(PCP)Pd] complexes. They found that the process is highly endothermic and, in contrast to Szabó's calculation with NCN derivatives, direct addition of PhBr to [(PCP)Pd-Cl] has a prohibitively high energy barrier (>60 kcal mol⁻¹). However, oxidative addition becomes less difficult when it is preceded by the dissociation of the chloride ligand from the Pd(II) complex (Figure 2.3). This process is still endothermic, but the energy barrier for the concerted addition of the C-Br bond to the T-shaped [(PCP)Pd]⁺ cation is only 20 kcal mol⁻¹. Since halide dissociation is favored by the polar solvents and the high temperatures used in the experimental setup of the Heck reaction, the authors concluded that mechanism involving a Pd(II)/Pd(IV) cycle could be thermally accessible. However, the unfavorable thermodynamic balance of oxidative addition would make the detection of Pd(IV) intermediates very difficult or impossible.

Reductive elimination reactions are responsible for the final C-C/C-X bond formation step in catalytic processes. In principle, C-bound or any other anionic pincer ligands could engage in reductive coupling reactions, bringing about the decomposition of the pincer complex. In order to enable catalysis by such complexes, it is mandatory to avoid reductive elimination reactions involving the pincer ligand itself. Fortunately, this seems to be usually the case. For example, reductive elimination of ethane from the Pd(IV) pincer complex **18** (Scheme 2.3) is preferred

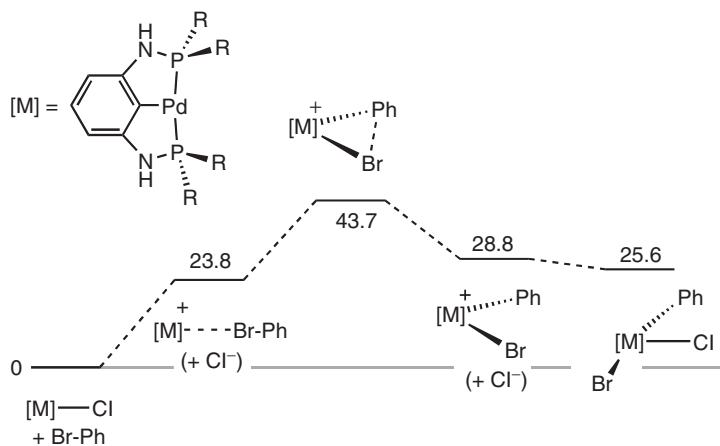
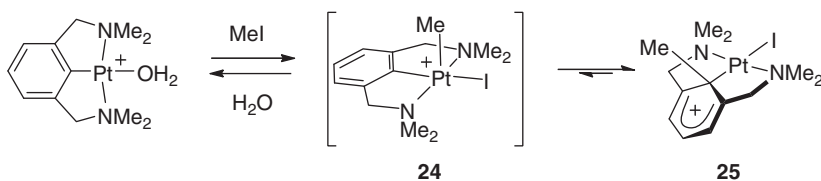


Figure 2.3 Computational energy profile for the oxidative addition of bromobenzene to a Pd PCP pincer complex. Energy is in kilocalories per mole.

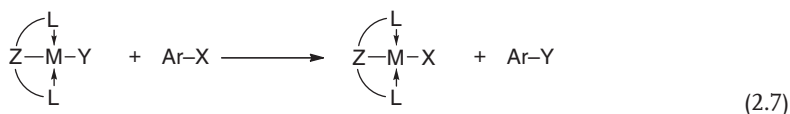
over coupling of the benzyl group of the pincer ligand and one of the methyl groups [36]. Another representative case is given in Scheme 2.4, where an unusual C–O bond formation is favored over coupling of the methyl group with the aryl group of the NCN ligand, which would be a more common type of reductive elimination [35]. The symmetrical configuration of NCN, PCP and related pincer ligands probably contributes, to preventing its participation in reductive coupling processes. However, the role of these aryl-based pincers in reductive elimination processes might be not as passive as it appears. van Koten [64] showed that oxidative addition of methyl iodide to cationic Pt(II) complexes is followed by migration of the alkyl group to the ipso carbon atom of the NCN ligand, affording stable complexes of type **25**, whose peculiar structure has been compared with the Wheland arenium intermediate of electrophilic substitution reactions (Scheme 2.6). Actually, the alkyl group can shift reversibly between the metal center and the aryl position [65]. The relative stabilities of Pt(IV) alkyls and Pt(II) “arenium” complexes are dictated by the other ligands present in the coordination sphere. Therefore, alkyl migration to the aryl ring does not involve the irreversible destruction of the pincer framework, and Pt(II) “arenium” complexes could be seen as a stabilized form of the Pt(IV) species [66]. Since cationic intermediates analogous to **24** have been proposed to participate in the oxidative addition of aryl halides to Pd(II) pincer complexes (see



Scheme 2.6 Formation of arenium-type Pt pincer complexes.

Figure 2.3) [62, 63], it is conceivable that the corresponding Pd–arenium complexes might also play some role in catalytic processes.

The overall outcome of reactions involving consecutive oxidative addition/reductive elimination, such as those represented in Schemes 2.4 and 2.6, is the exchange of groups between the pincer complex and the electrophile, as indicated in Eq. (2.7). These exchange reactions are rather common in the chemistry of nickel [54, 67–71] and palladium [13, 59, 72–74] pincer complexes, although they usually proceed without any detectable intermediates and do not necessarily involve a formal oxidative addition process. For example, Milstein [75] reported that the reaction of the PCP complex **2-Ph** with alkyl or aryl halides (R–I) proceeds in a nonselective manner, affording a mixture of coupling (Ph–R) and homocoupling products (Ph–Ph, R–R, sometimes in near-statistical ratio), and proposed that these are formed by the coupling of free radicals generated via an electron-transfer mechanism [75]. This redox mechanism is also well established for Ni complexes, as discussed in more detail in Section 2.3.3.

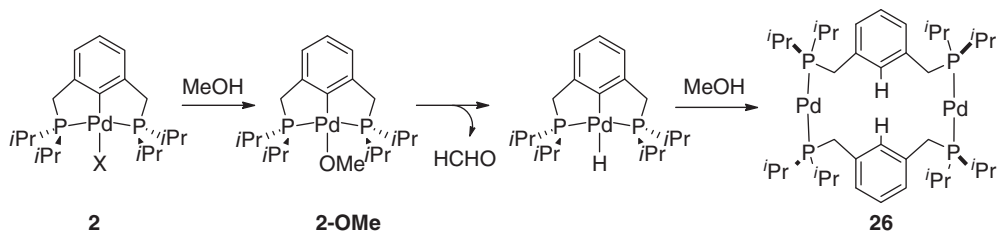


2.2.2

Reduced Complexes of Ni, Pd, and Pt with Pincer Ligands

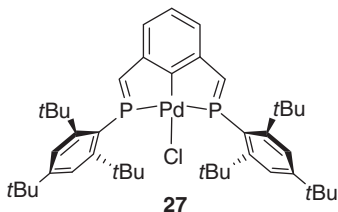
As discussed in Section 2.1, one of the main difficulties in providing a satisfactory explanation for the catalytic activity of anionic pincer ligands is their low capacity to support group 10 M(0) complexes, an essential part of many catalytic cycles. Leaving aside the fact that σ -carbon bonds are unusual among M(0) complexes of Ni, Pd, or Pt (except for carbene or carbonyl ligands), the geometric environment provided by pincer ligands is poorly adapted to the tetrahedral or trigonal configurations preferred by these d^{10} centers. In many cases, the catalytic properties of pincer complexes involve destructive reduction processes leading to ligand-free metal nanoparticles or colloids [12, 76]. The precise mechanisms responsible for to the breakdown of the metal-pincer framework are poorly understood, in general. Amines, sometimes added to the catalytic system as bases, induce the decomposition of palladium complexes with PCP or SCS ligands [77]. It has been suggested that the amine displaces one or both of the donor side arms of the pincer, and then undergoes β -hydrogen elimination. The ensuing decomposition process follows a sequence of reactions analogous to that described by Louie and Hartwig [23] for palladacycles. It has been recently shown that alcohols cleave the cyclometallated unit of very stable Pd PCP pincer complexes under mild conditions, affording a well-defined molecular Pd(0) complex **26** [78]. The reaction involves the intermediacy of an alkoxide species that decomposes by β -hydrogen elimination. The C–H coupling of the hydride and PCP ligands is an alcohol-induced reductive coupling that does not require dissociation of the very stable Pd–P interactions (Scheme 2.7) [78, 79].

Group 10 metal complexes with anionic pincer ligands can also undergo reduction reactions without losing the integrity of the metal–ligand framework. One of

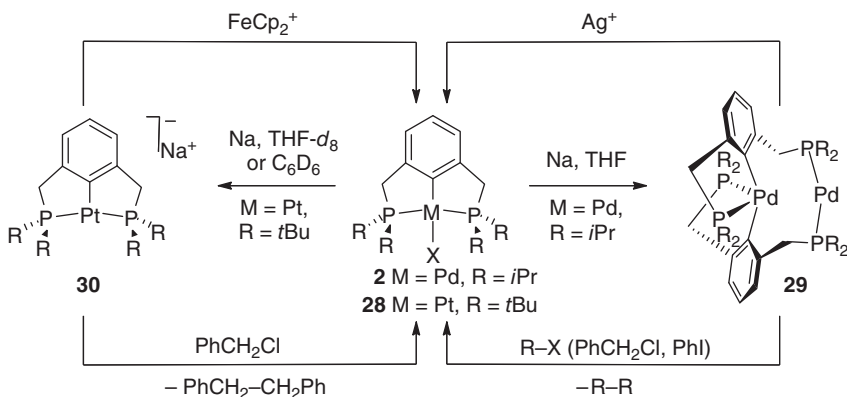


Scheme 2.7 Reduction of a Pd(II) pincer complex into a well-defined Pd(0) species.

the first examples of this type of processes dates back to 1992, when it was reported that complex **27** undergoes one-electron reversible electrochemical reduction [80]. The EPR signal of the reduced species exhibits hyperfine coupling to two phosphorus atoms, and its g value (2.0044) suggests that the unpaired electron is located in the ligand rather than in the metal center.



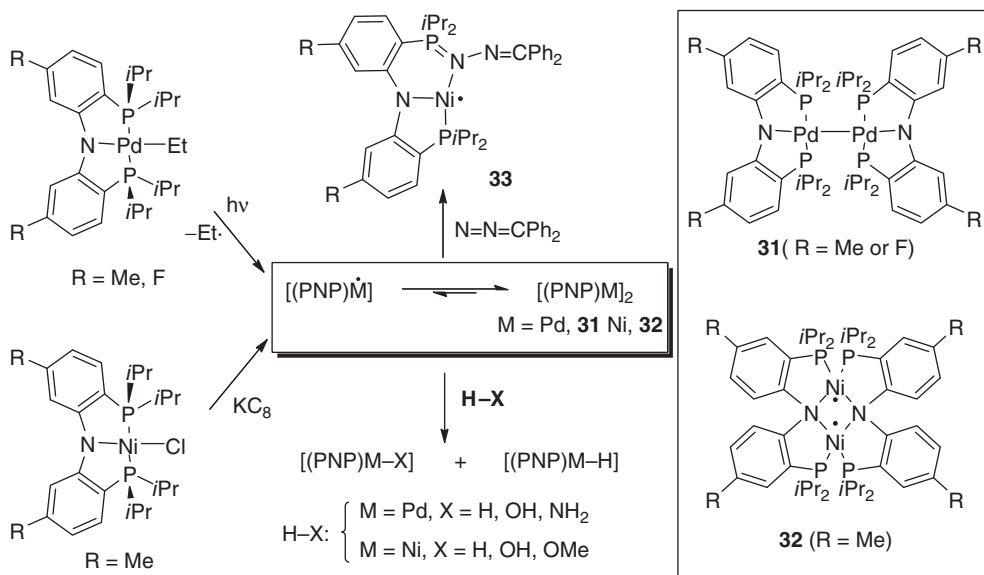
In recent years, a number of low-valent group 10 complexes with anionic pincer ligands have been isolated and characterized. Milstein investigated the chemical reduction of palladium [81] and platinum [82] complexes with PCP ligands with sodium (Scheme 2.8). The Pd-pincer framework of complex **2** does not resist reduction and collapses, giving rise to the unusual binuclear complex **29**. In this compound, both PCP ligands are covalently bound to one of the Pd atoms, which



Scheme 2.8 Reduction reactions of Pd(II) and Pt(II) pincer complexes and oxidation of the products thereof.

remains in the divalent state. The second metal center is reduced to Pd(0) and coordinates to one phosphine arm from each pincer unit. In contrast, the reduction of Pt complex **28** (containing a bulkier PCP ligand) afforded what is believed to be a genuine Pt(0) pincer complex (**30**) on the basis of spectroscopic data. Interestingly, both **29** and **30** are re-oxidized to the corresponding pincer M(II) precursors with one-electron oxidants (Ag^+ for $\text{M} = \text{Pd}$ and ferricinium for Pt). The oxidation can also be carried out with benzyl chloride, producing bibenzyl as the organic byproduct. In addition, complex **29** reacts similarly with PhI to give **2** and biphenyl.

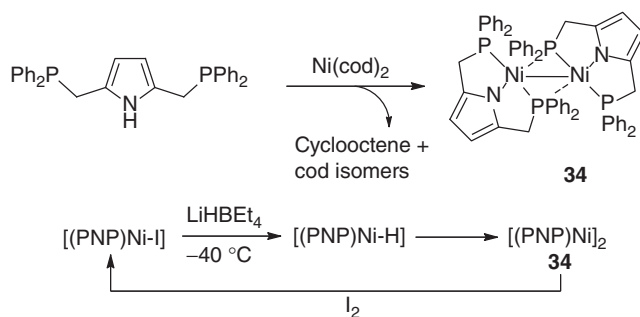
PNP ligands of the type *N,N*-bis(2-phosphinophenyl)amido can stabilize the monovalent state in both nickel and palladium complexes (Scheme 2.9). In 2007, Ozerov and Mindiola [83] reported that, upon irradiation with UV light, the ethyl Pd-complexes undergo Pd–C homolysis to afford binuclear Pd(I) complexes **31**, and shortly afterward Mindiola [84] described a Ni(I) derivative with the same kind of ligand, **32**, prepared by chemical reduction of the corresponding Ni(II) halocomplex with KC_8 . Although both compounds, **31** and **32**, correspond to the general formula $[(\text{PNP})\text{M}]_2$, their structures are very different. The palladium derivative is diamagnetic and its molecule is formed by two $[(\text{PNP})\text{M}]$ units singly bridged by a Pd–Pd bond. In the nickel complex, the PNP ligands are coordinate not in the usual pincer mode but bridge both nickel centers through the amido N atoms and donating one P unit to each metal atom. The complex is paramagnetic with a triplet ground state, consistent with the absence of a metal–metal bond. In spite of their structural differences, the reactivities of **31** and **32** exhibit remarkable analogies. Both undergo clean oxidative addition of small molecules containing X–H bonds (H_2 , H_2O , or even NH_3 in the case of **31**) to afford 1 : 1 mixtures of the



Scheme 2.9 Monovalent Ni and Pd species stabilized by PNP pincer ligands.

corresponding [(PNP)M–H] and [(PNP)M–X] products. This similarity stems from their tendency to reversibly dissociate into reactive monomeric units. The actual occurrence of such equilibrium is supported by the slow formation of a mixed ligand species [(PNP)Pd–Pd(PNP)'] when two homobinuclear Pd complexes containing different substituents in the PNP ligands are combined in solution and by measurements of the magnetic moment and cryoscopic molecular weight for the Ni complex. In addition, the nickel monomer can be trapped by reaction with N_2CPh_2 affording **33**, a monomeric species containing a tricoordinated Ni(I) center. A further example of monomeric Ni(I) “T-shaped” complex of the type [(PNP)Ni] was synthesized by Caulton by reduction of a Ni(II) precursor [(PNP)NiCl] with magnesium powder. It reacts with CO reversibly to afford a weakly bound carbonyl complex with a distorted square-planar structure [85].

The generation of the reduced species **29–32** requires very strong reducing conditions; therefore it is not obvious that such type of compounds can arise as intermediates in a catalytic process. However, Gade [86] has recently shown that a pyrrole-based PNP ligand reacts smoothly with $Ni(cod)_2$ (cod, cyclooctadiene) to afford a stable Ni(I) complex **34** (Scheme 2.10). This reaction presumably involves the intermediacy of an unstable hydride [(PNP)Ni–H]. When this hydride is generated by treating a Ni(II) iodide precursor with superhydride at low temperature, it spontaneously loses H_2 to afford **34**. Conversely, **34** is cleanly oxidized to the iodide precursor, demonstrating the chemical reversibility of this redox system.



Scheme 2.10 Generation of a Ni(I) complex containing a pyrrole-based PNP ligand.

2.3

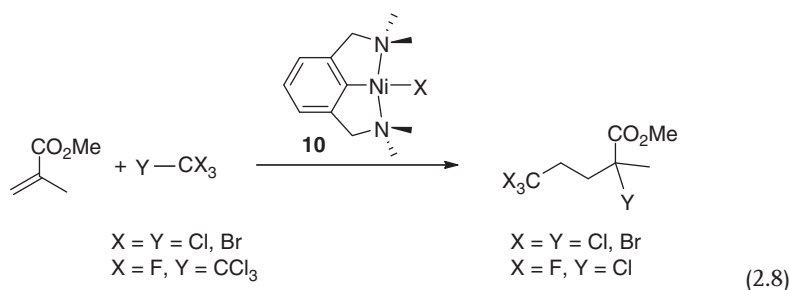
Catalytic Reactions Involving Redox Processes in the Pincer-Metal Framework

2.3.1

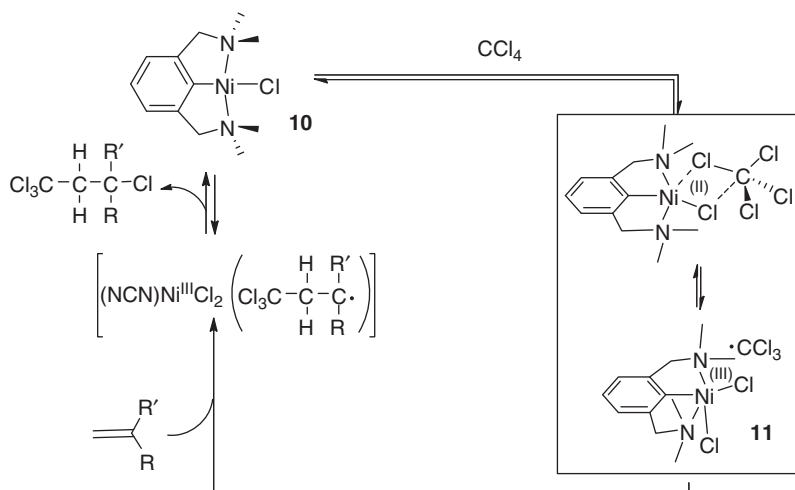
Atom-Transfer Radical Addition (ATRA) and Polymerization Reactions (ATRP)

One of the earliest applications of pincer complexes in catalysis is the ATRA of polyhaloalkanes (mainly CCl_4 , but also CBr_4 or CF_3CCl_3) to alkenes, also known as the *Kharasch reaction* (Eq. (2.8)) [33, 87]. Nickel complexes of type **10** (containing

NCN ligands) are among the most active catalysts for this type of reactions, operating at very mild temperatures (30 °C) [88, 89]. In contrast, the analogous Pd and Pt complexes are inactive for this type of process [89]. The outcome of the reaction depends on the ratio of the reagents, olefin and CCl_4 . When this is close to 1, the only observed product is the 1:1 Kharasch adduct (as shown in Eq. (2.8)). These reactions are very clean, and no sign of polymers or telomers is detected. However, when the concentration of CCl_4 is much lower than that of the olefin, living atom-transfer radical polymerization (ATRP) of the latter takes place [90].



It is believed that complexes of type **10** catalyze the Kharasch addition of CCl_4 to olefins through the mechanism outlined in Scheme 2.11 [91]. The process begins with the reversible oxidation of the Ni pincer complex by CCl_4 , which produces a stable Ni(III) complex **11** and a transient CCl_3 radical. This is accomplished by means of an inner-sphere electron transfer (i.e., involving prior coordination of CCl_4 to the metal center), followed by chlorine atom transfer to the metal. Formation of **11** was confirmed by the EPR spectra of the reaction mixtures [91]. Next, the $\cdot\text{CCl}_3$ radical adds to the olefin, generating a second radical intermediate.



Scheme 2.11 Mechanism of the Kharasch addition of CCl_4 to olefins catalyzed by Ni NCN complexes.

This is probably the rate-determining step, as the overall reaction kinetics is of first order on olefin. Rapid Cl atom delivery from the Ni(III) complex to the organic radical terminates the process, affording the Kharasch addition product. This step is analogous to the initial oxidation of **10** by CCl_4 , except that it proceeds in the reverse direction. The $\cdot\text{CCl}_3$ remains linked to the nickel(III) center during its short lifetime, in the sense that reversible electron transfer is much more rapid than the subsequent radical addition step. This explains why the reaction is not inhibited by free-radical traps such as Galvinoxyl and no cross-products are detected when a mixture of CCl_4 and CBr_4 is used [88]. When the CCl_4 concentration falls very low, ATRP is triggered by successive radical additions to the olefin.

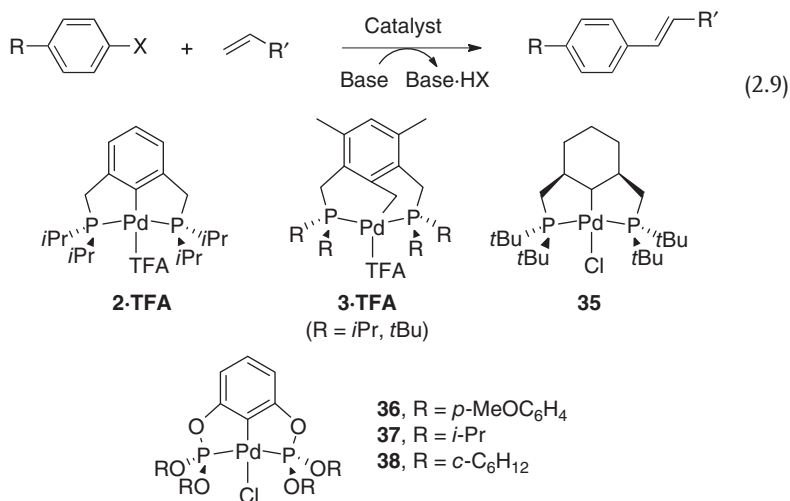
The catalytic activity of the Ni pincer complexes is linked to their unusually low oxidation potential. For a series of complexes containing different electron-donor or electron-withdrawing substituents, it has been shown that the catalytic activity is proportional to the oxidation potential of the complexes [46]. However, if the oxidation potential falls too low, free radicals can escape the metal complex, and irreversible oxidation of the Ni(II) complex to Ni(III) takes place rendering the system inactive. This was also found to occur when the catalyst is immobilized on a dendrimer, as closely packed $[(\text{NCN})\text{Ni}]$ units can easily interact with one another, lowering the oxidation potential (*dendritic effect*) [47]. Gradual radical decay is unavoidable during the ATRP, which gradually causes full oxidation of Ni(II) to Ni(III) complex with the concomitant loss of catalytic activity [90]. However, Zargarian [52, 53] has shown that Ni(III) complexes stabilized with PCP or PCN pincer ligands **14–16** are as active in the Kharasch addition reaction as their corresponding Ni(II) precursors. This might point to a somewhat different radical addition mechanism, or perhaps to the existence of a parallel redox process that allows the conversion of Ni(III) into Ni(II) complexes.

2.3.2

The Heck Reaction

The Heck reaction (Eq. (2.9)) is one of the most important processes catalyzed by palladium compounds. Nearly all sources of Pd catalyze this reaction, although their efficacy can vary widely. Thus, it is not surprising that the Heck reaction has become a benchmark proof for the catalytic ability of palladium complexes [9]. Many types of complexes with PCP [13, 62, 76, 77, 92–97], SCS [97–103], PNP [104], and other pincer systems [105, 106] have been shown to catalyze the Heck reaction. In general, they require very high temperatures (typically 140°C) and polar solvents (e.g., NMP (*N*-methylpyrrolidone), dimethylformamide (DMF), or dioxane). Optimum conversion is favored by the use of inorganic bases (Na_2CO_3 , NaHCO_3), but amines have also been employed. Mechanistic work has demonstrated that most Pd complexes, including palladacycles and, probably, most Pd pincer complexes, behave as precursors of nanoparticles or other ligand-free species that are the true catalysts, especially for the conversion the less reactive aryl bromides or chlorides [107, 108]. However, prompted by the special stability of pincer complexes, several authors have suggested that Pd pincer complexes could

act directly as molecular catalysts, as discussed below.

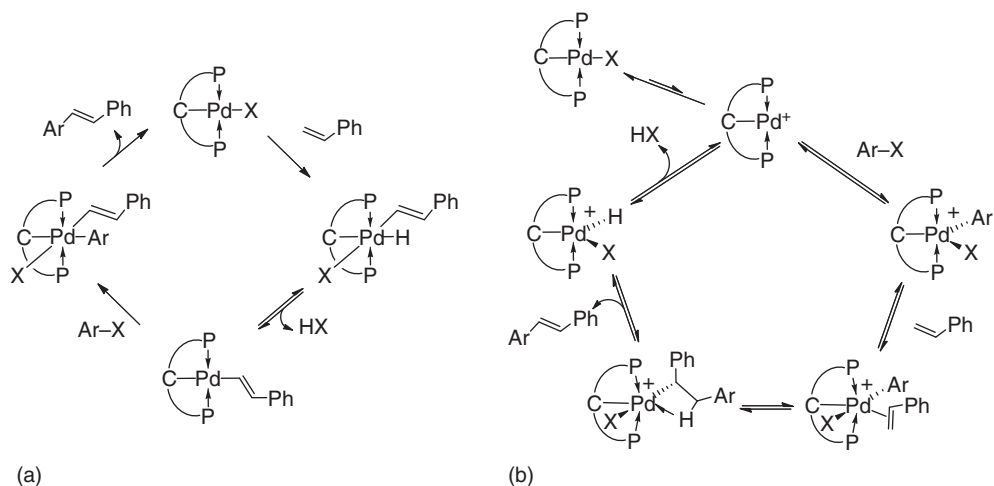


As mentioned in Section 2.1, Milstein described in 1997 [13] the first examples of Heck reactions catalyzed by Pd pincer complexes, **2-TFA** or **3-TFA** (TFA, trifluoroacetate). These are very active for the arylation of olefins (alkyl acrylates, styrene) with PhI, achieving TONs as high as 5×10^5 with PhI. They are somewhat less active with PhBr and essentially inactive with PhCl. **3-TFA** is appreciably more active than **2-TFA**. Neither of these complexes showed signs of decomposition at the temperatures used for the catalytic reaction (140 °C in NMP), which suggested that they could be directly involved in the catalytic process. However, the possible intermediacy of the phenyl (**2-Ph**) or the hydride (**2-H**) complexes was dismissed, since it was independently shown that these compounds undergo exchange reactions with iodobenzene affording biphenyl and benzene, which were not detected among the products of the Heck reaction. In addition, it was also shown that **2-Ph** fails to react with methyl acrylate. These findings are incompatible with a classical molecular mechanism involving a Pd(0)/Pd(II) cycle, and therefore an alternative mechanism involving a Pd(II)/Pd(IV) cycle was suggested, without commenting on the proposal in detail.

Another argument in favor of the direct involvement of molecular Pd complexes in the Heck reaction is the significant influence of the structure of the pincer ligand on the performance of catalysts. Milstein already pointed out that the higher activity of **3-TFA** as compared to **2-TFA** could be due to the higher electron density induced on the Pd center by the stronger σ -electron donor sp^3C donor center. Wendt [95] provided a better assessment of this effect by comparing **2-TFA** with a structurally more similar complex containing an sp^3C -bound pincer ligand, **35**, which also proved appreciably more active than **2-TFA**. Shibasaki [92] developed the POCOP catalyst **36**, which improves upon the mark of Milstein's PCP catalysts, attaining nearly full conversion for the PhI/*n*-butylacrylate coupling at Pd loadings of 1 ppm (i.e., TON $\approx 10^6$). Aryl chloride conversion was achieved by a closely related

POCOP catalyst, **37**, reported by Jensen [93]. Complex **37** is also more selective than conventional catalysts for the synthesis of trisubstituted olefins, which was also attributed to differences in the nature of the catalytically active species [94]. In the same vein, Bergbreiter showed that the closely related POCOP complex **38** does not catalyze the intramolecular Heck coupling of a substrate containing a diene functionality, while the intended transformation was performed by a conventional $\text{Pd}(\text{OAc})_2/\text{PPh}_3$ catalyst. Furthermore, the diene acts as a poison for **38**, suppressing its catalytic activity with regular olefinic substrates [99]. However, as Beletskaya [11] pointed out, comparing the performances of **38** and palladium acetate is not straightforward since the latter operates at a much higher Pd loading and requires the presence of an excess of PPh_3 , which may have an important effect in preventing the catalyst deactivation.

Two hypothetical mechanisms have been proposed to explain the Heck reaction on the basis of Pd(II)/Pd(IV) cycles (Scheme 2.12). As discussed in Section 2.2.1, oxidative addition of aryl halides to Pd(II) precursors is both kinetically and thermodynamically difficult. The Pd(II)/Pd(IV) mechanism proposed by Shaw for the Heck reaction (Scheme 2.1) tried to elude this problem by postulating the intermediacy of anionic Pd(II) complexes with increased nucleophilicity, but it is not evident how this mechanism could be adapted to complexes containing PCP or related pincer ligands. With this problem in mind, Jensen [93] made an alternative proposal (Scheme 2.12a), which starts with the oxidative addition of a C–H bond of the olefin to the Pd(II) pincer complex to afford a Pd(IV) vinyl-hydride intermediate. This idea was inspired by a similar reaction observed with an isostructural Ir(I) PCP complex, but such C–H bond activations are unusual in palladium chemistry. A theoretical analysis by Frech [63] ruled out such possibility, leading instead to the alternative Pd(II)/Pd(IV) cycle depicted in Scheme 2.12b. A key element

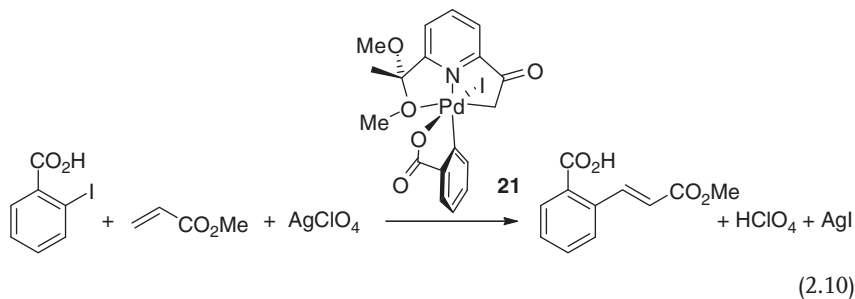


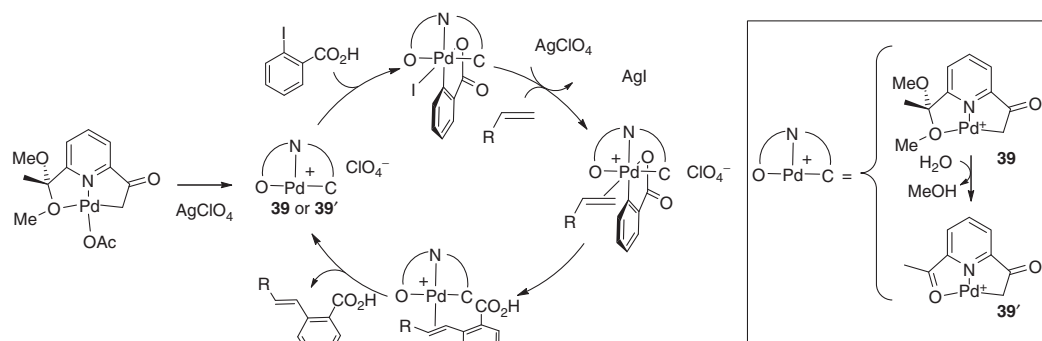
Scheme 2.12 Hypothetical Pd(II)/Pd(IV) mechanisms for the Heck reaction catalyzed by pincer complexes. (a) Jensen's proposal and (b) Frech's proposal.

of the latter mechanism is the generation of T-shaped cations $[(PCP)Pd]^+$ by electrolytic dissociation from the electrically neutral precursor, favored by the typical reaction conditions (i.e., polar solvents and high temperatures) commonly used for this type of catalysis. As already commented in Section 2.2.1 (Figure 2.3), a moderate energy barrier, about 23 kcal mol^{-1} , was calculated for the oxidative addition of bromobenzene to the $[(PCP)Pd]^+$ molecular fragment [62, 63]. The barrier for the subsequent reaction of the resulting 16-electron Pd(IV) species $[(PCP)Pd(Br)(Ph)]^+$ with the olefin to give the corresponding 18-electron species $[(PCP)Pd(Br)(Ph)(\eta^2\text{-olefin})]^+$ is comparable to that of the preceding oxidative addition, and the ensuing steps (including migratory insertion and β -hydrogen elimination) are thermodynamically downhill.

Apart from intuitions based on experimental observations and support from computational work, the arguments in favor of Pd(II)/Pd(IV) mechanisms in the Heck reactions catalyzed by Pd pincer complexes are scarce. On the contrary, there is conclusive evidence indicating that in many cases the actual catalytic species results from the decomposition of pincer complexes [62, 76, 77, 97, 100, 101, 103]. This conclusion can probably be extended to all systems that achieve exceptionally high TON numbers, such as **2** and **3**, since the rate of the processes based on Pd(II)/Pd(IV) cycles would be always limited by the low reactivity of Pd(II) toward aryl halides. The observed influence of pincer ligands on the catalytic activity or the ability to catalyze difficult couplings (e.g., with aryl chlorides) can be rationalized on the basis of their ability to regulate the production of the actual catalytic species [11, 12, 96]. This, however, does not prevent the possibility that, in some specific cases, pincer complexes could act as true molecular catalysts for the Heck reaction or other closely related processes. In recent years, a couple of examples have been provided that demonstrate this possibility, as discussed below.

The facile intramolecular oxidative addition of aryl halide which leads to Pd(IV) complex **22** (see Scheme 2.5) provided the basis for the development of a special type of Pd(II)/Pd(IV) Heck reaction [58, 109]. Although **22** fails to react with methyl acrylate at room temperature, an insertion reaction leading to the corresponding Heck product takes place in the presence of $AgClO_4$, which removes a iodide ligand generating the required coordination vacancy. Thus, complex **22** (10 mol%), or its Pd(II) precursor **20**, catalyzes a Heck-type coupling of 2-iodobenzoic acid with methyl acrylate, driven by iodide precipitation with silver salts (Eq. (2.10)). The reaction is completed within about 3.5 h at room temperature and, in contrast with the

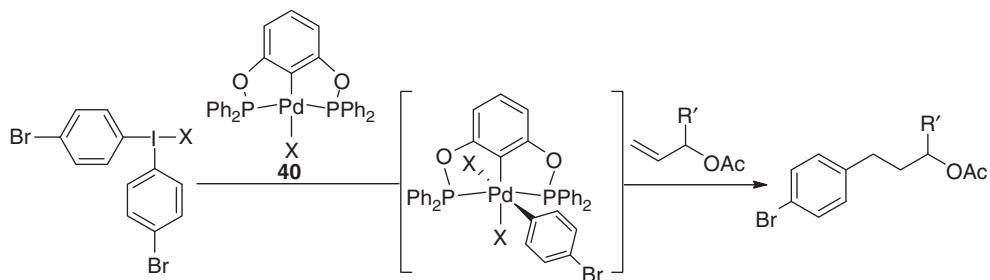




Scheme 2.13 Mechanism of a Heck-type reaction involving Pd(II) and Pd(IV) CNO pincer complexes.

typical Heck process, does not require added bases. Standard poisoning tests ruled out catalysis by palladium nanoparticles or other ligand-free palladium species. For example, the catalytic process is not quenched by mercury (Hg : Pd = 4000 : 1) or by 0.5–1 equiv of CS₂, PPh₃, or thiophene. Significantly, a strong drop in the catalytic activity was observed when the catalyst concentration was decreased from 10% to 1%, which is in stark contrast to the characteristic increase of TON numbers with dilution observed in reactions catalyzed by Pd nanoparticles. The proposed reaction mechanism is shown in Scheme 2.13. NMR monitoring of the reaction mixture showed that the catalyst remains mainly as a species identified as the solvated pincer complex [(ONC)Pd·S]⁺, **39**. The latter is gradually converted into **39'**, a related cationic species arising from the hydrolysis of the ketal group of the pincer ligand. It was shown that independently prepared **39** and **39'** are catalytically competent in this reaction. Therefore, both of them can be considered as the resting states of two independent catalytic systems, each of them based on its own ONC pincer system. Oxidative addition of the C–I bond leads to the corresponding Pd(IV) intermediate, which in the presence of AgClO₄ reacts with the olefin with consecutive insertion and β-hydrogen elimination to afford the organic product. Although this variation of the Heck reaction is probably of little practical interest, it represents the first authenticated example of a catalytic process involving aryl halide addition to a Pd(II) center. It is interesting to recall here that the cationic nature of the resting state is in good agreement with Frech's calculations for the PCP system, in the sense that the catalytic action of the pincer complex is facilitated by loss of the halide ligand. Noteworthy, the ClO₄[−] counteranion employed in this system has a critical role, and attempts to replace it by OTf[−] lead to a less stable catalytic system that operates through nanoparticles (positive Hg test).

Replacing aryl halides for bis(aryl)iodonium salts, Szabó [110] has developed another interesting variation of the Heck reaction that takes advantage of the known ability of these reagents to oxidatively add to Pd(II) centers (Scheme 2.14). The reaction is catalyzed by palladium acetate, or by pincer complexes with POCOP (**40**) or NCN (**8**) ligands at mild temperature (50 °C), using NaHCO₃ as a base. The existence Pd(IV) intermediates is supported by negative mercury drop tests (150 equiv Hg/Pd). ³¹P NMR spectra of reaction mixtures confirmed that the metal-pincer molecular framework of **40** remains unaltered after the substrates



Scheme 2.14 Redox Heck-type coupling of iodonium salts and alkenes.

have been fully converted. The efficient conversion of functionalized substrates such as allyl acetates or bromoaryliodonium reagents constitutes further evidence in favor of a Pd(II)/Pd(IV) cycle, since their functional groups would react with Pd(0) and are incompatible with a conventional Heck reaction. Apart from its mechanistic interest, the conversion of such functional substrates exemplifies the potential of Pd(IV)-based catalysis to expand the range of applications of Pd-catalyzed coupling reactions in organic synthesis.

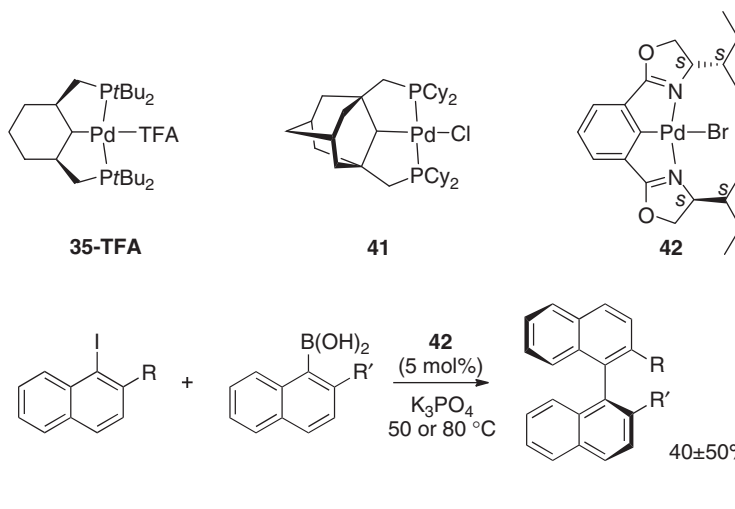
2.3.3

C–C Cross-Coupling Reactions

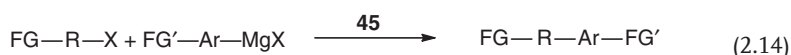
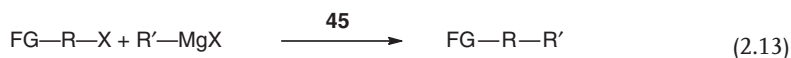
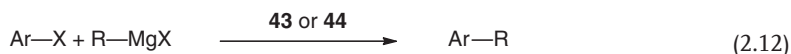
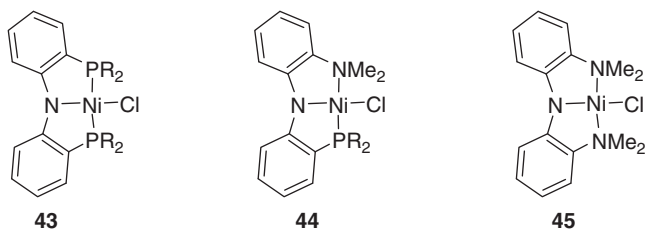
Nickel and palladium pincer complexes are largely complementary in their applications in cross-coupling reactions. Palladium derivatives, introduced first, typically catalyze Suzuki, Stille, or Negishi reactions, involving sp^2C – sp^2C couplings of aryl halides and aryl- or alkenyl-based soft nucleophiles, or Sonogashira couplings of alkyl halides and alkynes (a sp^2C – sp^3C coupling) [14, 15]. Nickel pincer complexes have found very interesting applications in Kumada-type reactions for the formation of sp^2C – sp^3C or sp^3C – sp^3C bonds, which rely on Grignard reagents as nucleophiles [17, 18].

As observed in Heck reactions, most C–C cross-couplings catalyzed by Pd pincer complexes require high temperatures ($>100^\circ\text{C}$) and achieve very high TON numbers at very low catalyst loads. This reaction profile suggests that also in cross-coupling reactions Pd pincer complexes behave as precursors for metal nanoparticles or other pincer ligand-free species. A typical example of this is the Suzuki synthesis of biaryls catalyzed with the complex **40-TFA** (see formula in Scheme 2.14), reported by Bedford in 2000 [111], which achieves TONs up to 2×10^5 at 130°C . Special pincer ligands with long [112] or hemilabile side arms [113, 114], designed to decrease the thermal stability of their complexes, give rise to Pd catalysts that operate at lower temperatures. In some of these reactions, the formation of black Pd material can be observed visually [112]. In some cases, the mercury drop and selective poisoning tests confirmed that either metal nanoparticles [115] or soluble Pd(0) species [116] are responsible for the observed catalytic activity. However, the results of such tests are not always clear-cut and the possible contribution of the molecular pincer complex as catalyst cannot be dismissed. Frech [117, 118], notes that the kinetics of Suzuki coupling reactions catalyzed by PCP pincer complexes with phosphoramidito ($-NPR_2$) arms exhibit a sigmoidal form that is typical of the generation of Pd nanoparticles, but the course of the reaction is not altered by Hg, nor is it improved by nanoparticle promoters (tetrabutylammonium salts). Mechanistic tests also leave some room for the contribution of molecular Pd catalysts in the case of the Suzuki coupling of aryls catalyzed by pincer complexes **41** [72] and **35-TFA** [74], reported by Frech and Wendt, respectively. Formation of catalytically active nanoparticles has been excluded in the case of **41**, since this catalyst is not affected by small amounts of PPh_3 or thiophene, and a nanoparticle stabilizer (tetrabutylammonium bromide) inhibits rather than promotes the reaction. The activity of **35-TFA** is only slightly affected

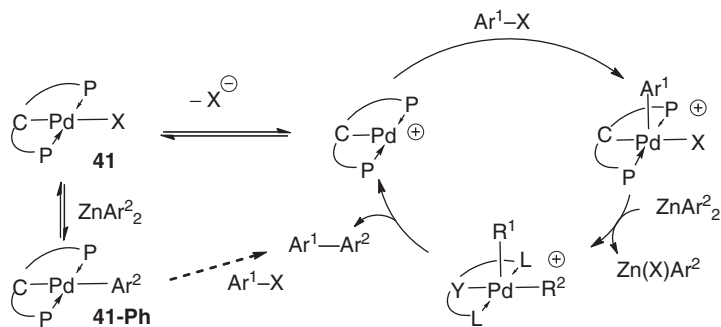
by the presence of mercury, which suggests that neither nanoparticles nor soluble Pd(0) species are involved in this case. With the chiral complex **42**, Nishiyama [119] provided a convincing argument for the involvement of the full metal-pincer moiety in the catalysis. This complex catalyzes the Suzuki coupling of binaphthyls with a significant enantiomeric excess (Eq. (2.11)), which is possible only if the chiral ligand remains attached to the active species. Asymmetric induction is not observed with related chiral Pd pincer complexes that presumably act as precursors of ligand-free catalytic species [120].



Nickel pincer complexes have been applied mainly in Kumada and less frequently in Negishi-type cross-coupling reactions. Some derivatives containing carbon-bound PCP [54, 121, 122] or PCN [123] pincers have been successfully tested in Kumada biaryl synthesis, but amido-type anionic pincer ligands have been more widely applied for this purpose (Eqs (2.12)–(2.14); FG = Functional Group). Representative examples of this structural type are the PNP or PNN complexes **43** and **44**, invented by Liang [124, 125], and the derivative **45**, termed *Nickamine* by Hu [17]. Other nickel catalysts containing exotic pincer ligands conformed by a central amido moiety and different side arm donors have also been tested [126, 127]. *Nickamine* is a versatile catalyst for the cross-coupling of functionalized, nonactivated haloalkanes [69, 128, 129] and polyhaloalkanes [68] with alkyl and aryl Grignards (including Knochel-type functionalized reagents) [68, 69, 128–130], as well as alkylnylmagnesiums [131]. Nickel catalysts allow the presence hydrogen atoms on the β positions of both the nucleophile and the electrophile. Significantly, most cross-coupling reactions catalyzed with Ni-pincer complexes take place at ambient temperature or below and are characterized by moderate TON numbers that are compatible with molecular mechanisms. Decomposition of the pincer framework appears less likely under such mild conditions, and in some cases mercury drop tests have been used to confirm that metal nanoparticles are not involved in these catalytic processes [130].



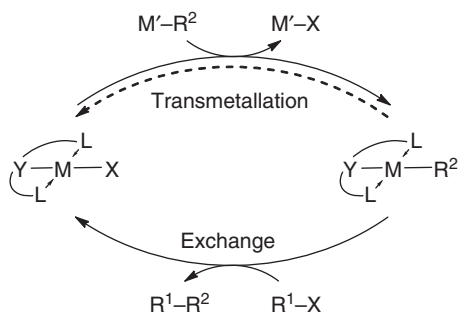
Mechanistic proposals for cross-coupling reactions catalyzed by pincer ligands encounter similar problems as those discussed for the Heck reaction in the preceding section. For palladium complexes, the most obvious possibility is a Pd(II)/Pd(IV) cycle. Frech has investigated the mechanism of Negishi cross-coupling reactions catalyzed by the Pd-PCP complex **41** (Scheme 2.15). He found that this compound catalyzes the coupling of aryl halides with arylzinc reagents (Negishi coupling) but, surprisingly, is not active with Grignard reagents (Kumada coupling). This compound reacts either with phenylmagnesium or diarylzinc reagent to afford the phenylnickel complex **41-Ph**. Treating the latter with an excess of ZnCl_2 leads back to **41**, indicating that Pd/Zn transmetalation is a reversible process. It was also shown that, under the reaction conditions (NMP, 100°C), **41-Ph** reacts with a fivefold excess of aryl bromide (Br-Ar , $\text{Ar} = p\text{-bromoanisole}$), yielding the coupling product Ar-Ph (dotted arrow). Although this result might suggest that



Scheme 2.15 Mechanism of the Negishi reactions catalyzed by complex **41**.

41-Ph is an intermediate in the coupling reaction, this is ruled out because **41** would then be active in the Kumada coupling. On the basis of DFT calculations, it was suggested that the Negishi coupling reaction involves the Pd(II)/Pd(IV) cycle shown in the right side of the scheme. As already mentioned in preceding sections, calculations show that direct oxidative addition of aryl bromide to 16-electron [(PCP)Pd-X] complexes, for example, **41** or **41-Ph**, are thermodynamically disfavored processes. However, the oxidative addition reaction would be less endothermic for the cationic 14-electron intermediate [(PCP)Pd]⁺, arising from halide dissociation from the initial Pd complex. The Pd(II)/Pd(IV) cycle would be completed with consecutive arylation of the Pd(IV) by the organozinc reagent and reductive elimination, which releases the cross-coupled product. These results provide an explanation as to why **41** is active in the Negishi reaction but inactive in the Kumada coupling. The difference lies in the reversibility of the reaction of **41** with organozinc compounds, in contrast to the irreversibility of the reaction with Grignard reagents. The latter prevents the generation of significant amounts of the key cationic species [(PCP)Pd]⁺, disabling the Pd(II)/Pd(IV) cycle. Significantly, transmetalations from arylboronic acids [72, 74] and organostannanes [132] to Pd pincer complexes have been shown to be reversible, which allows a similar mechanism for Suzuki or Stille cross-coupling reactions.

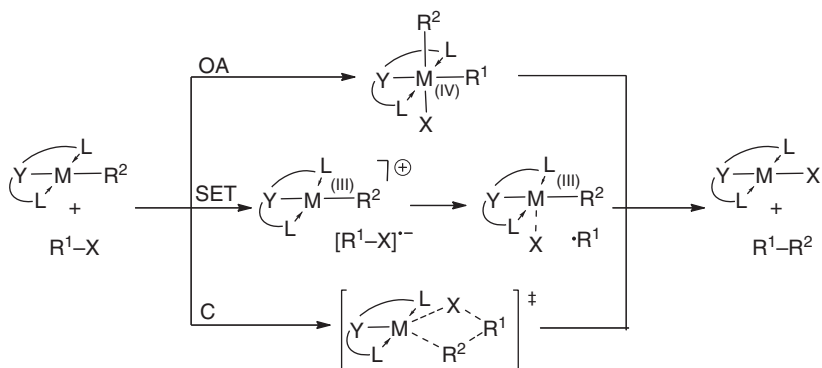
One of the less obvious aspects of the preceding mechanism is the reason that prevents complex **41-Ph** in participating in the catalytic process, since it was shown that this compound does in fact react with aryl halides affording the corresponding biaryls and **41**. Frech estimates that, if this reaction does actually take place under the catalysis conditions, it would be responsible at best for a small part of the total activity. The reaction of **41-Ph** with aryl halides is an example of exchange reactions, briefly mentioned in Section 2.2.1 (see Eq. (2.7)), that many pincer complexes undergo with different types of electrophiles (including aryl halides) to afford the corresponding cross-coupling products, usually with excellent selectivity [72–74]. Combining this exchange reaction with a transmetalation step leads to the alternative two-stage mechanism depicted in Scheme 2.16, which differs from that



Scheme 2.16 Basic two-stage transmetalation/exchange mechanism for cross-coupling reactions catalyzed by pincer complexes.

shown in Scheme 2.15 in that the attack by the nucleophile *precedes* the reaction with the electrophilic partner. This mechanism does not require the reversibility of the transmetalation step, and for this reason is particularly well adapted to explain the various types of Kumada couplings catalyzed by nickel pincer complexes. In these reactions, the nickel catalyst rests as a σ -alkyl or aryl species [69, 130]. Noteworthy, Ni alkyl complexes supported by amido-type pincers are resistant to β -hydrogen elimination, in good agreement with the ability of these compounds to couple aliphatic Grignard reagents [125, 133, 134].

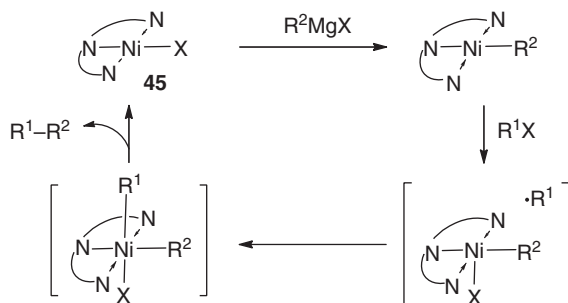
In most cases, both the transmetalation and the exchange processes are apparently simple processes involving no detectable intermediates. However, while the transmetalation step is mechanistically simple, the exchange reaction is complex (in the sense that it comprises two or more elemental steps) and can proceed through different mechanisms, summarized in the three main types shown in Scheme 2.17. Path OA corresponds to the oxidative addition/reductive elimination route, which finds some support in the Pd(IV) chemistry discussed in Section 2.2.1. As previously discussed, direct oxidative addition of aryl or vinyl halides is, in general, disfavored for most Pd(II) pincer complexes, but it can be feasible in specific cases (see Section 2.2.1). This is likely to be the case in a Negishi cross-coupling of aryl iodides catalyzed by an electron-rich Pd complex containing a dianionic pincer ligand, described by Lei [135]. It has also been suggested that the exchange step could take place without redox change on the metal center if it takes place through a concerted route C, involving a four-membered cyclic transition state [73, 74]. Some reactions of Pd pincer ligands, such as exchange reactions of η^1 -allyl complexes [(PCP)Pd-CH₂CH=CH₂] [136], or the hydrogenolysis of hydroxide or alkoxides [(PCP)Pd-OR] to afford HOR and [(PCP)Pd-H] [79], might proceed through non-redox mechanisms. However, these are special cases, because the exchanged ligands (η^1 -allyl, alkoxo) have a special reactivity of their own, and no mechanistic evidence has been provided in favor of this type of mechanisms when



Scheme 2.17 Mechanisms of exchange reactions: OA, oxidative addition; SET, single-electron transfer; C, concerted.

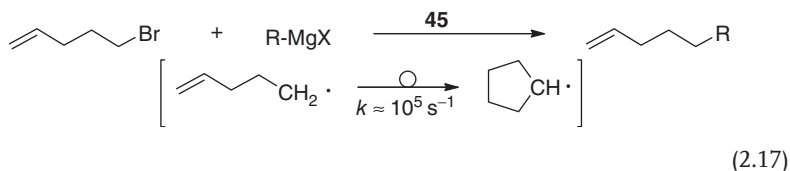
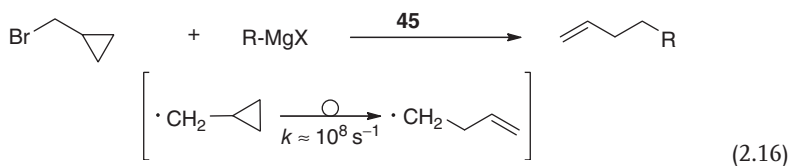
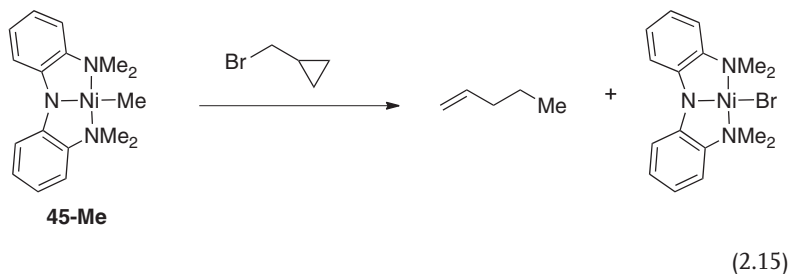
the exchange with electrophilic reagents involves simple σ -alkyl or aryl ligands, as required by the two-stage mechanism shown in Scheme 2.16. Thus, the most likely mechanism for these reactions is a free-radical process triggered by single-electron transfer, designated SET in Scheme 2.17. Milstein [75] found that the reaction of PCP palladium complex **2-Ph** with methyl iodide or iodoarenes affords mixtures of cross- and homocoupling products, and attributed this lack of selectivity to the generation of free radicals through an SET mechanism. As discussed in Section 2.3.1, SET reactions have special relevance for the chemistry of Ni pincer complexes. Zargarian [54] has shown that the ability of Ni complexes with PCP ligands to catalyze Kumada cross-couplings reactions correlates with the Ni(II)/Ni(III) oxidation potential of such complexes.

Hu [68, 128] has investigated the exchange of the Nickamine derivatives **45-Me** and **45-Et** with alkyl halides. These reactions afford the corresponding coupled products R-Me or R-Et. Chloroform and dichloromethane react with remarkable selectivity with **45-Me**, yielding isobutene and propane, respectively [68]. As expected for a radical mechanism, the rate of these reactions decreases in the presence of 2,2,6,6-tetramethylpiperidin-1-yl)oxy (TEMPO), a radical trap. Furthermore, treatment of **45-Me** with bromomethylcyclopropane, a well-known radical probe, yields the rearranged open-chain product 1-pentene (Eq. (2.15)). The high selectivity of these coupling reactions suggests that the radical pair formed in the SET reaction collapses into a high-valent (formally a Ni(IV)) species, which decomposes by reductive elimination. This leads to the catalytic cycle shown in Scheme 2.18 for the Kumada reaction. Accordingly, when **45** catalyzes Kumada coupling of bromomethylcyclopentane with Grignard reagents, the corresponding open-chain olefin products are obtained. However, if similar experiments are carried out with 5-bromo-1-pentene (another radical probe that cyclizes to afford cyclopentyl products), mainly “normal” products, instead of the expected products with a cyclic structure (non-transposed linear olefins) were obtained (Eqs (2.16) and (2.17)). Cyclopropylmethyl and 1-pentenyl radicals are “radical clocks” with characteristic rearrangement rate constants of 10^8 and 10^5 s⁻¹, respectively. Hence, the capture of the free radical by the Ni(III) intermediate complex must be slower than the



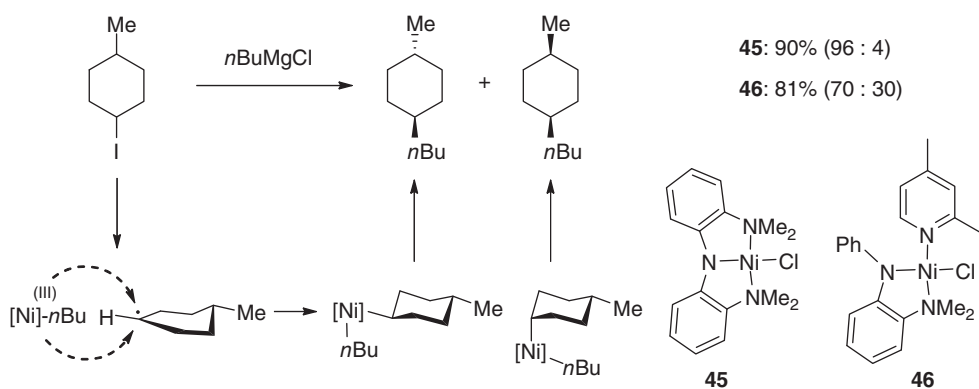
Scheme 2.18 Catalytic cycle for the Kumada reaction catalyzed by Nickamine (compound 45).

rearrangement of the cyclopropylmethyl radical but faster than that the cyclization of 1-pentenyl to cyclopentyl, which effectively prevents the latter process from taking place.



Very recently, Hu [129] has shown that cross-coupling reactions of alicyclic alkyl halides with Grignard reagents catalyzed with nickel catalysts exhibit a remarkable diastereoselectivity which depends markedly on the structure of the catalyst. Nickamine (**45**) has better performance than a second catalyst, **46** bearing a bidentate amino-amido ligand. The influence of the catalyst structure suggests that the diastereoselectivity of the reaction originates in the coordination sphere of the metal, that is, after capture of the radical by the transient Ni(III) intermediate has taken place, as shown in Scheme 2.19.

The Nickamine catalyst alone does not catalyze the coupling of aromatic Grignard reagents with alkyl halides, but becomes active in the presence of polydentate nitrogen bases (e.g., tetramethylethylenediamine or bis[2-(*N,N*-dimethylaminoethyl)]ether) [130]. Bidentate base auxiliaries were also found to be effective for the coupling of alkyl halides with alkynyl Grignards [131]. The cause of the lack of activity of Nickamine with aryl Grignards can be traced to the failure of arylnickel derivatives such as **45-Ph** to undergo exchange reactions with alkyl halides [69]. Electrochemical studies show that one-electron oxidation of alkyl complexes (e.g., **45-Me**) takes place more readily than that of **45-Ph**, which may be the cause of the lower reactivity of the latter. It is likely that the role of the nitrogen base is to enhance the nucleophilicity of the Grignard reagent by chelating the



Scheme 2.19 Diastereoselective Kumada couplings catalyzed by complexes **45** and **46**.

magnesium atom. This would enable the formation of small amounts of an electron-rich anionic species $[(\text{NNN})\text{NiR}_2]^-$ ($\text{R} = \text{aryl}$ or alkynyl) which can be more readily oxidized by the alkyl halide. The anionic intermediate has not been detected by NMR, which indicates that its formation is thermodynamically uphill. Liang [125] found a similar situation in a Kumada biaryl synthesis catalyzed by a Ni complex with a hybrid PNN pincer ligand.

Although neutral pincer ligands are outside the scope of this chapter, a brief reference to terpyridine nickel catalysts studied by Vici [137–139] is necessary in closing this section. The author reported that terpyridine monomethylnickel complexes **47**, formally Ni(I) complexes, are competent catalysts for the Kumada-type coupling of alkyl halides and alkyl Grignard reagents. Mechanistic investigations led to the original mechanistic proposal shown in Scheme 2.19, which was later adapted to the Nickamine catalyst, **45** [138]. Since the apparent oxidation state of Ni in **47** is +I and +II in **45**, the oxidation states of the successive intermediates $[(\text{NNN})\text{Ni}(\text{R}^2)(\text{X})]$ and $[(\text{NNN})\text{Ni}(\text{R}^2)(\text{R}^1)(\text{X})]$ are, respectively, +II and +III for the terpyridine system and +III and +IV for Nickamine-based intermediates. Apparently, the redox sequence fits better the known organometallic chemistry of Ni for **47** than for Nickamine. However, a detailed analysis of the electronic structure of **47** revealed that this type of compounds should be regarded as Ni(II) complexes containing a radical-anion terpy ligand rather than genuine Ni(I) complexes [139]. Other nitrogen ligands used in Ni-catalyzed cross-coupling reactions, for example, 2,6-bisoxazolinyipyridines (Pybox ligands), also exhibit a similar *non-innocent* behavior [140]. Ligand *non-innocence* allows redox changes to be ligand-centered as well as metal-based processes [141]. It also casts doubt on the actual oxidation state of the metal, in the sense that unusual formal oxidation states of the metal center can be deceptive (Figure 2.4). For example, in complex **17**, the PCP pincer ligand has undergone oxidation, therefore the effective oxidation state of the metal (II) is lower than the formal one (III) [57]. Therefore, it is not impossible that the unusual Ni(IV) suggested for the Nickamine system could be stabilized by partial oxidation of the NNN pincer ligand. It is thus important to stress that pincer ligands can have

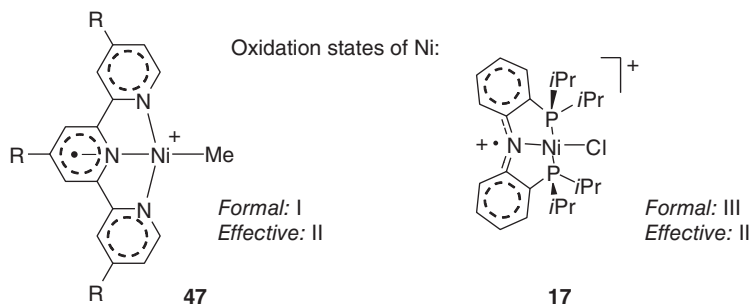


Figure 2.4 Formal and effective oxidation states of Ni in complexes **47** and **17**.

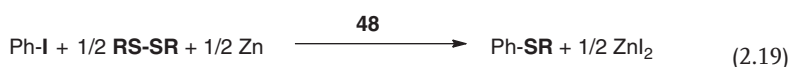
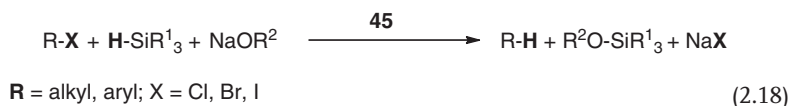
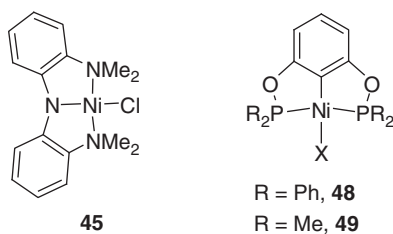
a very active role in catalysis, which goes beyond the stabilization of intermediates and can directly influence the ability of metal complexes to go through the different stages required to complete the catalytic process.

2.3.4

Carbon–Heteroatom Coupling Reactions

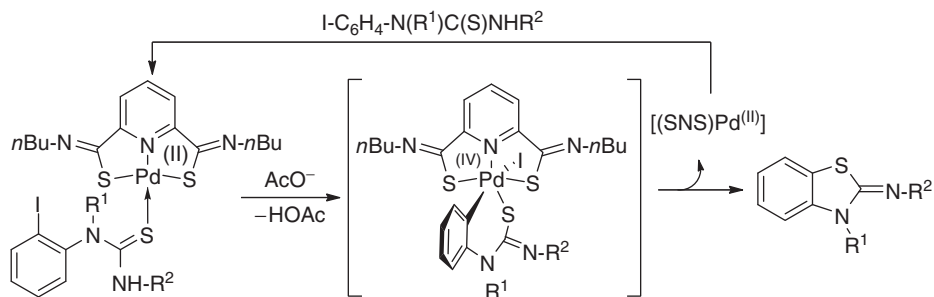
A number of carbon–heteroatom bond formation reactions are catalyzed by nickel or palladium pincer complexes. Some of these reactions operate through non-redox mechanisms analogous to that shown in Scheme 2.16, with a concerted non-exchange step (see route C, Scheme 2.17). For example, Szabó [142] has described an elegant method for the direct synthesis of propargylstannanes or propargylsilanes from propargyl halides catalyzed by the pincer complex [(NCN)Pd–Br], **8-Br**, in which the distannanes or disilanes $\text{Me}_3\text{E–E}\text{Me}_3$ ($\text{E} = \text{Sn}$ or Si) act as the organometallic transfer reagent. In this case, the exchange step involves the reaction of the corresponding [(NCN)Pd– ER_3] intermediate with propargyl halide. DFT calculations for the stannylation reaction show that the transition state for this exchange resembles that of a typical $\text{S}_{\text{N}}2$ reaction, except that the electron pair used by the attacking nucleophile is the one engaged in the sigma-Pd-Sn bond. A non-redox mechanism was also proposed for the exchange of alkyl iodides or bromides with silver fluoride, catalyzed by Ni and Pd fluoride pincer complexes with PCP ligands [67]. However, there are other cases in which mechanism of carbon–heteroatom bond formation requires redox capability of the pincer-complex catalyst. A good example is the hydrodehalogenation of alkyl and aryl halides with a combination of sodium alkoxide and the Nickamine catalyst (**45**), reported by Hu [143] (Eq. (2.18)). The scope of the reaction is very broad, and includes the selective reduction of C–X bonds ($\text{X} = \text{Cl}, \text{Br}, \text{I}$) in the presence of different FGs. The mechanism involves the generation of the nickel hydride intermediate **45-H** by successive X/OR metathesis with sodium alkoxide (NaOR^2), and substitution of the alkoxy group by hydride effected with a silane. Next, **45-H** undergoes exchange reaction with the organic halide, affording the hydrodehalogenated product and halide complex. The latter reaction was studied using pure samples of **45-H**. By using radical probes, such as bromomethyl cyclopropane, it was shown that this

reaction takes place through an SET mechanism involving free radicals. Morales-Morales [70] has described the thiolation of phenyl iodides with dithiols and zinc, depicted in Eq. (2.19), catalyzed by the Ni phosphinito POCOP complex **48**. Since the reaction involves the combined use of oxidizing organic disulfides (RSSR) and reducing reagents (Zn), it is tempting to suggest that the pincer complex must be undergoing some type of redox change. A Ni(I)/Ni(II) cycle has been suggested, invoking the formation of a reduced, T-shaped $[(\text{POCOP})\text{Ni}^{\text{I}}]$ intermediate, which is subsequently oxidized to the Ni(II) thiolate complex $[(\text{POCOP})\text{NiSR}]$. This, in turn, exchanges with the aryl iodide, affording Ar-SR and $[(\text{POCOP})\text{Ni}-\text{I}]$. The competitive formation of biphenyl as a minor byproduct can be readily accommodated in this mechanistic proposal. Guan has reported recently the related thiolation shown in Eq. (2.20), catalyzed by the closely related catalyst **48**. However, a mechanistic study showed that the phosphinite pincer complex is not stable under the basic conditions and decomposes releasing $\text{KP}(\text{O})\text{Me}_2$ and PPh_3 . That **49** is not the actual catalyst of this reaction is supported by the fact that this is catalyzed more efficiently by a combination of $\text{Ni}(\text{cod})_2$ and $\text{HP}(\text{O})\text{Me}_2$ [71].

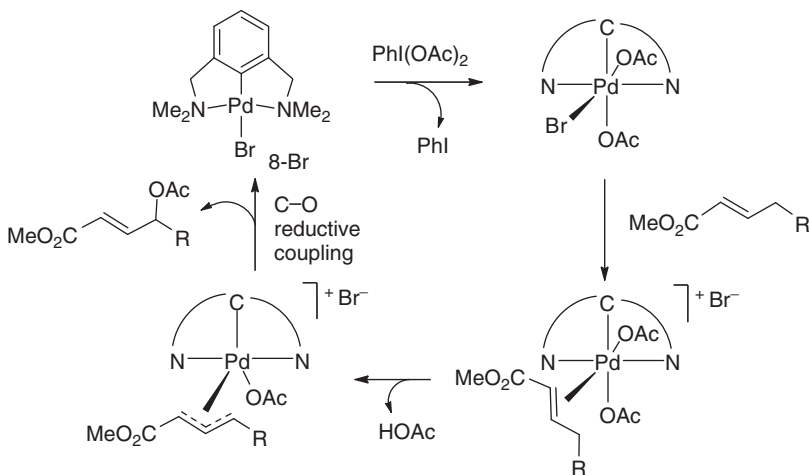


Very recently, Lei [144] has shown that a highly nucleophilic Pd complex containing a dianionic thioimido pincer ligand catalyzes the cyclization of 2-iodoaryl thioamides. The author suggests that the mechanism of this reaction could involve either an SET mechanism or intramolecular oxidative addition of the aryl iodide moiety to the Pd(II) center. The latter possibility (Scheme 2.20) is supported by its similarity to the intramolecular oxidative addition of 2-iodoarylcarboxylates reported almost simultaneously by Vicente [58].

Szabó has developed C–X bond formation reactions involving C–H bond activation and Pd(II)/Pd(IV) cycles, using iodonium salts as oxidants. One of them is a

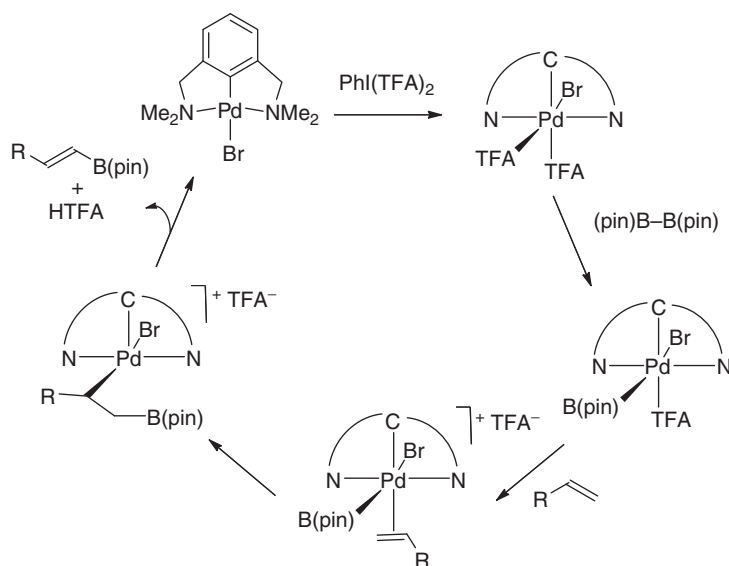


Scheme 2.20 Cyclization of 2-iodoarylamides catalyzed by SNS pincer Pd complexes.



Scheme 2.21 PCP-Pd complex catalyzed acyloxylation reaction.

special version of the acyloxylation reaction (Scheme 2.21), which allows the synthesis of allyl acetates or benzoates directly from the olefin and the corresponding iodobenzene dicarboxylate. This reaction is catalyzed with similar efficacy either by palladium acetate or a Pd pincer complex with of type 8-Br [41]. Isotopic labeling experiments carried out with the latter catalyst were used to demonstrate that this reaction involves intramolecular C–H activation and formation of a Pd(IV)- η^3 -allyl intermediate. The organic product is released in a reductive coupling step that has an immediate precedent in the decomposition of Pt(IV) and Pd(IV) pincer complexes with carboxylate derivatives investigated by Canty and van Koten [35] (see Scheme 2.4). A related reaction is the alkene borylation depicted in Scheme 2.22, which takes place when iodonium TFA is used in combination with diboron dipinacolate, $B_2(\text{pin})_2$ [145]. The scope of this borylation reaction is limited to cyclic olefins and some terminal alkenes. However, as compared to other methodologies for C–H activation/borylation, this one has the advantage of avoiding the formation of boranes as byproducts. Boranes add to the olefin, affording irresoluble mixtures



Scheme 2.22 NCN-Pd complex catalyzed alkene borylation reaction.

of alkyl- and alkenylboranes. Although the mechanism of this reaction was not studied in detail, it is likely that a Pd(IV) intermediate reacts with the diboron reagent, to afford a boryl complex. This intermediate undergoes a sequence alkene insertion into the Pd–B bond and β -hydrogen elimination reminiscent of the Heck reaction.

2.4

Concluding Remarks

Nickel and palladium complexes of anionic pincer ligands constitute a family of extremely effective and versatile catalysts for a number of C–C and C–X bond formation processes. Many of these processes, such as the Heck reaction or a variety of cross-coupling reactions, require the ability of the catalyst to undergo redox changes. In general, this type of compounds cannot be readily reduced without decomposition, and therefore they cannot perform through the usual M(0)/M(II) cycles. The nature of the mechanisms of these processes has been intensely debated. It is now widely assumed that, in the Heck as well as some cross-coupling reactions, the role of anionic pincer ligand complexes is limited to acting as precursors for minute amounts of metal nanoparticles or pincer ligand-free soluble species that perform as highly active catalysts, particularly in the case of Pd complexes. However, apart from imparting extreme stability to their M(II) complexes, anionic pincer ligands can also stabilize infrequent oxidation states of both nickel and palladium, which enables molecular catalysis processes taking place through unusual mechanisms. The discovery of these nonconventional catalytic routes has been fostered, to a large extent, by the impressive advance that the chemistry of

group 10 complexes has experienced in recent years. A good example of this is the discovery of oxidative addition reactions of iodonium reagents to Pt(II) or Pd(II) centers, which led to the development of conceptually new processes involving Pd(IV) intermediates, such as the Heck reaction, acetoxylation, or borination of C–H bonds. Nickel or palladium pincer complexes can also undergo reversible SET reactions, enabling M(II)/M(III) or M(II)/M(III)/M(IV) catalytic cycles that operate in various cross-coupling or radical addition reactions. Although the participation of the unusual M(I) oxidation state in processes catalyzed by Ni or Pd complexes with anionic pincer ligands is still hypothetical, the recent discovery of several M(I) derivatives of this type suggests that new processes including this oxidation state could be discovered soon. Furthermore, the role of pincer complexes may exceed the passive stabilization of the metal center as they can exhibit a *non-innocent* behavior, enabling what may appear as an apparently unusual redox behavior. Doubtless, complexes with anionic pincer ligands represent an opportunity for the design of innovative developments in catalysts, whose development we have just started to witness.

Acknowledgment

The authors wish to acknowledge the financial support from the Spanish Government, Junta de Andalucía and European Union (Projects CTQ2012-30962 and FQM6276).

References

1. Canty, A. (ed.) (2007) *Comprehensive Organometallic Chemistry III*, vol. 8, Elsevier, Oxford.
2. Oestreich, M. (ed.) (2009) *The Mizoroki-Heck Reaction*, John Wiley & Sons, Ltd, Chichester.
3. (a) Meijere, A.D. and Diedrich, F. (eds) (2004) *Metal-Catalyzed Cross-Coupling Reactions*, 2nd Completely Revised and Enlarged edn, Wiley-VCH Verlag GmbH, Weinheim; (b) Shi, W.S., Liu, C., and Lei, A. (2011) *Chem. Soc. Rev.*, **40** (5), 2761.
4. Marion, N. and Nolan, S.P. (2008) *Acc. Chem. Res.*, **41** (11), 1440.
5. Amatore, C. and Jutand, A. (2000) *Acc. Chem. Res.*, **33** (5), 314.
6. Mitsudo, T., Fischetti, W., and Heck, R.F. (1984) *J. Org. Chem.*, **49** (9), 1640.
7. (a) Herrmann, W.A., Brossmer, C., Öfele, K., Reisinger, C.P., Priermeier, T., Beller, M., and Fischer, H. (1995) *Angew. Chem., Int. Ed. Engl.*, **34** (17), 1844; (b) Beller, M., Fischer, H., Herrmann, W.A., Öfele, K., and Brossmer, C. (1995) *Angew. Chem., Int. Ed. Engl.*, **34**, 1848.
8. Herrmann, W.A., Böhm, V.P.W., and Reisinger, C.P. (1999) *J. Organomet. Chem.*, **576** (1-2), 23.
9. Beletskaya, I.P. and Cheprakov, A.V. (2000) *Chem. Rev.*, **100** (8), 3009.
10. Bedford, R.B. (2003) *Chem. Commun.*, (15), 1787.
11. Beletskaya, I.P. and Cheprakov, A.V. (2004) *J. Organomet. Chem.*, **689** (24), 4055.
12. Phan, N.T.S., Van Der Sluys, M., and Jones, C.W. (2006) *Adv. Synth. Catal.*, **348** (6), 609.
13. Ohff, M., Ohff, A., Van Der Boom, M., and Milstein, D. (1997) *J. Am. Chem. Soc.*, **119** (48), 11687.

14. Van Der Boom, M. and Milstein, D. (2003) *Chem. Rev.*, **103** (5), 1759.
15. Selander, N. and Szabó, K.J. (2011) *Chem. Rev.*, **111** (3), 2048.
16. Liang, L.-C. (2006) *Coord. Chem. Rev.*, **250** (9–10), 1152.
17. Hu, X. (2011) *Chem. Sci.*, **2** (10), 1867.
18. Wang, Z.-X. and Liu, N. (2012) *Eur. J. Inorg. Chem.*, (6), 901.
19. Herrmann, W.A., Reisinger, C.P., Öfele, K., Brossmer, C., Beller, M., and Fischer, H. (1996) *J. Mol. Catal. A.*, **108** (2), 51.
20. (a) Shaw, B.L. (1998) *New J. Chem.*, (2), 77; (b) Shaw, B.L., Perera, S.D., and Staley, E.A. (1998) *Chem. Commun.*, (13), 1361.
21. Muñiz, K. (2009) *Angew. Chem. Int. Ed.*, **48** (50), 9412.
22. Xu, L.M., Li, B.J., Yang, Z., and Shi, Z.J. (2010) *Chem. Soc. Rev.*, **39** (2), 712.
23. Louie, J. and Hartwig, J.F. (1996) *Angew. Chem., Int. Ed. Engl.*, **35** (20), 2359.
24. Böhm, V.P.W. and Herrmann, W.A. (2001) *Chem. Eur. J.*, **7** (19), 4191.
25. d'Orlyé, F. and Jutand, A. (2005) *Tetrahedron*, **61** (41), 9670.
26. van Koten, G. (1989) *Pure Appl. Chem.*, **61** (10), 1681.
27. Morales-Morales, D. and Jensen, C.M. (eds) (2007) *The Chemistry of Pincer Compounds*, Elsevier, Amsterdam.
28. Canty, A.J. (1992) *Acc. Chem. Res.*, **25** (2), 83.
29. Sehnal, P., Taylor, J.K., and Fairlamb, I.J.S. (2010) *Chem. Rev.*, **110** (2), 824.
30. Zhang, H. and Lei, A. (2011) *Dalton Trans.*, **40** (35), 8745.
31. Klein, H.F. and Kraikivskii, P. (2009) *Angew. Chem. Int. Ed.*, **48** (2), 260.
32. (a) Tsou, T.T. and Kochi, J.K. (1978) *J. Am. Chem. Soc.*, **100** (5), 1634; (b) Tsou, T.T. and Kochi, J.K. (1979) *J. Am. Chem. Soc.*, **101** (21), 6319. (c) Tsou, T.T. and Kochi, J.K. (1979) *J. Am. Chem. Soc.*, **101** (25), 7547.
33. Albrecht, M. and van Koten, G. (2001) *Angew. Chem. Int. Ed.*, **40** (20), 3750.
34. Terheijden, J., van Koten, G., De Booy, J., Ubbels, H.J.C., and Stam, C.H. (1983) *Organometallics*, **2** (12), 1882.
35. Canty, A.J., Denney, M.C., van Koten, G., Skelton, B.W., and White, A.H. (2004) *Organometallics*, **23** (23), 5432.
36. Alsters, P.L., Engel, P.F., Hogerheide, M.P., Copjin, M., Spek, A.L., and van Koten, G. (1993) *Organometallics*, **12** (5), 1831.
37. Vicente, J., Arcas, A., Juliá-Hernández, F., and Bautista, D. (2010) *Chem. Commun.*, **46** (38), 7253.
38. Vicente, J., Arcas, A., Juliá-Hernández, F., and Bautista, D. (2011) *Inorg. Chem.*, **50** (12), 5339.
39. Shabashov, D. and Daugulis, O. (2010) *J. Am. Chem. Soc.*, **132** (11), 3965.
40. Lagunas, M.C., Gossage, R.A., Spek, A.L., and van Koten, G. (1998) *Organometallics*, **17** (4), 731.
41. Pilarski, L.T., Selander, N., Böse, D., and Szabó, K.J. (2009) *Org. Lett.*, **11** (23), 5518.
42. Grove, D.M., van Koten, G., and Zoet, R. (1983) *J. Am. Chem. Soc.*, **105** (5), 1379.
43. Stol, M., Snelders, D.J.M., Godbole, M.D., Havenith, R.W.A., Haddelton, D., Clarkson, G., Lutz, M., Spek, A.L., Van Klink, G.P.M., and van Koten, G. (2007) *Organometallics*, **26** (16), 3985.
44. Grove, D.M., van Koten, G., Mul, P., Zoet, R., Van Der Linden, J.G.M., Legters, J., Schmitz, J.E., Murrall, N.W., and Welch, A.J. (1988) *Inorg. Chem.*, **27** (14), 2466.
45. Grove, D.M., van Koten, G., Mul, W., Van Der Zeijden, A.A.H., Terheijden, J., Zoutberg, M.C., and Stam, C.H. (1986) *Organometallics*, **5** (2), 322.
46. Van De Kuil, L.A., Luitjes, H., Grove, D.M., Zwikker, J.W., Van Der Linden, J.G.M., Roelofsen, A.M., Jenneskens, L.W., Drenth, W., and van Koten, G. (1994) *Organometallics*, **13** (2), 468.
47. (a) Kleij, A.W., Gossage, R.A., Klein Gebbink, R.J.M., Brinkmann, N., Reijerse, E.J., Kragl, U., Lutz, M., Spek, A.L., and van Koten, G. (2000) *J. Am. Chem. Soc.*, **122** (49), 12112; (b) Van De Kuil, L.A., Veldhizen, Y.S.J., Grove, D.M., Zwikker, J.W., Jenneskens, L.W., Drenth, W., Smeets, W.J.J., Spek, A.L., and van Koten, G. (1995) *J. Organomet. Chem.*, **488** (1–2), 191.

48. Van Beek, J.A.M., van Koten, G., Smeets, W.J.J., and Spek, A.L. (1986) *J. Am. Chem. Soc.*, **108** (16), 5010.
49. van Koten, G. (1990) *Pure Appl. Chem.*, **62** (6), 1155.
50. van Koten, G., Van Beek, J.a.M., Wehman-Ooyevaar, I.C.M., Muller, F., Stam, C.H., and Terheijden, J. (1990) *Organometallics*, **9** (4), 903.
51. Mills, A.M., Van Beek, J.A.M., van Koten, G., and Spek, A.L. (2002) *Acta Crystallogr., Sect. C.*, **58** (5), m304.
52. Pandaurus, V. and Zargarian, D. (2007) *Chem. Commun.*, **9**, 978.
53. Pandaurus, V. and Zargarian, D. (2007) *Organometallics*, **26** (17), 4321.
54. Castonguay, A., Beauchamp, A.L., and Zargarian, D. (2008) *Organometallics*, **27** (21), 5723.
55. Spasyuk, D.M., Zargarian, D., and Van Der Est, A. (2009) *Organometallics*, **28** (22), 6531.
56. Salah, A.B. and Zargarian, D. (2011) *Dalton Trans.*, **40** (35), 8977.
57. Adhikari, D., Mossin, S., Basuli, F., Huffman, J.C., Szilagyi, R.K., Meyer, K., and Mindiola, D. (2008) *J. Am. Chem. Soc.*, **130** (11), 3676.
58. Vicente, J., Arcas, A., Juliá-Hernández, F., and Bautista, D. (2011) *Angew. Chem. Int. Ed.*, **50** (30), 6896.
59. Canty, A.J., Rodemann, T., Skelton, B.W., and White, A.H. (2006) *Organometallics*, **25** (16), 3996.
60. Szabó, K.J. (2010) *J. Mol. Catal. A.*, **324** (1–2), 56.
61. (a) Portnoy, M. and Milstein, D. (1993) *Organometallics*, **12** (5), 1665; (b) Sundermann, A., Uzan, O., and Martin, J.M.L. (2001) *Chem. Eur. J.*, **7** (8), 1703.
62. Bolliger, J.L., Blacque, O., and Frech, C.M. (2008) *Chem. Eur. J.*, **14** (26), 7969.
63. Blacque, O. and Frech, C.M. (2010) *Chem. Eur. J.*, **16** (5), 1521.
64. Terheijden, J., van Koten, G., Vinke, I.C., and Spek, A.L. (1985) *J. Am. Chem. Soc.*, **107** (10), 2891.
65. Albrecht, M., Spek, A.L., and van Koten, G. (2001) *J. Am. Chem. Soc.*, **123** (30), 7233.
66. Madison, B.L., Thyme, S.B., Keene, S., and Williams, B.S. (2007) *J. Am. Chem. Soc.*, **129** (31), 9538.
67. Martínez-Prieto, L.M., Melero, C. *et al.* (2012) *Organometallics*, **31** (4), 1425.
68. Csok, Z., Vechorkin, O., Harkins, S.B., Scopelliti, R., and Hu, X. (2008) *J. Am. Chem. Soc.*, **130** (26), 8156.
69. Vechorkin, O., Csok, Z., Scopelliti, R., and Hu, X. (2009) *Chem. Eur. J.*, **15**, 3889.
70. Gómez-Benítez, V., Baldovino-Pantaleón, O., Herrera-Álvarez, C., Toscano, R.A., and Morales-Morales, D. (2006) *Tetrahedron Lett.*, **47** (29), 5059.
71. Zhang, J., Medley, C.M., Krause, J.A., and Guan, H. (2010) *Organometallics*, **29** (23), 6393.
72. Gerber, R., Blacque, O., and Frech, C.M. (2009) *ChemCatChem*, **1** (3), 393.
73. Gerber, R., Blacque, O., and Frech, C.M. (2011) *Dalton Trans.*, **40** (35), 8996.
74. Olsson, D. and Wendt, O.F. (2009) *J. Organomet. Chem.*, **694** (19), 3112.
75. Kraatz, H.B., Van Der Boom, M., Ben-David, Y., and Milstein, D. (2001) *Isr. J. Chem.*, **41** (3), 163.
76. Eberhard, E. (2004) *Org. Lett.*, **6** (13), 2125.
77. Sommer, W.J., Yu, K., Sears, J.S., Ji, Y., Zhang, X., Davis, R.J., Sherrill, D., Jones, C.W., and Weck, M. (2005) *Organometallics*, **24** (18), 4351.
78. Melero, C., Martínez-Prieto, L.M., Palma, P., Del Río, D., Álvarez, E., and Cámpora, J. (2010) *Chem. Commun.*, **46** (46), 8851.
79. Fulmer, G.R., Herndon, A.N., Kemp, R.A., and Goldberg, K.I. (2011) *J. Am. Chem. Soc.*, **133** (44), 17713.
80. Jouaiti, A., Geoffroy, M., Terron, G., and Bernardinelli, G. (1992) *J. Chem. Soc., Chem. Commun.*, (2), 155.
81. Frech, C.M., Shimon, L.J.W., and Milstein, D. (2005) *Angew. Chem. Int. Ed.*, **44** (11), 1709.
82. Schwartsburd, L., Cohen, R., Konstantinovski, L., and Milstein, D. (2008) *Angew. Chem. Int. Ed.*, **47** (19), 3603.
83. Fafard, C.M., Adhikari, D., Foxman, B.M., Mindiola, D., and Ozerov, O.V.

- (2007) *J. Am. Chem. Soc.*, **129** (34), 10318.
84. Adhikari, D., Mossin, S., Basuli, F., Dible, B.R., Chipara, M., Fan, H., Huffman, J.C., Meyer, K., and Mindiola, D. (2008) *Inorg. Chem.*, **47** (22), 10479.
 85. Ingleson, M.J., Fullmer, B.C., Buschhorn, D.T., Huffman, J.C., and Caulton, K.G. (2008) *Inorg. Chem.*, **47** (2), 407.
 86. Grüger, N., Wadepohl, H., and Gade, L. (2012) *Dalton Trans.*, **41** (46), 14028.
 87. Gossage, R.A., van de Kuil, L.A., and van Koten, G. (1998) *Acc. Chem. Res.*, **31** (7), 423.
 88. Grove, D.M., van Koten, G., and Verschuuren, A.H.M. (1988) *J. Mol. Catal.*, **45** (2), 169.
 89. Grove, D.M., Verschuuren, A.H.M., van Koten, G., and van Beek, J.A.M. (1989) *J. Organomet. Chem.*, **372** (1), C1.
 90. Granel, C., Dubois, P., Jérôme, R., and Teyssié, P. (1996) *Macromolecules*, **29** (27), 8576.
 91. Van De Kuil, L.A., Grove, D.M., Gossage, R.A., Zwikker, J.W., Jenneskens, L.W., Drenth, W., and van Koten, G. (1997) *Organometallics*, **16** (23), 4985.
 92. Miyazaki, F., Yamaguchi, K., and Shibasaki, M. (1999) *Tetrahedron Lett.*, **40** (41), 7379.
 93. Morales-Morales, D., Redón, R., Young, C., and Jensen, C.M. (2000) *Chem. Commun.*, (17), 1619.
 94. Morales-Morales, D., Grause, C., Kasaoka, K., Redón, R., Cramer, R.E., and Jensen, C.M. (2000) *Inorg. Chim. Acta*, **300–302**, 958.
 95. Sjövall, S., Wendt, O.F., and Andersson, C. (2002) *J. Chem. Soc., Dalton Trans.*, (7), 1241.
 96. Nilsson, P. and Wendt, O.F. (2007) *J. Organomet. Chem.*, **690** (18), 4197.
 97. Yu, K., Sommer, W.J., Richardson, J.M., Weck, M., and Jones, C.W. (2005) *Adv. Synth. Catal.*, **347** (1), 161.
 98. Bergbreiter, D.E., Osburn, P.L., and Liu, Y.S. (1999) *J. Am. Chem. Soc.*, **121** (41), 9531.
 99. Kiewel, K., Liu, Y., Bergbreiter, D.E., and Sulikowski, G.A. (1999) *Tetrahedron. Lett.*, **40** (51), 8945.
 100. Bergbreiter, D.E., Osburn, P.L., and Frels, J.D. (2005) *Adv. Synth. Catal.*, **347** (1), 172.
 101. da Costa, R.C., Jurisch, M., and Gladysz, J.A. (2008) *Inorg. Chim. Acta*, **361** (11), 3205.
 102. Suijkerbuijk, B.M.J.M., Herreras Martínez, S.D., van Koten, G., and Klein Gebbink, R.J.M. (2008) *Organometallics*, **27** (4), 534.
 103. Weck, M. and Jones, C.W. (2007) *Inorg. Chem.*, **46** (6), 1865.
 104. Huang, M.-H. and Liang, L.-C. (2004) *Organometallics*, **23** (11), 2813.
 105. Deux, M., Mézailles, N., Melaimi, M., Ricard, L., and Le Floch, P. (2002) *Chem. Commun.*, (15), 1566.
 106. Consorti, C.S., Ebeling, G., Flores, E.R., Rominger, F., and Dupont, J. (2004) *Adv. Synth. Catal.*, **346** (6), 617.
 107. de Vries, J.G. (2006) *Dalton Trans.*, (3), 421.
 108. de Vries, A.H.M., Mulders, J.M.C.A., Mommers, J.H.M., Hendrickx, H.J.W., and de Vries, J.G. (2003) *Org. Lett.*, **5** (18), 3285.
 109. Juliá-Hernández, F., Arcas, A., and Vicente, J. (2012) *Chem. Eur. J.*, **18** (25), 7780.
 110. Aydin, J., Larsson, J.M., Selander, N., and Szabó, K.J. (2009) *Org. Lett.*, **11** (13), 2852.
 111. Bedford, R.B., Draper, S.M., Scully, N.P., and Welch, S.L. (2000) *New J. Chem.*, **24** (10), 745.
 112. Lipke, M.C., Woloszynek, R.A., Ma, L., and Protasiewicz, J.D. (2009) *Organometallics*, **28** (1), 188.
 113. Zhang, B.-S., Wang, C., Gong, J.-F., and Song, M.-P.J. (2009) *J. Organomet. Chem.*, **694** (16), 2555.
 114. Kozolov, V.A., Aleksanyan, D.V., Nelyubina, Y.V., Lyssenko, K.A., Petrovskii, P.V., Vasil'ev, A.A., and Odinets, L. (2011) *Organometallics*, **30** (11), 2920.
 115. Olsson, D., Nilsson, P., El Massnouy, M., and Wendt, O.F. (2005) *Dalton Trans.*, (11), 1924.

116. Inés, B., San Martín, R., Moure, M.J., and Domínguez, E. (2009) *Adv. Synth. Catal.*, **351** (13), 2124.
117. Bolliger, J.L. and Frech, C.M. (2010) *Adv. Synth. Catal.*, **352** (6), 1075.
118. Bolliger, J.L. and Frech, C.M. (2009) *Adv. Synth. Catal.*, **351** (6), 891.
119. Takemoto, T., Iwasa, S., Hamada, H., Shibatomi, K., Kameyama, M., Motoyama, Y., and Nishiyama, H. (2007) *Tetrahedron Lett.*, **48** (19), 3397.
120. Zhang, B.-S., Wang, D.-D., Liu, J.-R., Wang, K.-L., Gong, J.-F., and Song, M.-P. (2010) *Organometallics*, **29** (11), 2579.
121. Xu, G., Li, X., and Sun, H. (2011) *J. Organomet. Chem.*, **696** (18), 3011.
122. Estudiante-Negrete, F., Hernández-Ortega, S., and Morales-Morales, D. (2012) *Inorg. Chim. Acta*, **387**, 58.
123. Sanford, J., Dent, C., Masuda, J.D., and Xia, A. (2011) *Polyhedron*, **30** (6), 1091.
124. Liang, L.-C., Chien, P.-S., Ling, J.-M., Huang, M.-H., Huang, Y.-L., and Liao, J.-H. (2006) *Organometallics*, **25** (6), 1399.
125. Liang, L.-C., Lee, W.-Y., Hung, Y.-T., Hsiao, Y.-C., Cheng, L.-C., and Chen, W.-C. (2012) *Dalton Trans.*, **41** (4), 1381.
126. Wang, Z.-X. and Wang, L. (2007) *Chem. Commun.*, (23), 2423.
127. Sun, K. and Wang, Z.-X. (2008) *Organometallics*, **27** (21), 5649.
128. Vechorkin, O. and Hu, X. (2009) *Angew. Chem. Int. Ed.*, **48** (16), 2937.
129. Pérez-García, P.M., Di Franco, T., Orsino, A., Ren, P., and Hu, X. (2012) *Org. Lett.*, **14** (16), 4286.
130. Vechorkin, O., Proust, V., and Hu, X. (2009) *J. Am. Chem. Soc.*, **131** (28), 9756.
131. Vechorkin, O., Godinat, A., and Hu, X. (2011) *Angew. Chem. Int. Ed.*, **50** (49), 11777.
132. Cotter, W.D., Barbour, L., Mcnamara, K.L., Hetcher, R., and Lachicotte, R.J. (1998) *J. Am. Chem. Soc.*, **120** (42), 11016.
133. Liang, L.C., Chien, P.S., and Lee, P.Y. (2008) *Organometallics*, **27** (13), 3082.
134. Breitenfeld, J., Vechorkin, O., Corminboeuf, C., Scopelliti, R., and Hu, X. (2010) *Organometallics*, **29** (17), 3686.
135. Wang, H., Liu, J., Deng, Y., Min, T., Yu, G., Wu, X., Yang, Z., and Lei, A. (2009) *Chem. Eur. J.*, **15** (6), 1499.
136. Solin, N., Kjellgren, J., and Szabó, K.J. (2004) *J. Am. Chem. Soc.*, **126** (22), 7026.
137. Jones, G.D., McFarland, C., Anderson, T.J., and Vivic, D.A. (2005) *Chem. Commun.*, (33), 4211.
138. Anderson, T.J., Jones, G.D., and Vivic, D.A. (2004) *J. Am. Chem. Soc.*, **126** (26), 8100.
139. Jones, G.D., Martín, J.L., Mcfarland, C., Allen, O.R., Hall, E.R., Haley, A.D., Brandon, R.J., Konovalova, T., Desrochers, P.J., Pulay, P., and Vivic, D.A. (2006) *J. Am. Chem. Soc.*, **128** (40), 13175.
140. (a) Phapale, V.B., Buñuel, E., García-Iglesias, M., and Cárdenas, D.J. (2007) *Angew. Chem. Int. Ed.*, **46** (46), 8790; (b) Phapale, V.B. and Cárdenas, D.J. (2009) *Chem. Soc. Rev.*, **38** (6), 1598.
141. (a) Van Der Vlugt, J.I. and Reek, J.N.H. (2009) *Angew. Chem. Int. Ed.*, **48** (47), 8832; (b) Blanchard, S., Derat, E., Desage-El Murr, M., Fensterbank, L., Malacria, M., and Mouriés-Masnuy, V. (2012) *Eur. J. Inorg. Chem.*, (3), 376.
142. Kjellgren, J., Sundén, H., and Szabó, K.J. (2005) *J. Am. Chem. Soc.*, **127** (6), 1787.
143. Breitenfeld, J., Scopelliti, R., and Hu, X. (2012) *Organometallics*, **31** (6), 2128.
144. Liu, J., Lin, C., and Lei, A. (2012) *Chem. Sci.*, **3** (4), 1211.
145. Selander, N., Willy, B., and Szabó, K.J. (2010) *Angew. Chem. Int. Ed.*, **49** (24), 4051.

3

Appended Functionality in Pincer Ligands

Cameron M. Moore and Nathaniel K. Szymczak

3.1

Introduction

As highlighted throughout this book, pincer-based metal complexes are capable of promoting remarkable reactivity toward small molecule substrates, and the utility of undecorated variants of this ligand framework should be apparent. To engage further substrate activation pathways, multifunctionality can be introduced within the secondary coordination sphere environment of a pincer-derived ligand. Secondary interactions are ubiquitous in biological systems and are responsible for promoting enhanced reactivity in many metalloenzymes, where a combination of hydrogen-bonding, steric, and electrostatic interactions are used synergistically to augment reactivity profiles [1, 2]. To emulate these principles, a growing number of synthetic complexes have targeted multifunctional ligand ensembles to directly probe how changes within a molecule's secondary coordination sphere can be used to influence and further modulate subsequent reactivity [3]. In addition to enhanced substrate activation, secondary coordination sphere interactions in synthetic systems have been utilized for the ground-state stabilization of otherwise unstable or reactive intermediates, and the combination of both of these strategies can be exploited for small molecule transformations [4].

In this chapter, we aim to introduce the reader to the motivations and strategies for appending cooperative functional groups (loosely termed *functionality* throughout this chapter) onto pincer-based ligand platforms, which are poised to cooperatively interact with a metal-coordinated substrate. Throughout this chapter, we highlight specific examples of rational ligand design that lead to measurable changes in chemical bonding and reactivity. The emphasis of our discussion will be on approaches to achieve directed interactions with metal-bound substrates and the ramifications on reactivity to which these interactions lead. A brief description of our nomenclature and overarching motivations for appending functionality, however, will first be discussed.

3.1.1

Design Criteria

The title of this chapter merits the question, “what defines *functionality*”? For the purposes of this discussion, we have limited our definition of *functionality* to a group, or groups, of polarizable units with an orientation suitable for cooperative substrate-directed interactions. In most cases, directed interactions should be considered to be toward a metal-bound substrate, but in some instances (i.e., supramolecular self-assemblies and sensors) metal ions may be absent from our discussion.

Pincer ligand frameworks are ideally suited for “decoration,” since these often rigid and redox-robust scaffolds preclude unproductive interaction of appended polar functional groups with the transition-metal center. Two limiting distinctions regarding the position of functionality relative to the plane defined by the donor atoms of the pincer framework can be made: functionality coplanar to the pincer chelate (Figure 3.1a), and functionality not coplanar to the pincer chelate (Figure 3.1b). In some cases, these distinctions may become less straightforward, especially in the case of trigonal-bipyramidal coordination geometry, and these aspects will be treated in more detail where necessary.

3.1.2

Motivations

In contrast to unmodified pincer ligands, comparatively few examples of pincer ligand frameworks appended with polar functionality have been reported. The overarching goals associated with such modifications are diverse and span the fields of catalysis, supramolecular assembly, and molecular recognition.

3.1.2.1 **Transition-Metal Catalysis**

Metal complexes featuring directed secondary coordination sphere interactions are highly topical for complexes containing bidentate [5], tripodal [4], or phosphine ligands [6], which can cooperatively promote a variety of catalytic transformations and/or stabilize highly reactive intermediate species. In contrast, only limited examples of catalysis involving pincer-ligated adducts that contain an appended functionality have been reported. One of the premier examples of cooperative catalysis that utilizes a pincer-derived framework for substrate-directed oxidation is the dimanganese complex **1** reported by Crabtree and Brudvig [7] (Figure 3.2).

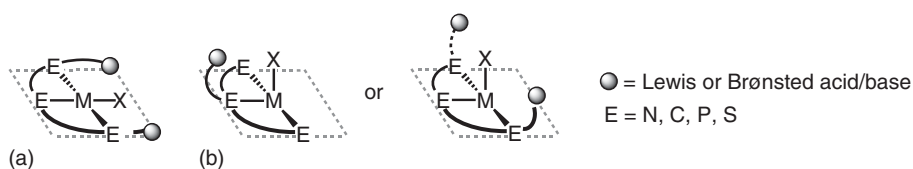


Figure 3.1 Representation of functionality coplanar (a) and not coplanar (b) to the pincer chelate.

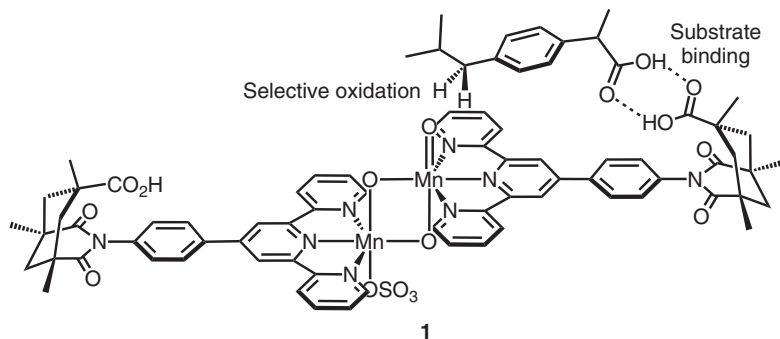


Figure 3.2 Selective C–H oxidation by a Mn-terpy complex featuring a remote molecular recognition site. (Reproduced from Ref. [8] with permission of The Royal Society of Chemistry.)

The design strategy of **1** features an oxidatively stable terpyridine ligand appended with a remote molecular recognition site (Kemp's triacid fragment) capable of binding a substrate such as ibuprofen, through hydrogen-bonding interactions, thus directing selective C–H oxygenation.

Oxygenation of ibuprofen using **1** as a catalyst and peroxomonosulfate as an oxidant provided >98% regioselectivity at the remote benzylic carbon with up to 700 turnovers. The substrate recognition is achieved through two hydrogen bonds between carboxylic acids of the substrate and the catalyst (Figure 3.2), which is preserved throughout the C–H oxidation reaction [8]. In support of a cooperative binding event that precedes substrate oxidation, the addition of exogenous carboxylic acids competitively inhibits the regioselectivity of ibuprofen oxygenation [9]. Furthermore, when the pendent carboxylic acid groups are removed from the terpyridine scaffold, the regioselectivity for oxygenation is diminished. This example highlights the potential of using secondary interactions to direct reactivity.

3.1.2.2 Supramolecular Architectures

Several elegant examples of appended pincer frameworks can be found in the field of supramolecular chemistry, where tridentate ligands have been used to design functional three-dimensional architectures, both in the presence and absence of metal ions [10, 11]. The ability to predict structural conformations a priori remains a key challenge within this field [12]. One strategy to overcome the apparent lack of predictability of self-assembly is to utilize noncovalent interactions to “guide” assembly into a predicted structure. For example, complementary hydrogen-bonding interactions between two molecules of a highly decorated terpyridine-derived framework generate **2**, a columnar helical scaffold in the solid state (Figure 3.3a). The appended NH₂ functionality engages in intermolecular hydrogen-bonding interactions with the pyridine groups of another molecule, and the fixed orientation of the three pyridine rings within each ligand serves to propagate a helical structure. Further utility of this system may be limited by its synthesis (eight steps, 5% overall yield) [13]. Complex architectures featuring pincer-type compounds have also been utilized as dynamic chemical devices which can respond to external

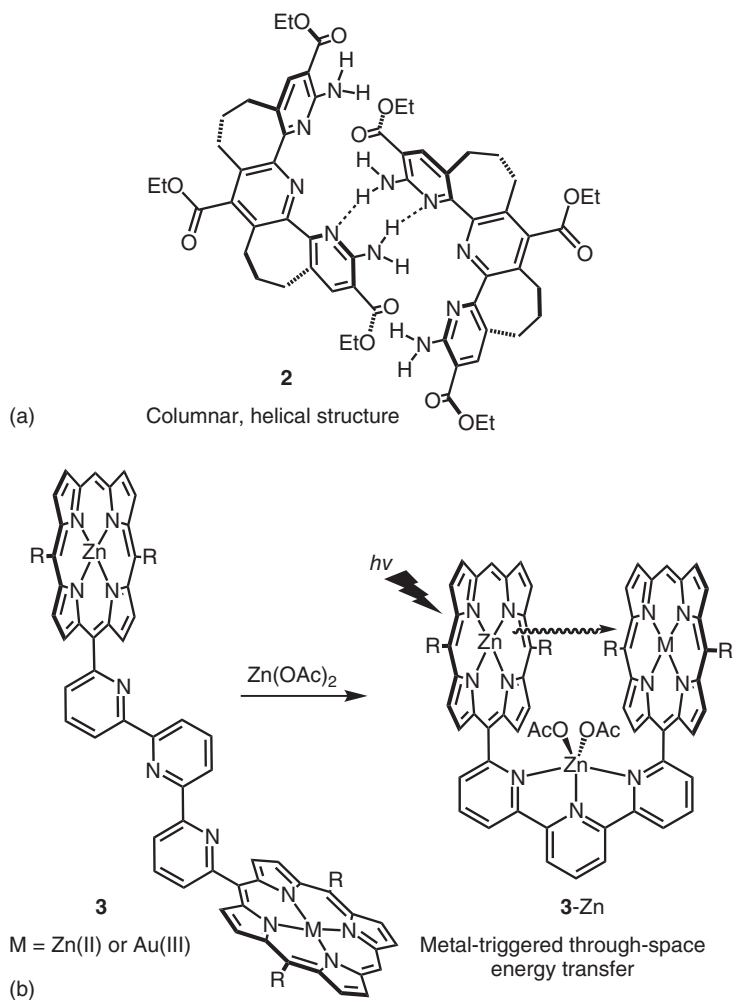


Figure 3.3 Self-complementary hydrogen bonding to yield a helical structure (a) and “butterfly-type” motion of a bis(porphyrin)terpyridine complex to give a species capable of through-space energy transfer (b).

stimuli, reminiscent of biological systems that undergo molecular-level changes to induce reactive states [14, 15]. Lehn and coworkers have designed a sophisticated porphyrin-functionalized terpyridine-based ligand to study metallation-triggered geometry changes (**3**, Figure 3.3b) [10]. In addition to conformation modulation mediated by ligand-binding events, efficient through-space energy transfer between the two porphyrin substituents was achieved when a metal ion was coordinated to the terpyridine chelate (**3-Zn**). The coordination of a metal ion at the terpyridine induces a change in geometry and orients the two porphyrin groups within close proximity to one another (Figure 3.3b).

The highly complex systems presented by supramolecular architectures demonstrate the ability to control individual components within a larger molecular ensemble. The functions of these supramolecular motifs often mirror the functions found in biological enzymes, that is, the unique ability to bind and orient molecules (or substrates) in a specific manner to achieve a more reactive state. These concepts parallel the efforts of organometallic chemists to perform selective reactions on challenging substrates. Incorporating design elements found in supramolecular chemistry enables the possibility to confer enzymatic-type function, such as specificity and high reaction rates, to synthetic systems [16]. Crabtree and Brudvig's dimanganese system exemplifies these principles upon which further systems may find inspiration. Our following discussions will focus on pincer systems where the functionality has been installed adjacent to the metal binding site, as opposed to remote sites, and the associated directed interactions that these functional groups provide to metal-bound substrates.

3.2

Appended Functionality Coplanar with the Pincer Chelate

3.2.1

Systems that Incorporate 2,2':6',2''-Terpyridine

Pincer-based ligands that incorporate the 2,2':6',2''-terpyridine (terpy) unit are attractive platforms upon which a diverse array of functional groups can be appended. Transition-metal complexes supported by terpy and terpy-based ligands have been used in a wide array of applications, including sensitizers for solar cells [17] and as catalysts for water oxidation [18, 19], cross-coupling reactions [20], hydrosilylation of alkenes [21, 22], and transfer hydrogenation [23–25]. In addition to the high rigidity of the terpy scaffold, which serves to lock appended groups in place (limiting intramolecular chelation and inhibiting undesired structural reorganization), the ability to exploit highly modular synthetic routes (early stage or late-stage ring assembly) contributes to the versatility of this ligand class.

3.2.1.1 Synthetic Strategies

The preparation of substituted terpyridine frameworks is well documented. Typical substitution patterns focus on functionalization at the 4'-positions [26, 27]. Here, we will focus on preparations of terpyridines specifically modified at the 6- and 6'-positions, because substituents at these positions are positionally disposed to interact with metal-bound substrates. For clarity, this section will be limited to discussions of two common strategies for the synthesis of appended terpyridine ligands, namely early and late-stage ring assembly approaches.

Early Stage Ring Assembly A highly useful synthon for the further modification of the terpyridine framework is 6,6''-dibromo-2,2':6',2''-terpyridine, which is commercially available. Standard cross-coupling methodologies can be readily employed

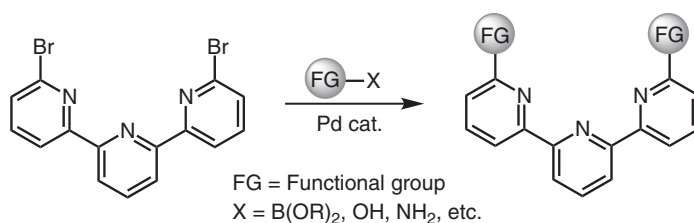


Figure 3.4 Cross-coupling approach to functionalize 6,6'-dibromoterpyridine.

with this substrate to introduce the desired functionality within a symmetric terpy ligand (Figure 3.4), and this approach has been utilized to synthesize terpy scaffolds for a wide variety of applications [25, 28–30].

Another class of useful terpy synthons are carbonitrile-substituted terpyridines. Incorporation of a carbonitrile group at the 6- and 6'-positions of terpy can be achieved from the pyridine di-*N*-oxide, using a modified Reissert–Henze reaction with Me₃Si(CN) and an acyl-chloride to provide the 6,6'-di(carbonitrile)terpyridine (**4**) [31, 32].

Further elaboration of **4** can be accomplished to install assorted functional groups of relevance for proton-transfer relays (Figure 3.5). For example, hydrolysis provides the dicarboxylic acid-appended terpy **5** [32], reduction with borane and hydrolysis yields the aminomethyl-terpy **6** [33], addition of azide provides the tetrazole-substituted terpy **7** [32], and treatment with hydrazine yields **8** [34]. Compounds **5–7** have been utilized as ligands for studying luminescence in lanthanide complexes [32, 33], but to our knowledge, have not yet been described in the catalysis literature.

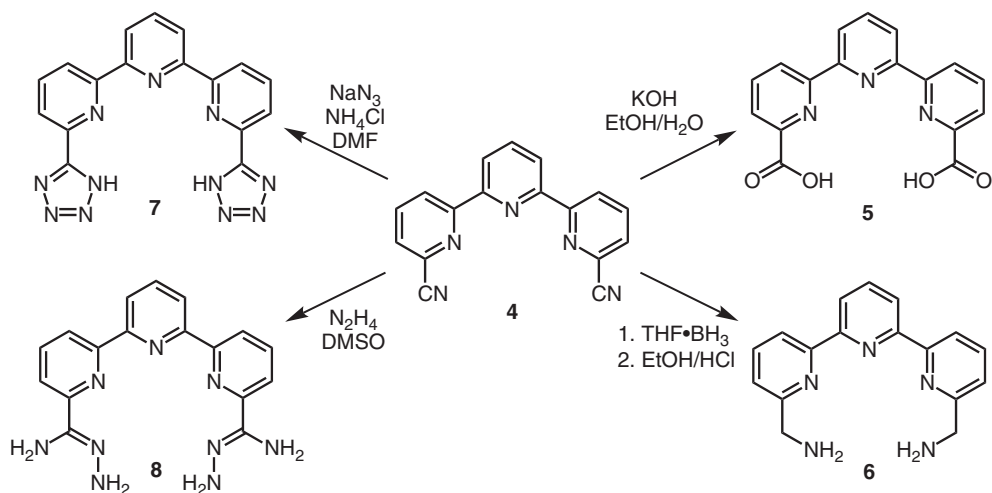


Figure 3.5 Utility of carbonitrile-terpyridines for functionalization.

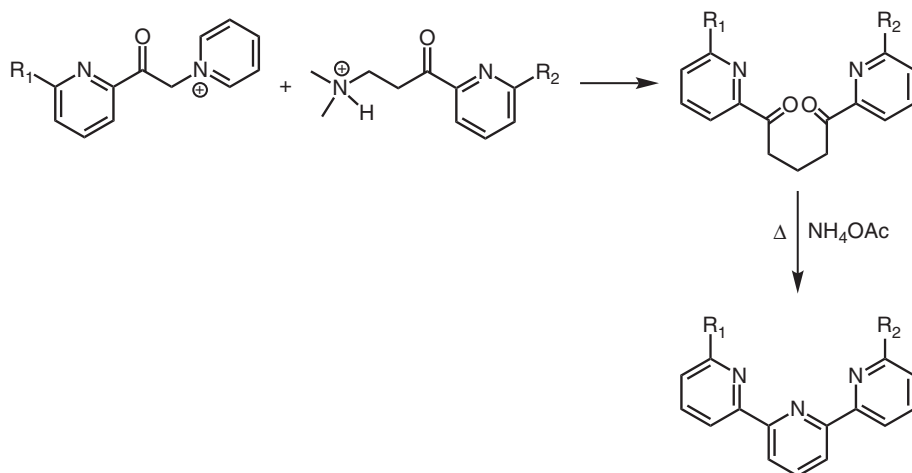


Figure 3.6 Kröhnke method for the synthesis of functionalized terpyridines.

Late-Stage Ring Assembly When an asymmetric terpy scaffold is desired, selective functionalization of a single Ar–X bond in terpy is difficult to achieve using cross-coupling and/or nucleophilic aromatic substitution, and late-stage ring assembly is particularly useful. This approach typically relies on the Kröhnke method (or variations thereof), which is a robust methodology and involves the construction of the central pyridine by aza-ring closure of a 1,5-diketone intermediate, generated following the condensation of pyridinium and ammonium salts (Figure 3.6) [35].

3.2.1.2 Appended Lewis Acid/Bases

We recently initiated efforts within our own laboratory to synthesize terpy-based ligands that incorporate appended Lewis acid/base pairs [36]. Motivated by metal-free systems of “frustrated Lewis pairs” (FLPs) which bind and form adducts with small molecules, we sought to couple the reactivity of FLPs to a transition-metal fragment to afford a metal Lewis acid/base triad (LABT). The combination of both partners with a transition-metal center opens up the possibility to synergistically use these systems for further activation and/or redox transformations – currently a limitation of metal-free FLP systems.

This concept is illustrated in Figure 3.7, where interaction of a hypothetical molecule “A=B” with the metal and FLP fragments in the secondary coordination sphere facilitates polarization of the A–B bond. Further weakening of the A–B bond may be promoted by interaction of a filled d orbital on the metal into anti-bonding orbitals of the A–B bond. Coupling these interactions with the ability of a redox-active metal center to promote proton and electron transfer events could lead to the release of the reduced A–B species. We are targeting this strategy to promote atypical reductive reactivity of typically inert substrates. To test these hypotheses, we have synthesized ligand architectures based on the terpyridine framework. Our first-generation design features a boronic ester and a morpholine group, as weakly

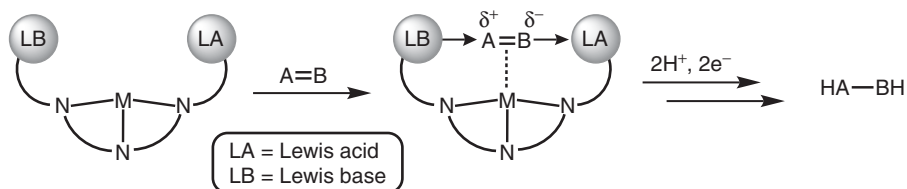


Figure 3.7 Hypothetical reduction of a substrate “A=B” using Lewis pairs in the secondary coordination sphere.

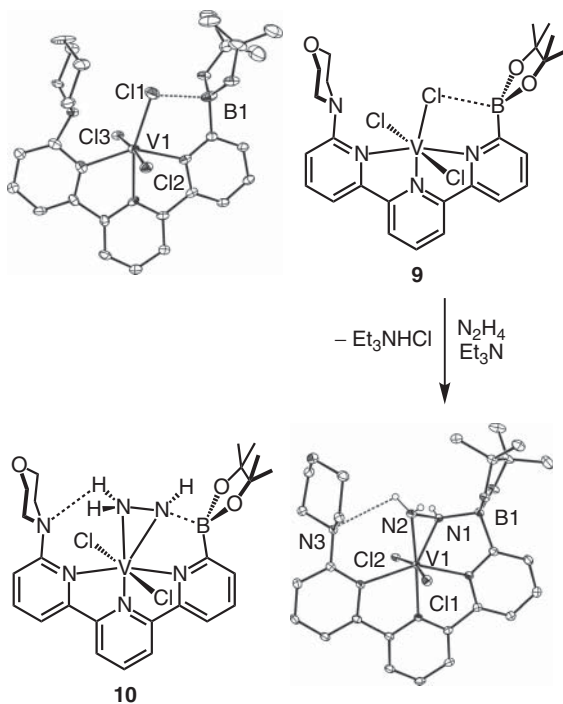


Figure 3.8 Reactivity of a vanadium complex featuring Lewis pairs in the secondary coordination sphere along with the solid-state structures of **9** (left) and **10** (right) [36].

Lewis acidic/basic partners appended to the terpy scaffold (Figure 3.8), synthesized by a late-stage ring assembly.

The ability of the appended functional groups to interact with a metal-bound substrate was confirmed by the interrogation of the associated V(III) adducts [36]. The structure of the VCl_3 adduct (**9**) contains an axial chloride ligand distorted toward the boronic ester group. The B1–Cl1 distance is consistent with a weak B–Cl interaction, and is further supported by the low degree of pyramidalization at boron ($\Sigma\text{B}_\alpha = 349.8(12)^\circ$). The appended functionality was confirmed as the major driver for these distortions: when the Lewis acid and base groups were replaced by CH_3 units, the axial chloride ligand was roughly equidistant from

both appended methyl groups. To synergistically engage both appended Lewis partners, hydrazine adducts were targeted, and a highly unusual complex (**10**) was obtained that featured deprotonated hydrazine in an unprecedented side-on coordination, stabilized by Lewis acid/base and hydrogen-bonding interactions. The N1–B1 separation is consistent with an elongated single bond, while the N3–H2 and N3–N2 separations are indicative of hydrogen bonding. This complex also mediates N₂-centered redox reactivity, and in the presence of CoCp*₂ and collidinium hydrochloride as a reductant and proton donor, respectively, ammonia was confirmed as a reduction product. The side-on binding mode and N–N bond scission reaction is of potential relevance to the N₂-fixation cycles since hydrazine is a known byproduct of N₂ reduction to ammonia by V-nitrogenase [37]. Future work on this scaffold will target redox transformations of other small molecule substrates amenable to reductive activation, for instance, CO₂, N₂, and CO, and seek to elucidate the intimate role of each Lewis partner to effect substrate activation.

3.2.1.3 Appended Hydrogen-Bond Acceptor/Donors

Complementary to Lewis acidic/basic groups, Brønsted acid/bases have also been incorporated within the secondary coordination sphere of pincer frameworks [38–40]. Incorporation of a Brønsted acid/base functionality may be pursued to provide sites for proton transfer to/from metal coordinated substrates and/or to modify electronic properties of a metal–ligand complex. Commonly, such architectures are designed with the intent of ground-state stabilization of coordinated substrates, such as metal-coordinated water or hydroxo molecules [41–43]. Recent reviews have detailed the effects of hydrogen bonding on metal–aquo ligands, especially within the context of hydrolysis reactivity [44, 45]. A particularly noteworthy example of a terpy-like framework appended with Brønsted acid/base functionality was reported by Anslyn and coworkers [46], who appended guanidinium groups to interact with metal-coordinated substrates. The zinc(II) complexes **11** and **12** (Figure 3.9) were examined for their reactivity in the stoichiometric hydrolysis of adenylyl (3'→5') phosphoadenine (ApA). The enhancement in ester hydrolysis from the secondary coordination sphere interactions was confirmed by comparison

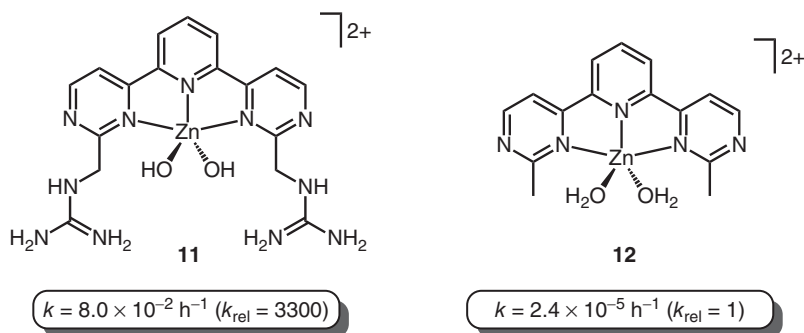


Figure 3.9 Zinc(II) complexes reported by Anslyn and coworkers and their rate constants for the hydrolysis of ApA at pH 7.4 [46].

with an analogous ligand structure that replaces the guanidinium units with functionally inert CH_3 groups (the rate of hydrolysis of ApA by **11** was about 3300 times greater than that of **12**).

Hydrolysis reactions measured as a function of pH of ApA by **11** established an optimal rate at a pH of 7.4, consistent with a zinc-bound hydroxo ($\text{p}K_a$ independently measured as 7.3 in **11**) as the active species in the hydrolysis reaction. Although the $\text{p}K_a$ of the zinc-bound aquo ligands in **12** was not determined, the guanidinium groups of **11** are thought to increase the rate of hydrolysis by (i) using noncovalent interactions to (a) acidify the zinc-bound aquo ligand and (b) bind and orient the phosphate groups during hydrolysis and/or (ii) acting as a general acid/base to facilitate proton transfer during hydrolysis. The impressive rate enhancement of ApA hydrolysis by appending guanidinium groups in the secondary coordination sphere demonstrates the effectiveness of this approach.

Appended functionality was also investigated as a means to mediate further transformations of a metal-coordinated aquo ligand. For instance, one of the first mononuclear ruthenium complexes reported for water oxidation was complex **13** by Zong and Thummel [47] (Figure 3.10). The ligand was prepared from a Friedländer condensation with 2-aminonicotinaldehyde and the corresponding 2,6-diacetylpyridine. Of particular note with regard to this chapter is that only the aquo complex (in contrast to the chloro) was produced under the reaction conditions from $\text{RuCl}_3 \cdot 3\text{H}_2\text{O}$.

The axial water ligand was shown to participate in hydrogen-bonding interactions with the nearby naphthyridine nitrogen atoms, which likely affords increased stabilization compared to a chloro ligand, which cannot engage in similar secondary-sphere interactions. The role, if any, of the hydrogen-bonding interactions to promote water oxidation is not well resolved, and recent reports demonstrate similar activity for water oxidation using several alternative mononuclear polypyridine complexes without additional assistance from the secondary coordination sphere [48].

We recently initiated studies using transition-metal complexes supported by the 6,6'-dihydroxyterpyridine (dhtp) ligand (**14**, Figure 3.11). This ligand is distinct from other terpy-based ligands described in this chapter because, in addition to presenting proton donors and acceptors that can interact with a metal-coordinated

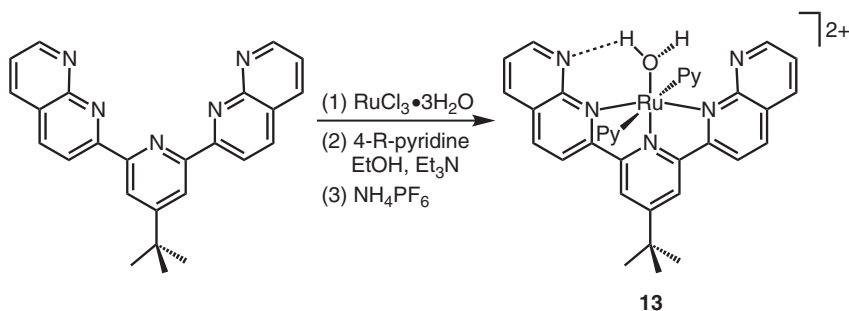


Figure 3.10 Mononuclear ruthenium(II) water oxidation catalysts reported by Thummel and coworkers.

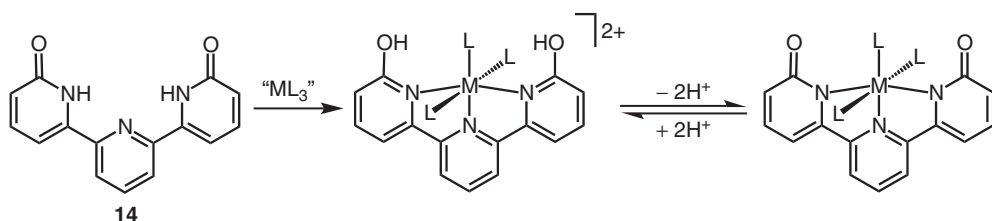


Figure 3.11 Proton-responsive ligand field of a hypothetical M-dhtp complex.

substrate, disparate ligand fields can be concomitantly conferred to a transition metal via two stable tautomeric forms. In biological systems, the 2-hydroxypyridine motif can be found in the Fe–S cluster-free hydrogenase metalloenzymes, which exploit the H_2 heterolytic cleavage reaction for substrate reduction [49]. Although the discrete mechanism by which H_2 is activated/utilized is currently an unresolved matter, the tautomeric duo 2-hydroxypyridine and 2-pyridone may participate to facilitate H_2 cleavage and transfer [49, 50].

The more stable “dione” tautomer (**14**) of the free ligand is favored in solution and the solid state. However, tautomerization can be induced upon metallation to afford the neutral “dihydroxy” tautomer. When coordinated to a metal fragment, this tautomerism provides a modifiable ligand field depending on the protonation state of the dhtp ligand. The neutral dihydroxy tautomer serving as an L_3 -type ligand and the dianionic dione tautomer providing an LX_2 -type coordination (Figure 3.11).

One consideration that must be taken into account when preparing transition-metal complexes of pincer ligands with appended polar functional groups is the formation of dimers and higher order oligomers. Polar functional groups serve as reasonable ligands themselves and, although rigid pincer frameworks provide a means to preclude interactions from these groups with a transition-metal ion in an *intramolecular* manner, *intermolecular* interactions can prove difficult to avoid. Subtle changes in metallation conditions can provide a means to control the formation of unwanted products, and an alternative and more robust strategy to avoid these complications is to include steric bulk around the polar functionality. As an example of the former strategy, reaction of dhtp with $RuCl_2(PPh_3)_3$ in the presence of sodium hydroxide provides **15**, as established by NMR spectroscopy and X-ray diffraction (Figure 3.12). The dimer is held together with hydrogen-bonding interactions of the bridging aquo-ligand and coordination of one pyridone oxygen to an adjacent ruthenium center. This bridging arrangement is kinetically inert and resists dissociation even under forcing conditions (Moore, C.M. and Szymczak, N.K. unpublished results).

In contrast, in the absence of a base, and through the use of a more polar solvent, reaction of dhtp with $RuCl_2(PPh_3)_3$ produces a monomeric species (**16**, Figure 3.12). Under the aforementioned conditions, the dhtp ligand tautomerizes upon metallation to afford a neutral terpy scaffold with appended hydroxyl groups. Notably, the solid-state structure of **16** displays hydrogen-bonding interactions

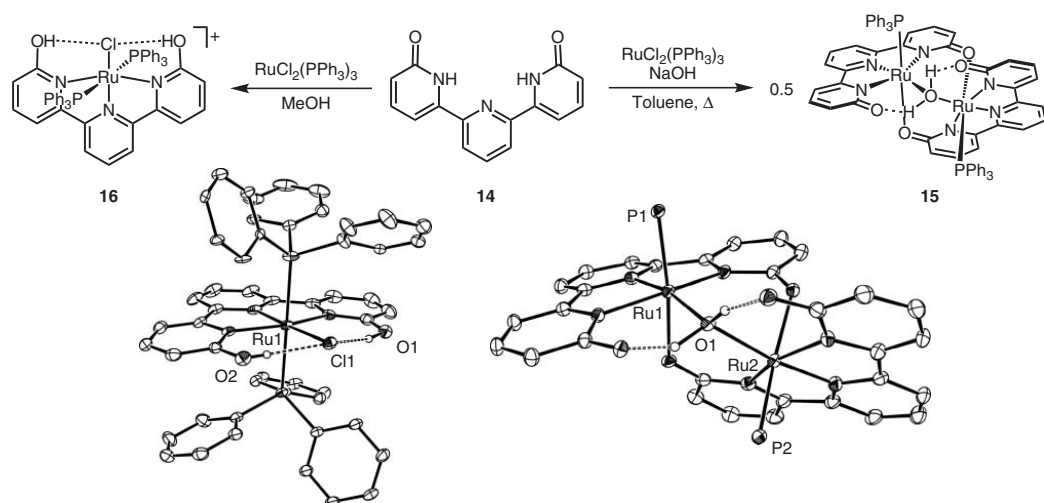


Figure 3.12 Synthesis and structures of monomeric and dimeric ruthenium complexes supported by the dhtp ligand (carbon atoms on the PPh_3 ligands of 15 have been omitted for clarity) [25].

between the hydroxyl groups of dhtp and the Ru-bound chloride ligand. The coplanarity of the metal-coordinated substrate and the appended O/OH groups suggests that minimal structural reorganizational is required for a proton-transfer event. To confirm the design strategy, catalysis involving proton transfer was targeted, and Ru-dhtp complexes were found to mediate ionic hydrogenation reactions. The complex, Ru(dhtp)(PPh₃)₂Cl (**16**) efficiently catalyzes the transfer hydrogenation of a variety of ketones, using 2-propanol as an H₂ surrogate [25]. High chemoselectivity was realized in the presence of substituted alkenes, and selective reduction of carbonyl groups was achieved in the presence of nonpolar olefins, consistent with an ionic-type hydrogenation pathway. These findings are consistent with an outer-sphere hydrogenation pathway where hydride/proton delivery is achieved through the transfer from the Ru-hydride and 2-hydroxypyridine motif, respectively, and experiments are ongoing in our laboratory to confirm this hypothesis.

Similar to dhtp pincer ligands, terpyridine ligands containing amine groups at the 6- and 6'-positions provide a complementary platform that contains hydrogen-bonding functionality with a decreased propensity for tautomerization [51]. Interestingly, the platinum(II)-methyl complex containing this terpy pincer ligand (**17**, Figure 3.13) can insert O₂ into the Pt–C bond and form a platinum(II)-methylperoxy species (**18**), which releases formaldehyde to afford a platinum(II)-hydroxo complex (**19**). A key intermediate in this transformation was identified. The amino groups of the terpyridine ligand participate in hydrogen-bonding interactions with the proximal oxygen atom of the methylperoxy unit. These interactions can be visualized in the solid state by X-ray crystallography, and were also demonstrated to persist in solution using NMR experiments.

The O₂ insertion reaction is light-dependent: the reaction proceeds to completion within minutes under ambient light, but only 50% conversion is obtained after prolonged reactions times in the absence of light. When the analogous unsubstituted terpyridine complex ([Pt(terpy)Me][SbF₆], **20**) is subjected to similar reaction conditions, no O₂ insertion products are observed. This finding is rationalized by examination of the electronic absorption spectra and photophysical properties of **17** and the terpyridine analog **20**. While the terpyridine analog **20** is not photoluminescent at room temperature, the substituted terpyridine complex **17**

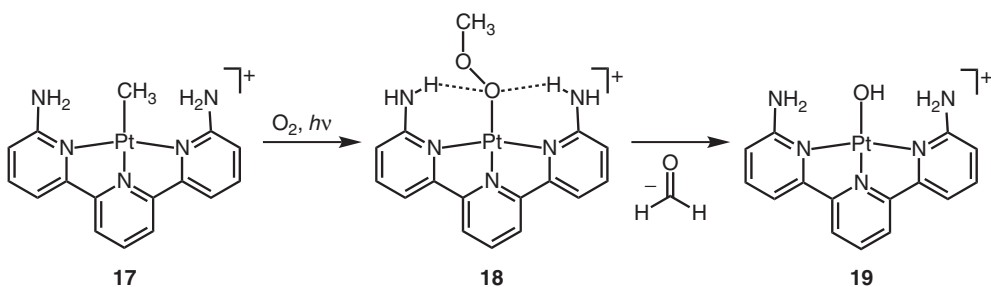


Figure 3.13 Insertion of O₂ into a Pt–CH₃ bond to produce a peroxo-species stabilized by hydrogen bonding. Decomposition results in the ultimate formation of a Pt–OH species.

exhibits photoluminescence under similar conditions. Additionally, the extinction coefficient for the metal-to-ligand charge-transfer band in the electronic absorption spectrum of **17** (~400 nm) is an order of magnitude greater than that of the parent complex **20**. These findings led Britovsek and coworkers to suggest that the observed reactivity of **17** is due to its ability to act as a photosensitizer for $^3\text{O}_2$ to afford $^1\text{O}_2$, the latter of which can insert into the Pt–Me bond. An important, and not unexpected, conclusion that can be drawn from this study is that the introduction of the functionality within pincer-derived ligands can modify not only the secondary coordination sphere properties but also photophysical properties of resulting complexes [52]. As such, the enhanced reactivity of **17** over **20** can be attributed to the synergistic ability to photosensitize O_2 concomitant with the ground-state stabilization of the Pt-methylperoxo unit through hydrogen-bonding interactions.

3.2.2

Pyridine-2,6-Dicarboxamide Systems

Pyridine-2,6-dicarboxamide ligands are a versatile class of pincer ligands [53] that present a dianionic ligand field upon metal coordination and can be appended with a wide range of substituents around the flanking amide donor units. Limited monomeric transition-metal complexes supported by pyridine-carboxamide ligands with appended functionality have been structurally characterized. This is in large part due to the propensity of these ligands to form multinuclear species (see below). Steric protection can inhibit higher nuclearity structures, but strategies to place these groups typically increase the synthetic complexity, and is likely a reason that so few monomeric pincer complexes exist in this class that feature appended functionality.

To enforce a monomeric complex of a pyridine-carboxamide ligand decorated with pyridine bases (**21**, Figure 3.14), methyl groups at the 6-positions of the pyridine groups were effectively used to sterically block intermolecular association [54]. The utility of the appended functionality within this system was highlighted within the context of Ru-mediated nitrite conversion to nitrosyl. Reaction of **21** with $\text{RuCl}_2(\text{PPh}_3)_3$ produces a ruthenium pincer adduct (**22**), where intramolecular proton transfer afforded the pendent pyridinium groups. The solid-state structure of **22** reveals that these pyridinium groups participate in hydrogen-bonding interactions with the ruthenium-bound chloride ligand. These secondary interactions were targeted to promote further reactivity of small molecules; for instance, the addition of nitrite furnished the ruthenium-nitrosyl complex **23**, presumably via a hydrogen-bonded intermediate. A traditional route to ruthenium-nitrosyls involves the reaction of ruthenium-nitrite complexes with an exogenous acid. In this case, the pyridinium units likely serve as internal acids to promote the conversion of nitrite to nitrosyl. The relative ease of the synthesis of **21** (one step) along with the potential to promote intramolecular proton transfer events in the secondary coordination sphere makes future catalytic studies with this architecture intriguing.

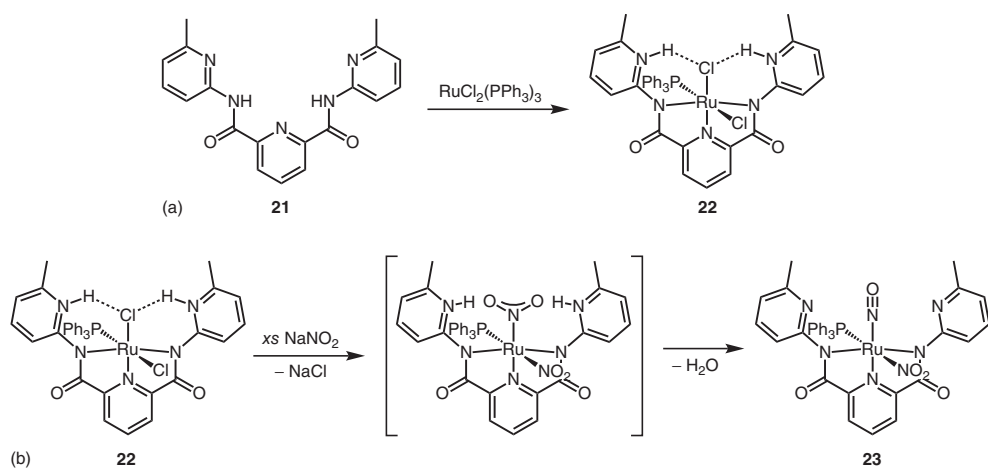


Figure 3.14 Metallation of Wright's pyridine-2,6-dicarboxamide ligand appended with pyridine groups (a) and formation of a ruthenium nitrosyl via proton transfer and water elimination (b).

3.3

Appended Functionality Not Coplanar to the Pincer Chelate

3.3.1

ENE Pincer Systems

ENE pincer systems ($E = \text{NR}_2$ or PR_2) containing a central pyridine ring have become prominent catalysts for numerous “hydrogen-borrowing” reactions. These systems exploit aromatization/dearomatization of the central pyridine for metal–ligand bifunctionality, and examples that incorporate appended functionality have recently appeared [55, 56]. A remarkable mode of C–C bond formation was recently reported via nucleophilic attack of a deprotonated methylene side arm on an electrophile such as CO_2 , accompanied by concomitant aromatization of the central pyridine [57, 58]. This mode of action was independently reported by two groups. Milstein and coworkers [59] disclosed this reaction as an equilibrium process when using a symmetric pincer ligand (**24**, $E = E' = \text{P}^t\text{Bu}_2$, Figure 3.15). In a related study, Sanford and coworkers [60] reported that the nonsymmetric pincer ligand (**25**, $E = \text{NEt}_2$, $E' = \text{P}^t\text{Bu}_2$) provides two distinct Ru-bound carboxylate complexes when exposed to an atmosphere of CO_2 , consistent with single carboxylation events on each of the methylene side arms.

These two products have distinct stabilities: the kinetic product (adjacent to P^tBu_2) undergoes facile exchange with isotopically labeled $^{13}\text{CO}_2$, whereas the thermodynamic product (adjacent to NEt_2) does not, and was stable toward exposure to vacuum. In the context of appended functionality, these reactions represent an intriguing approach to introduce a carboxylate group within the pincer framework. Although the emphasis of these reactions has been on their unique C–C bond-forming mechanism, the ligand architectures accessed through this transformation are appealing to promote further small molecule manipulations. The carboxylate-appended pincer frameworks bear resemblance to Hangman porphyrin systems in which carboxylic acid groups were utilized as proton relays [61]. Thus, these ligands are well suited to provide a new platform to examine catalytic reactions that feature a proton-transfer and/or proton-coupled electron-transfer processes for the conversion of small molecule substrates [62, 63].

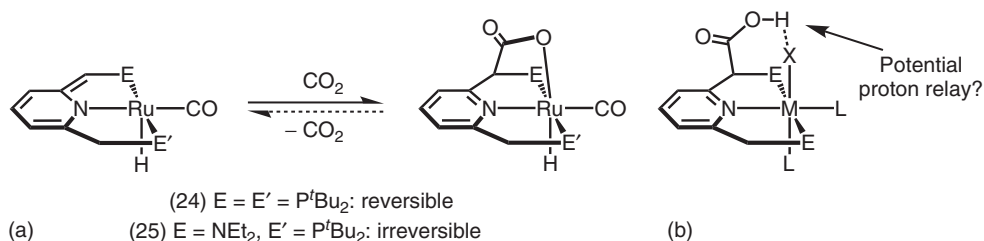


Figure 3.15 Formation of carboxylate compounds from CO_2 (a) and a hypothetical metal fragment supported by a pincer ligand with an appended carboxylic acid (b).

In addition to the reactivity directed at the methylene spacer in ENE pincers that contain a central pyridine unit, alternative catalytic reactivity can be promoted when the central N donor is a secondary amine. Although the N–H group of the central donor is not strictly “appended functionality,” these systems merit discussion in the light of recent reports where this N–H group serves to direct reactivity [64–66]. A notable example was described by Crabtree and Hazari [67] for CO₂ hydrogenation catalysis. The N–H functionality on a PNP pincer-ligated Ir(H)₃ fragment was found to substantially decrease the energy required for CO₂ insertion into an Ir–H bond. For example, insertion of CO₂ into the Ir–H bond trans to the central pyridine ring in **26** has a free-energy change of +65.5 kJ mol⁻¹, while insertion of CO₂ into the mutually trans Ir–H bonds is more favorable ($\Delta G^\circ = 3.1$ kJ mol⁻¹; Figure 3.16a), and likely due to the potent trans hydride ligand. In contrast, insertion of CO₂ into the Ir–H bond trans to the N–H group in **27** has a higher energetic barrier than the pyridine variant ($\Delta G^\circ = 76.8$ kJ mol⁻¹), which is consistent with the weaker trans-directing ability of the secondary amine. Unlike **26** where insertion of CO₂ into the mutually trans Ir–H bonds is identical, insertion of CO₂ into the Ir–H bond in **27** nearest to the N–H group is energetically downhill (-20.4 kJ mol⁻¹), in contrast to the other mutually trans Ir–H in **27** (+11.6 kJ mol⁻¹). Thus, the presence of the N–H group lowers the overall energy of CO₂ insertion by ~ 30 kJ mol⁻¹. This computational finding was supported with the structural characterization of the CO₂ insertion product (Figure 3.16b), which showed hydrogen-bonding interactions between the formate carbonyl and the pincer N–H group. In addition to lowering the barrier of CO₂ insertion into a metal hydride, the adjacent NH group has been implicated as an active participant to assist in the heterolytic cleavage of H₂ for hydrogenation reactions promoted by metal ENE pincer (PNP and SNS) complexes [68–70]. As such, these systems are promising multifunctional catalysts for transformations involving H₂ activation/delivery strategies.

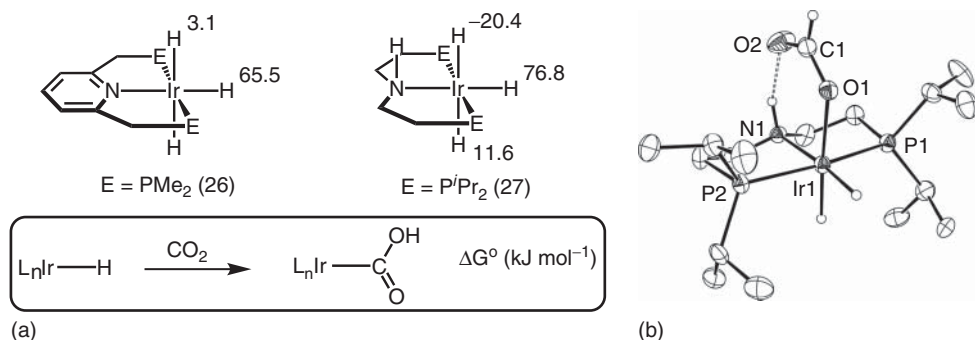


Figure 3.16 Gibbs free energies (in kilojoule per mol) for the insertion of CO₂ into various Ir–H bonds (a) and the solid-state structure of the CO₂ insertion product of **27** (b) [67].

3.3.2

PCP Pincer Systems

Unlike the majority of pincer ligands presented up to this point, which are predominantly planar, Gelman [71–73] recently reported $PC_{sp^3}P$ pincer constructs that are three dimensional. These ligands are based on dibenzobarrelene frameworks, and can be synthesized using highly modular Diels–Alder cycloaddition chemistry [74], which allows easy access to sterically and electronically varied sets of ligands within the same architecture. To highlight the potential of metal–ligand cooperativity within these systems, hydroxymethylene groups were incorporated within an Ir-PCP pincer to interact with metal-bound substrates (Figure 3.17) [75]. Solution-state NMR studies revealed an intramolecular close contact between the Ir–H and the methylene side arm in **28**. This species is only transiently stable, and upon standing, H_2 is eliminated to form the “arm-closed” species, **29**, presumably through an intermediate dihydrogen-bonded adduct (**28'**). The H_2 addition/elimination reaction is kinetically reversible, and the utility of this reaction was exploited for catalytic alcohol dehydrogenation. Both primary and secondary alcohols were dehydrogenated in the absence of an exogenous hydrogen acceptor to give esters and ketones, respectively. The structural versatility offered by this system, as well as the robustness presented by the highly aromatic scaffold, makes these systems exciting for future applications in catalysis.

3.3.3

PEP Pincer Systems

The central atom of a pincer ligand can be modified with acidic and/or basic groups, which may later engage in cooperative metal/ligand interactions. As noted previously for the case of the N–H unit in ENE pincers, a central phosphorus or sulfur can be further elaborated in PEP pincers (where E = P, S).

A recent example demonstrated that modification of the central atom of the pincer with acidic and basic functionality was possible with a mononuclear PPP pincer iridium(I) complex (Figure 3.18) [76]. In contrast to a meridional geometry typical of pincer ligands, the phosphido ligand in **30** is pyramidalized and, accordingly, affords a facial coordination mode. The geometry about the central phosphorus atom is consistent with predominantly σ -bonding character of the Ir–P unit,

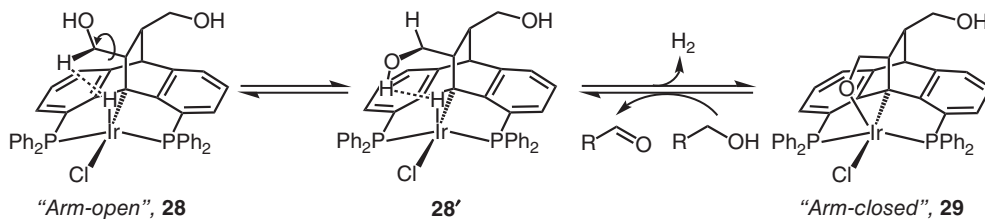


Figure 3.17 Acceptorless dehydrogenation of alcohols by Gelman’s Ir-PCP-pincer complex.

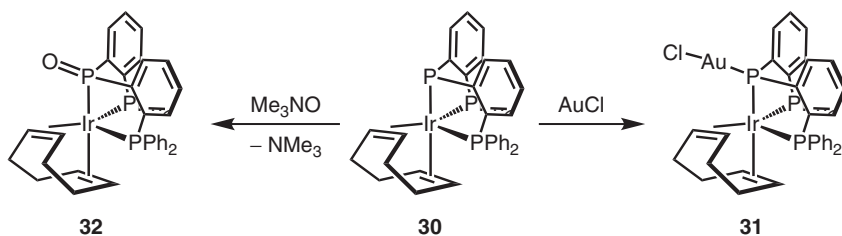


Figure 3.18 Functionalization of the central phosphide of a PPP pincer.

with an exposed lone pair. Further reactivity at this site provided pincer ligand manifolds that contain pendent acidic and basic groups. For example, **30** reacts with exogenous electrophiles, such as AuCl (**31**), $\text{BH}_3\cdot\text{SMe}_2$, and NH_4PF_6 , to provide discrete Lewis acid/base adducts. Alternatively, reaction with the O atom transfer reagent, trimethylamine-*N*-oxide, furnished the phosphine oxide complex **32**, which highlights the ability of the phosphido unit to support both Lewis acidic and basic groups in the secondary coordination sphere of the PPP pincer framework. Further reactivity studies were hindered by the tight binding of the cyclooctadiene ligand, which could not be eliminated under reductive conditions.

Although subsequent reactivity of the modified PPP ligands was not reported in this system, a related PP(O)P ligand featuring a central phosphine-oxide was recently reported by Bourissou and coworkers [77] (Figure 3.19a). Entry into the square-planar palladium(II) complex **34** can be achieved by formal insertion of the P–C bond of the free ligand **33** into a palladium(0) complex. The ability of the phosphine-oxide group in **34** to act as a Brønsted base was demonstrated by protonation using triflic acid to give the hydroxyl-phosphine complex, **35**. The addition of triflic acid to **34** modifies the ligand field of the central phosphorus atom from an X-type to an L-type donor, and is reversible using a sufficiently strong

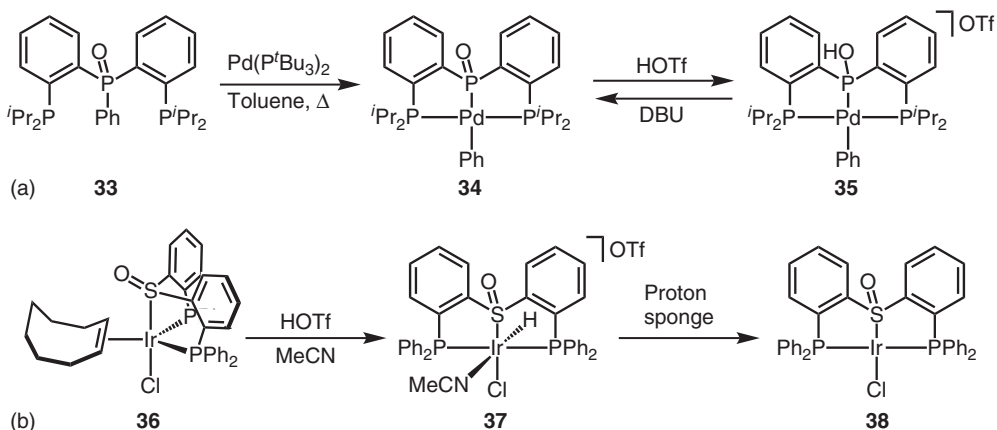


Figure 3.19 (a,b) PP(O)P and PS(O)P pincer complexes and their reactions with Brønsted acids and bases.

base such as DBU (1,8-diazabicycloundec-7-ene). Phosphine oxides and sulfoxides are both potent hydrogen-bond acceptor units, thus pincer-based PEP ligands that contain a central sulfoxide unit are highly complementary to the phosphine oxide PP(O)P ligands shown above. A PS(O)P pincer ligand was recently reported, in addition to its group 9 and 10 transition-metal complexes (Figure 3.19b) [78]. Similar to the PP(O)P ligands, the PS(O)P ligand supports meridional and facial coordination modes. Addition of Brønsted acids to iridium(I) complexes containing the PS(O)P ligand (**36**) results in the oxidative ligation of H⁺ to afford an iridium(III) hydride species (**37**). This finding suggests that the sulfoxide moiety in PS(O)P complexes has minimal Brønsted basicity, relative to the Ir(I) center. Protonation in this case is also reversible, and deprotonation affords a meridional isomer (**38**). Thus, the protonation/deprotonation sequence can be effectively used to induce facial/meridional isomerization. The utility of the proton-responsive phosphine oxide in **34** and the S=O functionality in **38** currently have limited demonstrated proficiency; however, these platforms might find application in catalytic cycles that feature proton-transfer events coupled with changes in the ligand field properties of a substrate. For this reason, future studies targeting proton-transfer reactivity in this complex, and related complexes, would be compelling.

3.3.4

Pyridine-2,6-Diimine Systems

Like Gelman's PC_{sp3}P pincer ligands, pyridine-2,6-diimine (PDI) ligands are a highly modular class of pincer ligands derived from commercially available starting materials [79]. An additional attribute of this ligand class is the *non-innocent* nature of the scaffold with respect to redox chemistry [80–82]. The synthesis of PDI ligands is amenable to the facile introduction of functionality in a symmetric and nonsymmetric manner, and can typically be achieved on multi-gram quantities. Symmetric PDI ligands featuring pendent Lewis basic (hydrazone) and acidic (pinacol boronate ester) sites have been reported with their iron(II) complexes, which were examined as catalysts for ethylene oligomerization [83, 84]. The specific role of the pendent functional groups during catalysis is not fully understood,

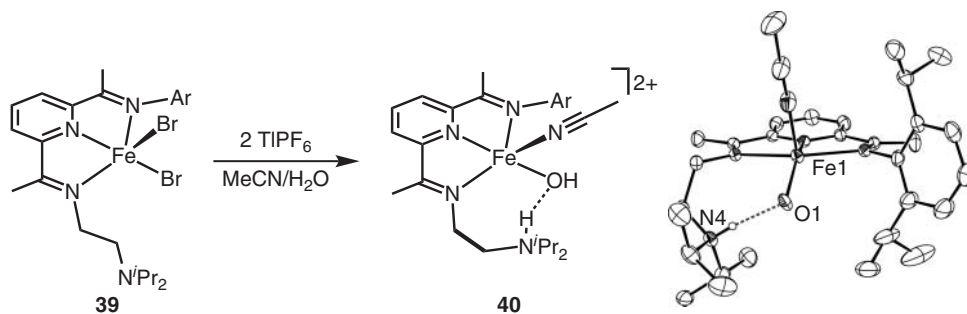


Figure 3.20 Formation of an iron(II)-hydroxo complex from water and the solid-state structure of **40** [85].

but it appears to contribute to enhanced thermal stability of the catalysts. A related nonsymmetric PDI ligand that features a pendent amine was reported by Gilbertson and coworkers [85] for metal–ligand cooperativity (**39**, Figure 3.20). In this case, the amine side arm is flexible and can engage in interactions with metal-coordinated substrates. The amine unit can be readily protonated, which presents a potent hydrogen-bond donor group capable of further interactions with coordinated ligands, for example, metal halides. Intramolecular proton transfer was also possible in this system, and was effected from a transiently formed iron(II)-aquo complex, which allowed the isolation of a rare iron(II)-hydroxo species, **40**. Of particular note, the subsequent hydrogen-bonding interaction with the protonated amine serves to stabilize the iron(II)-hydroxo complex. The highly flexible pendent amine is uniquely poised to act as a proton relay and/or to separately interact with a metal-coordinated substrate at two distinct sites. These features, in addition to possible participation in proton-coupled electron transfer reactions via ligand-centered redox events, make this a promising scaffold for further catalytic studies.

3.4

Future Outlook and Summary

Pincer frameworks provide a unique ligand scaffold that is amenable for further elaboration with appended functional groups, in large part due to the rigid nature of most pincer frameworks. Functionality can be directed collinear or orthogonal to a metal-coordinated substrate, and these distinct secondary structures can be targeted for substrate specificity within multifunctional architectures. Because of the potential coordinating ability of the introduced functionality, the selection of the metallation conditions requires careful attention to limit multinuclear metal–ligand ensembles. Once metallated, the appended functionality can serve to tune a ligand's physical properties and/or promote proton/electron transfer, which may concomitantly modify a pincer's ligand field strength. The recent explosion in reports of cooperative ligand frameworks demonstrates a high interest in the area of metal–ligand multifunctionality and, because of their geometrical constraints as well as unique tunable reactivity, pincer-based ligands are poised to continue to emerge as premier platforms upon which further elaboration is possible to uncover new reactivity profiles for small molecule activation.

References

1. Lippard, S.J. and Berg, J.M. (1994) *Principles of Bioinorganic Chemistry*, University Science Books, Mill Valley, CA.
2. Kaim, W. and Schwederski, B. (1994) *Bioinorganic Chemistry*, John Wiley & Sons Ltd, Chichester.
3. Crabtree, R.H. (2011) *New J. Chem.*, **35**, 18.
4. Shook, R.L. and Borovik, A.S. (2010) *Inorg. Chem.*, **49**, 3646.
5. Nieto, I., Livings, M.S., Sacci, J.B., Reuther, L.E., Zeller, M., and Papish, E.T. (2011) *Organometallics*, **30**, 6339.

6. Knapp, S.M.M., Sherbow, T.J., Yelle, R.B., Zakharov, L.N., Juliette, J.J., and Tyler, D.R. (2013) *Organometallics*, **32**, 824.
7. Das, S., Incarvito, C.D., Crabtree, R.H., and Brudvig, G.W. (2006) *Science*, **312**, 1941.
8. Balcells, D., Moles, P., Blakemore, J.D., Raynaud, C., Brudvig, G.W., Crabtree, R.H., and Eisenstein, O. (2009) *Dalton Trans.*, 5989.
9. Das, S., Brudvig, G.W., and Crabtree, R.H. (2008) *J. Am. Chem. Soc.*, **130**, 1628.
10. Linke-Schaetzel, M., Anson, C.E., Powell, A.K., Buth, G., Palomares, E., Durrant, J.D., Balaban, T.S., and Lehn, J.-M. (2006) *Chem. Eur. J.*, **12**, 1931.
11. Huang, C.-Y., Lynch, V., and Anslyn, E.V. (1992) *Angew. Chem. Int. Ed.*, **31**, 1244.
12. Disalvo, F.J. (1990) *Science*, **247**, 649.
13. Huang, C.Y., Cabell, L.A., Lynch, V., and Anslyn, E.V. (1992) *J. Am. Chem. Soc.*, **114**, 1900.
14. Barboiu, M., Prodi, L., Montalti, M., Zaccheroni, N., Kyritsakas, N., and Lehn, J.-M. (2004) *Chem. Eur. J.*, **10**, 2953.
15. Barboiu, M. and Lehn, J.-M. (2002) *Proc. Natl. Acad. Sci. U.S.A.*, **99**, 5201.
16. Meeuwissen, J. and Reek, J.N.H. (2010) *Nat. Chem.*, **2**, 615.
17. Nazeeruddin, M.K., Pechy, P., Renouard, T., Zakeeruddin, S.M., Humphry-Baker, R., Comte, P., Liska, P., Cevey, L., Costa, E., Shklover, V., Spiccia, L., Deacon, G.B., Bignozzi, C.A., and Graetzel, M. (2001) *J. Am. Chem. Soc.*, **123**, 1613.
18. Concepcion, J.J., Jurss, J.W., Norris, M.R., Chen, Z., Templeton, J.L., and Meyer, T.J. (2010) *Inorg. Chem.*, **49**, 1277.
19. Polyansky, D.E., Muckerman, J.T., Rochford, J., Zong, R., Thummel, R.P., and Fujita, E. (2011) *J. Am. Chem. Soc.*, **133**, 14649.
20. Anderson, T.J., Jones, G.D., and Vivic, D.A. (2004) *J. Am. Chem. Soc.*, **126**, 8100.
21. Kamata, K., Suzuki, A., Nakai, Y., and Nakazawa, H. (2012) *Organometallics*, **31**, 3825.
22. Tondreau, A.M., Atienza, C.C.H., Darmon, J.M., Milsmann, C., Hoyt, H.M., Weller, K.J., Nye, S.A., Lewis, K.M., Boyer, J., Delis, J.G.P., Lobkovsky, E., and Chirik, P.J. (2012) *Organometallics*, **31**, 4886.
23. Kelson, E.P. and Phengsy, P.P. (2000) *J. Chem. Soc., Dalton Trans.*, 4023.
24. Enthaler, S., Hagemann, B., Erre, G., Junge, K., and Beller, M. (2006) *Chem. Asian J.*, **1**, 598.
25. Moore, C.M. and Szymczak, N.K. (2013) *Chem. Commun.*, **49**, 400.
26. Schubert, U.S., Hofmeier, H., and Newkome, G.R. (2006) *Modern Terpyridine Chemistry*, Wiley-VCH Verlag GmbH, Weinheim.
27. Thompson, A.M.W.C. (1997) *Coord. Chem. Rev.*, **160**, 1.
28. Boddien, A., Loges, B., Gaertner, F., Torborg, C., Fumino, K., Junge, H., Ludwig, R., and Beller, M. (2010) *J. Am. Chem. Soc.*, **132**, 8924.
29. Annunziata, R., Benaglia, M., Puglisi, A., Raimondi, L., and Cozzi, F. (2008) *Eur. J. Org. Chem.*, 3976.
30. El-ghayoury, A. and Ziesel, R. (1998) *Tetrahedron Lett.*, **39**, 4473.
31. Fife, W.K. (1983) *J. Org. Chem.*, **48**, 1375.
32. Andreiadis, E.S., Demadrille, R., Imbert, D., Pecaut, J., and Mazzanti, M. (2009) *Chem. Eur. J.*, **15**, 9458.
33. Mukkala, V.M., Sund, C., Kwiatkowski, M., Pasanen, P., Hogberg, M., Kankare, J., and Takalo, H. (1992) *Helv. Chim. Acta*, **75**, 1621.
34. Lewis, F.W., Harwood, L.M., Hudson, M.J., Drew, M.G.B., Modolo, G., Sypula, M., Desreux, J.F., Bouslimani, N., and Vidick, G. (2010) *Dalton Trans.*, **39**, 5172.
35. Kroehnke, F. (1976) *Synthesis*, **1**, 1.
36. Tutusaus, O., Ni, C., and Szymczak, N.K. (2013) *J. Am. Chem. Soc.*, **135**, 3403.
37. Dilworth, M.J. and Eady, R.R. (1991) *Biochem. J.*, **277**, 465.
38. Champouret, Y.D.M., Maréchal, J.-D., Dadhiwala, I., Fawcett, J., Palmer, D., Singh, K., and Solan, G.A. (2006) *Dalton Trans.*, 2350.
39. Mai, E. and Schneider, C. (2007) *Chem. Eur. J.*, **13**, 2729.

40. Young, M.C., Liew, E., Ashby, J., McCoy, K. M., and Hooley, R.J. (2013) *Chem. Commun.*, **49**, 1627.
41. MacBeth, C.E., Hammes, B.S., Young, V.G. Jr., and Borovik, A.S. (2001) *Inorg. Chem.*, **40**, 4733.
42. Mukherjee, J., Lucas, R.L., Zart, M.K., Powell, D.R., Day, V.W., and Borovik, A.S. (2008) *Inorg. Chem.*, **47**, 5780.
43. Mareque-Rivas, J.C., Prabakaran, R., and Martin de Rosales, R.T. (2004) *Chem. Commun.*, **76**.
44. Berreau, L.M. (2006) *Activation of Small Molecules*, Wiley-VCH Verlag GmbH & Co. KGaA, Weinheim, p. 287.
45. Ahmed, T.J., Knapp, S.M.M., and Tyler, D.R. (2011) *Coord. Chem. Rev.*, **255**, 949.
46. Ait-Haddou, H., Sumaoka, J., Wiskur, S.L., Folmer-Andersen, J.F., and Anslyn, E.V. (2002) *Angew. Chem. Int. Ed.*, **41**, 4014.
47. Zong, R. and Thummel, R.P. (2005) *J. Am. Chem. Soc.*, **127**, 12802.
48. Kaveevivitchai, N., Zong, R., Tseng, H.-W., Chitta, R., and Thummel, R.P. (2012) *Inorg. Chem.*, **51**, 2930.
49. Hiromoto, T., Warkentin, E., Moll, J., Ermler, U., and Shima, S. (2009) *Angew. Chem. Int. Ed.*, **48**, 6457.
50. Shima, S. and Thauer, R.K. (2007) *Chem. Rec.*, **7**, 37.
51. Taylor, R.A., Law, D.J., Sunley, G.J., White, A.J.P., and Britovsek, G.J.P. (2009) *Angew. Chem. Int. Ed.*, **48**, 5900.
52. Mutai, T., Cheon, J.-D., Tsuchiya, G., and Araki, K. (2002) *J. Chem. Soc., Perkin Trans. 2*, 862.
53. Donoghue, P.J., Tehranchi, J., Cramer, C.J., Sarangi, R., Solomon, E.I., and Tolman, W.B. (2011) *J. Am. Chem. Soc.*, **133**, 17602.
54. Redmore, S.M., Rickard, C.E.F., Webb, S.J., and Wright, L.J. (1997) *Inorg. Chem.*, **36**, 4743.
55. Gunanathan, C. and Milstein, D. (2011) *Acc. Chem. Res.*, **44**, 588.
56. Schaub, T., Radius, U., Diskin-Posner, Y., Leitus, G., Shimon, L.J.W., and Milstein, D. (2008) *Organometallics*, **27**, 1892.
57. Montag, M., Zhang, J., and Milstein, D. (2012) *J. Am. Chem. Soc.*, **134**, 10325.
58. Vogt, M., Rivada-Wheelaghan, O., Iron, M.A., Leitus, G., Diskin-Posner, Y., Shimon, L.J.W., Ben-David, Y., and Milstein, D. (2013) *Organometallics*, **32**, 300.
59. Vogt, M., Gargir, M., Iron, M.A., Diskin-Posner, Y., Ben-David, Y., and Milstein, D. (2012) *Chem. Eur. J.*, **18**, 9194.
60. Huff, C.A., Kampf, J.W., and Sanford, M.S. (2012) *Organometallics*, **31**, 4643.
61. Rosenthal, J. and Nocera, D.G. (2007) *Prog. Inorg. Chem.*, **55**, 483.
62. Piers, W.E. (2011) *Organometallics*, **30**, 13.
63. Dempsey, J.L., Esswein, A.J., Manke, D.R., Rosenthal, J., Soper, J.D., and Nocera, D.G. (2005) *Inorg. Chem.*, **44**, 6879.
64. Clarke, Z.E., Maragh, P.T., Dasgupta, T.P., Gusev, D.G., Lough, A.J., and Abdur-Rashid, K. (2006) *Organometallics*, **25**, 4113.
65. Nielsen, M., Kammer, A., Cozzula, D., Junge, H., Gladiali, S., and Beller, M. (2011) *Angew. Chem. Int. Ed.*, **50**, 9593.
66. Bertoli, M., Choualeb, A., Lough, A.J., Moore, B., Spasyuk, D., and Gusev, D.G. (2011) *Organometallics*, **30**, 3479.
67. Schmeier, T.J., Dobreiner, G.E., Crabtree, R.H., and Hazari, N. (2011) *J. Am. Chem. Soc.*, **133**, 9274.
68. Spasyuk, D., Smith, S., and Gusev, D.G. (2012) *Angew. Chem. Int. Ed.*, **51**, 2772.
69. Spasyuk, D. and Gusev, D.G. (2012) *Organometallics*, **31**, 5239.
70. Spasyuk, D., Smith, S., and Gusev, D.G. (2013) *Angew. Chem. Int. Ed.*, **52**, 2538.
71. Azerraf, C. and Gelman, D. (2008) *Chem. Eur. J.*, **14**, 10364.
72. Azerraf, C. and Gelman, D. (2009) *Organometallics*, **28**, 6578.
73. Gelman, D. and Romm, R. (2013) *Top. Organomet. Chem.*, **40**, 289.
74. Azerraf, C., Shpruhman, A., and Gelman, D. (2009) *Chem. Commun.*, 466.
75. Musa, S., Shaposhnikov, I., Cohen, S., and Gelman, D. (2011) *Angew. Chem. Int. Ed.*, **50**, 3533.
76. Gloaguen, Y., Jacobs, W., de Bruin, B., Lutz, M., and van der Vlugt, J.I. (2013) *Inorg. Chem.*, **52**, 1682.
77. Derrah, E.J., Martin, C., Mallet-Ladeira, S., Miqueu, K., Bouhadir, G., and

- Bourissou, D. (2012) *Organometallics*, **41** (47), 14274–14280.
78. Suess, D.L.M. and Peters, J.C. (2012) *Organometallics*, **31**, 5213.
79. Gibson, V.C., Redshaw, C., and Solan, G.A. (2007) *Chem. Rev.*, **107**, 1745.
80. Tondreau, A.M., Stieber, S.C.E., Milsman, C., Lobkovsky, E., Weyhermuller, T., Semproni, S.P., and Chirik, P.J. (2013) *Inorg. Chem.*, **52**, 635.
81. Bart, S.C., Chlopek, K., Bill, E., Bouwkamp, M.W., Lobkovsky, E., Neese, F., Wieghardt, K., and Chirik, P.J. (2006) *J. Am. Chem. Soc.*, **128**, 13901.
82. Thammavongsy, Z., Seda, T., Zakharov, L.N., Kaminsky, W., and Gilbertson, J.D. (2012) *Inorg. Chem.*, **51**, 9168.
83. Britovsek, G.J.P., Gibson, V.C., Kimberley, B.S., Mastroianni, S., Redshaw, C., Solan, G.A., White, A.J.P., and Williams, D.J. (2001) *J. Chem. Soc., Dalton Trans.*, 1639.
84. Ionkin, A.S., Marshall, W.J., Adelman, D.J., Bobik, F.B., Fish, B.M., and Schiffhauer, M.F. (2008) *Organometallics*, **27**, 1902.
85. Kendall, A.J., Zakharov, L.N., and Gilbertson, J.D. (2010) *Inorg. Chem.*, **49**, 8656.

4

C–C, C–O, and C–B Bond Formation by Pincer Complexes Including Asymmetric Catalysis

Kálmán J. Szabó

4.1

Introduction – Pros and Cons of Using Pincer Complexes in Catalysis

Transition-metal catalysis has become one of the most powerful methodologies in organic synthesis [1, 2]. The main reason is that metal catalysts are able to transform organic substrates efficiently with high selectivity. The selectivity is very often controlled by the choice of the metal and the ligand applied in the catalytic process. In particular, palladium catalysis has been very successful in these applications, and by using ligand control remarkable selectivity including enantioselectivity can be achieved [1, 2]. The application and understanding of the rules of ligand control is usually difficult and requires sophisticated modeling and mechanistic studies. A basic problem is that, under the catalytic reactions, the ligands can coordinate and dissociate from the central metal atom, and therefore it is unclear which ligand exerts control in the selectivity-determining step of the reaction. In this respect, application of tridentate pincer complexes could be beneficial [3–10]. In these species, three of the coordination sites of the Pd(II) atom are occupied by the pincer ligand, and one coordination site is available for the organic substrate (Figure 4.1). The complex is usually very stable and has a well-defined stoichiometry. In most reactions, the pincer ligand and metal are firmly held together by the chemical reactions. The central Pd–C bond is usually electron rich, and the side arms can be easily varied. The steric and electronic effects of the side arms can be efficiently propagated to the reaction center. The Pd–C and Pd–Q bonds are forced to trans positions, and therefore reductive elimination (requiring cis position) can be avoided.

The above benefits of the application of pincer complexes are, of course, counterbalanced by a couple of disadvantages as well. Synthesis, and in particular the tuning of the reactivity and selectivity, of pincer complexes requires extra efforts. Although many pincer complexes, in particular Pd(II) complexes, are highly stable, change of the oxidation state of the metal atom may lead to stability issues. A typical problem is the reduction of Pd(II) to Pd(0) in pincer complexes. The Pd(0) form easily undergoes irreversible decomposition involving dissociation of the ligand [11, 12].

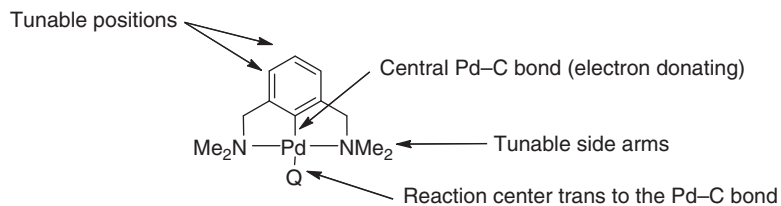


Figure 4.1 Example of a pincer complex catalyst.

This chapter focuses on some recent examples of the application of pincer complexes as catalysts in organic synthesis of C–C, C–O, and C–B formation reactions. We will show that these complexes can be employed as excellent catalysts or catalyst precursors, and they may help to explore important mechanistic details in catalytic processes. The examples mainly come from palladium chemistry, and, of course, this chapter does not fully cover this area.

4.2

Reaction of Imines and Isocyanoacetates

4.2.1

Stereoselective Synthesis of Imidazolines

The first example of the application of pincer complex catalysts for selective synthesis involves aldol type of reactions involving imines and isocyanoacetates. In aldol [13–27] and Michael addition [13, 28–34] reactions, palladium pincer complexes have usually been employed as Lewis acid catalysts, for the first time by Richards and coworkers [13, 28]. This also means that the palladium(II) atom in these processes is not involved in redox reactions, and therefore reduction to palladium(0) does not happen. The aldol and the Michael reactions are useful C–C bond-forming reactions. In these processes, new stereocenters are generated, and therefore the processes can be used for stereoselective synthesis. A typical example is the reaction of sulfonimines (**2**) with isocyanoacetate (**3**) to form imidazoline (**4**) derivatives. The imidazolines can be easily hydrolyzed to diamino acid derivatives in a one-pot process (Figure 4.2) [24].

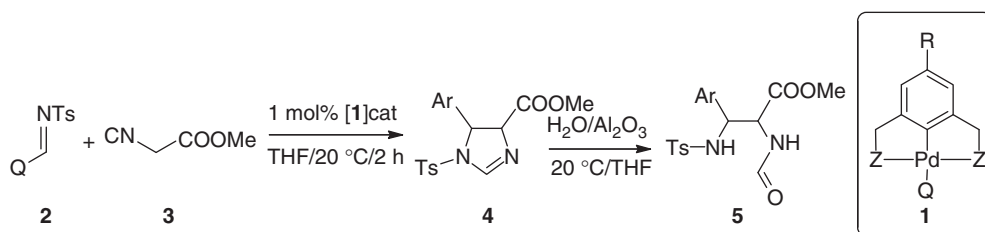
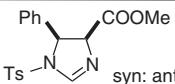
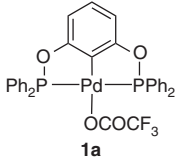
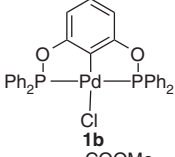
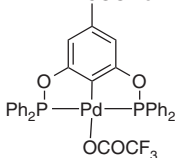
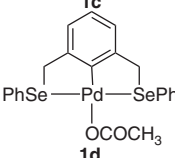
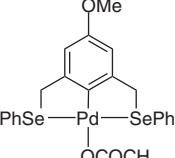
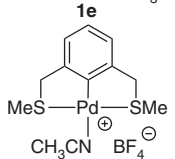
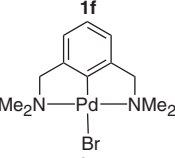


Figure 4.2 Pincer complex-catalyzed synthesis of imidazoline derivatives from sulfonimines and isocyanoacetates [24].

Table 4.1 Dependence of the stereoselectivity on the applied catalyst [24].

Pd-catalyst	 syn: anti	Yield (%)
$\text{Pd}(\text{OAc})_2$	1 : 2	82
 1a	10 : 1	98
 1b	7 : 1	99
 1c	8 : 1	99
 1d	1 : 3	98
 1e	1 : 4	99
 1f	2 : 3	98
 1g	2 : 3	98

When the cyclization reaction was performed in the presence of $\text{Pd}(\text{OAc})_2$ using a phenyl sulfonimine (**2**, $\text{Q} = \text{Ph}$) substrate, the imidazoline product (**4**, $\text{Ar} = \text{Ph}$) was formed with poor regioselectivity (Table 4.1). However, use of the PCP complex **1a** led to excellent regioselectivity with a *syn/anti* ratio of 10 : 1. This indicates that pincer complexes are more efficient catalysts for the cyclization reactions than simple palladium salt, as both the selectivity and the yield could be improved using **1a**.

An interesting feature of this study is the investigation of the effects of the counterions, the heteroatoms in the side arms, and the aromatic substituents on the selectivity. Replacement of the trifluoroacetate (TFA) (**1a**) to chloride (**1b**) leads to a decrease of the selectivity. This indicates that weakly coordinating ligands have a favorable effect on the selectivity and reactivity of the complex. Considering that palladium is supposed to act as a Lewis acid in the cyclization reaction, the effects of an electron-withdrawing group (COOMe) in the para position of the aromatic ring (**1c**) were also tested. However, the presence of the COOMe group did not improve the selectivity compared to the unsubstituted complex **1a**. Changing the heteroatom in the side arm from phosphorous (**1a**) to selenium (**1e**) considerably changed the selectivity. In contrast to the *syn* preference when using PCP complexes (**1a–c**), with the selenium complex **1d** the *anti* product formed in larger amounts. However, this *anti* selectivity was much lower than the *syn* selectivity with the PCP complexes. Interestingly, $\text{Pd}(\text{OAc})_2$ also gave the *anti* form in larger amount with poor selectivity. Change of the side arms to sulfur (**1f**) or nitrogen (**1g**) containing groups also leads to poor *anti* selectivity. It can be concluded that change of the π -acceptor phosphorous atom in the side arms to σ -donor selenium, sulfur, and nitrogen ligands (Table 4.1) leads to a decrease of the *syn/anti* selectivity of the above (Figure 4.1) cyclization reactions. This change of selectivity indicates mechanistic changes in the reaction (see below).

The reaction had a broad synthetic scope, as imines substrates with aromatic (**4a–d**), heteroaromatic (**4e**), and vinyl (**4f**) substituents gave high yield. Using the

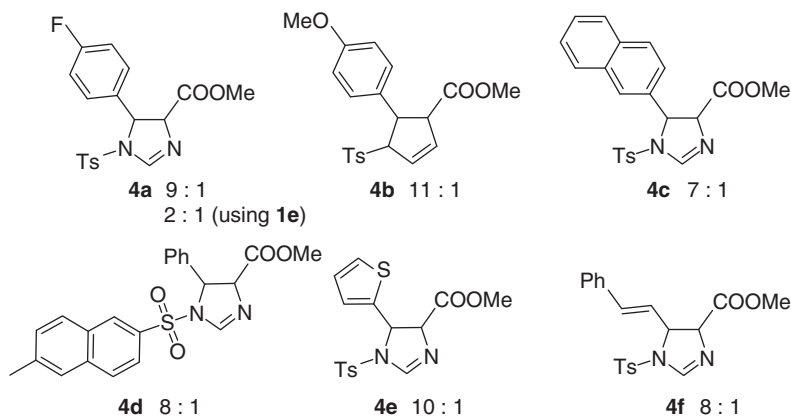


Figure 4.3 Synthetic scope of the reaction. Unless otherwise stated, the *syn/anti* ratio was obtained with **1a** as catalyst. The yields are in the range 93–99%.

PCP complex **1a** as a catalyst, high syn/anti selectivity was obtained (Figure 4.3). The electron-withdrawing substituent in the aryl group of the imine leads to a slight decrease of the selectivity (**4a**), while electron-donating substituents (**4b**, **4c**) give as high selectivity as that of the phenyl group. Interestingly, in the presence of a bulky naphthyl group (**4c**) the selectivity decreases, even if the bulky group is attached to the nitrogen of the imine (**4d**).

4.2.2

Application of Chiral Pincer Complexes

As the reaction creates two stereogenic carbons, it was appealing to develop an asymmetric version of the transformation. A particularly important reason is that the imidazoline product can easily be hydrolyzed to amino acids (Figure 4.2),

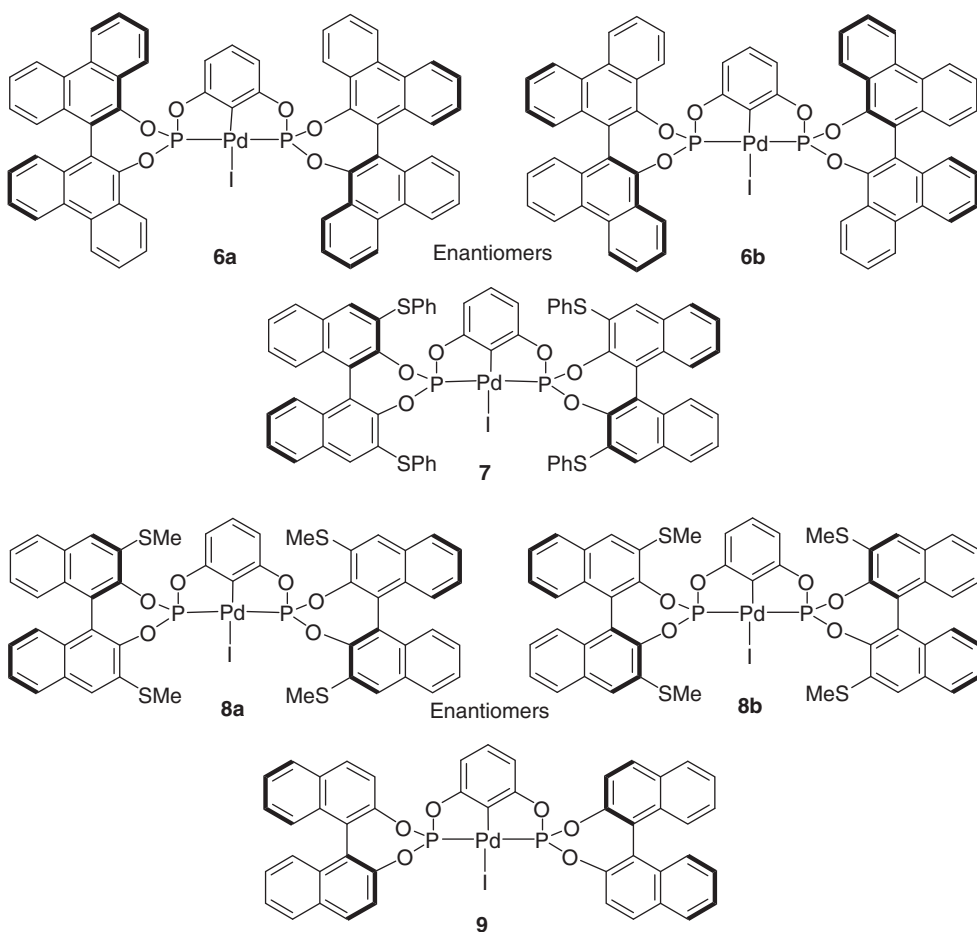


Figure 4.4 Chiral pincer complexes used as catalysts for the cyclization reaction.

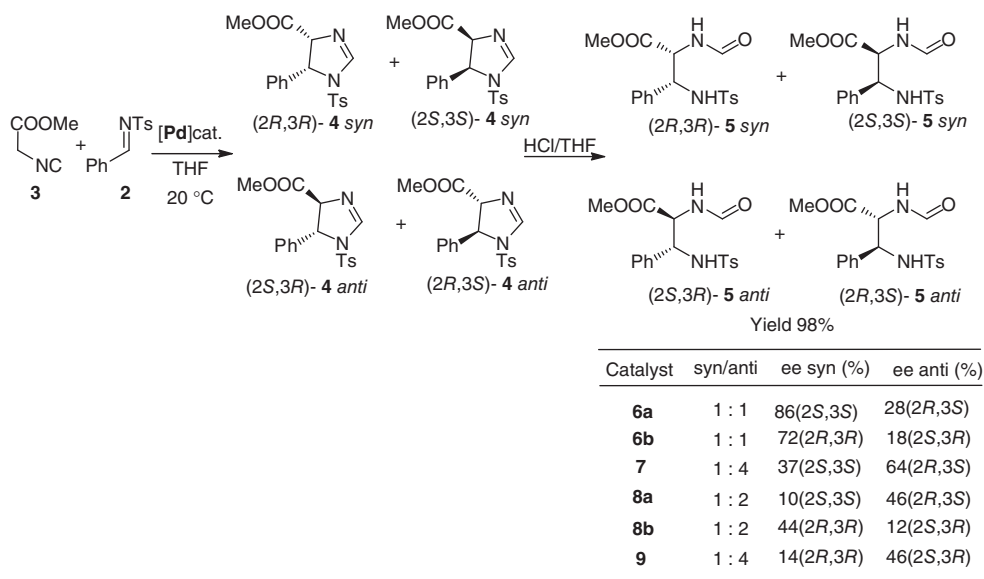


Figure 4.5 Enantioselectivity of the amino acid derivatives achieved by chiral pincer complexes 6–9.

and thus the procedure would be suitable for the synthesis of enantio-enriched amino acids. Therefore, chiral pincer complexes 6–9 (Figure 4.4) were employed to carry out asymmetric cyclization of 2 and 3 (Figure 4.5) [25]. These studies show that bisphenanthroline complexes, with bulky annelated phenyl groups **6a,b**, are more efficient in inducing enantioselectivity than 1,1'-bi-2-naphthol (BINOL) based complexes 7–9. The best enantioselectivity (86% ee) was achieved using the complex **6a**. Unfortunately, the high regioselectivity obtained with the achiral analogs **1a–c** was lowered, and **6a** resulted in a 1:1 mixture of syn and anti stereoisomers. Interestingly, the enantioselectivity (Figure 4.5) obtained for the syn isomer (86% ee) is significantly higher than for the anti isomer (28% ee). When **6b**, the enantiomer of **6a**, was used, the enantioselectivity slightly decreased. The main diastereomer was still the syn form but as expected the configuration of the major enantiomer (72% ee) was the opposite of the major enantiomer formed using **6a** (Figure 4.5). Interestingly, when S-Ph-substituted BINOL-based complex **7** was used, the diastereoselectivity increased benefiting the anti diastereomer. However, the enantioselectivity was lower than with bisphenanthroline complex **6a**. When the size of the substituent was decreased, or unsubstituted BINOL was employed in the side arms, the enantioselectivity was further decreased.

These studies show that variation of the steric bulkiness of the chiral ligands in the side arms strongly influences the selectivity of the cyclization reactions. However, obtaining full control over both the stereo and enantioselectivity of the reaction is still very challenging.

4.2.3

Mechanistic Considerations

A particularly interesting feature of the above reaction is the change of the stereoselectivity of the process upon changing the heteroatoms of the side arms (Table 4.1). In case of PCP complexes **1a–d**, a syn selectivity was obtained, while with σ -donor groups in the side arms **1a–g**, the stereoselectivity was reverted and decreased.

Szabó and coworkers [24] studied the mechanistic details of the cyclization reaction using PCP complex **1a** as catalyst. It was found that **1a** reacts with **3** even in the absence of the imine component **2** forming a new complex **10** (Figure 4.6). This complex was isolated and its structure determined by X-ray diffraction. Subsequently, complex **10** was reacted with imine **2**, which led to the expected cyclized product **4**. The integrity of pincer complex **1a** was preserved and it could be recovered without any decomposition after the reaction (Figure 4.6). This and the fact that PCP complex could also be recovered after the catalytic process [24] show that the palladium atom of **1a** does not undergo reduction to Pd(0), as this reaction would involve disintegration of the complex.

Based on the above results, a catalytic cycle was suggested for the cyclization reaction (Figure 4.7). Accordingly, complex **10** is the key intermediate of the process. Coordination of the isocyanate to the palladium atom facilitates the deprotonation of the CH₂ group of **3**. The carbanion center of **11** undergoes nucleophilic attack of the imine carbon leading to complex **12**, which after ring closure and deprotonation gives the final product and regenerates the catalyst. The stereo and enantioselectivity (with **6–9**) of the process is determined by formation of **12** from complex **11**.

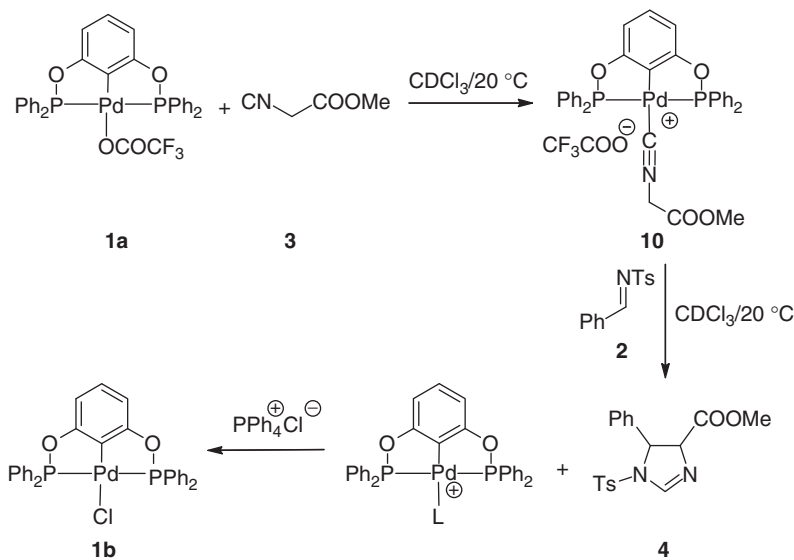


Figure 4.6 Cyclization proceeding via the pincer complex intermediate **10**.

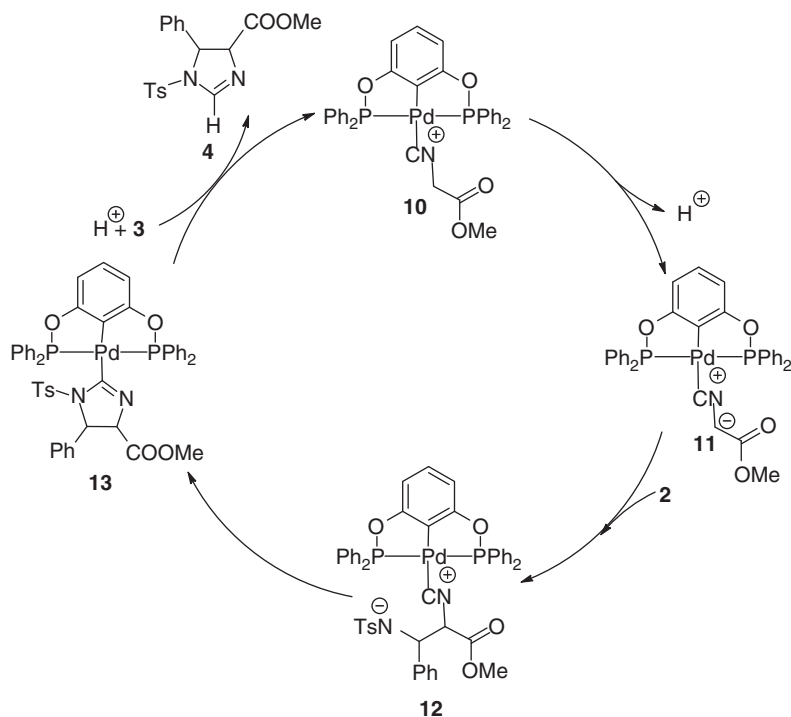


Figure 4.7 Suggested mechanism of the cyclization.

van Koten and coworkers [35] have shown that isocyanoacetate complexes with weakly coordinating side arms (such as **1e–g**) undergo insertion into the Pd–C bond, which leads to loss of the integrity of the pincer complex. This may explain the change of the stereoselectivity while using **1e–g** in condensation reactions.

4.3

C–H Functionalization of Organonitriles

4.3.1

Allylation of Imines

Another interesting application catalyzed by a palladium pincer complex for the transformation of sulfonimines involves allylation with allyl cyanides in the presence of a weak base (NaHCO_3) [36]. In this process, the allylic C–H bond adjacent to the CN group is replaced by a new C–C bond with excellent regioselectivity (Figure 4.8). The reactions proceed under mild conditions, typically at room temperature. Probably the most important feature of the reaction is that it requires the use of a very weak base (NaHCO_3). Application of stronger bases, such as Cs_2CO_3 , leads to allylic rearrangement of the product **15** by the formation of vinyl–CN

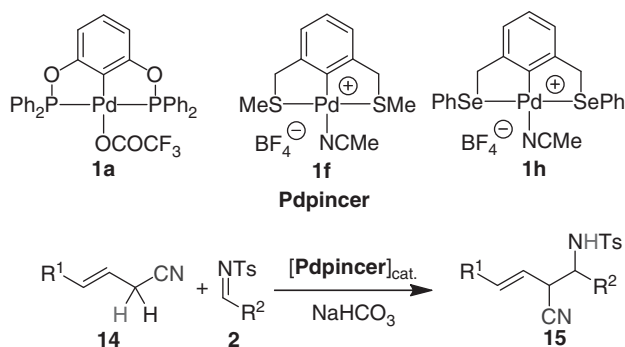


Figure 4.8 C–H functionalization-based allylation of sulfonimines.

derivatives [37]. The reaction is catalyzed by PCP complex **1a**, while common palladium catalysts, such as Pd(PPh₃)₄, Pd₂(dba)₃ (dba, dibenzylideneacetone), Pd(OAc)₂, or Pd(TFA)₂, are inactive.

Although, the regioselectivity of the process is excellent, the stereoselectivity is poor, which is probably due to the small size (and thus the poor directing ability) of the CN group. Interestingly, the variation of the pincer complex catalysts slightly changes the stereoselectivity. When the PCP catalyst **1a** was replaced by the SCS catalyst **1f**, the diastereoselectivity remained the same (cf. entries 1 and 2 in Table 4.2) but when the SeCSe catalyst **1h** was applied the stereoselectivity decreased (entry 3). For aryl-substituted sulfonimines, a faster reaction occurred with electron-withdrawing groups, such as **2b**, than with electron-donating substituents **2c** (cf. the reaction times in entries 4 and 5). The reaction works smoothly even with vinyl (**2d**) and alkyl (**2e**) sulfonimines (entries 6 and 7). The substrate scope involves both the parent allyl-CN (**14a**) and its substituted analogs, such as **14b–d** [36].

It is interesting to note that the same reaction catalyzed by palladium pincer complex can also be carried out using allylstannane derivatives [38]. A clear advantage of the above procedure (Figure 4.8) is that it does not require a tedious trialkyl tin prefunctionalization of the allylnitrile derivatives.

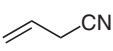
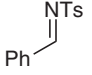
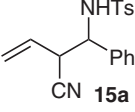
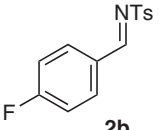
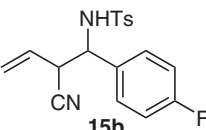
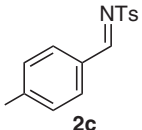
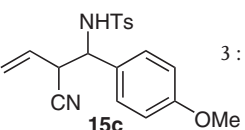
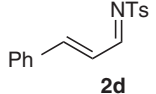
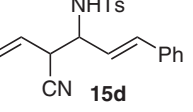
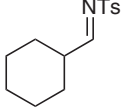
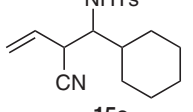
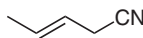
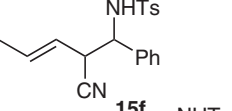
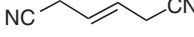
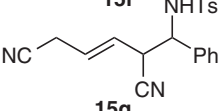
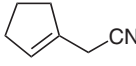
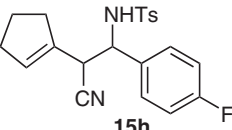
According to the mechanistic rationale given for the process [36], the reaction is supposed to proceed by NaHCO₃-aided deprotonation of the allyl-CN substrate, which is assisted by the palladium atom of **1a** (Figure 4.9). This process generates η¹-allyl complex **16**, which readily reacts with electrophiles [39–41], such as **2a**. η¹-Allyl palladium complexes preferentially react at the γ-position of the allylic moiety (**17**) to give the complex **18** [41, 42], which after decomplexation gives product **14a**.

4.3.2

Benzyl Amine Synthesis

A related study was carried out using benzyl-CN substrates and imines. The reaction was readily catalyzed by the PCP complex **1a** in the presence or absence of NaHCO₃ (Figure 4.10) [43].

Table 4.2 Catalytic allylation of imines with allyl cyanides.

Entry	Substrates	T (°C)/ t (h)	Catalyst	Products	dr	Yield	
1	 14a	 2a	20/5	1a	 15a	3 : 2	90
2	14a	2a	20/5	1f	15a	3 : 2	83
3	14a	2a	20/4	1h	15a	1 : 1	81
4	14a	 2b	20/1	1a	 15b	3 : 2	91
5	14a MeO	 2c	20/5	1a	 15c	3 : 2	91
6	14a	 2d	20/14	1a	 15d	2 : 1	93
7	14a	 2e	20/12	1a	 15e	1 : 1	90
8	 14b	3a	40/14	1a	 15f	1 : 1	98
9	 14c	3a	20/4	1a	 15g	1 : 1	97
10	 14d	3b	20/20	1a	 15h	3 : 2	94

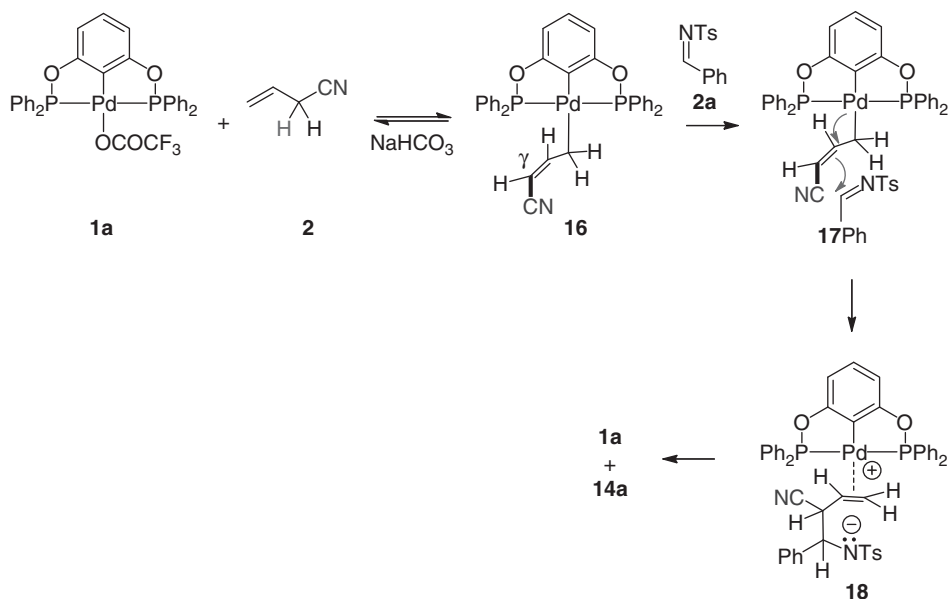


Figure 4.9 Suggested mechanism of the allylation of imines.

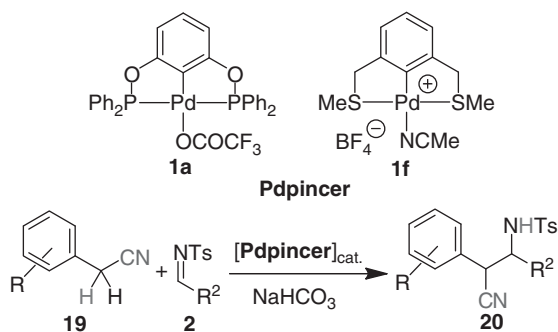
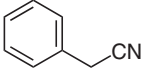
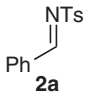
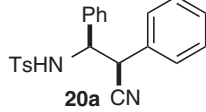
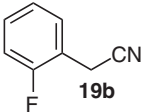
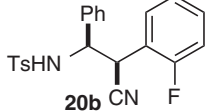
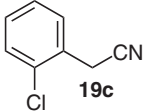
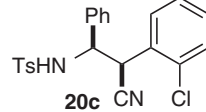
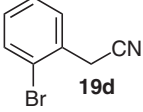
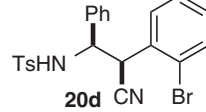
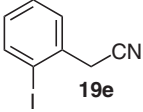
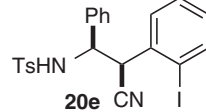
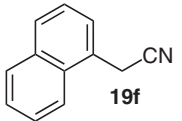
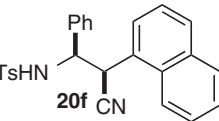
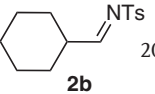
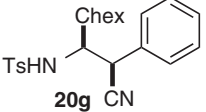


Figure 4.10 Pincer complex-catalyzed coupling of benzyl cyanides with sulfonimines.

The reaction proceeds under mild conditions, similar to the above catalytic transformations of sulfonimines. A relatively low diastereoselectivity occurred for coupling of the parent benzyl nitrile **19a** with **2a** (Table 4.3). However, the stereoselectivity increased for ortho-substituted derivatives **19b–f**. The degree of stereoselection was increased with increasing bulkiness of the ortho substituent, as shown for halogenated derivatives **19b–e** (entries 2–5). The lowest selectivity was obtained for the fluoro derivative **19b** (4.6:1), while the highest selectivity (10:1) occurred for the iodo derivative **19e**. Interestingly, the C–I bond remained unchanged in this process, suggesting that the $\text{Pd}(0)$ species (which readily

Table 4.3 Catalytic benzylation of sulfonimines.

Entry	Substrates	Temperature (°C) /time (h)	Catalyst	Product	dr	Yield
1	 19a	 2a	20/15 1a	 20a	2 : 1	99
2	 19b	2a 6/68	1a	 20b	4.6 : 1	95
3	 19c	2a 20/16	1a	 20c	8.4 : 1	99
4	 19d	2a 20/16	1a	 20d	10 : 1	83
5	 19e	2a 20/15	1a	 20e	10 : 1	99
6	2e	2a 20/16	1f	20e	10 : 1	70
7	 19f	2a 20/24	1a	 20f	10 : 1	83
8	19a	 2b	20/18 1a	 20g	1.4 : 1	91

undergoes oxidative addition to the C–I bond) did not form. The reaction also proceeded with high stereoselectivity for the naphthyl derivative **19f** (entry 7) as well, indicating the importance of the steric factor in the diastereoselection process.

Aliphatic sulfonimines also reacted smoothly, but the stereoselectivity with **19a** was poor. Variation of the pincer complex catalyst did not change the stereoselectivity (cf. entries 6 and 7). The reaction did not proceed while using commonly used (non-pincer) catalysts [43].

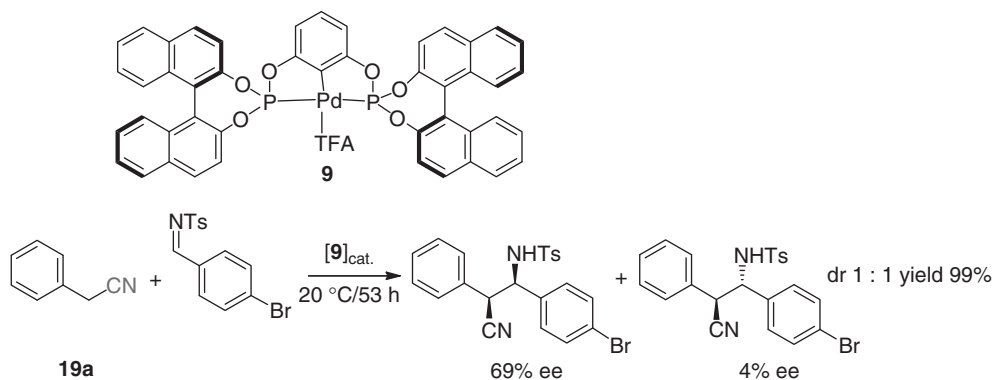


Figure 4.11 Asymmetric benzylation of sulfonamides.

An asymmetric version of the process was also developed (Figure 4.11) [43]. In this process, the BINOL-based catalyst **9** gave promising levels of enantioselectivity but the stereoselectivity of the reaction was poor.

The mechanism of the reaction was supposed to be similar to that of the allylation process. Deprotonation of benzyl cyanides requires very strong bases ($pK_a = 21.9$) [44]. However, coordination of the CN group to the palladium atom of **1a** allows easy deprotonation even with very weak bases, such as NaHCO_3 . The next step is a nucleophilic attack of the carbon atom of the imine group, which leads to C–C bond formation. This step determines the stereoselectivity of the process [43].

4.4 Reactions Involving Hypervalent Iodines

A particularly interesting catalytic feature of the above-discussed pincer complexes (**1a–h**) is that they comprise a Pd–C bond, rendering the Pd(II) atom electron rich. This allows oxidation of the Pd(II) atom to Pd(IV) without losing the pincer integrity of the complex [45–48]. This property can be exploited in catalytic applications, allowing a Pd(II)/Pd(IV) redox cycle [49–53]. Usually, oxidation of Pd(II) to Pd(IV) species requires strong oxidants, such as peroxides and hypervalent iodines. In the following section, we will show a couple of examples of the application of pincer-complex catalysis under oxidative conditions, in which a Pd(II)/Pd(IV) redox cycle is achieved. Another interesting application of pincer complexes is the relative ease by which the Pd(IV) oxidation state of the metal atom can be detected using ^1H NMR spectroscopy.

4.4.1 Arylation of Alkenes Using Pincer Complex Catalysis

Heck coupling is probably the most established catalytic method for the coupling of aryl compounds with alkenes [1, 54]. However, Heck coupling reactions are based

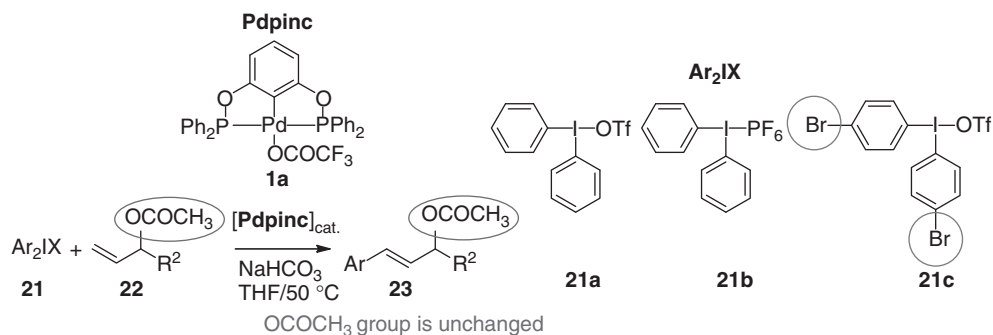


Figure 4.12 Arylation of allyl acetates.

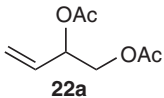
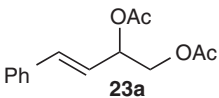
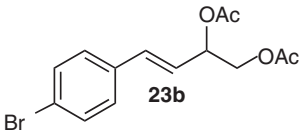
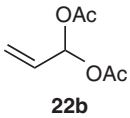
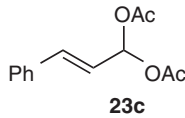
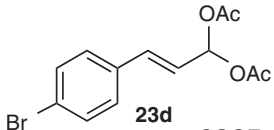
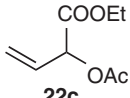
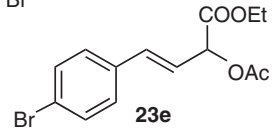
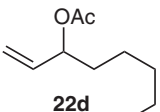
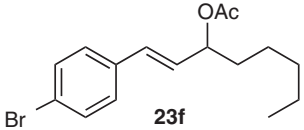
on a Pd(0)/Pd(II) redox cycle, meaning that certain functionalities that may undergo oxidative addition with Pd(0) are not tolerated. Typically, such functional groups are allylic acetates and aryl halides, which otherwise serve as prefunctionalized substrates in palladium-catalyzed allylic substitutions or cross-coupling reactions.

A possible solution for functionalization of allylic acetates involves the application of hypervalent iodones (**21**) as aryl source in the presence of a weak base (NaHCO₃) and pincer complex (**1a**) catalysis (Figure 4.12) [49]. Under these conditions, a regioselective arylation of the alkene takes place without altering the allylic acetate functionality.

After the reaction, the applied pincer complex **1a** can be recovered without any change, and the so-called mercury drop test [55] was negative. These findings suggest that the redox coupling took place via a Pd(II)/Pd(IV) mechanism without the involvement of Pd(0) species. The reaction has a broad synthetic scope, indicating that even diacetates **22a,b** smoothly undergo the desired coupling reaction (Table 4.4). Not only acetate but even COOEt or alkyl groups are tolerated in the allylic position (entries 5 and 6). A further attractive feature of the method is that aryl bromides can be transferred using hypervalent iodine **2c**, as Pd(0) species does not interfere with the cross-coupling process (entries 3 and 5–7). Based on the above experimental findings, a plausible catalytic cycle was suggested for the process (Figure 4.13) [49]. Probably the most important step is the oxidative addition of the hypervalent iodine to the PCP Pd(II) pincer complex catalyst to give the Pd(IV) complex **24**. This complex may react in the subsequent reaction steps, which are probably similar to the classical Heck coupling. The last step is the reduction of the Pd(IV) complex to the Pd(II) precursor of the catalytic cycle.

Density functional theory (DFT) modeling studies [56] pointed out the relatively high activation energy of the oxidative addition. Since carbopalladation of **24** is probably fast, complex **24** could not be detected. However, in the acetoxylation and the C–H borylation studies, the more strongly oxidizing iodine was used instead of **21**, and detection of the Pd(IV) intermediate could be realized (Sections 4.4.2 and 4.4.3).

Table 4.4 Application of palladium pincer complexes for arylation reactions.

Entry	Substrate	Ar ₂ IX	Product	Yield (%)
1		21a		94
2	22a	21b	23a	94
3	22a	21c		91
4		21a		91
5	22b	21a		89
6		21c		83
7		21c		90

4.4.2

Acetoxylation with Hypervalent Iodines

Palladium-catalyzed allylic C–H acetoxylation (acyloxylation) of alkenes is one of the synthetically most established C–H functionalization methods [57–62]. These reactions are conducted under oxidative reaction conditions. In the most commonly used approach, the reaction proceeds via a Pd(II)/Pd(0) catalytic cycle and benzoquinone (BQ) is used for reoxidation of Pd(0) and activation of the nucleophilic (acetate) attack [61, 62].

Application of BQ as oxidant and activator imposes some limitations to the reaction. Also, the active intermediate of the process is an allyl palladium(II)

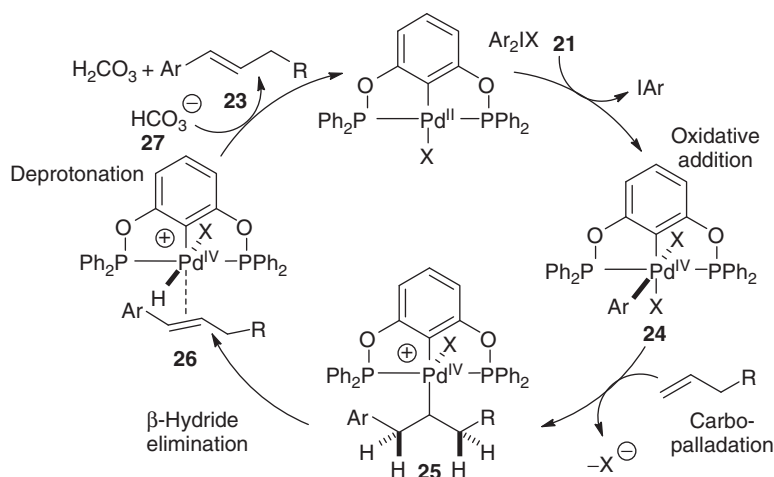


Figure 4.13 Plausible mechanism of the arylation using hypervalent iodines.

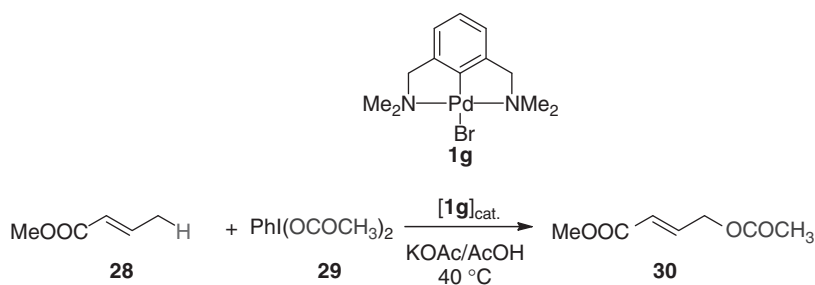


Figure 4.14 C–H acetoxylation with NCN complex **1g**.

species, which is reluctant to undergo reductive elimination without any activator (e.g., BQ). A possible alternative is implementing a Pd(II)/Pd(IV) redox cycle. This can be realized using strong oxidants, such as hypervalent iodine **29**, in the process (Figure 4.14) [50].

The reaction can be performed for a wide range of substrates, such as **28** (Figure 4.14), using Pd(OAc)₂ or the NCN pincer complex **1g** as catalyst. In these procedures, **1g** performs nearly as good as Pd(OAc)₂. However, using the pincer complex catalyst useful mechanistic information can be obtained. When the reaction of **1g** with hypervalent iodine **29** was monitored by ¹H NMR spectroscopy, systematic changes of the NMR shifts were observed. The signals for the CH₂ and CH₃ protons of the side arms of **1b** appeared as singlets resonating at 4.04 and 3.01 ppm, respectively (Figure 4.15). This arises from the fast inversion of the nitrogen atoms of the side arms, lending a time-averaged C_{2v} symmetry to the complex. Addition of **29** to the CDCl₃ solution of **1b** led to a color change from pale yellow to amber. Notable changes in the ¹H NMR spectrum were (i) the splitting of

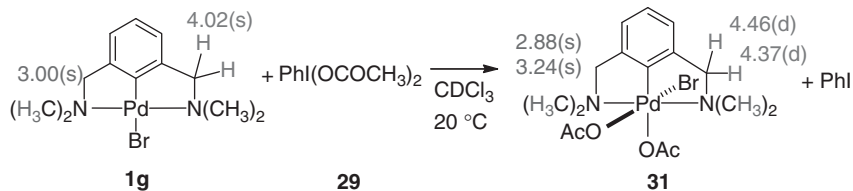


Figure 4.15 Systematic changes of the ^1H NMR shifts of the NCN complex **1g** indicating a Pd(II)-to-Pd(IV) oxidation.

the CH_3 signals into two distinct sharp singlets resonating at 2.88 and 3.24 ppm, and (ii) the emergence of two doublets ($J = 14$ Hz) at 4.46 and 4.37 ppm.

These results suggest that, under the applied catalytic conditions, the palladium atom of the catalyst **1g** is oxidized to Pd(IV) forming complex **31**. Thus pincer complex **1g** proved to be a useful handle for the detection of the Pd(II)-to-Pd(IV) oxidation [47]. Based on the above experiments, a plausible mechanism could be given for the palladium-catalyzed allylic C–H acetoxylation with hypervalent iodines (Figure 4.16) [50]. According to this mechanism, the first step is the oxidation of the Pd(II) atom of **1g** to Pd(IV) to give complex **31** (Figure 4.15). This is followed by coordination of alkene **28** and, via deprotonation, formation of allyl palladium(IV) complex **33**. This complex undergoes reductive elimination without any kind of external activation, as the high oxidation state of palladium can be regarded as an activation method.

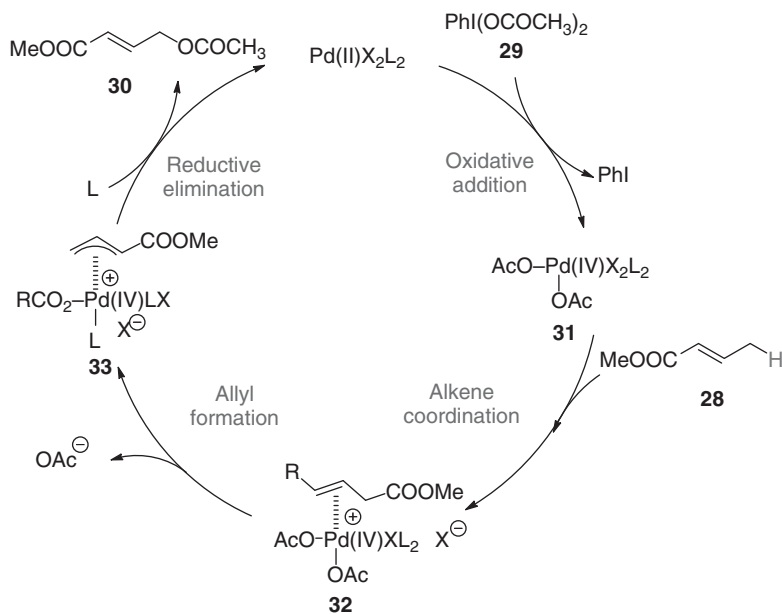


Figure 4.16 Suggested catalytic cycle of the C–H acetoxylation.

4.4.3

C–H Borylation of Alkenes

C–H borylation is a widely used methodology for the synthesis of organoboronates [63–65]. Most of the applications have been presented for the synthesis of arylboronates. However, functionalization of alkenes has also attracted much interest [66, 67]. In most applications, iridium catalysis was used. However, in case of alkenes, borohydride forms as a side product of the C–H borylation, which undergoes hydroboration with alkenes. This side reaction can be avoided using palladium catalysis under oxidative conditions. In a practically useful implementation of this reaction, pincer-complex catalysis (**1g**) was applied (Figure 4.17) [51]. The reaction can be carried out under mild reaction conditions at room temperature using the neat alkene **34** as solvent. In this reaction, hypervalent iodine **36**, the TFA analog of **29**, was employed. In the absence of **36**, borylation reaction did not occur.

The reaction works for both cyclic (**34a–c**) and acyclic (**34d,e**) alkenes (Table 4.5). In most processes, the product is a vinyl boronate (**37a–d**). However, the C–H functionalization of cycloheptene gives allyl boronate **38**. The mild neutral reaction conditions allow the synthesis of silyl and boronate functionalized species **37c,d** as well.

The first step of the reaction is oxidation of the palladium(II) central atom of **1g** to Pd(IV) by **36** (Figure 4.18). This process can be followed by ^1H NMR spectroscopy similar to the acetate analog (Figure 4.15). This step is followed by transmetalation of B_2pin_2 **35** with **37** to give complex **38**, which subsequently undergoes alkene coordination (**39**), insertion (**40**), and reductive deprotonation to give organoboronate **37**.

The reaction is also catalyzed by $\text{Pd}(\text{OAc})_2$ but the yields are much lower than with **1g**. Furthermore, application of the pincer complex **1g** allows the observation of the Pd(II)-to-Pd(IV) oxidation by ^1H NMR monitoring of the systematic changes of the NMR shifts and coupling constants (see Figure 4.15).

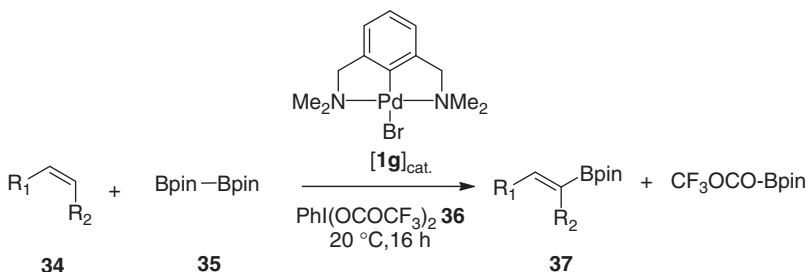

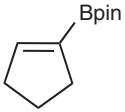

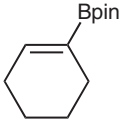

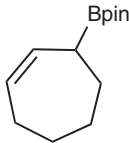
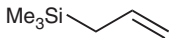
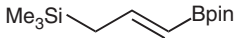
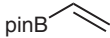
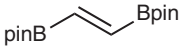


Figure 4.17 C–H borylation with NCN pincer complex **1g**.

Table 4.5 Examples for C–H borylation.

Entry	Substrate	Product	Yield (%)
1	 34a	 37a	73
2	 34b	 37b	61
3	 34c	 38	57
4	 34d	 37c	51
5	 34e	 37d	86

4.5

Summary and Outlook

By this chapter we wished to present some interesting application of palladium pincer complex catalysis for organic synthesis. A clear advantage of using pincer complexes is their well-defined metal/ligand stoichiometry. In particular, for palladium complexes, the integrity of the pincer complex is usually preserved during the catalytic process. This ensures that electronic/steric tuning implemented in the

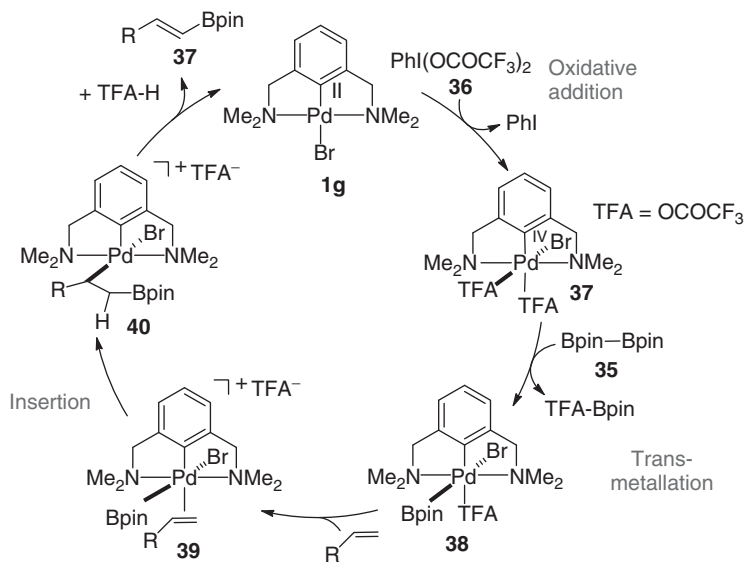


Figure 4.18 Mechanism suggested for the C–H borylation.

pincer ligand is transmitted to the metal atom, the active site of the catalyst, under the entire catalytic process. This is particularly useful for design of new asymmetric catalytic transformations, as shown in Sections 4.2.2 and 4.4.2. Pincer complexes usually decompose when the central atom is reduced to Pd(0), therefore Pd(0)/Pd(II) redox cycle-based transformations cannot be catalyzed by pincer complexes but these species may serve as catalyst precursors. However, the Pd(IV) state of the pincer complexes is stable. Thus, by using strong oxidants, such as hypervalent iodines, a Pd(II)/Pd(IV) redox cycle can be implemented with a preserved pincer complex architecture (Sections 4.4.1 and 4.4.2). In these processes, the pincer complex may serve as useful handle for the ^1H NMR monitoring of the formation of the Pd(IV) species. Pincer complexes have proven to be useful catalysts in C–H functionalization based processes, as shown in Sections 4.3.1, 4.3.2, 4.4.1, and 4.4.2 and diastereoselective synthesis (Section 4.2.1).

In the future applications, we will see generation of new pincer complexes in important application areas of organic synthesis, such as C–H functionalization and C–C and C–B bond-forming reactions. There is still a large unexploited potential for using pincer complexes in asymmetric catalysis. Design of the catalytic processes can be considerably facilitated by the rigid, well-defined structure of the chiral pincer complexes. The development of new catalytic procedures in pincer complex chemistry is, of course, very much dependent on the appearance of new powerful techniques for the synthesis of new pincer architectures. This makes pincer complex catalysis a fruitful interdisciplinary area of organic, organometallic, and inorganic chemistry.

References

- Hartwig, J. (2010) *Organotransition Metal Chemistry*, University Science Books, Sausalito, CA.
- Tsuji, J. (2004) *Palladium Reagents and Catalysts. New Perspectives for the 21st Century*, Wiley-VCH Verlag GmbH, Chichester.
- Morales-Morales, D. and Jensen, C.M. (2007) *The Chemistry of Pincer Compounds*, Elsevier, Amsterdam.
- Choi, J., MacArthur, A.H.R., Brookhart, M., and Goldman, A.S. (2011) *Chem. Rev.*, **111**, 1761.
- Selander, N. and Szabó, K.J. (2011) *Chem. Rev.*, **111**, 2048.
- Albrecht, M. and van Koten, G. (2001) *Angew. Chem. Int. Ed.*, **40**, 3750.
- Gunanathan, C. and Milstein, D. (2011) *Top. Organomet. Chem.*, **37**, 55.
- van der Boom, M.E. and Milstein, D. (2003) *Chem. Rev.*, **103**, 1759.
- Szabó, K.J. (2012) in *Topics in Organometallic Chemistry*, vol. **40** (eds G. van Koten and D. Milstein), Springer, p. 203.
- Pilarski, L.T. and Szabó, K.J. (2011) *Curr. Org. Chem.*, **15**, 3389.
- Eberhard, M.R. (2004) *Org. Lett.*, **6**, 2125.
- Sommer, W.J., Yu, K., Sears, J.S., Ji, Y., Zheng, X., Davis, R.J., Sherrill, C.D., Jones, C.W., and Weck, M. (2005) *Organometallics*, **24**, 4351.
- Stark, M.A. and Richards, C.J. (1997) *Tetrahedron Lett.*, **38**, 5881.
- Longmire, J.M., Zhang, X., and Shang, M. (1998) *Organometallics*, **17**, 4374.
- Schlenk, C., Kleij, A.W., Frey, H., and van Koten, G. (2000) *Angew. Chem. Int. Ed.*, **39**, 3445.
- Williams, B.S., Dani, P., Lutz, M., Spek, A.L., and van Koten, G. (2001) *Helv. Chim. Acta*, **84**, 3519.
- Giménez, R. and Swager, T.M. (2001) *J. Mol. Catal. A*, **166**, 265.
- Motoyama, Y., Kawakami, H., Shimozono, K., Aoki, K., and Nishiyama, H. (2002) *Organometallics*, **21**, 3408.
- Slagt, M.Q., Jastrzebski, J.T.B.H., Gebbink, R.J.M.K., van Ramesdonk, H.J., Verhoeven, J.W., Ellis, D.D., Spek, A.L., and van Koten, G. (2003) *Eur. J. Org. Chem.*, **2003**, 1692.
- Mehendale, N.C., Bezemer, C., van Walree, C.A., Gebbink, R.J.M.K., and van Koten, G. (2006) *J. Mol. Catal.*, **257**, 167.
- Gosiewska, S., Veld, M.H., de Pater, J.J.M., Bruijninx, P.C.A., Lutz, M., Spek, A.L., van Koten, G., and Gebbink, R.J.M.K. (2006) *Tetrahedron: Asymmetry*, **17**, 674.
- Soro, B., Stoccoro, S., Minghetti, G., Zucca, A., Cinellu, M.A., Manassero, M., and Gladiali, S. (2006) *Inorg. Chim. Acta*, **359**, 1879.
- Mehendale, N.C., Sietsma, J.R.A., de Jong, K.P., van Walree, C.A., Klein-Gebink, R.J.M., and van Koten, G. (2007) *Adv. Synth. Catal.*, **349**, 2619.
- Aydin, J., Kumar, K.S., Eriksson, L., and Szabó, K.J. (2007) *Adv. Synth. Catal.*, **349**, 2585.
- Aydin, J., Rydén, A., and Szabó, K.J. (2008) *Tetrahedron: Asymmetry*, **19**, 1867.
- Gosiewska, S., Herreras, S.M., Lutz, M., Spek, A.L., Havenith, R.W.A., van Klink, G.P.M., van Koten, G., and Gebbink, R.J.M.K. (2008) *Organometallics*, **27**, 2549.
- Gagliardo, M., Selander, N., Mehendale, N.C., van Koten, G., Klein-Gebink, R.J.M., and Szabó, K.J. (2008) *Chem. Eur. J.*, **14**, 4800.
- Stark, M.A., Jones, G., and Richards, C.J. (2000) *Organometallics*, **19**, 1282.
- Dijkstra, H.P., Meijer, M.D., Patel, J., Kreiter, R., van Klink, G.P.M., Lutz, M., Spek, A.L., Canty, A.J., and van Koten, G. (2001) *Organometallics*, **20**, 3159.
- Dijkstra, H.P., Slagt, M.Q., McDonald, A., Kruithof, C.A., Kreiter, R., Mills, A.M., Lutz, M., Spek, A.L., Klopper, W., van Klink, G.P.M., and van Koten, G. (2003) *Eur. J. Inorg. Chem.*, **2003**, 830.
- Fossey, J.S. and Richards, C.J. (2004) *Organometallics*, **23**, 367.
- Takenaka, K. and Uozumi, Y. (2004) *Org. Lett.*, **6**, 1833.
- Takenaka, K., Minakawa, M., and Uozumi, Y. (2005) *J. Am. Chem. Soc.*, **127**, 12273.

34. McDonald, A.R., Dijkstra, H.P., Suijkerbuijk, B.M.J.M., van Klink, G.P.M., and van Koten, G. (2009) *Organometallics*, **28**, 4689.
35. Zografidis, A., Polborn, K., Beck, W., Markies, B.A., and van Koten, G. (1994) *Z. Naturforsch., B: Chem. Sci.*, **49**, 1494.
36. Aydin, J. and Szabó, K.J. (2008) *Org. Lett.*, **10**, 2881.
37. Kisanga, P.B. and Verkade, J.G. (2002) *J. Org. Chem.*, **67**, 426.
38. Wallner, O.A. and Szabó, K.J. (2004) *Org. Lett.*, **6**, 1829.
39. Solin, N., Kjellgren, J., and Szabó, K.J. (2003) *Angew. Chem. Int. Ed.*, **42**, 3656.
40. Solin, N., Kjellgren, J., and Szabó, K.J. (2004) *J. Am. Chem. Soc.*, **126**, 7026.
41. Wallner, O.A. and Szabó, K.J. (2006) *Chem. Eur. J.*, **12**, 6976.
42. Szabó, K.J. (2000) *Chem. Eur. J.*, **6**, 4413.
43. Aydin, J., Conrad, C.S., and Szabo, K.J. (2008) *Org. Lett.*, **10**, 5175.
44. Kumagai, N., Matsunaga, S., and Shibasaki, M. (2004) *J. Am. Chem. Soc.*, **126**, 13632.
45. Canty, A.J., Denney, M.C., van Koten, G., Skelton, B.W., and White, A.H. (2004) *Organometallics*, **23**, 5432.
46. Lagunas, M.C., Gossage, R.A., Spek, A.L., and van Koten, G. (1998) *Organometallics*, **17**, 731.
47. Canty, A.J., Rodemann, T., Skelton, B.W., and White, A.H. (2006) *Organometallics*, **25**, 3996.
48. Canty, A.J. (2009) *Dalton Trans.*, 10409.
49. Aydin, J., Larsson, J.M., Selander, N., and Szabó, K.J. (2009) *Org. Lett.*, **11**, 2852.
50. Pilarski, L.T., Selander, N., Böse, D., and Szabó, K.J. (2009) *Org. Lett.*, **11**, 5518.
51. Selander, N., Willy, B., and Szabó, K.J. (2010) *Angew. Chem. Int. Ed.*, **49**, 4051.
52. Vicente, J., Arcas, A., Juliá-Hernández, F., and Bautista, D. (2010) *Chem. Commun.*, 7253.
53. Blacque, O. and Frech, C.M. (2010) *Chem. Eur. J.*, **16**, 1521.
54. Beletskaya, I.P. and Cheprakov, A.V. (2000) *Chem. Rev.*, **100**, 3009.
55. Anton, D.R. and Crabtree, R.H. (1983) *Organometallics*, **2**, 855.
56. Szabó, K.J. (2010) *J. Mol. Catal. A*, **324**, 56.
57. Hansson, S., Heumann, A., Rein, T., and Åkermark, B. (1990) *J. Org. Chem.*, **55**, 975.
58. Grennberg, H., Simon, V., and Bäckvall, J.-E. (1994) *J. Chem. Soc., Chem. Commun.*, 265.
59. Chen, M.S. and White, M.C. (2004) *J. Am. Chem. Soc.*, **126**, 1346.
60. McDonald, R.I., Liu, G., and Stahl, S.S. (2011) *Chem. Rev.*, **111**, 2981.
61. Popp, B.V. and Stahl, S.S. (2007) *Top. Organomet. Chem.*, **22**, 149.
62. Covell, D.J. and White, M.C. (2013) *Tetrahedron*, **69**, 7771.
63. Szabó, K.J. (2013) in *Cross Coupling and Heck Type Reactions 2* (ed J.P. Wolfe), Thieme, p. 485.
64. Mkhaliid, I.A.I., Murphy, J.M., Barnard, J.H., Marder, T.B., and Hartwig, J.F. (2010) *Chem. Rev.*, **110**, 890.
65. Hartwig, J.F. (2012) *Acc. Chem. Res.*, **45**, 864.
66. Olsson, V.J. and Szabó, K.J. (2008) *Org. Lett.*, **10**, 3129.
67. Olsson, V.J. and Szabó, K.J. (2007) *Angew. Chem. Int. Ed.*, **46**, 6891.

5

Nickel-Catalyzed Cross-Coupling Reactions

Anubendu Adhikary and Hairong Guan

5.1

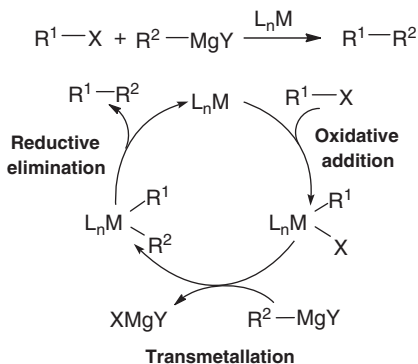
Introduction

Transition-metal-catalyzed cross-coupling reactions represent one of the most versatile and commonly utilized methods for the construction of carbon–carbon and carbon–heteroatom bonds. Their importance in modern organic synthesis has been highlighted by the 2010 Nobel Prize in Chemistry, which was awarded jointly to Heck, Negishi, and Suzuki for their pioneering contributions to the development of palladium-catalyzed C–C cross-coupling reactions. While palladium remains the metal of choice for catalyzing most of this type or related transformations, in recent years there has been intense interest in designing nickel-based catalysts for various cross-coupling reactions. If the cost of ligand is not overwhelmingly high and if the activity of a nickel catalyst can rival that of a palladium catalyst, the benefit of employing the former becomes obvious: nickel is significantly less expensive and more abundant than palladium. For the coupling of alkyl halides bearing β -hydrogens in particular, nickel catalysts are usually better choices because the key intermediates, nickel-alkyl species, are less prone to β -hydrogen elimination [1, 2]. In addition, one-electron process is more prevalent for nickel complexes, providing unique catalytic pathways that may not be readily accessible with the palladium analogs. A number of reviews and perspective articles have appeared in the literature emphasizing the new development of nickel-catalyzed cross-coupling reactions [3–8]. Coinciding with the advancement in this emerging field, the past decade has seen an explosive growth in pincer and pincer-type complexes as excellent catalysts for a wide range of synthetic applications. This chapter, therefore, will be focused specifically on cross-coupling reactions promoted by nickel pincer complexes and their derivatives. Special attention will be paid to the mechanistic aspects of these reactions. For the convenience of discussion, this chapter is organized according to the classification of different cross-coupling reactions.

5.2 Carbon–Carbon Bond-Forming Reactions

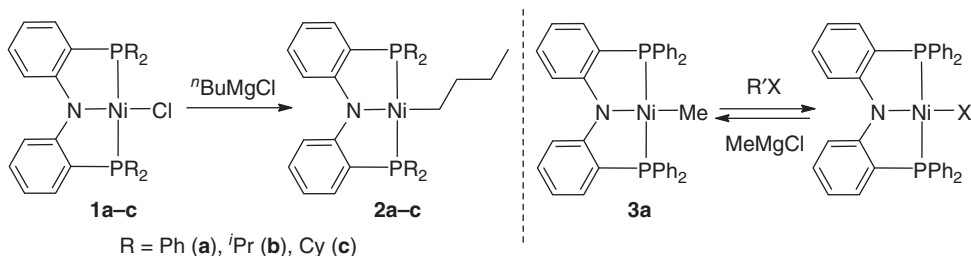
5.2.1 Kumada–Corriu–Tamao Coupling

The coupling of an aryl or alkyl halide with a Grignard reagent is among the earliest known cross-coupling reactions. Although it was dated back to a 1941 study by Kharasch and Fields showing that FeCl_3 , NiCl_2 , and, especially, CoCl_2 catalyzed the reaction of aryl Grignard reagents and organic halides [9], the more synthetically useful protocols were concurrently developed by the research groups of Corriu [10] and Kumada [11] in the early 1970s. Interestingly, the original Kumada–Corriu–Tamao coupling reactions were actually catalyzed by nickel complexes, namely $\text{Ni}(\text{acac})_2$ (acac, acetylacetonate) and $\text{Ni}(\text{dppe})\text{Cl}_2$ (dppe, 1,2-bis(diphenylphosphino)ethane). However, because of the high reactivity of Grignard reagents, for much of the modern history of cross-coupling reactions, Kumada–Corriu–Tamao coupling was not a preferred strategy for making C–C bonds as far as functional group tolerance was concerned [12]. Lowering the reaction temperature could render Grignard reagents compatible with more functional groups but make it more challenging for an organic halide to undergo oxidative addition (Scheme 5.1). Nevertheless, in the past a few years, significant progress has been made in developing highly active nickel systems for Kumada–Corriu–Tamao reactions, many of which use nickel pincer complexes and in some cases really showcase the advantages of employing such catalysts.



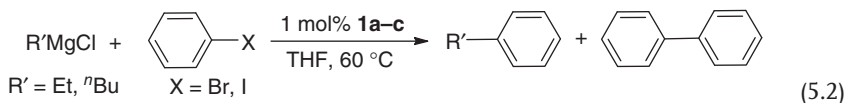
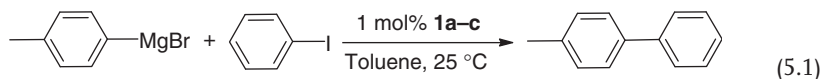
Scheme 5.1 A general mechanism for metal-catalyzed Kumada–Corriu–Tamao coupling reactions.

In 2003, Liang and coworkers [13] synthesized the nickel complex **2a** bearing a tridentate amido diphosphine ligand (known as a *PNP-pincer ligand*) from the corresponding chloride complex **1a** and $^n\text{BuMgCl}$ (Scheme 5.2). The isolation of this nickel alkyl species is notable, as β -hydrogen elimination to yield a nickel hydride complex might have been anticipated. Even more remarkable, similar complexes **2b** and **2c** (in benzene) are stable at 80°C for at least 3 days [14].



Scheme 5.2 Synthesis and reactivity of nickel PNP-pincer complexes.

Mixing the nickel methyl complex **3a** with various organic halides generates nickel halide complexes, suggesting that C–C bond formation can be carried out in a catalytic manner. Indeed, complexes **1a–c** are all excellent catalysts for Kumada–Corriu–Tamao coupling of *p*-tolylmagnesium bromide with PhI (Eq. (5.1)). Unfortunately, for the coupling of alkyl Grignard reagents, substantial amounts of homocoupling products (close to 50%) have been observed (Eq. (5.2)). Attempts to use alkyl halides as electrophiles have not been successful either; only 10% of the starting materials are converted to the cross-coupling products. In any case, the employment of alkyl nucleophiles in this case is noteworthy and may have influenced the later development of other nickel pincer catalysts for this type of cross-coupling reactions.



In 2008, Zargarian *et al.* [15] prepared several diphosphine-derived PCP-type pincer complexes of nickel (Figure 5.1) and explored their catalytic application to the coupling of MeMgCl and PhCl in tetrahydrofuran (THF). In the presence of 0.5 mol% **4b** under refluxing conditions, toluene can be obtained in 42% gas chromatography (GC) yield (84 turnovers). By comparison, compound **4d** with more bulky ^tBu substituents is less reactive and compound **5b** with an aromatic pincer backbone is almost inactive. Mechanistic study of the catalytic process suggests that nickel methyl species is the resting state of the catalysis. Exactly

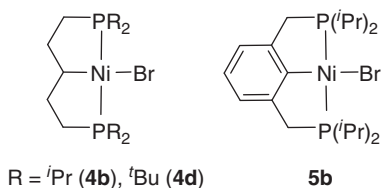
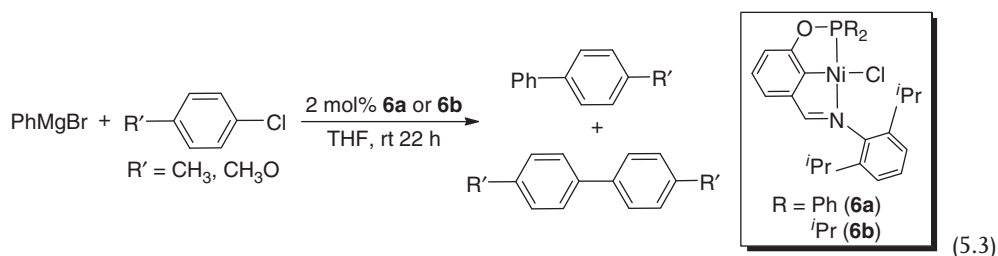


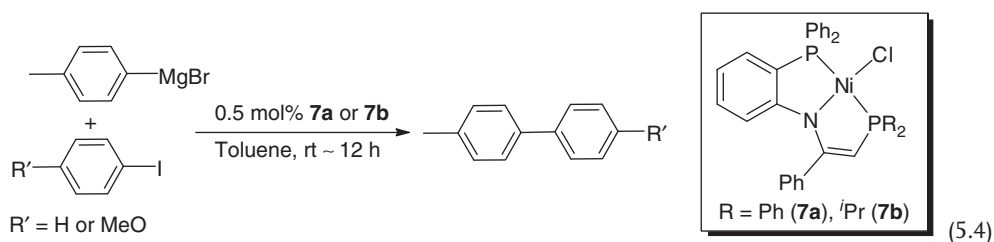
Figure 5.1 Diphosphine-derived nickel PCP-pincer complexes.

how the C–C bond is formed, or whether a Ni(IV) intermediate is ever involved in the reaction, remains uncertain. The relative catalytic activity of these pincer complexes, however, correlates nicely with the order of electron richness of the metal centers (**4b** > **4d** > **5b**), as measured by their oxidation potentials from cyclic voltammetry data. For the reaction catalyzed by **4b** or **4d**, a small amount of Ph–Ph has also been detected, implying that a radical intermediate may be involved in the catalytic process. More recently, the Zargarian group [16] has examined the catalytic activity of a bis(phosphinite)-based POCOP-type pincer complex (1 mol% loading) for Kumada–Corriu–Tamao coupling reactions. Similarly, mixtures of cross-coupling and homocoupling products have been obtained.

Xia and coworkers [17] have recently demonstrated that nickel complexes with an iminophosphinite-based pincer ligand catalyze the coupling of PhMgBr and aryl chlorides. The ⁱPr-substituted complex **6b** is more reactive than **6a** (Eq. (5.3)), which has been explained by the higher donor ability of P(ⁱPr)₂ as compared to PPh₂. In the presence of either catalyst, however, the expected cross-coupling products are contaminated with homocoupling byproducts, with an approximately 8 : 1 ratio favoring the former.



Shortly after Liang's report [14] on the PNP-pincer system, Wang and Wang [18] demonstrated that nickel complexes supported by a nonsymmetric amido diphosphine ligand were effective catalysts for the coupling of aryl Grignard reagents and aryl halides to form C_{sp²}–C_{sp²} bonds. When aryl iodides are employed as the coupling partners and the complex **7a** or **7b** is used as a catalyst (0.5 mol% loading), quantitative formation of the products can be observed within 12 h (Eq. (5.4)). These complexes also catalyze the coupling of more challenging substrates such as PhCl and *p*-MeOC₆H₄Cl, but a higher catalyst loading (2.5 mol%) is needed to achieve high yields. Generally speaking, complex **7b** is more active than **7a** in catalyzing the coupling of aryl chlorides, although their reactivity difference in promoting the reaction of aryl iodides is not obvious.



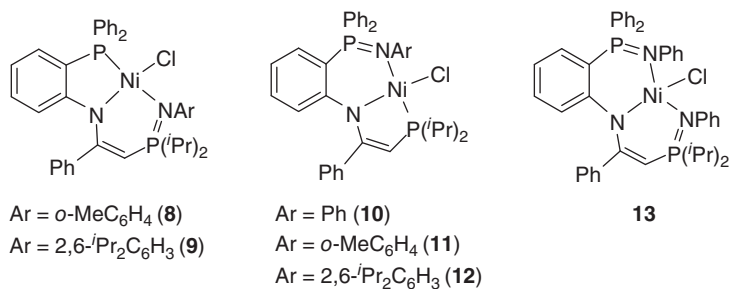


Figure 5.2 Phosphininimine-based nickel pincer complexes.

In the same study [18], phosphininimine–phosphine pincer complexes **8–12** and a bis(phosphininimine)-based pincer complex **13** (Figure 5.2) were tested for catalytic coupling of *p*-MeC₆H₄MgBr and *p*-RC₆H₄I (R = H or MeO). These pincer complexes are far more reactive than any of the amido diphosphine-based pincer complexes mentioned above (**1a–c**, **7a–b**). Especially in the case of **13**, the catalyst loading can be lowered to 0.005 mol%. Interestingly, for the coupling of *p*-MeC₆H₄MgBr and PhCl, complex **13** shows comparable activity to **7b**, **8**, and **12**, but lower activity than **9–11**, which cannot be straightforwardly rationalized.

Further structural modifications have been made to these amido diphosphine- or phosphininimine-based nickel pincer complexes to tune the catalytic activity. Complexes **14–19** depicted in Figure 5.3 represent a new class of pincer complexes lacking the enamine moiety that is characteristic of complexes **8–13** [19]. The reactivity order in coupling *p*-MeC₆H₄MgBr with *p*-MeOC₆H₄I (0.005 or 0.01 mol% catalyst) is **14** ~ **17** > **19** > **16** ~ **18**. When PhCl is used as the coupling partner for *p*-MeC₆H₄MgBr (2 or 4 mol% catalyst), the reactivity order is somewhat different:

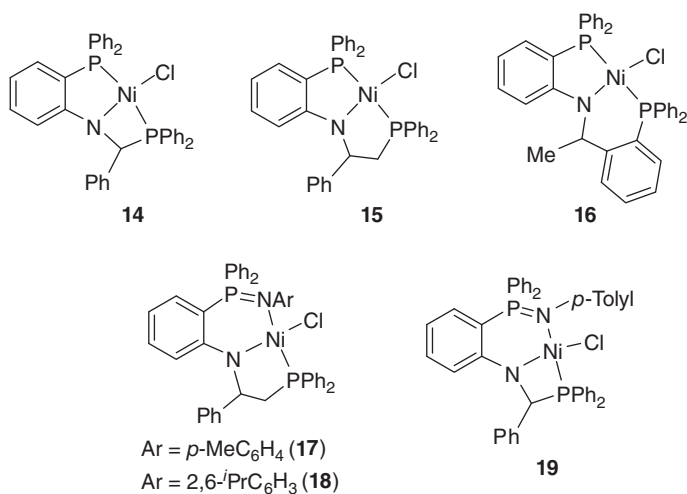


Figure 5.3 Different phosphine- or phosphininimine-based nickel pincer complexes.

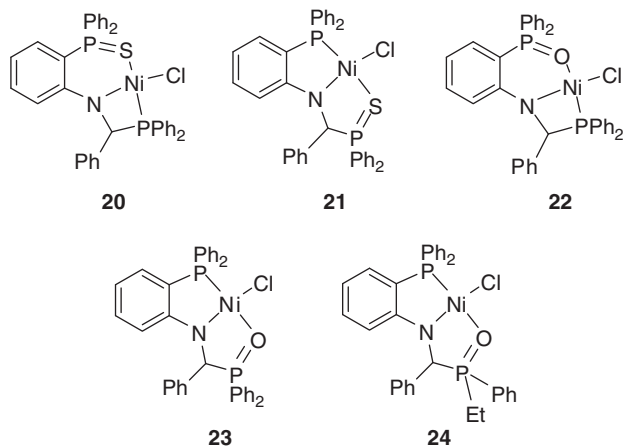
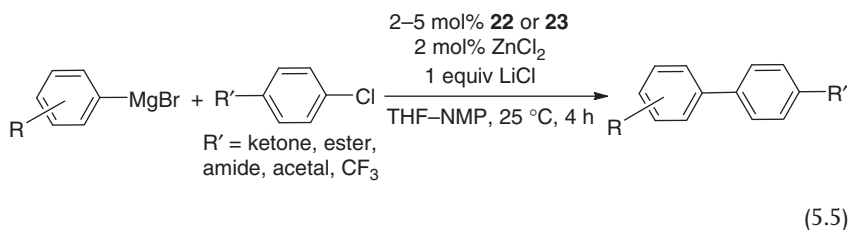


Figure 5.4 Nickel pincer complexes bearing a phosphine oxide or phosphine sulfide.

15 ~ 17 ~ 19 > 14 > 18 > 16. Explaining the reactivity differences is not an easy task; however, the large chelate ring in complex **16** and the sterically demanding phosphinimine aryl group in complex **18** appear to consistently decrease the efficiency of the catalysts.

A more recent report from the Wang group [20] has focused on derivatives of complex **14** featuring phosphine oxide or phosphine sulfide donors. Comparing their catalytic performance in coupling $p\text{-MeC}_6\text{H}_4\text{MgBr}$ with PhCl reveals that the PNO pincer complexes **22–24** are more active than the PNS pincer complexes **20** and **21** (Figure 5.4) [21]. The higher catalytic activity of **22–24** has been attributed to the more facile dissociation of the Ni–O bond (than the Ni–S bond) to create the necessary vacant coordination site for catalysis. With these PNO-pincer complexes, the scope of the electrophiles has been further expanded to heteroaryl and alkenyl chlorides. Using LiCl as an additive, ZnCl_2 as a co-catalyst, and THF–NMP (NMP, *N*-methyl-2-pyrrolidone) as a mixed solvent, this research group has demonstrated that even aryl chlorides bearing Grignard-sensitive functionalities are acceptable substrates (Eq. (5.5)). With added ZnCl_2 , whether these reactions should still be categorized as Kumada–Corriu–Tamao coupling or, instead, they should be called Negishi coupling is debatable.



Phosphine oxides and nitrones are isoelectronic with each other (Figure 5.5) and, therefore, an OCO-type nickel pincer complex such as **25** is closely related to the

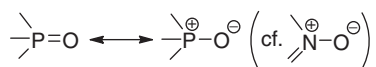
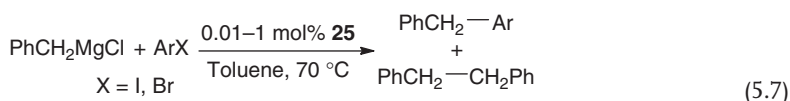
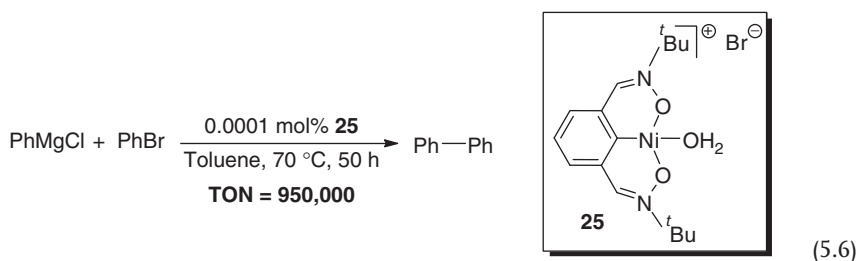


Figure 5.5 Nitrones being isoelectronic with phosphine oxides.

PNO-pincer complexes [22]. For the coupling of PhMgCl and PhBr, an impressively high turnover number of 950 000 has been achieved using only 0.0001 mol% catalyst **25** (Eq. (5.6)). The same compound also catalyzes the coupling of other aryl bromides or PhCl with aryl Grignard reagents very effectively. However, for the coupling of PhCH₂MgCl, in addition to the desired PhCH₂Ar, 6–9% of the final products are PhCH₂CH₂Ph (Eq. (5.7)). Of particular interest is that this homocoupling byproduct originated from the Grignard reagent rather than the electrophile as described in Eq. (5.2), suggestive of a different mechanistic pathway.



Recent interests in *N*-heterocyclic carbenes (NHCs) have prompted several research groups to synthesize NHC-derived nickel pincer complexes for various catalytic applications. Cationic NHC-based nickel pincer complexes **26–28** (Figure 5.6) have been reported to have good catalytic activity in coupling ArMgBr with aryl chlorides [23]. For the room temperature reaction involving PhCl, 1 mol% catalyst is sufficient, whereas for the more challenging substrates *p*-MeOC₆H₄Cl and *o*-MeC₆H₄Cl, 2 or 4 mol% catalyst is needed to ensure high yields, and in some cases a higher temperature of 80 °C is also required. The CNN-pincer complexes

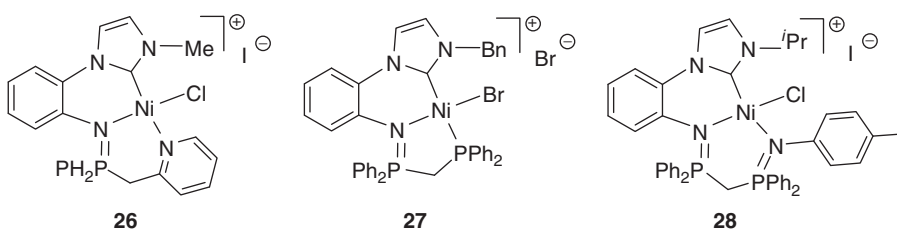
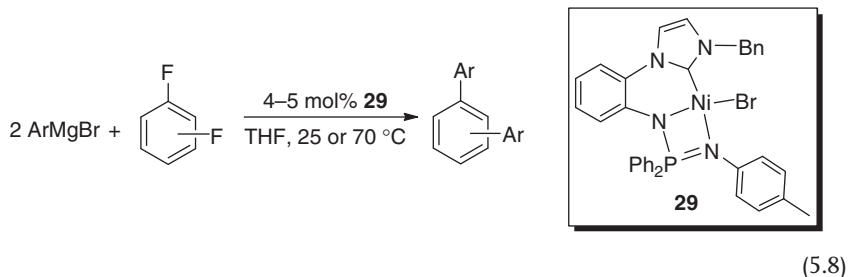
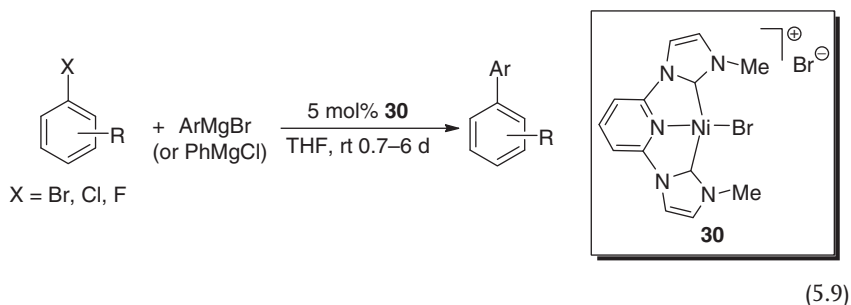


Figure 5.6 Cationic nickel pincer complexes bearing *N*-heterocyclic carbene and phosphinimine moieties.

26 and 28 are slightly more reactive than the CNP-pincer complex 27, which has been rationalized by the higher tendency of N-based pincer arms to dissociate from the nickel centers. A related *neutral* CNN-pincer complex 29 is much more reactive than these cationic complexes but comparable to PNO nickel complexes 22 and 23 [24]. A wide variety of aryl Grignard reagents and aryl chlorides can be used for cross-coupling reactions and the catalytic system is compatible with functional groups such as CN, NEt_2 , and OMe. Aryl fluorides are also viable electrophiles, although the catalyst loading is typically in the range of 2–5 mol% compared to 0.5–1 mol% for the coupling of aryl chlorides (Eq. (5.8)).



Nickel pincer complexes containing NHC donors but *without* the phosphinimine moiety have also been developed as catalysts for Kumada–Corriu–Tamao reactions. Inamoto and coworkers [25] have reported that cross-coupling of *p*-MeC₆H₄Br and PhMgBr (or PhMgCl) can be catalyzed by 0.1–5 mol% bis(carbene)-based nickel pincer complex 30. However, at least 10% of the products are identifiable as the homocoupling byproduct Ph–Ph. This specific catalytic system is applicable to various aryl bromides, chlorides, and fluorides, and tolerant to functional groups such as OMe, CF₃, OTBS, TBS (*tert*-butyldimethylsilyl acetal), and pyridyl ring (Eq. (5.9)). In contrast, NH₂ and OH groups interfere with the cross-coupling reactions.



The Chen group [26] has recently synthesized nickel complex 31 (Figure 5.7) with an NHC-tethered phenanthroline ligand. They have hypothesized that the NHC donor would increase the electron density at the nickel center while the phenanthroline unit could easily dissociate one of the N donors (presumably the outer one) to create a vacant coordination site, thereby facilitating the catalysis. This compound has proven to be a good catalyst (1 mol% loading) for the coupling of aryl chlorides

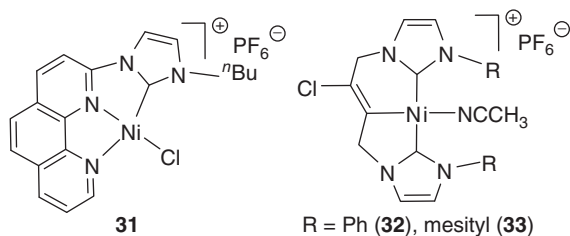


Figure 5.7 N-heterocyclic carbene ligated nickel pincer complexes.

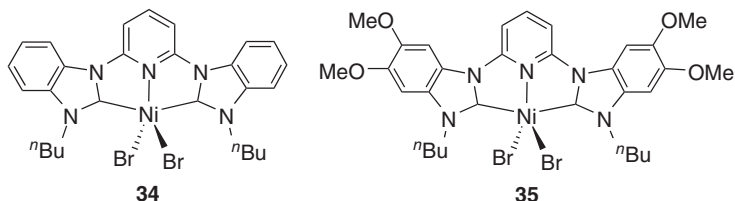


Figure 5.8 Five-coordinate nickel pincer complexes bearing a dicarbene ligand.

with $p\text{-MeC}_6\text{H}_4\text{MgBr}$ at room temperature. Substrates bearing CN, OMe, pyridyl, and pyrimidinyl groups have been successfully tested for the catalytic reactions. The same research group has also prepared the nickel pincer complexes **32** and **33** (Figure 5.7) via chloronickelation of an alkyne linking two NHC units [27]. These catalysts show better reactivity than **31** in aryl–aryl coupling; 0.5 mol% catalyst is usually sufficient to reach full conversion of the starting materials. In the case of coupling $p\text{-FC}_6\text{H}_4\text{Cl}$ with $p\text{-MeC}_6\text{H}_4\text{MgBr}$, C–C bond formation takes place at both halogenated sites.

Another NHC-based nickel pincer system involves five-coordinate nickel complexes with a bis(benzimidazol-2-ylidene)pyridine ligand (Figure 5.8). The corresponding four-coordinate cationic complexes (analogous to **31**) have been synthesized via salt metathesis, but catalysis-wise they do not offer any advantages [28]. Complexes **34** and **35** have showed moderate catalytic activity (5 mol% loading) for the coupling of aryl bromides and chlorides with PhMgBr or $p\text{-MeC}_6\text{H}_4\text{MgCl}$ at 30 °C. The GC yields for these reactions are less than 60%, mainly due to homocoupling of the Grignard reagents. Complex **34** is slightly more reactive than complex **35**, but neither of them is as efficient as the bis(imidazol-2-ylidene)pyridine complex **30**.

For all the catalytic systems discussed so far, the mechanistic details are not well understood. It is generally agreed that oxidation of the nickel center should be a critical step in nickel-catalyzed cross-coupling reactions, and therefore an electron-rich metal center would be ideal for catalysis. As argued by some of the studies [20, 23], facile dissociation of one of the pincer arms could be equally important. Degradation of Ni(II) pincer complexes to the more active Ni(0) species is also possible, and may be necessary, although there is no definitive evidence suggesting that this is the case for any of the reactions mentioned above. Moreover,

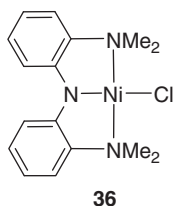
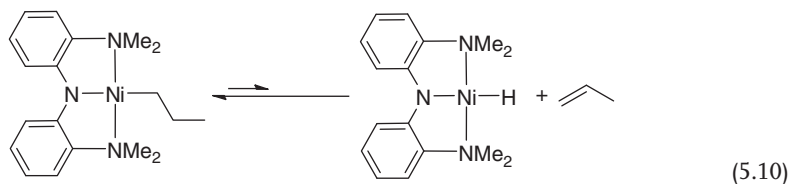


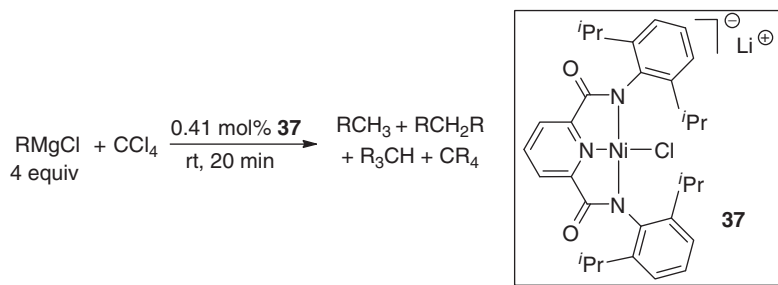
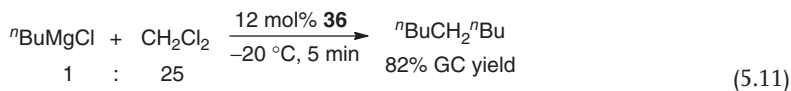
Figure 5.9 Amido bis(amine)-ligated nickel pincer complex.

it is not unreasonable to propose a Ni(II)/Ni(IV) catalytic cycle, given the fact that Ni(IV) complexes are known in the literature [29].

Replacing the phosphorous or NHC donors with relatively hard amine donors can potentially stabilize Ni(IV) intermediates and promote the catalytic reactions, if indeed they are involved in catalytic cycles. Guided by this hypothesis, Hu *et al.* [30] have designed a nickel catalyst **36** (Figure 5.9) with an amido bis(amine) (NNN-pincer) ligand. Viewed as potential intermediates of Kumada–Corriu–Tamao reactions, various nickel alkyl (or aryl) complexes have been isolated from the reaction between **36** and Grignard reagents including those containing β -hydrogens. A later study has revealed that the stability is a result of the thermodynamics and not kinetics [31]. The β -hydrogen elimination from a nickel propyl complex to generate a nickel hydride species is reversible, and the equilibrium predominantly lies on the side of the former (Eq. (5.10)). In any case, these alkyl complexes react with alkyl halides readily to release molecules with newly formed $C_{sp^3}-C_{sp^3}$ bonds and regenerate **36** (or its derivatives with other halides), proving the principle that cross-coupling reactions can be done catalytically with **36**.

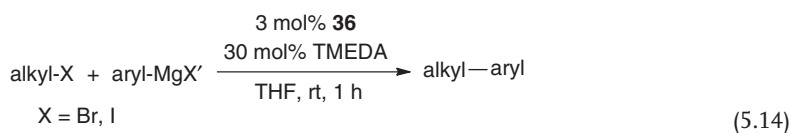
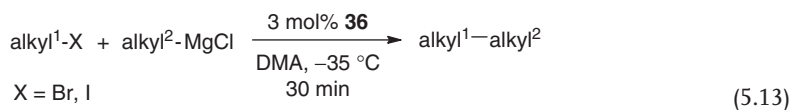


The initial catalytic study of **36** was focused on dual coupling of $n\text{BuMgCl}$ to CH_2Cl_2 (Eq. (5.11)), which gives rise to $n\text{BuCH}_2n\text{Bu}$ [30]. This catalytic system is also applicable to other linear-chain alkyl magnesium chlorides as well as $(\text{CH}_3)_2\text{CHCH}_2\text{MgCl}$, but not very effective for secondary and tertiary alkyl Grignard reagents [32]. The catalytic reaction with PhCH_2MgCl does not lead to the cross-coupling product but to the homocoupling product $\text{PhCH}_2\text{CH}_2\text{Ph}$. Interestingly, coupling of Ph_2CCL_2 with MeMgCl catalyzed by 3 mol% **36** generates $\text{Ph}_2\text{C}=\text{CPh}_2$ in 70% yield, suggesting that a radical mechanism is operative. One of the potential applications for this type of reactions is to convert halogenated wastes to less toxic non-halogenated chemicals. As demonstrated in a recent study by Ghosh *et al.* [33], an anionic NNN-pincer complex **37** catalyzes the cross-coupling of Grignard reagents and CCl_4 (or CHCl_3 , CH_2Cl_2) with turnover frequencies as high as 724 h^{-1} (Eq. (5.12)).



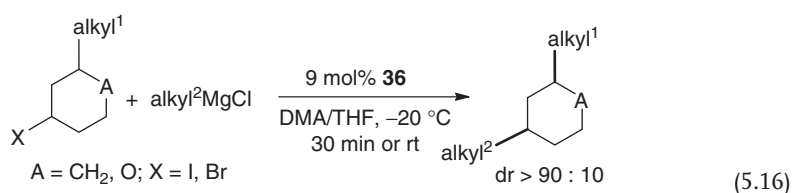
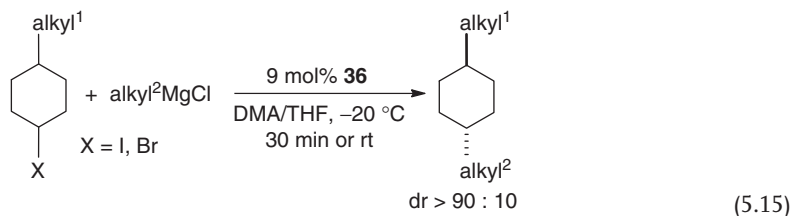
(5.12)

The more synthetically useful application is for the coupling of nonactivated, functionalized alkyl halides with Grignard reagents. The Hu group [32, 34] has shown that a diverse array of primary alkyl iodides and bromides can be successfully coupled to primary alkyl Grignard reagents at $-35\text{ }^\circ\text{C}$ (Eq. (5.13)) when dimethylacetamide (DMA) is used as the solvent and 3 mol% **36** is employed as catalyst. The low temperature provides high compatibility with sensitive functionalities such as chloride, ester, amide, nitrile, thioether, acetal, heterocycle, and ketone. A hydroxy group can also be tolerated, although one extra equivalent of Grignard reagent is needed as a sacrificial reagent. The results for allylic and benzylic halides or α -halocarbonyl compounds, on the other hand, are unsatisfactory. Coupling of alkyl halides with aryl Grignard reagents under the same conditions is problematic too, producing the cross-coupling products in low yields. However, replacing the solvent DMA with THF and adding 30 mol% tetramethylethylenediamine (TMEDA) or 60 mol% bis(2-dimethylaminoethyl) ether (O-TMEDA) drastically improves the yields (Eq. (5.14)) [35]. Under the modified catalytic conditions, even functionalized aryl Grignard reagents can be used to couple with a wide range of alkyl iodides and bromides.

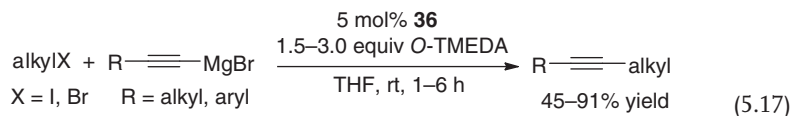


It should be mentioned that both protocols work well with a variety of primary alkyl iodides and bromides, but with a very limited number of secondary alkyl halides. The reaction of secondary alkyl iodides such as $i\text{PrI}$, 3-iodopentane, and

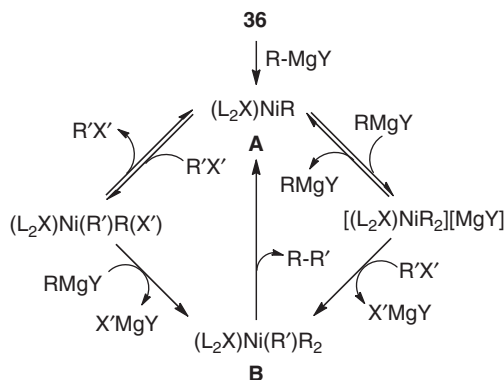
iodocyclopentane with ${}^n\text{C}_8\text{H}_{17}\text{MgCl}$ (or ${}^n\text{BuMgCl}$) produces negligible or low yields of cross-coupling products, although Hu and coworkers [36] have solved this problem by using a non-pincer-based catalytic system. In contrast to these secondary alkyl halides, catalytic reactions involving cyclohexyl iodides or bromides or analogous substituted tetrahydropyrans are not only high yielding but also highly diastereoselective (Eqs (5.15) and (5.16)) [37]. A radical pathway has been proposed to explain the high selectivity for *trans*-1,4- and *cis*-1,3-disubstituted products as well as the observation that diastereoselectivity is independent of the *cis/trans* ratios of the starting materials.



The Hu group [38] has further extended this chemistry by investigating the cross-coupling of primary alkyl iodides and bromides with alkynyl Grignard reagents catalyzed by **36** (Eq. (5.17)). Electrophiles including primary alkyl chlorides and secondary alkyl iodides (e.g., iodocyclohexane) are not viable coupling partners for this methodology. Once again, high functional group tolerance has been observed. Of particular note is the successful coupling of substrates bearing a thioether moiety, which can be an issue for the alternative Sonogashira coupling reactions.



All the experimental evidence for the NNN-pincer system is consistent with a generalized mechanistic scheme illustrated in Scheme 5.3. The interaction between **36** and a Grignard reagent leads to the rapid formation of a nickel alkyl, aryl, or alkynyl species **A**. In a number of the aforementioned studies [30, 32, 35, 38], these types of intermediates have been synthesized independently and have proven to be catalytically competent. From **A**, an alkyl halide $\text{R}'\text{X}'$ and a Grignard reagent RMgY can add to the nickel center in either order, resulting in an intermediate **B** which is formally a Ni(IV) species unless the pincer ligand (L_2X) is redox active.



Scheme 5.3 Mechanism for Kumada-Corriu-Tamao coupling reactions catalyzed by **36**.

Reductive elimination of the cross-coupling product from **B** regenerates the catalyst **A** and closes the catalytic cycle. The activation of an alkyl halide proceeds via single-electron transfer (SET) followed by the combination of a nickel-centered radical and an organic radical, which has been supported by radical clock experiments and the diastereoselective alkyl–alkyl coupling reactions shown in Eqs (5.15) and (5.16). The role of amine additives (TMEDA and O-TMEDA), however, remains unclear. It has been suggested that the coordination of the additives to Mg increases the nucleophilicity of Grignard reagents and may also help to stabilize functionalized Grignard reagents.

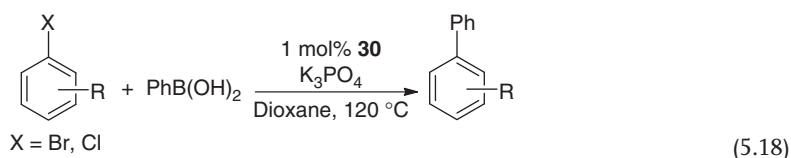
5.2.2

Suzuki–Miyaura Coupling

Suzuki–Miyaura coupling reaction is one of the most useful strategies to form C–C bonds, especially for the synthesis of biaryl compounds. The high availability, high air and moisture stability, and low toxicity of organoboron compounds make this method very attractive for both industrial and laboratory use. In contrast to well-developed palladium-catalyzed Suzuki–Miyaura coupling reactions, application of nickel complexes for this specific catalytic process is relatively unexplored. Several nickel-based systems such as Ni(dppe)Cl₂/phosphine [39], Ni(COD)₂/PCy₃ (COD, 1,5-cyclooctadiene) [40, 41], and Ni(PCy₃)₂Cl₂ [42, 43] have been developed to catalyze Suzuki–Miyaura-type reactions. Despite these advancements, there is much room for improvement, particularly on increasing the catalytic efficiency so that the catalyst loading can be further reduced from the typical level of 5 or 10 mol%. The use of pincer complexes can potentially address this issue, as demonstrated in many other types of cross-coupling reactions.

The Inamoto group [25, 44] has reported the first study of nickel pincer-catalyzed Suzuki–Miyaura reactions. In the presence of 1 mol% **30**, aryl bromides and activated aryl chlorides can be coupled with PhB(OH)₂ to generate the desired

diaryl products in high yields (Eq. (5.18)). For the reaction of *p*-BrC₆H₄CN, an activated aryl bromide, the catalyst loading can be reduced to 0.1 mol% without sacrificing the yield. Functional groups such as nitrile, ester, ketone, silyl ether, NH₂, and heterocycle are tolerated under the reaction conditions. Compared to **30**, the mixture of Ni(acac)₂ and pyridine-linked bis(imidazolium) salt does not show any catalytic activity, clearly highlighting the importance of having a presynthesized pincer complex as the catalyst.



Further modification of the catalyst structure has been made by introducing different substituents on NHCs or by expanding the chelate ring size from five to six (Figure 5.10). Complexes **38–41** are all efficient catalysts (1 mol%) for the coupling of aryl bromides and chlorides with arylboronic (or alkenylboronic) acids (Eq. (5.19)) [45]. Complexes with two five-membered metallacycles (**38** and **39**) are more active catalysts than those with two six-membered metallacycles (**40** and **41**). Crystal structures of these nickel pincer complexes suggest that the nickel centers in **38** and **39** are more crowded, which is expected to favor the reductive elimination step. Surprisingly, when aryl tosylates are used in place of aryl halides as the electrophiles, complexes **40** and **41** become better catalysts than **38** and **39** as well as the methyl-substituted complex **30** [46]. This has been explained as due to the change in the rate-determining step of the catalytic cycle, the details of which, however, remain to be uncovered. Nevertheless, the Suzuki–Miyaura coupling of aryl tosylates with various arylboronic or alkenylboronic acids can be smoothly catalyzed by 5 mol% **40** in dimethoxyethane (DME) at 120 °C in a sealed tube. The scope of the electrophiles has been expanded to activated alkenyl tosylates as shown in Eq. (5.20). Coupling of aryl mesylates is more challenging, which often gives low yields under the same catalytic conditions. Fortunately, switching the solvent from DME to dioxane improves the catalytic efficiency significantly and allows several

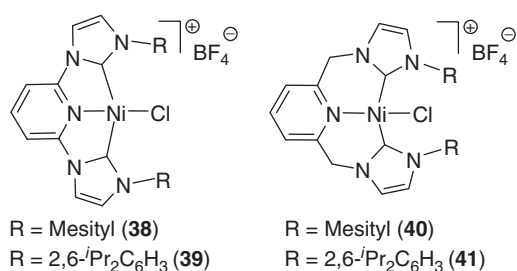
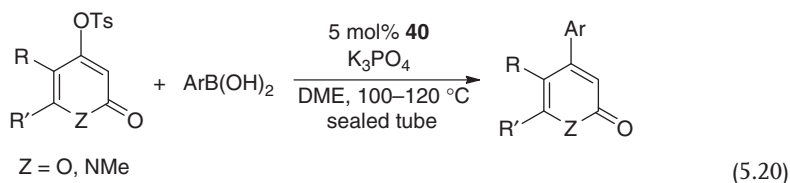
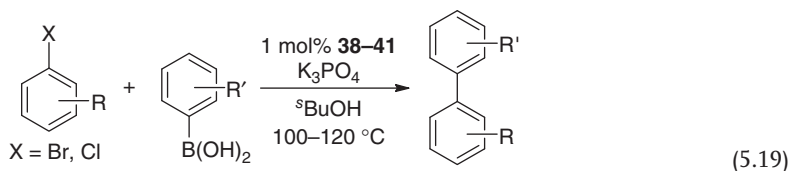
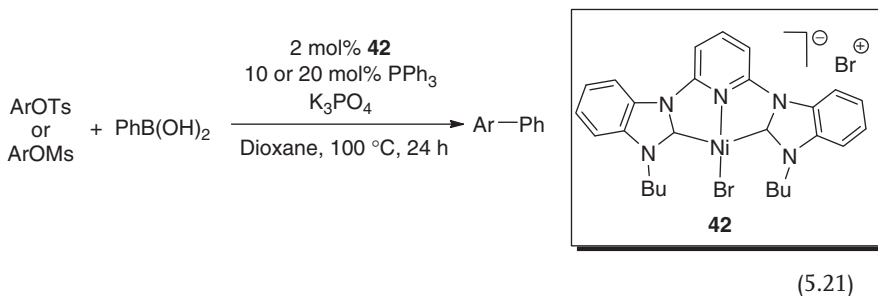


Figure 5.10 Carbene-based nickel CNC-pincer complexes.

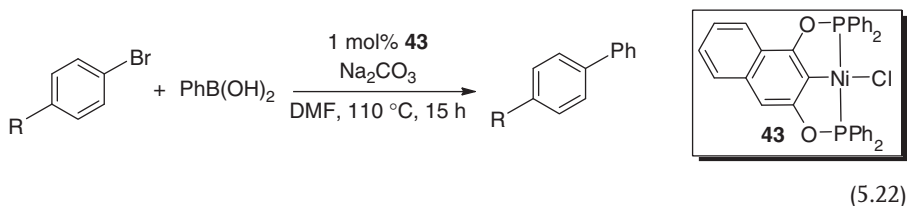
aryl mesylates to be coupled with different boronic acids.



Tu *et al.* [47] have reported a more active nickel pincer catalyst **42** (Eq. (5.21)), derived from pyridine-linked bis(benzimidazolium) bromide, for the Suzuki–Miyaura coupling of aryl tosylates and mesylates. The hypothesis is that the benzimidazole-based NHCs are stronger σ -donors and weaker π -acceptors than the imidazole-based NHCs, and therefore can promote catalytic reactions through the increase of electron density at the nickel center. The coupling of aryl tosylates and mesylates with $\text{PhB}(\text{OH})_2$ is thus accomplished with 2 mol% **42** combined with a catalytic amount of PPh_3 . The same protocol can also apply to the coupling of aryl bromides and chlorides. The role of added PPh_3 has been identified as a way to suppress the unwanted homocoupling process.



Beyond NHC-based nickel pincer systems, the Morales-Morales group [48] has examined the catalytic capability of bis(phosphinite)-based nickel pincer complex **43** in the cross-coupling of $\text{PhB}(\text{OH})_2$ and aryl bromides with varying electronic properties (Eq. (5.22)). As one might anticipate, substrates with electron-withdrawing groups ($\text{R} = \text{NO}_2$, CN , COCH_3 , CHO , and Cl) lead to higher conversions than those with electron-donating groups ($\text{R} = \text{CH}_3$, OCH_3 , and NH_2). The possibility of nanoparticles (released from catalyst degradation) catalyzing the reactions has been ruled out on the basis of a negative mercury test.

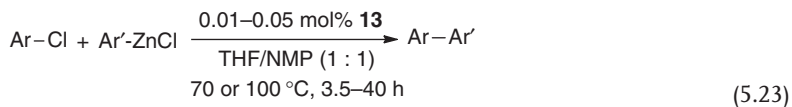


5.2.3

Negishi Coupling

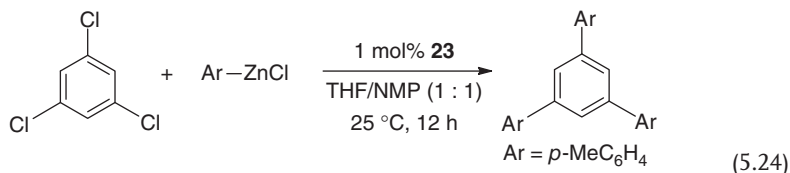
Organozinc reagents are much milder nucleophiles than their corresponding Grignard and organolithium reagents, making Negishi coupling one of the more attractive C–C bond-forming reactions when functional group tolerance is considered. Compared to Suzuki–Miyaura (or Hiyama) coupling, Negishi coupling does not require a Lewis or Brønsted base, which could erode stereoselectivity in asymmetric cross-coupling reactions. Not surprisingly, Negishi coupling has been the subject of intensive studies while exploring the catalytic applications of nickel pincer or pincer-like complexes.

As part of the efforts to develop efficient nickel catalysts for various cross-coupling reactions, the Wang group has shown that phosphinimine-derived or related nickel pincer complexes **7–13** [49] and **26–28** [23] catalyze the coupling of aryl chlorides and arylzinc chlorides at 70 °C. Using the coupling of PhZnCl and *p*-Me₂NC₆H₄Cl as the benchmark reaction [49], complexes **11** and **13** have proven to be more active than **7–10** and **12**. The cationic NHC-based complexes **26–28** also appear to be less reactive than **11** and **13**, judging by the catalyst loading required for a number of reactions. In all cases, reactivity trends for different substrates are the same; the Negishi reaction is favored by electron-deficient electrophiles (Ar–Cl) and electron-rich nucleophiles (Ar′–ZnCl). An ortho substituent on either substrate leads to a slower catalytic reaction. Catalytic reactions promoted by **13** are generally conducted with 0.01–0.05 mol% catalyst, and functional groups such as ester, amide, ether, amine, and ketone are tolerated (Eq. (5.23)). Substrates containing nitrile groups or heteroaromatic rings (e.g., furan) can be used as well, but they require a higher catalyst loading (>0.2 mol%) and in a few cases a high temperature (100 °C), possibly due to the coordination of heteroatoms to the nickel center. Substrates bearing NO₂ or CHO groups fail to react and form cross-coupling products. A mechanism analogous to the one shown in Scheme 5.1 has been proposed by the authors, and the oxidative addition of Ar–Cl has been postulated to take place at a Ni(I) center following the reduction of the starting Ni(II) complexes with organozinc reagents.

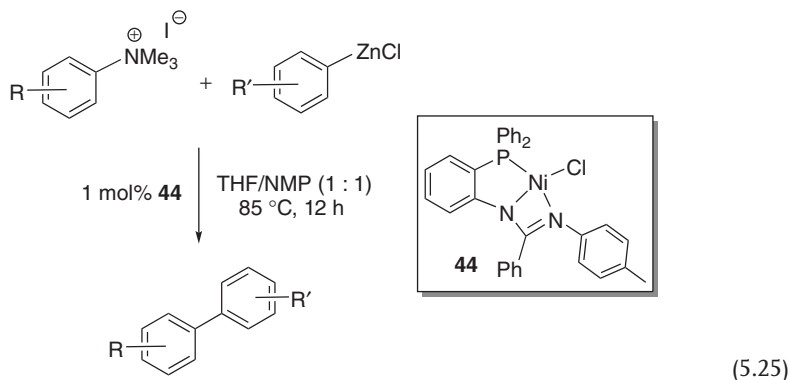


Compared to these phosphinimine-derived nickel pincer complexes, the PNS- and PNO-pincer complexes **20–24** show much higher activity, as Negishi coupling

reactions can be performed at room temperature [20]. The PNO-pincer systems are more effective than the PNS pincer systems, and give similar reactivity order as observed in Grignard reactions (Eq. (5.5)). The catalyst loading is in the 0.02–5 mol% range depending on the structures of the substrates, and the scope of the catalytic reactions is comparable to that of phosphinimine-based pincer systems. As a representative example, 1,3,5-trichlorobenzene has been successfully coupled with *p*-MeC₆H₄ZnCl at ambient temperature using 1 mol% **23** (Eq. (5.24)).



A very recent study from the Wang group [50] has focused on the coupling of aryl zinc chlorides with aryl ammonium salts, which are more challenging substrates for cross-coupling reactions but offer new opportunities for C–C bond formation. After some catalyst screening, they concluded that the PNN-pincer complex **44** can effectively catalyze the Negishi coupling of aryl ammonium salts to produce various diaryl compounds (Eq. (5.25)). The effects of counter anions have been examined, and halides work better than weak coordinating anions such as BF₄[−] and TfO[−]. The latest development in this chemistry has involved quinoline-based nickel catalysts **45**–**48** (Figure 5.11), among which complex **46** is the most active one for the catalytic reaction between aryl ammonium salts and ArZnCl [51]. This five-coordinate nickel complex, however, does not appear to perform better than the four-coordinate pincer complex **44** in terms of catalytic efficiency.



Bis(oxazoline)pyridine (Pybox) and terpyridine (terpy) belong to the family of tridentate ligands that are often excluded from the discussions on pincer chemistry. However, recent studies have shown that in some cases they are redox-active [52, 53] and exhibit properties closely resembling those of pincer ligands. Thus, cross-coupling reactions catalyzed by nickel complexes containing these ligands are also discussed in this chapter.

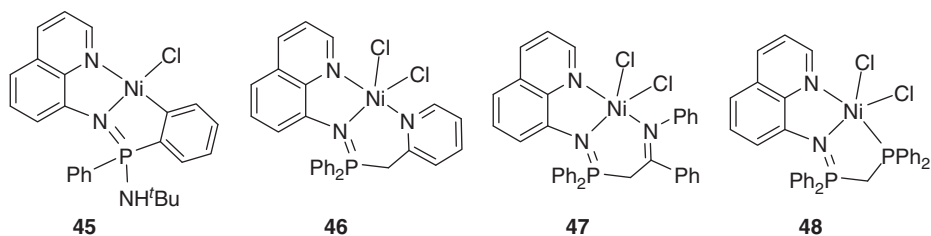
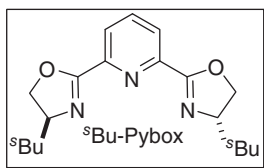
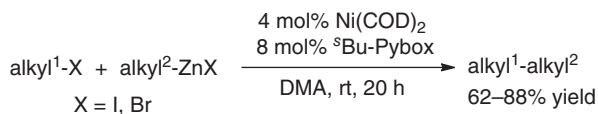


Figure 5.11 Quinoline-based nickel pincer complexes.

Since 2003, the Fu group has published a series of papers involving Negishi coupling of various organic halides with a special interest in forming $C_{sp^3}-C_{sp^3}$ bonds. Their initial study dealt with the cross-coupling of primary and secondary alkyl halides with alkylzinc halides [54]. An extensive catalyst optimization has revealed that $Ni(COD)_2$ mixed with 2 equiv of sBu -Pybox catalyze the targeted Negishi reactions in good yields (Eq. (5.26)). Functional groups tolerated in this particular catalytic system include sulfonamide, ether, acetal, ester, amide, imide, and ketone. Later on, efforts were directed to addressing the issue of enantioselectivity during the coupling of secondary alkyl species. For different electrophiles, fine-tuning of the catalytic conditions (nickel precursor, catalyst loading, Pybox ligand, solvent, and temperature) led to the formation of Negishi coupling products in high yields and high enantioselectivity. As summarized in Figure 5.12, a diverse array of activated electrophiles including α -bromo amides [55], α -bromo ketones [56], benzylic halides [57], allylic chlorides [58], and propargylic compounds [59, 60] are all viable substrates for highly enantioselective Negishi coupling reactions. All these processes are stereo-convergent, meaning that both enantiomers of the electrophile are converted to the same product. As expected, many functional groups are tolerated, illustrating the broad utility of this methodology.



(5.26)

The alkyl nucleophiles used in the reactions shown in Eq. (5.26) and Figure 5.12 are all prepared from primary alkyl halides. Similar reactions with *secondary* alkylzinc reagents are more difficult, not only because of the increased steric hindrance but also because of the possibility for a secondary metal-alkyl species to undergo isomerization. For the coupling of propargylic electrophiles specifically,

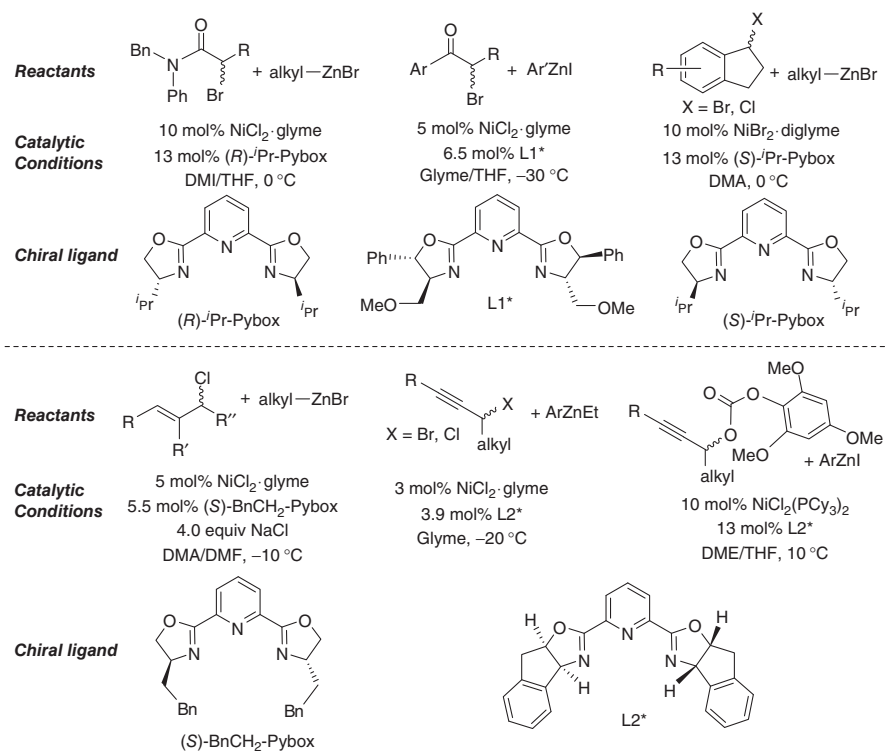
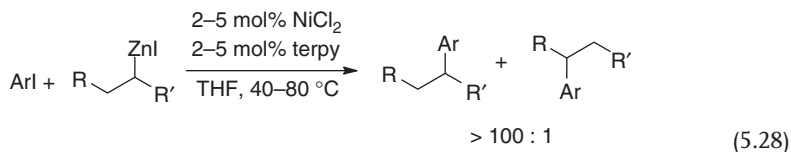
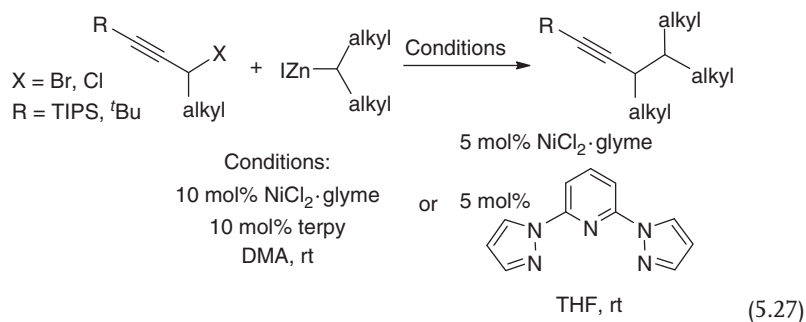


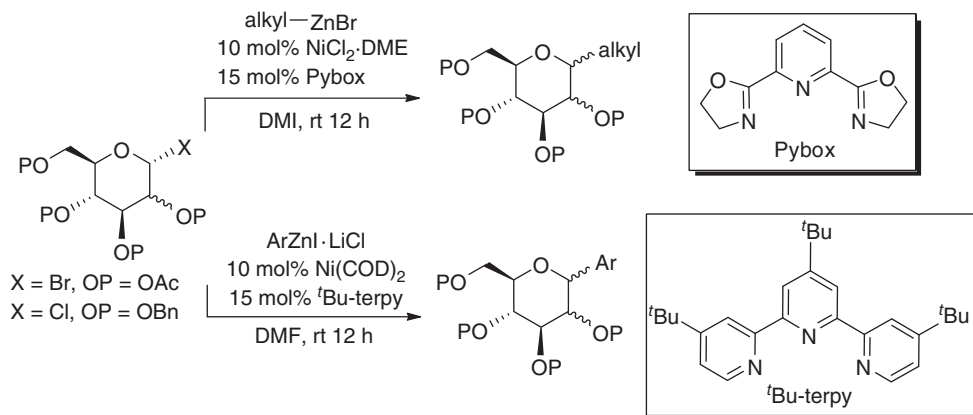
Figure 5.12 Nickel-catalyzed enantioselective Negishi coupling reactions.

the Fu group [61] has solved this problem by employing $\text{NiCl}_2 \cdot \text{glyme}$ and *terpy* (or 2,6-bis(*N*-pyrazolyl)pyridine for sterically more demanding substrates) as the catalytic mixture (Eq. (5.27)). Functional group tolerance for this method is high. For example, an unactivated alkyl chloride moiety is unaffected by the catalytic conditions. The Biscoe group [62] has also examined the cross-coupling of secondary alkylzinc reagents using aryl iodides as the electrophiles, instead. After considerable screening, they identified $\text{NiCl}_2/\text{terpy}$ in THF as the optimal catalyst system for the Negishi coupling reactions (Eq. (5.28)). Functional groups tolerated under the catalytic conditions include aldehyde, ester, phenol, aniline, alkyne, heterocycle, and boronic ester. The extent of alkyl isomerization during the reactions is minimal, reflecting the ability of the ligand to maintain the meridional configuration throughout catalysis.



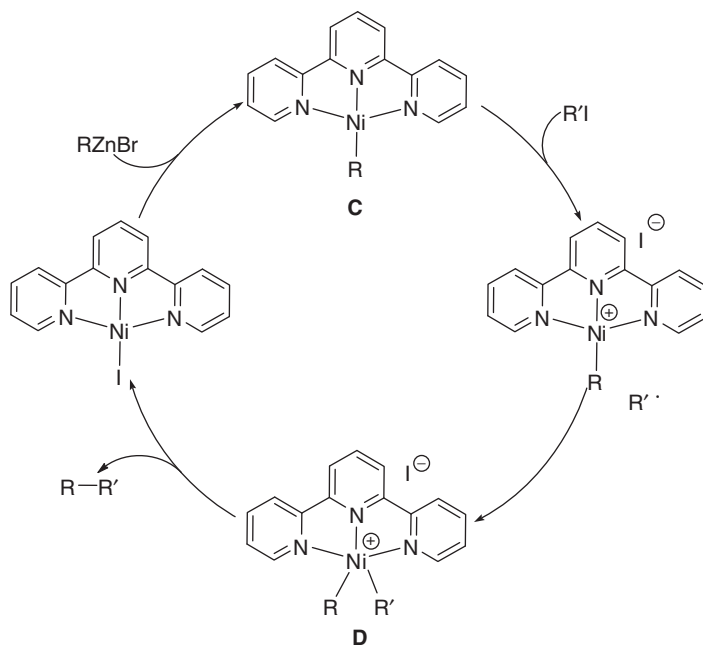
A further synthetic application of nickel-catalyzed Negishi reactions has been demonstrated by Gagné and coworkers for the synthesis of *C*-alkyl [63] and *C*-aryl glycosides [64] from acetate-protected α -bromo or benzyl-protected α -chloro sugars. For the coupling of alkylzinc bromides, $\text{NiCl}_2 \cdot \text{DME}$ with the unsubstituted PyBox ligand in DMI (*N,N'*-dimethylimidazolidinone) works the best at the catalytic conditions, whereas for arylation reactions $\text{Ni}(\text{COD})_2/{}^t\text{Bu-terpy}$ in dimethylformamide (DMF) proves to be a more effective catalytic system (Scheme 5.4). The competing β -OP and β -H elimination processes are negligible for most substrates. The diastereoselectivity observed in these reactions is substrate- and catalyst-dependent. Moderate to high α -selectivity has been obtained for *C*-mannosides in both alkylation and arylation reactions. In contrast, the formation of *C*-glucosides catalyzed by $\text{Ni}(\text{COD})_2/{}^t\text{Bu-terpy}$ often leads to the β -anomers.

The mechanisms for Negishi reactions catalyzed by a Ni(0) or Ni(II) species combined with a *terpy*- or Pybox-type ligand warrant some discussion. If the conventional cross-coupling mechanism (similar to the one shown in Scheme 5.1)

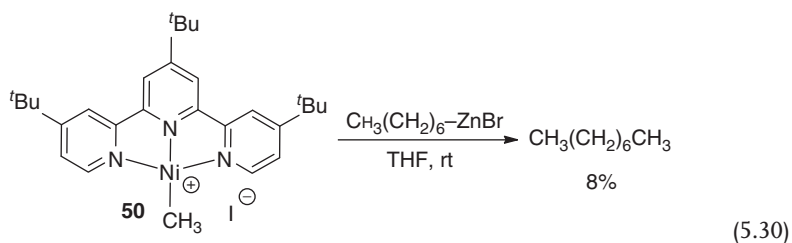
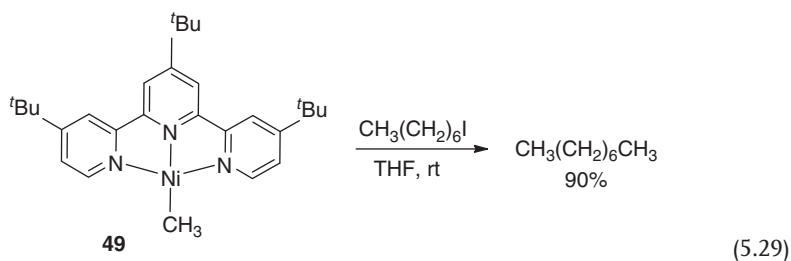


Scheme 5.4 Nickel-catalyzed Negishi cross-coupling approach to C-glycosides.

is operative here, a Ni(0)/Ni(II) catalytic cycle is expected. An alternative mechanism analogous to what Hu has proposed for Kumada–Corriu–Tamao coupling (Scheme 5.3) would invoke a Ni(II)/Ni(IV) catalytic cycle. In contrast to both mechanistic scenarios, Vicic *et al.* [65] have shown that mixing $\text{Ni}(\text{COD})_2$ with terpy (or ${}^t\text{Bu-terpy}$) and CH_3I (or EtI) produces $(\text{terpy})\text{NiI}$, for which the formal oxidation state of nickel is +1. This complex and nickel methyl complex **49** are active catalysts for Negishi coupling reactions forming $\text{C}_{\text{sp}^3}\text{--C}_{\text{sp}^3}$ bonds, suggesting that they may be involved in the catalytic cycle [66]. A stoichiometric reaction between **49** and 1-iodoheptane produces octane in 90% yield (Eq. (5.29)). Interestingly, the reaction between the cationic Ni(II) complex **50** and heptylzinc bromide gives octane in only 8% yield (Eq. (5.30)), implying that this transmetalation step is not catalytically relevant. These results, along with radical clock experiments and the observed homocoupling byproducts, have led to a mechanistic proposal illustrated in Scheme 5.5 [52]. An important implication is that intermediate **C** (or **49**), as confirmed by electron paramagnetic resonance (EPR) and density functional theory (DFT) studies, is a Ni(II) species with a reduced terpy ligand. Therefore, the subsequent reaction with $\text{R}'\text{I}$ appears to be a ligand-based reduction process, generating an organic radical that can potentially undergo dimerization or radical isomerization prior to its combination with the nickel center. Reductive elimination of the cross-coupling product from the resulting intermediate **D** generates $(\text{terpy})\text{NiI}$, which can close the cycle by reacting with an organic zinc reagent. The essential steps of this mechanism have been successfully modeled by DFT calculations [67], although there are some variations for the mechanism. For instance, the interaction between **C** and $\text{R}'\text{I}$ can occur through an inner-sphere iodine abstraction rather than an SET process. A similar computational study of Pybox-based chiral systems has supported the same reaction pathway [68]. The stereo-convergence observed in those asymmetric Negishi reactions can be easily rationalized, as the same radical species should be generated from both enantiomers.

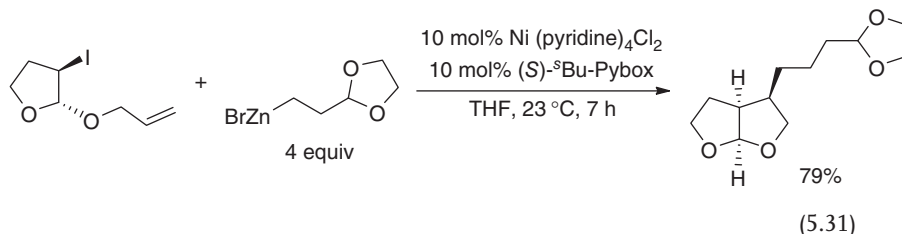


Scheme 5.5 Catalytic cycle for Negishi reactions catalyzed by terpy-ligated nickel complexes.



This radical mechanism can be exploited for cascade catalysis if the rate of radical cyclization (or other rearrangement reactions) for R^{\bullet} is significantly faster than the rate of R^{\bullet} attack on nickel. Cárdenas and coworkers [53] have proved this concept

by developing nickel-catalyzed cyclization/cross-coupling reactions of iodoalkanes with alkylzinc bromides. In addition to the example shown in Eq. (5.31), iodoalkanes with different ring structures as well as the acyclic ones can be incorporated into the synthesis. They have also calculated the structure of Me-Pybox nickel-methyl complex and have found a similar electronic structure as proposed by Vicić [52] for the (terpy)NiCH₃ complex.

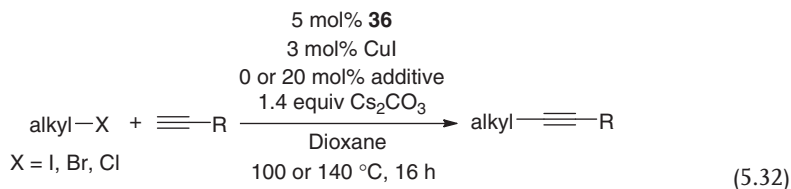


5.2.4

Sonogashira Coupling

Coupling of aryl or alkenyl halides with terminal alkynes, the Sonogashira reaction, is one of the most widely used methods for the synthesis of substituted alkynes [69]. The use of nickel complexes to catalyze such a transformation is surprisingly scarce. Beletskaya *et al.* [70] have reported that Ni(PPh₃)₂Cl₂ and CuI co-catalyze the cross-coupling of aryl iodides and aryl-substituted acetylenes. The catalytic system shows moderate activity (5 mol% Ni and 5 mol% Cu) with a limited substrate scope. Nickel particles (~100 nm) also exhibit some catalytic activity (10 mol%) for the Sonogashira coupling of aryl or alkenyl halides with various terminal alkynes [71].

Hu's NNN-pincer complex **36** is the only nickel pincer system that we are aware of for Sonogashira coupling reactions [72]. This compound shows excellent reactivity in catalyzing the coupling between primary alkyl halides and alkynes with high functional group tolerance (Eq. (5.32)). For the reaction of alkyl bromides and chlorides, a catalytic amount of an iodide salt (NaI or ⁿBu₄NI) is needed as an additive, which presumably undergoes Br/I or Cl/I exchange before the cross-coupling reaction takes place. The proposed mechanism is similar to the one proposed for Kumada–Corriu–Tamao coupling (Scheme 5.3) except that a nickel-alkynyl complex rather than a nickel alkyl species is the key intermediate.

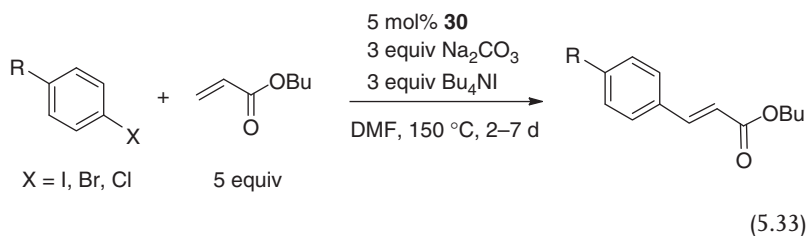


5.2.5

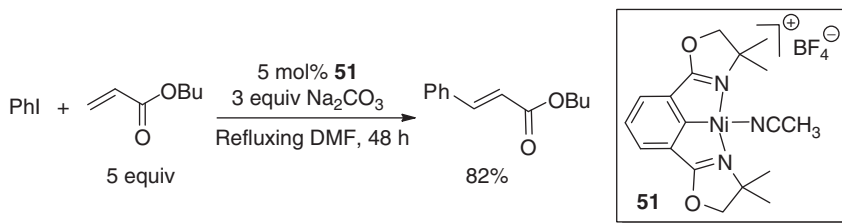
Mizoroki–Heck Reaction

Coupling of aryl or alkenyl halides (or pseudohalides) with olefins, the Mizoroki–Heck reaction, is another useful method for generating a new C–C bond. The main steps of the catalytic cycle are oxidative addition of aryl or alkenyl halides, insertion of olefins, and the subsequent β -hydride elimination. This type of cross-coupling reactions is generally carried out using palladium catalysts, but several nickel catalysts such as $\text{Ni}(\text{COD})_2/\text{dppf}$ [73, 74], $\text{Ni}[\text{P}(\text{OR})_3]_4$ ($\text{R} = \text{Ph}, \text{Et}$) [75], $\text{Ni}(\text{COD})_2/\text{PCy}_{3-x}\text{Ph}_x$ ($x = 1, 2$) [76], and $\text{Ni}(\text{PPh}_3)_4/\text{dppp}$ (dppp , 1,3-bis(diphenylphosphino)propane) [77, 78] have also been reported. The success of nickel pincer complexes in alkyl–alkyl coupling reactions has a lot to do with the reluctance of nickel–alkyl species to undergo β -hydride elimination, which becomes an indispensable step in Mizoroki–Heck reactions. Nevertheless, there have been two studies in the literature using nickel pincer complexes for Mizoroki–Heck reactions.

The Inamoto group [44] has reported that the NHC-based pincer complex **30** is an effective catalyst for the cross-coupling of aryl halides and butyl acrylate (Eq. (5.33)). This catalytic system is applicable to aryl iodides, aryl bromides, and activated aryl chlorides, and compatible with functional groups including nitrile, ketone, and aldehyde. Notably, the reaction of 4-bromobenzonitrile can be retarded by a drop of mercury, suggesting that the catalytic system may be heterogeneous.



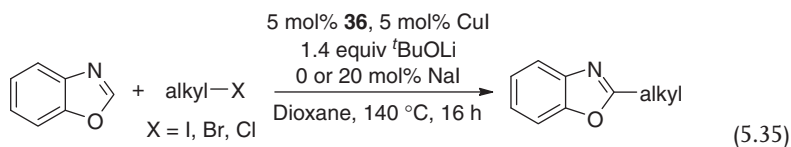
Mitsudo, Tanaka, and coworkers [79] have reported an air-stable cationic bis(oxazoline)-based nickel pincer complex **51** as a catalyst for the coupling of phenyl iodide and butyl acrylate (Eq. (5.34)). Stopping the reaction after 24 h gives the cross-coupling product in 25% yield, which is less than half of the yield for a 48 h reaction. This indicates an induction period during the catalytic reaction, possibly due to the conversion of **51** to a true catalytic species.



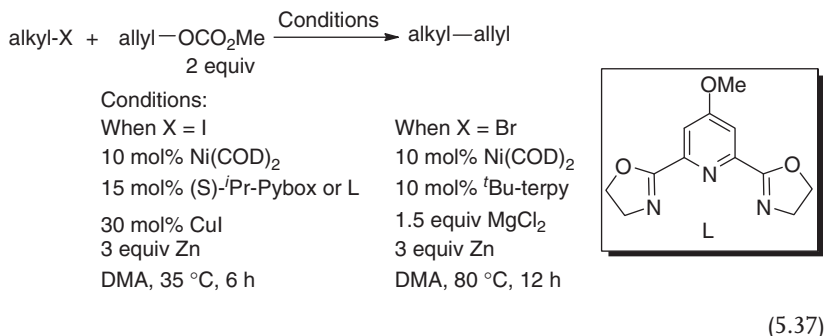
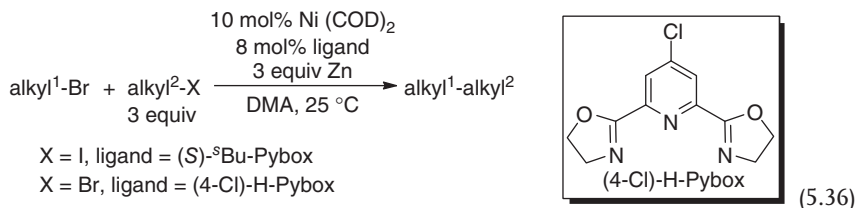
5.2.6

Other Miscellaneous Cross-Coupling Reactions

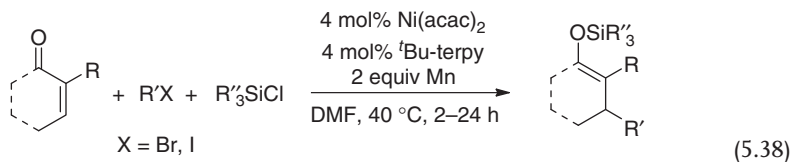
The Hu group [80] has extended the catalytic application of complex **36** to the coupling of heterocyclic compounds with various primary alkyl halides. The best catalytic conditions involve 5 mol% **36** and 5 mol% CuI with excess ^tBuOLi as a base in dioxane (Eq. (5.35)). Cross-coupling reactions take place without CuI, but if added, the yields for these reactions will improve. For the coupling of alkyl bromides and chlorides, 20 mol% NaI is also needed, possibly converting them to the more reactive alkyl iodides. A broad range of functional groups including aryl chloride, ether, thioester, nitrile, acetal, olefin, ester, ketone, indole, carbazole, and furan show no interference with the C–C bond-forming reaction. Other oxazoles as well as thiazole- and thiophene-based heterocyclic substrates can also be used by this method. Mechanistic investigations have revealed two important pieces of information: (i) heterocyclic substrates are deprotonated and transferred to nickel, and (ii) catalytic reactions are heterogeneous and inhibited by elemental mercury.



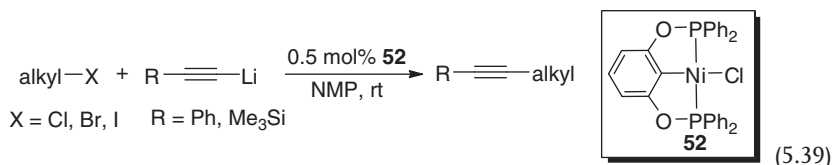
Another type of cross-coupling reactions worth mentioning is the reductive coupling of two different alkyl halides without converting one of them to an organometallic species. The real challenge is to minimize the formation of homocoupling products. With carefully chosen substrates and judicious choice of ligand, the Gong group [81] has been able to directly couple two unactivated alkyl halides in moderate yields (Eq. (5.36)). For almost all the examples presented, a secondary alkyl bromide and a large excess of a primary alkyl halide were chosen for the cross-coupling reactions. One might imagine that organozinc reagents can be generated *in situ* and therefore the reactions illustrated in Eq. (5.36) are simply a variation of Negishi reactions already demonstrated by Fu [54]. However, such a possibility has been ruled out on the basis of the observation that the Negishi reactions are not kinetically competitive. More recently, Gong *et al.* [82] have reported the reaction between alkyl iodides or bromides and allylic carbonates with various substitution patterns using slightly modified procedures (Eq. (5.37)). Likewise, the reaction of a pregenerated alkyl-ZnX with an allylic carbonate is too slow to account for the cross-coupling reactions shown in Eq. (5.37), thereby arguing against a Negishi-type mechanism. The role of zinc is believed to reduce Ni(I) and Ni(II) intermediates to lower oxidation states.



A closely related system has been reported by Weix *et al.* [83] for the cross-coupling of RX (R = aryl, alkyl; X = I, Br) and allylic acetates bearing a wide variety of functional groups. The best catalytic conditions have been identified as 5 mol% NiCl₂(DME)/^tBu-terpy with 2 equiv of Zn in THF/NEP (3:1) (NEP, N-ethylpyrrolidinone) at 40 °C. The same research group has also developed a method for the synthesis of silyl enol ethers from reductive conjugate addition of alkyl bromides or iodides to enones (Eq. (5.38)) [84]. Mechanistic studies have suggested that Mn serves as a reducing reagent for Ni(II) intermediates rather than as a precursor to R'MnX.



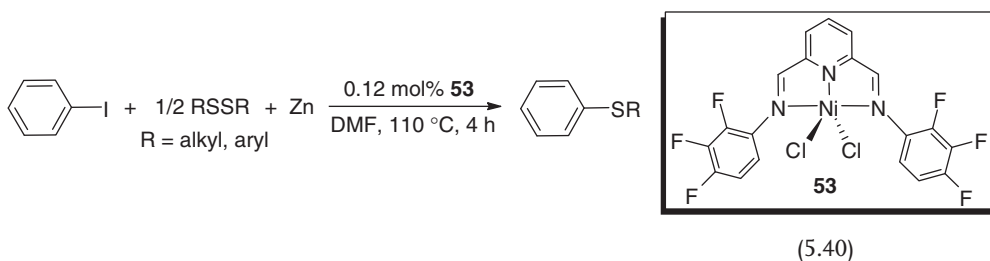
For the formation of C_{sp}-C_{sp}³ bonds, Sun and coworkers [85] have established a procedure for the coupling of primary alkyl halides and alkynyl lithium reagents (Eq. (5.39)). The hypothesized catalytic cycle is very much like the one proposed by Hu for Sonogashira coupling reactions (or analogous to Scheme 5.3), although oxidation of Ni(II) to Ni(IV) is expected to be much more difficult for the phosphinite-based pincer system than the electron-rich amine-based pincer system.



5.3

Carbon–Heteroatom Bond-Forming Reactions

Transition-metal-catalyzed cross-coupling of aryl or alkenyl halides with thiols or their derivatives constitutes an efficient way to construct C–S bonds. The resulting sulfide molecules are of high interest to the pharmaceutical industry. Nickel-catalyzed C–S cross-coupling reactions are known but not common [86–89]. In terms of catalysis of pincer-type complexes, the Morales-Morales group [90, 91] has reported that coupling of iodobenzene and disulfides can be catalyzed by bis(imino)-pyridine-based nickel complexes (Eq. (5.40)). The proposed mechanism involves the formation of a 17-electron Ni(I) species from the reduction of a Ni(II) intermediate with Zn. In a follow-up study, they have shown that complex **52** is a more active catalyst than **53**, particularly for the coupling of alkyl disulfides [92]. However, for the reaction with PhSSPh or a bulky alkyl disulfide such as ^tBuSS^tBu, the yield is lower because of the competitive homocoupling of PhI.

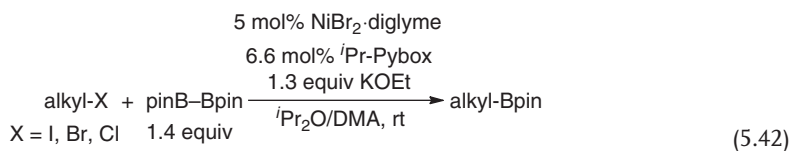


We have recently demonstrated that **52** effectively catalyzes the cross-coupling of aryl iodides and aryl thiols to produce diaryl sulfides in high yields (Eq. (5.41)) [93]. Our mechanistic investigations have confirmed that, during the catalytic reactions, the pincer complex is degraded to structurally ill-defined but catalytically more active species. The degradation process is initialized by the cleavage of O–P bonds with KOH, leading to the release of Ph₂POK, which could be the actual ligand promoting the cross-coupling reactions.



Another example of making carbon–heteroatom bonds through cross-coupling catalysis has come out of Fu's laboratory for the Miyaura borylation of alkyl halides (Eq. (5.42)) [94]. Alkyl iodides and bromides bearing functional groups such as olefin, carbamate, aniline, and amide are readily borylated with good isolated yields. In contrast, the reactions with simple alkyl chlorides and tosylates give only small amounts of cross-coupling products. The coupling of activated alkyl halides (e.g., allylic or benzylic chlorides), on the other hand, is successful. Remarkably, tertiary alkyl halides are also viable substrates as long as the catalytic loading is raised to 10 mol%. The proposed mechanism is similar to the one proposed for the Negishi reactions (Scheme 5.5). As an experimental evidence supporting

the radical process, both exo and endo isomers of 2-bromonorbornane, when subjected to the catalytic conditions, produce the borylated product with the same diastereoselectivity (exo/endo ratio > 20 : 1)



5.4 Summary and Outlook

In comparison to palladium chemistry, nickel-catalyzed cross-coupling reactions remain a less explored area of research. The utilization of pincer or pincer-type ligands, however, opens new doors to nickel catalysis by conferring unique electronic properties at the nickel center, which otherwise may be unreactive. As exemplified in Kumada–Corriu–Tamao reactions developed by Hu and Negishi reactions developed by Fu, the lower tendency of nickel to undergo β -hydrogen elimination offers a better chance to accommodate cross-coupling partners bearing β -hydrogens. Radical processes that are more commonly observed in nickel systems also provide the opportunity of conducting stereo-convergent reactions and add more sophistication to synthesis through cascade catalysis.

As illustrated by other chapters of this book, a diverse array of pincer and pincer-type ligands are known in the literature and can be incorporated to make new nickel complexes. Their catalytic activity in various cross-coupling reactions is likely to be the focus of future research. Another research direction that deserves more attention is carbon–heteroatom bond-forming reactions; very few nickel pincer complexes have been studied for these catalytic applications.

Acknowledgments

We thank the U. S. National Science Foundation (CHE-0952083) for support of our studies of nickel pincer complexes.

References

- Musaev, D.G. and Morokuma, K. (1999) *Top. Catal.*, **7**, 107.
- Lin, B.-L., Liu, L., Fu, Y., Luo, S.-W., Chen, Q., and Guo, Q.-X. (2004) *Organometallics*, **23**, 2114.
- Netherton, M.R. and Fu, G.C. (2004) *Adv. Synth. Catal.*, **346**, 1525.
- Terao, J. and Kambe, N. (2008) *Acc. Chem. Res.*, **41**, 1545.
- Lin, S. and Agapie, T. (2011) *Synlett*, **1**.
- Hu, X. (2011) *Chem. Sci.*, **2**, 1867.
- Wang, Z.-X. and Liu, N. (2012) *Eur. J. Inorg. Chem.*, 901.
- Mesganaw, T. and Garg, N.K. (2013) *Org. Process Res. Dev.*, **17**, 29.
- Kharasch, M.S. and Fields, E.K. (1941) *J. Am. Chem. Soc.*, **63**, 2316.

10. Corriu, R.J.P. and Masse, J.P. (1972) *J. Chem. Soc., Chem. Commun.*, 144a.
11. Tamao, K., Sumitani, K., and Kumada, M. (1972) *J. Am. Chem. Soc.*, **94**, 4374.
12. Knappke, C.E.I. and Jacobi von Wangelin, A. (2011) *Chem. Soc. Rev.*, **40**, 4948.
13. Liang, L.-C., Lin, J.-M., and Hung, C.-H. (2003) *Organometallics*, **22**, 3007.
14. Liang, L.-C., Chien, P.-S., Lin, J.-M., Huang, M.-H., Huang, Y.-L., and Liao, J.-H. (2006) *Organometallics*, **25**, 1399.
15. Castonguay, A., Beauchamp, A.L., and Zargarian, D. (2008) *Organometallics*, **27**, 5723.
16. Salah, A.B. and Zargarian, D. (2011) *Dalton Trans.*, **40**, 8977.
17. Sanford, J., Dent, C., Masuda, J.D., and Xia, A. (2011) *Polyhedron*, **30**, 1091.
18. Wang, Z.-X. and Wang, L. (2007) *Chem. Commun.*, 2423.
19. Sun, K., Wang, L., and Wang, Z.-X. (2008) *Organometallics*, **27**, 5649.
20. Liu, N., Wang, L., and Wang, Z.-X. (2011) *Chem. Commun.*, **47**, 1598.
21. Liu, N. and Wang, Z.-X. (2011) *J. Org. Chem.*, **76**, 10031.
22. Zhang, Y., Song, G., Ma, G., Zhao, J., Pan, C.-L., and Li, X. (2009) *Organometallics*, **28**, 3233.
23. Zhang, C. and Wang, Z.-X. (2009) *Organometallics*, **28**, 6507.
24. Guo, W.-J. and Wang, Z.-X. (2013) *J. Org. Chem.*, **78**, 1054.
25. Inamoto, K., Kuroda, J., Sakamoto, T., and Hiroya, K. (2007) *Synthesis*, 2853.
26. Gu, S. and Chen, W. (2009) *Organometallics*, **28**, 909.
27. Liu, A., Zhang, X., and Chen, W. (2009) *Organometallics*, **28**, 4868.
28. MaGee, K.D.M., Travers, G., Skelton, B.W., Massi, M., Payne, A.D., and Brown, D.H. (2012) *Aust. J. Chem.*, **65**, 823.
29. Sivaramakrishna, A., Clayton, H.S., and Muralikrishna, U. (2011) *J. Coord. Chem.*, **64**, 1309.
30. Csok, Z., Vechorkin, O., Harkins, S.B., Scopelliti, R., and Hu, X. (2008) *J. Am. Chem. Soc.*, **130**, 8156.
31. Breitenfeld, J., Vechorkin, O., Corminboeuf, C., Scopelliti, R., and Hu, X. (2010) *Organometallics*, **29**, 3686.
32. Vechorkin, O., Csok, Z., Scopelliti, R., and Hu, X. (2009) *Chem. Eur. J.*, **15**, 3889.
33. Gartia, Y., Biswas, A., Stadler, M., Nasini, U.B., and Ghosh, A. (2012) *J. Mol. Catal. A: Chem.*, **363-364**, 322.
34. Vechorkin, O. and Hu, X. (2009) *Angew. Chem. Int. Ed.*, **48**, 2937.
35. Vechorkin, O., Proust, V., and Hu, X. (2009) *J. Am. Chem. Soc.*, **131**, 9756.
36. Ren, P., Vechorkin, O., von Allmen, K., Scopelliti, R., and Hu, X. (2011) *J. Am. Chem. Soc.*, **133**, 7084.
37. Perez Garcia, P.M., Di Franco, T., Orsino, A., Ren, P., and Hu, X. (2012) *Org. Lett.*, **14**, 4286.
38. Vechorkin, O., Godinat, A., Scopelliti, R., and Hu, X. (2011) *Angew. Chem. Int. Ed.*, **50**, 11777.
39. Percec, V., Golding, G.M., Smidrkal, J., and Weichold, O. (2004) *J. Org. Chem.*, **69**, 3447.
40. Tang, Z.-Y. and Hu, Q.-S. (2004) *J. Am. Chem. Soc.*, **126**, 3058.
41. Tobisu, M., Shimasaki, T., and Chatani, N. (2008) *Angew. Chem. Int. Ed.*, **47**, 4866.
42. Guan, B.-T., Wang, Y., Li, B.-J., Yu, D.-G., and Shi, Z.-J. (2008) *J. Am. Chem. Soc.*, **130**, 14468.
43. Quasdorf, K.W., Tian, X., and Garg, N.K. (2008) *J. Am. Chem. Soc.*, **130**, 14422.
44. Inamoto, K., Kuroda, J., Hiroya, K., Noda, Y., Watanabe, M., and Sakamoto, T. (2006) *Organometallics*, **25**, 3095.
45. Inamoto, K., Kuroda, J., Kwon, E., Hiroya, K., and Doi, T. (2009) *J. Organomet. Chem.*, **694**, 389.
46. Kuroda, J., Inamoto, K., Hiroya, K., and Doi, T. (2009) *Eur. J. Org. Chem.*, **2009**, 2251.
47. Tu, T., Mao, H., Herbert, C., Xu, M., and Dötz, K.H. (2010) *Chem. Commun.*, **46**, 7796.
48. Estudiante-Negrete, F., Hernández-Ortega, S., and Morales-Morales, D. (2012) *Inorg. Chim. Acta*, **387**, 58.
49. Wang, L. and Wang, Z.-X. (2007) *Org. Lett.*, **9**, 4335.
50. Zhang, X.-Q. and Wang, Z.-X. (2012) *J. Org. Chem.*, **77**, 3658.

51. Zhang, Q., Zhang, X.-Q., and Wang, Z.-X. (2012) *Dalton Trans.*, **41**, 10453.
52. Jones, G.D., Martin, J.L., McFarland, C., Allen, O.R., Hall, R.E., Haley, A.D., Brandon, R.J., Konovalova, T., Desrochers, P.J., Pulay, P., and Vivic, D.A. (2006) *J. Am. Chem. Soc.*, **128**, 13175.
53. Phapale, V.B., Buñuel, E., García-Iglesias, M., and Cárdenas, D.J. (2007) *Angew. Chem. Int. Ed.*, **46**, 8790.
54. Zhou, J. and Fu, G.C. (2003) *J. Am. Chem. Soc.*, **125**, 14726.
55. Fischer, C. and Fu, G.C. (2005) *J. Am. Chem. Soc.*, **127**, 4594.
56. Lundin, P.M., Esquivias, J., and Fu, G.C. (2009) *Angew. Chem. Int. Ed.*, **48**, 154.
57. Arp, F.O. and Fu, G.C. (2005) *J. Am. Chem. Soc.*, **127**, 10482.
58. Son, S. and Fu, G.C. (2008) *J. Am. Chem. Soc.*, **130**, 2756.
59. Smith, S.W. and Fu, G.C. (2008) *J. Am. Chem. Soc.*, **130**, 12645.
60. Oelke, A.J., Sun, J., and Fu, G.C. (2012) *J. Am. Chem. Soc.*, **134**, 2966.
61. Smith, S.W. and Fu, G.C. (2008) *Angew. Chem. Int. Ed.*, **47**, 9334.
62. Joshi-Pangu, A., Ganesh, M., and Biscoe, M.R. (2011) *Org. Lett.*, **13**, 1218.
63. Gong, H., Sinisi, R., and Gagné, M.R. (2007) *J. Am. Chem. Soc.*, **129**, 1908.
64. Gong, H. and Gagné, M.R. (2008) *J. Am. Chem. Soc.*, **130**, 12177.
65. Anderson, T.J., Jones, G.D., and Vivic, D.A. (2004) *J. Am. Chem. Soc.*, **126**, 8100.
66. Jones, G.D., McFarland, C., Anderson, T.J., and Vivic, D.A. (2005) *Chem. Commun.*, 4211.
67. Lin, X. and Phillips, D.L. (2008) *J. Org. Chem.*, **73**, 3680.
68. Lin, X., Sun, J., Xi, Y., and Lin, D. (2011) *Organometallics*, **30**, 3284.
69. Negishi, E. and Anastasia, L. (2003) *Chem. Rev.*, **103**, 1979.
70. Beletskaya, I.P., Latyshev, G.V., Tsvetkov, A.V., and Lukashev, N.V. (2003) *Tetrahedron Lett.*, **44**, 5011.
71. Wang, L., Li, P., and Zhang, Y. (2004) *Chem. Commun.*, 514.
72. Vechorkin, O., Barmaz, D., Proust, V., and Hu, X. (2009) *J. Am. Chem. Soc.*, **131**, 12078.
73. Gøgsig, T.M., Kleimark, J., Nilsson Lill, S.O., Korsager, S., Lindhardt, A.T., Norrby, P.-O., and Skrydstrup, T. (2012) *J. Am. Chem. Soc.*, **134**, 443.
74. Ehle, A.R., Zhou, Q., and Watson, M.P. (2012) *Org. Lett.*, **14**, 1202.
75. Iyer, S., Ramesh, C., and Ramani, A. (1997) *Tetrahedron Lett.*, **38**, 8533.
76. Matsubara, R., Gutierrez, A.C., and Jamison, T.F. (2011) *J. Am. Chem. Soc.*, **133**, 19020.
77. Liu, C., Tang, S., Liu, D., Yuan, J., Zheng, L., Meng, L., and Lei, A. (2012) *Angew. Chem. Int. Ed.*, **51**, 3638.
78. Tang, S., Liu, C., and Lei, A. (2013) *Chem. Commun.*, **49**, 2442.
79. Mitsudo, K., Imura, T., Yamaguchi, T., and Tanaka, H. (2008) *Tetrahedron Lett.*, **49**, 7287.
80. Vechorkin, O., Proust, V., and Hu, X. (2010) *Angew. Chem. Int. Ed.*, **49**, 3061.
81. Yu, X., Yang, T., Wang, S., Xu, H., and Gong, H. (2011) *Org. Lett.*, **13**, 2138.
82. Dai, Y., Wu, F., Zang, Z., You, H., and Gong, H. (2012) *Chem. Eur. J.*, **18**, 808.
83. Anka-Lufford, L.L., Pinsell, M.R., and Weix, D.J. (2012) *J. Org. Chem.*, **77**, 9989.
84. Shrestha, R. and Weix, D.J. (2011) *Org. Lett.*, **13**, 2766.
85. Xu, G., Li, X., and Sun, H. (2011) *J. Organomet. Chem.*, **696**, 3011.
86. Percec, V., Bae, J.-Y., and Hill, D.H. (1995) *J. Org. Chem.*, **60**, 6895.
87. Millois, C. and Diaz, P. (2000) *Org. Lett.*, **2**, 1705.
88. Zhang, Y., Ngeow, K.C., and Ying, J.Y. (2007) *Org. Lett.*, **9**, 3495.
89. Jammie, S., Barua, P., Rout, L., Saha, P., and Punniyamurthy, T. (2008) *Tetrahedron Lett.*, **49**, 1484.
90. Baldovino-Pantaleón, O., Hernández-Ortega, S., and Morales-Morales, D. (2005) *Inorg. Chem. Commun.*, **8**, 955.
91. Baldovino-Pantaleón, O., Hernández-Ortega, S., and

- Morales-Morales, D. (2006) *Adv. Synth. Catal.*, **348**, 236.
92. Gómez-Benítez, V., Baldovino-Pantaleón, O., Herrera-Álvarez, C., Toscano, R.A., and Morales-Morales, D. (2006) *Tetrahedron Lett.*, **47**, 5059.
93. Zhang, J., Medley, C.M., Krause, J.A., and Guan, H. (2010) *Organometallics*, **29**, 6393.
94. Dudnik, A.S. and Fu, G.C. (2012) *J. Am. Chem. Soc.*, **134**, 10693.

6

PSiP Transition-Metal Pincer Complexes: Synthesis, Bond Activation, and Catalysis

Laura Turculeț

6.1

Introduction

Transition-metal-mediated reactivity plays a key role in addressing modern synthetic challenges, specifically with respect to the development of new chemical processes that are efficient, selective, high yielding, and environmentally friendly. A starting point for the discovery of new and/or improved metal-mediated syntheses is the design of metal complexes that exhibit novel reactivity, and key to this endeavor is the construction of new types of ancillary ligands that are able to stabilize a reactive metal center in a unique coordination environment while simultaneously conferring desirable reactivity properties. In this context, metal complexes supported by pincer-type LXL ligands (Figure 6.1), which feature a central anionic donor (X) flanked by two neutral donor groups (L), have been the subject of intense study in recent years [1–5]. The phosphine-based PCP pincer complexes **A** and **B** pioneered by Shaw [6–10] in the 1970s have been the most widely studied complexes of this type, and have become ubiquitous in organometallic chemistry. However, the modular nature of the tridentate pincer ligand design offers an attractive means of manipulating the steric and electronic features of the ensuing metal complexes. As such, significant effort has been devoted to the synthesis of systems where strategic alterations have been introduced to the pincer framework, including variation of the L donor fragments and of the ligand backbone [3, 4, 11–13]. By comparison, the central anionic donor (X) has largely been restricted to the elements C and N, the latter exemplified by structures of the type **C** and **D** [1–4, 14]. Thus, the study of pincer complexes that feature other types of central donor groups is an emerging area, with examples of pincer ligation featuring X = Si (see below), Ge [15, 16], Sn [15, 16], P [17–26], and B [27–33] (**E–K**) having been recently reported. Of these alternative pincer designs, silyl-based pincer-like bis(phosphino)silyl (PSiP) ligands, in particular those of types **E** and **F**, are the most established and well studied. This chapter will review the chemistry of such PSiP late transition-metal pincer complexes [34].

Silyl PSiP ligands were first reported by Stobart and coworkers [35, 36] in the 1980s, who prepared a series of platinum group metal complexes supported

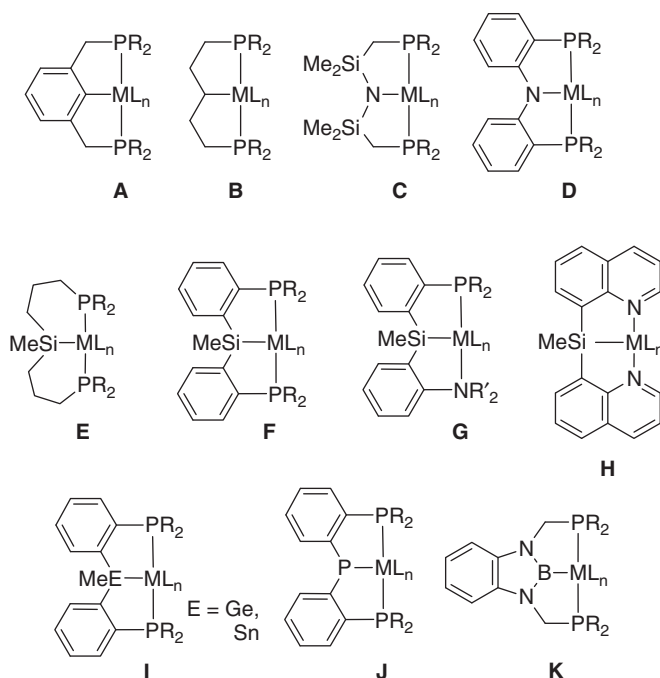


Figure 6.1 Examples of LXL tridentate pincer ligation.

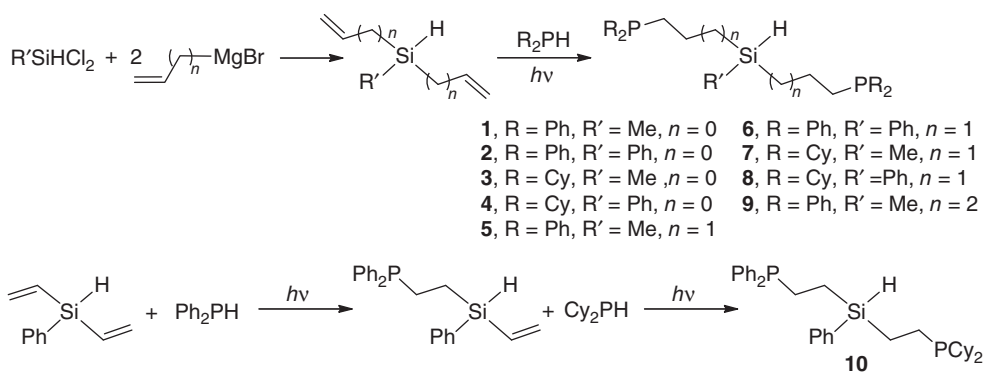
by bis(phosphino)silyl ligands featuring aliphatic and benzylic backbones. These early studies primarily addressed the fundamental coordination chemistry of such tridentate PSiP ligands. More recently, our group has developed PSiP (as well as PSiN) [37] derivatives featuring a phenylene backbone (**F**) [38, 39], and we, along with others, have begun exploring the reactivity and catalytic activity of such late metal PSiP species. These latter systems lack β -hydrogens in the ligand backbone, which removes the possibility of β -hydride elimination from the PSiP backbone. Although these somewhat more rigid phenylene-based ligands feature an sp^3 -hybridized central silyl donor, examples of both meridional and facial binding to a metal have been observed.

In comparing PSiP pincer ligation with the closely related PCP derivatives, the increased electron-donating character of Si relative to C is anticipated to lead to a more electron-rich late metal center. In addition, the stronger trans-labilizing ability of Si can better promote the generation of coordinatively unsaturated complexes [40]. Such features may lead to significant structural and reactivity differences between PCP- and PSiP-supported metal complexes. Indeed, PSiP ligation has been utilized to prepare unprecedented four-coordinate trigonal-pyramidal Ru complexes (see below), and computational studies have confirmed the key role of the strongly σ -donating silyl group in enforcing the unusual coordination geometry [41].

6.2 PSiP Ligand Syntheses

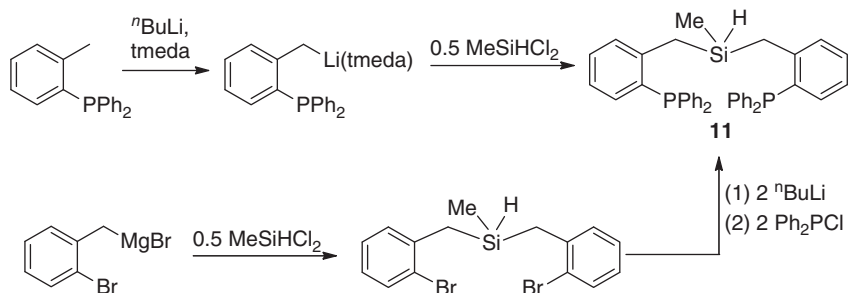
Several approaches have been utilized for the synthesis of bis(phosphino)hydrosilane precursors to PSiP pincer species. Two key steps in such syntheses involve the formation of Si–C and P–C bonds. The former is achieved readily by the reaction of an alkyl or aryl nucleophile (Grignard or organolithium reagent) with a chlorosilane. The formation of P–C bonds in this context has been achieved in a variety of ways, including P–H addition to bis(alkenyl)silanes, the alkylation of chlorophosphines with Grignard or organolithium reagents, and Pd cross-coupling catalysis. Once obtained, the metallation of such bis(phosphino)hydrosilane precursors is attained via chelate-assisted SiH oxidative addition at an appropriate late metal center.

Joslin and Stobart [42] were the first to report the synthesis of bis(phosphino)silanes by a route involving anti-Markovnikov P–H addition of secondary phosphines to bis(alkenyl)silanes (prepared by the reaction of the appropriate alkyl- or aryl-dichlorosilane with the corresponding Grignard reagent) under photochemical conditions (Scheme 6.1). A variety of bis(phosphino)silanes of the type $(R_2PCH_2CH_2(CH_2)_n)_2SiR'H$ (**1–9**; R = Ph, Cy; $n = 0–2$; R' = Me, Ph) were synthesized by this approach. Yields ranging from 60% to 98% were obtained upon UV irradiation for extended periods (e.g., 60 h for **1**). In one instance, the mono-addition product $(Ph_2PCH_2CH_2)(CH_2=CH)SiPhH$ was isolated in low yield and was subsequently reacted with Cy_2PH to provide the mixed bis(phosphinoethyl) analog $(Ph_2PCH_2CH_2)(Cy_2PCH_2CH_2)SiPhH$ (**10**). The mechanism of the P–H addition is proposed to involve nucleophilic attack by R_2P^{\bullet} radicals on the terminal alkene carbon. Slower reactions were observed for R = Cy versus R = Ph, as well as for allylsilane versus vinylsilane.



Scheme 6.1 Photochemical synthesis of bis(phosphino)hydrosilanes.

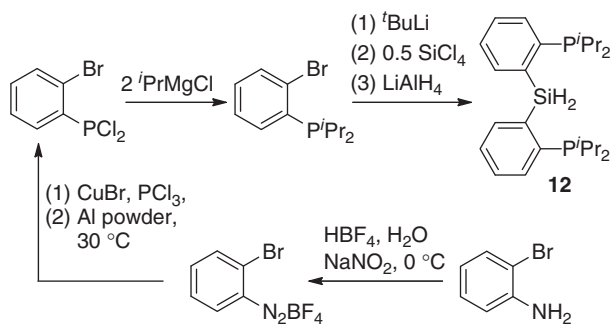
In a subsequent report, Stobart and coworkers [35] also reported the synthesis of a bis(phosphino)hydrosilane ligand precursor featuring a benzylic backbone (**11**, Scheme 6.2). Two routes were reported for the synthesis of **11**, both involving



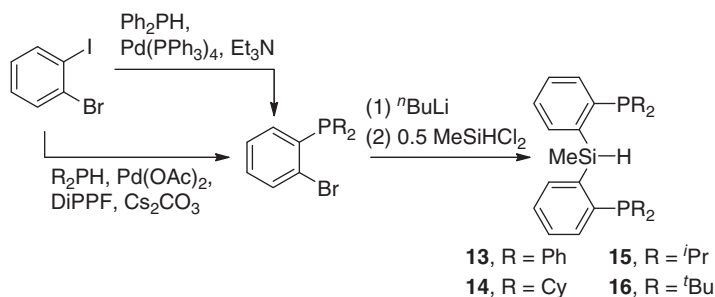
Scheme 6.2 Synthesis of a bis(phosphino)hydrosilane featuring a benzylic backbone.

the use of Grignard and/or organolithium reagents in order to form the desired Si–C and P–C linkages. Lithiation of *ortho*-tolylidiphenylphosphine and subsequent treatment with MeSiHCl_2 afforded **11** in 38% yield. Alternatively, the reaction of (2-bromobenzyl)magnesium chloride with MeSiHCl_2 provided bis(2-bromobenzyl)-methylsilane as a colorless oil, which after dilithiation and reaction with $\text{Ph}_2\text{P-Cl}$ gave the desired product **11** contaminated with about 20% $\text{Ph}_2\text{P}^n\text{Bu}$.

The synthesis of PSiP precursors featuring a phenylene ligand backbone was reported initially by both our group and that of Milstein. Milstein and coworkers [43] prepared the secondary silane $(2\text{-}^i\text{Pr}_2\text{PC}_6\text{H}_4)_2\text{SiH}_2$ (**12**) from *ortho*-dichlorophosphinobromobenzene, as shown in Scheme 6.3. The dichlorophosphine precursor is itself synthesized from 2-bromoaniline via a diazonium intermediate [44]. In total, seven synthetic steps are required for the synthesis of **12** by this route. By comparison, the synthesis of related PSiP ligand precursors of the type $(2\text{-R}_2\text{PC}_6\text{H}_4)_2\text{SiMeH}$ (**13**, $\text{R} = \text{Ph}$; **14**, $\text{R} = \text{Cy}$; **15**, $\text{R} = ^i\text{Pr}$; **16**, $\text{R} = ^t\text{Bu}$) can be readily achieved in three steps by utilizing Pd-catalyzed P–C cross-coupling of commercially available 2-bromiodobenzene with a secondary phosphine (Scheme 6.4) [38, 39, 45].



Scheme 6.3 Synthesis of a PSiP precursor featuring a phenylene ligand backbone.

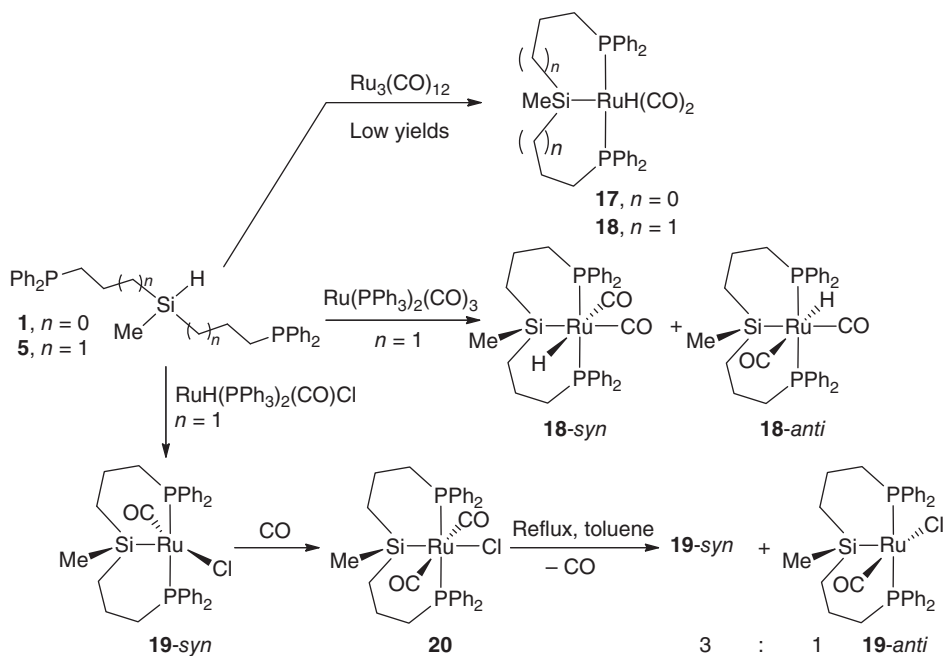


Scheme 6.4 Synthesis of PSiP precursors utilizing Pd-catalyzed P–C cross-coupling.

6.3

Group 8 Metal PSiP Chemistry

The published chemistry of group 8 metal PSiP complexes is thus far restricted to the synthesis of Ru^{II} complexes. PSiP complexes of Ru^{II} were first reported by Stobart and coworkers, who studied the complexation of the bis(phosphinoalkyl) silanes **1** and **5** with Ru carbonyl species. In an initial study, low yields of the 18-electron hydrido carbonyl complexes $[\kappa^3\text{-(Ph}_2\text{P(CH}_2\text{)}_n\text{)}_2\text{SiMe}] \text{Ru(H)(CO)}_2$ (**17**, $n=2$; **18**, $n=3$) were obtained upon reaction of either **1** or **5** with Ru₃(CO)₁₂ (Scheme 6.5) [36]. Complex **18** was crystallographically characterized and featured



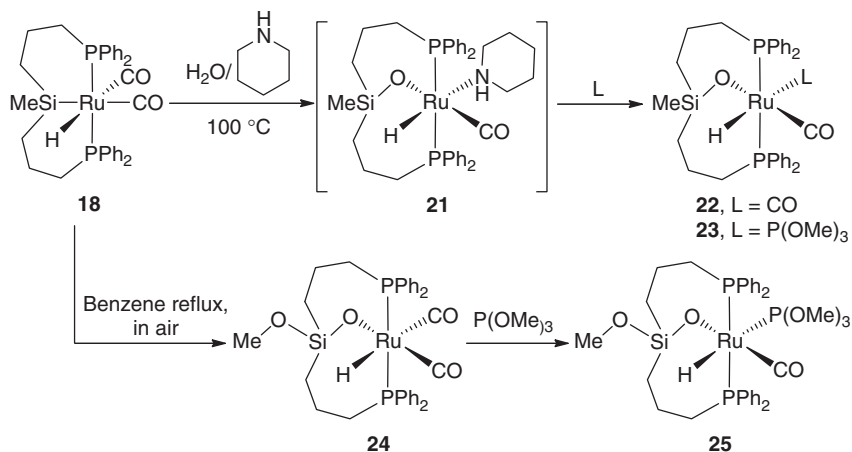
Scheme 6.5 Bis(phosphinoalkyl)silyl complexes of Ru.

cis-disposed carbonyl groups and mer-type coordination of the PSiP ligand (P–Ru–P angle of $174.5(2)^\circ$) in the solid state. The hydride ligand was not located, but clearly occupies the vacant coordination site trans to a carbonyl ligand and cis to Si and is oriented syn relative to the Si–Me group. In a subsequent report, the quantitative synthesis of **18** was achieved by the reaction of **5** with $\text{Ru}(\text{PPh}_3)_2(\text{CO})_3$ [46]. The latter synthesis results in the formation of a mixture of syn and anti diastereomers of **18**. Although the syn isomer can be selectively crystallized from this mixture, in solution it slowly reverts to an equilibrium mixture of the two diastereomers. Rate data obtained for this isomerization process provided activation parameters of $\Delta G^\ddagger_{295} = 102(5) \text{ kJ mol}^{-1}$, $\Delta H^\ddagger_{295} = 113(7) \text{ kJ mol}^{-1}$, and $\Delta S^\ddagger_{295} = 37(2) \text{ J K}^{-1} \text{ mol}^{-1}$. Despite repeated attempts, no evidence for the formation of the unsaturated five-coordinate species $[\kappa^3\text{-(Ph}_2\text{P(CH}_2)_n)_2\text{SiMe}] \text{Ru(H)(CO)}$ was observed, suggesting that CO dissociation from **18** does not occur readily. These data are consistent with an intramolecular pathway for the isomerization process that does not involve CO dissociation. Two possible mechanisms for the isomerization are (i) concerted exchange of H and CO and (ii) twisting of the Ru–H bond around the Ru–Si axis. The former proposal of a concerted exchange of H and CO may be accomplished via a trigonal twist and appears to be consistent with the energetics of **18-syn/18-anti** interconversion.

In a related study, Stobart and coworkers [47] found that the reaction of **5** with *mer*- $\text{RuH}(\text{PPh}_3)_3(\text{CO})\text{Cl}$ afforded the five-coordinate monocarbonyl chloride **19** (Scheme 6.5). Treatment of **19** with CO led to the formation of the six-coordinate dicarbonyl species **20**. Crystallographic characterization of **19** indicated that the complex adopts a Y-shaped coordination geometry in the solid state, featuring trans-disposed phosphino groups in the axial positions. The chloride ligand is oriented syn relative to the Si–Me group. The crystal structure obtained for **20** features octahedral geometry at Ru with *mer* coordination of the PSiP ligand and trans-disposed carbonyl ligands. The formation of the *trans*-dicarbonyl isomer of **20** suggests that an approach involving the binding of CO trans to the highly electron-releasing silyl group in **19** is disfavored, even though this binding site is the most accessible from a steric perspective, which highlights how the electronic influence of a silyl group can control substrate binding.

Interestingly, heating a toluene solution of **20** at reflux for 3 h led to the loss of CO and regeneration of **19** as a mixture of syn and anti diastereomers (about 3:1 ratio; Scheme 6.5) [47]. In contrast, reflux of pure **19-syn** did not result in the formation of any **19-anti**, nor was there any change in the **19-syn:19-anti** ratio on heating solutions that contained both species. Thus, it appears that the interconversion between the two five-coordinate isomeric structures (**19-syn/19-anti**) is effectively mediated in an associative manner by a coordinatively saturated intermediate (**20**). This represents an unusual reversal of the mechanistic premise that the isomerization of a rigid octahedral structure occurs dissociatively through a stereochemically nonrigid unsaturated species.

The reactivity of the hydrido dicarbonyl complex **18** with water and O_2 has been explored (Scheme 6.6) [48]. Although **18** does not react with either water (100°C , 17 h) or upon heating in dry piperidine, heating in wet piperidine (100°C , 17 h)



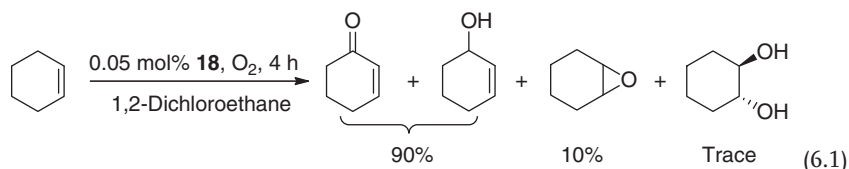
Scheme 6.6 Activation of water and O₂ by a bis(phosphinoalkyl)silyl complex of Ru.

led to the formation of a new product (**21**) which decomposed upon isolation. Treatment of **21** with CO or P(OMe)₃ afforded the isolable analogs **22** and **23**, respectively. Crystallographic characterization of **23** revealed the formation of a Ru-siloxo complex, where an oxygen atom has inserted in the Ru–Si linkage. Although the mechanism for the hydrolysis of **18** has not been elucidated, the requirement for a base in this transformation suggests that OH[−] attack at Si might play a role in the observed reactivity.

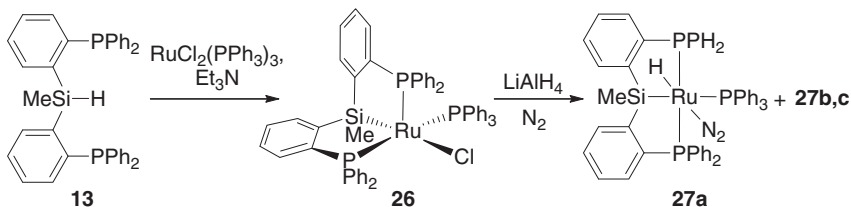
Although **18** did not react in air in the solid state, slow (>7 days) oxidation occurred in refluxing benzene solution under an ambient atmosphere to afford the new product **24** (Scheme 6.6) [48]. Addition of P(OMe)₃ to **24** afforded the trimethylphosphite analog (**25**), which was crystallographically characterized. Complex **25** features a Ru-siloxo linkage analogous to that observed for **23**, as well as insertion of a second oxygen atom into the Si–Me unit to generate a methoxysilyl in a rare example of partial oxidation of a typically inert Si–C bond. Interestingly, exposure of either **22** or **23** to O₂ does not lead to the formation of the Si–C oxidation products **24** or **25**, respectively. Although the mechanism for the formation of complexes **24** and **25** from **18** is not known, the authors propose a pathway involving outer-sphere electron transfer to give a cationic Ru^{III} analog of **18** and O₂[−]. Ensuing attack by superoxide at Si (or its addition across the Ru–Si bond) could effect the observed double insertion of O into the Ru–Si and Si–C linkages.

The activity of **18** in alkene oxidation catalysis was screened (Eq. (6.1)) [48]. Upon treatment of a cyclohexene/1,2-dichloroethane mixture with O₂ at ambient temperature and a catalyst loading of 0.05 mol%, about 15% conversion was obtained in 4 h, typically 90% to 2-cyclohexen-1-one and 2-cyclohexen-1-ol with about 10% cyclohexene oxide and a trace of *trans*-1,2-cyclohexanediol. Although varying the pressure of O₂ did not seem to drastically affect the outcome of the reaction, significantly lower conversion was observed at a higher catalyst loading

of 0.2 mol%. The reaction is shut down by the addition of 2,6-di-*tert*-butyl-4-methylphenol. These observations are consistent with a catalyzed autoxidation process.



More recently, our group has reported on the synthesis and reactivity of Ru^{II} complexes supported by phenylene-bridged PSiP ligands (Figure 6.1, F). Treatment of **13** with RuCl₂(PPh₃)₃ in the presence of Et₃N resulted in formation of the cyclometallated 16-electron Ru complex **26** (Scheme 6.7) [38]. The X-ray crystal structure of **26** (Figure 6.2) confirms the formation of a five-coordinate *fac*-(PSiP) complex with distorted square-pyramidal (Y-shaped) geometry at Ru, in which a phosphine ligand arm occupies the apical coordination site while the Si donor is positioned trans to Cl. These structural features differ somewhat from those of the related complex **19**, which features the PSiP ligand in a *mer*-type configuration with Si positioned trans to the vacant coordination site. Despite these differences, the Ru–Si distances in **19** and **26** are comparable (**19**, Ru–Si = 2.339(5) Å; **26**, Ru–Si = 2.3361(6) Å) [47].



Scheme 6.7 Synthesis of Ru complexes supported by a phenylene-bridged PSiP ligand.

Complex **26** reacted with LiEt₃BH to form a mixture of three Ru hydride species (**27a–c**) (Scheme 6.7) [38]. The ratio of **27a** : **b** : **c** observed *in situ* was approximately 2 : 1 : 1 and heating of the mixture did not change the observed ratio of these three complexes. Complex **27a** was isolated from this mixture and assigned as a dinitrogen adduct of the type (PSiP)RuH(N₂)(PPh₃). Facile formation of dinitrogen adducts has been reported in related PCP- and PNP-Ru pincer chemistry [49–51].

Both complexes **26** and **27a** function as precatalysts in the transfer hydrogenation of ketones employing basic ^{*i*}PrOH as the hydrogen source (Table 6.1) [38]. The activity of **26** as a precatalyst in this reaction is comparable to that of related Ru pincer catalysts that lack an NH functionality [51–55]. When employing 0.2 mol% of **26** with 2 mol% KO^{*t*}Bu at 82 °C, high conversion to the corresponding secondary alcohols was observed for several ketone substrates, including diaryl, dialkyl, and alkyl/aryl ketones. As is the case for most metal-catalyzed transfer hydrogenation processes conducted in ^{*i*}PrOH, <5% conversion was observed in the absence of

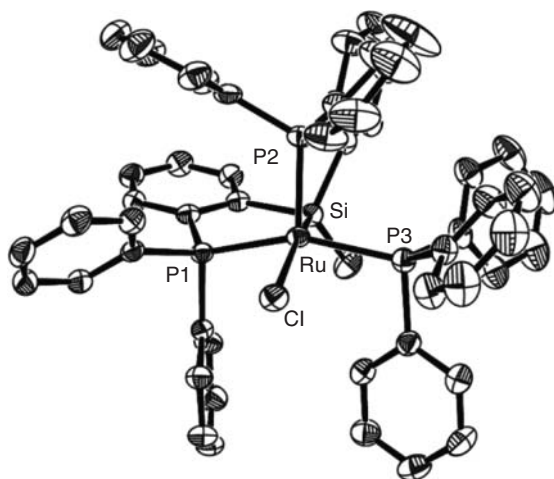
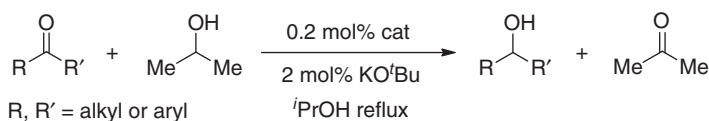


Figure 6.2 Crystallographically determined structure of **26**.

Table 6.1 Transfer hydrogenation of ketones.^a



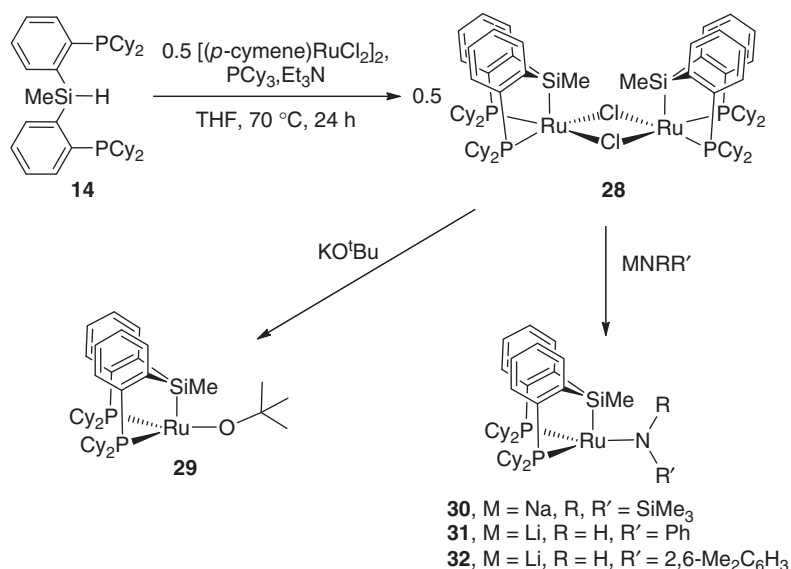
Entry	Catalyst	Substrate	Time (h)	Conversion (%) ^b
1	26	Acetophenone	6	96
2	26	Benzophenone	6	92
3	26	2-Heptanone	4.5	99
4	26	Cyclopentanone	3	> 99
5	26	Cyclohexanone	3	> 99
6	27a	Cyclohexanone	3	94

^aReactions were performed on 1 ml scale (0.1 M ketone, 0.2 mol% Ru, 2 mol% KO^tBu) in ⁱPrOH at 82 °C under N₂.

^bDetermined on the basis of GC-FID (gas chromatography with flame ionization detector) data.

KO^tBu as base. The preformed Ru hydride **27a** was similarly inactive in the absence of added KO^tBu, although 94% conversion was obtained in the hydrogenation of cyclohexanone when using 2 mol% KO^tBu (entry 6, Table 6.1). These preliminary results establish the catalytic utility of such (PSiP)Ru^{II} complexes in ketone transfer hydrogenation.

The synthesis of Ru^{II} complexes supported by the cyclohexylphosphino PSiP ligand analog **14** was subsequently pursued [41]. The tertiary silane **14** reacted



Scheme 6.8 Synthesis of four-coordinate (PSiP)Ru^{II} complexes.

with 0.5 equiv of [(*para*-cymene)RuCl₂]₂ in the presence of Et₃N and PCy₃ to afford the diamagnetic dinuclear species [(Cy-PSiP)RuCl]₂ (**28**; Cy-PSiP = [κ^3 -(2-R₂PC₆H₄)₂SiMe]⁻; Scheme 6.8). Complex **28** serves as a useful precursor for the synthesis of novel diamagnetic four-coordinate formally 14-electron Ru amido and alkoxo complexes of the type (Cy-PSiP)RuX (**29**, X = O^{*t*}Bu; **30**, X = N(SiMe₃)₂; **31**, X = NHPh; **32**, X = NH(2,6-Me₂C₆H₃); Scheme 6.8), of which **29**, **30**, and **32** were crystallographically characterized (Figure 6.3). Although unsaturated 14-electron species are often proposed as reactive intermediates in metal-mediated chemistry, such isolable four-coordinate Ru^{II} species are extremely rare [56–58], especially in the absence of stabilizing agostic interactions. Remarkably, no evidence for such

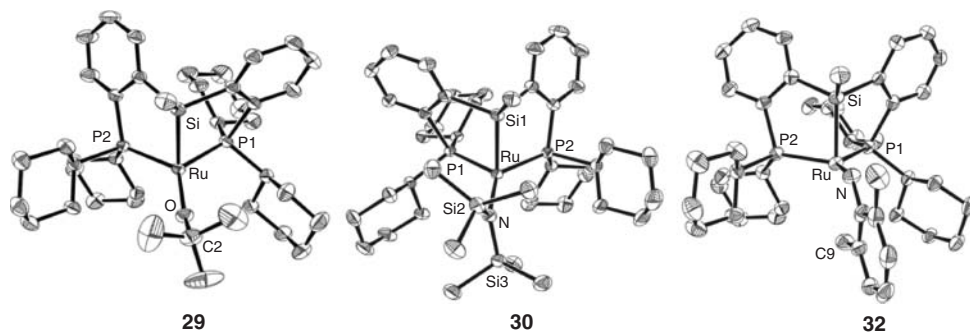


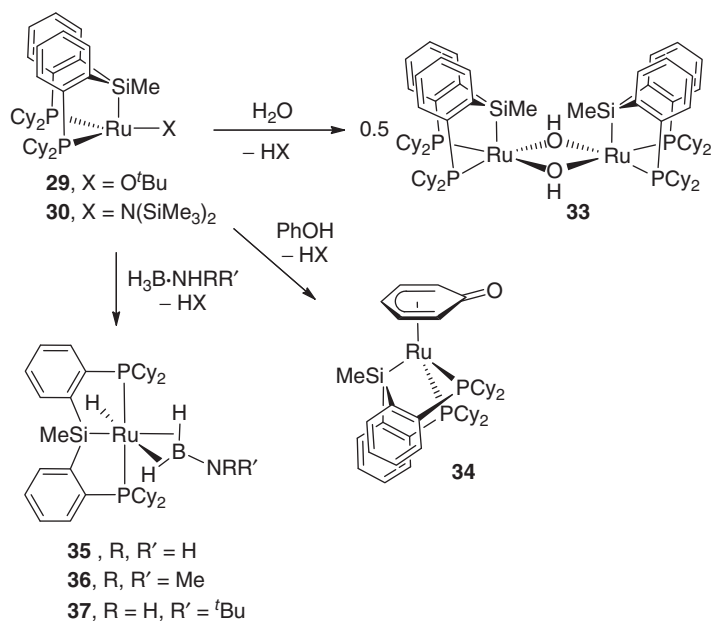
Figure 6.3 Crystallographically determined structures of **29**, **30**, and **32**.

agostic interactions was observed for **29–31** either in solution or in the solid state. The X-ray crystal structure of **32** features a short Ru...C contact of 2.749(3) Å to one of the anilido methyl substituents, which is consistent with a C–H agostic interaction. Computational data confirms a weak (about 2.3 kcal mol⁻¹) agostic interaction in **32** [41]. Despite the prevalence of square-planar and tetrahedral geometries for four-coordinate transition-metal complexes, the X-ray crystal structures of **29**, **30**, and **32** each exhibit slightly distorted trigonal-pyramidal coordination geometry at Ru, with Si in the apical site. The relatively short Ru–X distances observed in the solid state for these complexes (**29**, Ru–O = 1.9090(14); **30**, Ru–N = 2.0465(12); **32**, Ru–N = 1.995(2) Å) are consistent with Ru–X π -bonding.

Density functional theory (DFT) studies of **29**, **30**, and **32** confirmed the slightly distorted trigonal-pyramidal geometry that was observed for these complexes, where the alternative *mer*- κ^3 -pincer–Ru^{II} coordination mode is significantly (on the order of 30 kcal mol⁻¹) higher in energy [41]. Taking complex **29** as an example, optimized Ru–O distances of 1.91 and 1.98 Å for *fac*- κ^3 and *mer*- κ^3 forms, respectively, are suggestive of stronger Ru^{II}–O π interactions in the former. The stability of these four-coordinate complexes cannot be attributed to a triplet spin state, as has been invoked in the case of square-planar Ru^{II} species [56–58]. Rather, for **29**, **30**, and **32**, a triplet spin state, which also favors a *fac*- κ^3 -(PSiP)Ru^{II} ligation, is higher in energy by more than 24 kcal mol⁻¹. The strong metal $d_{x^2-y^2}$ character of the highest occupied molecular orbital (HOMO), together with a smaller metal d_{xz} component that is involved in some Ru–X π bonding, is not particularly well suited to accommodate an agostic interaction at the vacant axial coordination site, while the lowest unoccupied molecular orbital (LUMO) exhibits Ru–X π^* character featuring a strong metal d_{xy} component. Hence, agostic C–H interactions are not essential for stabilizing the singlet ground state.

Analogues of **29**, **30**, and **32** which have the central silyl X-group replaced by C(sp³)–Me (**29c–32c**), phosphido (**29p–32p**), or amido (**29n–32n**) donor groups were also studied computationally [41]. The assessed natural bond orbital (NBO) charge distribution reveals the following order of descending donating ability: PSiP > PPP > PCP > PNP. DFT reveals that the strength of the C–H agostic interaction in complexes of the type (PXP)Ru(NH(2-MeC₆H₄)) (**32***, X = Si; **32*p**, X = P; **32*c**, X = C(sp³)–Me; **32*n**, X = N) directly correlates with the degree of electron deficiency at Ru and hence increases in the following order (kcal mol⁻¹): **32*** (2.3) < **32*p** (3.8) < **32*c** (4.4) < **32*n** (7.3). The nature of the central donor group also has a profound influence on the gap in stability between *fac*- κ^3 - and *mer*- κ^3 -(PXP)Ru^{II} forms, which follows a regular trend as exemplified for complex **32** (kcal mol⁻¹): **32** (32.0) > **32p** (25.3) > **32c** (17.5) > **32n** (10.8). Of particular importance is the marked dependency revealed by DFT between the charge density at Ru and the size of the gap between the singlet and triplet spin states. The $\Delta E(S-T)$ gap decreases regularly for the silylamido complex from 24.2 (**30**) to 23.6 (**30p**), 22.7 (**30c**), and 20.5 kcal mol⁻¹ (**30n**), thereby reinforcing the pivotal role of a strongly donating silyl donor for the stabilization of the singlet state in such complexes.

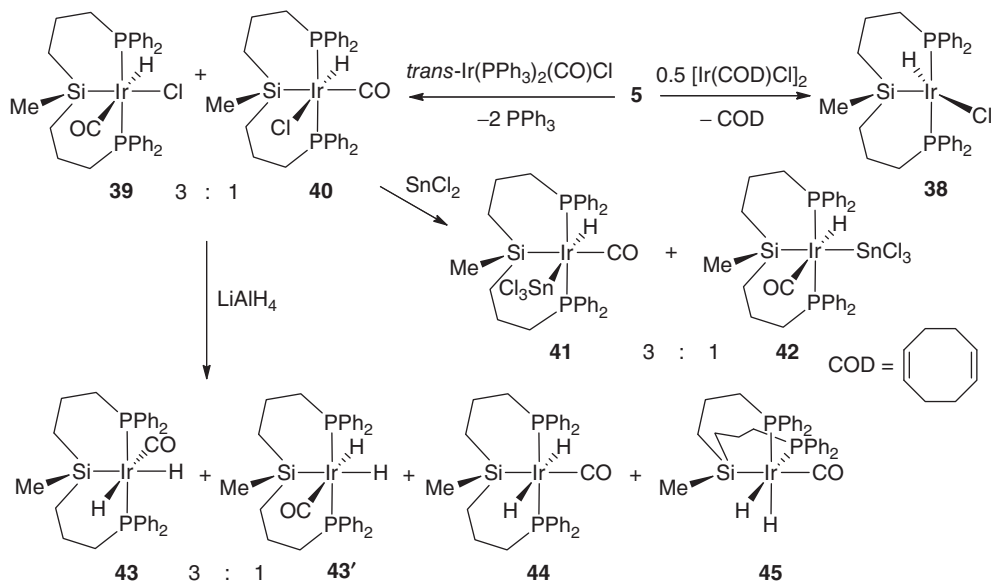
Although such trigonal-pyramidal (PSiP)Ru^{II} species are stabilized by the strongly donating silyl group, they are nonetheless reactive toward E–H bonds (E = main group element). Each of complexes **29** and **30** underwent protonolysis with water to form the dinuclear hydroxo-bridged dimer **33** (Scheme 6.9) [41]. The dimeric nature of **33** relative to monomeric **29** confirms that steric bulk plays an important role in attaining a monomeric structure for complexes of the type (PSiP)RuX. The attempted synthesis of a phenoxo analog by treatment of either **29** or **30** with PhOH led instead to the synthesis of the 18-electron η^5 -oxocyclohexadienyl complex **34** (Scheme 6.9). Complexes **29** and **30** also underwent multiple E–H bond activation steps upon treatment with H₃B·NH₃ to form quantitatively the bis(σ -B–H) complex (PSiP)RuH(η^2 : η^2 -H₂BNH₂) (**35**) [41], a rare example of a bis(σ -B–H) aminoborane complex [59, 60]. The substituted aminoboranes H₃B·NHMe₂ and H₃B·NH₂^tBu reacted in a similar manner (Scheme 6.9) to form the related bis(σ -B–H) complexes (**36**, **37**). The mechanism of the activation of ammonia-borane by such low-coordinate (PSiP)RuX species was studied computationally and was determined to proceed most favorably in a stepwise manner via intramolecular deprotonation of ammonia and subsequent borane B–H bond oxidative addition [41]. These studies confirm that such four-coordinate formally 14-electron (R-PSiP)RuX complexes are capable of promoting multiple bond activation steps in a manner that may be synthetically useful in the transformation of main group substrates.



Scheme 6.9 Reactivity of trigonal-pyramidal (PSiP)Ru^{II} complexes.

6.4 Group 9 Metal PSiP Chemistry

The first examples of group 9 complexes supported by tridentate PSiP ligation were reported by Stobart and coworkers in 1997 [36]. Treatment of the hydrosilane **5** with $[\text{Ir}(\text{COD})\text{Cl}]_2$ (COD, 1,5-cyclooctadiene) afforded the five-coordinate hydrido chloride complex **38** (Scheme 6.10). Alternatively, treatment of **5** with *trans*- $\text{Ir}(\text{PPh}_3)_2(\text{CO})\text{Cl}$ afforded a 3:1 mixture of the six-coordinate hydrido carbonyl chloride isomers **39** and **40**. Reaction of the **39/40** mixture with SnCl_2 led to the synthesis of the six-coordinate Ir–SnCl₃ complex as another pair of stereoisomers (**41** and **42**) in the same 3:1 ratio. Treatment of the **39/40** mixture with LiAlH_4 led to the formation of a mixture of dihydrido carbonyl stereoisomers (**43**–**45**, Scheme 6.10), which is proposed to include the *fac*-PSiP complex **45** as a minor component. Complexes **38** and **42** were crystallographically characterized.

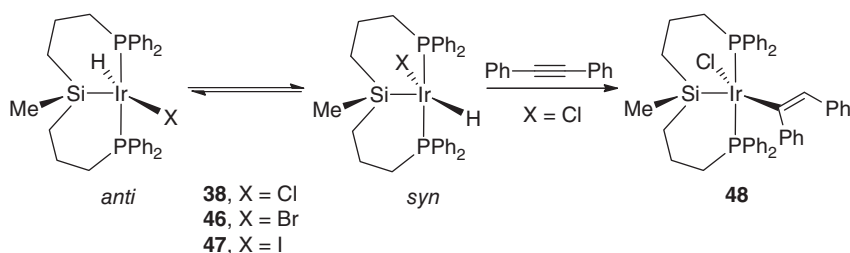


Scheme 6.10 Bis(phosphinoalkyl)silyl complexes of Ir.

Although **38** was initially assigned as a single isomer exhibiting an anti orientation of the Ir–H and Si–Me groups, a subsequent recent study by Sola and coworkers [61] determined that equilibrium mixtures of anti and syn isomers are established over the course of several days in a room-temperature solution. While the equilibrium ratio of isomers is solvent dependent, the anti isomer appears to be the major component. The bromo (**46**) and iodo (**47**) analogs of **38** were also synthesized, and exhibit similar isomerization behavior, with the exception that **47-syn** is the major stereoisomer in the case of the iodo-substituted complex. Complexes **46-anti** and **46-syn** were each crystallographically characterized, and exhibit subtle differences in coordination geometry, such that the geometry in **46-anti** is best described as

Y-shaped, while **46-syn** is best described as T-shaped. Computational modeling studies suggest that the structure of **46-anti** is the electronically preferred one, whereas that of **46-syn** results from distortions provoked by sterics. Such small structural differences lead to more significant differences in reactivity between syn and anti isomers. Thus, syn isomers of **38**, **46**, and **47** form six-coordinate adducts with chlorinated solvents, CO, and P(OMe)₃ after coordination of the incoming ligand trans to Si. The anti isomers do not form detectable adducts with chlorinated solvents and coordinate CO or P(OMe)₃ either trans to Si (kinetic product) or trans to hydride (thermodynamic product). The equilibrium distribution of isomers for such six-coordinate adducts is dependent on the nature of the halide ligand, such that in the case of CO adducts, the replacement of chloride by iodide inverts the stereochemistry of the reaction product and switches the CO coordination position from trans to hydride (98%) to trans to Si (100%).

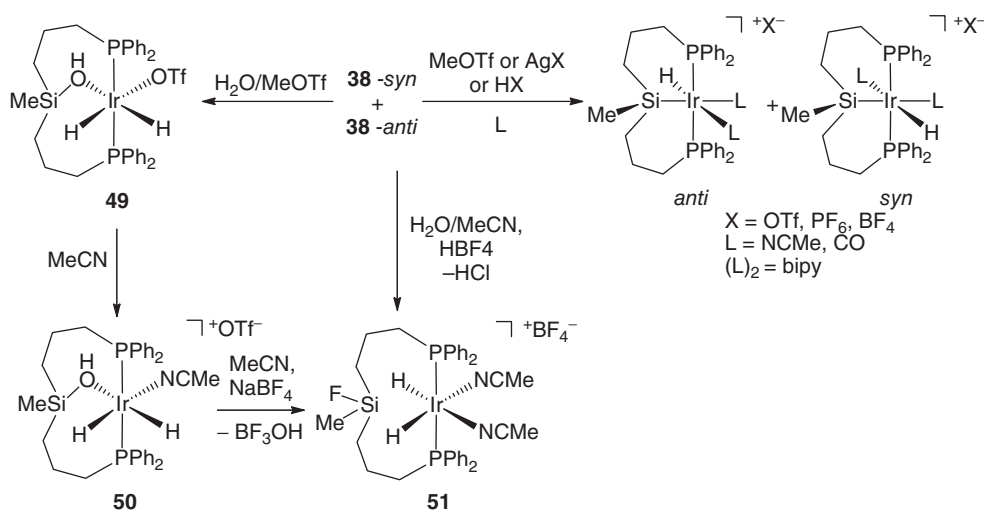
The differing coordination properties of syn and anti isomers for **38**, **46**, and **47** have a significant effect on the insertion chemistry exhibited by such complexes [61]. Thus, diphenylacetylene reacts selectively with **38-syn** to form the corresponding five-coordinate *syn*-alkenyl complex **48** (Scheme 6.11). Although it is nonreactive in such insertion processes, the anti isomer slowly isomerizes to form **38-syn**, thus leading to the eventual quantitative formation of **48**. The rate of syn/anti isomerization is actually dependent on the nature of the insertion reactant (e.g., diphenylacetylene leads to much slower isomerization than acetylene). Interestingly, added H₂ has a profound effect on the syn/anti isomerization process, resulting in extremely rapid rates (on the same order than as NMR timescale) even though no new product resulting from a reaction of the hydrido halide complex with H₂ is observed. A possible isomerization mechanism involving H₂ oxidative addition to form an Ir^V intermediate has been proposed. The isomerization occurs when a hydride ligand passes from one face of the Ir^V complex to the other (through the plane defined by the *mer*-PSiP ligand) via a transition state involving an Ir-(η²-SiH) interaction. In the absence of H₂, such syn/anti isomerization process can still occur if the key Ir-(η²-SiH) transition state can be generated through reductive elimination involving Ir^{III} species.



Scheme 6.11 Isomerization of five-coordinate bis(phosphinoalkyl)silyl complexes of Ir.

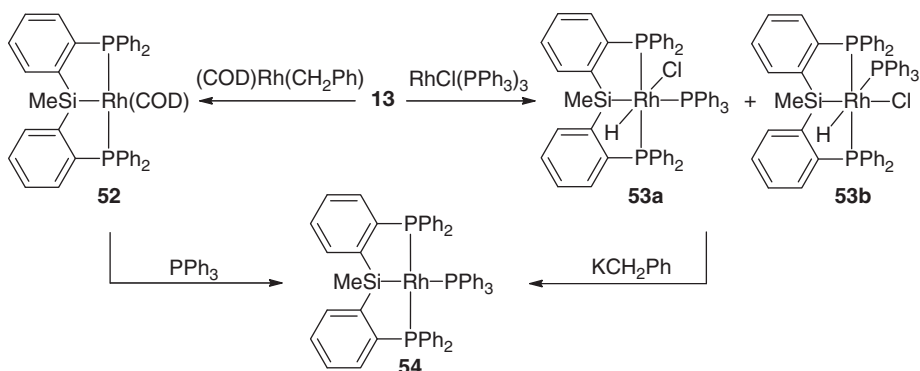
In a subsequent study, Sola and coworkers [62] reported the synthesis of cationic Ir^{III} complexes supported by bis(phosphinoalkyl)silyl PSiP ligation. Thus, treatment

of equilibrium mixtures of **38-syn**/**38-anti** with various electrophilic reagents such as MeOTf or AgPF₆ in the presence of donor ligands such as CO or acetonitrile leads to chloride abstraction and the formation of six-coordinate cationic complexes of the type [(PSiP)IrHL₂]⁺, which are formed as mixtures of syn and anti isomers (Scheme 6.12). In the presence of water, reactions with such electrophilic reagents result in water activation to form Ir dihydride complexes that contain the neutral L₃-silanol ligand κ³-(Ph₂P(CH₂)₃)₂Si(Me)OH (**49**, Scheme 6.12). As in the case of water activation by related (PSiP)Ru^{II} species (see above), the mechanism of this reaction is not known. In the presence of anions that are susceptible to hydrolysis, such as PF₆⁻ and BF₄⁻, the final products obtained featured Si–F rather than Si–O linkages (**51**, Scheme 6.12). The same Si–F-containing species could be accessed by treatment of the water activation product **50** with NaF or NaBF₄.

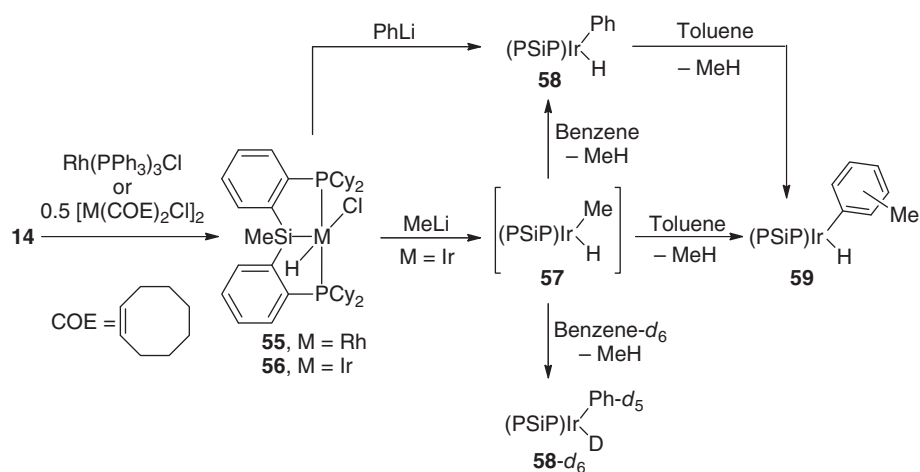


Scheme 6.12 Water activation by cationic (PSiP)Ir^{III} complexes.

Our group reported the first examples of PSiP ligated Rh complexes featuring phenylene-bridged bis(phosphino)silyl ligands. Although we initially utilized the diphenylphosphino ligand precursor **13** to target such complexes, including in the synthesis of **52**, **53a,b**, and **54** (Scheme 6.13) [38], we quickly discovered that the more electron-releasing dicyclohexylphosphino derivative **14** leads to the formation of more reactive Group 9 metal species that can undergo a variety of challenging E–H bond activation processes [39]. In contrast to the formation of the six-coordinate hydrido chloride species **53a,b** (Scheme 6.13) upon treatment of **13** with Rh(PPh₃)₃Cl [38], employing **14** under similar conditions resulted in formation of the five-coordinate complex **55** (Scheme 6.14) [39]; the Ir analog **56** was also prepared. The X-ray crystal structures of **55** and **56** confirm the formation of five-coordinate square-planar (Y-shaped) complexes with Si in the apical site, similar to the structure of the related complex **46-anti**. Unlike the reactivity observed



Scheme 6.13 Synthesis of (PSiP)Rh complexes.



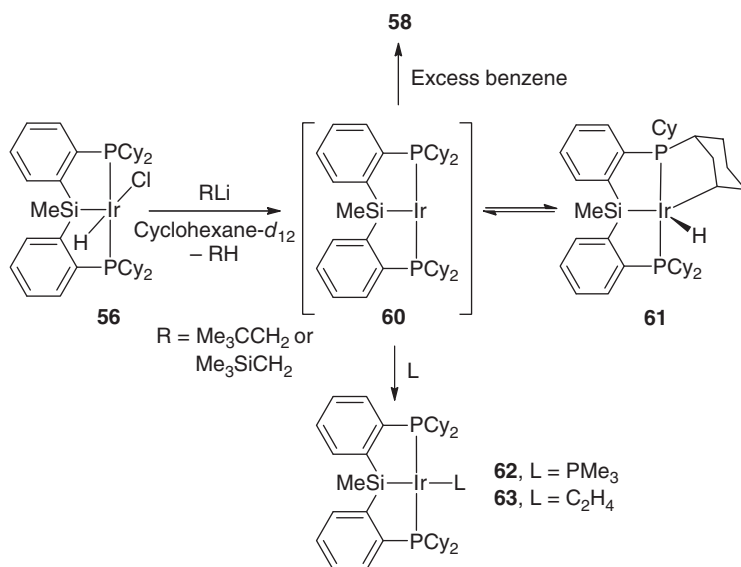
Scheme 6.14 Arene CH bond activation by (PSiP)Ir complexes.

for **38**, which features an aliphatic PSiP ligand backbone and diphenylphosphino donors, no *syn/anti* isomerization has been observed for **55** and **56** or their derivatives (see below), which suggests that the phenylene-bridged PSiP ligand framework can better restrict the coordination geometry in the ensuing metal complexes.

The attempted alkylation of **56** with MeLi in benzene solution resulted in quantitative formation of the phenyl hydride complex **58** with concomitant evolution of methane (Scheme 6.14) [39]. The targeted methyl hydride complex **57** can be observed *in situ* and rapidly reacts to generate **58** via CH bond activation of the benzene solvent. Complex **58** also undergoes facile arene exchange, as indicated by the formation of tolyl hydride species (**59**) upon treatment of **58**

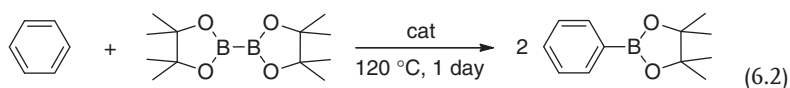
with excess toluene. Although Ir pincer complexes, especially those supported by PCP ligation, are well established in CH bond activation chemistry [1, 63, 64], this represents the first example of intermolecular CH bond cleavage by a silyl pincer Ir complex. While sp^2 -CH bond activation occurs readily in this system, no evidence for the intermolecular activation of sp^3 -CH bonds was observed. Reactivity commencing from the Rh analog **55** does not lead to such CH bond cleavage chemistry.

Based on the precedent related PCP and PNP Ir chemistry [63–66], we proposed that reductive elimination from **57** should provide access to a highly reactive 14-electron (PSiP)Ir^I intermediate (**60**, Scheme 6.15) which undergoes oxidative addition of CH bonds. Attempts to observe this intermediate species in cyclohexane- d_{12} solution provided evidence for a cyclometallated variant of **60** (i.e., **61**) that serves as a source of (PSiP)Ir^I [39]. Thus, treatment of *in situ* generated **61** with a large excess of benzene led to the formation of **58**, and (PSiP)IrL complexes (**62**, L = PMe₃; **63**, L = C₂H₄) were formed upon addition of donor ligands to **61** (Scheme 6.15) [67]. Treatment of **61** with benzene- d_6 led to the formation of **58-*d*₆**, with no evidence for ²H incorporation into the P-Cy substituents. Interestingly, although no CH bond cleavage chemistry was observed for (PSiP)Rh, a Rh analog of **60** (i.e., **64**) appears to be accessible, as treatment of **55** with an alkyl lithium reagent in cyclohexane solution results in rapid alkane formation and the generation of a new (PSiP)Rh species that features very broad NMR resonances and reacts with donor ligands such as PMe₃ and CO to form isolable Rh^I complexes of the type (PSiP)RhL (**65**, L = CO; **66**, L = PMe₃) [39, 67].

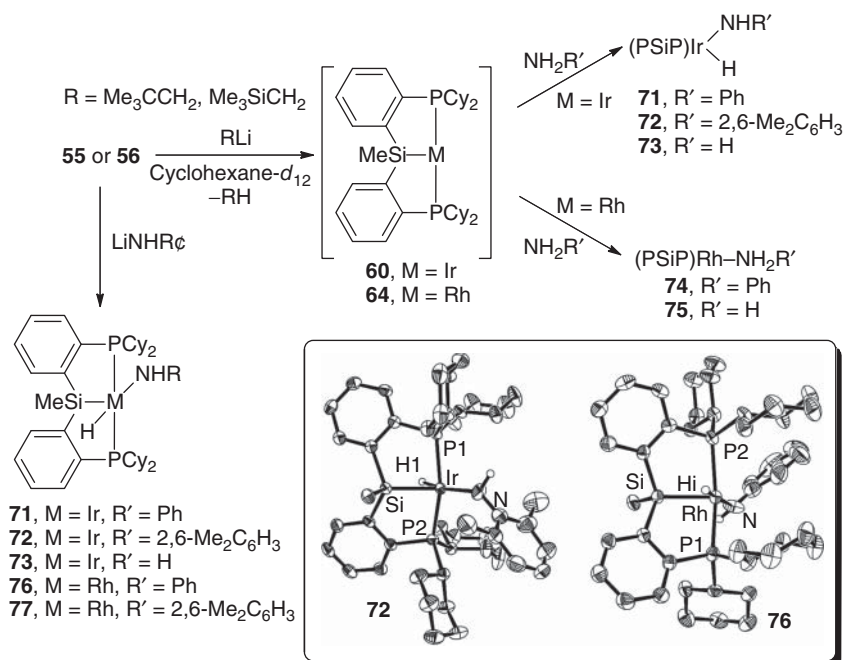


Scheme 6.15 Generation of (PSiP)Ir^I.

Activation of sp^2 -CH bonds has also been observed when complexes of the type $(R\text{-PSiP})\text{Ir}(\text{H})_4$ ($R\text{-PSiP} = [\kappa^3\text{-(2-R}_2\text{PC}_6\text{H}_4)_2\text{SiMe}]^-$; **67**, $R = \text{Cy}$; **68**, $R = {}^i\text{Pr}$; **69**, $R = {}^t\text{Bu}$) were heated in benzene solution in the presence of *tert*-butylethylene as a hydrogen acceptor to generate $(R\text{-PSiP})\text{IrH}(\text{Ph})$ (**58**, $R = \text{Cy}$; **58-}^i\text{Pr}, $R = {}^i\text{Pr}$; **58-}^t\text{Bu}, $R = {}^t\text{Bu}$) [45]. Treatment of **67** with 3 equiv of norbornene (nbe) resulted in the formation of the Ir^{I} norbornene adduct $(\text{Cy-PSiP})\text{Ir}(\text{nbe})$ (**70**), which indicates that such Ir^{I} tetrahydride complexes are dehydrogenated in the presence of alkenes to generate Ir^{I} species. The catalytic borylation of benzene with bis(pinacolato) diboron was examined using complexes **58**, **58-}^i\text{Pr}, and **58-}^t\text{Bu} as catalysts (Eq. 6.2) [45]. Yields of the product 2-phenyl-4,4,5,5-tetramethyl-1,3,2-dioxaborolane ranging from 20% to 88% were obtained at a catalyst loading of 5 mol% upon heating at 120°C for 1 day. Complex **58-}^t\text{Bu} is the most efficient catalyst, providing a yield of 82% at 1 mol% catalyst loading after heating at 120°C for 1 day.**********



In addition to sp^2 -CH bond cleavage, *in situ* generated **60** is also capable of mediating N–H bond oxidative addition processes (Scheme 6.16) [67]. N–H bond oxidative addition of anilines and, remarkably, ammonia occurred under mild

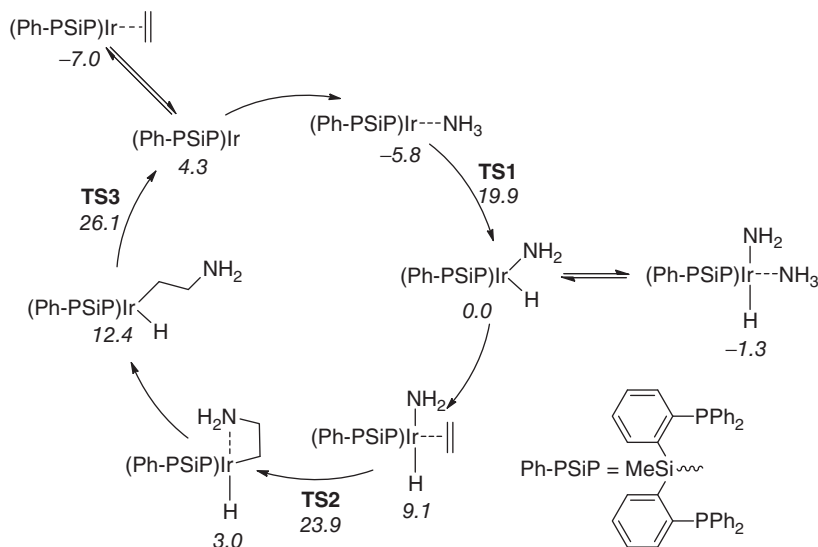


Scheme 6.16 N–H bond activation by $(\text{PSiP})\text{Ir}$ species.

conditions to form isolable (PSiP)Ir(H)(NHR') complexes (**71–73**). In comparison to the previously reported (PCP)Ir systems [68–70], **71–73** are significantly more resistant to N–H bond reductive elimination, even in the presence of alkene and arene substrates. Such well-documented examples of N–H bond oxidative addition are rare, especially in the case of ammonia [69, 70], and may provide inroads into new atom-economical chemical transformations that incorporate N–H bond oxidative addition steps, such as hydroamination. In the case of Rh, treatment of *in situ* generated **64** with aniline and ammonia resulted in the formation of Rh^I amine adducts which were stable only in the presence of excess amine and decomposed upon attempted isolation [67]. Since Rh^{III} anilido hydride complexes of the type (PSiP)RhH(NHR') (**76**, R' = Ph; **77**, R' = 2,6-Me₂C₆H₃) are synthetically accessible from the reaction of **55** with Li anilide reagents and are resistant to N–H reductive elimination, the formation of the adducts **74** and **75** from treatment of **64** with the corresponding amine indicates that the barrier to N–H oxidative addition in such Rh species is prohibitively high.

DFT studies of the N–H activation chemistry mediated by (PSiP)Ir species have been carried out. An initial report calculated the relative stabilities of the amido hydride complexes **71** and **73** and the corresponding amine complexes that would result from N–H reductive elimination [71]. ΔG^\ddagger was determined to be 33.4 kcal mol⁻¹ for **71** and 29.0 kcal mol⁻¹ for **73** in the gas phase at 298 K. The inclusion of solvent effects had minimal impact on these results. In the case of **71**, the Gibbs energy of the N–H reductive elimination reaction, $\Delta G_{\text{reaction}}$, was determined to be 10.1 kcal mol⁻¹ in the gas phase, indicating that the Ir^{III} amido hydride was more stable than the Ir^I aniline complex. For **73**, the $\Delta G_{\text{reaction}}$ was calculated to be 3.2 kcal mol⁻¹ in the gas phase. Interestingly, both ΔG^\ddagger and $\Delta G_{\text{reaction}}$ were reduced as the net result of substituting C for Si in **71** and **73**, which reflects the experimentally observed trend that more electron-releasing pincer ligands favor the formation of Ir^{III} amido hydride species over Ir^I amine adducts.

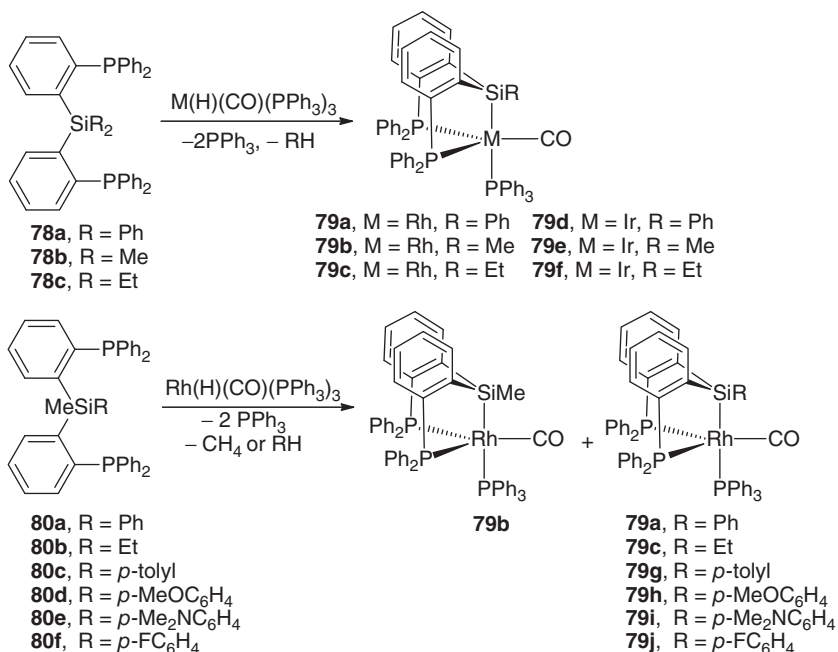
A second DFT study also determined that the amido hydride complex **73** was more stable than the corresponding ammine adduct ($\Delta G_{\text{reaction}} = -2.6$ kcal mol⁻¹ for N–H oxidative addition in the gas phase) [72]. This study also examined the relative energies of (PCP)Ir analogs and determined that [κ^3 -(^tBu₂PCH₂CH₂)₂CH]IrH(NH₂) was also more stable than the corresponding ammine adduct, while changing the pincer ligand to [κ^3 -1,3-(^tBu₂PCH₂)₂C₆H₃]⁻ led to a reversal in this trend, which is in agreement with experimental results. Catalytic cycles for the hydroamination of ethylene with ammonia were also examined computationally for (PSiP)- as well as (PCP)Ir pincer species. In the case of [κ^3 -(^tBu₂PCH₂CH₂)₂CH]IrH(NH₂), all energy spans calculated are on the order of about 40 kcal mol⁻¹ or higher, which suggests that such a catalytic process is not viable. By comparison, although the energy spans (on the order of about 35 kcal mol⁻¹) determined for hydroamination cycles involving **73** are significantly lower in some cases, these values are still quite high, suggesting that no turnover would be expected here either. The effect of modifications to the PSiP ligand was evaluated in this context, and it was determined that the substitution of Ph for Cy



Scheme 6.17 Optimized catalytic pathway for the hydroamination of ethylene; calculated Gibbs free energies (in kilocalories per mole).

substituents on the pincer phosphorus donors (Ph-PSiP) resulted in an energetic span low enough for catalytic turnover (Scheme 6.17). The ethylene complex $(\text{Ph-PSiP})\text{Ir}(\text{C}_2\text{H}_4)$ can serve as both a catalyst precursor and a resting state in the proposed cycle. The resulting predicted turnover frequency (TOF) was determined to be 17 h^{-1} at 140°C . When solvent effects (cyclohexane) were included in the calculation, a TOF of 6.0 h^{-1} was determined at 140°C .

Building on the Si–C bond cleavage reactivity that has been documented in Group 10 metal (Ni, Pd, Pt) PSiP complexes (see below), Nakazawa and coworkers [73] have reported on related Si–C bond activation processes involving Rh and Ir (Scheme 6.18). The bis(phosphino)silanes **78a–c** reacted with $\text{Rh}(\text{H})(\text{CO})(\text{PPh}_3)_3$ to form trigonal-bipyramidal Rh silyl complexes (**79a–c**). No intermediates were observed during the course of these reactions, and the reaction rates at 60°C increased in the order Si–Et < Si–Me < Si–Ph. Similar reactivity was observed when $\text{Ir}(\text{H})(\text{CO})(\text{PPh}_3)_3$ was reacted with **78a–c**. In an effort to assess the relative selectivity for sp^2 -SiC versus sp^3 -SiC bond activation, related reactions were carried out with the bis(phosphino)silanes **80a–f** which feature two different substituents at Si. In the case of **80a**, which features a SiMePh unit, both **79a** and **79b** were obtained in 39:61 ratio upon heating at 60°C , while an analogous reaction utilizing $\text{Ir}(\text{H})(\text{CO})(\text{PPh}_3)_3$ resulted in a reversal of this selectivity. Furthermore, the selectivity for Si–Me versus Si–Ph activation was found to be dependent on the reaction temperature, so that in the reaction of **80a** with $\text{Rh}(\text{H})(\text{CO})(\text{PPh}_3)_3$ a reversal in selectivity was observed upon heating at 160°C leading to a **79a** : **79b** ratio of 59 : 41. The incorporation of electron-donating substituents in **80c–e** resulted in the inhibition of Si–C(sp^2) activation.



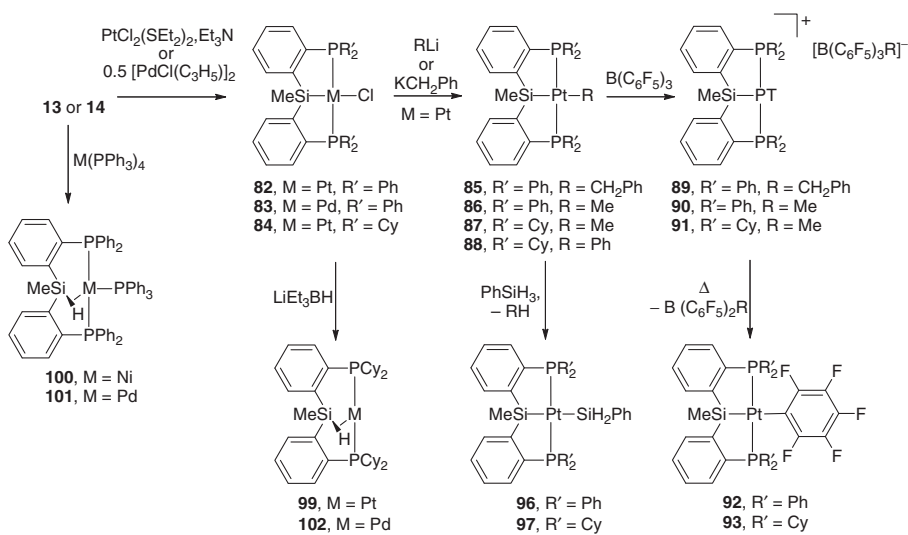
Scheme 6.18 Si–C bond activation by Rh and Ir hydride complexes.

6.5

Group 10 Metal PSiP Chemistry

The first examples of group 10 metal complexes supported by bis(phosphino)silyl ligation were reported by Stobart and coworkers [35, 36] who studied the reactivity of the silanes **1**, **3–7**, **10**, and **11** with (COD)PtCl₂ in the presence of Et₃N. Square-planar (PSiP)PtCl complexes (**81a–h**) were isolated from these reactions in yields ranging from 27% to 84%. Subsequent to this study, our group reported the first example of related Pt^{II} and Pd^{II} chloride complexes (**82**, M = Pt; **83**, M = Pd) supported by the phenylene-bridged PSiP ligand [κ^3 -(2-Ph₂PC₆H₄)₂SiMe][−] (Ph-PSiP) derived from **13** (Scheme 6.19) [38]. The reactivity of **83** and related derivatives has since been explored extensively by Iwasawa and coworkers [74, 75], who have utilized such silyl pincer Pd^{II} complexes in a variety of catalytic applications, including the hydrocarboxylation of allenes and 1,3-dienes, reductive aldol reactions [16], and the dehydrogenative borylation of alkenes and 1,3-dienes [76]. This work is reviewed in an accompanying chapter.

Our group has explored in detail the reactivity of **82** and the dicyclohexylphosphino analog **84** (Scheme 6.19). These Pt^{II} chloride complexes were utilized as precursors for the synthesis of Pt^{II} alkyl complexes and cations of the type [(PSiP)Pt]⁺, with the goal of accessing highly reactive metal complexes that would engage in E–H bond activation chemistry [77]. Indeed, square planar Pt^{II} alkyl and aryl complexes of the type (R′-PSiP)PtR (**85**, R′ = Ph, R = CH₂Ph; **86**,



Scheme 6.19 Synthesis of group 10 metal PSiP complexes.

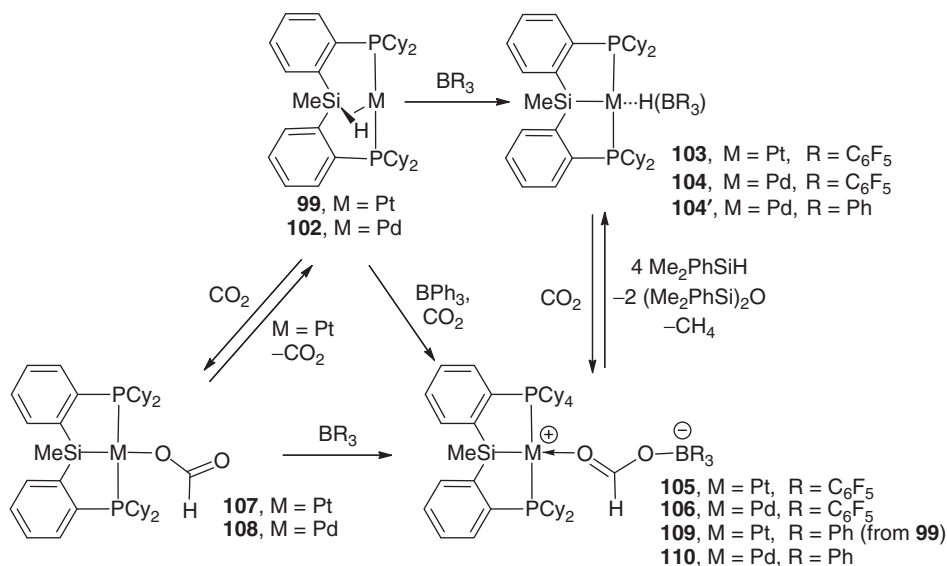
$R' = \text{Ph}$, $R = \text{Me}$; **87**, $R' = \text{Cy}$, $R = \text{Me}$; **88**, $R' = \text{Cy}$, $R = \text{Ph}$) were readily prepared (Scheme 6.19). Treatment of **85–87** with $\text{B}(\text{C}_6\text{F}_5)_3$ resulted in abstraction of the alkyl group to form cationic species of the type $[(R'-\text{PSiP})\text{Pt}]^+[\text{RB}(\text{C}_6\text{F}_5)_3]^-$ (**89**, $R' = \text{Ph}$, $R = \text{CH}_2\text{Ph}$; **90**, $R' = \text{Ph}$, $R = \text{Me}$; **91**, $R' = \text{Cy}$, $R = \text{Me}$). Although there is significant precedent for arene CH bond activation by cationic Pt^{II} species [78], including pincer-type Pt cations [79, 80], no such CH bond cleavage chemistry was observed for **89–91**. Complex **89** proved highly insoluble in benzene solution even at elevated temperatures. By comparison, **90** and **91** are both fully soluble in benzene, but underwent facile transfer of a C_6F_5^- group from B to Pt to form $[(R'-\text{PSiP})\text{Pt}(\text{C}_6\text{F}_5)]$ (**92** and **93**). The related cationic complex $[(\text{Ph-PSiP})\text{Pt}(\text{OEt}_2)]^+[\text{B}(\text{C}_6\text{F}_5)_4]^-$ (**94**) and triflate derivative $(\text{Cy-PSiP})\text{PtOTf}$ (**95**) also proved to be unreactive toward benzene CH bonds.

By comparison, complexes **85–87** mediated facile SiH bond cleavage, reacting readily with PhSiH_3 to form Pt^{II} silyl complexes (**96**, $R' = \text{Ph}$; **97**, $R' = \text{Cy}$) with concomitant formation of the corresponding alkane (Scheme 6.19) [77]. Interestingly, **96** and **97** represent rare examples of Pt^{II} bis(silyl) species featuring trans-disposed silyl ligands [81]. This unusual geometry is likely enforced by the chelating nature of the PSiP silyl pincer ligand. The activation of SiH bonds by complexes **85–87** is sensitive to the steric profile of the hydrosilane, and bulky secondary silanes such as Mes_2SiH_2 do not react. By comparison, divergent reactivity toward hydridochlorosilanes was observed based on the substitution at phosphorus ($R = \text{Ph}$ vs $R = \text{Cy}$). Thus, while **85** and **86** reacted with Ph_2SiHCl to form the silyl complex $(\text{Ph-PSiP})\text{PtSiPh}_2\text{Cl}$ (**98**) with loss of either toluene or methane, respectively, **87** reacted with Ph_2SiHCl , ${}^i\text{Pr}_2\text{SiHCl}$, or Me_3SiCl to form **84** with concomitant evolution of Ph_2SiMeH , ${}^i\text{Pr}_2\text{SiMeH}$, or Me_4Si , respectively. A mechanism invoking direct Si–Cl oxidative addition to **87** followed by Si–C reductive elimination appears unlikely for these reactions, as SiH oxidative addition to Pt^{II} is anticipated to be preferred [82–90]. Nonetheless, the divergent reactivity with hydridochlorosilanes exhibited by **85–87** reveals that changes in the substitution at phosphorus in the PSiP ligand can significantly alter the course of reactions involving such substrates.

Surprisingly, treatment of **84** with LiEt_3BH did not result in the formation of a terminal Pt–H, but rather led to the formation of $[\text{Cy-PSi}(\mu\text{-H})\text{P}]\text{Pt}$ (**99**), which was identified on the basis of NMR and IR spectroscopic data as a bis(phosphino) Pt derivative of $(\text{Cy-PSiP})\text{H}$ that features $\eta^2\text{-SiH}$ coordination involving the tethered silicon fragment (Scheme 6.19) [77]. The formation of the $\eta^2\text{-SiH}$ complex was unexpected given that complexes of the type *trans*- $\text{Pt}(\text{PCy}_3)_2(\text{H})(\text{SiR}_3)$ are known [91–93]. Complex **99** can be viewed as the product of an “arrested” reductive elimination from the unobserved terminal Pt^{II} hydride species. Such an elimination may be envisioned to proceed via an initial distortion of the square-planar structure [94, 95], which would serve to bring the hydride ligand into the proximity of the silyl group. Although attempts to probe the solution behavior of **99** by variable-temperature ${}^1\text{H}$ and ${}^{31}\text{P}$ NMR spectroscopy revealed no appreciable changes in spectroscopic features in the range of -80 to 90°C , it is possible that a small equilibrium concentration of the terminal Pt–H can be accessed via a reversible SiH oxidative addition–reductive elimination process.

Related Ni (**100**) and Pd (**101**) complexes bearing a PPh₃ co-ligand and featuring η^2 -SiH coordination of the silane **13** were subsequently reported and crystallographically characterized by Takaya and Iwasawa [96, 97]. We have also reported the synthesis of a Pd analog of **99** (i.e., **102**) [98]. Although we did not obtain X-ray quality crystals of **102**, the NMR and IR features of this complex are consistent with its formulation as an η^2 -SiH complex of **14**. Namely, while the ¹H NMR spectrum of isolated **102** does not feature a high-field resonance in the region characteristic of a terminal Pd–H (typically <0 ppm), ¹H–²⁹Si HMQC (heteronuclear multiple quantum correlation) spectroscopic analysis revealed a Pd–H resonance at 1.28 ppm (in benzene-*d*₆ solution this resonance is obscured by resonances associated with the P-Cy substituents) that correlates with a ²⁹Si NMR resonance at 62.5 ppm (¹J_{SiH} = 47 Hz). The reduced ¹J_{SiH} value (typical ¹J_{SiH} values in free silanes fall near 200 Hz) observed for **102** falls in the range commonly associated with η^2 -silane complexes [99]. Furthermore, in keeping with η^2 -SiH coordination to a metal center, the IR spectrum of **102** (film) exhibits a broad, intense band at 1623 cm⁻¹, a region characteristic of an η^2 -SiH metal species. Concurrent with our publication of the synthesis of **102**, Hazari and coworkers [100] reported an identical synthesis but assigned **102** as a terminal Pd^{II} hydride complex on the basis of an X-ray crystal structure indicating a terminal Pd–H, albeit with the comment that “although the hydride was located in the difference Fourier map, due to the high level of residual electron density around the Pd center the assignment of the hydrogen atom cannot be guaranteed”. There is precedent for such differing SiH binding modes in solution versus in the solid state [101, 102], which suggests that it is possible for the η^2 -SiH structure of **102** to be the major species in solution at room temperature whereas the terminal hydride structure is adopted in the solid state. DFT evaluation of the terminal Pd–H and η^2 -SiH structures proposed for **102** indicated that the former is thermodynamically favored ($\Delta G^\circ = 11$ kcal mol⁻¹) [100]. Hazari [100] also reported the synthesis and crystallographic characterization of the analogous (Cy-PSiP)NiH, which is also apparently a terminal Ni^{II} hydride in the solid state.

Treatment of complexes **99** and **102** with the strong Lewis acid B(C₆F₅)₃ afforded the hydride abstraction products **103** and **104**, respectively (Scheme 6.20) [98]. Complexes **103** and **104** react with CO₂ gas (about 1 atm) to form the corresponding Pt and Pd formatoborate complexes (**105**, M = Pt; **106**, M = Pd). The formatoborate complexes were readily distinguished from the corresponding Pt and Pd formate species (**107**, M = Pt; **108**, M = Pd) on the basis of their NMR spectroscopic features [98, 100]. Furthermore, unlike complex **105**, which was readily isolated in high yield, the Pt formate complex **107** was only observable under a CO₂ atmosphere and re-formed **99** upon removal of CO₂. Conversely, the Pd formate complex **108** proved isolable, and treatment of **108** with an equivalent of B(C₆F₅)₃ resulted in quantitative conversion to **106**. BPh₃ analogs of **105** (i.e., **109**) and **106** (i.e., **110**) were also synthesized. Such transition-metal formatoborate complexes are quite rare. A previous late metal example was reported by Bercau and Labinger [103] for [HNi(dmpe)₂]⁺ (dmpe, 1,2-bis(dimethylphosphino)ethane), which was shown to form formate-borane adducts in the presence of trialkyl boranes upon reaction



Scheme 6.20 Synthesis of Pd and Pt formatoborate complexes (only one resonance structure is shown for formatoborate complexes **105**, **106**, **109**, and **110**).

with CO₂. By comparison, B(C₆F₅)₃ exhibited only hydride transfer from Ni to B and no CO₂ reduction in this system. Thus, it appears that the facile reduction of CO₂ by **103** and **104** to form late metal formatoborate species is unprecedented. Subsequent to our report, Piers and coworkers [104] published an example of a d⁰ Sc formatoborate complex formed by the reaction of [Cp*₂Sc][HB(C₆F₅)₃] with CO₂.

Complexes **105** and **106** reacted with 4 equiv of Me₂PhSiH to reform **103** or **104**, respectively, with the concomitant evolution of methane and (Me₂PhSi)₂O (Scheme 6.20) [98]. A catalytic variant of this reaction was pursued [104–107], using *in situ* generated **103** or **104** as the catalyst (Table 6.2). Using **103** as the catalyst afforded 1063 turnovers after 4 h, while the Pd analog at the same loading resulted in 469 turnovers with heating at 85 °C (Table 6.1, entries 1 and 6). In the case of the more active Pt-based catalyst **103**, the TOF after 0.5 h at 65 °C was determined to be 956 h⁻¹. As expected, the TOF was observed to decrease over the course of the reaction (TOF = 616 h⁻¹ after 1 h and 266 h⁻¹ after 4 h). Notably, the use of BPh₃ in place of B(C₆F₅)₃ under comparable conditions afforded no catalytic turnover. Control experiments carried out in the absence of CO₂ confirmed that the observed silyl ether formation cannot be attributed to side reactions involving adventitious water or O₂ (entry 5), and further control experiments confirmed the key role of both the platinum group metal complex and B(C₆F₅)₃ in achieving efficient catalytic reduction of CO₂ (entries 7–10). The catalytic productivity (TON, turnover number) and rates (TOF) exhibited by **103** are comparable in magnitude to those observed by Brookhart and coworkers [105] in a related cationic (POCOP)Ir^{III} pincer system.

Table 6.2 Reduction of CO₂ with trialkylsilanes.^a

$$4 \text{ R}_3\text{SiH} + \text{CO}_2 (1 \text{ atm}) \xrightarrow[\text{C}_6\text{H}_5\text{F}, 65^\circ\text{C}]{\text{Catalyst}} 2 (\text{R}_3\text{Si})_2\text{O} + \text{CH}_4$$

Entry	Catalyst	Mol% of catalyst	Silane	Time (h)	(R ₃ Si) ₂ O (mmol) ^b	TON ^c
1	103	0.065	Me ₂ PhSiH	4	3.4	1063 ^d
2 ^e	103	0.016	Me ₂ PhSiH	8	5.7	1781
3 ^f	103	0.016	Me ₂ PhSiH	16	6.9	2156
4	103	0.065	Et ₃ SiH	4	0.07	22
5 ^g	103	0.065	Me ₂ PhSiH	4	0	0
6 ^h	104	0.065	Me ₂ PhSiH	4	1.5	469
7 ⁱ	NaH/B(C ₆ F ₅) ₃ /15-c-5	0.4	Me ₂ PhSiH	4	1.2	57
8	LiEt ₃ BH/B(C ₆ F ₅) ₃	0.1	Me ₂ PhSiH	4	0.1	16
9	99	0.0065	Me ₂ PhSiH	4	0	0
10	102	0.0065	Me ₂ PhSiH	4	0	0

^aReaction conditions: 2 ml C₆H₅F, 1 atm CO₂, 9.78 mmol silane, 65 °C.

^bDetermined on the basis of calibrated GC data.

^cCalculated based on moles of SiH reacted per moles of catalyst.

^dTOF of 956 h⁻¹ (0.5 h), 616 h⁻¹ (1 h), and 266 h⁻¹ (4 h).

^eReaction carried out using 39.16 mmol of silane; CO₂ (1 atm) was reintroduced to the reaction mixture after 4 h at 65 °C.

^fReaction carried out using 39.16 mmol of silane; CO₂ (1 atm) was reintroduced to the reaction mixture after 4, 8, and 12 h at 65 °C.

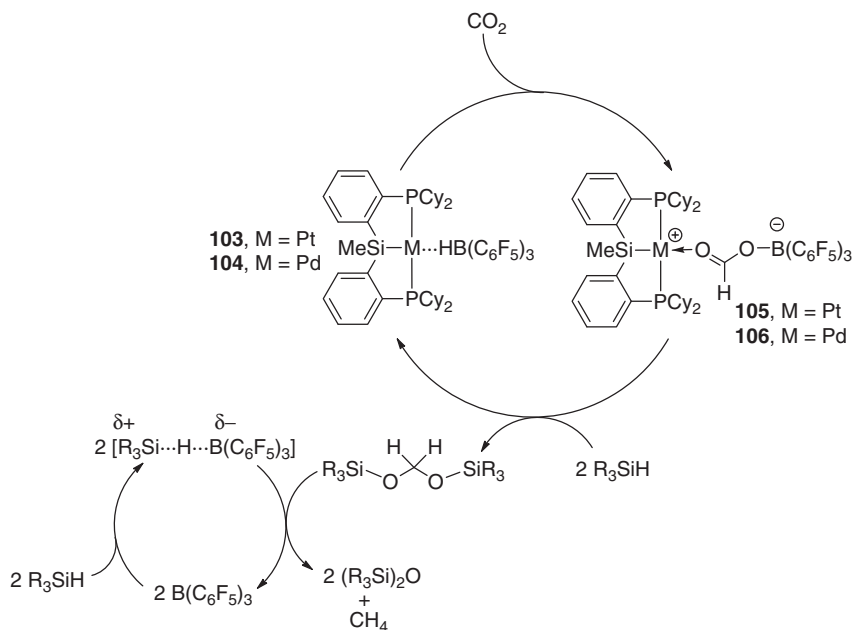
^gReaction conducted in absence of CO₂.

^hReaction carried out at 85 °C.

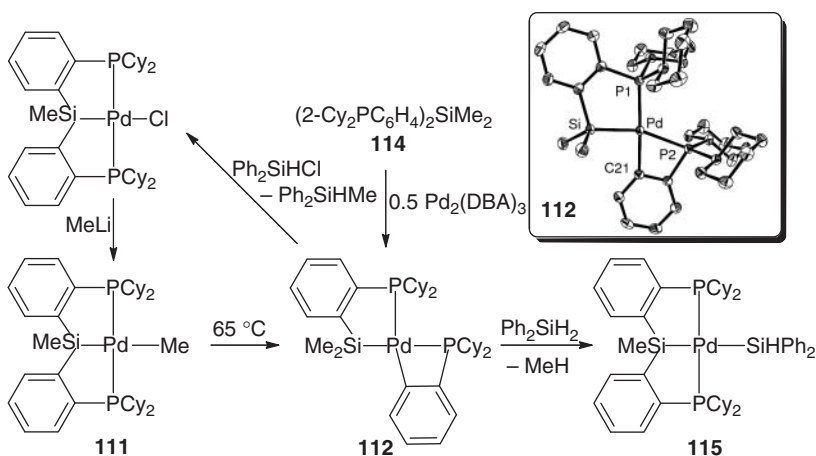
ⁱ15-c-5, 15-Crown-5.

A proposed catalytic cycle for the reduction of CO₂ with tertiary silanes in the presence of **103** and **104** is shown in Scheme 6.21. We postulated that **103** and **104** initially react with CO₂ to form the corresponding formatoborate complexes **105** and **106**, respectively, which subsequently react with 2 equiv of silane to re-form **103** and **104** and generate an equivalent of CH₂(OSiR₃)₂. Subsequent reduction of the bis(silyl)acetal to form methane and the corresponding bis(silyl)ether is achieved by the previously reported route involving B(C₆F₅)₃-mediated hydrosilylation [104, 106–109]. A sufficient amount of free B(C₆F₅)₃ is likely present in solution, possibly as a result of its dissociation from complexes **103** and **104** and/or **105/106**. Upon addition of excess B(C₆F₅)₃ (10%) to a catalytic run involving **103**, the yield of (R₃Si)₂O produced actually decreased relative to the reaction run in the absence of excess borane.

Our investigations on the reactivity of Group 10 metal pincer complexes supported by [κ³-(2-Cy₂PC₆H₄)₂SiMe]⁻ (Cy-PSiP) ligation also led to the discovery of unusual Si–C bond activation chemistry (Scheme 6.22) [110, 111]. The alkylation of (Cy-PSiP)PdCl with MeLi led to the formation of the corresponding Pd–Me complex (**111**) in good yield [110]. Complex **111** underwent a subsequent rearrangement



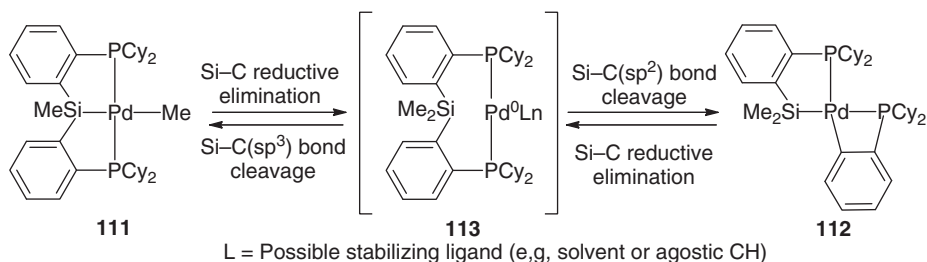
Scheme 6.21 Proposed catalytic cycle for CO_2 hydrosilylation.



Scheme 6.22 Si-C bond cleavage involving (Cy-PSiP)Pd species.

involving net transfer of the Pd-Me group to Si and cleavage of a Si-C(sp²) bond in the pincer ligand backbone to yield a four-membered Pd-C-C-P metallacycle (Scheme 6.22). The resulting complex (**112**) was isolated and crystallographically characterized. A possible mechanism for the formation of **112** could involve the intermediacy of a Pd⁰ species (**113**; not directly observed and likely stabilized by

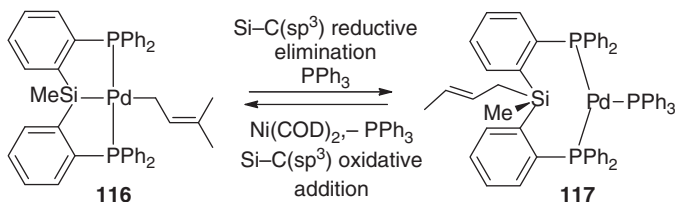
solvent coordination or an agostic interaction) which undergoes Si–C(sp²) oxidative addition (Scheme 6.23). Given that direct reductive elimination from **111** to afford **113** is unlikely due to the trans-disposed Pd–Si and Pd–Me groups, it is plausible that Si–C(sp³) bond formation is preceded by Pd–P dissociation or a tetrahedral distortion in **111**. Support for this mechanistic proposal was obtained by the quantitative generation of **112** from the reaction of (2-Cy₂PC₆H₄)₂SiMe₂ (**114**) with half an equivalent of Pd₂(DBA)₃ (DBA, dibenzylideneacetone; Scheme 6.22). Remarkably, the Si–C(sp²) bond cleavage process is reversible, as indicated by the reaction of **112** with Ph₂SiH₂, which afforded the Pd silyl complex **115** [110]. As well, treatment of **112** with Ph₂SiHCl led to the formation of (Cy-PSiP)PdCl with the concomitant generation of Ph₂SiHMe. These reactions require cleavage of a Si–C(sp³) linkage within the rearranged species **112** in order to re-form the Cy-PSiP framework. Although Si–C(sp²) bond activation is well documented [112–116], examples of unstrained Si–C(sp³) bond cleavage within the coordination sphere of a mononuclear metal complex are extremely rare [73, 117–125]. It is plausible that Si–C(sp²) reductive elimination in **112** regenerates **113**, which undergoes subsequent Si–C(sp³) bond cleavage to re-form **111** (Scheme 6.23). The terminal Pd–Me species then undergoes SiH bond oxidative addition to ultimately provide the observed products. The Si–C(sp³) bond cleavage step may involve an initial CH bond oxidative addition of a Si–Me group, as precedent for such a transformation exists in related Pt Si–C(sp³) bond cleavage chemistry [122, 124, 125].



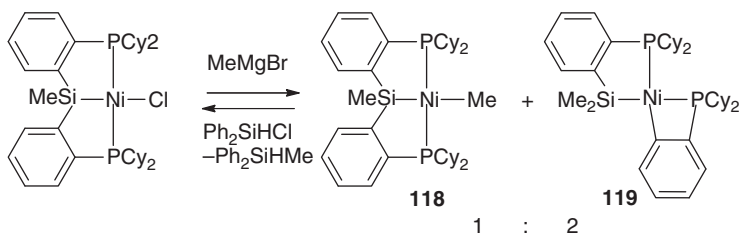
Scheme 6.23 Proposed mechanism of reversible Si–C bond activation by (Cy-PSiP)Pd.

In a subsequent publication, Takaya and Iwasawa [96] reported a related example of reversible Si–C(sp³) bond cleavage involving Ph-PSiP-ligated Pd species (Scheme 6.24). Treatment of the prenylpalladium complex **116** with PPh₃ resulted in Si–C(sp³) reductive elimination to form a Pd⁰ tris(phosphine) complex that featured an allylsilane unit in the ligand backbone (**117**). Subsequent treatment of **117** with the phosphine scavenger Ni(COD)₂ resulted in Si–C(sp³) bond cleavage and regeneration of **116**. These observations lend support to the mechanistic proposal put forward for the reversible Si–C bond cleavage processes observed for (Cy-PSiP)Pd.

Our attempt to access a Ni analog of **112** led to the generation of an equilibrium mixture comprised of the terminal Ni–Me complex (**118**) and the complex resulting from Si–C(sp²) bond cleavage in the ligand backbone (**119**, Scheme 6.25),



Scheme 6.24 Si-C(sp³) bond cleavage involving (Ph-PSiP)Pd.

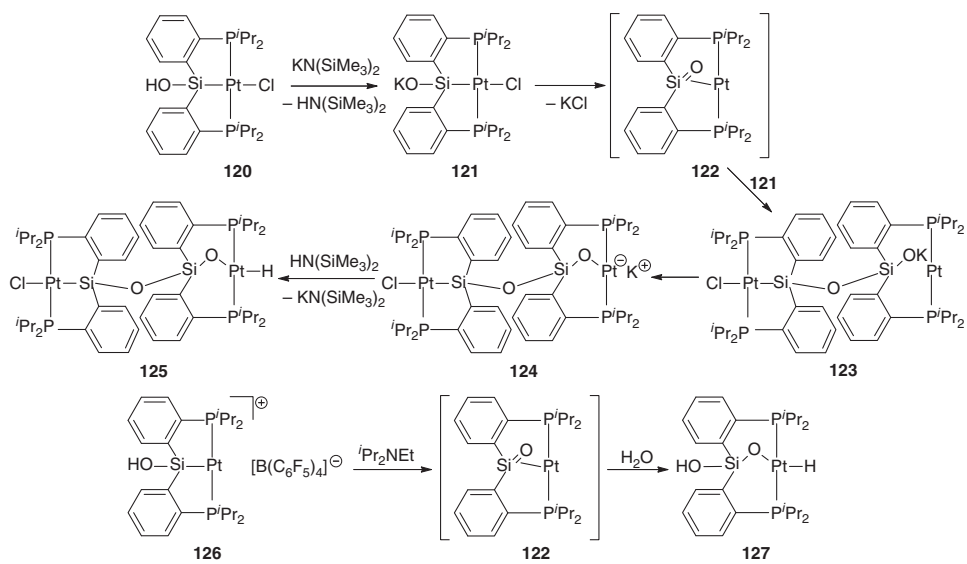


Scheme 6.25 Si-C bond cleavage involving (Cy-PSiP)Ni.

which were observed in a nearly 1:2 ratio [110]. Notably, ³¹P-³¹P EXSY NMR (EXSY, Exchange Spectroscopy) spectra of the **118/119** mixture revealed chemical exchange between the magnetically nonequivalent phosphorus environments in **119** (in keeping with reversible Si-C(sp²) bond cleavage), as well as cross-peaks indicative of exchange involving **118** and **119** (in keeping with reversible Si-C(sp³) bond cleavage). Under similar conditions, no chemical exchange between the magnetically nonequivalent phosphorus environments in **112** was observed. The interconversion of **118** and **119** was further confirmed by ¹H-¹H EXSY NMR experiments, which revealed chemical exchange between the SiMe and NiMe environments in **118** and **119** [110]. Thus, remarkably, in the case of Ni, these Si-C bond activation processes are reversible on the NMR timescale in solution.

Interestingly, contrary to these observations for Ni and Pd alkyl complexes supported by Cy-PSiP ligation, the analogous Pt alkyl complexes do not appear to engage in such Si-C bond cleavage processes [77]. However, treatment of Pt(PPh₃)₄ with (2-Cy₂PC₆H₄)₂SiMe₂ (**114**) resulted in Si-C(sp³) bond cleavage and quantitative formation of (Cy-PSiP)PtMe (**87**) [111]. The analogous reaction with a Pd⁰ source afforded **112**, the product of Si-C(sp²) bond cleavage (see above) [110], indicating that the choice of metal influences the outcome of Si-C bond cleavage in this system.

Milstein and coworkers [43] have also contributed to group 10 metal PSiP chemistry, having attempted to stabilize Pt silanone (R₂Si=O) species in the framework of a PSiP pincer. The attempted deprotonation of the silanol Pt^{II} complex **120** with a strong base resulted in an unusual rearrangement process that afforded the dinuclear Pt hydride complex **125** (Scheme 6.26). A proposed



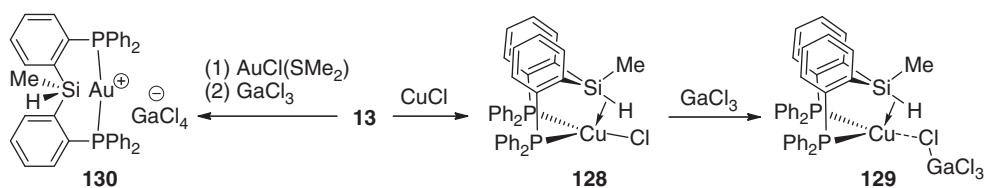
Scheme 6.26 Attempted generation of a Pt silanone complex.

mechanism for the formation of **125** invokes the generation of an intramolecularly coordinated silanone species (**122**) that undergoes nucleophilic attack by the silanolate species **121** to form the dinuclear siloxy-silanolate intermediate **123**. Complex **123** subsequently undergoes an intramolecular attack on the metal to give the anionic dinuclear intermediate **124**, which is subsequently protonated by $\text{HN}(\text{SiMe}_3)_2$ to form the observed product **125** (Scheme 6.26). Alternatively, **123** could be protonated by $\text{HN}(\text{SiMe}_3)_2$ to form the corresponding silanol, which could then undergo intramolecular OH oxidative addition to afford **125**. Treatment of the cationic Pt^{II} silanol complex **126** with the weak base ${}^i\text{Pr}_2\text{NEt}$ led to related reactivity involving the nucleophilic attack of adventitious water on the intermediate silanone **122** to form the mononuclear silanolate Pt^{II} hydride species **127** (Scheme 6.26). Thus it appears that the targeted silanone complex **122** is not sufficiently protected from nucleophilic attack, which prevents its isolation.

6.6

Group 11 Metal PSiP Chemistry

Bourissou and coworkers [126] have studied the complexation of **13** to Cu and Au (Scheme 6.27). In the case of complexation to CuCl, a weak $\sigma\text{-SiH}$ complex (**128**) appears to form, as indicated by a reduced ${}^1J_{\text{SiH}}$ value (180 Hz vs 204 Hz in free **13**) and ν_{SiH} stretching frequency (1996 cm^{-1} vs 2142 cm^{-1} in free **13**). In an attempt to increase the electrophilicity of the Cu center, complex **128** was treated with GaCl_3 to form complex **129**, where the Lewis acid had partially abstracted the Cu–Cl ligand to form a tight ion pair, as indicated by an elongated Cu–Cl distance ($2.359(1)\text{ \AA}$ vs $2.229(1)\text{ \AA}$ in **128**) in the X-ray crystal structure of **129**. The σ -coordination of the SiH bond appears to strengthen in **129**, as indicated by further reduction of both ${}^1J_{\text{SiH}}$ (170 Hz) and the ν_{SiH} stretching frequency (1973 cm^{-1}), which is consistent with pure $\sigma\text{-SiH}\rightarrow\text{Cu}$ donation. DFT calculations confirm the formation of $\sigma\text{-SiH}$ complexes of Cu that feature negligible $\text{Cu}\rightarrow\sigma^*\text{-SiH}$ back-donation. Complexes **128** and **129** thus represent rare examples of σ -bond coordination to Cu. In contrast, the reaction of **13** with $\text{AuCl}(\text{SMe}_2)$ and GaCl_3 led to the formation of a cationic bisphosphino Au^I complex (**130**), in which the Au center does not interact with the SiH bond contained in the ligand backbone.



Scheme 6.27 Synthesis of Cu $\sigma\text{-SiH}$ complexes.

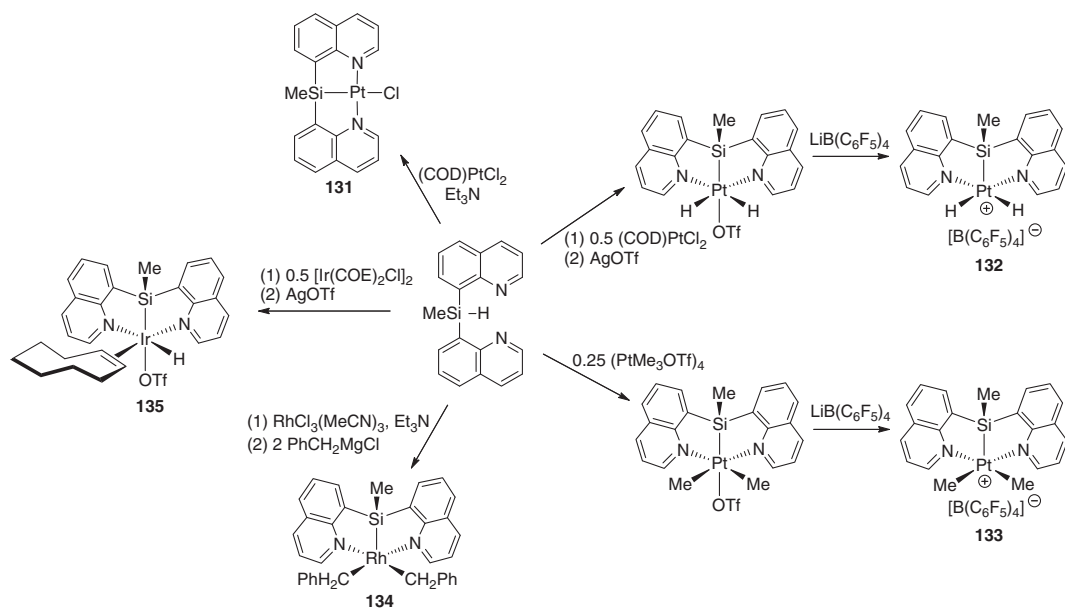
6.7

Alternative Silyl Pincers

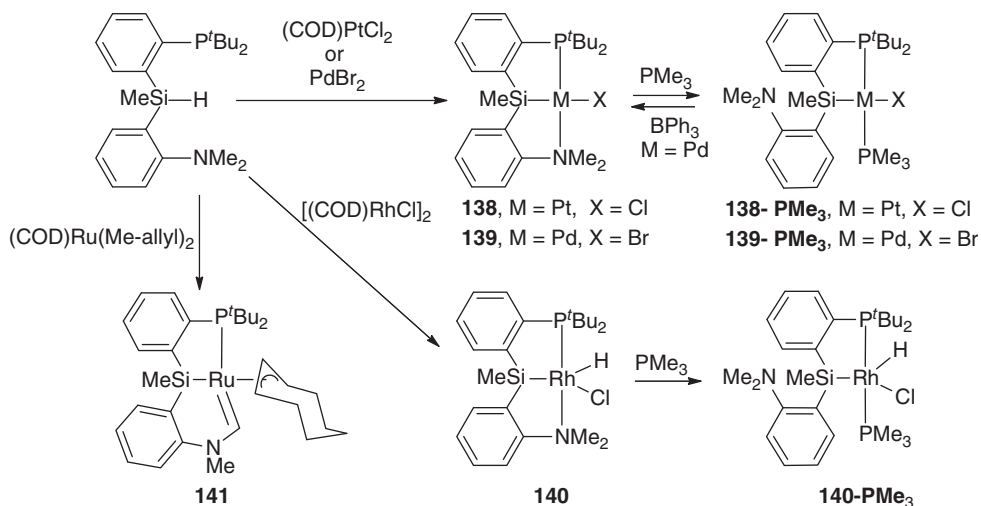
While PSiP silyl pincer complexes have received the most attention, several alternative silyl pincer motifs have also been developed in recent years. Among the most prominent are the bis(quinolyl)silyl (NSiN) complexes developed by Tilley and coworkers. Tridentate coordination of NSiN to Rh, Ir, and Pt has been reported, affording both neutral and cationic complexes (Scheme 6.28) [127–130]. Such complexes typically exhibit *fac*-NSiN coordination, although square-planar (NSiN)PtCl (**131**) has also been isolated [130]. Interestingly, NSiN promotes the formation of five-coordinate complexes, including examples of five-coordinate Pt^{IV} species (**132** and **133**) of the type often proposed as intermediates in Pt-mediated CH bond activation chemistry [130], and an unusual example of a 16-electron Rh^{III} dialkyl complex, (NSiN)Rh(CH₂Ph)₂ (**134**) [128]. The Ir^{III} triflate complex (NSiN)Ir(H)(OTf)(COE) (**135**; COE, cyclooctene) catalyzes both aryl silane redistribution and the dehydrogenative silylation of arenes [129]. Attempts to prepare (NSiN)Ni complexes led to the formation of the silyl nickel cluster (NSiN)₂Ni₃Cl₂ (**136**) [131]. As well, an unusual Fe complex [(NSiN)H]Fe[N(SiMe₃)₂]₂ (**137**) which features an η¹-SiH interaction with the Fe center has been reported [132].

Our group has recently reported the first example of hemilabile PSiN mixed donor pincer ligation (Scheme 6.29) [37]. Square-planar complexes of the type (PSiN)MX (**138**, M = Pt, X = Cl; **139**, M = Pd, X = Br) were engaged in dynamic processes in solution involving decomplexation of the amine arm and inversion and rotation at N, which rendered the NMe groups equivalent at elevated temperatures. The amino PSiN ligand arm could also be displaced from the metal coordination sphere in **138**, **139**, and the five-coordinate Rh complex (PSiN)Rh(H)Cl (**140**) by the introduction of a more strongly coordinating donor ligand such as PMe₃. In the case of (κ²-PSiN)Pd(Br)(PMe₃) (**138**-PMe₃), treatment with BPh₃ as a PMe₃ scavenger led to the quantitative regeneration of **139**, which further highlights the hemilabile character of PSiN ligation. This reversible coordination of the amine pincer arm is anticipated to render PSiN-ligated complexes more responsive to the changing electronic and coordinative requirements at a metal center that arise during substrate transformations, and may provide access to new and/or enhanced reactivity. Surprisingly, attempts to prepare (PSiN)Ru complexes by utilizing (COD)Ru(2-methylallyl)₂ as the Ru source led instead to the formation of a cyclooctenyl (PSiC)Ru carbene complex (**141**) resulting from CH bond activation of an NMe group in the PSiN ligand and of the 1,5-cyclooctadiene. Remarkably, this transformation requires three CH bond activation steps, as well as SiH bond activation at a single Ru center.

Lastly, there have been two reports of tridentate SSiS ligation. Takeda and coworkers [133] have reported on the synthesis of dihydrosilanes substituted with two thioether groups (**142**–**144**, Scheme 6.30). The reaction of **143** with (COD)PtCl₂ in the presence of Et₃N afforded the bis(silyl) Pt complex **145** in low

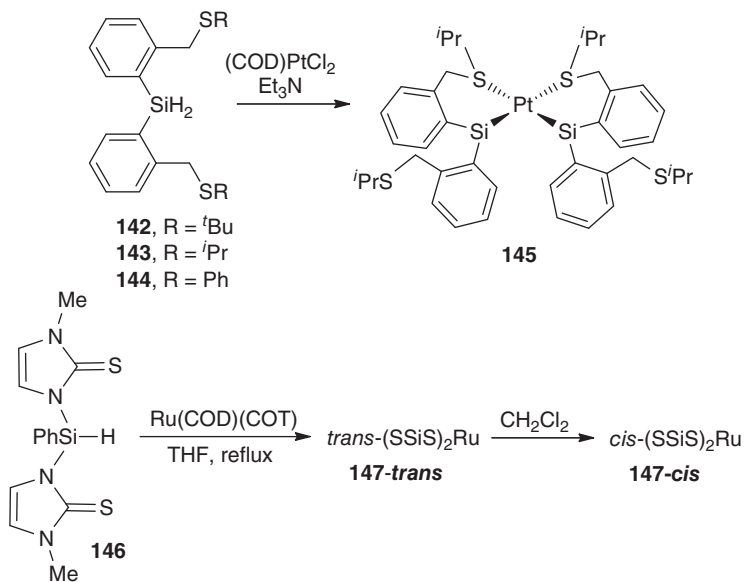


Scheme 6.28 Synthesis of late metal NSiN complexes.



Scheme 6.29 Synthesis of late metal PSiN complexes.

yield. As well, Hill and coworkers [134] have reported on the reactivity of the bis(methimazolyl)silane **146** with $\text{Ru}(\text{COD})(\text{COT})$ (COD, 1,5-cyclooctadiene; COT, 1,3,5,7-cyclooctatetraene), which led to the formation of two isomeric forms of the Ru^{II} species $(\text{SSiS})_2\text{Ru}$ (**147**, Scheme 6.30).



Scheme 6.30 Examples of tridentate SSiS late metal complexes.

6.8

Summary

PSiP ligands have emerged as a versatile, new class of tridentate ligands that can accommodate a variety of reactive late metal centers. PSiP complexes have been shown to display unique structural features and reactivity which result directly from the incorporation of a strongly donating silyl group into the pincer ligand architecture, including the stabilization of square-pyramidal Ru^{II} complexes and the synthesis of highly robust amido hydride Ir complexes by NH bond oxidative addition. Although the catalytic applications of late metal PSiP complexes are in their infancy, the promising stoichiometric reactivity that has been observed thus far for such complexes is anticipated to lead to new breakthroughs in synthetic chemistry.

References

- Albrecht, M. and van Koten, G. (2001) *Angew. Chem. Int. Ed.*, **40**, 3750–3781.
- van der Boom, M.E. and Milstein, D. (2003) *Chem. Rev.*, **103**, 1759–1792.
- Morales-Morales, D. and Jensen, C. (eds) (2007) *The Chemistry of Pincer Compounds*, Elsevier, Oxford.
- van Koten, G. and Milstein, D. (eds) (2013) *Organometallic Pincer Chemistry*, Topics in Organometallic Chemistry, vol. 40, Springer, New York.
- Singleton, J.T. (2003) *Tetrahedron*, **59**, 1837–1857.
- Alsalem, N.A., Empsall, H.D., Markham, R., Shaw, B.L., and Weeks, B. (1979) *J. Chem. Soc., Dalton Trans.*, 1972–1982.
- Crocker, C., Errington, R.J., Markham, R., Moulton, C.J., Odell, K.J., and Shaw, B.L. (1980) *J. Am. Chem. Soc.*, **102**, 4373–4379.
- Crocker, C., Errington, R.J., McDonald, W.S., Odell, K.J., Shaw, B.L., and Goodfellow, R.J. (1979) *J. Chem. Soc., Chem. Commun.*, 498–499.
- Empsall, H.D., Hyde, E.M., Mentzer, E., and Shaw, B.L. (1977) *J. Chem. Soc., Dalton Trans.*, 2285–2291.
- Moulton, C.J. and Shaw, B.L. (1976) *J. Chem. Soc., Dalton Trans.*, 1020–1024.
- Leis, W., Mayer, H.A., and Kaska, W.C. (2008) *Coord. Chem. Rev.*, **252**, 1787–1797.
- Gunanathan, C. and Milstein, D. (2011) *Acc. Chem. Res.*, **44**, 588–602.
- Pugh, D. and Danopoulos, A.A. (2007) *Coord. Chem. Rev.*, **251**, 610–641.
- Liang, L.C. (2006) *Coord. Chem. Rev.*, **250**, 1152–1177.
- Kameo, H., Ishii, S., and Nakazawa, H. (2012) *Dalton Trans.*, **41**, 11386–11392.
- Takaya, J., Nakamura, S., and Iwasawa, N. (2012) *Chem. Lett.*, **41**, 967–969.
- Mazzeo, M., Lamberti, M., D'Auria, I., Milione, S., Peters, J.C., and Pellicchia, C. (2010) *J. Polym. Sci., Part A: Polym. Chem.*, **48**, 1374–1382.
- Derrah, E.J., Ladeira, S., Bouhadir, G., Miqueu, K., and Bourissou, D. (2011) *Chem. Commun.*, **47**, 8611–8613.
- Day, G.S., Pan, B., Kellenberger, D.L., Foxman, B.M., and Thomas, C.M. (2011) *Chem. Commun.*, **47**, 3634–3636.
- Pan, B., Bezpalko, M.W., Foxman, B.M., and Thomas, C.M. (2011) *Organometallics*, **30**, 5560–5563.
- Gloaguen, Y., Jacobs, W., de Bruin, B., Lutz, M., and van der Vlugt, J.I. (2013) *Inorg. Chem.*, **52**, 1682–1684.
- Derrah, E.J., Martin, C., Mallet-Ladeira, S., Miqueu, K., Bouhadir, G., and Bourissou, D. (2013) *Organometallics*, **32**, 1121–1128.
- Mazzeo, M., Strianese, M., Kuhl, O., and Peters, J.C. (2011) *Dalton Trans.*, **40**, 9026–9033.

24. Mankad, N.P., Rivard, E., Harkins, S.B., and Peters, J.C. (2005) *J. Am. Chem. Soc.*, **127**, 16032–16033.
25. Mazzeo, M., Lamberti, M., Massa, A., Scettri, A., Pellicchia, C., and Peters, J.C. (2008) *Organometallics*, **27**, 5741–5743.
26. Bauer, R.C., Gloaguen, Y., Lutz, M., Reek, J.N.H., de Bruin, B., and van der Vlugt, J.I. (2011) *Dalton Trans.*, **40**, 8822–8829.
27. Ogawa, H. and Yamashita, M. (2013) *Dalton Trans.*, **42**, 625–629.
28. El-Zaria, M.E., Arii, H., and Nakamura, H. (2011) *Inorg. Chem.*, **50**, 4149–4161.
29. Hill, A.F., Lee, S.B., Park, J., Shang, R., and Willis, A.C. (2010) *Organometallics*, **29**, 5661–5669.
30. Spokoyny, A.M., Reuter, M.G., Stern, C.L., Ratner, M.A., Seideman, T., and Mirkin, C.A. (2009) *J. Am. Chem. Soc.*, **131**, 9482–9483.
31. Hasegawa, M., Segawa, Y., Yamashita, M., and Nozaki, K. (2012) *Angew. Chem. Int. Ed.*, **51**, 6956–6960.
32. Segawa, Y., Yamashita, M., and Nozaki, K. (2009) *J. Am. Chem. Soc.*, **131**, 9201–9203.
33. Segawa, Y., Yamashita, M., and Nozaki, K. (2009) *Organometallics*, **28**, 6234–6242.
34. Balakrishna, M.S., Chandrasekaran, P., and George, P.P. (2003) *Coord. Chem. Rev.*, **241**, 87–117.
35. Gossage, R.A., McLennan, G.D., and Stobart, S.R. (1996) *Inorg. Chem.*, **35**, 1729–1732.
36. Brost, R.D., Bruce, G.C., Joslin, F.L., and Stobart, S.R. (1997) *Organometallics*, **16**, 5669–5680.
37. Ruddy, A.J., Mitton, S.J., McDonald, R., and Turculet, L. (2012) *Chem. Commun.*, **48**, 1159–1161.
38. MacInnis, M.C., MacLean, D.F., Lundgren, R.J., McDonald, R., and Turculet, L. (2007) *Organometallics*, **26**, 6522–6525.
39. MacLean, D.F., McDonald, R., Ferguson, M.J., Caddell, A.J., and Turculet, L. (2008) *Chem. Commun.*, 5146–5148.
40. Aizenberg, M. and Milstein, D. (1995) *J. Am. Chem. Soc.*, **117**, 6456–6464.
41. MacInnis, M.C., McDonald, R., Ferguson, M.J., Tobisch, S., and Turculet, L. (2011) *J. Am. Chem. Soc.*, **133**, 13622–13633.
42. Joslin, F.L. and Stobart, S.R. (1993) *Inorg. Chem.*, **32**, 2221–2223.
43. Korshin, E.E., Leitus, G., Shimon, L.J.W., Konstantinovski, L., and Milstein, D. (2008) *Inorg. Chem.*, **47**, 7177–7189.
44. Xu, Y.J., Alcock, N.W., Clarkson, G.J., Docherty, G., Woodward, G., and Wills, M. (2004) *Org. Lett.*, **6**, 4105–4107.
45. Fang, H.Y., Choe, Y.K., Li, Y.H., and Shimada, S. (2011) *Chem. Asian J.*, **6**, 2512–2521.
46. Zhou, X.B. and Stobart, S.R. (2001) *Organometallics*, **20**, 1898–1900.
47. Bushnell, G.W., Casado, M.A., and Stobart, S.R. (2001) *Organometallics*, **20**, 601–603.
48. Stobart, S.R., Zhou, X.B., Cea-Olivares, R., and Toscano, A. (2001) *Organometallics*, **20**, 4766–4768.
49. Zhang, J., Gandelman, M., Shimon, L.J.W., Rozenberg, H., and Milstein, D. (2004) *Organometallics*, **23**, 4026–4033.
50. Gusev, D.G., Dolgushin, F.M., and Antipin, M.Y. (2000) *Organometallics*, **19**, 3429–3434.
51. Amoroso, D., Jabri, A., Yap, G.P.A., Gusev, D.G., dos Santos, E.N., and Fogg, D.E. (2004) *Organometallics*, **23**, 4047–4054.
52. Gagliardo, M., Chase, P.A., Brouwer, S., van Klink, G.P.M., and van Koten, G. (2007) *Organometallics*, **26**, 2219–2227.
53. Weng, W., Parkin, S., and Ozerov, O.V. (2006) *Organometallics*, **25**, 5345–5354.
54. Danopoulos, A.A., Winston, S., and Motherwell, W.B. (2002) *Chem. Commun.*, 1376–1377.
55. Dani, P., Karlen, T., Gossage, R.A., Gladiali, S., and van Koten, G. (2000) *Angew. Chem. Int. Ed.*, **39**, 743–745.
56. Askevold, B., Khusniyarov, M.M., Herdtweck, E., Meyer, K., and Schneider, S. (2010) *Angew. Chem. Int. Ed.*, **49**, 7566–7569.
57. Walstrom, A., Pink, M., and Caulton, K.G. (2006) *Inorg. Chem.*, **45**, 5617–5620.

58. Watson, L.A., Ozerov, O.V., Pink, M., and Caulton, K.G. (2003) *J. Am. Chem. Soc.*, **125**, 8426–8427.
59. Alcaraz, G., Vendier, L., Clot, E., and Sabo-Etienne, S. (2010) *Angew. Chem. Int. Ed.*, **49**, 918–920.
60. Alcaraz, G. and Sabo-Etienne, S. (2010) *Angew. Chem. Int. Ed.*, **49**, 7170–7179.
61. Sola, E., Garcia-Camprubi, A., Andres, J.L., Martin, M., and Plou, P. (2010) *J. Am. Chem. Soc.*, **132**, 9111–9121.
62. Garcia-Camprubi, A., Martin, M., and Sola, E. (2010) *Inorg. Chem.*, **49**, 10649–10657.
63. Choi, J., MacArthur, A.H.R., Brookhart, M., and Goldman, A.S. (2011) *Chem. Rev.*, **111**, 1761–1779.
64. Jensen, C.M. (1999) *Chem. Commun.*, 2443–2449.
65. Zhu, Y.J., Fan, L., Chen, C.H., Finnell, S.R., Foxman, B.M., and Ozerov, O.V. (2007) *Organometallics*, **26**, 6701–6703.
66. Kanzelberger, M., Singh, B., Czerw, M., Krogh-Jespersen, K., and Goldman, A.S. (2000) *J. Am. Chem. Soc.*, **122**, 11017–11018.
67. Morgan, E., MacLean, D.F., McDonald, R., and Turculet, L. (2009) *J. Am. Chem. Soc.*, **131**, 14234–14236.
68. Cartwright Sykes, A., White, P., and Brookhart, M. (2006) *Organometallics*, **25**, 1664–1675.
69. Zhao, J., Goldman, A.S., and Hartwig, J.F. (2005) *Science*, **307**, 1080–1082.
70. Kanzelberger, M., Zhang, X.W., Emge, T.J., Goldman, A.S., Zhao, J., Incarvito, C., and Hartwig, J.F. (2003) *J. Am. Chem. Soc.*, **125**, 13644–13645.
71. Cho, H., Woo, H.Y., and Hwang, S. (2010) *Bull. Korean Chem. Soc.*, **31**, 1421–1423.
72. Uhe, A., Hoelscher, M., and Leitner, W. (2013) *Chem. Eur. J.*, **19**, 1020–1027.
73. Kameo, H., Ishii, S., and Nakazawa, H. (2013) *Dalton Trans.*, **42**, 4663–4669.
74. Takaya, J. and Iwasawa, N. (2008) *J. Am. Chem. Soc.*, **130**, 15254–15255.
75. Takaya, J., Sasano, K., and Iwasawa, N. (2011) *Org. Lett.*, **13**, 1698–1701.
76. Takaya, J., Kirai, N., and Iwasawa, N. (2011) *J. Am. Chem. Soc.*, **133**, 12980–12983.
77. Mitton, S.J., McDonald, R., and Turculet, L. (2009) *Organometallics*, **28**, 5122–5136.
78. Fekl, U. and Goldberg, K.I. (2003) *Adv. Inorg. Chem.*, **54**, 259–320.
79. Liang, L.C., Lin, J.M., and Lee, W.Y. (2005) *Chem. Commun.*, 2462–2464.
80. Harkins, S.B. and Peters, J.C. (2002) *Organometallics*, **21**, 1753–1755.
81. Kim, Y.J., Park, J.I., Lee, S.C., Osakada, K., Tanabe, M., Choi, J.C., Koizumi, T., and Yamamoto, T. (1999) *Organometallics*, **18**, 1349–1352.
82. Gatard, S., Chen, C.H., Foxman, B.M., and Ozerov, O.V. (2008) *Organometallics*, **27**, 6257–6263.
83. Yoo, H., Carroll, P.J., and Berry, D.H. (2006) *J. Am. Chem. Soc.*, **128**, 6038–6039.
84. Stohr, F., Sturmayer, D., Kickelbick, G., and Schubert, U. (2002) *Eur. J. Inorg. Chem.*, **2002** (9), 2305–2311.
85. Levy, C.J. and Puddephatt, R.J. (1997) *J. Am. Chem. Soc.*, **119**, 10127–10136.
86. Levy, C.J., Vittal, J.J., and Puddephatt, R.J. (1996) *Organometallics*, **15**, 2108–2117.
87. Levy, C.J., Puddephatt, R.J., and Vittal, J.J. (1994) *Organometallics*, **13**, 1559–1560.
88. Zlota, A.A., Frolow, F., and Milstein, D. (1989) *J. Chem. Soc., Chem. Commun.*, 1826–1827.
89. Yamashita, H., Tanaka, M., and Goto, M. (1997) *Organometallics*, **16**, 4696–4704.
90. Yamashita, H., Hayashi, T., Kobayashi, T., Tanaka, M., and Goto, M. (1988) *J. Am. Chem. Soc.*, **110**, 4417–4418.
91. Ebsworth, E.A.V., Marganian, V.M., Reed, F.J.S., and Gould, R.O. (1978) *J. Chem. Soc., Dalton Trans.*, 1167–1170.
92. Grumbine, S.D., Tilley, T.D., Arnold, F.P., and Rheingold, A.L. (1993) *J. Am. Chem. Soc.*, **115**, 7884–7885.
93. Chan, D., Duckett, S.B., Heath, S.L., Khazal, I.G., Perutz, R.N., Sabo-Etienne, S., and Timmins, P.L. (2004) *Organometallics*, **23**, 5744–5756.
94. Tsuji, Y., Nishiyama, K., Hori, S., Ebihara, M., and Kawamura, T. (1998) *Organometallics*, **17**, 507–512.

95. Obora, Y., Tsuji, Y., Nishiyama, K., Ebihara, M., and Kawamura, T. (1996) *J. Am. Chem. Soc.*, **118**, 10922–10923.
96. Takaya, J. and Iwasawa, N. (2009) *Organometallics*, **28**, 6636–6638.
97. Takaya, J. and Iwasawa, N. (2011) *Dalton Trans.*, **40**, 8814–8821.
98. Mitton, S.J. and Turculet, L. (2012) *Chem. Eur. J.*, **18**, 15258–15262.
99. Corey, J.Y. (2011) *Chem. Rev.*, **111**, 863–1071.
100. Suh, H.W., Schmeier, T.J., Hazari, N., Kemp, R.A., and Takase, M.K. (2012) *Organometallics*, **31**, 8225–8236.
101. Chen, W.Z., Shimada, S., Tanaka, M., Kobayashi, Y., and Saigo, K. (2004) *J. Am. Chem. Soc.*, **126**, 8072–8073.
102. Boyle, R.C., Mague, J.T., and Fink, M.J. (2003) *J. Am. Chem. Soc.*, **125**, 3228–3229.
103. Miller, A.J.M., Labinger, J.A., and Bercaw, J.E. (2011) *Organometallics*, **30**, 4308–4314.
104. Berkefeld, A., Piers, W.E., Parvez, M., Castro, L., Maron, L., and Eisenstein, O. (2013) *Chem. Sci.*, **4**, 2152–2162.
105. Park, S., Bezier, D., and Brookhart, M. (2012) *J. Am. Chem. Soc.*, **134**, 11404–11407.
106. Matsuo, T. and Kawaguchi, H. (2006) *J. Am. Chem. Soc.*, **128**, 12362–12363.
107. Berkefeld, A., Piers, W.E., and Parvez, M. (2010) *J. Am. Chem. Soc.*, **132**, 10660–10661.
108. Thompson, D.B. and Brook, M.A. (2008) *J. Am. Chem. Soc.*, **130**, 32–33.
109. Parks, D.J., Blackwell, J.M., and Piers, W.E. (2000) *J. Org. Chem.*, **65**, 3090–3098.
110. Mitton, S.J., McDonald, R., and Turculet, L. (2009) *Angew. Chem. Int. Ed.*, **48**, 8568–8571.
111. Mitton, S.J., McDonald, R., and Turculet, L. (2013) *Polyhedron*, **52**, 750–754.
112. Beck, R. and Johnson, S.A. (2012) *Organometallics*, **31**, 3599–3609.
113. Mintcheva, N., Nishihara, Y., Tanabe, M., Hirabayashi, K., Mori, A., and Osakada, K. (2001) *Organometallics*, **20**, 1243–1246.
114. Gilges, H. and Schubert, U. (1998) *Organometallics*, **17**, 4760–4761.
115. Temple, K., Lough, A.J., Sheridan, J.B., and Manners, I. (1998) *J. Chem. Soc., Dalton Trans.*, 2799–2805.
116. Steenwinkel, P., Gossage, R.A., Maunula, T., Grove, D.M., and van Koten, G. (1998) *Chem. Eur. J.*, **4**, 763–768.
117. Hua, R., Akita, M., and Moro-oka, Y. (1996) *Chem. Commun.*, 541–542.
118. Lin, W.B., Wilson, S.R., and Girolami, G.S. (1994) *Organometallics*, **13**, 2309–2319.
119. Hendriksen, D.E., Oswald, A.A., Ansell, G.B., Leta, S., and Kastrup, R.V. (1989) *Organometallics*, **8**, 1153–1157.
120. Fullmer, B.C., Fan, H.J., Pink, M., Huffman, J.C., Tsvetkov, N.P., and Caulton, K.G. (2011) *J. Am. Chem. Soc.*, **133**, 2571–2582.
121. Safa, M., Jennings, M.C., and Puddephatt, R.J. (2012) *Organometallics*, **31**, 3539–3550.
122. Heyduk, A.F., Labinger, J.A., and Bercaw, J.E. (2003) *J. Am. Chem. Soc.*, **125**, 6366–6367.
123. Thomson, S.K. and Young, G.B. (1989) *Organometallics*, **8**, 2068–2070.
124. Hofmann, P., Heiss, H., Neiteler, P., Muller, G., and Lachmann, J. (1990) *Angew. Chem., Int. Ed. Engl.*, **29**, 880–882.
125. Ong, C.M., Burchell, T.J., and Puddephatt, R.J. (2004) *Organometallics*, **23**, 1493–1495.
126. Joost, M., Mallet-Ladeira, S., Miqueu, K., Amgoune, A., and Bourissou, D. (2013) *Organometallics*, **32**, 898–902.
127. Stradiotto, M., Fujdala, K.L., and Tilley, T.D. (2001) *Chem. Commun.*, 1200–1201.
128. Sangtrirutnugul, P., Stradiotto, M., and Tilley, T.D. (2006) *Organometallics*, **25**, 1607–1617.
129. Sangtrirutnugul, P. and Tilley, T.D. (2007) *Organometallics*, **26**, 5557–5568.
130. Sangtrirutnugul, P. and Tilley, T.D. (2008) *Organometallics*, **27**, 2223–2230.

131. Yang, J.A., Del Rosal, I., Fasulo, M., Sangtrirutnugul, P., Maron, L., and Tilley, T.D. (2010) *Organometallics*, **29**, 5544–5550.
132. Yang, J.A., Fasulo, M., and Tilley, T.D. (2010) *New J. Chem.*, **34**, 2528–2529.
133. Takeda, N., Nakamura, T., Imamura, A., and Unno, M. (2011) *Heteroat. Chem.*, **22**, 438–445.
134. Hill, A.F., Neumann, H., and Wagler, J. (2010) *Organometallics*, **29**, 1026–1031.

7 Electronic Structures of Reduced Manganese, Iron, and Cobalt Complexes Bearing Redox-Active Bis(imino)pyridine Pincer Ligands

Paul J. Chirik

7.1 Introduction

Bis(imino)pyridines, first explored as modular terpyridine mimics [1], have recently evolved into a privileged class of tridentate meridional [NNN] pincer ligands [2]. The introduction of sterically demanding aryl substituents on the imine positions by Bennet [3], Brookhart [4], and Gibson [5] has resulted in highly active iron and cobalt catalysts, following activation with alkyl aluminums, for the oligomerization and polymerization of ethylene and α -olefins [6]. The ease of preparation, modularity, and air stability of these pincer ligands make them attractive for both transition-metal and main-group compounds [7, 8]. Expectedly, many intriguing stoichiometric and catalytic transformations have since been realized.

In addition to these synthetic attributes, bis(imino)pyridines are also redox-active, a feature that distinguishes them from many other tridentate pincer-type ligands [9, 10]. The ability to act as classic π -acceptor (non-innocent form) or undergo reversible one to three electron transfer with a metal or main-group element (redox-active form) often presents a challenge for electronic structure elucidation and generates compounds whose low formal oxidation state assignment is often deceptive [11]. On the other hand, it is these unique electronic properties that are often responsible for the interesting bond activation and catalytic chemistry observed with bis(imino)pyridine compounds [12]. This chapter will overview the chemistry of bis(imino)pyridine pincer ligands with reduced complexes of manganese, iron, and cobalt. Fundamental questions such as “when is the ligand or the metal oxidized or reduced?” and “what are the properties of the metal complex that induce redox non-innocence or redox activity?” are the themes throughout.

7.2 Reduced Manganese, Iron, and Cobalt Complexes with Redox-Active Bis(imino)pyridines

During the past decade, our group has been interested in developing base metal catalysts as alternatives to precious metal complexes for transformations such

as alkene hydrogenation, hydrosilylation, and cycloaddition reactions [13, 14]. In addition to providing potentially less expensive and more environmentally benign alternatives to established precious metal catalysts, we sought to exploit the unique electronic structure of the first-row metals to discover new chemistry. Based on the precedented thermal [15] and photochemical [16] activation of $\text{Fe}(\text{CO})_5$, reduced manganese, iron, and cobalt compounds were targeted. Given the established redox activity of the bis(imino)pyridine chelate [17–19], we anticipated a range of interesting electronic structures and potential applications in small molecule activation and group-transfer chemistry.

7.2.1

Reduced Bis(imino)pyridine Manganese Chemistry

Preparation and elucidation of the electronic structure of bis(imino)pyridine manganese compounds was pioneered by Wieghardt and coworkers [15a]. One-electron reduction of the six-coordinate bis(chelate) Mn(II) complex $[(^{4\text{-OMe}}\text{PDI})_2\text{Mn}^{\text{II}}](\text{PF}_6)_2$ ($^{4\text{-OMe}}\text{PDI} = 2,6\text{-}(4\text{-OMe-C}_6\text{H}_4\text{N=CMe})_2\text{C}_5\text{H}_3\text{N}$) resulted in two ligand-centered reductions with concomitant oxidation of the metal and furnished the low-spin Mn(III) compound $[(^{4\text{-OMe}}\text{PDI}^{\cdot-})_2\text{Mn}^{\text{III}}](\text{PF}_6)$ (Figure 7.1). The oxidation state of both the chelates and the metal were assigned on the basis of spectroscopic and metrical parameters from crystallographic data. The bond distortions to the bis(imino)pyridines reported in this study were some of the first examples to define the experimental parameters for identifying ligand participation.

Inspired by the polymerization activity of the analogous iron and cobalt compounds, Gambarotta and coworkers [20] prepared $(^{i\text{Pr}}\text{PDI})\text{MnCl}_2$ ($^{i\text{Pr}}\text{PDI} = 2,6\text{-}(2,6\text{-C}_6\text{H}_3\text{N=CMe})_2\text{C}_5\text{H}_3\text{N}$) and studied its alkylation chemistry. Treatment with methyl lithium yielded the four-coordinate distorted planar complex $(^{i\text{Pr}}\text{PDI})\text{MnCH}_3$, a compound best described as a high-spin Mn(II) compound with a bis(imino)pyridine radical anion, based on the metrical parameters from X-ray diffraction (Figure 7.1). Alkylation with $\text{LiCH}_2\text{SiMe}_3$ resulted in characterization of two complexes: the anionic, four-coordinate manganese alkyl

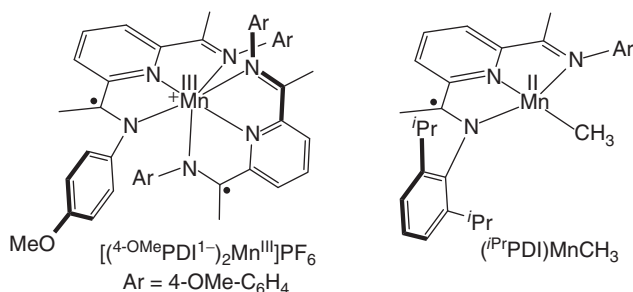


Figure 7.1 Early examples of manganese complexes with redox-active bis(imino)pyridine ligands.

$[(iPrPDI)MnCH_2SiMe_3]^-$, and a bimetallic alkyl complex resulting from C–C coupling following deprotonation of the imine methyl groups in the backbone. Such reactivity demonstrates the chemical non-innocence of bis(imino)pyridines in addition to their interesting electronic properties.

The success of reduced bis(imino)pyridine iron dinitrogen complexes as precursors in various catalytic processes prompted attempts in the preparation of the analogous manganese compounds [21]. The preference for the formation of high-spin Mn(II) ions suggested that coordination of a weak π -acid such as N_2 may be challenging [22]. Stirring a tetrahydrofuran (THF) slurry of $(iPrPDI)MnCl_2$ with excess sodium in the presence of a catalytic quantity (0.5 mol%) of naphthalene resulted in isolation of a dark brown solid identified as $(iPrPDI)Mn(THF)_2$ (Figure 7.2). Superconducting quantum interference device (SQUID) magnetometry along with electron paramagnetic resonance (EPR) spectroscopy in a pentane–toluene glass established an $S = 3/2$ ground state with three principally Mn-based electrons. These data, in combination with the metrical parameters from X-ray diffraction, indicated that $(iPrPDI)Mn(THF)_2$ is best described as a high-spin Mn(II) compound with a bis(imino)pyridine chelate diradical. Antiferromagnetic coupling between the metal and ligand spins gives rise to the observed quartet ground state. Notably, the high-spin Mn(II) configuration is preserved upon two-electron reduction.

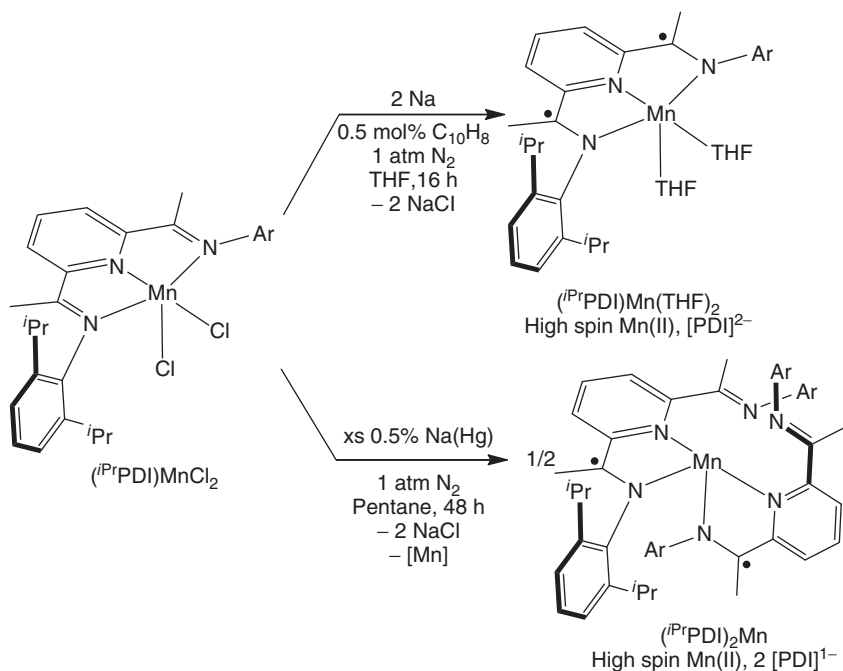


Figure 7.2 Synthesis and electronic structure of reduced aryl-substituted bis(imino)pyridine manganese complexes.

Unfortunately, $(^{iPr}\text{PDI})\text{Mn}(\text{THF})_2$ exhibited little activity for the hydrogenation of alkenes or $[2 + 2]$ cyclization of dienes. In an attempt to synthesize an active bis(imino)pyridine manganese precatalyst, alternative reduction conditions were explored. Sodium amalgam reduction of $(^{iPr}\text{PDI})\text{MnCl}_2$ in pentane yielded the red bis(chelate) complex $(^{iPr}\text{PDI})_2\text{Mn}$. X-ray diffraction established a cis-divacant octahedral compound where one imine arm on each of the chelates is dissociated from the metal center. The metrical parameters from X-ray diffraction in conjunction with SQUID magnetic and EPR spectroscopic data established that the overall $S = 3/2$ compound is best described as a high-spin Mn(II) species ($S_{\text{Mn}} = 5/2$) with two bis(imino)pyridine radical anions.

To determine whether bis(imino)pyridine manganese complexes with lower spin and spectroscopic oxidation states could be synthesized, the preparation of carbonyl complexes was carried out. Exposure of $(^{iPr}\text{PDI})\text{Mn}(\text{THF})_2$ to CO gas resulted in the isolation of the neutral manganese dicarbonyl complex $(^{iPr}\text{PDI})\text{Mn}(\text{CO})_2$. Unlike the other bis(imino)pyridine manganese complexes discussed thus far, $(^{iPr}\text{PDI})\text{Mn}(\text{CO})_2$ is a low-spin complex with a doublet ground state. Accordingly, a rhombic signal was observed by EPR spectroscopy with relatively small ^{55}Mn hyperfine coupling constants ($A_{xx} = 23 \times 10^{-4} \text{ cm}^{-1}$, $A_{yy} = 8.0 \times 10^{-4} \text{ cm}^{-1}$, $A_{zz} = 32.5 \times 10^{-4} \text{ cm}^{-1}$). These data, in combination with broken symmetry (BS) density functional theory (DFT) calculations established a low-spin Mn(I) complex with a bis(imino)pyridine radical as the singly occupied molecular orbital (SOMO). The observation of an essentially ligand-based radical by spectroscopic methods provides definitive experimental evidence for the redox activity of the bis(imino)pyridine chelate. These observations follow those previously reported by Gambarotta and coworkers [7] who provided direct experimental observation, again by EPR spectroscopy, of bis(imino)pyridine radicals in the reduced aluminum complex $(^{iPr}\text{PDI})\text{AlMe}_2$.

The oxidation and reduction of $(^{iPr}\text{PDI})\text{Mn}(\text{CO})_2$ was explored to determine whether such redox events were ligand- or metal-based or, perhaps, a combination of both. Treatment of $(^{iPr}\text{PDI})\text{Mn}(\text{CO})_2$ with $[\text{Cp}_2\text{Fe}][\text{BPh}_4]$ under N_2 atmosphere resulted in the isolation of the *tricarbonyl* complex $[(^{iPr}\text{PDI})\text{Mn}(\text{CO})_3][\text{BPh}_4]$ in modest yield. A more appropriate protocol was developed where the oxidation was conducted under a CO atmosphere. A combination of metrical parameters from X-ray diffraction, IR, and NMR studies in conjunction with DFT methods established a low-spin Mn(I), d^6 compound with a neutral bis(imino)pyridine chelate (Figure 7.3). The anionic complex $[\text{Na}(\text{OEt}_2)_3][(^{iPr}\text{PDI})\text{Mn}(\text{CO})_2]$ was also prepared and, using the same combination of spectroscopic, diffraction, and computational techniques, was established as an overall $S = 0$ compound best described as a low-spin, Mn(I), d^6 compound with the closed-shell form of the dianionic bis(imino)pyridine (Figure 7.3). The redox series of bis(imino)pyridine manganese complexes is therefore illustrative of an important concept in coordination chemistry with redox-active ligands. More often than not, the preferred oxidation state of the metal complex in a specific coordination environment is both dominant and familiar and often times readily predicted. From decades of organometallic manganese carbonyl chemistry [23] and more recent PNP-pincer compounds [24], formation

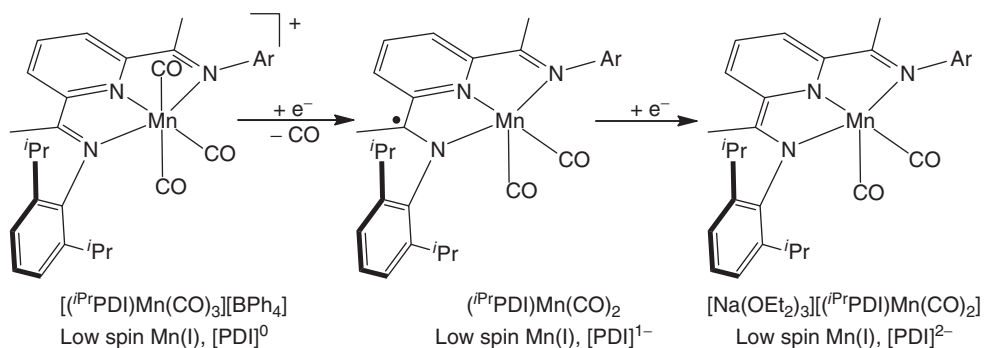


Figure 7.3 Synthesis and electronic structure of bis(imino)pyridine manganese carbonyl complexes over three oxidation states.

of low-spin Mn(I) carbonyl complexes is hardly surprising. It is also perhaps therefore anticipated that all of the redox chemistry in the three bis(imino)pyridine manganese carbonyl compounds is ligand-based. As such, the strong-field carbonyl ligands and not the bis(imino)pyridine pincer dictate the overall electronic structure.

7.2.2

Reduced Bis(imino)pyridine Iron Chemistry

Because of our motivations in base metal catalysis [12], the synthesis and electronic structure determination of bis(imino)pyridine iron complexes have been of longstanding interest in our laboratory. In 2004, we reported the synthesis and initial investigations of the catalytic activity of $(\textit{iPr}\text{PDI})\text{Fe}(\text{N}_2)_2$ [25]. Following this report, Gambarotta and coworkers [26] prepared a family of bis(imino)pyridine iron dinitrogen compounds from the treatment of $(\textit{iPr}\text{PDI})\text{FeCl}_2$ with various quantities of NaH. A family of anionic iron dinitrogen complexes was isolated and structurally characterized. In many cases, the imine methyl groups were deprotonated.

The exceptional catalytic activity of $(\textit{iPr}\text{PDI})\text{Fe}(\text{N}_2)_2$ and its variants [27–29] prompted detailed investigation into its electronic structure. Although $(\textit{iPr}\text{PDI})\text{Fe}(\text{N}_2)_2$ was isolated in the solid state, the four-coordinate iron dinitrogen complex $(\textit{iPr}\text{PDI})\text{FeN}_2$ predominates in solution under standard laboratory conditions (22 °C, ~1 atm N_2). To avoid this complication in spectroscopic studies, we prepared a series of neutral ligand complexes $(\textit{iPr}\text{PDI})\text{FeL}_n$ ($L_n = 4\text{-}N$, N -dimethylaminopyridine (DMAP), NH_3 , ketones, etc.) which exhibited greater fidelity in solution [30]. One example, $(\textit{iPr}\text{PDI})\text{Fe}(\text{DMAP})$, was studied in detail and is best described as an intermediate-spin Fe(II) compound with the triplet diradical form of the bis(imino)pyridine dianion. Antiferromagnetic coupling between the metal and ligand spin centers gives rise to the observed diamagnetic ground state. An energetically similar triplet excited state was also identified computationally and mixing of this state into the ground state by spin–orbit coupling. This gives rise to temperature-independent paramagnetism and was invoked to explain the unusual shifts in the ^1H NMR spectrum (Figure 7.4).

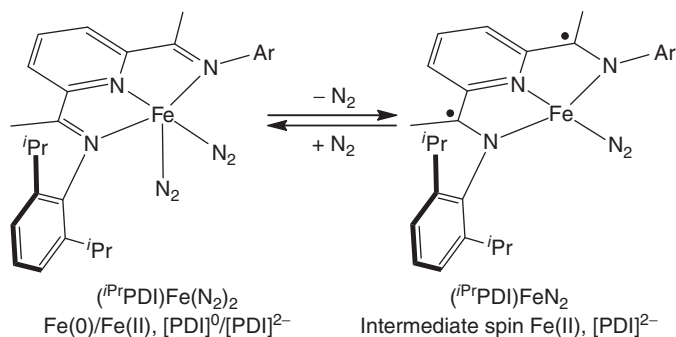


Figure 7.4 Synthesis and electronic structure of four- versus five-coordinate bis(imino)pyridine iron dinitrogen complexes.

For several years, we transposed the electronic structure of $(iPrPDI)Fe(DMAP)$ onto the mixture of $(iPrPDI)Fe(N_2)_2$ and $(iPrPDI)FeN_2$. This seemed reasonable given that the 1H NMR spectrum of a mixture of four- and five-coordinate iron complexes also has unusual shifts for the in-plane bis(imino)pyridine resonances. However, it is important to note that these shifts were opposite in field than $(iPrPDI)Fe(DMAP)$. For the mixture of iron dinitrogen complexes, the imine methyl groups appeared downfield in the vicinity of 15 ppm while for $(iPrPDI)Fe(DMAP)$ an upfield shift to -6 ppm was observed. Two nearly simultaneous discoveries prompted us to revisit the electronic structure of these compounds. First, it was discovered that the substitution of the imine methyl group with a slightly larger ethyl or isopropyl group allowed the isolation and crystallographic characterization of the four-coordinate iron dinitrogen compounds $(iPrRPDI)FeN_2$ ($R = Et, iPr$) (Figure 7.5) [31]. Thus, authentic bond distances for the four-coordinate complexes were now in hand and provided a benchmark for subsequent computational and spectroscopic studies.

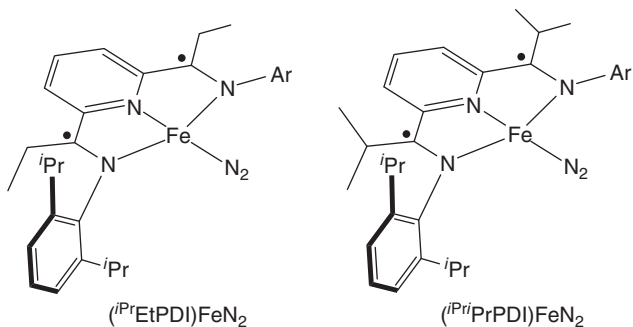


Figure 7.5 Isolable and crystallographically characterized four-coordinate bis(imino)pyridine iron dinitrogen complexes.

The second development was the application of high-energy X-ray spectroscopic techniques to reduced bis(imino)pyridine iron compounds. One of the key experiments was the observation of different X-ray absorption spectra for $(^{iPr}PDI)Fe(N_2)_2$ and $(^{iPr}PDI)FeN_2$ [31]. Mössbauer and X-ray emission spectroscopies also supported different electronic structure descriptions for the four- and five-coordinate compounds. Computational studies reproduced the experimental data and established that the five-coordinate iron complex $(^{iPr}PDI)Fe(N_2)_2$ was a covalent molecule, with the bis(imino)pyridine chelate acting as a π -acceptor and the iron as a hybrid between Fe(0) and Fe(II) oxidation states. There is no evidence for ligand-centered radicals in this electronic structure description. Comparison of these data to those on other five-coordinate iron neutral ligand complexes with strong-field π -acids such as $(^{iPr}PDI)Fe(CO)_2$ and $(^{iPr}PDI)Fe(CN^tBu)_2$ also demonstrated that this description of the bonding is appropriate and is general among the formally 18-electron family of compounds.

The four-coordinate bis(imino)pyridine iron dinitrogen complex $(^{iPr}PDI)FeN_2$ has a different electronic structure. The computational output that best reproduces the computational data is a BS (2,2) solution corresponding to an intermediate-spin iron(II) center and the triplet diradical form of the bis(imino)pyridine dianion. This electronic structure description is similar to that observed for four-coordinate complexes such as $(^{iPr}PDI)Fe(DMAP)$ and $(^{iPr}PDI)FeNH_3$ with one important difference. In cases with essentially σ -donating ligands, strong antiferromagnetic coupling between the iron and ligand diradicals occurs. Introduction of a weakly π -acidic N_2 ligand stabilizes and hence lowers the energy of the iron d_{xz} orbital (z is defined perpendicular to the idealized plane of the molecule, and x contains the Fe–N \equiv N vector). This orbital becomes doubly occupied and hence unable to engage in an antiferromagnetic coupling interaction. As a consequence, the d_{z^2} orbital becomes one of the iron SOMOs and has the incorrect symmetry to interact with either of the bis(imino)pyridine SOMOs. This produces a low spatial overlap in one pair of magnetic orbitals and likely accounts for the population of excited states observed at higher temperatures.

It is useful to compare the molecular and electronic structures of the bis(imino)pyridine iron dinitrogen complexes with those of the ruthenium congeners reported by Berry and coworkers [32]. Stirring $\kappa^2\text{-}(^{Mes}PDI)Ru(\eta^6\text{-arene})$ complexes in non-arene solvents under a dinitrogen atmosphere furnished the bimetallic ruthenium dinitrogen complex $[(^{Mes}PDI)Ru]_2(\mu_2, \eta^1, \eta^1-N_2)$. The dimeric complex is composed of two 4-coordinate ruthenium centers and contrasts the analogous iron compound $[(^{Mes}PDI)Fe(N_2)]_2(\mu_2, \eta^1, \eta^1-N_2)$, which contains two formally 18-electron, coordinatively saturated, five-coordinate iron subunits. In describing the electronic structure of the ruthenium compound, Berry recognized the possibility of a redox-active or non-innocent bis(imino)pyridine ligand and a potentially higher oxidation state for the metal but also argued that the formal Ru(0) description was informative. The distortions to the metrical parameters of the chelate, a key piece of experimental data in assigning both ligand and metal oxidation state, are consistent with bis(imino)pyridine reduction and are likely a

result of π -back-bonding between the electron-rich metal center and the chelate in a square-planar ligand field.

We note that there is a difference between the favored electronic structures between *four-coordinate* iron and ruthenium dinitrogen compounds. In both cases, diamagnetic ground states are observed, with unusual ^1H NMR shifts being noted for hydrogens in the metal-chelate plane [25, 33]. For iron, antiferromagnetic coupling between metal and pincer triplet diradicals has been invoked to account for the $S=0$ ground state, while for ruthenium a more classical π -back-bonding description is favored. If these descriptions are correct, why does the electronic structure differ between the first- and second-row transition metals? The differences may be traced to the relative diffusivity and energy of electrons in 3d versus 4d orbitals [34]. A redox-active biradical-type metal–ligand interaction arises from relatively poor overlap (weak interaction) between metal and ligand orbitals resulting in greater accessibility of higher-spin excited states. This situation is observed with first-row transition metals where the valence orbitals are relatively contracted. By contrast, when the bis(imino)pyridine acts as a π -acceptor, a bonding situation where there is strong overlap between metal and ligand orbitals arises and produces an energetically separated M–L bonding and antibonding pair. This situation is encountered with more reducing second- and third-row metals with more energetic and diffuse valence orbitals. We do note, however, that Berry [35] has synthesized a bis(imino)pyridine ruthenium hydride complex where pincer-radical character is invoked.

As with manganese, the oxidation and reduction of the neutral bis(imino)pyridine iron dinitrogen complex ($^{i\text{Pr}}\text{PDI})\text{FeN}_2$ was explored (Figure 7.6) [36]. Treatment of ($^{i\text{Pr}}\text{PDI})\text{FeN}_2$ with $[\text{Cp}_2\text{Fe}][\text{BAR}^{\text{F}}_4]$ ($\text{BAR}^{\text{F}}_4 = \text{B}(3,5\text{-}(\text{CF}_3)\text{-C}_6\text{H}_3)_4$) in diethyl ether solution resulted in N_2 dissociation and isolation of $[(^{i\text{Pr}}\text{PDI})\text{Fe}(\text{OEt}_2)][\text{BAR}^{\text{F}}_4]$. This compound has an $S=3/2$ ground state and is best described as a high-spin Fe(II) derivative with a bis(imino)pyridine radical anion. Accordingly, a rhombic EPR signal with large g anisotropy was observed ($g_x = 2.11$, $g_y = 2.22$, $g_z = 2.03$), consistent with a majority contribution from an iron-centered spin. The overall oxidation event is therefore ligand-based because the diradical dianionic bis(imino)pyridine in ($^{i\text{Pr}}\text{PDI})\text{FeN}_2$ converts to the radical anion in $[(^{i\text{Pr}}\text{PDI})\text{Fe}(\text{OEt}_2)]^+$.

Reduction of ($^{i\text{Pr}}\text{PDI})\text{FeN}_2$ was accomplished with sodium naphthalenide in THF in the presence of 15-crown-5 and yielded $[\text{Na}(15\text{-crown-5})(\text{THF})_2][(^{i\text{Pr}}\text{PDI})\text{FeN}_2]$ (Figure 7.6). Solid-state magnetic susceptibility measurements established an $S=1/2$ ground state, and, accordingly, a rhombic EPR spectrum with large g -anisotropy ($g_x = 1.95$, $g_y = 2.15$, $g_z = 2.24$), consistent with an iron-centered spin, was observed. Most notably, the solid-state structure of $[\text{Na}(15\text{-crown-5})(\text{THF})_2][(^{i\text{Pr}}\text{PDI})\text{FeN}_2]$ established an essentially planar compound with significant distortions to the bis(imino)pyridine chelate. These values, in conjunction with computational data, support a *trianionic* version of the chelate, demonstrating that the reduction of ($^{i\text{Pr}}\text{PDI})\text{FeN}_2$ to $[(^{i\text{Pr}}\text{PDI})\text{FeN}_2]^-$ is chelate-based where the intermediate-spin iron configuration is preserved. The only other examples of trianionic bis(imino)pyridines are the trilithium salt

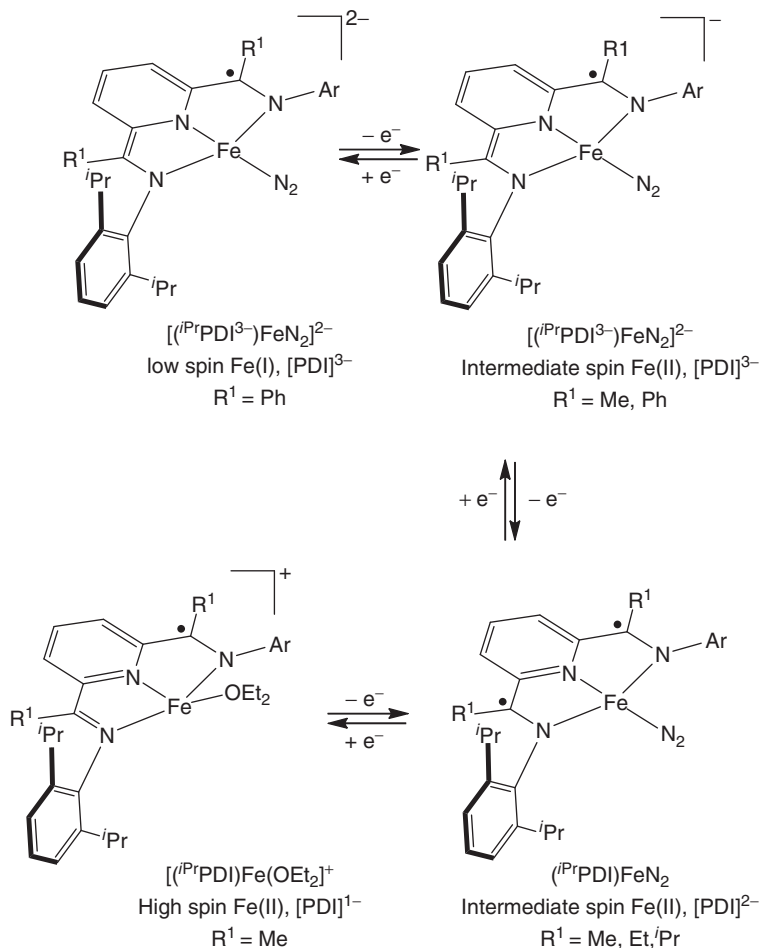


Figure 7.6 Electronic structure of bis(imino)pyridine iron dinitrogen and diethyl ether complexes over four oxidation states.

prepared by Gambarotta [33] and a cyclopentadienyl uranium complex more recently described by Bart and coworkers [37].

An analogous bis(imino)pyridine iron dinitrogen anion was prepared with the phenylated version of the pincer $[Na(15\text{-crown-5})(THF)_2][(iPrBPDI)FeN_2]$. The X-band EPR spectrum of this compound was similar to that of the methylated variant, consistent with an identical electronic structure description. Significantly, $[(iPrBPDI)FeN_2]^-$ was reduced by an additional electron to yield the bis(imino)pyridine iron dinitrogen dianion $[Na(15\text{-crown-5})(THF)_2][(iPrBPDI)FeN_2]^{2-}$ (Figure 7.6). Because of the extreme sensitivity and poor solubility of the compound, characterization was limited to X-ray diffraction, infrared spectroscopy, and combustion analysis. The metrical data, in combination with the measured

diamagnetism of the compound, were consistent with a low-spin Fe(I) centered structure and maintenance of the trianionic bis(imino)pyridine. Perhaps most notably, a series of dinitrogen complexes (with one diethyl ether derivative) was prepared over four oxidation states, highlighting the electronic flexibility of the bis(imino)pyridine.

An analogous series of bis(imino)pyridine iron dicarbonyl complexes was also synthesized (Figure 7.7) [38]. Unlike $(iPrPDI)FeN_2$, $(iPrPDI)Fe(CO)_2$ exhibits clean and reversible electrochemistry, allowing quantitative measurement of the potentials for one-electron oxidation and reduction. The combined metrical, spectroscopic, and computational data established that the cationic iron dicarbonyl complex $[(iPrPDI)Fe(CO)_2][BAR^F_4]$ is best described as a low-spin iron(I) compound with a neutral bis(imino)pyridine chelate. Both EPR and DFT calculations support a principally iron-based SOMO with significant d_{z^2} character. In the limit where the neutral iron dicarbonyl $(iPrPDI)Fe(CO)_2$ is viewed in its low-spin Fe(II) canonical form, one-electron oxidation to $[(iPrPDI)Fe(CO)_2]^+$ is pincer-based and results in a net *reduction* of the metal to Fe(I).

One-electron reduction of $(iPrPDI)Fe(CO)_2$ was accomplished with 0.5% Na(Hg) in the presence of 15-crown-5 and yielded $[Na(15-crown-5)][(iPrPDI)Fe(CO)_2]$ as a green powder. The ^{57}Fe Mössbauer isomer shift of -0.01 mm s^{-1} is almost identical to the value measured for the neutral compound ($\delta = 0.01 \text{ mm s}^{-1}$), suggesting little perturbation to the electronic environment of the iron nucleus upon reduction. The X-band EPR spectrum of the compound exhibited an axial signal consistent with an $S = 1/2$ ground state with little g anisotropy, suggesting a ligand- rather than iron-based SOMO. DFT calculations supported this electronic structure description with a low-spin iron(I) center and the triplet diradical form of the bis(imino)pyridine. The spectroscopic and computational data also indicate a high degree of covalency in the molecule, suggesting that the $[(iPrPDI^{2-})Fe(CO)_2]^-$ description is probably an oversimplification.

As discussed above, introduction of alkyl substituents larger than methyl onto the imine carbon resulted in a preference for four-coordinate iron dinitrogen

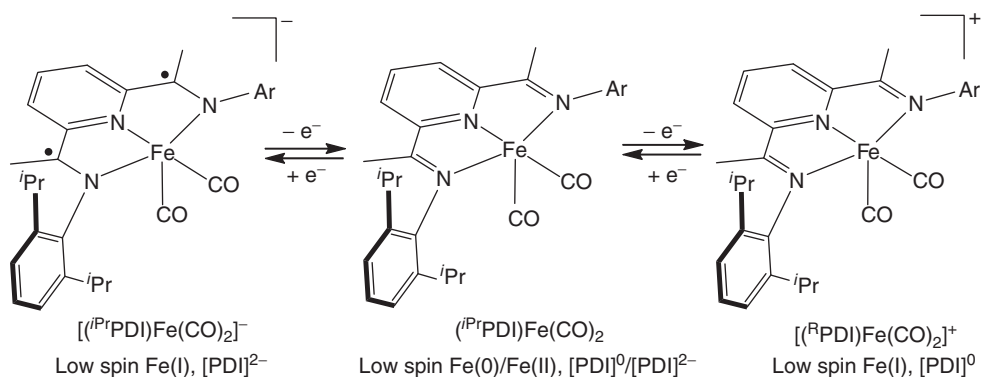


Figure 7.7 Electronic structure of bis(imino)pyridine iron dicarbonyl complexes over three oxidation states.

complexes. These observations, along with presence of a triplet diradical form of the bis(imino)pyridine in the electronic structure of the iron dinitrogen compounds, motivated the preparation of the aldimine-supported iron dihalides [6, 39]. As with the ketimine variant of the pincer, we initiated this chemistry by the reduction of the iron dibromide complex ($i^{\text{Pr}}\text{PDAI})\text{FeBr}_2$ ($i^{\text{Pr}}\text{PDAI} = 2,6(2,6\text{-}i^{\text{Pr}}_2\text{-C}_6\text{H}_3\text{N}=\text{CH})_2\text{C}_5\text{H}_3\text{N}$) [40].

Performing the sodium amalgam reduction in toluene solution resulted in the isolation of a diamagnetic compound identified as the κ^2 -bis(aldimino)pyridine iron toluene complex ($i^{\text{Pr}}\text{PDAI})\text{Fe}(\eta^6\text{-C}_7\text{H}_8)$ (Figure 7.8). When dissolved in benzene- d_6 , the analogous iron benzene- d_6 complex was isolated, demonstrating that the arene ligands are labile. Berry and coworkers [32] have reported a similar structural type in bis(imino)pyridine ruthenium chemistry with the 2,6-dimethyl aryl variant of the pincer. Placing the iron arene compounds in solvents such as diethyl ether or pentane for 24 h resulted in the formation of a brown crystalline solid identified as the paramagnetic bis(chelate) complex $[(i^{\text{Pr}}\text{PDAI})\text{Fe}]_2$.

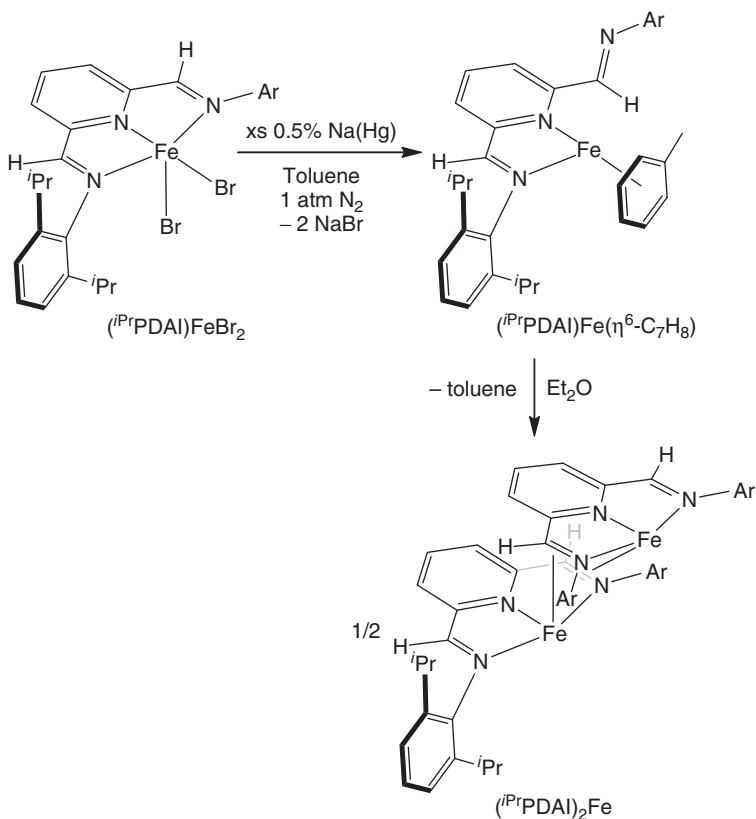


Figure 7.8 Reduced bis(aldimino)pyridine iron chemistry.

The dimeric iron compound proved to be robust both in solution and the solid state. Although catalytically inactive, the electronic structure of $[(^{iPr}PDAI)Fe]_2$ was of interest. Observation of a single Mössbauer doublet with an isomer shift of 0.84 mm s^{-1} established equivalent high-spin iron centers. These data, in combination with the distortions to the pincer ligand observed by X-ray diffraction, established overall two-electron reduction of the chelate, one in the unperturbed portion of the ligand and the other in the η^2 -imine coordinated to the adjacent iron.

The unusual structure of $[(^{iPr}PDAI)Fe]_2$ presented a unique opportunity to study electronic communication between two iron centers bearing redox-active bis(aldimino)pyridine pincer ligands. Variable-temperature solid-state magnetic susceptibility measurements established an essentially invariant effective magnetic moment of $4.3 \mu_B$ between 100 and 300 K. Below 100 K, μ_{eff} decreases monotonically from $4.1 \mu_B$ at 100 K to $1.5 \mu_B$ at 2 K, the lowest temperature where data were recorded. Initial fits of the data using two noninteracting $S = 1$ $[(^{iPr}PDAI)Fe]$ subunits failed to reproduce the temperature dependence of the data with physically reasonable values for the zero-field splitting parameter $|D|$ and the isotropic coupling constant J .

A more complex model was developed involving four spin centers resulting from two high-spin ferrous ions (each $S = 2$) and two triplet pincer dianions (each $S = 1$). In principle, all coupling pathways, metal–ligand and metal–metal, are antiferromagnetic and represent competing pathways for the alignment of the spin on the iron centers. To reduce the number of independent parameters, and because of the symmetry of compound, equivalent g and D values were assumed for the two iron centers, while neglecting g -anisotropy ($g_{\text{PDAI}} = 2.00$) and zero-field splitting ($|D_{\text{PDAI}}| = 0 \text{ cm}^{-1}$) for the pincers. The best fit obtained from this model successfully reproduced the experimental data and variable field measurements [37].

The preferred model corresponds to very strong antiferromagnetic coupling between each of the high-spin Fe(II) ions and its accompanying triplet diradical pincer ligand $[PDAI]^{2-}$ ($S = 1$). This results in essentially two uncoupled $S = 1$ $[(^{iPr}PDAI)Fe]$ subunits in the high-temperature regime (100–300 K). At temperatures below 100 K, weaker antiferromagnetic coupling between the two subunits produces the lower observed magnetic moments and accounts for the temperature dependence of μ_{eff} . The metal–metal interaction is mediated via a superexchange pathway and is an essential component of the model. Notably, the magnetic data and the associated spin-coupling model provide strong experimental evidence for the presence of a triplet diradical bis(aldimino)pyridine pincer ligand.

7.2.3

Reduced Bis(imino)pyridine Cobalt Chemistry

Reduced cobalt compounds have been of longstanding interest in bis(imino)pyridine chemistry. Following the reports of ethylene polymerization activity, efforts were focused on the preparation of various cobalt alkyl derivatives with the goal of understanding the nature of the active species formed upon treatment with methyl

aluminoxane (MAO) and other aluminum alkyls. Treatment of (i^{Pr} PDI)CoCl₂ with 1 equiv of alkyl lithiums [41], Grignard reagents [42], or zinc metal [42a] yielded the corresponding cobalt chloride (i^{Pr} PDI)CoCl. Subsequent alkylation with alkyl lithium or Grignard reagents furnished a variety of diamagnetic cobalt alkyl complexes (i^{Pr} PDI)CoR (R = Me, Et, n^{Pr} , n^{Bu}) [43]. The electronic structure of this class of compounds has been established, which are best described as low-spin Co(II) derivatives with bis(imino)pyridine radical anions [44]. Thus, the reduction of (i^{Pr} PDI)CoCl₂ to (i^{Pr} PDI)CoCl is ligand-based, reducing the neutral bis(imino)pyridine chelate to its radical form where the cobalt(II) oxidation state is preserved. A change of the spin state from high to low accompanies the chelate reduction because of the increased field strength of the chelate radical anion (Figure 7.9).

Our laboratory subsequently explored the influence of changing the imine substituent from aryl to an alkyl group on the overall electronic structure of the reduced bis(imino)pyridine cobalt compounds [45]. Treatment of ($^{\text{R}}$ APDI)CoCl₂ ($^{\text{R}}$ APDI = 2,6-(RN=CMe)₂C₅H₃N, R = Cy, i^{Pr}) [46] with 1 equiv of NaBEt₃H in toluene followed by recrystallization from pentane yielded ($^{\text{R}}$ APDI)CoCl as red-brown (R = Cy) and mauve (R = i^{Pr}) solids. In contrast to the aryl-substituted bis(imino)pyridine cobalt halide compounds, ($^{\text{R}}$ APDI)CoCl are paramagnetic. The solid-state structure of (i^{Pr} APDI)CoCl was determined by X-ray diffraction, which

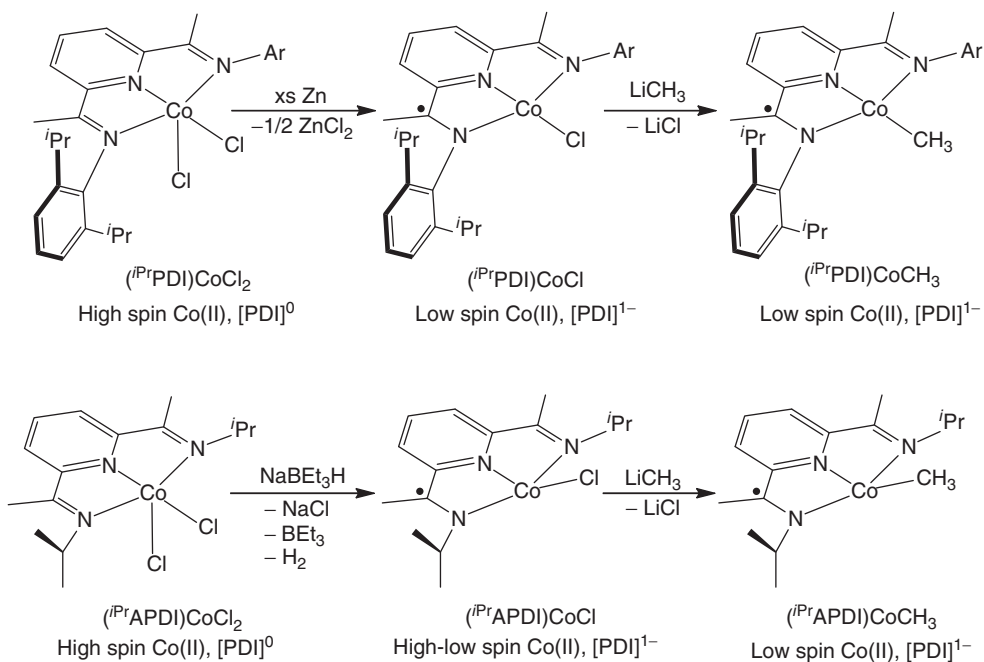


Figure 7.9 Synthesis and electronic structures of aryl- versus alkyl-substituted bis(imino)pyridine cobalt chloride and methyl complexes.

established a distorted geometry where the chloride ligand is lifted with an $N_{\text{pyr}}\text{-Co-Cl}$ angle of $150.73(5)^\circ$. The metrical parameters of the pincer ligand established bond length distortions that are consistent with one-electron reduction of the chelate. Thus, in analogy with the planar ($i^{\text{Pr}}\text{PDI})\text{CoCl}$, distorted ($i^{\text{Pr}}\text{APDI})\text{CoCl}$ is a cobalt(II) compound.

The magnetic properties of both ($^{\text{Cy}}\text{APDI})\text{CoCl}$ and ($i^{\text{Pr}}\text{APDI})\text{CoCl}$ were studied in more detail by SQUID magnetometry. The data for ($^{\text{Cy}}\text{APDI})\text{CoCl}$ established an effective magnetic moment of $2.67 \mu_B$ at 300 K, approaching the spin-only value for two unpaired electrons and an $S = 1$ ground state. Cooling the sample resulted in a steep decrease of the magnetic moment, which dropped to a value of $0.23 \mu_B$ at temperatures below 50 K, indicating a greater population of the singlet state. The data for ($i^{\text{Pr}}\text{APDI})\text{CoCl}$ exhibited the same general features but were overall less pronounced. The value of μ_{eff} reached a maximum of $1.0 \mu_B$ at 300 K, consistent with the narrower chemical shift dispersion for this compound observed by ^1H NMR spectroscopy. The magnetic data and variable temperature NMR studies established the spin crossover behavior between $S = 0$ and $S = 1$ states for both compounds.

Methylation of the ($^{\text{R}}\text{APDI})\text{CoCl}$ was accomplished by straightforward salt metathesis with methyl lithium and furnished ($^{\text{Cy}}\text{APDI})\text{CoCH}_3$ and ($i^{\text{Pr}}\text{APDI})\text{CoCH}_3$ as red solids. Both ^1H NMR spectroscopic studies and magnetic measurements established diamagnetic compounds, analogous to ($i^{\text{Pr}}\text{PDI})\text{CoCH}_3$. The solid-state structure of ($i^{\text{Pr}}\text{APDI})\text{CoCH}_3$ was determined by X-ray diffraction, and the overall molecular geometry was similar to that of the chloride derivative with the methyl ligand displaced from the idealized metal-chelate plane. The $N_{\text{py}}\text{-Co-CH}_3$ angle of $147.11(8)^\circ$ was slightly contracted from the value of $150.73(5)^\circ$ observed in the chloride compound. The distortions to the chelate bond distances were also consistent with formation of a bis(imino)pyridine radical anion. It is therefore important to realize that, even though the geometries of ($i^{\text{Pr}}\text{APDI})\text{CoCl}$ and ($i^{\text{Pr}}\text{APDI})\text{CoCH}_3$ are similar, the electronic structures are different.

These studies raised several fundamental questions about the effects of pincer substituents on the overall electronic structure of the resulting cobalt halide or alkyl compound. First, why are the electronic structures of N -aryl and N -alkyl substituted bis(imino)pyridine cobalt chloride complexes different? Second, why for the N -alkyl derivatives is the chloride compound spin crossover and the methyl diamagnetic? What role does the distortion of the ligand play on the overall electronic structure?

To answer these questions, a series of BS DFT calculations were conducted. Initially we sought to examine the influence of the imine substituents on the preferred geometry and spin state of the various species. Calculations were conducted on the full molecule as well as model compounds where the N -imine isopropyl groups were replaced with methyl substituents and another where the methyl groups in the backbone of the pincer were replaced with hydrogen atoms. In both model complexes, planar geometries were obtained following optimization of $S = 0$ states, demonstrating that the observed distortion in the experimental structure of ($i^{\text{Pr}}\text{APDI})\text{CoCl}$ is a result of steric interactions.

Calculations were conducted on $S = 1$ descriptions of (^{iPr}APDI)CoCl to elucidate the nature of the observed higher spin state. A BS (3,1) solution was found that was 6.6 kcal mol⁻¹ more stable than the corresponding BS (1,1) open-shell singlet state. This corresponds to a high-spin Co(II) center ($S_{\text{Co}} = 3/2$) engaged in an antiferromagnetic coupling interaction with a bis(imino)pyridine radical anion ($S_{\text{APDI}} = 1/2$). The optimized geometry for the BS(3,1) triplet for the model compound, where the isopropyl groups have been replaced by methyl groups, is significantly bent with a N_{pyr}-Co-Cl angle of 153.55°. Because of the absence of large imine substituents, the distortion is likely due to electronic effects. Analysis of the resulting molecular orbital (MO) diagram from full molecule calculations on triplet (^{iPr}APDI)CoCl with a bent N_{pyr}-Co-Cl linkage revealed that the d_{yz} orbital (z is defined as orthogonal to the idealized metal-chelate plane with x along the N_{pyr}-Co bond) is destabilized by strong Cl π -donation and the d_{x²-y²} is stabilized by removing the chloride from the metal-ligand plane. Accordingly, the energy difference between these two orbitals decreases and favors a high-spin Co(II) center.

By contrast, the related methyl derivative (^{iPr}APDI)CoCH₃ has a purely σ -donating hydrocarbyl ligand and the destabilization of the d_{yz} orbital is absent. Accordingly, the energetic gap between this orbital and d_{x²-y²} is larger and as such the triplet state is less accessible. Therefore, it is the field strength of the X-type ligand, not the geometry of the molecule, that dictates the overall spin state of the molecule.

Two-electron reduction chemistry of both aryl- and alkyl-substituted bis(imino)pyridine cobalt compounds was also explored. Stirring (^{iPr}PDI)CoCl₂ with excess sodium amalgam under a dinitrogen atmosphere furnished (^{iPr}PDI)CoN₂ [47]. The cobalt dinitrogen compound was also prepared by the treatment of (^{iPr}PDI)CoCl₂ with 2 equiv of NaBEt₃H. Both synthetic routes were extended to the preparation of the phenylated derivative (^{iPr}BPDI)CoN₂ (Figure 7.10).

The solid-state structure of (^{iPr}PDI)CoN₂ was determined by X-ray diffraction, which established a planar molecule with distortions to the bis(imino)pyridine chelate consistent with one-electron reduction. SQUID magnetic measurements confirmed an $S = 1/2$ ground state. Taken together, these data indicate a Co(I), d⁸ compound, which is a common electronic configuration for planar four-coordinate cobalt. If this electronic structure was indeed correct, the SOMO of (^{iPr}PDI)CoN₂ should be bis(imino)pyridine-based. The X-band EPR spectrum of (^{iPr}PDI)CoN₂ in fluid toluene solution at 23 °C exhibits an isotropic g_{iso} value of 2.003 with small hyperfine interactions from the coupling of the principally ligand-based radical to the ⁵⁷Co nucleus. This view of the electronic structure was also supported by DFT calculations. The Mulliken spin density established that the unpaired electron was almost exclusively localized on the bis(imino)pyridine pincer. The synthesis and electronic structure determination of (^{iPr}PDI)CoN₂ are notable in that they provide direct experimental evidence for the formation of bis(imino)pyridine radicals in reduced transition-metal chemistry.

The reactivity of (^{iPr}PDI)CoN₂ was also examined. Exposure to 1 atm of CO furnished the red-brown cobalt carbonyl compound (^{iPr}PDI)CoCO, which exhibits a strong C≡O stretch centered at 1975 cm⁻¹. Notably, substitution of the carbonyl

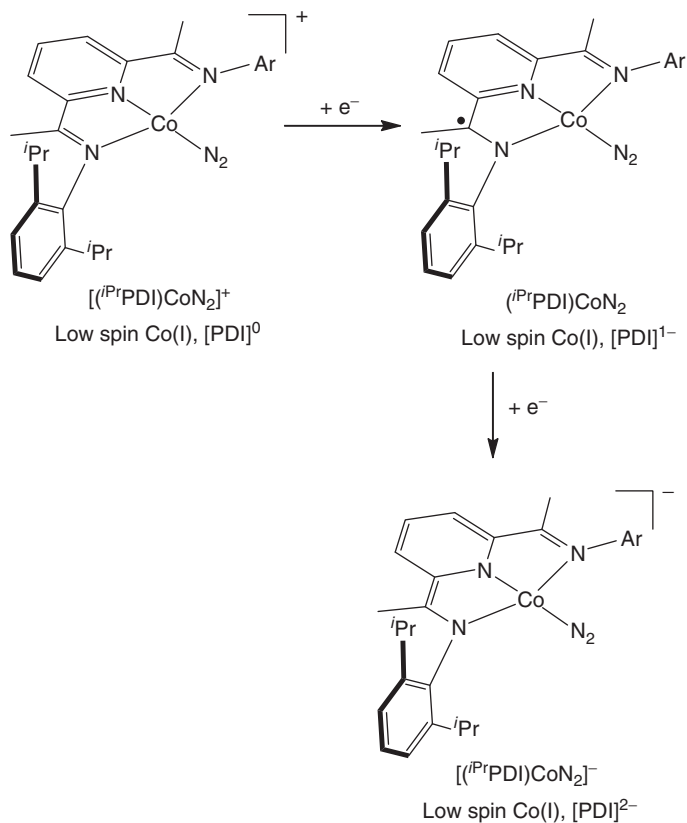


Figure 7.10 Electronic structures of a series of bis(imino)pyridine cobalt dinitrogen complexes across three formal oxidation states.

ligand was achieved by re-exposure of $(i^{\text{Pr}}\text{PDI})\text{CoCO}$ to 1 atm of N_2 at 23 °C over the course of 6 h, supporting the lability of the neutral ligand in the Co(II) compound.

Because $(i^{\text{Pr}}\text{PDI})\text{CoN}_2$ contains a one-electron-reduced bis(imino)pyridine and the chelate can accept up to three electrons, additional reduction chemistry was explored. Stirring a THF solution of $(i^{\text{Pr}}\text{PDI})\text{CoCl}_2$ with excess sodium naphthalenide followed by filtration and recrystallization from diethyl ether resulted in the isolation of the anionic bis(imino)pyridine cobalt dinitrogen compound $[\text{Na}(\text{Solv})_3][(i^{\text{Pr}}\text{PDI})\text{CoN}_2]$ (Solv = THF, Et_2O). The ^1H NMR spectrum of the THF-solvate in $\text{THF-}d_8$ exhibited the number of resonances expected for a diamagnetic, C_{2v} symmetric compound. Evaluation of the electronic structure by computational methods established a low-spin Co(I) d^8 compound with a doubly reduced bis(imino)pyridine ligand. The calculations indicate that both the metal and the $[(i^{\text{Pr}}\text{PDI})]^{2-}$ ligand are in their closed-shell forms, providing no evidence for redox activity in this compound. Comparing the d^6 Fe(II) iron dinitrogen compound with the anionic d^8 Co(I) derivative reveals interesting differences in the electronic

structure preferences of the bis(imino)pyridine dianion [${}^{iPr}PDI]^{2-}$. In the neutral iron dinitrogen complex (${}^{iPr}PDI)FeN_2$, the intermediate spin d^6 electronic configuration ($S=1$) is well poised to antiferromagnetically couple to a triplet pincer dianion. By contrast, the d^8 anionic cobalt dinitrogen complex is ill equipped to engage in antiferromagnetic coupling and hence the closed-shell form of the dianionic ligand is preferred.

The preparation of (${}^{iPr}PDI)CoN_2$ and [${}^{iPr}PDI)CoN_2]^-$ completes a series of four-coordinate cobalt dinitrogen complexes over three different oxidation states as [${}^{iPr}PDI)CoN_2]^+$ was reported previously by Gibson and coworkers [42a]. Following our report, Peters and coworkers [48] described a similar series of iron dinitrogen complexes in three oxidation states and the role of each in the functionalization of N_2 . Holland and coworkers [49] have also described sequential reduction of β -diketiminate cobalt N_2 complexes with bridging end-on dinitrogen ligands and have demonstrated the influence of alkali metal coordination on N_2 activation. In the series of bis(imino)pyridine cobalt dinitrogen complexes, the reduction events are principally ligand-based and preserve the Co(I) d^8 electronic configuration in all three compounds. This is perhaps unsurprising given that, in a square-planar ligand field, the metal-based lowest unoccupied molecular orbital (LUMO) is $d_{x^2-y^2}$ and is energetically inaccessible as compared to the low-lying a_2 and b_2 MOs of the coordinated bis(imino)pyridine.

Budzelaar and coworkers [50] have reported the two-electron reduction chemistry of the corresponding bis(imino)pyridine nickel dihalide derivative. Stirring (${}^{iPr}PDI)NiBr_2$ with 2 equiv of NaH in THF under a dinitrogen atmosphere furnished a yellow-brown compound identified as (${}^{iPr}PDI)NiN_2$. The solid-state structure established a planar molecule with an extremely short N–N bond of 0.92 Å, indicating no dinitrogen activation. Accordingly, a high-frequency N_2 band was observed at 2156 cm^{-1} by infrared spectroscopy. The planar geometry of the nickel, the observed diamagnetism, and the metrical parameters of the bis(imino)pyridine are consistent with an electronic structure identical to [${}^{iPr}PDI)CoN_2]^-$ where the Ni(II) d^8 center is coordinated by an $S=0$ bis(imino)pyridine dianion (Figure 7.11).

The synthesis of the reduced bis(imino)pyridine cobalt dinitrogen complex (${}^{iPr}PDI)CoN_2$ and related derivatives has prompted studies into the oxidative

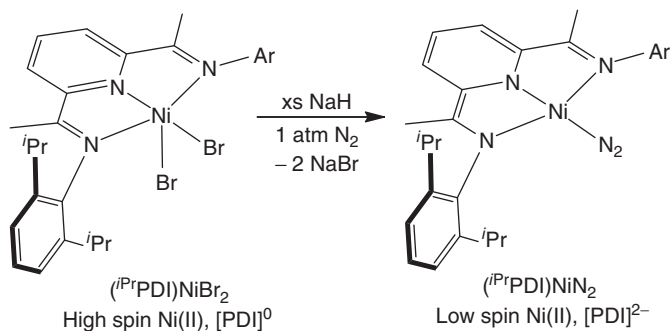


Figure 7.11 Synthesis and electronic structure of (${}^{iPr}PDI)NiN_2$.

addition of various substrates. During the course of these studies, Zhu and Budzelaar [51] reported that treatment of cobalt alkyl complexes containing the dimethyl variant of the pincer (^{Me}PDI)CoCH₂SiMe₃ with dihydrogen, followed by exposure to N₂, was also a route to the dinitrogen compound (^{Me}PDI)CoN₂. Treatment of (^RPDI)CoN₂ compounds with various alkyl or aryl halides R¹-X produced a mixture of the cobalt alkyl (aryl) and halide species (^RPDI)CoR¹ and (^RPDI)CoX, respectively. Investigation into the mechanism with cyclopropylmethyl halides and DFT calculations supported the intermediacy of free alkyl and aryl radicals [52]. Notably, the overall two-electron oxidation occurs into two discreet one-electron steps and results in an oxidation of Co(I) to Co(II) (Figure 7.12).

The rich two- and three-electron reduction of (^{iPr}PDI)CoCl₂ prompted similar studies with *N*-alkylated bis(imino)pyridine cobalt compounds. Recall that the monohalide complexes (^RAPDI)CoCl exhibited spin crossover behavior distinct from their *N*-arylated counterparts. Stirring (^RAPDI)CoCl₂ (R = Cy, ^{iPr}) with excess sodium amalgam under a dinitrogen atmosphere – the conditions used to prepare (^{iPr}PDI)CoN₂ – furnished the bis(chelate) compound compounds (^RAPDI)₂Co

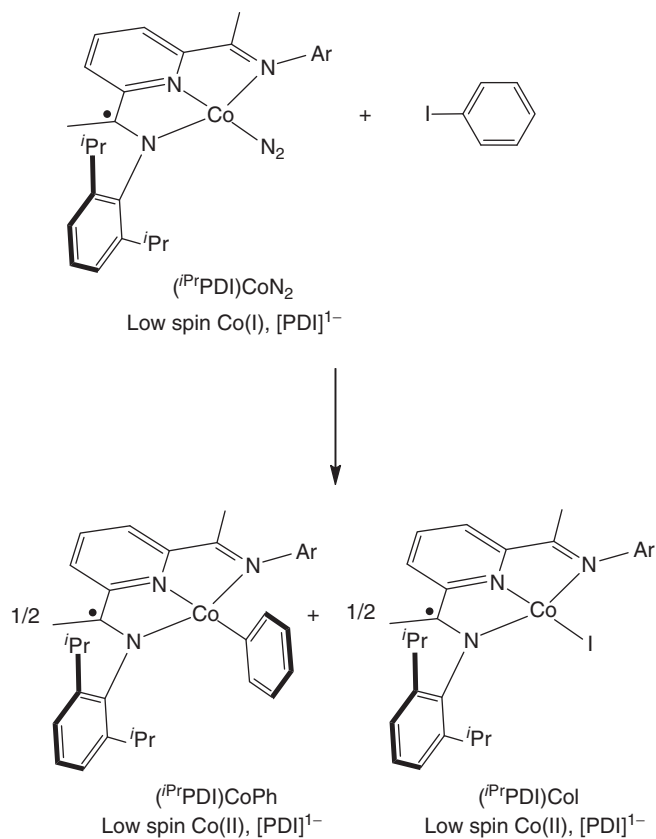


Figure 7.12 Oxidative addition of iodobenzene to (^{iPr}PDI)CoN₂.

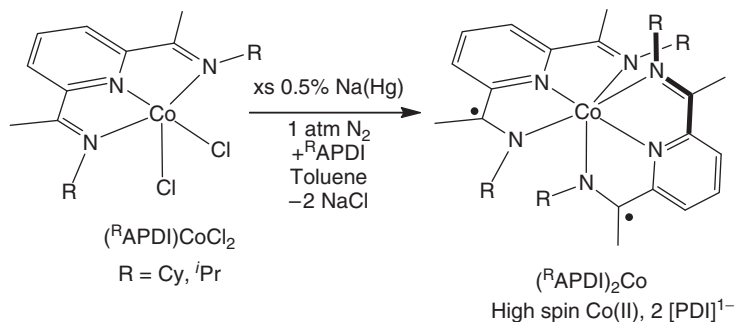


Figure 7.13 Two-electron reduction of $(^R\text{APDI})\text{CoCl}_2$ compounds to yield $(^R\text{APDI})_2\text{Co}$.

in poor yield. Following identification of the product, the synthetic procedure was modified to include an additional equivalent of the free bis(imino)pyridine and, accordingly, the yields were increased to 63% ($\text{R} = \text{Cy}$) and 70% ($\text{R} = \textit{i}\text{Pr}$) (Figure 7.13). In either case, no evidence for the formation of neutral cobalt dinitrogen compound was obtained.

The solid-state structures were determined by X-ray diffraction, which established six-coordinate compounds with idealized D_{2d} symmetry with orthogonal bis(imino)pyridine chelates. Examination of the metrical parameters revealed the appropriate bond length distortions for a monoreduced bis(imino)pyridine radical anion. Both $(^R\text{APDI})_2\text{Co}$ complexes are paramagnetic and exhibit interesting variable-temperature magnetic behavior. From 150 to 300 K, the μ_{eff} of $(\textit{i}\text{Pr}\text{APDI})_2\text{Co}$ is essentially temperature dependent with a value of $4.1 \mu_B$, which is close to the spin-only value for three unpaired electrons. Below 150 K, the magnetic moment *increases* to a maximum at 20 K before the values again decrease as a result of the normal effects of zero field splitting and magnetic saturation domination. The origin of the unusual behavior between 20 and 150 K was attributed to mechanical torquing, where small particles of the powder sample are aligned in the magnetic field.

The electronic structure of $(^R\text{APDI})_2\text{Co}$ was also investigated by EPR spectroscopy. The 10 K EPR spectrum of a powder sample of $(\textit{i}\text{Pr}\text{APDI})_2\text{Co}$ exhibits axial symmetry with effective g values of $g_{\perp}^{\text{eff}} = 4.5$ and $g_{\parallel}^{\text{eff}} = 2.1$. These values are as expected for a compound with an $S = 3/2$ ground state with large axial zero-field splitting and low rhombicity. Both EPR spectroscopy and SQUID magnetic measurements firmly established an $S = 3/2$ ground states for the $(^R\text{APDI})_2\text{Co}$ compounds. In comparison with the related iron complex $(\textit{i}\text{Pr}\text{APDI})_2\text{Fe}$ [53], the quartet ground state for the cobalt derivative is counterintuitive. In the iron example, antiferromagnetic coupling of the two bis(imino)pyridine radicals to a high-spin iron(II) center forces the radical spins into a parallel alignment and results in an overall $S = 1$ ground state. Based on this electronic structure, an $S = 1/2$ ground state for the cobalt complex would be expected arising from antiferromagnetic coupling of the ligand-centered radicals to the high-spin Co(II) center. The observation of an overall $S = 3/2$ spin state indicates that ligand–radical antiferromagnetic coupling

must dominate over metal–ligand coupling. This is perhaps even more surprising given the almost idealized orthogonal arrangement of the two chelate planes.

To gain additional insight into the intriguing electronic structures of the $(^R\text{APDI})_2\text{Co}$ compounds, BS DFT calculations were carried out [45]. The preferred solution was consistent with a high-spin Co^{II} ion ($S_{\text{Co}} = 3/2$) and two ligand-centered radicals. Notably, the two pincer-localized spins are antiparallel, where the spin density on each ligand approaches one but are of opposite sign. The qualitative MO diagram obtained from this calculation revealed that the high-spin $\text{Co}(\text{II})$ configuration mediates the antiferromagnetic coupling interaction between the ligand-centered radicals. One SOMO, a formally t_{2g} -type d_{yz} orbital, is available for antiferromagnetic coupling to a ligand-centered radical while the remaining two SOMOs are of e_g symmetry (d_{z^2} and $d_{x^2-y^2}$) and are orthogonal to the remaining π -radical SOMO of the remaining bis(imino)pyridine radical. Thus, the overall $S = 3/2$ spin state can be viewed as arising from two Co-centered spins and one ligand-centered radical. This, of course, is a gross oversimplification of the true ground state and is a manifestation of the failure of BS wavefunction to accurately describe the multireference character of such systems. Because of the symmetry of the complex, a second degenerate solution exists in which the ligand spin densities

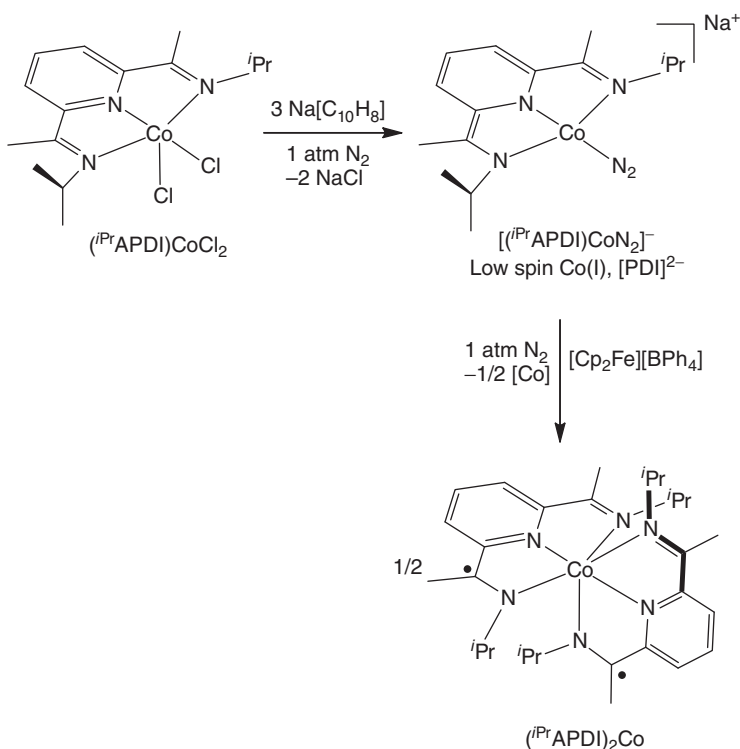


Figure 7.14 Synthesis and electronic structure of compounds to yield $[(i\text{PrAPDI})\text{CoN}_2]^-$ and $(i\text{PrAPDI})_2\text{Co}$.

are inverted and one of the unpaired electrons resides in a d_{xy} orbital while the d_{yz} is doubly occupied. Accordingly, the true ground state of the molecule is in fact a superposition of both states where the ligand radicals are antiferromagnetically coupled to each other and form a diamagnetic pair that carries no net spin density.

Even though two-electron reduction of (*i*PrAPDI)CoCl₂ furnished a bis(chelate) cobalt compound, three-electron chemistry of the same compound was also explored with the goal of exploring the possibility of dinitrogen coordination in an “over reduced” cobalt species. Stirring a THF solution of (*i*PrAPDI)CoCl₂ with 3 equiv of NaC₁₀H₈ under a dinitrogen atmosphere followed by extraction into and recrystallization from Et₂O furnished [Na(Solv)₃][(*i*PrAPDI)CoN₂] as a mixture of ether and THF solvates (Figure 7.14). Analysis of the compound by ¹H NMR spectroscopy established a diamagnetic molecule with no evidence for contribution from paramagnetic excited states. Attempts to oxidize this compound to furnish the corresponding neutral cobalt dinitrogen complex were unsuccessful, resulting in the isolation of (*i*PrAPDI)₂Co with no evidence for any other cobalt species. It is notable that the *N*-alkylated bis(imino)pyridine ligand will support an anionic cobalt dinitrogen complex where the pincer is in a closed-shell π -accepting form but not a neutral cobalt–N₂ complex where presumably a pincer π -radical would be accessed.

7.3

Conclusions and Outlook

The coordination chemistry of reduced bis(imino)pyridine manganese, iron, and cobalt complexes has proven to be rich. In some instances, compounds that are active base metal precatalysts for important transformations such as alkene hydrogenation, hydrosilylation, and cycloaddition have been synthesized. Other examples include bis(chelate) complexes of manganese, iron, and cobalt, which, although catalytically inactive, still exhibit rich spectroscopic and magnetic properties. Furthermore, it is these compounds that have proven to yield the most interesting electronic structures and in many cases have provided the definitive experimental evidence for the formation of both radical and diradical forms of the bis(imino)pyridine pincers. From these studies, there is little doubt that bis(imino)pyridines engage in radical chemistry when coordinated to first-row transition metals. Having established these foundations, the future for this ligand class is bright. Their ease of synthesis, modularity, and unique electronic properties suggest that some of the most interesting chemistry is yet to be discovered.

References

1. (a) Lions, F. and Martin, K.V. (1957) *J. Am. Chem. Soc.*, **79**, 2733. (b) Figgins, P.E. and Busch, D.H. (1960) *J. Am. Chem. Soc.*, **82**, 820. (c) Stouffer, R.C., Hadley, W.B., and Busch, D.H. (1961) *J. Am. Chem. Soc.*, **83**, 3732.
2. Gibson, V.C., Redshaw, C., and Solan, G.A. (2007) *Chem. Rev.*, **107**, 1745.

3. (a) Bennett, A.M.A. (1998) Ligands and catalyst systems thereof for ethylene oligomerization to linear alpha olefins. (DuPont) WO 98/27124; *Chem. Abstr.*, **129**, (1998), 122973x; (b) Bennett, A.M.A. (1999) *ChemTech*, **29**, 24.
4. (a) Small, B.L. and Brookhart, M. (1998) *J. Am. Chem. Soc.*, **120**, 7143. (b) Small, B.L., Brookhart, M., and Bennett, A.M.A. (1998) *J. Am. Chem. Soc.*, **120**, 4049.
5. (a) Britovsek, G.J.P., Gibson, V.C., Kimberly, B.S., Maddox, P.J., McTavish, S.J., Solan, G.A., White, A.J.P., and Williams, D.J. (1998) *Chem. Commun.*, 849. (b) Britovsek, G.J.P., Bruce, M., Gibson, V.C., Kimberly, B.S., Maddox, P.J., Mastroianni, S., McTavish, S.J., Redshaw, C., Solan, G.A., Strömberg, S., White, A.J.P., and Williams, D.J. (1999) *J. Am. Chem. Soc.*, **121**, 8728.
6. Small, B.L. and Brookhart, M. (1999) *Macromolecules*, **32**, 2120.
7. Scott, J., Gambarotta, S., Korobkov, I., Knijnenburg, Q., de Bruin, B., and Budzelaar, P.H.M. (2005) *J. Am. Chem. Soc.*, **127**, 17204.
8. For representative examples see: (a) Magdzinski, E., Gobbo, P., Martin, C.D., Workentin, M.S., and Ragogna, P.J. (2012) *Inorg. Chem.*, **51**, 8425. (b) Martin, C.D. and Ragogna, P.J. (2012) *Inorg. Chem.*, **51**, 2947. (c) Jurca, T., Lummiss, J., Burchell, T.J., Gorelsky, S.I., and Richeson, D.S. (2009) *J. Am. Chem. Soc.*, **131**, 4608. (d) Reeske, G. and Cowley, A.H. (2006) *Chem. Commun.*, 1784. (e) Reger, D.L., Wright, R.D., Smith, M.D., Rheingold, A.L., Kassel, S., Concolino, T., and Rhagitan, B. (2002) *Polyhedron*, **21**, 1795.
9. Caulton, K.G. (2012) *Eur. J. Inorg. Chem.*, **2012**, 435.
10. Butin, K.P., Beloglazkina, E.K., and Zyk, N.V. (2005) *Russ. Chem. Rev.*, **74**, 531.
11. Chirik, P.J. (2011) *Inorg. Chem.*, **50**, 9737.
12. Chirik, P.J. and Wieghardt, K. (2010) *Science*, **327**, 794.
13. Bullock, R.M. (ed.) (2010) *Catalysis without Precious Metals*, Chapter 4, Wiley-VCH Verlag GmbH, Weinheim, pp. 83–106.
14. Enthaler, S., Junge, K., and Beller, M. (2008) *Angew. Chem. Int. Ed.*, **47**, 3317.
15. (a) Frankel, E.N., Emken, E.A., Peters, H.M., Davison, V.K., and Butterfield, R.O. (1964) *J. Org. Chem.*, **29**, 3292. (b) Frankel, E.N., Emken, E.A., and Davison, V.K. (1965) *J. Org. Chem.*, **30**, 2739.
16. (a) Wrighton, M. (1974) *Chem. Rev.*, **74**, 401. (b) Schroeder, M.A. and Wrighton, M.S. (1976) *J. Am. Chem. Soc.*, **98**, 551. (c) Mitchener, J.C. and Wrighton, M.S. (1981) *J. Am. Chem. Soc.*, **103**, 975. (d) Whetten, R.L., Fu, K.-J., and Grant, E.R. (1982) *J. Am. Chem. Soc.*, **104**, 4270. (e) Weiller, B.H. and Grant, E.R. (1987) *J. Am. Chem. Soc.*, **109**, 1051. (f) Wu, Y.-M., Bentsen, J.G., Brinkley, C.G., and Wrighton, M.S. (1987) *Inorg. Chem.*, **26**, 530. (g) Kismartoni, L.C., Weitz, E., and Cedeño, D.L. (2005) *Organometallics*, **24**, 4714.
17. (a) Kuwabara, I.H., Comninou, F.C.M., Pardini, V.L., Viertler, H., and Toma, H.E. (1994) *Electrochim. Acta*, **39**, 2401. (b) Toma, H.E. and Chavel-Gil, T.E. (1997) *Inorg. Chim. Acta*, **257**, 197.
18. (a) de Bruin, B., Bill, E., Bothe, E., Weyhermüller, T., and Wieghardt, K. (2000) *Inorg. Chem.*, **39**, 2936. (b) Budzelaar, P.H.M., de Bruin, B., Gal, A.W., Wieghardt, K., and van Lenthe, J.H. (2001) *Inorg. Chem.*, **40**, 4649. (c) Knijnenburg, Q., Gambarotta, S., and Budzelaar, P.H.M. (2006) *Dalton Trans.*, 5442.
19. Zhu, D. and Budzelaar, P.H.M. (2008) *Organometallics*, **27**, 2699.
20. (a) Reardon, D., Aharnian, G., Gambarotta, S., and Yap, G.P.A. (2002) *Organometallics*, **21**, 786. (b) Sugiyama, H., Reardon, D., Aharnian, G., Gambarotta, S., Yap, G.P.A., and Budzelaar, P.H.M. (2002) *J. Am. Chem. Soc.*, **124**, 12268.
21. Russell, S.K., Bowman, A.C., Lobkovsky, E., Wieghardt, K., and Chirik, P.J. (2012) *Eur. J. Inorg. Chem.*, **2012**, 535.
22. (a) MacKay, B.A. and Fryzuk, M.D. (2004) *Chem. Rev.*, **104**, 385. (b) Fryzuk, M.D. and Johnson, S.A. (2000) *Coord. Chem. Rev.*, **200**, 379. (c) King, W.A., Scott, B.L., Eckert, J., and Kubas, G.J. (1999) *Inorg. Chem.*, **38**, 1069. (d) Lu, C.C. and Peters, J.C. (2006) *Inorg. Chem.*, **45**, 8597.

23. Cotton, F.A. and Wilkinson, G. (1988) *Advanced Inorganic Chemistry*, 5th edn, John Wiley & Sons, Inc., New York, pp. 1021–1050.
24. Radosevich, A.T., Melnick, J.G., Stoian, S.A., Bacciu, D., Chen, C.-H., Foxman, B.M., Ozerov, O.V., and Nocera, D.G. (2009) *Inorg. Chem.*, **48**, 9214.
25. Bart, S.C., Lobkovsky, E., and Chirik, P.J. (2004) *J. Am. Chem. Soc.*, **126**, 13794.
26. Scott, J., Vidyaratne, I., Korobkov, I., Gambarotta, S., and Budzelaar, P.H.M. (2008) *Inorg. Chem.*, **47**, 896.
27. Archer, A.M., Bouwkamp, M.W., Cortez, M.-P., Lobkovsky, E., and Chirik, P.J. (2006) *Organometallics*, **25**, 4269.
28. Russell, S.K., Darmon, J.M., Lobkovsky, E., and Chirik, P.J. (2010) *Inorg. Chem.*, **49**, 2782.
29. Darmon, J.M., Turner, Z.R., Lobkovsky, E., and Chirik, P.J. (2012) *Organometallics*, **31**, 2275.
30. (a) Bart, S.C., Chlopek, C., Bill, E., Bouwkamp, M.W., Lobkovsky, E., Neese, F., Wieghardt, K., and Chirik, P.J. (2006) *J. Am. Chem. Soc.*, **128**, 13901. (b) Bart, S.C., Lobkovsky, E., Bill, E., Wieghardt, K., and Chirik, P.J. (2007) *Inorg. Chem.*, **46**, 7055.
31. Stieber, S.C.E., Milsmann, C., Hoyt, J.M., Turner, Z.R., Finkelstein, K.D., Wieghardt, K., Debeer, S., and Chirik, P.J. (2012) *Inorg. Chem.*, **51**, 3770.
32. Gallagher, M., Wieder, N.L., Dioumaev, V.K., Carroll, P.J., and Berry, D.H. (2010) *Organometallics*, **29**, 591.
33. Enright, D., Gambarotta, S., Yap, G.P.A., and Budzelaar, P.H.M. (2002) *Angew. Chem. Int. Ed.*, **41**, 3873.
34. Wang, S.G., Qiu, Y.X., Fang, H., and Schwarz, W.H.E. (2006) *Chem. Eur. J.*, **12**, 4101.
35. Wieder, N.L., Gallagher, M., Carroll, P.J., and Berry, D.H. (2010) *J. Am. Chem. Soc.*, **132**, 4107.
36. Tondreau, A.M., Stieber, S.C.E., Milsmann, C., Lobkovsky, E., Weyhermüller, T., Semproni, S.P., and Chirik, P.J. (2013) *Inorg. Chem.*, **52**, 635.
37. Cladis, D.P., Kiernicki, J.J., Fanwick, P.E., and Bart, S.C. (2013) *Chem. Commun.*, **49**, 4169–4171. doi: 10.1039/C2CC37193F
38. Tondreau, A.M., Milsmann, C., Lobkovsky, E., and Chirik, P.J. (2011) *Inorg. Chem.*, **50**, 9888.
39. (a) Britovsek, G.J.P., Mastroianni, S., Solan, G.A., Baugh, S.P.D., Redshaw, C., Gibson, V.C., White, A.J.P., Williams, D.J., and Elsegood, M.R. (2000) *Chem. Eur. J.*, **6**, 2221.
40. Russell, S.K., Milsmann, C., Lobkovsky, E., Weyhermüller, T., and Chirik, P.J. (2011) *Inorg. Chem.*, **50**, 3159.
41. Kooistra, T.M., Knijnenburg, Q., Smits, J.M.M., Horton, A.D., Budzelaar, P.H.M., and Gal, A.W. (2001) *Angew. Chem. Int. Ed.*, **40**, 4719.
42. (a) Gibson, V.C., Humphries, M.J., Tellmann, K.P., Wass, D.F., White, A.J.P., and Williams, D.J. (2001) *Chem. Commun.*, 2252. (b) Steffen, W., Blömker, T., Kleigrewe, N., Kehr, G., Fröhlich, R., and Erker, G. (2004) *Chem. Commun.*, 1188.
43. (a) Gibson, V.C., Tellmann, K.P., Humphries, M.J., and Wass, D.F. (2004) *Chem. Commun.*, 2316. (b) Tellmann, K.P., Humphries, M.J., Rzepa, H.S., and Gibson, V.C. (2004) *Organometallics*, **23**, 5503. (c) Kleigrewe, N., Steffen, W., Blömker, T., Kehr, G., Fröhlich, R., Wibbeling, B., Erker, G., Wasilke, J.-C., Wu, G., and Bazan, G.C. (2005) *J. Am. Chem. Soc.*, **127**, 13955.
44. Knijnenburg, Q., Hettterscheid, D., Kooistra, T.M., and Budzelaar, P.H.M. (2004) *Eur. J. Inorg. Chem.*, 1204.
45. Bowman, A.C., Milsmann, C., Bill, E., Lobkovsky, E., Weyhermüller, T., Wieghardt, K., and Chirik, P.J. (2010) *Inorg. Chem.*, **49**, 6110.
46. Davis, R.N., Tanski, J.M., Adrian, J.C., and Tyler, L.A. (2007) *Inorg. Chim. Acta*, **360**, 3061.
47. Bowman, A.C., Milsmann, C., Atienza, C.C.H., Lobkovsky, E., Wieghardt, K., and Chirik, P.J. (2010) *J. Am. Chem. Soc.*, **132**, 1676.
48. Lee, Y., Mankad, N.P., and Peters, J.C. (2010) *Nat. Chem.*, **2**, 558.
49. Ding, K., Pierpont, A.W., Brennessel, W.W., Lukat-Rodgers, G., Rodgers, K.R., Cundari, T.R., Bill, E., and Holland, P.L. (2009) *J. Am. Chem. Soc.*, **131**, 9471.

50. Zhu, D., Thapa, I., Korobkov, I., Gambarotta, S., and Budzelaar, P.H.M. (2011) *Inorg. Chem.*, **50**, 9879.
51. Zhu, D. and Budzelaar, P.H.M. (2010) *Organometallics*, **29**, 5759.
52. Zhu, D., Budzelaar, P.H.M., and Korobkov, I. (2012) *Organometallics*, **31**, 3958.
53. Wile, B.M., Trovitch, R.J., Bart, S.C., Tondreau, A.M., Lobkovsky, E., Milsman, C., Bill, E., Wieghardt, K., and Chirik, P.J. (2009) *Inorg. Chem.*, **48**, 4190.

8

Pincer Complexes with Saturated Frameworks: Synthesis and Applications

Klara J. Jonasson and Ola F. Wendt

8.1

Introduction

Since the early work by Moulton and Shaw [1], the family of tridentate chelate complexes with transition metals, currently known as *pincer complexes*, has grown tremendously in size and variety [2].

In their initial publications [1, 3], Shaw and coworkers introduced PCP-type ligands with both aromatic and aliphatic backbones (Figure 8.1), but the former has almost completely dominated the literature since. This reflects the higher activation energy of the C(sp³)-H bond relative to the C(sp²)-H bond, along with the higher coordination stability of the planar and more rigid aromatic pincer backbone, giving an overall more straightforward metallation process. The aromatic ligands are also usually relatively easy to synthesize from readily available starting materials.

After their establishment as potent catalysts for several chemical transformations, the interest in steric and electronic tuning of the pincer complexes has increased, making the hybridization of the coordinated central carbon a possible variable [4]. Thus, over the past decades a slowly growing collection of pincer ligands with saturated backbones has been reported (Figure 8.2). Along with the straight alkyl chain featured already in Shaw's work, examples of cyclohexane- [5], arylmethane- [6], adamantane- [7], dibenzobarrelene- [8], cycloheptatriene- [9], and diarylmethane-based [10] scaffolds are known from the literature.

8.2

Synthesis of the Ligands

Generally, the phosphinite type of pincer ligands with saturated frameworks can be obtained by reacting a suitable diol with the chlorophosphine of choice in the presence of a base (Scheme 8.1). A number of diols are commercially available, and this is a straightforward reaction that often proceeds in high yields [11–13]. The synthesis of trialkylphosphine pincer ligands displays a higher complexity and

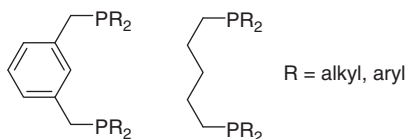


Figure 8.1 Shaw's original pincer ligands.

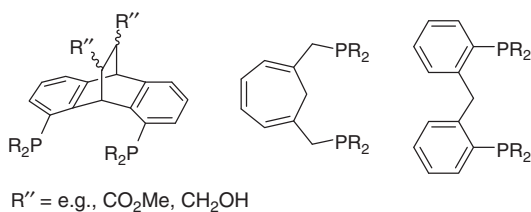
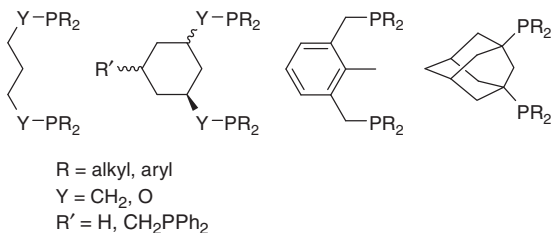
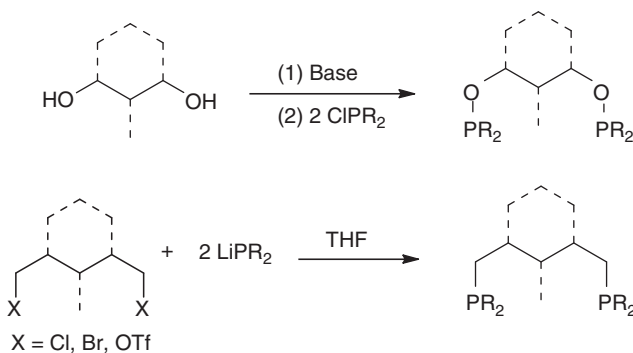


Figure 8.2 Examples of pincer ligands with an sp^3 -hybridized central carbon atom.



Scheme 8.1 Synthesis of aliphatic pincer ligands.

variety of reagents, but the highest yields are usually reported for the substitution reaction between an alkyl dihalide and the corresponding lithium phosphide [5, 14]. In general, the synthetic procedures are more cumbersome than what is observed for making aromatic pincer phosphine ligands.

8.3

Synthesis and Coordination Behavior of Carbometallated PC(sp³)P Complexes

The first reports on pincer chemistry by Shaw and coworkers included the synthesis of cyclometallated diphosphine PC(sp³)P complexes with Rh, Ir, Pd, and Pt [15], and these were later accompanied by examples of Ru, Os [16], and Ni complexes [17]. The phosphinite counterparts appeared later on the scene, but today complexes with Ni [13], Fe, Co [18], and Ir [19] are known. Typical examples are given in Figure 8.3.

With higher backbone flexibility, side products in the form of 16-ring cyclic dimers or di-coordinated eight-membered ring systems are more frequently reported for the complexations with aliphatic pincer ligands than for their aromatic counterparts [3, 20]. Shaw and coworkers [21] reported on the conversion of a 16-atom cyclic Rh dimer to the corresponding PCP coordinated pincer complex upon treatment with 2-methylpyridine. Seligson and Trogler [22] similarly reported on the cyclometallation of a 16-atom cyclic Pd dimer upon heating to 260 °C, and the group of Zargarian [23] achieved the same conversion of a Ni dimer at 110 °C in presence of 4-dimethylaminopyridine (DMAP). As opposed to the aromatic systems, aliphatic phosphinites have consistently been much more reluctant to cyclometallate than the corresponding phosphines. Thus, although the cyclohexyl phosphine ligands in Figure 8.2 are fairly straightforward to carbometallate with palladium and platinum precursors, the corresponding phosphinites resisted all attempts to cyclometallation, exclusively forming 16-ring cyclic dimers or dicoordinated eight-membered rings, instead [5b, 24]. The eight-membered rings always display a diaxial conformation and, as a possible explanation, Wendt and coworkers [25] have proposed that the inability of the phosphinite ligands to cyclometallate is due to a kinetic barrier, possibly involving an axial–equatorial conformational change necessary for the C–H activation process. The shorter bond distances in the phosphinite can prevent a ring-flip of the type shown in Scheme 8.2. Gusev and coworkers have investigated the coordination behavior of *cis*- and *trans*-substituted cyclohexyl phosphine ligands, achieving cyclometallation with Rh and Pd with both types of ligands. Although density functional theory (DFT) calculations predicted a more strained system in the *trans* case (by 9–11 kcal mol⁻¹), structural characterization confirmed almost identical, near-ideal chair conformations adopted by the cyclohexyl ring in both the *cis* and *trans* complexes [5b].

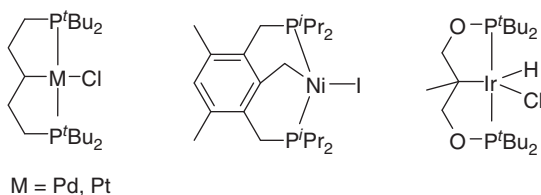
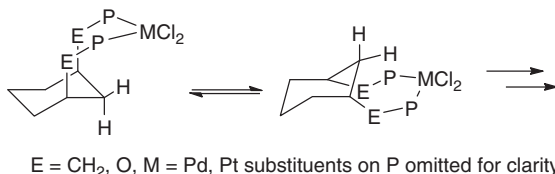


Figure 8.3 Examples of pincer complexes with an sp³-hybridized central carbon atom.

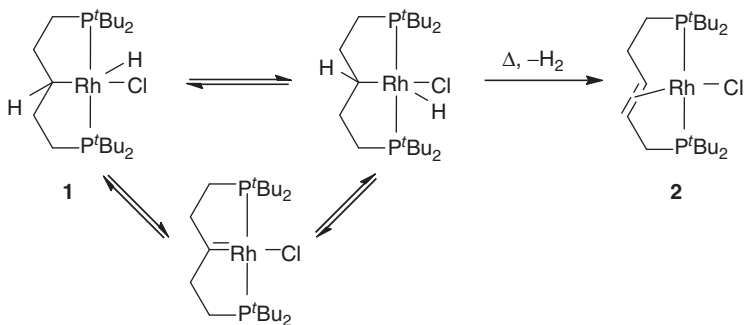


Scheme 8.2 Suggested ring-flip in the cyclometallation of cyclohexylbased pincer ligands.

8.3.1

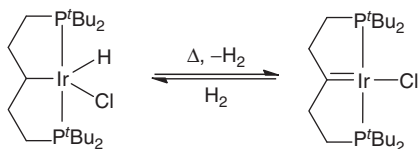
Coordination Flexibility in Acyclic PC(sp³)P Complexes

With a strongly σ -donating C(sp³) in a flexible pincer backbone, and with hydrogens present in both α - and β -positions, pincer complexes with saturated ligands are typically exposed to elimination reactions. In their pioneering studies, Shaw and coworkers [20, 21] reported on the β -elimination of Rh(III) chloro hydride complex **1** through thermolysis and H₂ formation, giving rise to the olefin chelate complex **2**. They also suggested a reversible interconversion of **1** via an α -elimination process on the basis of an observed fluxionality on the NMR timescale (Scheme 8.3). The analogous Ir complex also releases H₂ upon thermolysis although, instead, forming the PCP carbene complex through a presumed α -H elimination (Scheme 8.4) [3]. Gusev and Lough [16] reported on similar complexation behavior for the analogous Ru and Os complexes in presence of a base (Scheme 8.5), and later they found a cyclohexyl-based Ru complex to form the olefin and carbene complex in the same manner. An α -H elimination is also suggested to initiate the backbone aromatization observed for the cyclohexyl-based POC(sp³)OP iridium complex, as reported by the group of Wendt [26] (Scheme 8.6).

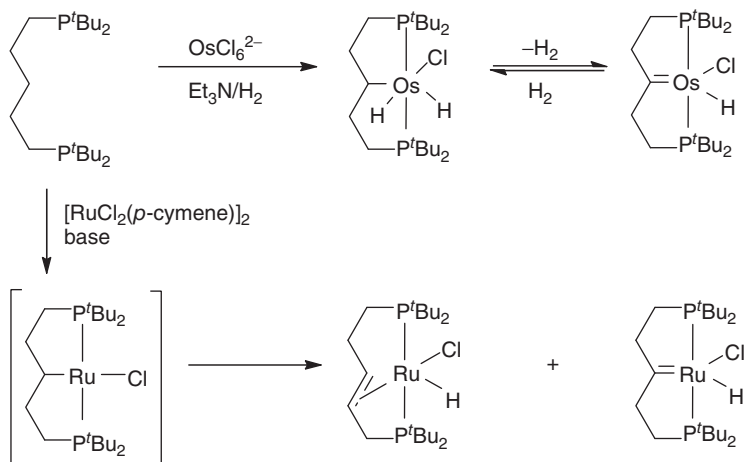


Scheme 8.3 Elimination reactions in ligands with α - and β -hydrogens

Introducing a methyl substituent on the coordinating carbon resulted in selective β -elimination of the Rh(III) chloro hydride complex **3** upon thermolysis, forming **4**. NaH reduction to a terminal nitrogen Rh(I) complex also induces a reversible β -elimination forming the hydride complex **5** (Scheme 8.7) [27].



Scheme 8.4 Formation of a pincer carbene complex.



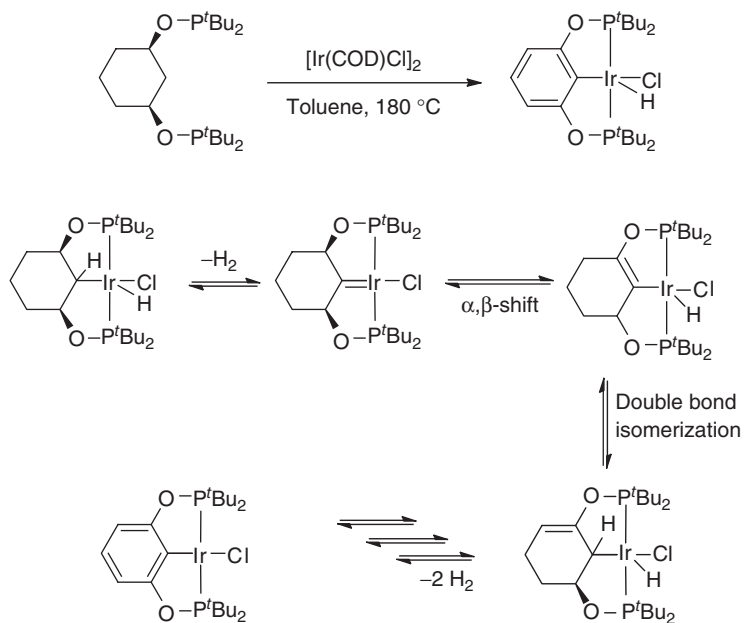
Scheme 8.5 Backbone reactivity in Ru- and Os-complexes.

8.4 Reactivity and Catalytic Applications of PC(sp³)P Complexes

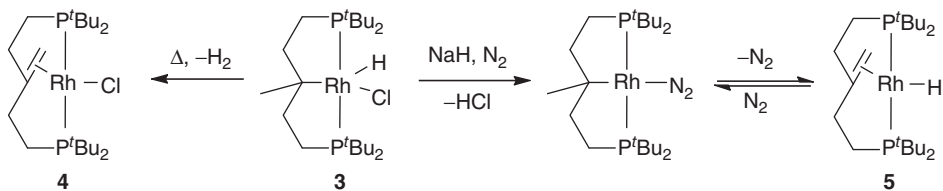
8.4.1

Ammonia Activation

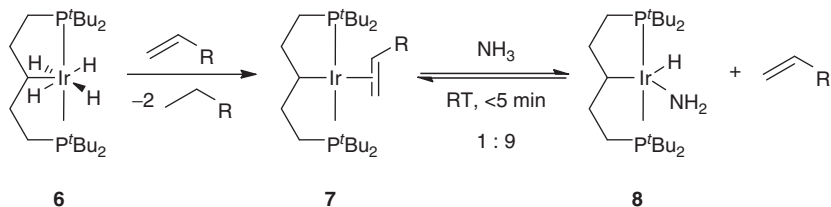
Hartwig and coworkers [28] have reported on the N–H activation of NH₃ utilizing an all-aliphatic Ir pincer complex, which displays reactivity contrary to the aromatic analog that is known to form the common Lewis acid–base ammonia complex. This underlines how an increased electron density at the metal center can favor the thermodynamics of an oxidative addition. Starting from the tetrahydride complex **6**, via the olefin complex **7** by treatment with an alkene, the amido hydride complex **8** was formed within minutes in a ratio 9:1 (Scheme 8.8). Isotopic labeling of the NH₃ has supported the suggested mechanism and, as indicated by kinetic experiments, the reaction follows a dissociative pathway. N–H activation under mild conditions is a key step toward a future catalytic transformation of NH₃ in, for example, olefin hydroamination. The Hartwig group has also used compound **7** to achieve N–H activation of both hydrazine and 1-aminopiperidine to form the



Scheme 8.6 Suggested mechanism for the aromatization reaction in an iridium cyclohexyl pincer complex.



Scheme 8.7 A methyl substituent in the α -position favors β -elimination.



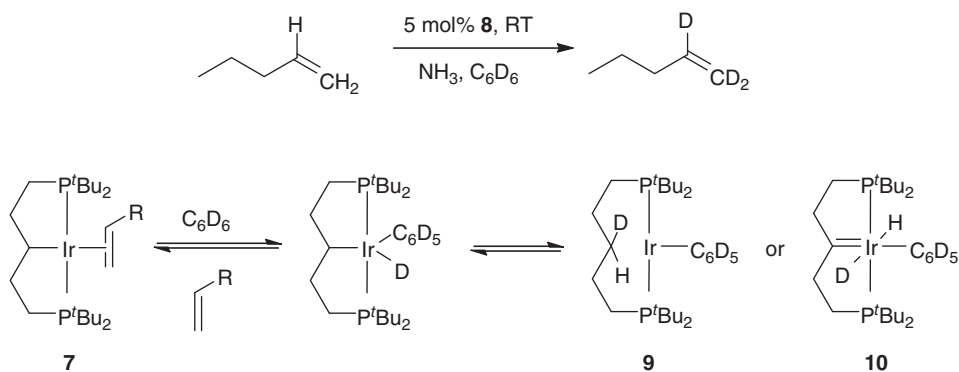
Scheme 8.8 Fast and reversible activation of ammonia in an iridium complex.

corresponding hydrido-iridium amido complexes. These compounds are stable, as opposed to the analogous aromatic pincer compounds, which in the case of N–H activation of 1-aminopiperidine undergoes a subsequent N–H bond cleavage to form an aminonitrene compound [29].

8.4.2

Isotopic Labeling

Hartwig [30] has also utilized the amido hydride complex **8** as a catalyst for H/D exchange at vinyl groups, operating at mild conditions without isomerization of the double bonds. This is an important transformation because of the value of deuterated compounds in studies of reaction mechanisms or biological processes. The Hartwig protocol displays an absolute regioselectivity along with high functional group compatibility. Aromatic pincer complexes activate C–H bonds but only at an elevated temperature, and for complex **8** a mechanism has been suggested where the methine position acts as a shuttle, in consistency with an observed deuterium incorporation in that position (Scheme 8.9). Complex **8** also catalyzes H/D exchange in arenes and, after oxidative addition of an aryl deuterium bond, the resulting complex can either undergo a reversible C–D reductive elimination or a reversible α -H elimination, forming the Ir(I) aryl complex **9** and the Ir(III) carbene **10**, respectively. A parallel process with the vinylic C–H bonds would lead to deuteration of the olefinic substrates.



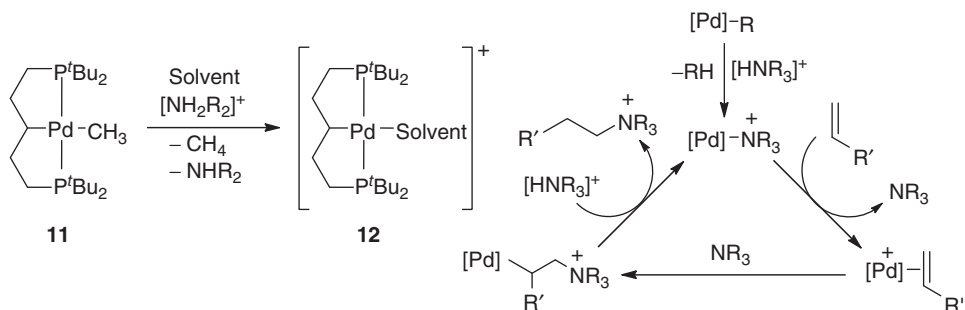
Scheme 8.9 Deuterium labeling catalysed by an iridium complex.

8.4.3

Reactions with Coordinated Olefins

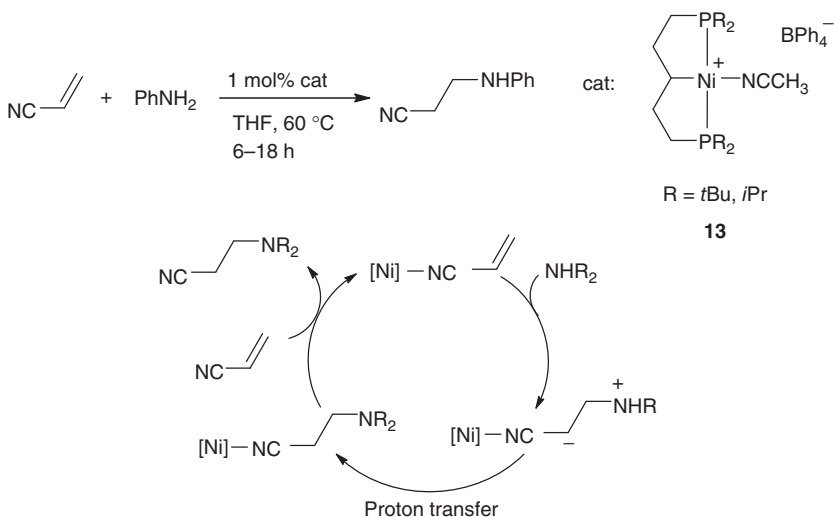
Seligson and Troglor [31] reported the catalytic amination of activated olefins with Pd(II) complex **11** (Scheme 8.10), with turnover numbers in the range of 10² with no observed loss of reactivity. The larger robustness of the pincer scaffold is responsible for the increased activity as compared to PdR₂(R'₂PCH₂CH₂PR'₂)-based catalysts with bidentate phosphine ligands. The mechanistic pathway is suggested to go via a coordination of the activated olefin and a subsequent nucleophilic attack of the amine. Initial reaction of the methyl complex **11** with a trialkyl ammonium salt with a noncoordinating anion affords cleavage of the Pd–C bond under the formation of methane and a catalytically active cationic species. In the reaction

of **11** with alkylammonium salts, the corresponding amine complexes are never observed irrespective of whether a tertiary or secondary amine is used and, instead, the solvent-coordinated complex **12** is obtained [22].



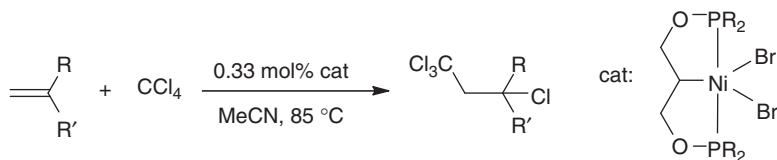
Scheme 8.10 Amination of olefins catalyzed by a palladium(II) complex.

Later studies by the group of Zargarian reported the same transformation, using the cationic Ni(II) pincer complex **13**, although postulating a so-called Lewis acid mechanism where the Ni center coordinates the nitrile group, thereby activating the coordinated olefin toward nucleophilic attack (Scheme 8.11). Aromatic analogs, however, were found to be more efficient catalysts for the transformation [32].



Scheme 8.11 Amination of olefins catalyzed by a nickel(II) complex.

The Zargarian group [13, 33] has also utilized the unusual Ni(III) phosphinite pincer complex as catalyst in the Kharasch addition (Scheme 8.12), reporting ~200 turnovers in 1 h and yields of around 65%.

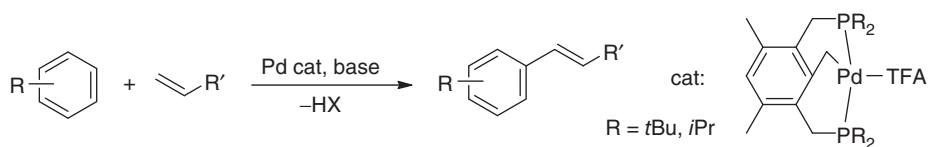


Scheme 8.12 Kharasch addition catalysed by a nickel(III) complex.

8.4.4

Carbon–Carbon Coupling Reactions

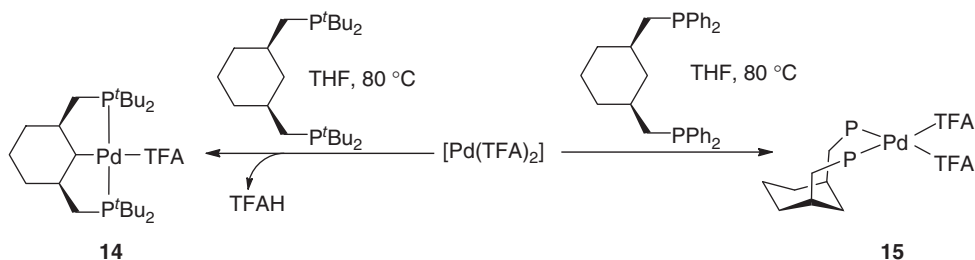
Several d⁸ Pd complexes have been reported as active catalysts for the Heck olefin arylation, and it was the group of Milstein [34] that first applied PCP Pd pincer complexes for this task (Scheme 8.13). High yields and turnover numbers above 100 000 and up to 500 000 were reported, and a slightly higher catalytic activity of the PC(sp³)P pincer complexes relative to its aromatic counterparts was observed, which was attributed to the more electron-rich metal center. A tendency of increased reactivity with less sterically hindering substituents on the coordinating phosphorus was also noted. Catalysis with the aromatic pincer complexes was originally proposed to involve a Pd(II)–Pd(IV) cycle [34, 35], but several kinetic studies could convincingly show that pincer complexes are only precatalysts to the highly active Pd(0) species that undergo a traditional Pd(0)–Pd(II) cycle [36].



Scheme 8.13 Mizoroki-Heck reaction catalysed by a palladium pincer pre-catalyst.

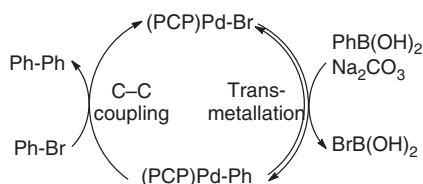
Later, Sjövall *et al.* [24] introduced an all-aliphatic cyclohexyl-based pincer complex **14** as catalyst for the Heck coupling reaction, allowing direct comparison between sp² and sp³ hybridization of the PCP coordinating carbon without altering the chelate ring size, underpinning the increased activity in the aliphatic case. Complex **14** was synthesized from the corresponding pincer ligand in complexation with the precursor Pd(TFA)₂ (TFA, trifluoroacetate); altering the phosphorus substituents to phenyl groups resulted in the nonmetallated complex **15** (Scheme 8.14, Ph substituent omitted for clarity) – an observation not made for the aromatic analogs [5a]. This again underpins the greater difficulty in cyclometallating aliphatic ligands. Initially, the catalysis was believed to be based on molecular Pd(II) and Pd(IV) species as evidenced by the seemingly full recovery of the intact pincer complex after catalysis [24]; but, again, detailed kinetic studies could convincingly show that the actual catalysis is dominated by leached Pd(0) species [37]. The kinetics shows a saturation behavior with respect to styrene concentration, and a mechanism involving a fast pre-equilibrium with styrene followed by an irreversible reaction

with aryl halide was proposed. This is a reversed order of entry of the substrates as compared to the classical Heck mechanism, where the aryl halide is activated before the olefin [38].



Scheme 8.14 The outcome of attempted cyclometallation with a cyclohexyl-based ligand depend on the phosphorus substituents.

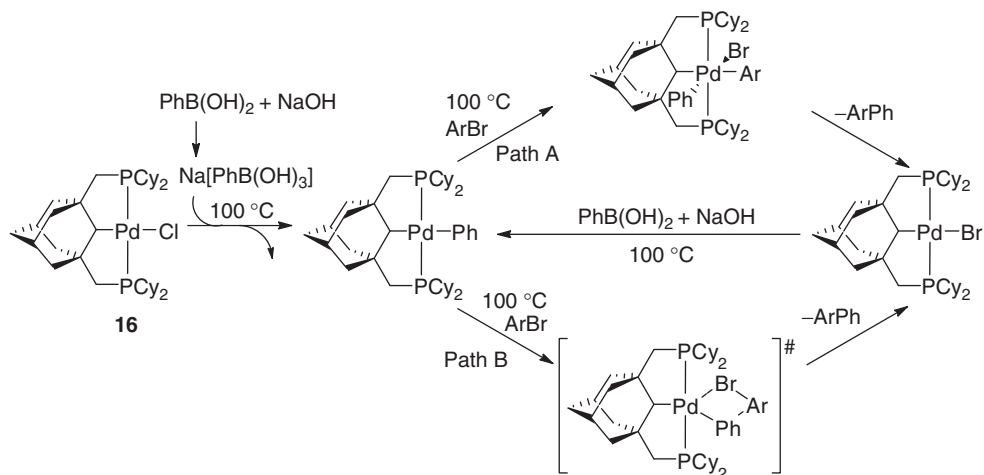
Olsson and Wendt [39] also utilized complex **14** as catalyst in the Suzuki–Miyaura coupling reaction though with moderate conversions and yields and high activation temperatures. Contrary to previous findings in the Heck coupling, there was no evidence of Pd(0) formation in this reaction and, instead, a catalytic cycle involving a homogeneous Pd complex in a higher formal oxidation state was proposed (Scheme 8.15). Stoichiometric precedence for the individual reaction was shown, but the mechanism for the step involving the aryl halide was not elucidated more closely.



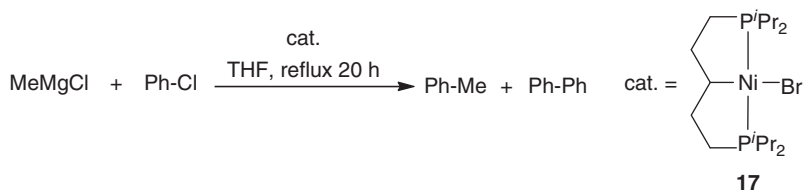
Scheme 8.15 Suzuki–Miyaura reaction catalysed by a palladium pincer complex.

Frech and coworkers [7] published a more successful protocol using their adamantyl-based PC(sp³)P pincer complex **16** in H₂O/NaOH or toluene/K₃PO₄ at 100 °C in presence of air, reporting conversions >95% and turnovers in the order of 10⁴ for a wide variety of substrates. The suggested catalytic cycle (Scheme 8.16) is similar to Scheme 8.15: the phenyl Pd complex is formed in a transmetalation on the halide complex, which then reacts with the aryl halide in a C–C bond-forming reaction. Again, the exact nature of the latter reaction is not clear. It proceeds either via an oxidative addition of an aryl bromide to the phenyl Pd complex, forming a neutral hexacoordinated Pd(IV) intermediate, followed by a reductive elimination of the biaryl product (Scheme 8.16, path A), or through direct product formation via a four-centered transition state (path B).

Having observed how Grignard reagents converted their aliphatic pincer Ni–Br complex **17** to the corresponding Ni–R complex, the group of Zargarian [23] applied **17** as a catalyst for the Kumada coupling reaction (Scheme 8.17). As opposed to its



Scheme 8.16 Proposed mechanism for the Suzuki-Miyaura reaction catalysed by a palladium pincer complex.



Scheme 8.17 Kumada coupling catalysed by a nickel(II) complex.

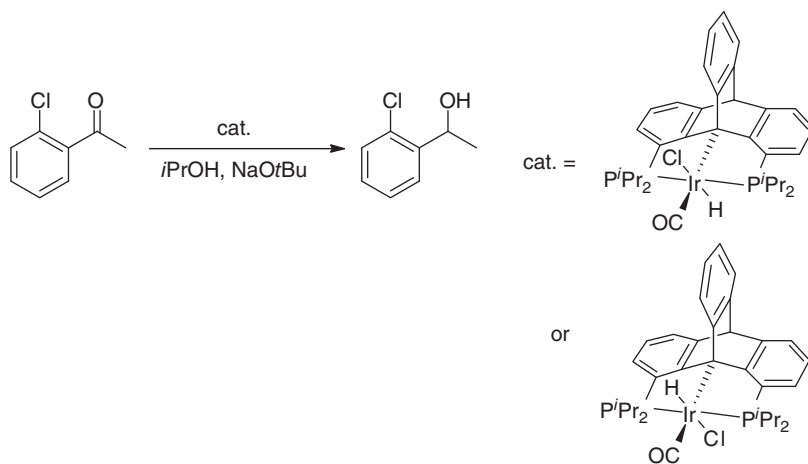
aromatic analog, **17** successfully catalyzed the desired coupling with turnovers up to 84, although minor amounts of the homocoupling product were also observed. A slightly reduced activity was observed when altering the phosphorus substituents for more sterically hindering ^tBu groups. The mechanism was suggested to not involve any Ni⁰ intermediates.

8.4.5

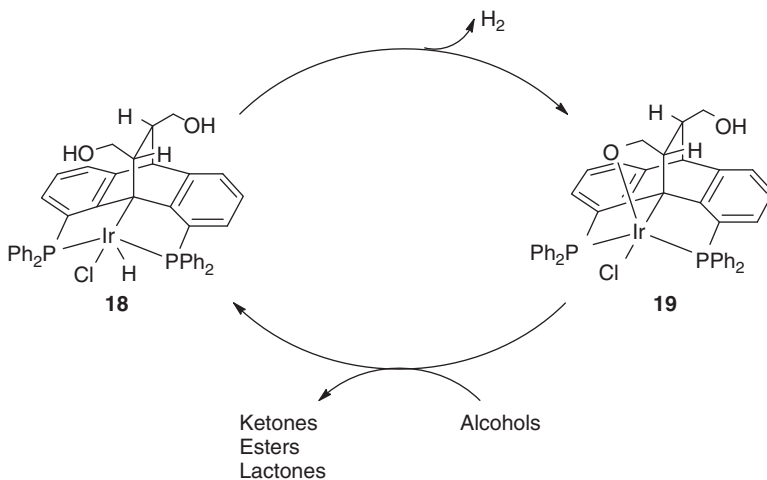
Hydrogenation and Dehydrogenation

The group of Gelman has successfully accomplished the design of a pincer complex based on the dibenzobarrelene framework, which gives an sp³-hybridized coordination without α - or β -hydrogens present and thus a very high robustness [8]. Ir(III) complexes of this type have been successfully applied as catalysts for transfer hydrogenations (Scheme 8.18), reporting full conversion and a turnover frequency (TOF) of 6000 with 0.1% catalyst loading [40].

By introducing functional groups on the dibenzobarrelene scaffold, Gelman and coworkers could isolate complexes with cooperative ligands, as shown in Scheme 8.19. Complex **18** with acidic side arms was found to slowly convert into the ring-closed compound **19** under extrusion of dihydrogen, and, moreover,



Scheme 8.18 Acceptorless dehydrogenation of alcohols catalysed by dibenzobarrelene based iridium complexes.



Scheme 8.19 Proposed mechanism for the reaction in Scheme 8.18.

addition of isopropanol led to the recovery of **18**. Based on this observation, a catalytic cycle was proposed for acceptorless alcohol dehydrogenation with **18**, starting with H_2 release and formation of **19**. Ligand substitution with the substrate then forms an arm-open iridium alkoxide species, followed by product formation and regeneration of **18** through a β -hydride elimination. Catalytic studies confirmed the conversion of secondary alcohols to ketones, and primary alcohols and diols to esters and lactones, respectively. Reported yields of the oxidized products were $\sim 90\%$ within 10 h upon refluxing in *p*-xylene under N_2 in presence of 0.1 mol% **18**. No presence of acid or base was needed, and no activity was observed under the same conditions when using an analogous nonfunctionalized pincer complex [41].

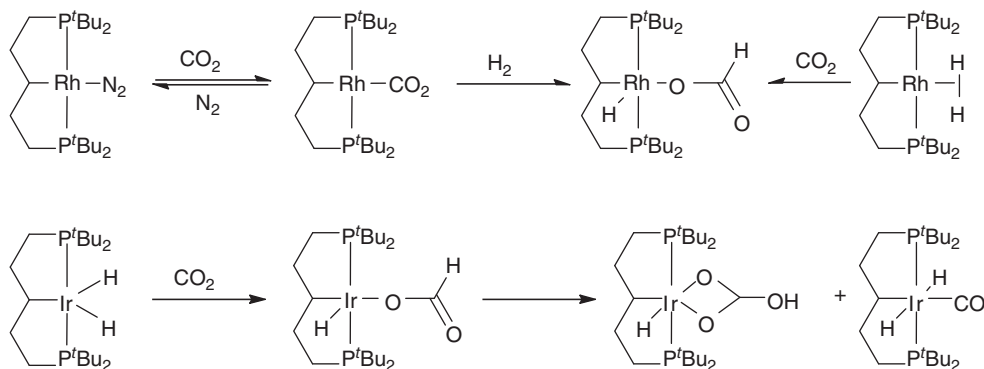
The catalyst **18** has also been immobilized on a silica sol gel and applied in the same acceptorless dehydrogenation reaction, resulting in a slower reaction although with a clear advantage in recyclability and stabilization compared to the nonheterogenized protocol [42].

Dibenzobarrelene-based PC(sp³)P complexes of Pd and Pt have also been reported recently by the same group, although they were found to be only moderately active catalysts for H/D exchange of benzene, indicating a lower potential as catalysts than their Ir analogs [43].

8.4.6

CO₂ Activation

The reduction of CO₂ to a valuable liquid fuel such as methanol is a much wanted reaction and has attracted interest also from the pincer community. An attractive first step of such a transformation is the hydrogenation of CO₂. The group of Milstein [44] has accomplished this with aliphatic Rh(I) complexes, starting from either an η²-dihydrogen complex or the corresponding terminal dinitrogen complex going via an unusual “side-on” bound Rh–CO₂ complex (Scheme 8.20). The analogous iridium formate complex was synthesized by Kaska and coworkers by reacting CO₂ with a Ir(III) dihydride complex. However, in this case, the formate complex proved to be unstable, undergoing disproportionation to form the hydrogen carbonate complex and the carbonyl dihydride, overall corresponding to the reverse water gas shift reaction CO₂ + H₂ → CO + H₂O [45]. Reduction of CO₂ to the methanol level has since been effected using an aromatic nickel pincer complex and a cascade reaction involving a ruthenium pincer complex in one step [46].



Scheme 8.20 Difference in interaction of carbon dioxide and dihydrogen with rhodium and iridium pincer complexes.

References

1. Moulton, C.J. and Shaw, B.L. (1976) *J. Chem. Soc., Dalton Trans.*, 1020.
2. van der Boom, M.E. and Milstein, D. (2003) *Chem. Rev.*, **103**, 1759.

3. Empsall, H.D., Hyde, E.M., Markham, R., McDonald, W.S., Norton, M.C., Shaw, B.L., and Weeks, B. (1977) *J. Chem. Soc., Chem. Commun.*, 589.
4. Albrecht, M. and Lindner, M.M. (2011) *Dalton Trans.*, **40**, 8733.
5. (a) Sjövall, S., Johansson, M.H., and Andersson, C. (2001) *Eur. J. Inorg. Chem.*, 2907. (b) Sjövall, S., Andersson, C., and Wendt, O.F. (2001) *Inorg. Chim. Acta*, **325**, 182. (c) Mayer, H.A. and Kaska, W.C. (1990) *Chem. Ber.*, **123**, 1827. (d) Mayer, H.A., Fawzi, R., and Steimann, M. (1993) *Chem. Ber.*, **126**, 1341. (e) Kuznetsov, V.F., Lough, A.J., and Gusev, D.G. (2006) *Inorg. Chim. Acta*, **359**, 2806.
6. Gozin, M., Weisman, A., Bendavid, Y., and Milstein, D. (1993) *Nature*, **364**, 699.
7. Gerber, R., Blacque, O., and Frech, C.M. (2009) *ChemCatChem*, **1**, 393.
8. (a) Azerraf, C. and Gelman, D. (2008) *Chem. Eur. J.*, **14**, 10364. (b) Azerraf, C. and Gelman, D. (2009) *Organometallics*, **28**, 6578.
9. Nemeš, S., Flesher, R.J., Gierling, K., Maichle-Mossmeyer, C., Mayer, H.A., and Kaska, W.C. (1998) *Organometallics*, **17**, 2003.
10. (a) Hoskins, S.V., Rickard, C.E.F., and Roper, W.R. (1984) *J. Chem. Soc., Chem. Commun.*, 1000. (b) Weng, W., Parkin, S., and Ozerov, O.V. (2006) *Organometallics*, **25**, 5345.
11. Eberhard, M.R., Matsukawa, S., Yamamoto, Y., and Jensen, C.M. (2003) *J. Organomet. Chem.*, **687**, 185.
12. Ozerov, O.V., Guo, C.Y., and Foxman, B.M. (2006) *J. Organomet. Chem.*, **691**, 4802.
13. Pandarus, V. and Zargarian, D. (2007) *Organometallics*, **26**, 4321.
14. (a) Geier, S., Goddard, R., Holle, S., Jolly, P.W., Kruger, C., and Lutz, F. (1997) *Organometallics*, **16**, 1612. (b) Gusev, D.G. and Lough, A.J. (2002) *Organometallics*, **21**, 5091.
15. Errington, R.J., McDonald, W.S., and Shaw, B.L. (1982) *J. Chem. Soc., Dalton Trans.*, 1829.
16. (a) Gusev, D.G. and Lough, A.J. (2002) *Organometallics*, **21**, 2601. (b) Kuznetsov, V.F., Abdur-Rashid, K., Lough, A.J., and Gusev, D.G. (2006) *J. Am. Chem. Soc.*, **128**, 14388.
17. (a) Castonguay, A., Sui-Seng, C., Zargarian, D., and Beauchamp, A.L. (2006) *Organometallics*, **25**, 602. (b) van der Boom, M.E., Liou, S.Y., Shinion, L.J.W., Ben-David, Y., and Milstein, D. (2004) *Inorg. Chim. Acta*, **357**, 4015.
18. Xu, G.Q., Sun, H.J., and Li, X.Y. (2009) *Organometallics*, **28**, 6090.
19. Jonasson, K.J., Ahlsten, N., and Wendt, O.F. (2011) *Inorg. Chim. Acta*, **379**, 76.
20. Crocker, C., Errington, R.J., Markham, R., Moulton, C.J., Odell, K.J., and Shaw, B.L. (1980) *J. Am. Chem. Soc.*, **102**, 4373.
21. Crocker, C., Errington, R.J., McDonald, W.S., Odell, K.J., Shaw, B.L., and Goodfellow, R.J. (1979) *J. Chem. Soc., Chem. Commun.*, 498.
22. Seligson, A.L. and Trogler, W.C. (1993) *Organometallics*, **12**, 738.
23. Castonguay, A., Beauchamp, A.L., and Zargarian, D. (2008) *Organometallics*, **27**, 5723.
24. Sjövall, S., Wendt, O.F., and Andersson, C. (2002) *J. Chem. Soc., Dalton Trans.*, 1396.
25. Olsson, D., Arunachalampillai, A., and Wendt, O.F. (2007) *Dalton Trans.*, 5427.
26. (a) Arunachalampillai, A., Olsson, D., and Wendt, O.F. (2009) *Dalton Trans.*, 8626. (b) Gelman, D. and Musa, S. (2012) *ACS Catal.*, 2456.
27. Vigalok, A., Kraatz, H.B., Konstantinovskiy, L., and Milstein, D. (1997) *Chem. Eur. J.*, **3**, 253.
28. Zhao, J., Goldman, A.S., and Hartwig, J.F. (2005) *Science*, **307**, 1080.
29. Huang, Z., Zhou, J.R., and Hartwig, J.F. (2010) *J. Am. Chem. Soc.*, **132**, 11458.
30. Zhou, J.R. and Hartwig, J.F. (2008) *Angew. Chem. Int. Ed.*, **47**, 5783.
31. Seligson, A.L. and Trogler, W.C. (1993) *Organometallics*, **12**, 744.
32. Castonguay, A., Spasyuk, D.M., Madern, N., Beauchamp, A.L., and Zargarian, D. (2009) *Organometallics*, **28**, 2134.
33. Pandarus, V. and Zargarian, D. (2007) *Chem. Commun.*, 978.
34. Ohff, M., Ohff, A., van der Boom, M.E., and Milstein, D. (1997) *J. Am. Chem. Soc.*, **119**, 11687.
35. Shaw, B.L. (1998) *New J. Chem.*, **22**, 77.

36. (a) Yu, K.Q., Sommer, W., Weck, M., and Jones, C.W. (2004) *J. Catal.*, **226**, 101. (b) Eberhard, M.R. (2004) *Org. Lett.*, **6**, 2125. (c) Similar results were obtained for other C–C coupling reactions: Olsson, D., Nilsson, P., El Masnaouy, M., and Wendt, O.F. (2005) *Dalton Trans.*, 1924. (d) For an excellent review, see: Weck, M. and Jones, C.W. (2007) *Inorg. Chem.*, **46**, 1865.
37. Nilsson, P. and Wendt, O.F. (2005) *J. Organomet. Chem.*, **690**, 4197.
38. Amatore, A. and Jutand, A. (2000) *Acc. Chem. Res.*, **33**, 314.
39. Olsson, D. and Wendt, O.F. (2009) *J. Organomet. Chem.*, **694**, 3112.
40. Levy, R., Azerraf, C., Gelman, D., Rueck-Braun, K., and Kapoor, P.N. (2009) *Catal. Commun.*, **11**, 298.
41. Musa, S., Shaposhnikov, I., Cohen, S., and Gelman, D. (2011) *Angew. Chem. Int. Ed.*, **50**, 3533.
42. Oded, K., Musa, S., Gelman, D., and Blum, J. (2012) *Catal. Commun.*, **20**, 68.
43. Musa, S., Shpruhman, A., and Gelman, D. (2012) *J. Organomet. Chem.*, **699**, 92.
44. Vigalok, A., Ben-David, Y., and Milstein, D. (1996) *Organometallics*, **15**, 1839.
45. McLouglin, M.A., Keder, N.L., Harrison, W.T.A., Flesher, R.J., Mayer, H.A., and Kaska, W.C. (1999) *Inorg. Chem.*, **38**, 3223.
46. (a) Chakraborty, S., Zhang, J., Krause, J.A., and Guan, H. (2010) *J. Am. Chem. Soc.*, **132**, 8872. (b) Huff, C.A. and Sanford, M.S. (2011) *J. Am. Chem. Soc.*, **133**, 18122.

9

Heavier Group 14 Elements-Based Pincer Complexes in Catalytic Synthetic Transformations of Unsaturated Hydrocarbons

Jun Takaya and Nobuharu Iwasawa

9.1

Introduction

Transition metal complexes with LXL-type pincer ligands (L, neutral ligand; X, anionic ligand) have been widely utilized as versatile catalysts in synthetic organic chemistry [1–6]. Among numerous types of pincer complexes, synthesis and reaction of anionic carbon and nitrogen-based systems such as PCP- and PNP-complexes have been extensively studied. These pincer complexes generally have high thermal stability due to the rigid tridentate structure and show unique reactivity induced by the anionic X ligand. Fine-tuning of electronic and steric environments is also possible by manipulation of substituents, rendering these complexes highly attractive in developing new catalytic synthetic reactions.

On the contrary, little attention has been paid to the utilization of silicon-based pincer complexes in synthetic chemistry although the basic organometallic chemistry on silicon–metal bonds has been studied extensively as the key reactive element of hydrosilylation [7]. Stobart [8, 9] reported the synthesis of metal complexes with PSiP-pincer ligands, some of which were employed as catalysts for the hydroformylation reaction. Tilley [10] developed an NSiN-type pincer ligand and demonstrated that its iridium complex catalyzed dehydrogenative silylation of arenes. In view of the unique character of silicon as an anionic donor ligand, further utilization of silicon-based pincer complexes is highly desirable in developing innovative synthetic reactions.

In 2007, synthesis and complexation of a PSiP-pincer ligand, in which a silicon atom and two phosphorus atoms are tethered by a phenylene group, was first reported by Turculet and coworkers [11–19]. They reported that the PSiP-ruthenium complex exhibited catalytic activity for transfer hydrogenation of ketones [11], and the PSiP-platinum and -palladium complexes efficiently catalyzed reduction of CO₂ to methane by silanes [18]. Shortly after the Turculet's first report in 2007, we reported the first example of utilization of the phenylene-bridged PSiP-pincer complex in carbon–carbon bond formation reactions of unsaturated hydrocarbons [20].

In this chapter, we describe several synthetic transformations of unsaturated hydrocarbons catalyzed by palladium complexes bearing the phenylene-bridged

PSiP-pincer ligands and their analogs developed in our laboratory [20–27]. The unique structural and electronic nature of the PSiP-ligands enables these catalytic reactions to proceed through the generation and reaction of palladium hydride species as a key intermediate. Some mechanistic aspects of the reactions are also described based on the synthesis and reaction of η^2 -(Si–H)Pd(0) complex as an equivalent to the palladium hydride species [28–33].

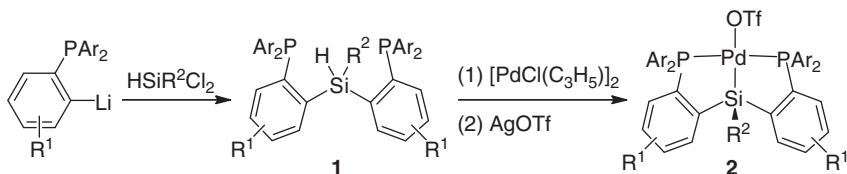
9.2

Synthesis of Palladium Complexes Bearing PXP-Pincer Ligands (X = Si, Ge, Sn)

9.2.1

Synthesis

A variety of palladium complexes **2** bearing PSiP-pincer ligands can be synthesized by the complexation of $[\text{PdCl}(\text{C}_3\text{H}_5)]_2$ with silanes **1** (Scheme 9.1) [23, 27]. Introduction of various substituents on the diarylphosphine, silicon, and phenylene linker moieties enables fine-tuning of electronic and steric nature of the complexes (Figure 9.1). Moreover, replacement of the central silicon atom by germanium and tin was also possible with modified procedures to afford PGeP- and PSnP-pincer complexes **3** and **4** [25].



Scheme 9.1 General procedure for the synthesis of PSiP-palladium complexes.

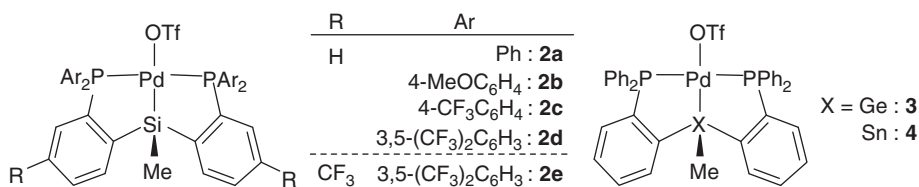
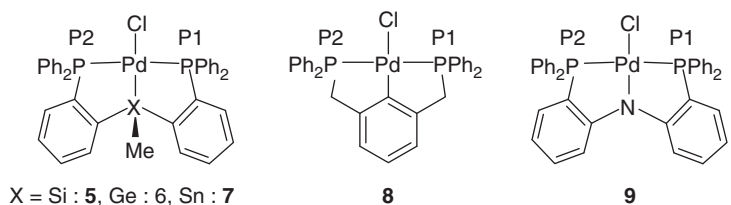


Figure 9.1 PSiP-, PGeP-, and PSnP-pincer palladium complexes.

9.2.2

Structural Analyses

X-ray analyses were performed for palladium chloride complexes **5–7** with PSiP-, PGeP-, and PSnP-ligands [25]. The characteristic features of these complexes are observed in the Pd–Cl length and dihedral angle of P1–Pd–X–P2 (θ), which are

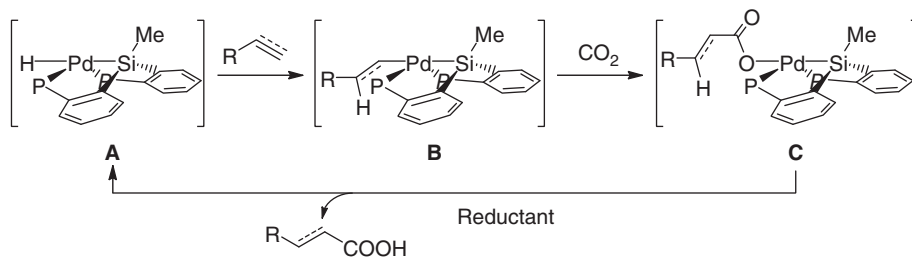
Table 9.1 Structural analyses of PXP-pincer palladium complexes.

X		Pd–Cl (Å)	P1–Pd–X–P2 (°)
Si	5	2.4414(17)	157.2
Ge	6	2.4219(11)	157.5
Sn	7	2.4270(8)	158.1
C	8	2.367(3)	177.9
N	9	2.313(5)	180.0

listed in Table 9.1 and compared with those of common PCP- and PNP-palladium complexes **8** and **9** [34, 35]. Heavier group 14 element-based pincer complexes, especially the PSiP-complex **5**, exhibit longer Pd–Cl bond length compared with **8** and **9**, demonstrating the strong trans influence of Si to enhance the reactivity of the trans substituent [36]. Moreover, it should be noted that the dihedral angles θ of PSiP-, PGeP-, and PSnP-complexes are around 158° whereas those of **8** and **9** are almost 180° , showing that the geometry of **5–7** is distorted square planar where phosphine atoms bended from 180° .

9.3 Hydrocarboxylation

Development of transition metal-catalyzed CO_2 -fixation reactions using easily available unsaturated hydrocarbons as starting material is highly desirable as a practical method for the synthesis of carboxylic acids [37–40]. However, such catalytic reactions have mostly been limited to those based on Ni(0)-promoted oxidative cyclization of rather specific substrates such as α,ω -diynes and bis(1,3-diene)s [41]. We designed PSiP-palladium hydride **A**, which we expected to catalyze hydrocarboxylation reaction of unsaturated hydrocarbons with CO_2 (Scheme 9.2). Hydrometallation of unsaturated hydrocarbons by **A** would generate new metal complexes **B** bearing a carbon–palladium bond. Nucleophilic addition of **B** to CO_2 affords palladium carboxylate complexes **C**, which could be reconverted to the palladium hydride **A** by an appropriate stoichiometric reductant. We envisioned several advantages of utilizing the PSiP-palladium as a catalyst as follows (Figure 9.2): (i) Nucleophilic carboxylation would be enhanced as a result of the strong electron-donating nature and trans influence of the silicon atom. (ii) The



Scheme 9.2 Hydrocarboxylation of unsaturated hydrocarbons.

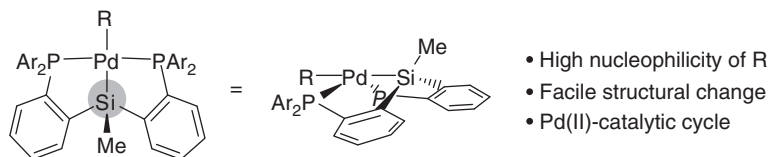


Figure 9.2 Expected features of the phenylene-bridged PSiP-palladium.

strained square planar structure of the PSiP-linkage would facilitate structural change to a trigonal bipyramidal geometry, which might allow coordination of CO_2 for facile carboxylation. (iii) The pincer structure would enable a catalytic cycle based on Pd(II) without liberation of Pd(0), which causes side reactions through oxidative cyclization of unsaturated hydrocarbons.

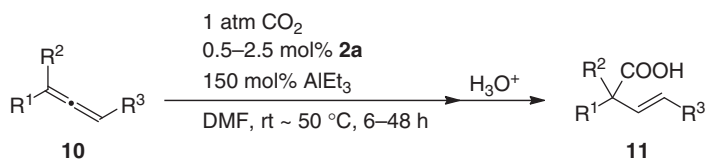
9.3.1

Hydrocarboxylation of Allenes

PSiP-pincer palladium complex **2a** was found to catalyze the hydrocarboxylation of allenes by using AlEt_3 as a stoichiometric reductant under atmospheric pressure of CO_2 (Table 9.2) [20]. The reaction proceeded regioselectively to give α -substituted β,γ -unsaturated carboxylic acids **11** in high yield. A variety of functional groups such as alkene, ether, ester, ketone, ketal, and carbamate are tolerated under the reaction conditions, demonstrating high synthetic utility of this reaction as a practical method for carboxylic acid synthesis. The reaction is thought to start with generation of the palladium hydride complex **13** bearing a PSiP-pincer ligand through transmetalation of AlEt_3 to **2a** followed by β -hydride elimination (Scheme 9.3). Hydrometallation of allenes forms σ -allylpalladium complexes **14**, which undergo nucleophilic addition to CO_2 at the γ -position to yield palladium carboxylates **15** regioselectively. Transmetalation of **15** with AlEt_3 regenerates the palladium hydride complex **13** accompanied by the release of the hydrocarboxylation products as Al-carboxylates **16**.

By NMR analyses, prenylpalladium complex **17**, derived from palladium chloride **5** and prenylmagnesium chloride *in situ*, was confirmed to take a σ -allyl form with the C–Pd bond at the less substituted carbon atom (Scheme 9.4) [21]. This result strongly supports the proposed structure of **14** and its carboxylation at γ -position.

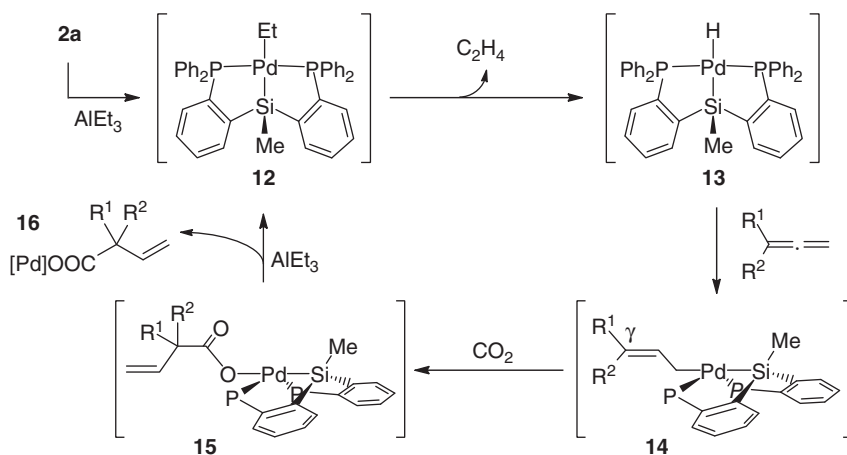
Table 9.2 Hydrocarboxylation of allenes.



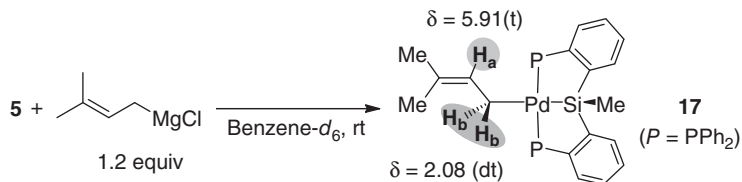
Entry	Product	R or X		Yield (%)
1		-CH ₂ OSi ^t BuPh ₂	11a	94
2		-CH ₂ OBz	11b	Quantitative
3		-CH=CMe ₂	11c	85
4		NBoc	11d	75
5		C=O	11e	63
6		C(CH ₂ O) ₂	11f	89
7		-H	11g	65 ^{a,b}
8		-CH ₂ CH ₂ Ph	11h	51 ^{a,b}

^aUsing ZnEt₂ instead of AlEt₃.

^bIsolated after Me-esterification.



Scheme 9.3 Proposed mechanism.



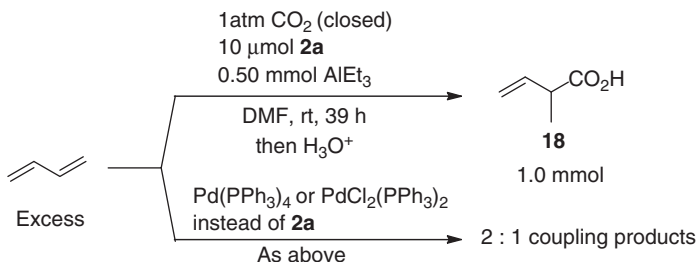
Scheme 9.4 Structure of PSiP-prenylpalladium complex.

The anionic, tridentate pincer structure suppresses the formation of an electrophilic π -allylpalladium intermediate as established by Prof. Szabó [42] in the PCP-pincer system. It is assumed that the nucleophilicity of the σ -allylpalladium is further enhanced by strong trans influence and electron-donating nature of the Si atom, realizing a facile nucleophilic addition to less reactive CO_2 .

9.3.2

Hydrocarboxylation of 1,3-Dienes

The hydrocarboxylation reaction of allenes can be extended to 1,3-dienes as substrate, some of which are abundant, easily available chemical feedstock in industrial chemistry (Scheme 9.5) [24]. For example, 1,3-butadiene reacted with 1 atm CO_2 and $AlEt_3$ in the presence of a catalytic amount of **2a** to give 2-methyl-3-butenoic acid **18** in high yield (200% based on Al). Interestingly, comparative experiments using $Pd(PPh_3)_4$ or $PdCl_2(PPh_3)_2$ as a catalyst instead of **2a** gave a mixture of 2 : 1 coupling products of 1,3-butadiene and CO_2 . This result indicates the importance of the PSiP-pincer ligand in suppressing the generation of $Pd(0)$ species that promote oxidative coupling of two molecules of 1,3-butadiene leading to 2 : 1 coupling products [37].



Scheme 9.5 Hydrocarboxylation of 1,3-butadiene catalyzed by PSiP-palladium complex.

Various substituted dienes such as isoprene, piperylene, 1,3-cyclohexadiene, and 3-methyl-1,3-pentadiene were employable as substrates to give corresponding β,γ -unsaturated carboxylic acids **19–22** with high turnover number (TON) (up to 506) (Table 9.3). This reaction also showed good compatibility with various functional groups as seen in the reaction of allenes. It should be noted that the reaction of dienamide **23** afforded α -amino acid derivative **24** selectively, demonstrating promising utility as an efficient protocol for α -amino acid synthesis using CO_2 .

Table 9.3 Generality of 1,3-dienes.

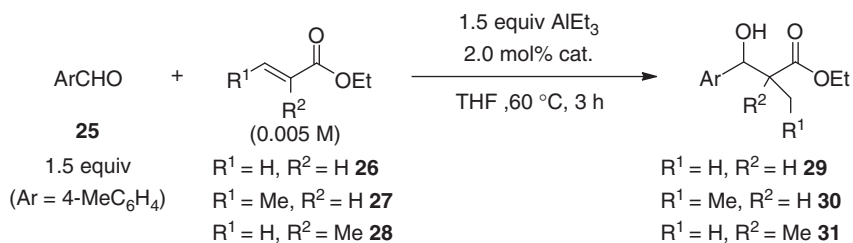
Entry	1,3-Diene	Product
1 ^a		19 1.22 mmol TON = 245
2 ^a	 (<i>E</i> : <i>Z</i> = 67:33)	20 2.53 mmol TON = 506 (<i>E</i> : <i>Z</i> = 93:7)
3 ^a		21 1.98 mmol TON = 396
4 ^a	 (<i>E</i> : <i>Z</i> = 70:30)	22 1.51 mmol TON = 302 (<i>E</i> : <i>Z</i> = 67:33)
5 ^b		24 81%

^a20 mmol 1,3-diene, 5.0 mmol AlEt₃, 5 μmol **2a**, 1 atm CO₂ in DMF at rt or 40 °C.

^b1.05 equiv AlEt₂(OEt), 2.5 mol% **2a**, 1 atm CO₂ in THF at 40 °C.

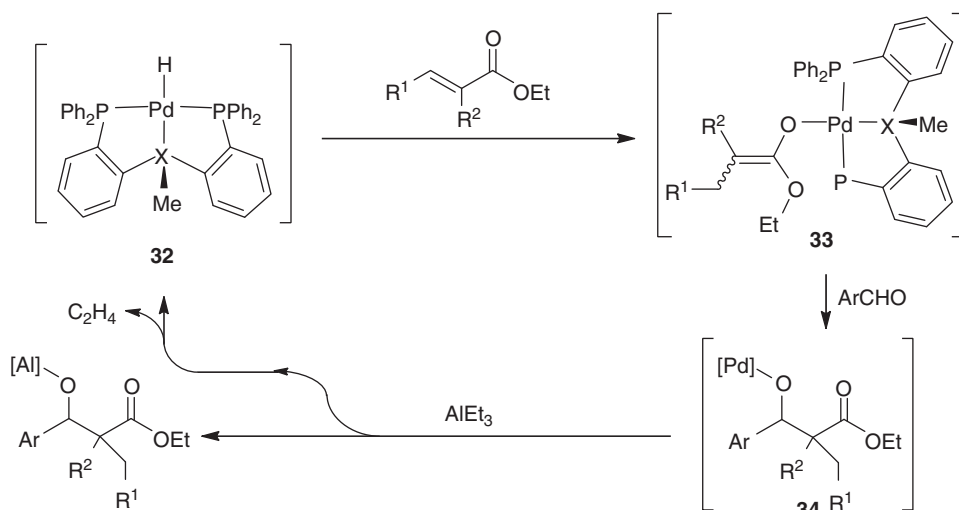
9.4 Reductive Aldol Type Reaction

The combination of group 14 element-based pincer palladium catalysts and AlEt₃ as a stoichiometric reductant was proven to be effective for a catalytic reductive aldol-type reaction [25]. Not only P*Si*P-palladium **2a**, but also its heavier analogs P*Ge*P- and P*Sn*P-complexes efficiently catalyzed the reaction. Thus, treatment of *p*-tolualdehyde **25**, α,β-unsaturated esters **26–28**, and 1.5 equiv of AlEt₃ in the presence of 2.0 mol% of palladium complexes **2a**, **3**, **4** afforded β-hydroxyesters **29–31** in good to high yield (Table 9.4). It should be noted that the P*Sn*P-complex **4** showed the highest activity for all reactions regardless of the substitution pattern of α,β-unsaturated esters. This is the first example of utilization of Ge- or Sn-containing multidentate ligands for a catalytic synthetic reaction. The reaction is proposed to proceed through hydrometallation of α,β-unsaturated esters to generate palladium enolates **33** followed by nucleophilic addition to aldehydes (Scheme 9.6). Transmetalation of the resulting alkoxy-palladiums **34** with AlEt₃ followed by β-hydride elimination regenerates palladium hydride **32**. The wider coordination sphere around the palladium of the P*Sn*P-complex may facilitate hydrometallation and/or nucleophilic addition steps more efficiently. These results demonstrate

Table 9.4 PXP-palladium-catalyzed reductive aldol reaction.

Entry	Catalyst	X	Substrate	Product	Yield (%) ^a
1	2a	Si	26	29	86
2	3	Ge	26	29	49
3	4	Sn	26	29	82
4	2a	Si	27	30	94
5	3	Ge	27	30	54
6	4	Sn	27	30	95
7	2a	Si	28	31	52
8	3	Ge	28	31	47
9	4	Sn	28	31	93

^adr = 65 : 35 ~ 72 : 28 for product 29 and 30.

**Scheme 9.6** Proposed mechanism.

promising utility of Ge- and Sn-based pincer complexes for developing catalytic synthetic reactions.

9.5

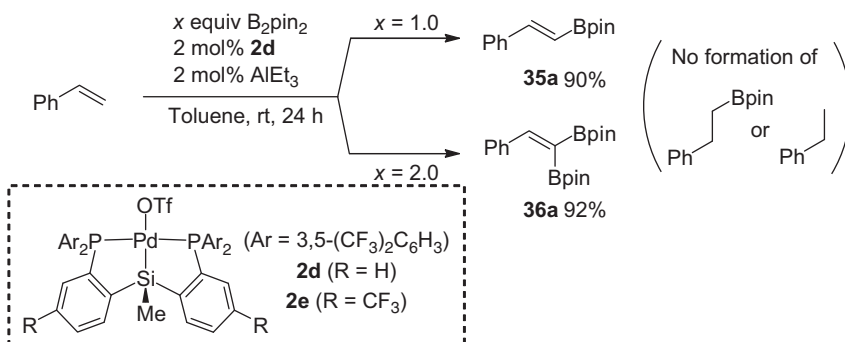
Dehydrogenative Borylation

Dehydrogenative borylation of alkenes proceeds through insertion of alkenes into the M–B bond of borylmetal complexes followed by β -hydride elimination [43]. This reaction is a formal direct borylation reaction of olefinic C–H bonds with diboron or borane, providing the most straightforward method for the preparation of synthetically useful alkenylboronic esters. However, most of previous reports require excess alkenes because sacrificial hydroboration and/or hydrogenation of alkenes are inevitable problems, and the substrate scope is rather limited. These side-reactions are caused by coordinatively unsaturated hydrido(boryl)- or dihydridometal species generated from the metal catalysts and boranes or dihydrogen produced during the reaction. Thus, the development of a new type of dehydrogenative borylation reaction unaccompanied by such side reactions is highly desirable for an efficient and general synthesis of alkenylboronic esters [44, 45].

9.5.1

Dehydrogenative Borylation of Alkenes and 1,3-Dienes

An efficient, stereoselective synthesis of (*E*)- β -styrylboronic ester **35a** was achieved by treatment of a 1 : 1 mixture of styrene and B_2pin_2 with a catalytic amount of $AlEt_3$ and the PSiP-palladium complex **2d** bearing 3,5-(CF_3) $_2C_6H_3$ groups on phosphorus atoms in toluene at room temperature (Scheme 9.7) [23, 27]. Catalytic activity is highly dependent on the electronic nature of palladium complexes and greatly increases as the PSiP-ligand becomes more electron-deficient (**2d** > **2c** > **2a** > **2b**). Moreover, it was discovered that the same reaction with 2 equiv of B_2pin_2 enabled double borylation at the alkene terminus to give β,β -diborylstyrene **36a** selectively in high yield. These results indicate that this reaction enables the selective synthesis

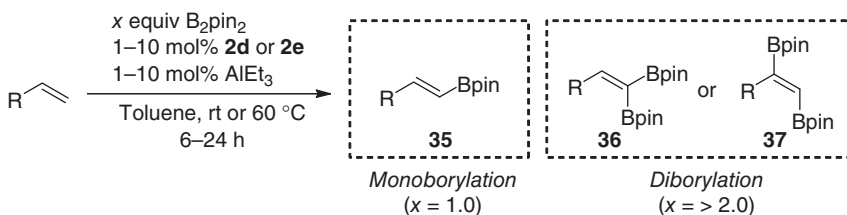


Scheme 9.7 Dehydrogenative borylation of styrene catalyzed by PSiP-palladium complex.

of mono- or diborylalkenes simply by changing the amount of B_2pin_2 . It should be noted that analysis of the crude mixture by GC–MS showed formation of HBpin, but neither hydroboration nor hydrogenation products were observed at all in contrast to the previously reported dehydrogenative borylation reactions.

These protocols for selective synthesis of mono- and 1,1-diborylalkenes were applicable to various alkenes by using **2d** or more active, electron-deficient PSiP-palladium **2e** as catalysts (Table 9.5). Vinylferrocene, *N*-vinylphthalimide, and 1,3-dienes selectively afforded 1,1-diborylalkenes **36b–d** in high yield by the use of 2–3 equiv of B_2pin (entries 1–3). Interestingly, another mode of diborylation, *trans*-1,2-diborylation, was found to proceed to give (*Z*)-1,2-diborylalkenes **37**

Table 9.5 Selective monoborylation/diborylation.



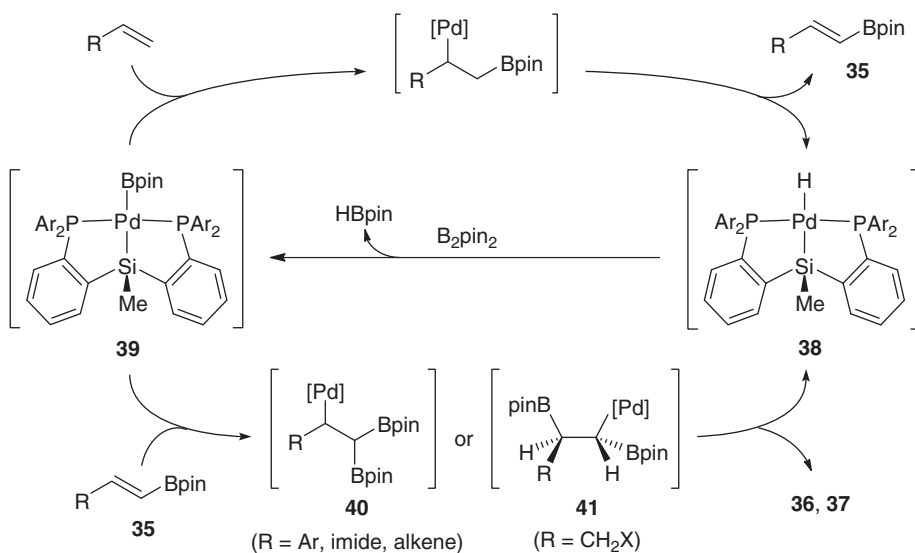
Entry	R	Monoborylation ($x = 1.0$) Yield (<i>E</i> : <i>Z</i>)	Diborylation ($x \geq 2.0$) Yield (<i>E</i> : <i>Z</i>)
1		35b 93% (<i>E</i> only)	36b 92% —
2		35c 91% (<i>E</i> only)	36c 86% —
3		35d 98% (87:13)	36d 98% —
4	$n-C_6H_{13}-$	35e 85% (93:7)	— 37e 63% (19:81)
5		35f 62% (88:12)	— 37f 68% (11:89)
6		35g 53% (92:8)	— 37g 48% (9:91)
7		35h 87% (86:14)	— 37h 59% (<i>Z</i> only)

selectively when sterically less demanding, non-electronically activated terminal alkenes were employed as substrates (entries 4–7). Not only simple alkenes but also alkenes having functional groups such as silyl ether, chloro, and acid anhydride were employable as substrates, giving synthetically useful functionalized (*Z*)-1,2-diborylalkenes **37e–h** in good yield. Selective synthesis of monoborylalkenes **35** from these substrates was also achieved with good (*E*)-selectivity under monoborylation conditions using 1 equiv of B_2pin_2 . These are the first examples of a general, direct synthesis of 1,1- and *trans*-1,2-diborylalkenes from alkenes, which are not easily accessible by the previous diboration protocols [44, 46, 47]. Moreover, a selective route to synthetically useful diboryl- and monoborylalkenes would find abundant use in organic synthesis.

9.5.2

Mechanistic Considerations

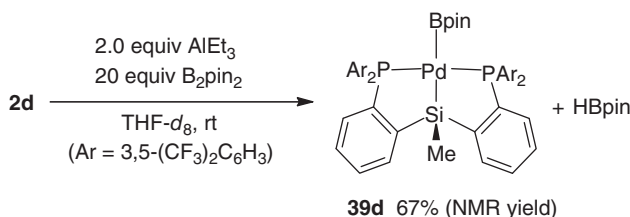
In view of the formation of HBpin during the reaction, it is assumed that the reaction starts with the generation of palladium hydride complex **38** via transmetalation of **2** with $AlEt_3$ followed by β -hydride elimination, and the palladium hydride complex **38** further reacts with B_2pin_2 to give a borylpalladium complex **39** and HBpin (Scheme 9.8). The borylpalladium **39** undergoes insertion of alkenes followed by β -hydride elimination, affording (*E*)-alkenylboronic esters **35** preferentially with regeneration of the palladium hydride **38**. Second borylation of **35** in the presence of excess B_2pin_2 proceeds regioselectively to avoid steric repulsion between Bpin on the palladium and substituents on the alkenes, leading to the 1,1- or 1,2-diborylation products **36** or **37**. The predominant *trans*-selectivity



Scheme 9.8 Proposed mechanism.

in 1,2-diborylation is reasonably explained by considering the syn-insertion/syn-elimination mechanism via alkylpalladium(II) intermediates **41**.

In support of this mechanism, it was found that treatment of palladium triflate **2d** with AlEt_3 in the presence of excess B_2pin_2 afforded a borylpalladium complex **39d** along with the generation of HBpin (Scheme 9.9). X-ray analysis of analogous compound **39a** ($\text{Ar} = \text{Ph}$) disclosed that the Pd–B distance is 2.11 Å, which is longer than those of previously reported borylpalladium complexes (1.97–2.08 Å for Pd– BX_2 ($\text{X} = \text{O}, \text{N}$)) due to the strong trans influence of Si (Figure 9.3) [48–51]. Thus, the PSiP-borylpalladium showed high reactivity for borylpalladation to enable the second dehydrogenative borylation.



Scheme 9.9 Formation of PSiP-borylpalladium complex.

Investigation of the reactivity of these borylpalladium complexes demonstrated that the electron-deficient borylpalladium **39d** ($\text{Ar} = 3,5\text{-(CF}_3)_2\text{C}_6\text{H}_3$) smoothly reacted with (*E*)- β -methylstyrene to give (*Z*)- β -boryl- β -methylstyrene **42** quantitatively whereas normal **39a** ($\text{Ar} = \text{Ph}$) caused no reaction (Scheme 9.10) [27]. Thus, electron-withdrawing nature of the PSiP-ligand clearly accelerates the borylpalladation step, leading to high catalytic activity of **39d**. Additionally, the stereospecific formation of (*Z*)-alkenylboronic ester **42** from (*E*)- β -methylstyrene supports the proposed mechanism for borylation of alkenes via syn-insertion/syn-elimination.

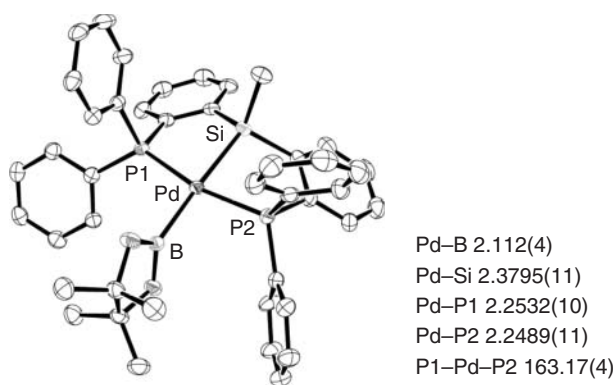
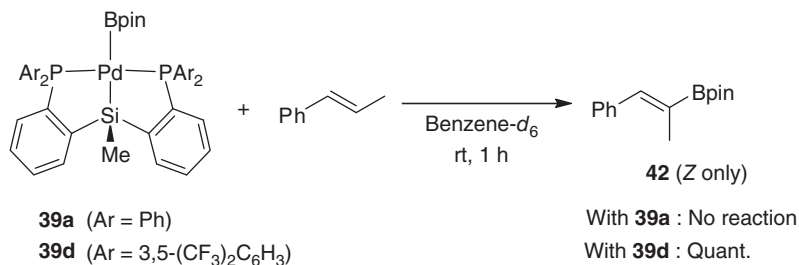


Figure 9.3 Oak ridge thermal ellipsoid plot (ORTEP) diagram of **39a** ($\text{Ar} = \text{Ph}$) at the 50% probability level.



Scheme 9.10 Electronic effect of phosphine ligands.

As described in the beginning of this section, sacrificial hydroboration and hydrogenation of alkenes have often been a problem in previous dehydrogenative borylation reactions. On the contrary, this new catalytic cycle consists of monohydrido- and monoborylpalladium(II) complexes (**38** and **39**) and does not generate hydrido(boryl)- or dihydridometal species because of the characteristics of the anionic tridentate pincer ligand. The PSiP-pincer ligand also enhances the reactivity of the B–Pd bond of the borylpalladium complex. These features have enabled an efficient reaction without using excess alkenes, leading to successful development of the double dehydrogenative borylation.

9.6

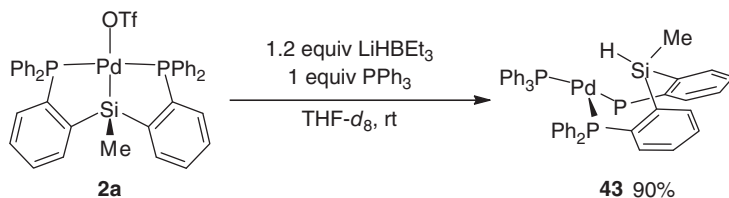
Synthesis and Reaction of η^2 -(Si-H)Pd(0) Complex as an Equivalent to PSiP-Palladium Hydride Complexes

The palladium hydride species bearing PSiP-pincer ligands are the common, key intermediates in all reactions described so far. Synthesis, structural analyses, and investigation of reactivity of the PSiP-palladium hydride complexes have been highly desired to elucidate these reaction mechanisms. During such investigations, we discovered that a silane-coordinated palladium(0) complex could be obtained unexpectedly, which worked as a synthetic equivalent to the palladium hydride complex. Detailed investigations on the reactivity of the η^2 -(Si-H)Pd(0) complex disclosed novel aspects of the PSiP-palladium complexes and provided useful mechanistic insights into the catalytic reactions.

9.6.1

Synthesis and Structure of η^2 -(Si-H)Pd(0)

Reduction of **2a** by LiBEt₃H in the presence of PPh₃ afforded η^2 -(Si-H)Pd(0) complex **43** bearing a Si–H σ -bond coordinated to Pd(0) although the same reaction without PPh₃ resulted in some decomposition reactions probably via palladium hydride (Scheme 9.11) [21, 22]. X-ray and NMR analyses disclosed that the η^2 -(Si-H)Pd(0) structure is retained both in solid and solution (Figure 9.4). The Si–H, Pd–H, and Pd–Si distances are 1.60(3), 1.67(3), and 2.4283(8) Å, respectively.



Scheme 9.11 Formation of η^2 -(Si-H)Pd(0) complex.

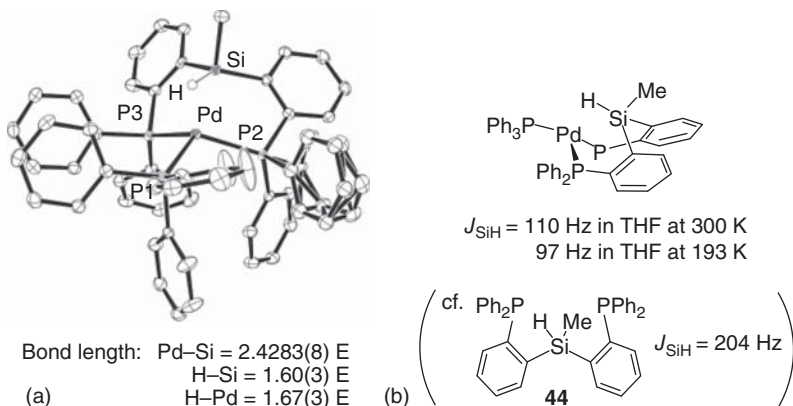


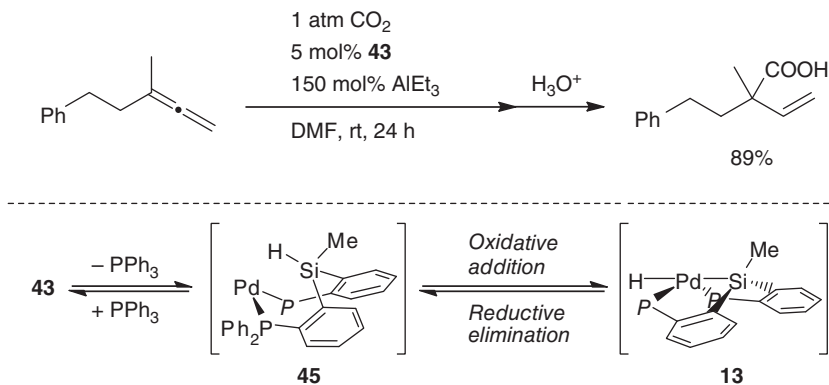
Figure 9.4 Oak ridge thermal ellipsoid plot (ORTEP) diagram of **43** at the 50% probability level.

The $^1J_{\text{HSi}}$ coupling constant is observed to be 110 Hz by non ^1H -decoupled ^{29}Si NMR in tetrahydrofuran (THF) at room temperature, which is much larger than typical values found for H-M-Si complexes ($< \sim 20$ Hz) but significantly smaller than that of silane **44** itself ($J_{\text{HSi}} = 204$ Hz), supporting weakening of the Si-H bond by η^2 -(Si-H) coordination to the metal [52–54]. Silane-coordinated complexes can be regarded as a frozen intermediate of oxidative addition of the Si-H bond and are usually difficult to isolate especially in the Ni triad [55, 56]. Therefore, this is quite a rare example of the synthesis, isolation, and structural analyses of a mononuclear silane-coordinated palladium(0) complex. Formation of η^2 -(Si-H)Pt(0) and Pd(0) complexes without monophosphine ligand was reported by Turculet [13, 18] with the P*Si*P-pincer ligand having cyclohexyl groups on phosphorus atoms although no fine X-ray structures were provided.

9.6.2

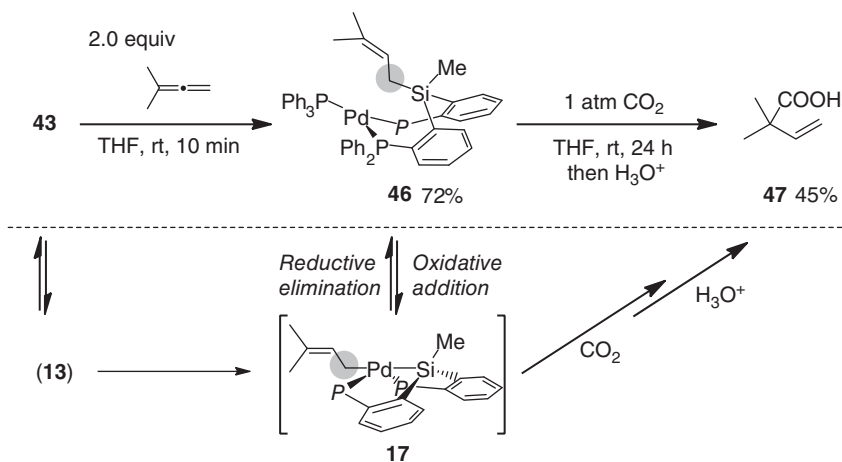
Reaction of η^2 -(Si-H)Pd(0) Complex with an Allene

The η^2 -(Si-H)Pd(0) **43** was found to catalyze the hydrocarboxylation reaction of allenes, indicating that **43** worked as the palladium hydride complex **13** in solution via reversible oxidative addition/reductive elimination of the Si-H bond after dissociation of PPh_3 (Scheme 9.12) [21]. This result prompted us to investigate a



Scheme 9.12 Fluxional behavior of Si-H bond with palladium.

stoichiometric reaction of **43** with 3-methyl-1,2-butadiene expecting the formation of prenylpalladium intermediate **17**. However, to our great surprise, the reaction afforded trisphosphine-palladium(0) complex **46** bearing a prenyl substituent on the silicon atom in good yield (Scheme 9.13). Furthermore, when a THF solution of **46** was allowed to stand under atmospheric pressure of CO₂ at room temperature, the hydrocarboxylation product **47** was obtained after acidic hydrolysis. Thus, not only the Si-H bond in **43** but also the Si-C(sp³) bond in **46** undergoes reversible oxidative addition/reductive elimination with palladium at room temperature. Related reversible cleavage and formation of Me-Si bond on Ni was also reported by Turculet and coworkers [15]. These results demonstrate the unusual “flexibility” of this PSiP-pincer ligand that enables facile oxidative addition/reductive elimination of trans substituents whereas common PCP-pincer complexes rarely cause such reversible reactions.

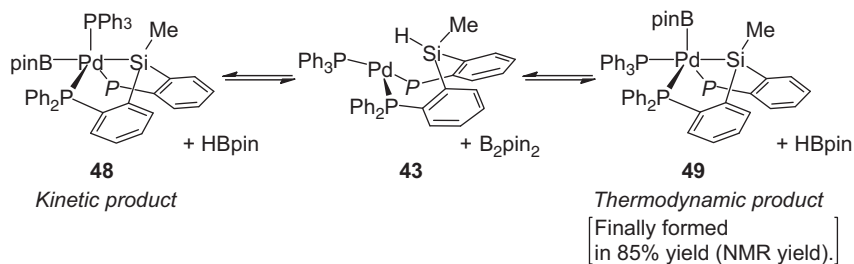


Scheme 9.13 Fluxional behavior of sp³C-Si bond with palladium.

9.6.3

Reaction of $\eta^2\text{-(Si-H)Pd(0)}$ Complex with Diboron

During investigations on the reaction of $\eta^2\text{-(Si-H)Pd(0)}$ complexes with B_2pin_2 , it was discovered that the reaction of $\eta^2\text{-(Si-H)Pd(0)}$ complex **43** with B_2pin_2 initially gave a trans five-coordinate borylpalladium complex **48** as a kinetic product and finally afforded its stereoisomer, cis five-coordinate borylpalladium complex **49**, as the thermodynamically most stable product (Scheme 9.14) [26]. The structures of these complexes were elucidated by X-ray and NMR analyses (Figure 9.5). Detailed mechanistic studies by several experiments and density functional theory (DFT) calculations suggested that coordinatively unsaturated $\eta^2\text{-(Si-H)Pd(0)}$ complex **45** undergoes a new reversible σ -bond metathesis reaction between H–Pd bond and B–B bond via transition state **50** to give square planar borylpalladium **39a**, which is converted to the trans five-coordinate borylpalladium **48** by coordination of PPh_3 (Scheme 9.15). The formation of **39a** is reversible to regenerate **45**. Oxidative addition of the Si–H bond of **45** proceeds via transition state **51** to afford palladium hydride complex **13** as proposed before, which undergoes another σ -bond metathesis leading to the formation of *cis*-**49**. These results provide a



Scheme 9.14 Selective formation of two stereoisomeric five-coordinate borylpalladium complexes.

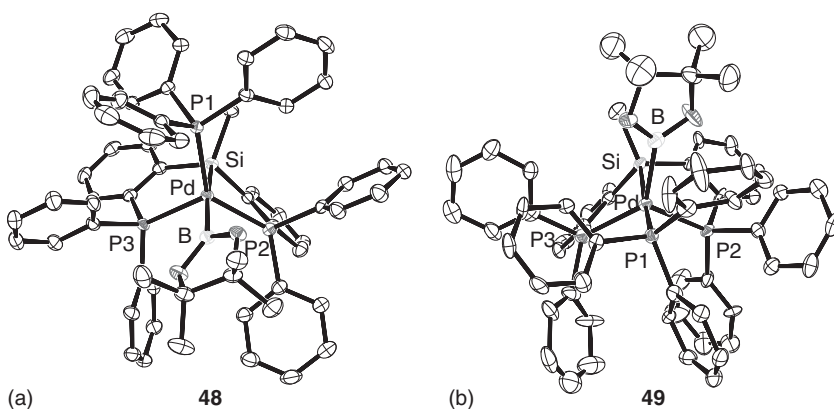
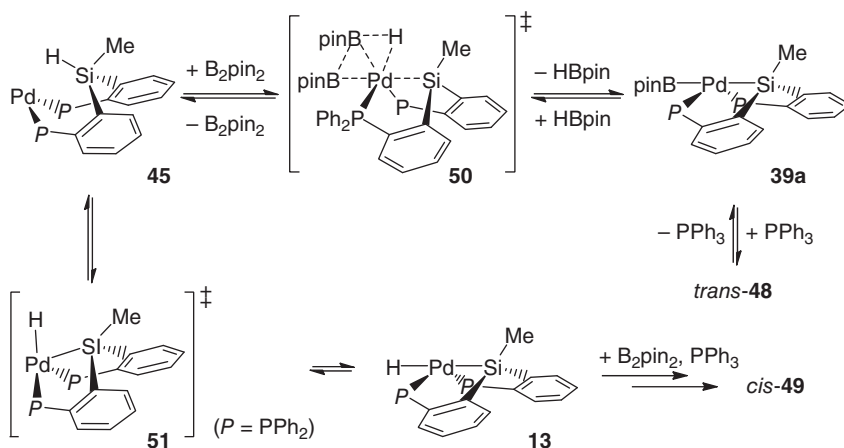


Figure 9.5 ORTEP diagram of (a) **48** and (b) **49**.



Scheme 9.15 Proposed mechanism.

useful mechanistic insight into the formation of the borylpalladium complex in the catalytic dehydrogenative borylation of alkenes and also demonstrate novel reactivity of silane-coordinated palladium(0) complexes via σ -bond metathesis.

We believe that realization of these unique reactions is attributed to the structural features of the phenylene-bridged PSiP-pincer ligand, which enables facile structural change to trigonal bipyramidal-like geometry around palladium as seen in **50** and **51** because of its strain in square planar geometry. It is conceivable that such structural effect would facilitate interaction and reaction of the metal catalyst with other substrates, leading to the development of new types of transformations.

9.7

Conclusions

We have developed new synthetic reactions catalyzed by phenylene-bridged PSiP-palladium complexes and their analogs. The hydrocarboxylation reaction of allenes and 1,3-dienes with CO_2 provides an efficient method for the synthesis of synthetically useful β,γ -unsaturated carboxylic acids. Dehydrogenative borylation of alkenes with B_2pin_2 enables an expedient synthesis of mono- and diborylalkenes simply by changing the amount of B_2pin_2 . Both reactions are highly efficient transformations of unsaturated hydrocarbons to synthetically valuable compounds realized by utilizing the electronic and structural features of the PSiP-pincer ligands. Furthermore, unique organometallic reactions are also discovered, providing deeper mechanistic insights into reaction mechanisms. These results open up a new possibility of rational design of catalytic synthetic reactions based on characteristic properties of the phenylene-bridged PSiP-pincer ligands.

References

- Albrecht, M. and Kotten, G. (2001) *Angew. Chem. Int. Ed.*, **40**, 3750–3781.
- Singleton, J.T. (2003) *Tetrahedron*, **59**, 1837–1857.
- Boom, M.E. and Milstein, D. (2003) *Chem. Rev.*, **103**, 1759–1792.
- Selander, N. and Szabó, K.J. (2010) *Chem. Rev.*, **111**, 2048–2076.
- Choi, J., MacArthur, A.H.R., Brookhart, M., and Goldman, A.S. (2011) *Chem. Rev.*, **111**, 1761–1779.
- Morales-Morales, D. and Jensen, C.M. (2007) *The Chemistry of Pincer Compounds*, Elsevier.
- Balakrishna, M.S., Chandrasekaran, P., and George, P.P. (2003) *Coord. Chem. Rev.*, **241**, 87–117.
- Stobart, S.R., Grundy, S.L., and Joslin, F.L. (1990) Process for catalytic hydroformylation. US Patent 4,950,798.
- Gossage, R.A., McLennan, G.D., and Stobart, S.R. (1996) *Inorg. Chem.*, **35**, 1729–1732.
- Sangtrirutnugul, P. and Tilley, T.D. (2007) *Organometallics*, **26**, 5557–5568.
- MacInnis, M.C., MacLean, D.F., Lundgren, R.J., McDonald, R., and Turculet, L. (2007) *Organometallics*, **26**, 6522–6525.
- MacLean, D.F., McDonald, R., Ferguson, M.J., Caddell, A.J., and Turculet, L. (2008) *Chem. Commun.*, 5146–5148.
- Mitton, S.J., McDonald, R., and Turculet, L. (2009) *Organometallics*, **28**, 5122–5136.
- Morgan, E., MacLean, D.F., McDonald, R., and Turculet, L. (2009) *J. Am. Chem. Soc.*, **131**, 14234–14236.
- Mitton, S.J., McDonald, R., and Turculet, L. (2009) *Angew. Chem. Int. Ed.*, **48**, 8568–8571.
- MacInnis, M.C., McDonald, R., Ferguson, M.J., Tobisch, S., and Turculet, L. (2011) *J. Am. Chem. Soc.*, **133**, 13622–13633.
- Mitton, S.J., McDonald, R., and Turculet, L. (2012) *Polyhedron*. doi: 10.1016/j.poly.2012.07.072
- Mitton, S.J. and Turculet, L. (2012) *Chem. Eur. J.*, **18**, 15258–15262.
- Ruddy, A.J., Mitton, S.J., McDonald, R., and Turculet, L. (2012) *Chem. Commun.*, **48**, 1159–1161.
- Takaya, J. and Iwasawa, N. (2008) *J. Am. Chem. Soc.*, **130**, 15254–15255.
- Takaya, J. and Iwasawa, N. (2009) *Organometallics*, **28**, 6636–6638.
- Takaya, J. and Iwasawa, N. (2011) *Dalton Trans.*, **40**, 8814–8821.
- Takaya, J., Kirai, N., and Iwasawa, N. (2011) *J. Am. Chem. Soc.*, **133**, 12980–12983.
- Takaya, J., Sasano, K., and Iwasawa, N. (2011) *Org. Lett.*, **13**, 1698–1701.
- Takaya, J., Nakamura, S., and Iwasawa, N. (2012) *Chem. Lett.*, **41**, 967–969.
- Kirai, N., Takaya, J., and Iwasawa, N. (2013) *J. Am. Chem. Soc.*, **135**, 2493–2496.
- Kirai, N., Iguchi, S., Itoh, T., Takaya, J., and Iwasawa, N. (2013) *Bull. Chem. Soc. Jpn.*, **86**, 784–799, accepted.
- For other examples of synthesis and utilization of phenylene-bridged PSiP-pincer complexes, see: Korshin, E.E., Leitus, G., Shimon, L.J.W., Konstantinovski, L., and Milstein, D. (2008) *Inorg. Chem.*, **47**, 7177–7189.
- Fang, H., Choe, Y.-K., Li, Y., and Shimada, S. (2011) *Chem. Asian J.*, **6**, 2512–2521.
- Li, Y.-H., Zhang, Y., and Ding, X.-H. (2011) *Inorg. Chem. Commun.*, **14**, 1306–1310.
- Li, Y.-H., Ding, X.-H., Zhang, Y., He, W.-R., and Huang, W. (2012) *Inorg. Chem. Commun.*, **15**, 194–197.
- Suh, H.-W., Schmeier, T.J., Hazari, N., Kemp, R.A., and Takase, M.K. (2012) *Organometallics*, **31**, 8225–8236.
- Kameo, H., Ishii, S., and Nakazawa, H. (2012) *Dalton Trans.*, **41**, 11386–11392.
- Gorla, F., Venanzi, L.M., and Albinati, A. (1994) *Organometallics*, **13**, 43–54.
- Huang, M.-H. and Liang, L.-C. (2004) *Organometallics*, **23**, 2813–2816.
- Appleton, T.G., Clark, H.C., and Manzer, L.E. (1973) *Coord. Chem. Rev.*, **10**, 335–422.
- Braunstein, P., Matt, D., and Nobel, D. (1988) *Chem. Rev.*, **88**, 747–764.

38. Sakakura, T., Choi, J.-C., and Yasuda, H. (2007) *Chem. Rev.*, **107**, 2365–2387.
39. Aresta, M. (ed.) (2010) *Carbon Dioxide as Chemical Feedstock*, Wiley-VCH Verlag GmbH, Weinheim.
40. Tsuji, Y. and Fujihara, T. (2012) *Chem. Commun.*, **48**, 9956–9964.
41. Mori reported several catalytic carboxylation reactions of bis(1,3-diene)s, alkynes, and allenes using Ni catalyst and organozinc reagents, see: Mori, M. and Takimoto, M. (2005) in *Modern Organonickel Chemistry* (ed. Y. Tamaru), Wiley-VCH Verlag GmbH, Weinheim, pp. 205–223.
42. Solin, N., Kjellgren, J., and Szabó, K.J. (2004) *J. Am. Chem. Soc.*, **126**, 7026–7033.
43. Mkhaliid, I.A.I., Barnard, J.H., Marder, T.B., Murphy, J.M., and Hartwig, J.F. (2009) *Chem. Rev.*, **110**, 890–931.
44. For examples of Dehydrogenative borylation reaction without sacrificial hydroboration and hydrogenation, see: Coapes, R.B., Souza, F.E.S., Thomas, R.L., Hall, J.J., and Marder, T.B. (2003) *Chem. Commun.*, 614–615.
45. Selander, N., Willy, B., and Szabó, K.I. (2010) *Angew. Chem. Int. Ed.*, **49**, 4051–4053.
46. Mkhaliid, I.A.I., Coapes, R.B., Edes, S.N., Coventry, D.N., Souza, F.E.S., Thomas, R.L., Hall, J.J., Bi, S.-W., Lin, Z., and Marder, T.B. (2008) *Dalton Trans.*, 1055–1064.
47. Takaya, J. and Iwasawa, N. (2012) *ACS Catal.*, **2**, 1993–2006.
48. Onozawa, S., Hatanaka, Y., Sakakura, T., Shimada, S., and Tanaka, M. (1996) *Organometallics*, **15**, 5450–5452.
49. Onozawa, S. and Tanaka, M. (2001) *Organometallics*, **20**, 2956–2958.
50. Braunschweig, H., Gruss, K., Radacki, K., and Uttinger, K. (2008) *Eur. J. Inorg. Chem.*, **2008**, 1462–1466.
51. Zhu, Y., Chen, C.-H., Fafard, C.M., Foxman, B.M., and Ozerov, O.V. (2011) *Inorg. Chem.*, **50**, 7980–7987.
52. Schubert, U. (1990) *Adv. Organomet. Chem.*, **30**, 151–187.
53. Schubert, U. and Gilges, H. (1996) *Organometallics*, **15**, 2373–2375.
54. Lachaize, S. and Sabo-Etienne, S. (2006) *Eur. J. Inorg. Chem.*, **2006**, 2115–2127.
55. Chen, W., Shimada, S., Tanaka, M., Kobayashi, Y., and Saigo, K. (2004) *J. Am. Chem. Soc.*, **126**, 8072–8073.
56. Tanabe, M., Ito, D., and Osakada, K. (2008) *Organometallics*, **27**, 2258–2267, and references cited therein.

10

Experimental and Theoretical Aspects of Palladium Pincer-Catalyzed C–C Cross-Coupling Reactions

Christian M. Frech

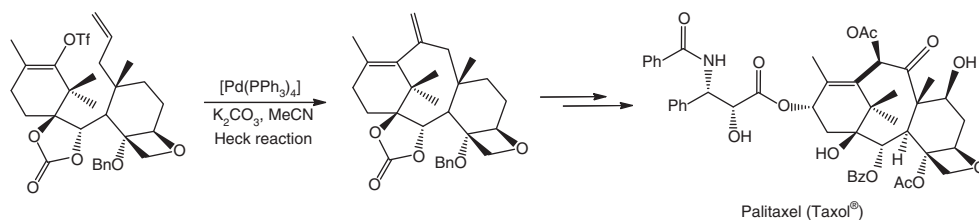
10.1

C–C Cross-Coupling Reactions – an Indispensable Tool for the Synthesis of Complex Organic Molecules

Palladium-catalyzed C–C cross-coupling reactions, for which the Nobel Prize in Chemistry 2010 was jointly given to Heck, Negishi, and Suzuki – the inventors of such cross-coupling reactions – belong to the most important types of catalytic carbon–carbon bond-forming reactions and are nowadays an indispensable tool for the target-oriented synthesis of complex organic molecules across all research fields and industrial segments. From new materials (e.g., polymers) research to pharmaceutical production, these types of reactions have been extensively applied throughout the past decades, propelling advances capable of effecting beneficial changes in modern life. Their success and hence widespread use in organic synthetic applications are due to the mild conditions associated with the reactions together with their tolerance to a wide range of functional groups. For example, the Heck reaction has been used in more than 100 different syntheses of natural products and biologically active compounds, such as Taxol[®] [1], a mitotic inhibitor used in cancer chemotherapy (Scheme 10.1), or the herbicide Prosulforon[®] [2].

The anti-inflammatory drug Naproxen and the asthma drug Singulair are other examples of industrially manufactured pharmaceuticals involving a Heck reaction step. The Heck reaction has also been used in the synthesis of other complex organic molecules such as steroids, strychnine, and the diterpenoid scopadulcic acid B with cytotoxic and antitumor activity [3–5]. Examples in the literature of natural product syntheses which include a Negishi coupling step in their total syntheses are the natural marine antiviral product hennoxazole A (Figure 10.1) and pumiliotoxin A (Scheme 10.2), a toxic alkaloid found in the skin of frogs from the Dendrobatidae family that it uses for self-defense [6, 7].

The antiviral bromoindole alkaloid dragmacidin F and the potent natural anti-tumor agent (+)-dymemicin A involve a Suzuki coupling in one of the key carbon–carbon bond-forming steps (Figure 10.1) [8, 9]. Further examples of industrially prepared fine chemicals involving palladium-catalyzed cross-coupling



Scheme 10.1 Palitaxel (Taxol[®]) synthesis with a Heck coupling as the key step [1].

reaction steps are Cyclotene[®], a monomer for high-performance electronic resins [10], 5-HT_{1A} agonist (an agonist for a subtype of the 5-hydroxytryptamine (serotonin) receptor) [11], and the fungicide Boscalid (Figure 10.1) [12].

The inherent green nature of catalysis (green chemistry is the utilization of a set of principles that reduce or eliminate the use or generation of hazardous substances in the design, manufacture, and application of chemical products) [13], where small amounts of a transition-metal complex enables reactions to be accomplished in an atom- and energy-economic as well as environmentally friendly way, further underlines the great importance and indispensability of palladium-catalyzed C–C cross-coupling reactions for the target-oriented synthesis of complex organic molecules.

Various types of palladium complexes are known to promote these processes, of which many follow the “classical” Pd⁰/Pd^{II} mechanism, as it is, for example, the case for [Pd(PPh₃)₂(OAc)₂] or [Pd(PPh₃)₄]. Other catalysts, such as [Pd(OAc)₂] serve as sources of palladium nanoparticles. Among the plethora of catalytic systems available to perform C–C cross-coupling reactions, phosphorus ligands and their palladium complexes constitute the vast majority of the promoters of choice. Most of the demand for such ligands and catalysts comes from pharmaceutical industry and academic research, and both have expressed growing interest in latest innovations in this area. Accordingly, also pincer-type complexes have been applied in these processes.

10.2

Palladium Pincer Complexes as C–C Cross-Coupling Catalysts

The first pincer-catalyzed cross-coupling reaction was published in 1997 by Milstein and coworkers [14] who successfully applied xylene-derived phosphine-based palladium pincer complexes such as [$\{(\text{C}_6\text{H}_3)\text{-2,6-(CH}_2\text{PPr}_i)_2\}\text{Pd(TFA)}\}$] (TFA, trifluoroacetate) (**1**, Figure 10.2) as Heck catalysts in the coupling of iodobenzene with alkyl acrylates. Two years later, Shibasaki and coworkers [15] applied the highly efficient bis(phosphinito) pincer complex [$\{(\text{C}_6\text{H}_3)\text{-2,6-(OP(OC}_6\text{H}_4\text{-4-OMe))}_2\}\text{Pd(I)}\}$] (**2**, Figure 10.2) in the Heck coupling of iodobenzene and *n*-butyl acrylate at catalyst loadings down to 0.1 ppm, for which turnover numbers (TONs) of up to 8 900 000 have been obtained. Excellent catalytic activities and the formation of trisubstituted olefins from acrylates and aryl halides, as well as conversions of aryl chlorides

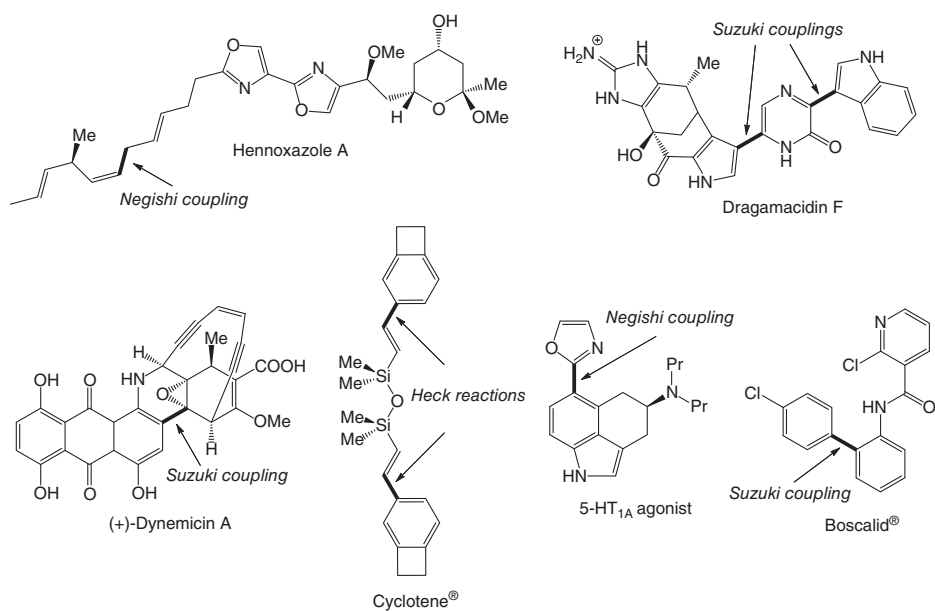
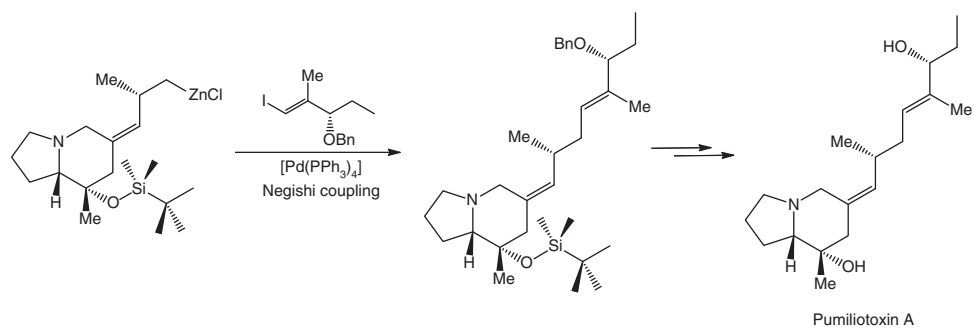


Figure 10.1 Palladium-catalyzed cross-coupling reactions in natural product synthesis and industrially prepared fine chemicals.



Scheme 10.2 Synthesis of pumiliotoxin A involving Negishi coupling as the key step [6].

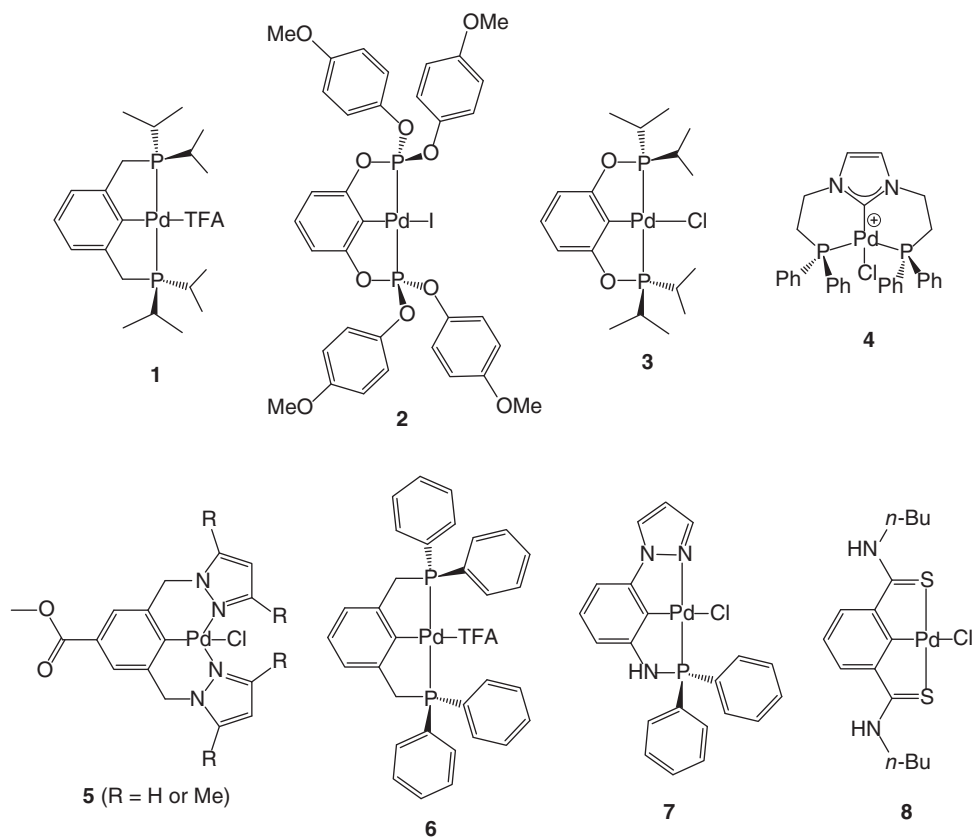


Figure 10.2 Palladium pincer complexes applied in C–C cross-coupling reactions.

with styrene into *trans*-stilbenes, have been reported by Jensen and coworkers [16] in 2000 for the closely related xylene-derived phosphinito pincer complex $\{[(C_6H_3)-2,6-(OP(iPr)_2)_2Pd(Cl)]\}$ (**3**, Figure 10.2).

These results impressively demonstrated that seemingly slight structural changes on pincer-type (Heck) cross-coupling catalysts can dramatically influence their catalytic activity, and hence indicated their great potential in Heck as well as other cross-coupling reactions. Accordingly, Lee and coworkers [17] reported in 2004 the first pincer-catalyzed Suzuki–Miyaura cross-coupling reaction, which was catalyzed by cationic NHC-derived (NHC, *N*-heterocyclic carbene), phosphine-based pincer complexes of the type $[(NHC)-N,N-(CH_2CH_2PPh_2)_2Pd(MeCN)]^+$ (**4**, Figure 10.2). While only moderate catalytic activities were obtained in the Suzuki–Miyaura reaction, excellent TONs of up to 56 000 000 have been achieved in the Heck reaction between phenyl iodide and styrene. A year later, Dominguez and coworkers [18] introduced xylene-derived pyrazole-based NCN pincer catalysts of type **5** (Figure 10.2), which were found to efficiently catalyze the Heck, Suzuki, and Sonogashira cross-coupling reaction, and hence are rare examples of generally applicable pincer-type cross-coupling catalysts and the first ones to be applied in the cross-coupling of aryl halides and alkynes, the so-called Sonogashira reaction. The first report on a pincer-catalyzed Stille reaction was published in the same year by Wendt and coworkers [19] who successfully coupled aryl bromides with trimethylphenyltin in the presence of $\{[(C_6H_3)-2,6-(CH_2PPh_2)_2Pd(TFA)]\}$ (**6**, Figure 10.2), a xylene-derived, phosphine-based PCP pincer complex, at loadings as low as 0.0001 mol% (and TONs of up to 690 000). Palladium pincer-catalyzed versions of the Hiyama reaction (cross-coupling of aryl halides and arylsilicon compounds) were for the first time reported by SanMartin and Dominguez and coworkers in 2008 [20]. The authors reported on the synthesis and catalytic activity of a nonsymmetric PCN-based pincer palladium complex **7** (Figure 10.2) in Suzuki, Sonogashira, and Hiyama couplings in neat water and NaOH as base. In 2009, Lei and coworkers [21] successfully applied the alkylpyridine-2,6-dicarbothioamide SNS-based pincer complex **8** (Figure 10.2) in the Negishi coupling of aryl iodides with alkylzinc reagents under very mild reaction conditions at loadings down to 0.00001 mol%.

Even though various C–C cross-coupling reactions have been successfully catalyzed with palladium pincer complexes, often with excellent performances [22], their primarily application nowadays lies in the Heck reaction, of which the role of pincer-type catalysts in this reaction still is unclear and therefore under debate.

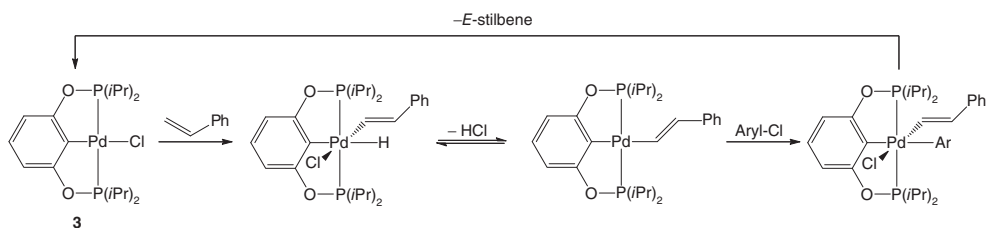
10.3

The Role of Palladium Pincer Complexes in Heck Reactions

Apart from their high catalytic activity in the Heck reaction, palladium pincer-catalyzed C–C cross-coupling reactions are of particular interest from mechanistic points of view. While “classical” Pd⁰/Pd^{II} cycles and mechanisms in which the palladium center of pincer-type cross-coupling catalysts does not change its oxidation state and has in most cases been excluded to be operative [23], considerable

experimental evidence for both heterogeneous mechanisms and catalytic cycles involving the Pd^{II}/Pd^{IV} redox pair have been obtained for Heck cross-coupling reactions [22]. This is the reason why the latter mechanisms are controversially discussed and still are an important part of current research [24].

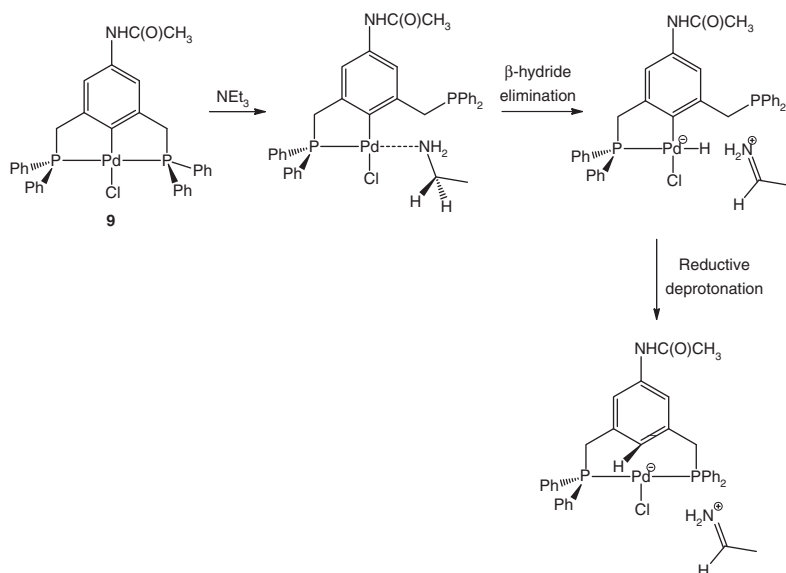
Even though the oxidation of Pd^{II} centers to Pd^{IV} intermediates is thermodynamically disfavored and therefore is usually considered to require strong oxidants, Milstein and coworkers [14] suggested that the xylene-derived phosphine-based palladium pincer complex [$\{(C_6H_3)-2,6-(CH_2PPr_2)_2Pd(TFA)\}$] (**1**) (and closely related systems) operate via catalytic cycles involving the Pd^{II}/Pd^{IV} redox pair. Pd^{II}/Pd^{IV} mechanisms have primarily been proposed because homogeneous Pd⁰/Pd^{II} cycles could have been excluded to be operative for these systems (as indicated by the reactivity pattern of possible intermediate compounds of such mechanisms) and because of the high thermal stability of palladium pincer complexes, for which no decomposition was observed at temperatures up to 180 °C and after heating solutions of **1** for 2 weeks at 140 °C under the reaction conditions applied. The pincer complexes also did not show any sensitivity toward oxygen and moisture, and that is why the reactions could also be carried out in air without noticeable changes in efficiencies or yields. In addition, the catalysts were shown to remain highly active after completion of the reaction, and, upon addition of more substrates, catalysis was found to be resumed, leading to the coupling products in the same yields and rates. Further experimental results, derived from competitive experiments using (electronically) different aryl iodides and methyl acrylate, gave a linear correlation with the respective Hammett σ values and a ρ value which was found to be too low to fit a rate-determining nucleophilic aromatic substitution but did account for a subsequent reaction step, such as olefin insertion into the palladium–aryl bond, instead. The same mechanism was suggested to be operative by Shibasaki and coworkers [15] for the bis(phosphino) pincer complex [$\{(C_6H_3)-2,6-(OP(OC_6H_4-4-OMe)_2)_2Pd(I)\}$] (**2**). A Pd^{II}/Pd^{IV} cycle with initial oxidative addition of a vinyl C–H bond of the alkene on the Pd^{II} center of **3** and formation of vinyl Pd^{IV} intermediates was proposed to be operative for the resorcinol-derived, phosphine-based PCP pincer complex [$\{(C_6H_3)-2,6-(OP(iPr)_2)_2Pd(Cl)\}$] (**3**) by Jensen and coworkers. Sequential reductive elimination of HCl, oxidative addition of the aryl halide, and reductive elimination of the coupling product were proposed to close the catalytic cycle (Scheme 10.3) [16b]. The significantly higher catalytic activity



Scheme 10.3 Proposed catalytic cycle for the Heck reaction of aryl chlorides catalyzed by [$\{(C_6H_3)-2,6-(OP(iPr)_2)_2Pd(Cl)\}$] (**3**).

of the phosphinito PCP complex **3** when compared with their xylene-derived, phosphine-based analogs, such as **1**, did account for a reductive elimination step to be rate-determining one in this process.

In 2004, Eberhard [25] demonstrated that phosphinito-based pincer-type Heck catalysts such as $[(C_6H_3)-2,6-(OP(iPr)_2)_2Pd(Cl)]$ (**3**) and related systems serve as sources of nanoparticles. Sigmoidal-shaped reaction kinetics, positive quantitative poisoning experiments with CS_2 , thiophene, and PPh_3 , mercury drop tests, and NMR studies indicated their involvement in the catalytic cycle [26]. Moreover, it was found that pincer complexes possessing only phosphinito donors decomposed more easily under Heck reaction conditions than those containing phosphine units, thereby providing an explanation for their higher catalytic activities. However, a year later, also Weck, Jones, and coworkers [27] proposed the involvement of palladium nanoparticles in the catalytic cycle of the Heck reaction for xylene-derived phosphine-based pincer Heck catalysts such as $[(4-(NHCOCH_3)(C_6H_2)-2,6-(CH_2P(iPr)_2)_2Pd(Cl)]$ (**9**) for which complex degradation was observed at elevated reaction temperatures in the presence of tertiary aliphatic amines (Scheme 10.4). Computational studies showed that the lowest energy decomposition path involves sequential β -hydride elimination of a coordinated amine and formation of an iminium ion and an anionic hydride complex that subsequently undergoes “reductive deprotonation” to give anionic halide bisphosphine palladium(0) complexes, which are suggested to serve as sources of palladium nanoparticles under Heck reaction conditions.



Scheme 10.4 Proposed decomposition path of a xylene-derived phosphine-based pincer complexes in the presence of triethylamine.

High reaction temperatures were found to be crucial for their irreversible decomposition into nanoparticles, because recent investigations on xylene-derived

phosphine-based pincer complexes recently showed that reduction of **1** (with metallic sodium) can induce a collapse of the pincer framework and lead to the formation of dinuclear palladium complexes, containing Pd⁰ and Pd^{II} centers, which readily undergo reoxidation in the presence of aryl halides upon regeneration of the pincer framework [28]. However, palladium nanoparticles were also found to be the catalytically active form of xylene-derived SCS-based pincer catalysts (in which the sulfur donor atoms bear fluorine alkyl substituents), as observed by Gladysz's research group in 2008 [29]. Nanoparticle formation was indicated by the reddish color of the reaction mixtures in *N,N*-dimethylformamide (DMF), which is characteristic for palladium nanoparticles [30] as seen also from mercury drop tests and transmission electron microscopy (TEM). The same conclusion was independently drawn by Curran and coworkers [31] with a closely related system in the same year. Palladium nanoparticles were also demonstrated to be the catalytically active form of Frech's aminophosphine-based pincer palladium complex [$\{C_6H_3-2,6-(NHP(piperidinyl)_2)_2\}Pd(Cl)$] (**10**), even though experimental and computational evidence for the thermal accessibility of pincer-type Pd^{IV} intermediates in halide exchange reactions with phenylbromide (to yield the bromo derivative [$\{C_6H_3-2,6-(NHP(piperidinyl)_2)_2\}Pd(Br)$] (**11**)) at 140 °C have been obtained as well [24].

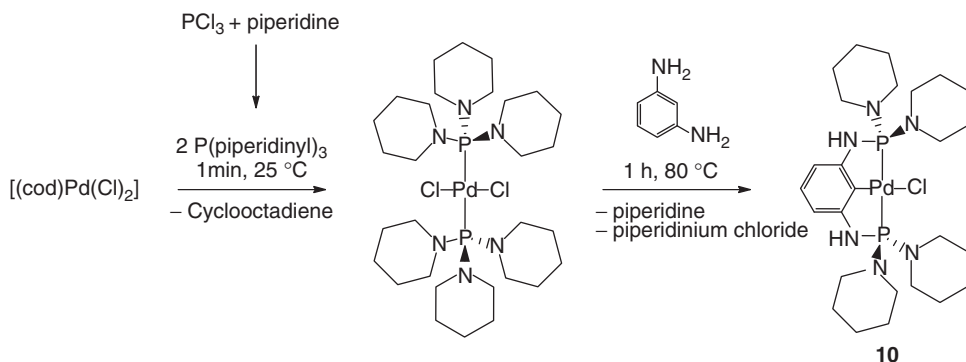
Finally, it should be mentioned that two years later, an enantioselective oxidative (boron) Heck-type reaction was reported by Jung and coworkers [32] for a dinuclear NHC-derived CNO-based pincer complex for which for the first time a Pd⁰/Pd^{II} mechanism was suggested to be operative with palladium pincer-type cross-coupling catalysts. Reaction mechanisms without a change of the palladium's oxidation state have never been proposed to be operative for Heck cross-coupling reactions, but have been shown to be operative for xylene-derived selenium-based pincer complexes and related systems in the cross-coupling of vinyl epoxides (and aziridines) with organoboronic acids [24d, 33].

10.3.1

Pd^{II}/Pd^{IV} Cycles and Palladium Nanoparticle Formation

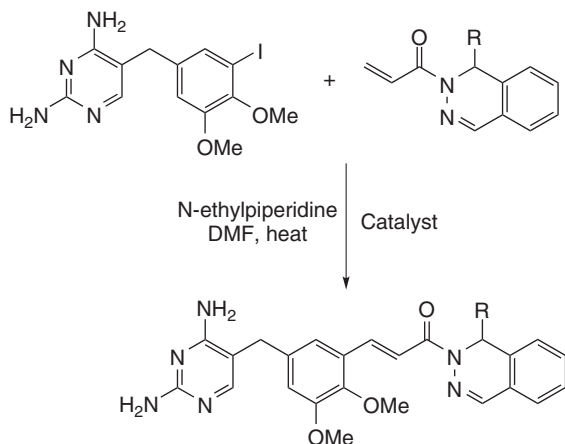
A mechanistically interesting example of a highly efficient Heck catalyst is the aminophosphine-based pincer palladium complex [$\{C_6H_3-2,6-(NHP(piperidinyl)_2)_2\}Pd(Cl)$] (**10**) [24a], which was introduced by Frech's research group in 2007 [34]. The aminophosphine-based ligand system of **10** was shown to have the same steric bulk and the σ -donor strength when compared to its phosphine-based analog but allows (in contrast to phosphines) the donation of additional electron density from the nitrogen lone pairs toward the P atom, which was expected to facilitate the thermal accessibility of Pd^{IV} intermediates and hence promote catalytic cycles where Pd^{II}/Pd^{IV} redox pairs are involved. On the other hand, the labile character of P–N bonds in aminophosphine-based ligand systems (sensitivity toward protons; e.g., in form of water) also offers the possibility to efficiently promote the formation of nanoparticles and hence reactions that are catalyzed by nanoparticles. An additional advantage of Frech's cross-coupling catalyst is its simple and cheap synthesis, which uses

the dichloro(bis(1,1',1''-(phosphinetriyl)tripiperidine))palladium complex as a template for the reaction with 2,6-diaminobenzene to build up the aromatic pincer core directly on the metal center (Scheme 10.5). This makes Frech's pincer catalyst also attractive from the synthetic (and economic) points of view, because an independent synthesis of the pincer-type ligand system is unnecessary.



Scheme 10.5 Synthesis of Frech's aminophosphine-based pincer complex $[\{\text{C}_6\text{H}_3\text{-2,6-}(\text{NHP}(\text{piperidinyl})_2)_2\}\text{Pd}(\text{Cl})]$ (**10**).

Despite of its cheap and easy accessibility, **10** was found to show excellent catalytic activities in the Heck, Suzuki, and Sonogashira cross-coupling reactions and effectively coupled to a wide range of different aryl bromides and boronic acids/potassium trifluoroborates in air at loadings as low as 0.05 mol%. While Frech's pincer catalyst demonstrates high catalytic activity in the Suzuki coupling [34], its performance in both the Heck reaction and Sonogashira coupling [24a, 35] – the latter reaction even performed under amine- and copper-free reaction conditions – requires even lower amounts of catalyst. Excellent product yields with different substrates were obtained at parts per million levels (between 0.2 and 50) reaching TONs of up to 4 900 000 for the Heck reaction and 2 000 000 for the Sonogashira coupling. The potential applicability of Frech's pincer catalyst in organic syntheses was recently impressively demonstrated in a comparative study with two conventional catalysts ($[\text{Pd}(\text{OAc})_2]$ and $[\text{Pd}(\text{Cl})_2(\text{PPh}_3)_2]$) in the Heck Synthesis of a series of highly functionalized 2,4-diaminopyrimidine-based antibiotics, which have demonstrated activity against inhalation anthrax [36] and multi-drug resistant staph [37] (Scheme 10.6). It was found that Frech's pincer catalyst was without exception superior to conventional palladium-based Heck catalysts, giving the desired products in higher yields and with fewer contaminants that were more easily purified by using catalytic loadings by a factor lower than ten compared to the other catalysts examined [38]. Moreover, the potential use of Frech's pincer catalyst in industrial processes was demonstrated in exemplary "large scale" Heck reactions, where 210 ml (2.0 mol) of phenyl bromide and 250 ml (2.4 mol) of styrene were quantitatively coupled within 36 h at 140°C in DMF and K_2CO_3 in the presence of only ~ 0.25 mg (0.00002 mol%) of catalyst; for example,



Scheme 10.6 Heck-type cross-coupling of allylacetates and hypervalent iodines catalyzed by $[(C_6H_3-2,6-(OPPh_2)_2Pd(TFA))] (15)$.

100% conversion into 1,1',1''-ethene-1,1,2-triyltribenzene was achieved at 160 °C within 24 h upon addition of 1.1 equiv of phenyl bromide to DMF solutions of (*E*)-stilbene or 1,1-diphenylethene or by adding 2.2 equiv of phenyl bromide to DMF solutions of styrene [24a].

An additional advantage of Frech's palladium pincer cross-coupling catalyst includes its well-defined fate after catalysis. Treatment of **10** with aqueous hydrochloric acid and thus under work-up conditions led to a rapid and complete catalyst degradation, accompanied by the formation of phosphonate, piperidinium salts, 1,3-diaminobenzene, and other insoluble palladium-containing products, which were easily separable from the coupling products – an important issue to be considered in particular for pharmaceutical applications. All these advantages make, $[(C_6H_3-2,6-(NHP(piperidinyl)_2)_2Pd(Cl)] (10)$ attractive for industrial applications. Indeed, **10** was successfully applied in industry, and nowadays is commercially available.

Mechanistic studies performed with Frech's pincer catalyst in the Heck reaction excluded catalytic cycles with the involvement of homogeneous palladium(0) species, as indicated by the results obtained from the (recently developed) dibenzyl-test, which is directly applicable under the reactions conditions applied [24a]. Dibenzyl formation was – in contrast to Heck reactions catalyzed by palladium(0) complexes of type $[Pd(PR_3)_2]$, where Pd^0/Pd^{II} cycles are operative – not detectable by gas chromatography-mass spectrometry (GC/MS) when reaction mixtures of aryl bromide, olefin, benzyl chloride (~10 mol% relative to aryl bromide), catalyst, and base were thermally treated. On the other hand, experimental observations, such as quantitative poisoning experiments with metallic mercury and CS_2 , which were shown to efficiently inhibit catalysis, as well as analysis of the reaction profiles showed sigmoidal-shaped kinetics with induction periods and hence indicated that palladium nanoparticles are the catalytically active form

of Frech's pincer catalyst. However, even though pincer-type Pd^{IV} intermediates were not involved in the catalytic cycle of the Heck reaction catalyzed by [$\{C_6H_3-2,6-(NHP(piperidinyl)_2)\}Pd(Cl)$] (**10**), their thermal accessibility as reactive intermediates was demonstrated by a smooth halide exchange reaction with **10** and phenyl bromide (and formation of **11**) in DMF at 100 °C, which was not observable for phosphine- and phosphite-based pincer complexes, such as **1** or **3** [24a]. The involvement of Pd^{IV} intermediates in the halide exchange reaction was confirmed by density functional theory (DFT) calculations: chloride dissociation from **10** and formation of [$\{C_6H_3-2,6-(NHP(piperidinyl)_2)\}Pd$]⁺ (**10a**), which is endothermic by +23.8 kcal mol⁻¹, was found to initiate the reaction sequence and is followed by the oxidative addition of phenyl bromide on the palladium(II) center of **10a** and formation of the cationic Pd^{IV} intermediate [$\{C_6H_3-2,6-(NHP(piperidinyl)_2)\}Pd(Br)(C_6H_5)$]⁺ (**10b**). The oxidative addition process is only slightly endothermic (+28.8 kcal mol⁻¹) and revealed an energetic barrier of only +19.9 kcal mol⁻¹. Re-coordination of the chloride ligand and formation of **10c** (+25.6 kcal mol⁻¹), and the subsequent reductive elimination of chlorobenzene, yield [$\{C_6H_3-2,6-(NHP(piperidinyl)_2)\}Pd(Br)$] (**11**), which was found to be exothermic by -5.3 kcal mol⁻¹ and is accompanied by a calculated barrier of +27.8 kcal mol⁻¹ [24a].

In this context, it is interesting to note that aryl palladium(IV) pincer complexes have been recently isolated (or characterized in solution) from stoichiometric oxidations of the corresponding pincer palladium(II) derivatives with hypervalent iodines. Canty and coworkers and van Koten and coworkers [39, 40] successfully oxidized xylene-derived amine-based palladium(II) NCN pincer complexes with the general formula of [$\{(C_6H_2)-2,6-(NMe_2)_2Pd(X)\}$] (**12**, X = OAc or OBz) to the corresponding octahedral six-coordinated palladium(IV) complexes [$\{(C_6H_2)-2,6-(NMe_2)_2Pd(Cl)_2(X)\}$] (**13**, X = OBz or OAc) and [$\{(C_6H_2)-2,6-(NMe_2)_2Pd(CCSiMe_3)(OTf)(X)\}$] (**14**, X = OBz or OAc) by using PhICl₂ and (Me₃SiCC)I(Ph)(OTf), respectively, as oxidants. These results, however, inspired Szabo and coworkers [24b] in the development of a new palladium pincer-catalyzed version of the Heck cross-coupling reaction with allyl acetates and hypervalent iodines of type (Ar)₂I(X) as coupling partners, probing Heck cross-coupling reactions that follow Pd^{II}/Pd^{IV} mechanisms (Scheme 10.6).

Pincer complexes of type [$\{(C_6H_2)-2,6-(NMe_2)_2Pd(X)\}$] (**12**, X = OAc or OBz) and [$\{(C_6H_3)-2,6-(OPPh_2)_2Pd(TFA)\}$] (**15**) successfully catalyzed this process. Moreover, palladium nanoparticles were excluded to be involved in this process, as indicated by the mercury drop test, and thereby gave the first piece of evidence that catalytic cycles with the Pd^{IV}/Pd^{II} redox pair were operative. DFT calculations verified an eased oxidative addition of hypervalent iodines (when compared to aryl iodides) on (pincer-type) Pd^{II} centers, and consequently supported Pd^{II}/Pd^{IV} catalytic cycles to be operative for this process [24b]. The oxidative addition of (Ph)₂I(OTf) on the palladium center of **12** and formation of [$\{(C_6H_2)-2,6-(NMe_2)_2Pd(Ph)(OTf)(OAc)\}$] (**16**, Figure 10.3) was found to be an exothermic process (-6.2 kcal mol⁻¹) with an activation barrier of 28.1 kcal mol⁻¹. Although the transition state of the oxidative addition of phenyl iodide on **12** (to form [$\{(C_6H_2)-2,6-(NMe_2)_2Pd(Ph)(I)(OAc)\}$])

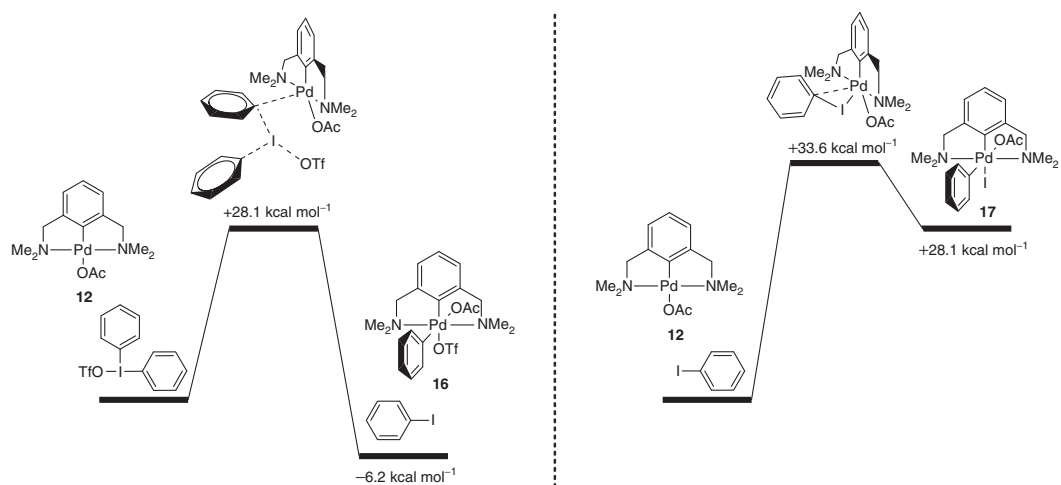
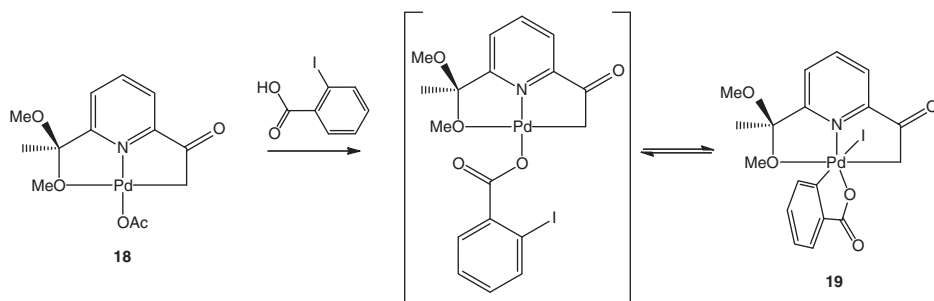


Figure 10.3 DFT reaction profiles of oxidative additions of (Ph)₂I(OTf) (left) and phenyliodide (right) on the palladium(II) centers of 12.

(17)) was only 5 kcal mol⁻¹ higher in energy, the overall process was strongly endothermic (+24.9 kcal mol⁻¹), instead (Figure 10.3). The authors concluded that such small activation barriers for the reverse reaction and the reductive elimination of aryl iodides from intermediates could generally inhibit the coupling process under catalytic reaction conditions.

A year later, Blacque and Frech [24c] performed comprehensive DFT studies on the thermal feasibility of Pd^{II}/Pd^{IV} cycles in pincer-catalyzed Heck reactions and convincingly showed that pincer-type Pd^{IV} intermediates are indeed thermally accessible with aryl bromides at elevated temperatures and hence are generally to be considered as reactive intermediates in pincer-catalyzed reactions with aryl halides at elevated reaction temperatures (for details, see below). Shortly thereafter, Vicente and coworkers [41] published the first oxidative addition of an aryl iodide on the metal center of a palladium(II) pincer complex: 2-iodobenzoic acid was found to smoothly undergo oxidative addition on the palladium(II) center of [(ONC)Pd(OAc)] (18) to give two isomeric forms of the respective palladium(IV) complex with the general formula of [(ONC)Pd(II)(C₆H₄C(O)O)] (19) (Scheme 10.7). Moreover, mixtures of both isomers showed (although only very poor) catalytic activity in the cross-coupling of 2-iodobenzoic acid with methyl acrylate (in the presence of AgClO₄), and hence indicated that pincer Pd^{IV} complexes of type 19 could indeed be intermediates in this process catalyzed by 18.



Scheme 10.7 Oxidative addition of 2-iodobenzoic acid on the palladium(II) center of [(ONC)Pd(OAc)] (18).

Even though aminophosphine- and phosphite-based pincer complexes, as well as other systems such as SCS-based pincer-type Heck catalysts, were shown to serve as stable and clean sources of palladium nanoparticles in Heck reactions [24a, 25], and also xylene-derived phosphine-based systems were found to decompose under Heck reaction conditions in the presence of organic bases and hence palladium nanoparticles generally are considered to be the catalytically active form of palladium pincer Heck catalysts [27], catalytic cycles with the involvement of Pd^{IV} intermediates could not have been excluded to be operative in pincer-catalyzed versions of the Heck reaction. In contrast, experimental observations, such as halide exchange reactions

between phenyl bromide and the aminophosphine-based pincer complex $[\{C_6H_3-2,6-(NHP(piperidinyl)_2\}Pd(Cl)]$ (**10**) and the stoichiometric oxidative addition of 2-iodobenzoic acid on the palladium(II) center of $[(ONC)Pd(OAc)]$ (**18**) and formation of the palladium(IV) pincer complex $[(ONC)Pd(II)(C_6H_4C(O)O)]$ (**19**), indicated that catalytic cycles with the involvement of the Pd^{II}/Pd^{IV} redox pair are thermally feasible and hence a mechanistic option to nanoparticle-catalyzed versions of Heck- (and other) cross-coupling reactions [24a, 38]. In order to verify (or disprove) the thermal feasibility of Pd^{II}/Pd^{IV} Heck cycles, detailed theoretical investigations have been performed by Frech's research group. These studies are described below and demonstrated for the first time (on a computational basis) that Pd^{II}/Pd^{IV} cycles could indeed be operative in polar nonprotic solvents at elevated temperatures under Heck reaction conditions with pincer-type Heck catalysts and that mechanisms with Pd^{IV} intermediates are a true alternative to catalytic cycles involving palladium nanoparticles in the Heck reaction.

10.4

Computational Investigations on the Thermal Feasibility of Pd^{II}/Pd^{IV} Cycles of Palladium Pincer-Catalyzed Heck Reactions

Frech's research group presented in 2010 detailed quantum chemical calculations using DFT on the experimentally applied aminophosphine-, phosphite-, and phosphine-based pincer-type Heck catalysts $[2,6-C_6H_3(XPR_2)_2Pd(Cl)]$ ($X = NH$, $R = piperidinyl$, **10**; $X = O$, $R = piperidinyl$, **20**; $X = O$, $R = isopropyl$, **3**; $X = CH_2$, $R = isopropyl$, **21**) with the sterically demanding $P(piperidinyl)_2$ and $PiPr_2$ groups (Figure 10.4) and the substrates styrene and phenyl bromide, and *E*-stilbene as the coupling product and demonstrate the thermal feasibility of Pd^{II}/Pd^{IV} cycles of palladium pincer-catalyzed Heck reactions.

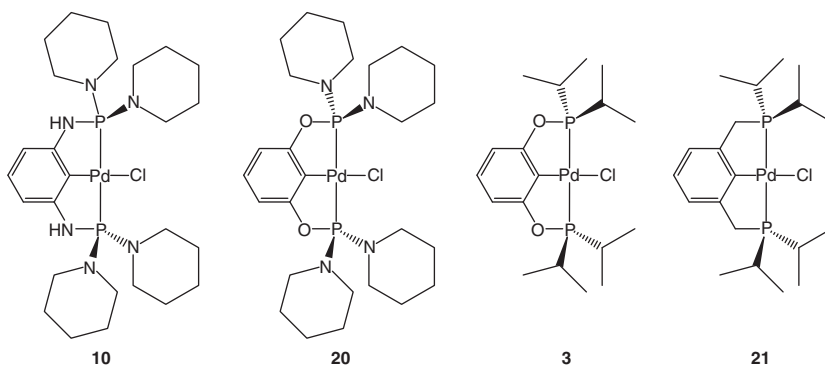


Figure 10.4 Experimentally applied pincer-type Heck catalysts $[2,6-C_6H_3(XPR_2)_2Pd(Cl)]$ ($X = NH$, $R = piperidinyl$, **10**; $X = O$, $R = piperidinyl$, **20**; $X = O$, $R = isopropyl$, **3**; $X = CH_2$, $R = isopropyl$, **21**) selected for the computational study published by Frech in 2010.

10.4.1

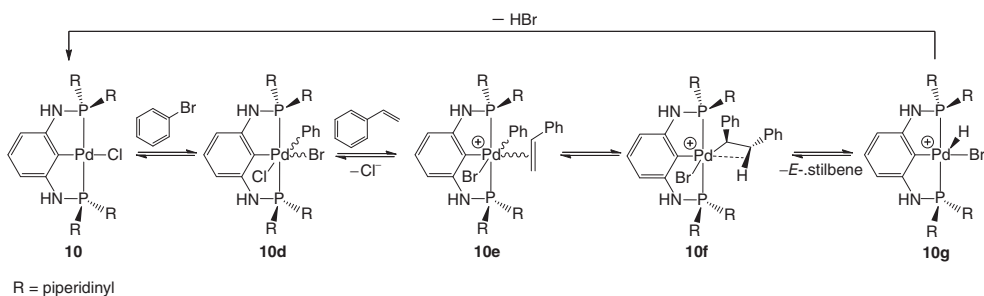
Possible Initial Reaction Steps of Pd^{II}/Pd^{IV} Mechanisms

Pincer-type Heck catalysts, following Pd^{II}/Pd^{IV} mechanisms, are initiated by styrene coordination or oxidative addition of phenyl bromide on either the neutral, square-planar 16e⁻ complexes of type [2,6-C₆H₃(XPR₂)₂Pd(Cl)] or their cationic, T-shaped 14e⁻ analogs with the general formula of [2,6-C₆H₃(XPR₂)₂Pd]⁺. All possible initiation steps as well as subsequent transformations were preliminarily investigated with **10**, the pincer complex with the largest electron density on the palladium(II) center used in this study (and, hence, where the most favorable energies for Pd^{IV} intermediates and the corresponding transition states were expected to be obtained). The energetically most favorable reaction paths were then recalculated with the other pincer complexes to figure out whether Pd^{IV} intermediates are thermally accessible in at least one of the selected systems and how strong the influence of the modifications on the ground-state energies and the transition states is.

10.4.2

Investigations on Mechanisms Initiated by Oxidative Addition of Phenyl Bromide on the Palladium(II) Center of [2,6-C₆H₃-2,6-(NHP(piperidinyl))₂]Pd(Cl)] (10**)**

The first Pd^{II}/Pd^{IV} cycle that was investigated includes initial oxidative addition of phenyl bromide on the palladium(II) center of [2,6-C₆H₃(NHP(piperidinyl))₂Pd] (**10**) and formation of the neutral, six-coordinated phenyl pincer complexes of type [2,6-C₆H₃(NHP(piperidinyl))₂Pd(Br)(Cl)(C₆H₅)] (**10d**) with the metal center in the oxidation state of +IV. Subsequent halide dissociation followed by the coordination of styrene (in cis position relative to the phenyl ligand to form **10e**) and migration of the phenyl ligand into the olefinic bond gives the cationic, penta-coordinated 1,2-diphenylethyl complex [2,6-C₆H₃(NHP(piperidinyl))₂Pd(Br)(CHPhCH₂Ph)] (**10f**), which could undergo β-hydride elimination and liberate *E*-stilbene to give the cationic hydride complex [2,6-C₆H₃(NHP(piperidinyl))₂Pd(Br)(Cl)(H)] (**10g**). Deprotonation of **10g** closes the catalytic cycle (Scheme 10.8).



Scheme 10.8 Possible catalytic cycle of pincer-catalyzed Heck reactions (involving Pd^{IV} intermediates), initiated by the direct oxidative addition of phenyl bromide on the palladium(II) center of [2,6-C₆H₃(NHP(piperidinyl))₂Pd(Cl)] (**10**).

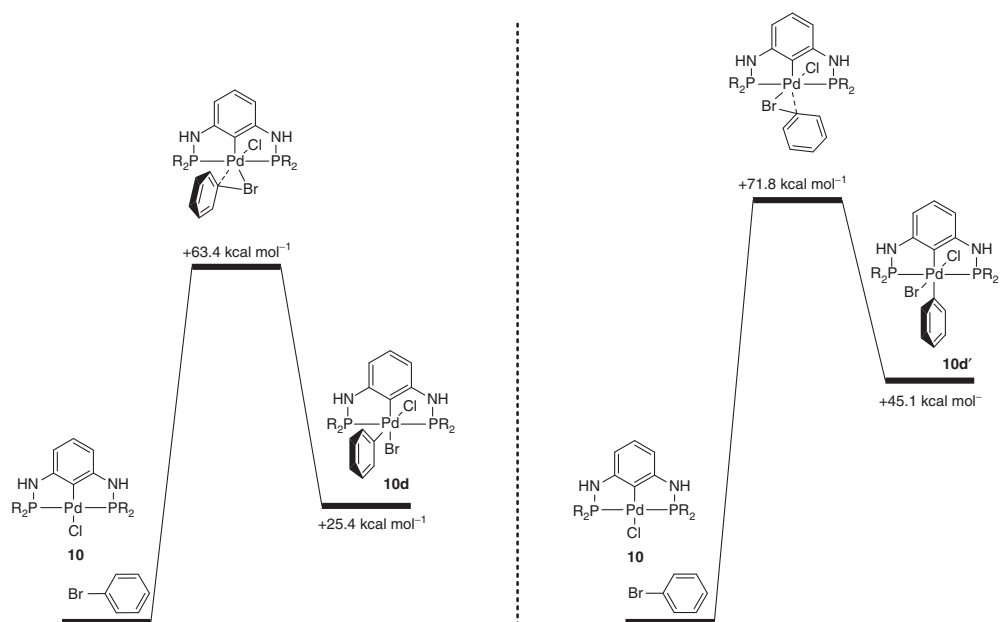


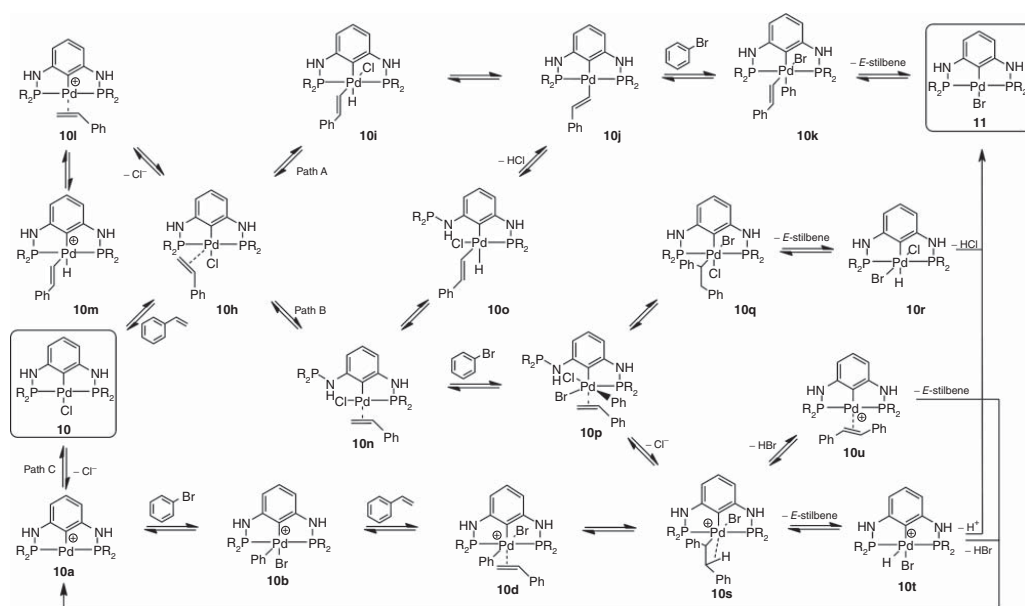
Figure 10.5 DFT reaction profiles of oxidative additions of phenyl bromide on the palladium(II) centers of **10** (with R = piperidiny) to form **10c** (left) and **10c'** (right).

Oxidative addition of phenyl bromide on **10** and the formation of complexes of type **10d** and **10d'** (to enter the catalytic cycle shown in Figure 10.5) was found to be strongly endothermic: the transition state traversed for the formation of **10d**, characterized by a significant elongation of the Br–C bond and a relative trans position of the phenyl group with respect to the chloride ligand and perpendicular to the equatorial plane between the halogens, was calculated to be 63.4 kcal mol⁻¹ relative to the ground-state energies of the isolated reactants (Figure 10.5). Thus, even though subsequent Br–C bond breakage and formation of the neutral, octahedral [2,6-C₆H₃(NHP(piperidinyl))₂Pd(Br)(Cl)(C₆H₅)] (**10d**) with the palladium center in the oxidation state of +IV is stabilized by 38.0 kcal mol⁻¹ relative to the transition state (the ground state energy of **10d** is 25.4 kcal mol⁻¹), the oxidative addition process is thermally not accessible. The situation is the same for its structural isomer **10d'** (with the phenyl ligand in trans position relative to the aromatic pincer core), which was found to have a significantly higher ground-state energy than **10c** (the ground-state energy of **10d'** is 45.1 kcal mol⁻¹) with an energetic barrier of 71.8 kcal mol⁻¹ above the energy of the ground-state reactants (Figure 10.5). Accordingly, catalytic cycles involving oxidative addition processes of aryl bromides on the palladium(II) centers of neutral, four-coordinated 16e⁻ pincer-type Heck catalysts are too high in energy and hence cannot be operative in the Heck reaction, and that is why subsequent transformations involving **10d** or **10d'** were not investigated further.

10.4.3

Investigations on Mechanisms Initiated by Styrene Coordination and/or Chloride Dissociation

Other mechanisms that were envisaged to be operative in the Heck coupling include cycles initiated by the coordination of styrene on **10** with the formation of neutral, square-pyramidal complexes of type [2,6-C₆H₃(NHP(piperidinyl))₂Pd(Cl)(CH₂=CHPh)] (**10h**). Subsequent reaction steps that were investigated included the oxidative addition of the vinyl C–H bond of coordinated styrene (to yield the phenylethenyl hydride complex **10i**), HCl elimination (to form **10j**) followed by the oxidative addition of phenyl bromide with formation of **10k**, reductive elimination of *E*-stilbene yielding **11** (path A, Scheme 10.9), chloride dissociation (to give the cationic, square-planar styrene adducts of type [2,6-C₆H₃(NHP(piperidinyl))₂Pd(CH₂=CHPh)]⁺ (**13l**)), and further reaction steps, such as the oxidative addition of the vinyl C–H bond and formation of type [2,6-C₆H₃(NHP(piperidinyl))₂Pd(H)(CH=CHPh)]⁺ (**10m**). Although seemingly less likely, alternative routes including the dissociation of one of the phosphine arms from **10h** and the formation of neutral, square-planar styrene complexes of type **10n** (path B, Scheme 10.9) which either could undergo oxidative addition of the vinyl C–H bond of styrene to yield phenylethenyl hydride complexes such as **10o** and HCl elimination to merge into reaction path A or oxidatively add phenyl bromide to give the neutral, hexa-coordinated phenyl pincer complexes with the general formula [2,6-C₆H₃(NHP(piperidinyl))₂Pd(Br)(Cl)(CH₂=CHPh)(C₆H₅)]



Scheme 10.9 Possible catalytic cycles and intermediates traversed of pincer-catalyzed Heck reactions, exemplarily evaluated with **10**.

(**10p**) were considered as well. Subsequent migration of the phenyl ligand into the olefinic bond of **10p** (to give **10q**), β -hydride elimination (either prior to phosphine re-coordination or after halide dissociation), and consecutive liberation of *E*-styrene with the formation of the neutral palladium hydride complex [2,6-C₆H₃(NHP(piperidinyl)₂)₂Pd(Br)(Cl)(H)] (**10r**) and HCl elimination would close the catalytic cycle. An alternative path to close the catalytic cycle includes chloride dissociation from **10p** and formation of the cationic phenylethenyl complexes with the general formula [2,6-C₆H₃(NHP(piperidinyl)₂)₂Pd(Br)(CHPhCH₂Ph)(C₆H₅)] (**10s**), sequential β -hydride elimination, *E*-stilbene liberation, and deprotonation via either the penta-coordinated cationic [2,6-C₆H₃(NHP(piperidinyl)₂)₂Pd(Br)(H)]⁺ (**10t**) or the cationic styrene adduct [2,6-C₆H₃(NHP(piperidinyl)₂)₂Pd(PhHC=CHPh)]⁺ (**10u**). Also, combined routes such as the formation of [2,6-C₆H₃(NHP(piperidinyl)₂)₂Pd(Br)(CHPhCH₂Ph)(C₆H₅)] (**10s**) via migration of the phenyl ligand into the olefinic bond of **10d** were considered to be operative. An overview with all the reaction steps investigated is given in Scheme 10.9.

Coordination of styrene on the palladium(II) center of **10** and formation of its styrene adduct [2,6-C₆H₃(NHP(piperidinyl)₂)₂Pd(Cl)(CH₂=CHPh)] (**10h**) was found to be endothermic by 26.8 kcal mol⁻¹. However, even though the initial styrene adduct formation might occur under Heck reaction conditions, subsequent oxidative addition of the vinyl C-H bond (path A, Scheme 10.9) and formation of the octahedral palladium phenylethenyl hydride complex [2,6-C₆H₃(NHP(piperidinyl)₂)₂Pd(Cl)(H)(CH=CHPh)] (**10i**), similar to the mechanism proposed for the resorcinol-derived, phosphine-based PCP pincer complex [2,6-(OP(*i*Pr)₂)₂Pd(Cl)] (**3**) (Scheme 10.3), cannot occur. The corresponding energetic barrier (TS_{10h/10i}) is 70.5 kcal mol⁻¹ relative to the energy of the isolated reactants and 43.7 kcal mol⁻¹ relative to **10h** which is far too high to be part of the catalytic cycle. Although breakage of the C-H bond would lead to a stabilization of 8.2 kcal mol⁻¹, the formation of **10i** was found to remain greatly endothermic (by 35.5 kcal mol⁻¹ relative to **10h**). Thus, reaction paths traversing phenylethenyl hydride intermediates of type [2,6-C₆H₃(XPR)₂Pd(Cl)(H)(CH=CHPh)] were excluded to be operative in pincer-catalyzed Heck reactions.

Similarly, although dissociation of one of the phosphine arms of [2,6-C₆H₃(NHP(piperidinyl)₂)₂Pd(Cl)(CH₂=CHPh)] (**10h**) and formation of **10n** might indeed occur under catalytic reaction conditions (the formation of **10n** was calculated to be endothermic by 9.7 kcal mol⁻¹), phosphine arm dissociation is not relevant for the catalytic cycle because chloride dissociation (from **10h**) and formation of the cationic square-planar styrene adduct [2,6-C₆H₃(NHP(piperidinyl)₂)₂Pd(CH₂=CHPh)]⁺ (**10l**) is thermodynamically and kinetically favored over the formation of **10n**. Notably, the formation of **10l** was found to be even more favored by the initial dissociation of the chloride ligand from **10** (to yield **10a**) and subsequent coordination of styrene (see below); thus, reaction paths involving **10n** are not relevant for the catalytic cycle. Indeed, ground-state energies of two exemplary isomeric structures with the general formula [2,6-C₆H₃(NHP(piperidinyl)₂)₂Pd(H)(CH=CHPh)] (**10o**) and [2,6-C₆H₃(NHP(piperidinyl)₂)₂Pd(Br)(Cl)(CH₂=CHPh)(C₆H₅)] (**10p**) showed that

oxidative addition of either the vinyl C–H bond of styrene or phenyl bromide on the palladium(II) center of **10n** is strongly endothermic: their ground-state energies were calculated to be 64.7 and 71.0 kcal mol⁻¹, respectively, which are too high to be part of catalytic cycles in palladium pincer-catalyzed Heck reactions.

Similarly, although dissociation of the chloride ligand of **10** (prior to an oxidative addition of phenyl bromide or a coordination of styrene) resulted in the cationic, T-shaped 14e⁻ complex [2,6-C₆H₃(NHP(piperidinyl))₂Pd]⁺ (**10a**) with a ground-state solvent-corrected energy of only 23.8 kcal mol⁻¹, the subsequent styrene coordination (to yield the cationic square planar styrene complex [2,6-C₆H₃(NHP(piperidinyl))₂Pd(CH₂=CHPh)]⁺ (**10l**)) is exothermic by 13.6 kcal mol⁻¹ (with a relative ground-state energy of 10.2 kcal mol⁻¹) and hence indicated that styrene adducts of **10a** (**10l**) are present in the reaction mixtures of the Heck reaction, either as an intermediate in the catalytic cycle or more likely as resting states of the catalytic mechanism to provide more facile access to **10a**. Subsequent oxidative addition of the vinyl C–H bond on their palladium(II) centers and formation of the cationic palladium phenylethenyl hydride complexes with the general formula of [2,6-C₆H₃(XPR₂)₂Pd(H)(CH=CHPh)]⁺ (**10m**) was found to be far too high in energy to be thermally accessible under Heck reaction conditions: the ground-state energy of the phenylethenyl hydride complex **10m** was calculated to be 72.3 kcal mol⁻¹ higher than those calculated for the reactants (Figure 10.6).

On the other hand, the oxidative addition of phenyl bromide on **10a** to give the cationic five-coordinated Pd^{IV} complex [2,6-C₆H₃(NHP(piperidinyl))₂Pd(Br)(C₆H₅)]⁺ (**10b**) with the phenyl ligand positioned *cis* to the aromatic unit of the pincer core is only slightly endothermic. Complex **10b** has a computed ground-state energy of only 28.8 kcal mol⁻¹, which lies 5.0 kcal mol⁻¹ above the sum of the ground-state energies of the reactants. The corresponding transition state was found to be only 19.9 kcal mol⁻¹ higher than the calculated energy for the isolated reactants, and thus is thermally accessible. Oxidative addition of phenyl bromide on the palladium(II) center of **10a** results in the cationic penta-coordinated bromo phenyl pincer complex **10b**. Subsequent coordination of styrene trans to the aromatic unit of the pincer core (*cis* coordination of styrene relative to the phenyl ligand is required for an ensuing phenyl migration into the olefinic bond of styrene) yielded the hexa-coordinated 18e⁻ complex [2,6-C₆H₃(NHP(piperidinyl))₂Pd(Br)(C₆H₅)(CH₂=CHPh)]⁺ (**10d**) with a relative ground-state energy of 45.1 kcal mol⁻¹. Migration of the phenyl ligand into the olefinic bond was found to be strongly exothermic ($\Delta E = 38.2$ kcal mol⁻¹) and gives the cationic 1,2-diphenylethyl palladium complex [2,6-C₆H₃(NHP(piperidinyl))₂Pd(Br)(CHPhCH₂Ph)]⁺ (**10s**) with a relative ground-state energy of only 6.9 kcal mol⁻¹. An agostic interaction of one of the CH₂ hydrogen atoms of the 1,2-diphenylethyl ligand eases the subsequent β -hydride elimination and hence the formation of cationic pincer hydride complex with the formula [2,6-C₆H₃(NHP(piperidinyl))₂Pd(H)(Br)(PhCH=CHPh)]⁺, which was found to undergo direct deprotonation. The resulting cationic *E*-stilbene complex [2,6-C₆H₃(NHP(piperidinyl))₂Pd(PhCH=CHPh)]⁺ (**10u**) has a ground-state

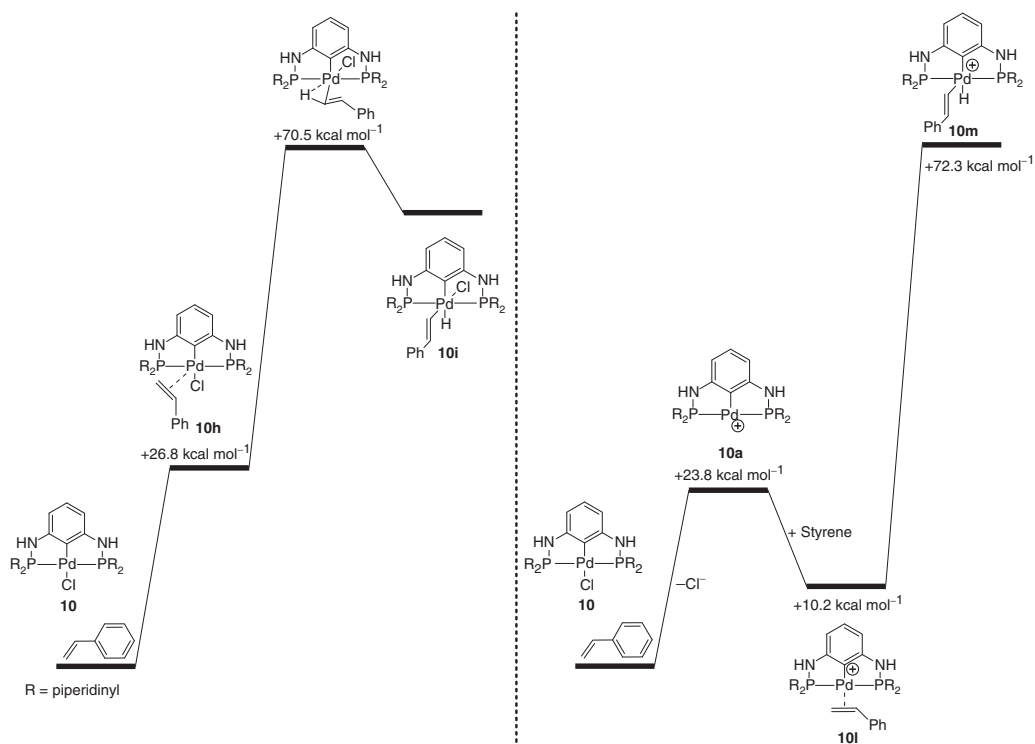


Figure 10.6 DFT reaction profiles of oxidative addition of the vinyl C-H bond of coordinated styrene on the palladium(II) centers of neutral penta-coordinated **10i** (left) and its cationic analog **10m** (right).

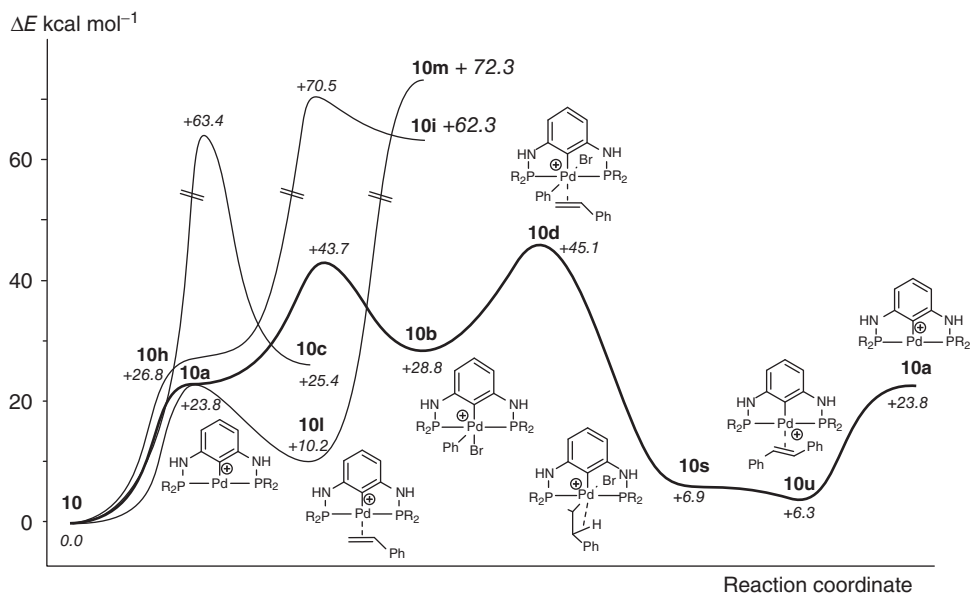


Figure 10.7 Potential energy surfaces for the calculated reactions of **10** with styrene and/or phenyl bromide. (Energies are in kcal mol^{-1} and relative to the ground-state reactants.)

energy of $6.3 \text{ kcal mol}^{-1}$. Subsequent *E*-stilbene liberation and formation of **10a** is endothermic by $17.5 \text{ kcal mol}^{-1}$ and closes the catalytic cycle (Figure 10.7).

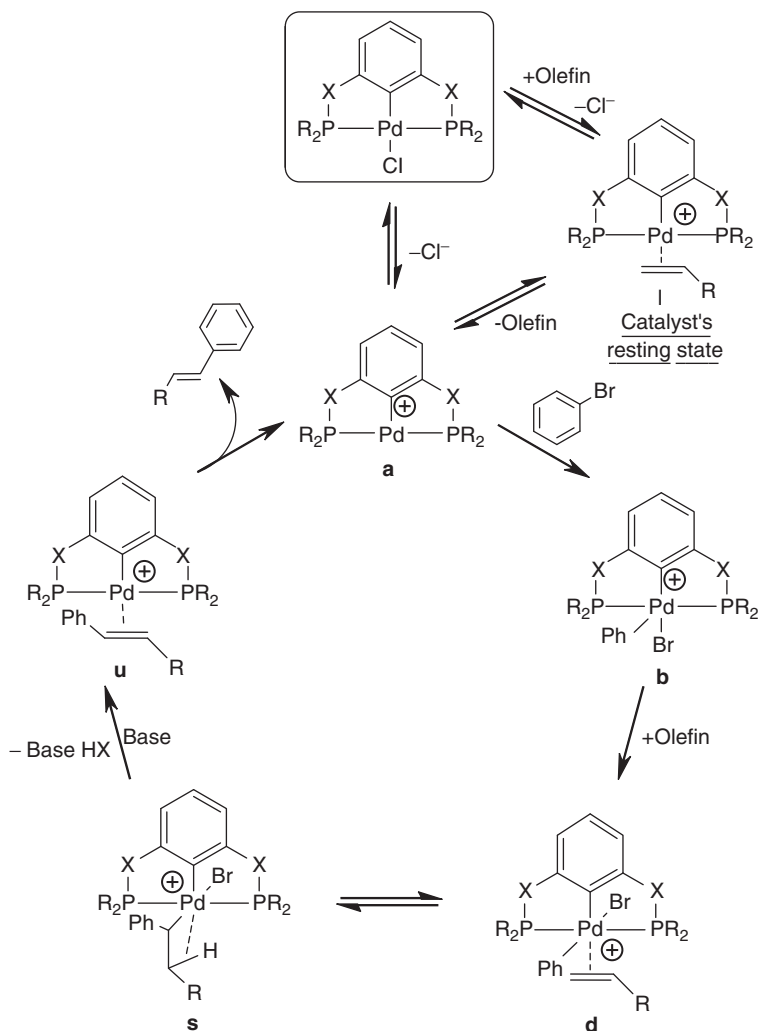
The energetic situation is similar with phenyl iodide as substrate: the ground-state, solvent-corrected energy of **10a** is $22.2 \text{ kcal mol}^{-1}$ higher than those of **10** and phenyl iodide. Subsequent oxidative addition of phenyl iodide on the palladium(II) center of **10a** and formation of $[2,6\text{-C}_6\text{H}_3\{\text{NHP}(\text{piperidiny})_2\}_2\text{Pd}(\text{I})(\text{C}_6\text{H}_5)]^+$ (**10b₁**), the iodide derivative of **10b**, has a computed ground-state energy of $26.3 \text{ kcal mol}^{-1}$, which is $4.1 \text{ kcal mol}^{-1}$ higher than the sum of the ground-state energies of the reactants. The corresponding transition state is $16.3 \text{ kcal mol}^{-1}$ higher in energy than calculated for the isolated reactants and thus compares well with the results obtained for phenyl bromide.

10.4.4

Pd^{II}/Pd^{IV} Cycle Proposed for Palladium Pincer-Catalyzed Heck Reactions

The lowest energy reaction path for *E*-stilbene formation (path C, Scheme 10.9) is the only thermally accessible catalytic cycle calculated for **10** and hence the generally proposed mechanism for palladium pincer complex-catalyzed Heck reactions (Scheme 10.10).

This reaction sequence was recalculated for **3**, **20**, and **21** (Figure 10.4) and shows the expected trend: the higher the electron density on the metal center, the lower the ground state energies and energetic barriers (Figure 10.8).



Scheme 10.10 Generally proposed catalytic cycle of the Heck reaction catalyzed by palladium pincer complexes involving Pd^{IV} intermediates and cationic styrene complexes as resting state.

For example, whereas chloride dissociation from the aminophosphine catalyst **10** and the phosphine-based palladium pincer complex [2,6-C₆H₃(CH₂PiPr₂)₂Pd(Cl)] (**21**) were found to be endothermic by only 23.8 and 23.7 kcal mol⁻¹, respectively, a ground-state energy of 27.5 kcal mol⁻¹ was calculated for [2,6-C₆H₃(OP(piperidinyl))₂Pd(Cl)] (**20**). The highest ground-state energy was found for the phosphinito pincer complex [2,6-C₆H₃(OPiPr₂)₂Pd(Cl)] (**3**) (30.7 kcal mol⁻¹), the one with the lowest electron density on the metal center. The situation is the same for the oxidative addition of phenyl bromide and formation

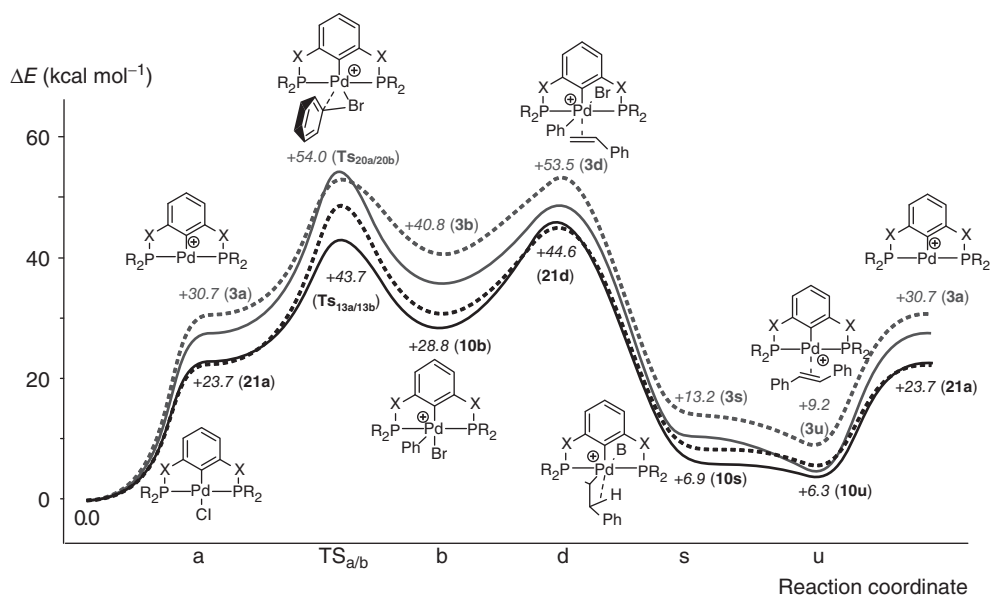
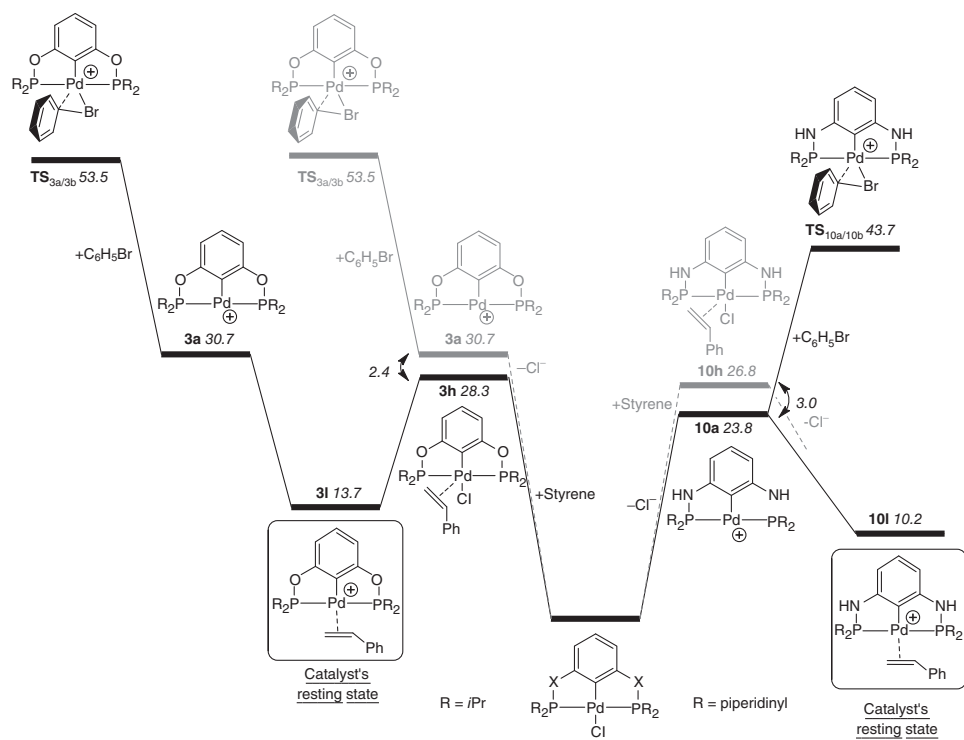


Figure 10.8 Comparison of the lowest energy path of the Heck coupling of phenyl bromide and styrene to form *E*-stilbene promoted by **3**, **10**, **20**, and **21**. (Energies are in kilocalories per mole and relative to the ground-state reactants.)

of the cationic phenyl pincer complexes of type $[2,6\text{-C}_6\text{H}_3(\text{XPR}_2)_2\text{Pd}(\text{Br})(\text{Ph})]^+$ ($\text{X} = \text{NH}$, $\text{R} = \text{piperidinyl}$, **10b**; $\text{X} = \text{O}$, $\text{R} = \text{piperidinyl}$, **20b**; $\text{X} = \text{O}$, $\text{R} = \text{isopropyl}$, **3b**; $\text{X} = \text{CH}_2$, $\text{R} = \text{isopropyl}$, **21b**), whose formations were found to be endothermic only slightly ($<10 \text{ kcal mol}^{-1}$) but accompanied by energetic barriers within the range of $20\text{--}25 \text{ kcal mol}^{-1}$. Even though styrene coordination on the palladium(II) centers of **10a**, **20a**, **3a**, and **21a** was found to be exothermic by $13.6 \text{ kcal mol}^{-1}$ for **10a**, 17.6 and $17.0 \text{ kcal mol}^{-1}$ for **20a** and **3a**, respectively, and $10.6 \text{ kcal mol}^{-1}$ for **21a** and therefore generally favored over the oxidative addition of phenyl bromide on cationic, T-shaped $14e^-$ complexes of type $[2,6\text{-C}_6\text{H}_3(\text{XPR}_2)_2\text{Pd}]^+$, styrene adduct formation did not prevent the oxidative addition process. In contrast, styrene coordination and formation of complexes of type $[2,6\text{-C}_6\text{H}_3(\text{XPR}_2)_2\text{Pd}(\text{CH}_2=\text{CHPh})]^+$ ($\text{X} = \text{NH}$, $\text{R} = \text{piperidinyl}$, **10l**; $\text{X} = \text{O}$, $\text{R} = \text{piperidinyl}$, **20l**; $\text{X} = \text{O}$, $\text{R} = \text{isopropyl}$, **3l**; $\text{X} = \text{CH}_2$, $\text{R} = \text{isopropyl}$, **21l**) was found to be crucial for electron-poor pincer complexes such as **20** and **3** because their styrene adducts provide an energetically more favorable access to the cationic, T-shaped $14e^-$ complexes of type $[2,6\text{-C}_6\text{H}_3(\text{XPR}_2)_2\text{Pd}]^+$ – the key intermediates of

Figure 10.9 DFT reaction profiles of the initial reaction steps of the Heck cycle catalyzed by pincer-type Heck catalysts (according to Scheme 10.10), exemplarily depicted for **3** for electron-poor palladium pincer-complexes (left)

and for **10** for electron-rich pincer complexes (right), demonstrating the importance of the catalyst's resting state. (Energies (in italics) are in kilocalories per mole and relative to the ground-state reactants.)



the catalytic cycle. Hence, complexes of type $[2,6\text{-C}_6\text{H}_3(\text{XPR}_2)_2\text{Pd}(\text{CH}_2=\text{CHPh})]^+$ are the catalysts' resting states (Figure 10.9 and Scheme 10.10). Moreover, whereas chloride dissociation from **10** and **21** was found to be energetically favored over styrene adduct formation (by $\sim 3 \text{ kcal mol}^{-1}$), coordination of styrene and consecutive dissociation of the chloride ligand and styrene is energetically preferred for pincer complexes with low electron densities on the metal center: styrene adduct formation on the palladium(II) centers of $[2,6\text{-C}_6\text{H}_3(\text{XPR}_2)_2\text{Pd}(\text{Cl})]$ (X = O, R = piperidinyl, **20**; X = O, R = isopropyl, **3**) is endothermic by 23.3 and 28.3 kcal mol^{-1} , respectively, and hence favored over chloride dissociation by 4.2 and 2.4 kcal mol^{-1} , respectively.

However, the next reaction steps, the coordination of styrene on the palladium(IV) centers of the phenyl pincer complexes of type $[2,6\text{-C}_6\text{H}_3(\text{XPR}_2)_2\text{Pd}(\text{Br})(\text{C}_6\text{H}_5)]^+$ (X = NH, R = piperidinyl, **10b**; X = O, R = piperidinyl, **20b**; X = O, R = isopropyl, **3b**; X = CH₂, R = isopropyl, **21b**) and formation of the hexa-coordinated phenyl styrene complexes with the general formula of $[2,6\text{-C}_6\text{H}_3(\text{XPR}_2)_2\text{Pd}(\text{Br})(\text{C}_6\text{H}_5)(\text{CH}_2=\text{CHPh})]^+$, are endothermic by only 16.3 kcal mol^{-1} for **10d**, 12.1 kcal mol^{-1} for **20d**, 12.7 kcal mol^{-1} for **3d**, and 14.2 kcal mol^{-1} for **21d**. In contrast, migration of the phenyl ligand into the olefinic bond to give the cationic penta-coordinated phenylethenyl complexes of type $[2,6\text{-C}_6\text{H}_3(\text{XPR}_2)_2\text{Pd}(\text{Br})(\text{CHPhCH}_2\text{Ph})]^+$ and subsequent β -hydride elimination leads to the direct liberation of HBr and thus to the formation of cationic *E*-stilbene complexes $[2,6\text{-C}_6\text{H}_3(\text{XPR}_2)_2\text{Pd}(\text{PhCH}=\text{CHPh})]^+$ (X = NH, R = piperidinyl, **10u**; X = O, R = piperidinyl, **20u**; X = O, R = isopropyl, **3u**; X = CH₂, R = isopropyl, **21u**), which is greatly exothermic (by $\sim 40 \text{ kcal mol}^{-1}$) for all derivatives. *E*-stilbene liberation regenerates the catalyst and is endothermic by $\sim 20 \text{ kcal mol}^{-1}$ (Figure 10.8).

10.4.5

Heck Reactions Catalyzed by Palladium Pincer Complexes: Pd^{II}/Pd^{IV} Cycles and/or Palladium Nanoparticle Formation

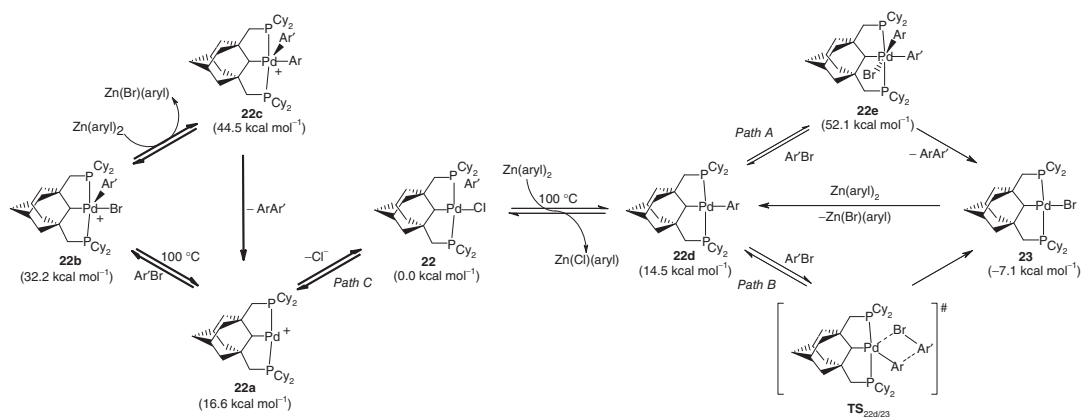
These computational investigations showed for the first time that catalytic cycles with the involvement of Pd^{IV} intermediates are indeed thermally accessible for palladium pincer complexes under Heck reaction conditions and hence are a true alternative to palladium nanoparticle-catalyzed versions of the Heck reaction. This, however, does not imply that Pd^{II}/Pd^{IV} mechanisms are operative in any case for palladium pincer complexes in the Heck reaction. In contrast, palladium nanoparticles have been often shown to be the catalytically active form of pincer-type Heck catalysts, as it is, for example, the case for the aminophosphine-based palladium pincer Heck catalyst $[2,6\text{-C}_6\text{H}_3(\text{NHP}(\text{piperidinyl})_2)_2\text{Pd}(\text{Cl})]$ (**10**) (under the reaction conditions applied) – the pincer complex with the highest electron density on the metal center and thus where the lowest energy path was calculated. Therefore, it is reasonable to anticipate that palladium pincer Heck catalysts exist that operate via Pd^{II}/Pd^{IV} mechanisms whereas others serve as sources of palladium nanoparticles. This hypothesis got strong experimental support from

Heck reactions catalyzed by **10**, performed with phenyl bromide and *n*-butyl acrylate in NMP at 140 °C with 0.01 mol% of catalyst and K₂CO₃ as base. Whereas dramatically retarded conversion rates were observed with the phosphine-based pincer complex **21** in the presence of 1-methyl-1,4-cyclohexadiene [42], only a marginal effect was noticed under identical reaction conditions with catalyst **10** (as well as with **3**). These results exclude the possibility that the catalytically active species derived from **10** (or **3**) and from **21** are of the same type, and in turn imply that different reaction mechanisms can indeed be operative with different pincer complexes in Heck reactions (and most probably also in other cross-coupling reactions). Therefore, it is reasonable to anticipate that palladium pincer Heck catalysts can operate via homogeneous (Pd^{II}/Pd^{IV}) mechanisms and serve as sources of palladium nanoparticles, depending on the reaction conditions applied.

10.5

Theoretical Investigations on a Pincer-Catalyzed Negishi Cross-Coupling Reaction

The proposed catalytic cycle for palladium pincer-catalyzed Heck reactions was supported by experimental and computational investigations performed with the recently introduced adamantyl-derived phosphine-based palladium pincer Negishi catalyst [C₁₀H₁₃-1,3-(CH₂P(Cy₂)₂)Pd(Cl)] (**22**, Scheme 10.11) for which a strongly related mechanism was found to be operative [43]. Whereas experimental investigations, including analysis of kinetic reaction profiles, quantitative poisoning experiments performed with PPh₃ and thiophene, and the mercury drop test, excluded biaryl formation mediated by palladium nanoparticles, a homogeneous mechanism with initial chloride dissociation and formation of the cationic, T-shaped 14e-complex [C₁₀H₁₃-1,3-(CH₂P(Cy₂)₂)Pd]⁺ (**22a**) and subsequent oxidative addition of aryl bromides (Ar'Br) with formation of cationic, penta-coordinated palladium(IV) aryl pincer complex [C₁₀H₁₃-1,3-(CH₂P(Cy₂)₂)Pd(Br)(aryl')]⁺ (**22b**) was found to initiate the Negishi cross-coupling reaction. These initial reaction steps are the same as those found for pincer-catalyzed Heck reactions (Scheme 10.10). However, subsequent transmetalation with Zn(aryl)₂ and formation of cationic diaryl pincer complexes of type [C₁₀H₁₃-1,3-(CH₂P(Cy₂)₂)Pd(aryl)(aryl')]⁺ (**22c**), followed by reductive elimination of the coupling products (path C, Scheme 10.11), closes the catalytic cycle of the Negishi reaction and is the only mechanism that explains all experimental observations, such as the rarely observed formation of homocoupled side products, the prominent solvent and temperature effects, the effects observed upon addition of tetrabutylammonium bromide, the dramatic drop in activity when {2-[(dimethylamino)methyl]phenyl}(phenyl)zinc instead of diarylzinc or chloro(aryl)zinc reagents was used, the absence of Schlenk equilibria and hence [44] the smooth product formation obtained in cross-coupling reactions performed with zinc reagents prepared from their lithiated precursors, and the retarding effect observed upon addition of MgBr₂·Et₂O or why the Kumada reaction is not promoted by **22**.



Scheme 10.11 Possible mechanisms of the Negishi reaction catalyzed by the adamantyl-derived, phosphine-based palladium pincer complex [C₁₀H₁₃-1,3-(CH₂P(Cy₂)₂)Pd(Cl)] (**22**), of which only path C (bold arrows) explains all the experimental observations. The relative energies are given for aryl Ar = Ar' = phenyl.

The experimentally deduced mechanism was confirmed by DFT studies, which showed (although Pd halide–Zn interactions were not included in these calculations) that, even though the neutral phenyl pincer complex $[(C_{10}H_{13}-1,3-(CH_2P(Cy_2)_2)Pd(C_6H_5)]$ (**22d**) is formed under Negishi reaction conditions (its solvent-corrected ground state energy lies $+14.5 \text{ kcal mol}^{-1}$ above the sum of energies calculated for the reactants), **22d** is not relevant for the catalytic cycle, as subsequent oxidative addition of phenyl bromide and formation of the neutral, hexa-coordinated diphenyl pincer complex **22e** or one of its structural isomer (path A in Scheme 10.11) is strongly endothermic. The solvent-corrected ground-state energies are $+37\text{--}41 \text{ kcal mol}^{-1}$ higher than the sum of the ground-state energies calculated for the reactants and hence are thermally not accessible. Similarly, even though biaryl formation via four-center transition states, such as $TS_{22d/23}$ (path B, Scheme 10.11), neither could be verified nor disproved by DFT calculations, such mechanisms would imply (high) catalytic activity of **22** in the Kumada reaction and hence were excluded to be operative. On the other hand, initial chloride dissociation and formation of the cationic, T-shaped $14e^-$ complex **22a** and the subsequent oxidative addition of phenyl bromide and formation of the cationic penta-coordinated palladium(IV) phenyl pincer complex $[(C_{10}H_{13}-1,3-(CH_2PCy_2)_2)Pd(Br)(C_6H_5)]^+$ (**22b**) with the aromatic unit positioned cis to the aliphatic pincer core (path C, Scheme 10.11) have computed ground-state energies of $+16.6 \text{ kcal mol}^{-1}$ (**22a**) and $+32.2 \text{ kcal mol}^{-1}$ (**22b**), and hence are only slightly endothermic. The energetic barrier of the oxidative addition of an aryl bromide on the metal center of **22a** (the rate-determining step of the catalytic cycle) was not calculated in this study but is expected to be between 25 and 30 kcal mol^{-1} , which is of the same order of magnitude as that calculated for the xylene-derived, phosphine-based palladium pincer complex $TS_{21a/21b}$ (Figure 10.8). However, the subsequent transmetallation with diphenylzinc and formation of the cationic penta-coordinated Pd^{IV} diphenyl complex $[(C_{10}H_{13}-1,3-(CH_2PCy_2)_2)Pd(C_6H_5)_2]^+$ (**22c**) and bromo(phenyl)zinc has a computed solvent-corrected ground-state energy of $+44.5 \text{ kcal mol}^{-1}$, which is only $+12.3 \text{ kcal mol}^{-1}$ higher than the sum of the ground-state energies of the reactants. The reductive elimination of biphenyl is strongly exothermic ($\Delta E = -28.0 \text{ kcal mol}^{-1}$) and closes the catalytic cycle. The slight structural change for the reductive elimination of biphenyl from **22c** indicates a significantly smaller energetic barrier for the reductive elimination process than for a second transmetallation step and hence would explain why homocoupling has only rarely been observed as side a reaction.

10.6

Concluding Remarks

Palladium-catalyzed C–C cross-coupling reactions belong to the most important types of catalytic carbon–carbon bond-forming reactions and are nowadays an indispensable tool for the target-oriented synthesis of complex organic molecules across all research fields and industrial segments. Various types of palladium

complexes are known to promote these processes, which either follow Pd⁰/Pd^{II} mechanisms or serve as sources of palladium nanoparticles. Accordingly, also pincer complexes have been applied in these processes. However, even though pincer complexes typically are considered to serve as stable sources of palladium nanoparticles, controversial Pd^{II}/Pd^{IV} mechanisms have often been proposed to be operative, even though oxidation of Pd^{II} centers to Pd^{IV} intermediates is a thermodynamically disfavored process for which strong oxidants usually are assumed to be required. In order to confirm the thermal accessibility of such mechanisms under Heck reaction conditions, computational investigations were performed, which demonstrated the thermal accessibility of Pd^{II}/Pd^{IV} mechanisms in polar nonprotic solvents at elevated temperatures and identified cationic complexes of type [2,6-C₆H₃(XPR₂)₂Pd]⁺ (**a**, Scheme 10.10) as key intermediates in such processes. Therefore, it is reasonable to anticipate that palladium pincer (Heck) cross-coupling catalysts can operate via Pd^{II}/Pd^{IV} mechanisms whereas others serve as sources of nanoparticles. Moreover, it is possible that palladium pincer Heck catalysts either operate via homogeneous (Pd^{II}/Pd^{IV}) mechanisms or serve as sources of palladium nanoparticles, depending on the reaction conditions applied.

References

- Danishefsky, S.J., Masters, J.J., Young, W.B., Link, J.T., Snyder, L.B., Magee, T.V., Jung, D.K., Isaacs, R.C.A., Bornmann, W.G., Alaimo, C.A., Coburn, C.A., and Di Grandi, M.J. (1996) *J. Am. Chem. Soc.*, **118**, 2843.
- Baumeister, P., Seifert, G., and Steiner, H. (1994) Process for the preparation of substituted benzenes and benzene sulfonic acid and derivatives thereof and a process for the preparation of N'N-substituted ureas. European Patent EP584043.
- Chang, Y., Wu, G., Agnel, G., and Negishi, E.-I. (1990) *J. Am. Chem. Soc.*, **112**, 8590.
- Rawal, V.H. and Iwasa, S. (1994) *J. Org. Chem.*, **59**, 2685.
- (a) Overman, L.E., Ricca, D.J., and Tran, V.D. (1993) *J. Am. Chem. Soc.*, **115**, 2042. (b) Kucera, D.J., O'Connor, S.J., and Overman, L.E. (1993) *J. Org. Chem.*, **58**, 5304.
- Wipf, P. and Lim, S. (1995) *J. Am. Chem. Soc.*, **117**, 558.
- Hirashima, S., Aoyagi, S., and Kibayashi, C. (1999) *J. Am. Chem. Soc.*, **121**, 9873.
- Garg, N.K., Caspi, D.D., and Stoltz, B.M. (2004) *J. Am. Chem. Soc.*, **126**, 9552.
- Myers, A.G., Tom, N.J., Fraley, M.E., Cohen, S.B., and Madar, D.J. (1997) *J. Am. Chem. Soc.*, **119**, 6072.
- Schrock, A.K. (1989) Polyorganosiloxane-bridged bisbenzocyclobutene monomers. US Patent 4812588.
- Anderson, B.A., Becke, L.M., Booher, R.N., Flaugh, M.E., Harn, N.K., Kress, T.J., Varie, D.L., and Wepsiec, J.P. (1997) *J. Org. Chem.*, **62**, 8634.
- (a) Eicken, H., Rang, Harreus, A., Götze, N., Ammermann, E., Lorentz, G., and Strathmann, S. (1997) Bisphenylamide. German Patent DE19531813; (b) Eicken, K., Rack, M., Wetterich, F., Ammermann, E., Lorentz, G., and Strathmann, S. (1999) New bi:phenylamide derivatives are active against wide range of phytopathogenic fungi. German Patent DE19735224; (c) Rouhi, A.M. (2004) *Chem. Eng. News*, **82** (36), 49–58.
- Anastas, P.T. and Warner, J.C. (1998) *Green Chemistry: Theory and Practice*, Oxford University Press, New York, p. 30.

14. Ohff, M., Ohff, A., van der Boom, M., and Milstein, D. (1997) *J. Am. Chem. Soc.*, **119**, 11687.
15. Miyazaki, F., Yamaguchi, K., and Shibasaki, M. (1999) *Tetrahedron Lett.*, **40**, 7379.
16. (a) Morales-Morales, D., Grause, C., Kasaoka, K., Redon, R., Cramer, R.E., and Jensen, C.M. (2000) *Inorg. Chim. Acta*, **300-302**, 958. (b) Morales-Morales, D., Redon, R., Yung, C., and Jensen, C.M. (2000) *Chem. Commun.*, 1619.
17. Lee, H.M., Zeng, J.Y., Hu, C.-H., and Lee, M.-T. (2004) *Inorg. Chem.*, **43**, 6822.
18. Churruca, F., SanMartin, R., Tellitu, I., and Dominguez, E. (2005) *Synlett*, 3116.
19. Olsson, D., Nilsson, P., El Masnaouy, M., and Wendt, O.F. (2005) *Dalton Trans.*, 1924.
20. Inés, B., SanMartin, R., Churruca, F., Dominguez, E., Urtiaga, M.K., and Arriortua, M.I. (2008) *Organometallics*, **27**, 2833.
21. Wang, H., Liu, J., Deng, Y., Min, T., Yu, G., Wu, X., Yang, Z., and Lei, A. (2009) *Chem. Eur. J.*, **15**, 1499.
22. Selander, N. and Szabo, K.J. (2011) *Chem. Rev.*, **111**, 2048, and references therein.
23. (a) Olsson, D. and Wendt, O.F. (2009) *J. Organomet. Chem.*, **694**, 3112. (b) Takemoto, T., Iwasa, S., Hamada, H., Shibatomi, K., Kameyama, M., Motoyama, Y., and Nishiyama, H. (2007) *Tetrahedron Lett.*, **48**, 3397.
24. (a) Bolliger, J.L., Blacque, O., and Frech, C.M. (2008) *Chem. Eur. J.*, **14**, 7969. (b) Aydin, J., Larsson, J.M., Selander, N., and Szabo, K.J. (2009) *Org. Lett.*, **11**, 2852. (c) Blacque, O. and Frech, C.M. (2010) *Chem. Eur. J.*, **16**, 1521. (d) Bonnet, S., van Lenthe, J.H., Siegler, M.A., Spek, A.L., van Koten, G., and Klein Gebbink, R.J.M. (2009) *Organometallics*, **28**, 2325. (e) Szabo, K.J. (2010) *J. Mol. Catal. A: Chem.*, **324**, 56.
25. Eberhard, M.R. (2004) *Org. Lett.*, **6**, 2125.
26. Widegren, J.A. and Finke, R.G. (2003) *J. Mol. Catal. A*, **198**, 317.
27. (a) Sommer, W.J., Yu, K., Sears, J.S., Ji, Y., Zheng, X., Davis, R.J., Sherrill, C.D., Jones, C.W., and Weck, M. (2005) *Organometallics*, **24**, 4351. (b) Yu, K., Sommer, W., Richardson, J.M., Weck, M., and Jones, C.W. (2005) *Adv. Synth. Catal.*, **347**, 161. (c) Yu, K.Q., Sommer, W., Weck, M., and Jones, C.W. (2004) *J. Catal.*, **226**, 101. (d) Weck, M. and Jones, C.W. (2007) *Inorg. Chem.*, **46**, 1865.
28. Frech, C.M., Shimon, L.J.W., and Milstein, D. (2005) *Angew. Chem. Int. Ed.*, **44**, 1709.
29. da Costa, R.C., Jurisch, M., and Gladysz, J.A. (2008) *Inorg. Chim. Acta*, **361**, 3205.
30. Reetz, M.T. and Westermann, E. (2000) *Angew. Chem. Int. Ed.*, **39**, 165.
31. Curran, D.P., Fischer, K., and Moura-Letts, G. (2004) *Synlett*, 1379.
32. Yoo, K.S., O'Neill, J., Sakaguchi, S., Giles, R., Lee, J.H., and Jung, K.W. (2010) *J. Org. Chem.*, **75**, 95.
33. (a) Kjellgren, J., Aydin, J., Wallner, O.A., Saltanova, I.V., and Szabo, K.J. (2005) *Chem. Eur. J.*, **11**, 5260. (b) Bonnet, S., Lutz, M., Spek, A.L., van Koten, G., and Klein Gebbink, R.J.M. (2010) *Organometallics*, **29**, 1157.
34. (a) Bolliger, J.L., Blacque, O., and Frech, C.M. (2007) *Angew. Chem. Int. Ed.*, **46**, 6514. (b) Bolliger, J.L. and Frech, C.M. (2010) *Adv. Synth. Catal.*, **352**, 1075.
35. Bolliger, J.L. and Frech, C.M. (2009) *Adv. Synth. Catal.*, **351**, 891.
36. (a) Nammalwar, B., Bunce, R.A., Berlin, K.D., Bourne, C.R., Bourne, P.C., Barrow, E.W. and Barrow, W.W. (2012) *Eur. J. Med. Chem.*, **54**, 387; (b) Bourne, C.R., Bunce, R.A., Bourne, P.C., Berlin, K.D., Barrow, E.W., Barrow, W.S., and Barrow, W.W. (2009) *Antimicrob. Agents Chemother.*, **53**, 3065; (c) Barrow, E.W., Drier, J., Reinelt, S., Bourne, P.C., and Barrow, W.W. (2007) *Antimicrob. Agents Chemother.*, **51**, 4447.
37. Bourne, C.R., Barrow, E.W., Bunce, R.A., Bourne, P.C., Berlin, K.D., and Barrow, W.W. (2010) *Antimicrob. Agents Chemother.*, **54**, 3825.
38. Nammalwar, B., Bunce, R.A., Darrell Berlin, K., Bourne, C.R., Bourne, P.C., Barrow, E.W., and Barrow, W.W. (2013) *Org. Prep. and Proc. Int.*, **45**, 66.
39. Canty, A.J., Denney, M.C., van Koten, G., Skelton, B.W., and White, A.H. (2004) *Organometallics*, **23**, 5432.
40. Lagunas, M.C., Gossage, R.A., Spek, A.L., and van Koten, G. (1998) *Organometallics*, **17**, 731.

41. Vicente, J., Arcas, A., Julia-Hernandez, F., and Bautista, D. (2011) *Angew. Chem. Int. Ed.*, **50**, 6896.
42. Kiewel, K., Liu, Y., Bergbreiter, D.E., and Sulikowski, G.A. (1999) *Tetrahedron Lett.*, **40**, 8945.
43. Gerber, R., Blacque, O., and Frech, C.M. (2011) *Dalton Trans.*, **40**, 8996.
44. Schlenk, W. and Schlenk, W. Jr., (1929) *Ber. Dtsch. Chem. Ges. B*, **62**, 920.

11

Reactions of Square-Planar d^8 Pincer Complexes with Oxygen and Hydrogen

Wilson D. Bailey, Marie V. Parkes, Richard A. Kemp, and Karen I. Goldberg

11.1

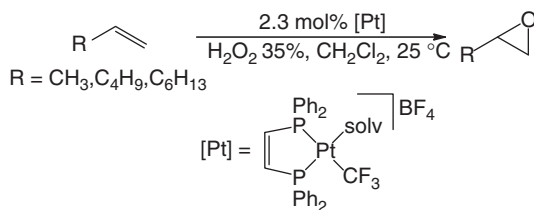
Introduction

Pincer complexes of the late transition metals have found significant use in catalysis [1–10]. Not only do pincer ligands commonly provide catalysts with unusually high degrees of thermal stability, but the ease by which these ligands can be electronically and sterically tuned allows them to be very effective in improving the reactivity and selectivity of catalytic systems [11]. The optimization of late-metal pincer systems for particular catalytic reactions is often assisted by mechanistic understanding of the fundamental reaction steps that comprise the catalytic cycle. In turn, the highly stable pincer-ligated complexes are ideally suited for the detailed mechanistic work needed to gain this knowledge. Using pincer complexes as model compounds researchers have carried out numerous kinetic and mechanistic studies on a wide variety of essential reactions in organometallic chemistry. The fundamental understanding of reactions ranging from small molecule insertions, to β -hydride eliminations and abstractions, to oxidative additions and reductive eliminations has benefited from the rigid and robust pincer framework [12].

In particular, pincer ligands have been very useful for studying reactions of transition-metal complexes with oxygen and hydrogen. For example, studies have been carried out on reactions of late-metal hydrides with molecular oxygen to generate metal hydroperoxide complexes and the reaction of late-metal hydroxides with hydrogen to release water and regenerate the metal hydride. These two reactions are particularly important as they may be key transformations in the direct partial oxidation of organic substrates by O_2 . General methods for the selective oxidation of organics by molecular oxygen have the potential to streamline chemical production with minimal environmental impact. There have been extensive research efforts in both academic and industrial laboratories focused on this formidable goal [13–21]. An ambitious target is the selective oxidation of alkenes to epoxides using molecular oxygen, a heterogeneously catalyzed reaction that is effective only for ethylene and 1,3-butadiene, two alkenes that do not contain allylic hydrogens [22]. Partial oxidation of propylene to propylene oxide (PO) is one of the many important industrial processes that could be revolutionized by a direct oxygen oxidation route. Current

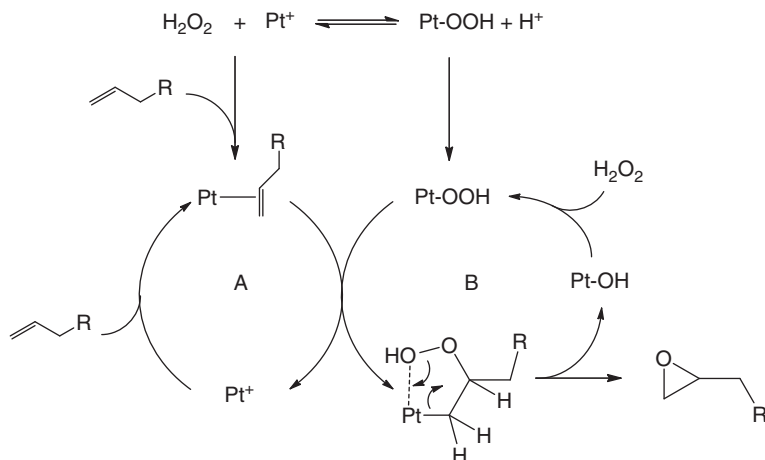
methods for PO production involve the use of more expensive and/or hazardous oxidants such as chlorine, organic hydroperoxides, or hydrogen peroxide [21]. In 2008, the world production of PO was over 8 billion kg/year, making it one of the top five mass-produced chemicals by oxidation [21]. Establishing a catalytic route to PO production through partial oxidation of propylene by clean, abundant, and readily available O_2 would be of great benefit to the chemical industry.

In 1984, Strukul *et al.* documented the first group VIII metal epoxidation catalyst [23], followed by in-depth studies of that system [24, 25]. This study garnered particular interest because of the fact that most previous epoxidation catalysts were oxophilic early transition-metal complexes (Mo, V, W, Cr, Ti, Mn) [26–31]. While Strukul's system used H_2O_2 rather than O_2 as the oxidant, the use of a less oxophilic late-transition metal such as platinum in a homogeneous catalytic system was a remarkable advance. Strukul demonstrated that the square-planar $[(\text{diphoe})Pt(\text{CF}_3)(\text{solv})]BF_4$ (diphoe, *cis*-1,2-bis(diphenylphosphino)ethane; solv = CH_2Cl_2) complex could epoxidize $R-\text{CH}=\text{CH}_2$ ($R = \text{CH}_3, \text{C}_4\text{H}_9, \text{C}_6\text{H}_{13}$) with H_2O_2 as the oxidant achieving turnover numbers (TONs) up to 325 (Scheme 11.1) [25]. Investigations in his laboratory led to the mechanistic proposal that the system operated in a bimolecular manner. The Pt^{II} center performed two different tasks: one platinum complex coordinated the olefin (A), thus increasing its electrophilicity, while another platinum center activated H_2O_2 (B) by forming a nucleophilic platinum hydroperoxide ($Pt-\text{OOH}$) species (Scheme 11.2). This hydroperoxo species attacked the bound olefin, eliminating the desired epoxide, and a platinum hydroxide ($Pt-\text{OH}$) species which was then converted back to the $Pt-\text{OOH}$ using H_2O_2 [25].

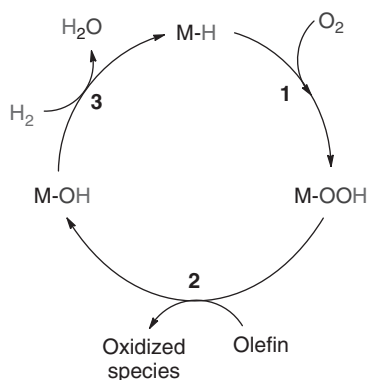


Scheme 11.1 Epoxidation of olefins by $[(\text{diphoe})Pt(\text{CF}_3)(\text{solv})]BF_4$ catalyst [25].

Soon after Strukul's Pt^{II} system for olefin epoxidation was published, Wenzel proposed a catalytic cycle for epoxidation employing a similar Pt^{II} center but using molecular oxygen rather than hydrogen peroxide as the oxidant [32]. The proposed cycle with a general metal M is shown in Scheme 11.3. The cycle begins with a metal hydride ($M-\text{H}$) species undergoing a reaction with O_2 to form a $M-\text{OOH}$ species (1). Next, O-atom transfer to an olefin occurs, forming the epoxide and $M-\text{OH}$ products (2). This $M-\text{OH}$ species can then undergo hydrolysis to re-form the $M-\text{H}$ and water, which is the only byproduct (3). While this exciting proposal incorporated Strukul's observation of oxygen transfer from a platinum hydroperoxide to an olefin, the other steps in the cycle – insertion of molecular oxygen into a late-metal hydride bond and hydrolysis of a late metal hydroxide

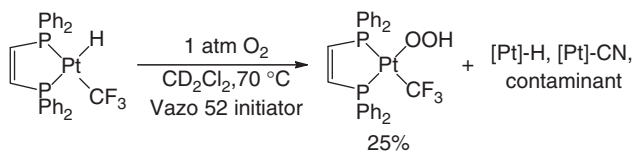


Scheme 11.2 Bimolecular catalytic epoxidation mechanism of [(diphoe)Pt(CF₃)(sol)]BF₄ [25]. (Adapted with permission from [25]. Copyright 2012, American Chemical Society.)



Scheme 11.3 Proposed catalytic cycle for the epoxidation of olefins by molecular oxygen.

[32–38] – have limited precedent in the literature [20, 39–54]. Furthermore, Wenzel [32] found that the key insertion of O₂ into the Pt–H bond of (diphoe)Pt(H)CF₃ was challenging (Scheme 11.4). At elevated temperatures in the presence of radical initiators, a Pt–OOH species could be detected, but only in minor amounts (25%).



Scheme 11.4 Attempt at O₂ insertion into a Pt–H bond (Wenzel's system) [32].

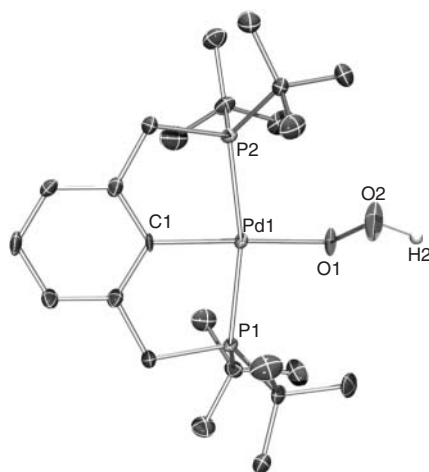
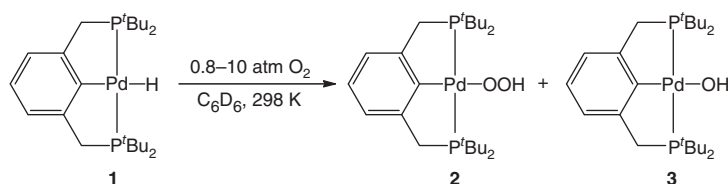
However, this experiment provided a proof of principle that, under appropriate conditions, O_2 can insert into a late-metal hydride bond.

A notable aspect of the Strukul system is that only one of the sites in the square plane of the metal center is utilized. Thus, a pincer ligand could be an ideal partner for this application, as it could lend the potential metal catalyst a high degree of robustness and still allow for reactivity at one site in the square plane. Wenzel's investigations pointed out the challenge of insertion of molecular oxygen into a $Pt^{II}-H$ bond, but oxygen insertion into $Pd^{II}-H$ bonds may be an easier reaction. In fact, insertion of molecular oxygen into $Pd^{II}-H$ bonds has been proposed as a key step in a number of palladium-catalyzed oxidations [15]. In 2006, utilizing a pincer ligand framework, we reported the first direct observation of molecular oxygen insertion into a $Pd^{II}-H$ bond [47]. The pincer complex (t^Bu PCP) PdH (t^Bu PCP, 2,6-bis(di t butylphosphino)methylbenzene) (**1**) underwent insertion of molecular oxygen to generate the palladium hydroperoxide complex (t^Bu PCP) $PdOOH$ (**2**). The pincer ligand stabilized both the starting complex and the product and, as such, allowed for a detailed study of the mechanism of the insertion reaction. Furthermore, the pincer motif was used to show the generality of this dioxygen insertion reaction with a variety of palladium pincer hydride complexes [48, 55, 56]. Experimental and computational results presented some notable trends and predictions for this reaction [57, 58]. The same pincer motif also allowed detailed studies of hydrogenolysis reactions of $Pd-O$ bonds, and information about this reaction is presented below [37, 38]. Importantly, the hydrogenolysis of a $Pd-OH$ bond would represent the last step in Wenzel's proposed olefin epoxidation cycle using molecular oxygen as an oxidant and a late-metal hydride as a catalyst. The strongly binding tridentate pincer ligand again provided the various complexes with high stability, which allowed a full study of the mechanism of hydrogenolysis [38]. The use of a hemilabile pincer ligand illustrated the importance of the more typical tridentate configuration in achieving the desired reactivity [59]. As the hydrogenolysis of metal hydroxides has been proposed in other important transformations [60, 61], the mechanistic insight obtained from these studies should also assist in the design of more efficient catalysts for a variety of reactions.

11.2

Insertion of Molecular Oxygen into Late-Transition Metal Hydride Bonds

Our nascent understanding of the mechanisms of dioxygen insertion into late-metal hydrides has grown significantly in the past several years. Discrete examples of this relatively uncommon reaction have been observed and studied in detail, and common mechanisms are beginning to emerge. The first reported example of direct insertion of O_2 into a $Pd^{II}-H$ bond was observed by our groups using the pincer complex (t^Bu PCP) PdH (**1**), which reacted with molecular oxygen to form the η^1 -hydroperoxo species (t^Bu PCP) $PdOOH$ (**2**) (Scheme 11.5) [47]. The hydroperoxide complex was fully characterized, including by X-ray crystallography. The hydroxide species (t^Bu PCP) $PdOH$ (**3**) was detected as a minor product in the reaction (with the



Scheme 11.5 Direct insertion of O₂ into the Pd–H bond of **1** [47]. (Adapted with permission from [47]. Copyright 2006, American Chemical Society.)

ratio of 2 : 3 being 25 : 1). Notably, the palladium hydroperoxide PdOOH **2** gradually decomposed to the palladium hydroxide complex **3** over time.

The insertion of O₂ into the Pd–H bond of **1** was readily monitored by ¹H and ³¹P{¹H} NMR spectroscopy, and the reaction was found to proceed with a second-order rate law, first order in [**1**] and first order in [O₂]. No experimental evidence for a radical process was found; the rates were reproducible and no effects of light or radical inhibitors on the reaction were observed. A kinetic isotope effect (KIE) of $k_{\text{H}}/k_{\text{D}} = 5.8(5)$, measured using the analogous palladium deuteride complex, (^tBuPCP)PdD, implicated the breaking of the Pd–H bond in the rate-determining step of the reaction.

The unsaturated nature of the square planar d⁸ palladium(II) center in the starting hydride could allow molecular oxygen to bind prior to insertion. In this way, a pathway similar to CO migratory insertion could be envisioned. However, computations found no evidence for such coordination of molecular oxygen to the open site at palladium [57]. Instead, a weak interaction between the hydride and free O₂ occurred. This interaction initiated an elongation of the Pd–H bond, which ultimately resulted in the breaking of the Pd–H bond and formation of an O–H bond (Figure 11.1). The resulting [•]OOH fragment then rapidly recombined with the Pd[•] to form the Pd–OOH product. This pathway has been referred to as a *hydrogen*

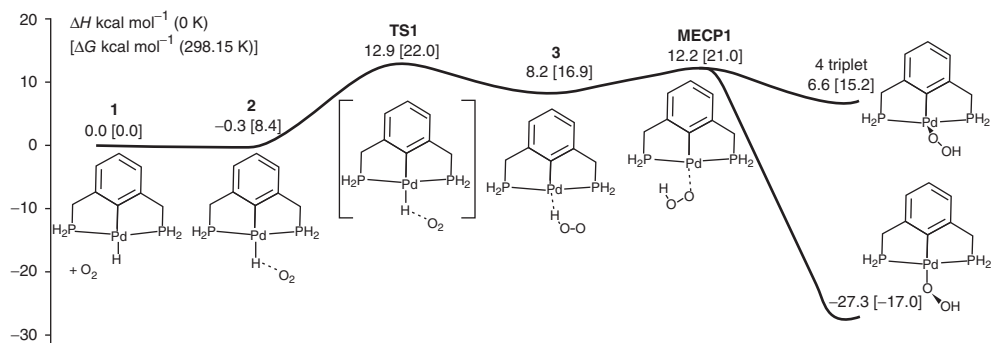
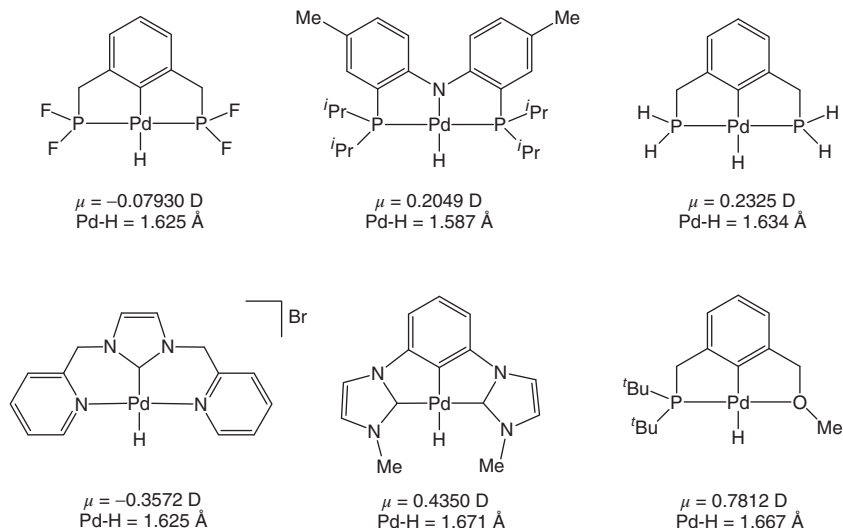


Figure 11.1 Computed reaction coordinate for the insertion of O_2 into the $Pd^{II}-H$ bond of the pincer complex $(PCP)PdH$ [57]. (Reprinted with permission from [57]. Copyright 2006, American Chemical Society.)

atom abstraction (HAA) pathway because the hydrogen atom is formally abstracted from the palladium by the oxygen. A similar type of insertion mechanism was recently proposed for an $Ir^{III}-H$ molecular oxygen reaction [49, 62]. As described below, a key factor in the ease of this reaction for $(^{i}Bu)PCP)PdH$ appears to be the strong trans donor ability of the aryl within the pincer ligand.

Notably, insertion of molecular oxygen into a $Pd^{II}-H$ bond in which the ancillary ligand was not a pincer was observed by Stahl [63–66]; however, a very different mechanism was found in this system. The biscarbene complex *trans*- $(IMes)_2Pd(H)(X)$ ($X = O_2CAR$) was reported to insert molecular oxygen by a pathway involving HX reductive elimination (HXRE), followed by O_2 coordination, and finally protonation of the Pd^0 peroxo complex to form the final *trans*- $(IMes)_2Pd(OOH)(X)$ species. Following these initial results, the Stahl group [66] reported a Hammett study of the reaction, wherein they investigated substitution of the benzoate ligand in the para position. They found that, by increasing the electron-donating ability of the ligand trans to the hydride, a mechanistic crossover from an HXRE pathway to an HAA pathway was observed. In essence, a strong trans donor promotes an HAA pathway for the insertion of molecular oxygen into the $Pd-H$ bond.

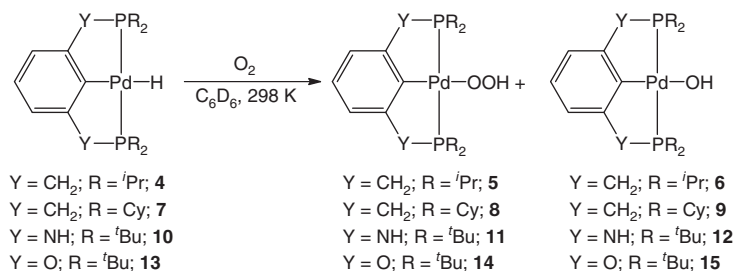
The initial experimental results of O_2 insertions were followed with computational studies of pincer ligated $Pd^{II}-H$ complexes [58]. Both the $Pd-H$ dipoles and the $Pd-H$ bond lengths were evaluated for a series of complexes with varying pincer donor atoms (CNC, NNN, PNP, PPP, PCP, NCN, SCS, PCN, CCC, PCO, PSiP, and OCO). Of the 49 complexes evaluated for O_2 insertion, 6 were chosen for detailed reaction coordinate calculations (Scheme 11.6). The six compounds spanned a range of calculated $Pd-H$ bond dipoles, μ , found by multiplying the differences in atomic charge between the palladium and hydride by the bond length. No correlation between $Pd-H$ bond dipole and transition state energy was found, indicating that a proton abstraction mechanism was unlikely. Instead, a correlation between $Pd-H$ bond lengths and the transition state energy was noted. An inverse relationship was revealed: as the bond length increased, the transition state barrier



Scheme 11.6 Compounds chosen for reaction coordinate study based on CHELPG-charge derived palladium(II) hydride bond dipole [58, 67].

decreased. This dependence of the reaction facility on palladium hydride bond length supports the HAA mechanism and also emphasizes the importance of a strong trans donor.

A series of pincer ligated palladium(II) complexes containing a strong σ -donor aryl ring trans to the hydride were examined experimentally for their O_2 reactivity (Scheme 11.7). The palladium(II) hydride complexes of $^i\text{PrPCP}$ (2,6-bis(di i propylphosphino)methylbenzene) [55], $^{\text{Cy}}\text{PCP}$ (2,6-bis(dicyclohexylphosphino)methylbenzene) [55], PNCNP (2,6-bis(di t butylphosphino)aminobenzene) [56], and POCOP (2,6-bis(di t butylphosphino)oxybenzene) [56] were synthesized and were each exposed to molecular oxygen. The isopropyl and cyclohexyl analogs of **1** were found to react similar to **1**, each producing the corresponding hydroperoxide in good yield [55]. For example, with 3.4 atm of O_2 at room temperature, 50% of the ($^i\text{PrPCP}$)Pd-H **4** reacted to form the hydroperoxide



Scheme 11.7 Insertion of O_2 into $\text{Pd}^{\text{II}}\text{-H}$ bonds of pincer complexes containing aryl backbones [55, 56].

($i\text{Pr}$ PCP)Pd–OOH **5** (40%) and hydroxide ($i\text{Pr}$ PCP)Pd–OH **6** (10%) complexes within 20 min. The reaction of the pincer bearing nitrogen bridges in the backbone, PNCNP complex **10**, with 7 atm of O_2 went to completion in 1 h, forming the corresponding hydroperoxide and hydroxide complexes (PNCNP)PdOOH (**11**) and (PNCNP)PdOH (**12**), respectively [56]. While this reaction occurred at a similar rate as that of **1**, the stability of the product species was greatly reduced compared to **1**, and further decomposition to intractable products was observed in a span of 10 h. The oxygen-bridged complex **13** reacted considerably more slowly with oxygen when compared to **1** or the PNCNP derivative **10**. With 7 atm of molecular oxygen, nearly 10 h was required to produce the corresponding hydroperoxide and hydroxide, (POCOP)PdOOH (**14**) and (POCOP)PdOH (**15**), respectively. Perhaps because of the longer reaction times, the product mixtures after complete conversion of the starting hydride **13** contained a large amount of palladium hydroxide **15** (about 25%). When a sample of **13** was pressurized with only 1 atm of O_2 , the only product that was observed was the hydroxide **15**. It appeared that the hydroperoxide species **14** was reasonably unstable, and decomposed to the hydroxide **15** at a similar rate as its formation under 1 atm of O_2 . Similar to the PNCNP system, the completed reaction mixture was monitored over 10 h and further decomposition to intractable products was observed.

The O_2 reactivity of the analogous platinum complex ($t\text{Bu}$ PCP)PtH [68] (**16**) was also investigated [56]. When a solution of **16** in C_6D_6 was subjected to O_2 pressures up to 7 atm at room temperature, no evidence of any reaction was detected. Heating of the reaction mixture to 100 °C yielded no reaction over 3 days, and further heating to 125 °C ultimately yielded degradation of **16**, with no hydroxo or hydroperoxo species ever observed. Thus, while the *trans*-aryl group of the ($t\text{Bu}$ PCP) ligand is a strong enough donor to promote the insertion of molecular oxygen into the palladium hydride of **1**, the greater strength of the platinum(II) hydride bond appears to inhibit a similar reaction for **16**. In contrast to the platinum complex, (R PCP)NiH ($\text{R} = i\text{Pr}, \text{Cy}$) complexes reacted quickly with molecular oxygen at room temperature [55]. Within minutes, multiple unidentified products were observed by NMR spectroscopy, as well as signal broadening, presumably from paramagnetic species. No Ni(II) hydroperoxide species were isolated or observed in these reactions. It was proposed that the (R PCP)NiH complexes reacted with molecular oxygen to produce highly reactive Ni–OOH species that quickly decomposed into intractable products. Analysis of the reaction mixtures by GC/MS showed evidence for acetone when $\text{R} = i\text{Pr}$, and cyclohexanone when $\text{R} = \text{Cy}$. It was suggested that a Ni–OOH species was generated and was responsible for oxidation of the pincer ligand substituents, as no degradation was observed when the analogous Ni^{II}–Cl complexes were exposed to O_2 . A similar trend, with respect to Ni, Pd, and Pt, was found in a series of group 10 hydrides employing an anionic asymmetric PhPNP^{R} pincer ligand based on a bis(tolyl)amine framework ($\text{R} = i\text{Pr}, \text{Cy}$) [69]. While the hydride (PhPNP^{R})NiH reacted very quickly with O_2 to form intractable products, the Pd^{II} analog was found to react over a day with O_2 (5 atm) to form (PhPNP^{R})PdOOH and (PhPNP^{R})PdOH complexes. Similar to observations with ($t\text{Bu}$ PCP)PtH, the platinum analog (PhPNP^{R})PtH showed no reactivity with O_2 over several days.

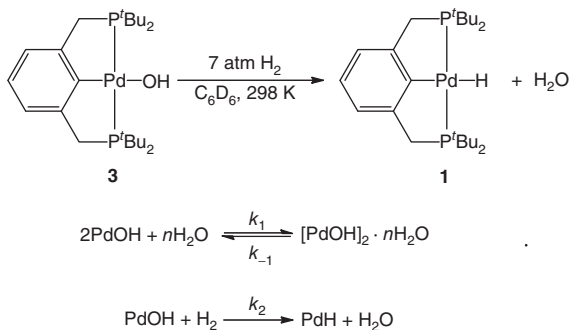
Notable in the reactions discussed above involving hydride complexes of palladium, nickel, and platinum is that no cooperative reactivity of the pincer ligands with molecular oxygen was observed. The structure of the pincer ligands presented is presumably important in promoting reaction at the M–H bond (e.g., trans influence of the aryl group) and also in inhibiting reactions of the ligands directly with molecular oxygen. Previous studies of molecular oxygen reactions involving five-coordinate platinum(IV) species with anionic bidentate ligands were shown to be susceptible to backbone oxidation by formal cycloaddition [70, 71]. Other small molecule activations through metal–ligand cooperativity have been observed by systems with similar reactive sites in the backbone of pincer ligands [5, 72, 73]. Thus, the choice of the pincer ligand will be critical to promoting specific reactions of metal centers with molecular oxygen. Pincer ligands lacking basic sites in the backbone and bearing a strong central donor atom are likely to be the most favorable for directing the insertion of molecular oxygen into a late-transition metal hydride bond.

11.3

Hydrogenolysis of Late-Transition Metal Hydroxide and Alkoxide Complexes

Hydrogenolysis of a palladium hydroxide species would release water and generate a palladium hydride complex, while hydrogenolysis of a palladium alkoxide would release an alcohol. Notably, hydrogenolysis of a M–O bond is the catalyst regeneration step in Wenzel's proposed catalytic cycle for olefin epoxidation [32]. A hydrogenolysis reaction wherein a metal hydride is generated from a metal hydroxide or metal alkoxide could also serve as a general catalyst regeneration step for other transformations. However, there are few well-characterized examples of this fundamental reaction in the literature. This scarcity may be due in part to the paucity of mononuclear hydroxide and alkoxide complexes of the late metals [74–76]. The tridentate design and the stability of the pincer motif has allowed the isolation and study of such mononuclear complexes of late transition metals [38, 59, 77–79]. The hydrogenolysis reactions of (^tBuPCP)PdOR (R = H, Me, Ph, Np, CH₂CF₃, CH₂CHF₂, and CH₂CH₂F) [38] and (PCO)PdOH (^tBuPCO, 2-(di^tbutylphosphino)methyl-6-(methoxy)methylbenzene) [59] have been investigated and mechanisms for these reactions have been proposed.

Upon pressurization of a solution of the palladium hydroxide complex (^tBuPCP)Pd–OH (**3**) in C₆D₆ with 7 atm of H₂ at room temperature, quantitative conversion to the Pd–H complex **1** was observed over 60 h (Scheme 11.8) [37, 38]. Unusual kinetics were observed for this reaction as the reaction rate was first order in [H₂] but only half-order in [**3**] [38]. Well-behaved kinetic behavior was also observed only when the reaction was carried out in the presence of an excess of water. Notably, water was found to inhibit the reaction rate and, with water being a product of the reaction, it was important to keep the concentration of water constant through the use of an excess of water. It was initially thought that the inhibition by water was due to an equilibrium effect, essentially pushing



Scheme 11.8 Hydrogenolysis of $(t\text{BuPCP})\text{PdOH}$ (**3**) [38]. (Adapted with permission from [38]. Copyright 2011, American Chemical Society.)

the reaction backwards toward palladium hydroxide. However, it was later determined that the half-order term with respect to **3** and the effect of water on the reaction could be explained by the formation of a water-bridged dimer of **3**. X-ray structures of both the monomeric Pd–OH **3** and a water-bridged dimer (grown in the presence of water) were also reported (Figure 11.2) [38, 80]. Under the reaction conditions, an equilibrium between the water-bridged dimer and the monomer was established. The kinetic behavior was shown to be consistent with hydrogenolysis occurring by reaction of the monomeric species **3** with hydrogen.

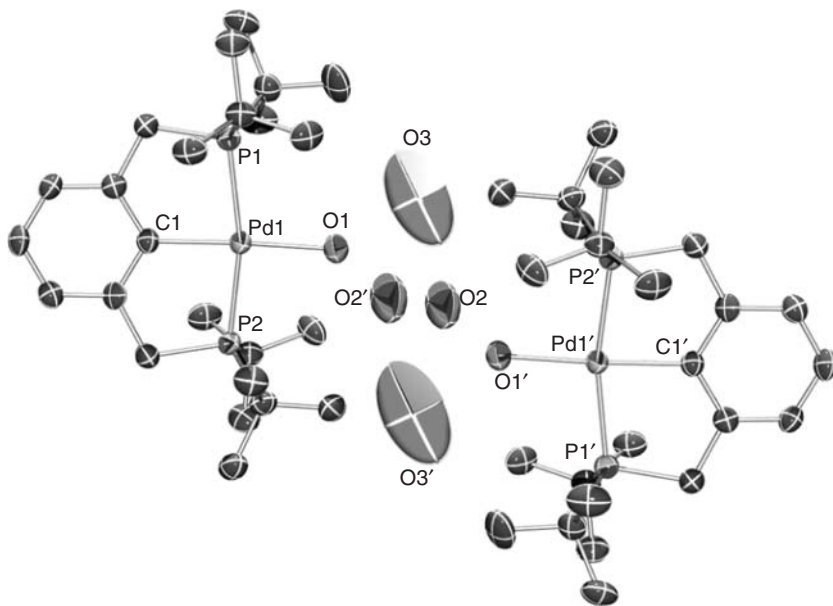
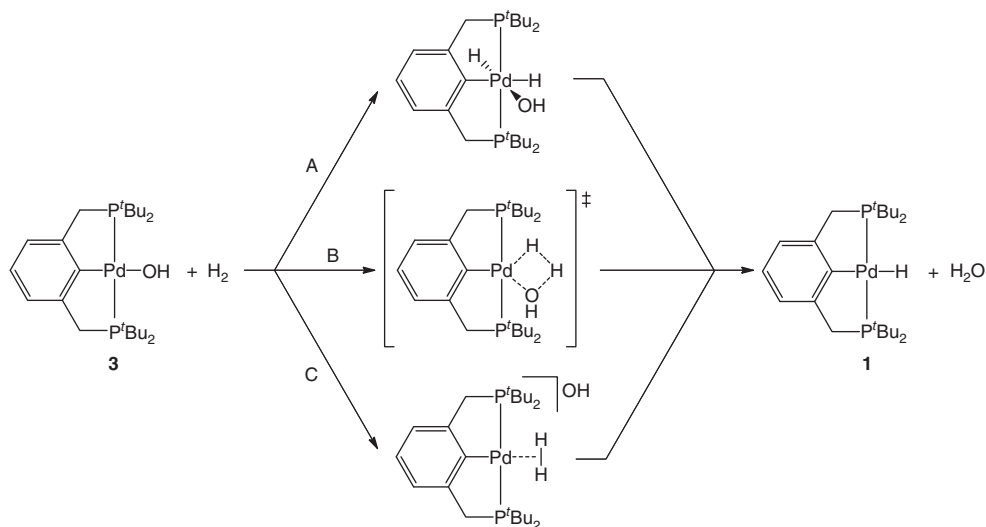


Figure 11.2 Single-crystal structure of the water-bridged dimer of **3**. Ellipsoids are shown at 50% probability, and hydrogen atoms are omitted for clarity [38, 80]. (Adapted with permission from [38]. Copyright 2011, American Chemical Society.)

Several mechanisms were proposed for the actual hydrogenolysis of the monomeric Pd–OH complex **3**: (A) oxidative addition of hydrogen, (B) a four-centered transition state with an intramolecular proton transfer (internal electrophilic substitution, IES) [81, 82], or (C) the deprotonation of a four-coordinate dihydrogen complex by dissociated hydroxide (Scheme 11.9) [38]. With excess water slowing the rate of hydrogenolysis, a mechanism involving dissociation of hydroxide (path C) was considered unlikely. No experimental evidence was available to distinguish between paths A and B. The results of density functional theory (DFT) computations at the B3LYP/LACVP** level of theory on this ^tBuPCP–Pd system supported that the reaction proceeds via the four-centered transition state shown in path B ($\Delta G^\ddagger = 25.7 \text{ kcal mol}^{-1}$). Oxidative addition of hydrogen to produce the Pd(IV) intermediate ($\Delta G = 40.9 \text{ kcal mol}^{-1}$) shown in Scheme 11.9 was far too high in energy.



Scheme 11.9 Possible mechanistic pathways for the hydrogenolysis of **3** [38]. (Adapted with permission from [38]. Copyright 2011, American Chemical Society.)

To complement the PCP work described above, further calculations were performed to examine the effects of commonly used donor atoms other than phosphorus cis to the palladium–hydride bond [58]. Neutral two-electron donor atoms or groups investigated included nitrogen (NCN), sulfur (SCS), heterocyclic carbenes (CCC), and ethers (OCO). Consistent with the results found with ^tBuPCP, in all cases the IES pathway B was significantly favored over the oxidative addition route A. Quite interestingly, in the case of the less strongly bound OCO ligand (hemilabile ether groups), an IES transition state could not be located. Rather, the calculations found hydrogenation across the Pd–OH bond with concomitant dissociation of a pincer ether arm. This difference in reactivity between ligands

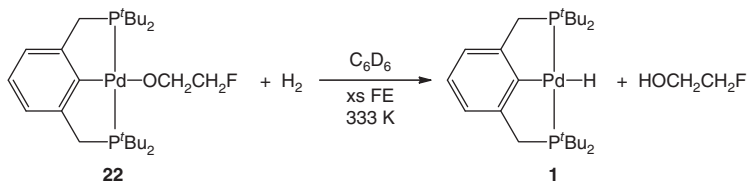
with and without hemilabile groups foreshadowed the unexpected experimental reactivity seen using the related hemilabile PCO ligand (see below).

The strongly binding $^t\text{BuPCP}$ pincer ligand also provided the opportunity to study the mechanism of hydrogenolysis of palladium alkoxide complexes [38]. Hydrogenolysis would yield an alcohol and generate a metal hydride, a reaction that could potentially be incorporated as a catalyst regeneration step in the production of alcohols. Without the tridentate chelation of the pincer ligand, β -hydride elimination might be expected to be favored over the proposed hydrogenolysis. The hydrogenolysis of the simple methoxide analog of **3**, $(^t\text{BuPCP})\text{PdOCH}_3$ (**17**), was investigated. Under a pressure of 7 atm of H_2 , a solution of **17** in C_6D_6 converted to **1** and methanol in high yield (96%) over a period of 3 days. However, kinetic studies of this reaction were complicated by a hydrolysis reaction wherein adventitious water resulted in the formation of **3** and methanol. Attempts to minimize the hydrolysis reaction by adding methanol to shift the equilibrium back toward **17** led instead to alcohol-assisted dissociative β -hydride abstraction (DBHA) [83]. Thus, the pincer ligand was able to adequately protect the complex from ancillary ligand loss which led to β -hydride elimination, but the propensity of the alkoxide to dissociate in the presence of alcohol promoted the DBHA pathway.

Further studies of Pd-OR hydrogenolysis were conducted with $-\text{OR}$ substituents lacking β -hydrogens to prevent any complications due to DBHA. The phenoxide and neopentoxide analogs $(^t\text{BuPCP})\text{PdOPh}$ (**18**) and $(^t\text{BuPCP})\text{PdONp}$ (**19**) were synthesized and their reactions with hydrogen studied. The phenoxide **18** was found to be resistant not only to DBHA (lacking any β -hydrogens) but also to hydrolysis. Unfortunately, the hydrogenolysis reaction was thermodynamically unfavored. Under conditions of 7 atm of hydrogen in a C_6D_6 solution at room temperature, the hydrogenolysis of **18** to the hydride **1** only proceeded to 20% conversion. The thermodynamics of this reaction was convincingly demonstrated by the reaction of phenol with the palladium hydride **1** which proceeded to form the palladium phenoxide **18** and H_2 . The difference in the thermodynamics of the reaction compared to that of the hydrogenolysis of the palladium methoxide was explained by the difference of the $\text{p}K_{\text{a}}$ of phenol versus methanol. Surprisingly, the neopentoxide analog **19** also did not undergo hydrogenolysis under 7 atm of H_2 , even after heating above 100°C . In this case, the steric bulk about the Pd(II) center was proposed to hinder the four-centered transition state postulated for the less hindered hydroxide and methoxide complexes **3** and **17**, respectively.

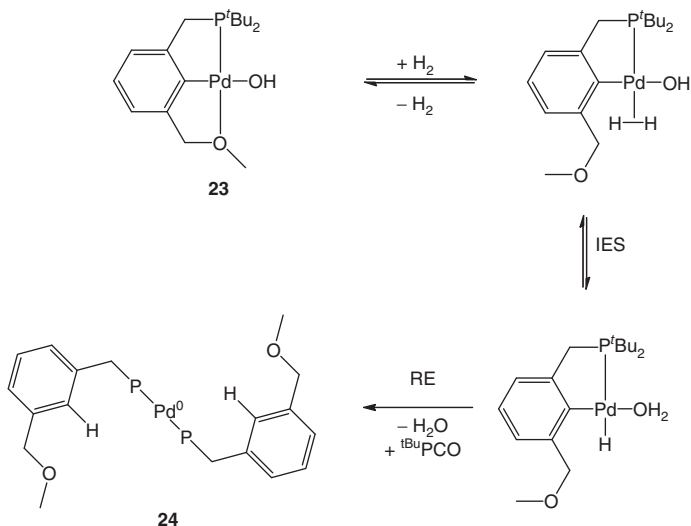
The hydrogenolysis of pincer palladium alkoxide complexes containing electron-withdrawing fluorine groups was also investigated. The fluorinated ethoxide ligands were expected to disfavor the DBHA decomposition pathway [84]. Unfortunately, the more heavily fluorinated derivatives 2,2,2-trifluoroethanol ($\text{p}K_{\text{a}} = 12.4$) and 2,2-difluoroethanol ($\text{p}K_{\text{a}} = 13.3$) were acidic enough to make the thermodynamics of hydrogenolysis unfavorable [85]. Addition of either of these alcohols to the hydride **1** led to complete conversion to hydrogen and the alkoxy species $(^t\text{BuPCP})\text{PdOCH}_2\text{CF}_3$ (**20**) or $(^t\text{BuPCP})\text{PdOCH}_2\text{CHF}_2$ (**21**) [38]. However, the monofluorinated species $(^t\text{BuPCP})\text{PdOCH}_2\text{CH}_2\text{F}$ (**22**) was found to be stable to both hydrolysis and DBHA decomposition, and susceptible to hydrogenolysis in excess 2-fluoroethanol (FE)

(Scheme 11.10). Kinetic studies found that the hydrogenolysis reaction was first order in both [22] and $[H_2]$. A mechanism similar to that proposed for the hydrogenolysis of the hydroxide **3** was then invoked for the hydrogenolysis of the pincer palladium alkoxide complexes.



Scheme 11.10 Hydrogenolysis of $(t\text{BuPCP})\text{PdOCH}_2\text{CH}_2\text{F}$ (**22**) [38].

The importance of a strongly binding pincer system in these hydrogenolysis reactions became evident when the reaction of H_2 with $(t\text{BuPCO})\text{PdOH}$ (**23**), a complex bearing a hemilabile pincer, was studied [59]. In contrast to the reaction of $(t\text{BuPCP})\text{PdOH}$ (**3**) with H_2 , exposure of **23** to 7 atm of H_2 at room temperature did not yield a palladium(II) hydride product. Instead, a palladium(0) bisphosphine complex (**24**) was formed as shown in Scheme 11.11. The difference in reactivity between the two palladium hydroxide complexes was attributed to the hemilabile ether arm, which can dissociate allowing the operation of other reaction pathways. Following deuterium labeling studies, it was proposed that the reaction of **23** with H_2 likely operates by displacement of the ether arm by dihydrogen, followed by IES. Reductive elimination of the aryl and the hydride ligands leads to palladium(0)



Scheme 11.11 Possible mechanism for the decomposition of $(t\text{BuPCO})\text{PdOH}$ (**23**) to $(t\text{BuPCO})_2\text{Pd}^0$ (**24**) under 7 atm of H_2 [59]. (Adapted with permission from [59]. Copyright 2011, American Chemical Society.)

(Scheme 11.11). As both palladium black and free ligand are observed in this reaction, it was proposed that the monophosphine palladium(0) species binds an additional $^t\text{BuPCO}$ ligand to form the observed product. The identity of the product ($^t\text{BuPCO}$)₂Pd⁰ (**24**) was confirmed by independent synthesis. Note that this different behavior of a hemilabile ligand in a hydrogenolysis reaction was also found computationally (see above).

11.4

Summary

The pincer ligand framework provides a powerful motif for the stabilization of late-transition metal complexes. The rigid tridentate design has allowed detailed studies of the insertion of molecular oxygen into palladium hydride bonds to form palladium hydroperoxide moieties and of hydrogenolysis reactions of palladium hydroxide and alkoxide bonds to regenerate palladium hydrides. Both these reaction classes are potential key players in methods for the selective partial oxidation of organics. For example, a pathway for olefin epoxidation is proposed to involve insertion of molecular oxygen into a late-transition metal hydride bond to produce a late-metal hydroperoxide species. Following transfer of the oxygen to the olefin substrate, hydrogenolysis of the resulting late-metal hydroxide would regenerate the metal hydride complex. The cycle as pictured in Scheme 11.3 for a square-planar d^8 metal center involves using only one site in the square plane for reactions. The system is perfectly set up for a pincer ligand design that protects the metal center by strongly binding to the three remaining sites.

As detailed above, a strong trans influence donor in the central site of the pincer lengthens the palladium hydride bond, making it more susceptible to insertion of molecular oxygen via an HAA pathway. Hydrogenolysis of palladium hydroxide and alkoxide complexes are proposed to operate through a four-centered transition state by an IES pathway. The strongly coordinating tridentate structure of the pincer ligand is key to preventing alternative decomposition pathways. Of note is the fact that the hydrogenolysis of alkoxide complexes can be complicated by competitive hydrolysis and DBHA pathways that can operate even with the strongly binding pincer ligand motif. Overall, the pincer ligands through their stabilization of the reactants and products have allowed the detailed mechanistic study of the reactions of late-metal complexes with molecular oxygen and hydrogen. The robust nature of these ligands in turn will allow them to be incorporated into catalytic cycles to accomplish such challenging reactions as organic oxidations using molecular oxygen.

Acknowledgment

We thank the Department of Energy (DE-FG02-06ER15765) for support.

References

- van der Boom, M.E. and Milstein, D. (2003) *Chem. Rev.*, **103**, 1759.
- Singleton, J.T. (2003) *Tetrahedron*, **59**, 1837.
- Benito-Garagorri, D. and Kirchner, K. (2008) *Acc. Chem. Res.*, **41**, 201.
- Milstein, D. (2010) *Top. Catal.*, **53**, 915.
- Gunanathan, C. and Milstein, D. (2011) *Acc. Chem. Res.*, **44**, 588.
- Niu, J.-L., Hao, X.-Q., Gong, J.-F., and Song, M.-P. (2011) *Dalton Trans.*, **40**, 5135.
- Albrecht, M. and Lindner, M.M. (2011) *Dalton Trans.*, **40**, 8733.
- Haibach, M.C., Kundu, S., Brookhart, M., and Goldman, A.S. (2012) *Acc. Chem. Res.*, **45**, 947.
- St John, A., Goldberg, K.I., and Heinekey, D.M. (2013) *Top. Organomet. Chem.*, **40**, 271.
- Van Koten, G. and Milstein, D. (eds) (2013) *Organometallic Pincer Chemistry*, Topics Organometallic Chemistry, vol. **40**, Springer, Heidelberg.
- Roddick, D.M. (2013) *Top. Organomet. Chem.*, **40**, 49.
- Albrecht, M. and van Koten, G. (2001) *Angew. Chem. Int. Ed.*, **40**, 3750, and references therein.
- Arndtsen, B.A., Bergman, R.G., Mobley, T.A., and Peterson, T.H. (1995) *Acc. Chem. Res.*, **28**, 154.
- Stahl, S.S. (2005) *Science*, **309**, 1824.
- Stahl, S.S. (2004) *Angew. Chem. Int. Ed.*, **43**, 3400.
- Wu, W. and Jiang, H. (2012) *Acc. Chem. Res.*, **45**, 1736.
- Punniyamurthy, T., Velusamy, S., and Iqbal, J. (2005) *Chem. Rev.*, 2329.
- McCoy, M. (2001) *Chem. Eng. News*, **43**, 19.
- Mills, G.A. (1994) *Catal. Today*, **22**, 179.
- Boisvert, L. and Goldberg, K.I. (2012) *Acc. Chem. Res.*, **45**, 899.
- Cavani, F. and Teles, J.H. (2009) *ChemSusChem*, **2**, 508.
- Monnier, J.R. (2001) *Appl. Catal. A*, **221**, 73.
- Strukul, G. and Michelin, R.A. (1984) *J. Chem. Soc., Chem. Commun.*, 1538.
- Strukul, G. and Michelin, R.A. (1985) *J. Am. Chem. Soc.*, **107**, 7563.
- Sgarbossa, P., Scarso, A., Strukul, G., and Michelin, R.A. (2012) *Organometallics*, **31**, 1257.
- Sheldon, R.A. (1980) *J. Mol. Catal.*, **7**, 107.
- Katsuki, T. and Sharpless, K.B. (1980) *J. Am. Chem. Soc.*, **102**, 5974.
- Zhang, W., Loebach, J.L., Wilson, S.R., and Jacobsen, E.N. (1990) *J. Am. Chem. Soc.*, **112**, 2801.
- De Vos, D.E., Sels, B.F., and Jacobs, P.A. (2003) *Adv. Synth. Catal.*, **345**, 457.
- Mizuno, N., Yamaguchi, K., and Kamata, K. (2005) *Coord. Chem. Rev.*, **249**, 1944.
- Sumitomo Chemical Co., Ltd (2006) Development of New Propylene Oxide Process, Vol. 2006-I.
- Wenzel, T.T. (1991) *Stud. Surf. Sci. Catal.*, **66**, 545.
- Böhler, C., Avarvari, N., Schönberg, H., Wörle, M., Rügger, H., and Grützmacher, H. (2001) *Helv. Chim. Acta*, **84**, 3127.
- Thompson, J.S., Randall, S.L., and Atwood, J.D. (1991) *Organometallics*, **10**, 3906.
- Thompson, J.S., Bernard, K.A., Rappoli, B.J., and Atwood, J.D. (1990) *Organometallics*, **9**, 2727.
- Goeden, G.V. and Caulton, K.G. (1981) *J. Am. Chem. Soc.*, **103**, 7354.
- Fulmer, G.R., Muller, R.P., Kemp, R.A., and Goldberg, K.I. (2009) *J. Am. Chem. Soc.*, **131**, 1346.
- Fulmer, G.R., Herndon, A.N., Kaminsky, W., Kemp, R.A., and Goldberg, K.I. (2011) *J. Am. Chem. Soc.*, **133**, 17713.
- Bayson, J.H. and Winfield, M.E. (1964) *J. Catal.*, **3**, 123.
- Roberts, H.L. and Symes, W.R. (1968) *J. Chem. Soc. A*, 1450.
- Johnston, L.E. and Page, J.A. (1969) *Can. J. Chem.*, **47**, 4241.
- Gillard, R.D., Heaton, B.T., and Vaughan, D.H. (1970) *J. Chem. Soc. A*, 3126.

43. Endicott, J.F., Wong, C.L., Inoue, T., and Natarajan, P. (1979) *Inorg. Chem.*, **18**, 450.
44. Wick, D.D. and Goldberg, K.I. (1999) *J. Am. Chem. Soc.*, **121**, 11900.
45. Thyagarajan, S., Incarvito, C.D., Rheingold, A.L., and Theopold, K.H. (2001) *Chem. Commun.*, 2198.
46. Gligorich, K.M. and Sigman, M.S. (2006) *Agnew. Chem. Int. Ed.*, **45**, 6612.
47. Denney, M.C., Smythe, N.A., Cetto, K.L., Kemp, R.A., and Goldberg, K.I. (2006) *J. Am. Chem. Soc.*, **128**, 2508.
48. Lansing, R.B. Jr., Goldberg, K.I., and Kemp, R.A. (2011) *Dalton Trans.*, **40**, 8950.
49. Heiden, Z.M. and Rauchfuss, T.B. (2007) *J. Am. Chem. Soc.*, **129**, 14303.
50. Szajna-Fuller, E. and Bakac, A. (2010) *Inorg. Chem.*, **49**, 781.
51. Look, J.L., Wick, D.D., Mayer, J.M., and Goldberg, K.I. (2009) *Inorg. Chem.*, **48**, 1356.
52. Teets, T.S., Cook, T.R., McCarthy, B.D., and Nocera, D.G. (2011) *J. Am. Chem. Soc.*, **133**, 8114.
53. Teets, T.S. and Nocera, D.G. (2011) *J. Am. Chem. Soc.*, **133**, 17796.
54. Keith, J.M., Teets, T.S., and Nocera, D.G. (2012) *Inorg. Chem.*, **51**, 9499.
55. Boro, B.J. (2009) Investigations of Pincer-Ligated Transition Metal Complexes for the Activation of Molecular Oxygen. PhD Dissertation. University of New Mexico.
56. Fulmer, G.R. (2010) Investigations of Palladium Pincer Complexes Towards a Catalytic Olefin Epoxidation Process. PhD Dissertation. University of Washington.
57. Keith, J.M., Muller, R.P., Kemp, R.A., Goldberg, K.I., Goddard, W.A. III, and Oxgaard, J. (2006) *Inorg. Chem.*, **45**, 9631.
58. Parkes, M.V. (2012) A Proposed Palladium-Catalyzed Cycle for the Epoxidation of Alkenes. PhD Dissertation. University of New Mexico;
59. Fulmer, G.R., Kaminsky, W., Kemp, R.A., and Goldberg, K.I. (2011) *Organometallics*, **30**, 1627.
60. Roberts, H.L. and Symes, W.R. (1968) *J. Chem. Soc. A*, 1450.
61. Johnston, L.E. and Page, J.A. (1969) *Can. J. Chem.*, **47**, 4241.
62. Chowdhury, S., Himo, F., Russo, N., and Sicilia, E. (2010) *J. Am. Chem. Soc.*, **132**, 4178.
63. Konnick, M.M., Gandhi, B.A., Guzei, I.A., and Stahl, S.S. (2006) *Angew. Chem. Int. Ed.*, **45**, 2904.
64. Popp, B.V. and Stahl, S.S. (2007) *J. Am. Chem. Soc.*, **129**, 4410.
65. Konnick, M.M. and Stahl, S.S. (2008) *J. Am. Chem. Soc.*, **130**, 5753.
66. Konnick, M.M., Decharin, N., Popp, B.V., and Stahl, S.S. (2011) *Chem. Sci.*, **2**, 326.
67. Breneman, C.M., Wiberg, K.B. (1990) *J. Comput. Chem.*, **11**, 361.
68. Kimmich, B.F.M. and Bullock, R.M. (2002) *Organometallics*, **21**, 1504.
69. Lansing, R.B. Jr., Goldberg, K.I., and Kemp, R.A. (2011) *Dalton Trans.*, **40**, 8950.
70. Scheuermann, M.L., Fekl, U., Kaminsky, W., and Goldberg, K.I. (2010) *Organometallics*, **29**, 4749.
71. Grice, K.A., Scheuermann, M.L., and Goldberg, K.I. (2011) *Top. Organomet. Chem.*, **35**, 1.
72. Schwartsburd, L., Iron, M.A., Konstantinovski, L., Ben-Ari, E., and Milstein, D. (2011) *Organometallics*, **30**, 2721.
73. Vogt, M., Rivada-Wheelaghan, O., Iron, M.A., Leitus, G., Diskin-Posner, Y., Shimon, L.J.W., Ben-David, Y., and Milstein, D. (2013) *Organometallics*, **13**, 300.
74. Bryndza, H.E. and Tam, W. (1988) *Chem. Rev.*, **88**, 1163.
75. Fulton, J.R., Holland, A.W., Fox, D.J., and Bergman, R.G. (2002) *Acc. Chem. Res.*, **35**, 44.
76. Roesky, H.W., Singh, S., Yusuff, K.K.M., Maguire, J.A., and Hosmane, N.S. (2006) *Chem. Rev.*, **106**, 3813.
77. Johansson, R. and Wendt, O.F. (2007) *Organometallics*, **26**, 2426.
78. Arunachalampillai, A., Loganathan, N., and Wendt, O.F. (2012) *Polyhedron*, **32**, 24.
79. Kloek, S.M., Heinekey, D.M., and Goldberg, K.I. (2007) *Agnew. Chem. Int. Ed.*, **46**, 4736.

80. Johansson, R., Öhrström, L., and Wendt, O.F. (2007) *Cryst. Growth Des.*, **7**, 1974.
81. Cundari, T.R., Grimes, T.V., and Gunnoe, T.B. (2007) *J. Am. Chem. Soc.*, **129**, 13172.
82. Oxgaard, J., Tenn, W.J. III, Nielsen, R.J., Periana, R.A., and Goddard, W.A. III, (2007) *Organometallics*, **26**, 1565.
83. Smythe, N.A., Grice, K.A., Williams, B.S., and Goldberg, K.I. (2009) *Organometallics*, **28**, 277.
84. Smith, M.B. and March, J. (2001) *March's Advanced Organic Chemistry: Reactions, Mechanisms, and Structure*, 5th edn, John Wiley & Sons, Inc., New York, p. 1176.
85. Ballinger, P. and Long, F.A. (1960) *J. Am. Chem. Soc.*, **82**, 795.

Index

a

- acetoxylation 109–111
- alkenes
 - arylation 107–109
 - C–H borylation 112–114
- allyl acetates arylation 108
- amides synthesis 15
 - from alcohols and amines 15–18
 - from esters and amines 18–20
 - polyamides synthesis from diols and diamines 20–24
- ammonia activation 217–218
- appended functionality 71
 - coplanar with pincer chelate
 - pyridine-2,6-dicarboxamide systems 84–85
 - systems incorporating 2,2':6',2''-terpyridine 75–84
- design criteria 72
 - supramolecular architectures 73–75
 - transition-metal catalysis 72–73
- not coplanar to pincer chelate
 - ENE pincer systems 86–87
 - PCP pincer systems 88
 - PEP pincer systems 88–90
 - pyridine-2,6-diimine systems 90–91
- atom-transfer radical addition (ATRA) and polymerization reactions (ATRP) 46–48
- carbon–heteroatom coupling reactions 62–65
- C–C cross-coupling reactions 54–62
- Heck reaction 48–54

b

- benzyl amine synthesis 103, 105–107
- bond activation by metal–ligand cooperation 3–4

c

- carbometallated PC(sp³) P complexes
 - synthesis and coordination behavior 215–216
- acyclic PC(sp³) P complexes coordination flexibility 216–217
- carbon–carbon bond-forming reactions 141–142
 - Kumada–Corriu–Tamao coupling 118–129
 - Mizoroki–Heck reaction 140
 - Negishi coupling 132–139
 - Sonogashira coupling 139
 - Suzuki–Miyaura coupling 129–132
- carbon–carbon coupling reactions 221–223
- carbondioxide
 - activation 225
 - reduction with trialkylsilanes 174
- carbon–heteroatom
 - bond-forming reactions 143–144
 - coupling reactions 62–65
- catalysis, by pincer complexes 1–2
 - amides synthesis 15
 - from alcohols and amines 15–18
 - from esters and amines 18–20
 - polyamides synthesis from diols and diamines 20
- bond activation by metal–ligand cooperation 3–4
- esters synthesis 4
 - cross-esters synthesis from primary and secondary alcohols 9–11
 - polyesters synthesis from diols 11, 13–15
 - from primary alcohols 4–9
 - by secondary alcohols acylation 9, 11–13
- peptides synthesis from β-amino alcohols 24–26

- C–C, C–O, and C–B bond formation 95–96
- C–H functionalization of organonitriles
 - – benzyl amine synthesis 103, 105–107
 - – imines allylation 102–105
 - hypervalent iodines reactions 107
 - – acetoxylation 109–111
 - – alkenes arylation 107–109
 - – alkenes C–H borylation 112–114
 - imines and isocyanoacetates reactions
 - – chiral pincer complexes application 99–100
 - – imidazolines stereoselective synthesis 96–99
 - – mechanistic considerations 101–102
 - C–C cross-coupling reactions 54–62
 - cyclic peptides 24–25
- d**
- dehydrogenative borylation 237
 - of alkenes and 1,3-dienes 237–239
 - mechanistic considerations 239–241
 - dendritic effect 48
 - density function theory (DFT) studies 159, 167, 172, 259–261, 264, 269, 272
- e**
- ENE pincer systems 86–87
 - esters synthesis 4
 - cross-esters synthesis from primary and secondary alcohols 9–11
 - from primary alcohols 4–9
 - polyesters synthesis from diols 11, 13–15
 - by secondary alcohols acylation 9, 11–13
- f**
- frustrated Lewis pairs 77
- g**
- Grignard reagents 54–61, 118–120, 122–129, 132, 133, 151, 152, 201, 222
- h**
- Heck reactions 32, 34, 41, 48–54, 253–256
 - computational investigations on thermal feasibility of cycles 262
 - – cycles and nanoparticle formation 274–275
 - – phenyl bromide oxidative addition and investigations on mechanisms 263–265
 - – possible initial reaction steps 263
 - – proposed cycles 270–274
 - – styrene coordination and chloride dissociation and investigations on mechanisms 265–270
 - intermediates and nanoparticle formation promoted by single system 256–262
 - hydrocarboxylation 231–232
 - of 1,3-dienes 234–235
 - of allenes 232–234
 - hydrogenation and dehydrogenation 223–225
 - hydrogen atom abstraction (HAA) 285, 286
 - hydrogenolysis of late-transition-metal hydroxide and alkoxide complexes 289–294
 - hypervalent iodines reactions 107
 - acetoxylation 109–111
 - alkenes arylation 107–109
 - alkenes C–H borylation 112–114
- i**
- imidazolines stereoselective synthesis 96–99
 - imines allylation 102–105
 - imines and isocyanoacetates reactions
 - chiral pincer complexes application 99–100
 - imidazolines stereoselective synthesis 96–99
 - mechanistic considerations 101–102
 - isotopic labeling 219
- k**
- ketones transfer hydrogenation 157
 - Kharasch reaction 46–48
 - Kumada synthesis 54–59, 61
 - Kumada–Corriu–Tamao coupling 118–129
- l**
- LXL tridentate pincer ligation 150
- m**
- Mizoroki–Heck reaction 140
 - Mulliken spin density 203
- n**
- Negishi coupling 54–58, 132–139
 - Negishi cross-coupling reaction 275–277
 - Ni, Pd, and Pt pincer complexes in oxidation states 34
 - higher oxidation states complexes (III, IV) 34–43
 - reduced complexes with pincer ligands 43–46
 - nickel-catalyzed cross-coupling reactions 117
 - carbon–carbon bond-forming reactions 141–142
 - – Kumada–Corriu–Tamao coupling 118–129

- – Mizoroki–Heck reaction 140
 - – Negishi coupling 132–139
 - – Sonogashira coupling 139
 - – Suzuki–Miyaura coupling 129–132
 - carbon–heteroatom bond-forming reactions 143–144

 - o**
 - olefins reactions 219–221
 - organonitriles C–H functionalization
 - benzyl amine synthesis 103–107
 - imines allylation 102–105

 - p**
 - palladium complexes synthesis bearing
 - PXP-pincer ligands (X=Si, Ge, Sn)
 - structural analyses 230–231
 - synthesis 230
 - palladium pincer-catalyzed C–C cross coupling reactions 250, 252–253
 - complex organic molecules synthesis 249–251
 - computational investigations on thermal feasibility of cycles of pincer-catalyzed Heck reactions 262
 - – cycles and nanoparticle formation 274–275
 - – phenyl bromide oxidative addition and investigations on mechanisms 263–265
 - – possible initial reaction steps 263
 - – proposed cycles 270–274
 - – styrene coordination and chloride dissociation and investigations on mechanisms 265–270
 - Heck reactions 253–256
 - – intermediates and nanoparticle formation promoted by single system 256–262
 - theoretical investigations on pincer-catalyzed Negishi cross-coupling reaction 275–277
- PCP pincer systems 88
- PC(sp³) P complexes reactivity and catalytic applications
- ammonia activation 217–218
 - carbon–carbon coupling reactions 221–223
 - – CO₂ activation 225
 - coordinated olefins reactions 219–221
 - hydrogenation and dehydrogenation 223–225
 - isotopic labeling 219
- PEP pincer systems 88–90
- peptides synthesis from β -amino alcohols 24–26
- phenyl bromide oxidative addition and investigations on mechanisms 263–265
- PNP-pincer ligand 118
- polyamides synthesis from diols and diamines 20–24
- polyesters synthesis from diols 11, 13–15
- PSiP chemistry
- group 8 metal 153–160
 - group 9 metal 161–169
 - group 10 metal 169–179
 - group 11 metal 179
- pyridine-2,6-diimine systems 90–91
-
- r**
- redox-active bis(imino)pyridine pincer ligands 189
- reduced manganese, iron, and cobalt complexes 189–190
- – reduced bis(imino)pyridine cobalt chemistry 200–209
- – reduced bis(imino)pyridine iron chemistry 193–200
- – reduced bis(imino)pyridine manganese chemistry 190–193
- redox process 31–34
- atom-transfer radical addition (ATRA) and polymerization reactions (ATRP) 46–48
 - – carbon–heteroatom coupling reactions 62–65
 - – C–C cross-coupling reactions 54–62
 - – Heck reaction 48–54
 - Ni, Pd, and Pt pincer complexes in oxidation states 34
 - – higher oxidation states complexes (III, IV) 34–43
 - – Ni, Pd, and Pt reduced complexes with pincer ligands 43–46
- reductive aldol type reaction 235–237
-
- s**
- η^2 -(Si–H)Pd(0) complex synthesis and reaction as equivalent to PSiP-palladium hydride complexes 241
- reaction with allene 242–243
- reaction with diboron 244–245
- synthesis and structure 241–242
- saturated frameworks and pincer complexes 213
- carbometallated PC(sp³) P complexes synthesis and coordination behavior 215–216

- saturated frameworks and pincer complexes
(*contd.*)
- – acyclic PC(sp³) P complexes coordination flexibility 216–217
 - ligands synthesis 213–214
 - PC(sp³) P complexes reactivity and catalytic applications
 - – ammonia activation 217–218
 - – carbon–carbon coupling reactions 221–223
 - – CO₂ activation 225
 - – coordinated olefins reactions 219–221
 - – hydrogenation and dehydrogenation 223–225
 - – isotopic labeling 219
 - silyl-based pincer-like bis(phosphino)silyl (PSiP) transition-metal pincer complexes 149–150
 - alternative silyl pincers 180–182
 - group 10 metal PSiP chemistry 169–179
 - group 11 metal PSiP chemistry 179
 - group 8 metal PSiP chemistry 153–160
 - group 9 metal PSiP chemistry 161–169
 - syntheses 151–153
 - Sonogashira coupling 54, 139
 - square-planar d⁸ pincer complexes with oxygen and hydrogen 281–284
 - hydrogenolysis of late-transition-metal hydroxide and alkoxide complexes 289–294
 - molecular oxygen insertion into-late-transition-metal hydride bonds 284–289
 - Stille coupling 32, 54, 57
 - styrene coordination and chloride dissociation and investigations on mechanisms 265–270
 - sulfonimines
 - asymmetric benzylation 107
 - catalytic benzylation 106
 - Suzuki coupling 31, 54, 55, 57
 - Suzuki–Miyaura coupling 129–132
- t**
- 2,2':6',2''-terpyridine incorporating systems 75
 - appended hydrogen-bond acceptor/donors 79–84
 - appended Lewis acid/bases 77–79
 - synthetic strategies 75–77
 - transesterification reaction 9
- u**
- unsaturated hydrocarbons catalytic synthetic transformations 229–230
 - η²-(Si–H)Pd(0) complex synthesis and reaction as equivalent to PSiP-palladium hydride complexes 241
 - – reaction with allene 242–243
 - – reaction with diboron 244–245
 - – synthesis and structure 241–242
 - – mechanistic considerations 239–241
 - – of alkenes and 1,3-dienes 237–239
 - hydrocarboxylation 231–232
 - – of 1,3-dienes 234–235
 - – of allenes 232–234
 - palladium complexes synthesis bearing PXP-pincer ligands (X=Si, Ge, Sn)
 - – structural analyses 230–231
 - – synthesis 230
 - reductive aldol type reaction 235–237